Acta Geodaetica, Geophysica et Montanistica Hungarica

VOLUME 25, NUMBERS 1–2, 1990

MINING SAFETY PROJECT REPORT

Edited by F Martos †

Akadémiai Kiadó, Budapest
AGGM 25 (1–2) 1–225 (1990) HU ISSN 0236-5758

ACTA GEODAETICA, GEOPHYSICA et MONTANISTICA HUNGARICA
A Quarterly Journal of the Hungarian Academy of Sciences

Acta Geodaetica, Geophysica et Montanistica (AGGM) publishes original reports on geodesy, geophysics and minings in English.

AGGM is published in yearly volumes of four numbers by

AKADÉMIAI KIADÓ
Publishing House of the Hungarian Academy of Sciences
H-1054 Budapest, Alkotmány u. 21.

Manuscripts and editorial correspondence should be addressed to

AGGM Editorial Office
H-9401 Sopron P.O. Box 5

Subscription information

Orders should be addressed to

KULTURA Foreign Trading Company
H-1389 Budapest P.O. Box 149

INSTRUCTIONS TO AUTHORS

Manuscripts should be sent to the editors (MTA Geodéziai és Geofizikai Kutató Intézete, AGGM Editorial Office, H-9401 Sopron, P.O.Box 5, HUNGARY). Only articles not submitted for publication elsewhere are accepted.

Manuscripts should be typewritten in duplicate, double-spaced, 25 lines with 50 letters each. The papers generally include the following components, which should be presented in the order listed.

1. Title, name of author(s), affiliation, dateline, abstract, keywords
2. Text, acknowledgements
3. References
4. Footnotes
5. Legends
6. Tables and illustrations

1. The *affiliation* should be as concise as possible and should include the complete mailing address of the authors. The *date of receipt* of the manuscript will be supplied by the editors. The abstract should not exceed 250 words and should clearly and simply summarize the most important methods and results. 5–10 significant expressions describing the content are used as *keywords*. Authors may recommend these keywords.

2. The *text* should be generally in English and as short and clear as possible. From Hungarian authors papers are also accepted in Hungarian.

The section heading should *not* be underlined or in capitals.

Please note that underlining denotes special types:

— single underlining: italics
— double underlining: bold-face roman

ACTA GEODAETICA, GEOPHYSICA et MONTANISTICA
A Quarterly Journal of the Hungarian Academy of Sciences

VOLUME 25

AKADÉMIAI KIADÓ, BUDAPEST
1990

CONTENTS

Book Reviews

Report for the International Lithosphere Program

General Section

Book Reviews

AUTHOR INDEX

KEYWORD INDEX

CONTENTS

Book reviews

FOREWORD

IMPROVEMENT OF MINING SAFETY VIA SCIENTIFIC RESEARCH

Normally the Editor-in-Chief does not write introduction or preface to numbers or volumes of Acta. When he has done it is for two reasons. These are:

1. The Editor-in-Chief, being a researcher himself, is the project leader and coordinator of the scientific activity reviewed in this volume.
2. The present issue contains results of fundamental research under the financial support of the so-called Hungarian Scientific Research Fund (OTKA) which will be presented at the first time.

It should be added that these papers only deal with the first partial results of a large-scale complex research planned for several years and, due to the limited size of this volume, selected passages are only offered from the scientific production of the first two-three years.

WHAT IS THE MATTER AT ALL?

On the initiative of the Hungarian Academy of Sciences a special financial fund was established by the Hungarian Government in 1986 which provides the possibility of support for all branches of science in the field of fundamental research of greatest importance. This financial fund is the Hungarian Scientific Research Fund (OTKA). Financial support may be obtained through a competition system. Within the scope of mining science the exploitation safety of mineral raw materials represents a field which consists of problems reguiring a lot of fundamental research to be solved. The understanding of the character of the field and tasks may be easier by drafting the accepted subject of mining science in a schematic way. This might be needed even for the reason that in all those cases when any branch of material production is in question (e.g. mining, metallurgy, architecture, etc.), normally the technical

and economic processes of the technological development of production can hardly be separated from the specific human activity which is qualified as scientific research. It is easier to distinguish them in the field of the natural and social sciences. In these cases the research and especially its phase called fundamental research can be separated in a much clearer and easier way (if such a "distinction" is necessary at all) from the development and application process of the results, the latter being the ultimate object of every scientific research.

WHAT IS TO BE UNDERSTOOD UNDER MINING SCIENCE?

In our opinion mining science deals with laws of phenomena which are the results of the fact that the exploration and especially the exploitation of mineral raw materials and sometimes their processing as well represent rather "drastic" interventions into the natural environment including not only the solid crust of the earth (as the natural host medium of these materials) but also significant zones of the hydro- and atmosphere.

Namely, mining science is a coherent system of knowledge about the laws of material- and energy-flows which proceed in space and time as a consequence of the establishment and abandonment of caverns caused by the exploitation of minable mineral raw materials from the three-phase crust of the earth. With their knowledge - in connection and in interaction with a number of other branches of science - these laws can be disclosed, recognized and interpreted. Based on these laws operations can be selected which help to prevent and avert the consequences of these movements, or to control, influence and eliminate their effects. It is obvious that in our interpretation an open pit and a deep borehole are the same "caverns" developed in the earth's crust like the roadway system of an underground mine and large-size workings. The intrusion into the earth's crust results, first of all, in a disturbance of the original stress conditions. The consequence of this

disturbance is a "reaction", some kind of "answer" of both materials in solid and fluid phase and in form of rather complicated interactions. The reaction of the original material in a relative equilibrium manifests itself in response to cavern-building and abandonment in processes of motion, in changes of quality and condition, in transport processes of materials and energy. The three-phase medium in which these processes take place is neither homogeneous, nor isotropic at all and naturally it is not a continuum.

That means that the analysis of material behaviour, the recognition of its laws of operation, and the development of possible process control methods are by no means simple tasks. Essentially, however, this is the subject of mining science.

Due to the processes in motion mentioned above the following natural hazards endangering mining activity appear:
- deterioration of rock environment (faults, collapses),
- gas phenomena (gas outbursts, damp explosions),
- water hazard (water inrush),
- mine fires due to self-ingition,

and other sources of hazards.

These may cause not only damages and sometimes destruction of material values, but endanger the health and life of people working in the mine.

In the Hungarian mining the influence of natural hazards, the frequency of their occurrence are potentially increasing with the operations moving towards greater depths and geologically and tectonically more disturbed areas, and with the operations carried out below the static level of water stored in karstic rocks. With them the risk of production is strongly increasing. The influence of environmental effects and the processes endangering the natural environment are also added to them. Essentially these are the circumstances which led to the support of our fundamental research in this field from state financial sources and by the Fund mentioned.

The exact and official title of the project is: "Complex research works establishing and supporting the increase of mining safety to disclose control possibilities based on the

interactions of the natural system". It is planned for five years and is based in principle on experiences and scientific results obtained in several decades.

The research is carried out in several fields by the staff of a number of institutions (research institutes, university departments). To give a better idea on the subject a brief explanation will be given in the followings about the main relations and connections among the elements of the system. The increase of mining safety requires the availability or establishment of the corresponding conditions. A common feature of these conditions is that a definite kind of balance of factors interacting with each other should be obtained, very often, even nearly in all cases, by compromise solutions. In actual cases, however, there is a possibility of making choice among different alternatives, a well selected compromise will represent the optimum solution.

In our case the factors to be taken into account form a coherent system divided into two groups:

1. System of natural factors
- in their original, undisturbed condition, and
- in the changed and continuously changing condition due to mining interventions.

2. System of the technical-technological factors of production
- a chain of caverns of varying lifetime developed in the earth's crust in space and time with different sizes and locations, and
- structures ensuring the stability of caverns, the relative balance of the host rock, solutions, methods and means to influence the state of rocks, further their material (water, gas) and heat conductivity conditions as well.

These system groups of factors are not treated here in detail. We refer to them by means of some obvious examples. These are:
- the geometry, the physical state, material properties of the mineral occurrence,
- changes due to mining interventions, intrusions, as

a) loosening, displacement of rocks,
b) flow of fluids, gases and heat,
c) the change of flow in space and time,
d) effects appearing at the surface, further

- means to keep the underground areas open
  a) supporting structures,
- consolidating and scaling procedures to modify the characteristics of permeability and rock conditions respectively,
- reduction of heat by means of ventilation, and simultaneously the decrease and provention of the possibilities of self-ignition, etc.

At this point it should be emphasized that there are manifold interactions between the natural and technical systems, and what is more, such interactions are continuously arising from the operation of the production process, because the technical system of mining (production) provides the constant conditions of changes of the natural system as well as the boundary conditions defining these changes continuously.

The task is just the detection of these interactions to influence deliberately and last but not least to control expediently the activity of the elements of the natural system, by applying the appropriate technical means. If we know better the character of the natural system elements and the changes of their active mechanism, then it will be possible to influence, with hope of success, the different forms of natural hazards not only separately in each case, but together, too. This is the more important, as they have a common reason of development. Namely: the underground cavern-system is the general and necessarily inseparable consequence of mineral exploration and exploitation.

The method of research should undoubtedly be an approximate formulation of the physics of processes on one hand and a statistical elaboration of data obtained partly from laboratory tests (e.g. from material models), but mostly from observations of the nature on the other hand. In the next step simulation models of the individual subsystems should be established and finally these models connected. This way a real process control

would be reached.

From the papers in this volume it is easy to recognise that they deal with some considerable factors of the natural and technical systems, they include the investigation of some essential elements of these systems as well as the results.

After having finished the present stage, in one or maybe two further issues of the Acta, it should be possible to report on the final results in a more complete and more comprehensive way and in a more detailed form.

Thanks are to be expressed to the Hungarian Academy of Sciences and to the Hungarian Government for the financial support.

F Martos†

Acta Geod. Geoph. Mont. Hung., Vol. 25 (1-2), pp. 9-23 (1990)

AUTHENTICITY OF DETERMINATION OF TECTONIC CHARACTERISTICS IN COAL DEPOSITS

F Kovács

Department of Mining, Technical University for Heavy Industry,
H-3515 Miskolc, Egyetemváros, Hungary

The author characterizes the reliability of the parameters determined by geological prospecting on the basis of a comparison between the predicted and actual tectonic data of various coal deposits. Geological prospecting can only predict 10 to 20 percent of the actual faults.

It is verified by means of a statistical analysis that the throw of faults as a probability variable has lognormal statistical distribution.

The analysis proves that it is possible to determine the rate of predicted and actual tectonic parameters as a function of throw. Using regression functions the probable tectonic parameters (frequency of faults, specific strike-length and fault plane area) can be estimated on the basis of geological prediction.

Keywords: coal deposits; faults; Hungarian coal mines; predicted tectonics; tectonic structure

The tectonic structure of coal-occurrences is of outstanding importance among the factors determining the complexity of exploitation. The exposure of the set of workings and of the individual working faces, the length of drift driving in the country rock and the conditions of drift driving are largely determined by the tectonic situation (the site and size of faults and other geological discontinuities).

It is the task of geological prospecting - and partly that of mining exploration - to carry out a preliminary exploration of the spatial situation of the layer. But, naturally, this preliminary exploration is limited. On the one hand, the number of prospecting drill-holes cannot be increased beyond a certain limit, and, on the other hand, only quantitative characteristics can be obtained by geophysical methods in some instances.

On the basis of experiences of mining exploration, the

actual tectonic situation is very often considerably different from the one predicted by geological prospecting data. The predicted tectonic situation usually contains some uncertainty, the reliability of tectonic parameters is of a relatively low level.

According to data relating to the Karaganda basin, 5 to 17.1 percent of tectonic disturbances is detected by geological prospecting. In the period of planning and mine construction the rate of detection rises by 3.5 to 10.6 percent. The majority of the faults (72.3 to 91.6 percent) becomes only known during exploitation. The rate of preliminary detection - relating to the total number of faults - is 10 to 15 percent (Kovács 1988).

The present examination covered in Hungary the territory of six mining works (Lyukóbánya, Oroszlány shaft 21, Balinka, Márkushegy, Nagyegyháza, Mány). An evaluation of the data of the "reliability" of geological prospecting in predicting the tectonic situation led to the fact that the geological prospecting using deep-drilled holes was able to detect 7.3 to 47.8 percent of the actual faults with more or less accuracy as regards location. The mean value of the reliability of the prediction of faults was 15.2 percent in the territories examined.

The rate of the preliminary detection rises with the increase in the throw of faults. According to the data on the Karaganda basin the majority (88.9 to 93.1 percent) of the faults with a throw of less than five meters were only discovered in the period of mining exploration and exploitation. The faults with a throw of more than 10 m are detected in a considerable extent (17.6 percent) already in the period of geological prospecting. The rate of the preliminary detection is only acceptable for throws of more than 15 m, where geological prospecting detects tectonic disturbances with a reliability of 60 percent.

On the basis of the exhaustive examination of the six Hungarian territories it was found that prospecting predicted

faults with a throw of less than 5 m with a reliability of 5 to 8 percent, faults with a throw of 6 to 10 m with a reliability of 25 to 29 percent, faults with a throw of 11 to 20 m with a reliability of 33 to 38 percent and faults with a throw of over 20 m with a reliability of 83 to 90 percent.

The relatively low reliability level of geological prospecting manifests itself not only regarding the sites and number of faults, but also regarding the throws. The throw of the faults found at the site predicted by prospecting is on an average only 84 percent of the predicted value. A comparison of the mean throws of all predicted faults to those of the actual faults shows that the throw of the actual faults is only 30 to 70 percent (47 percent on an average) of the predicted mean value.

On the basis of the data presented, the tectonic characteristics given by the preliminary geological prospecting do not give a realistic picture (in an absolute sense) of the disturbance of the occurrences or of the mining conditions to be expected. Only 10 to 20 percent of the actual faults are predicted, only big tectonic disturbances (with a throw of more than 20 m) are indicated exactly as regards locality. At the same time the prediction gives a higher value of throw than the one that can actually be expected.

To characterize the tectonic intensity of deposits in the horizontal direction the number of faults (number) or the specific number of faults, density (number/km^2) can be used. This parameter, however, does not give a complete picture of the tectonic situation in itself, as it does not contain the size of the faults, the length of the strike or of the throw.

Another characteristic of the tectonic intensity in the horizontal direction is the specific value of the strike-length of the faults (km/km^2) which gives the total amount of strike--lengths in a unit area. This parameter reflects the general character of the tectonic situation, informs about the probable technical and economic conditions of exploitation.

The third useful parameter is the specific area of fault planes (km^2/km^2) which shows the area in km^2 of fault planes

per unit area of the deposit. This last parameter is naturally determined by the specific strike-length (km/km^2) and the throw of the faults.

DETERMINATION OF THE PROBABLE THROW OF FAULTS

In a first step the probable throw of faults is determined as statistical analyses show that the throw is decisive in determining the reliability of geological prediction. The reliability of the prediction (prediction of the number and location of faults) rises with an increase in the throw of faults, and vice versa.

The first three columns of figures in Table I show - by giving full details of the actual data - the prediction and the actual throw for the faults predicted during prospecting and for the actual faults which appeared at the predicted sites. The second three columns of figures in the table give the average throw of all the predicted and all the actual faults.

Thus the prediction by geological prospecting does not give an exact approximation of the actual situation. A method is to be found to determine parameters characterising the probable actual tectonic situation from the data of the prediction.

This analysis can be performed by using a statistical method on the basis of the probability theory. In investigations of this kind the first thing to do is - on the basis of examination of the fitting and theoretical considerations - to determine the statistical distribution of the set of data (in this case: the throw of faults). Namely, the computational relations are determined by the character of the statistical distribution.

The examination of the hypothesis was carried out on the basis of the predicted and actual data of five territories (Oroszlány shaft No. 21, Balinka, Márkushegy, Nagyegyháza, Mány).

On the basis of the mathematical statistical examination of the throws of the faults predicted by preliminary geological prospecting and of those of the actual faults, the throw of the

Table I. The predicted and actual mean values of throw of faults

Number	Territory	The mean throw of faults (m) whose accurate site was indicated during geological prospecting			Throw of total faults (m)		
		Predicted mean value	Average of actual values	Reality / Prediction	Predicted mean value	Average of actual values	Reality / Prediction
1.	Lyukóbánya	10	6	60	10	3	30
2.	Oroszlány, shaft No. 21	43	35	81	30	23	77
3.	Balinka	34	24	71	34	13	38
4.	Márkushegy	85	62	73	54	21	39
5.	Nagyegyháza	54	57	105	32	13	41
6.	Mány	40	39	98	31	19	61
7.	Total	44	37	84	32	15	47

faults as a probability variable has a lognormal statistical distribution. The hypothesis was verified by the Kolmogorov--Smirnov test (Rényi 1954).

The empirical distribution functions were first determined for the throw values then the parameters of the lognormal distribution were calculated by regression calculation.

According to Kolmogorov's law, if a 99 percent probability level is desired,

$$\sup \left[F_n(x) - F(x)\right] = DF_{max}$$

must be less than

$$\frac{1.63}{\sqrt{N}}$$

with a probability of 99 percent. If this requirement is satisfied, the hypothesis is accepted.

On the basis of the data of Table II, the condition

$$DF_{max} < \frac{1.63}{\sqrt{N}}$$

Table II. Calculated data of fitting

Mining works	Predicted value			Actual value		
	DF_{max}	N'	$\frac{1.63}{\sqrt{N'}}$	DF_{max}	N	$\frac{1.63}{\sqrt{N}}$
Oroszlány	0.161	21	0.356	0.214	20	0.364
Balinka	0.113	22	0.348	0.120	65	0.202
Márkushegy	0.211	24	0.333	0.208	79	0.183
Nagyegyháza	0.205	21	0.356	0.074	124	0.146
Mány	0.124	18	0.384	0.190	52	0.226

is satisfied in nine cases; the hypothesis of lognormal distribution is not valid for the actual data of Márkushegy (where

the two calculated values are nearly equal). The reason for this is that all the faults with low throws (M < 1 to 1.5 m), discovered in a large number in individual areas during exploitation, were included in the data.

It was verified on a high probability level in nine cases (90 percent of all cases) that the throw distribution of the faults has a lognormal distribution. From the character of the distribution it follows that

- the probable value M can be approximated by the arithmetical mean
- the probable value can be calculated from the parameters m and σ of the distribution function by the relation

$$M = e^{m+\frac{\sigma^2}{2}} .$$

Three of the results of the detailed calculations will be presented here. Figure 1 shows the distribution function calculated from the data predicted for shaft No. 21. The number of data (faults) N', the probable value m' and the standard deviation σ' of the distribution function are given in the figure. The value M'_0 gives the degree of the displacement of the function in the direction of the x-axis what means that the function does not start from x = 0, but from x = M'_0. Figure 2 presents the distribution function determined by the actual faults.

The "displacement" of the function in the direction of the range of smaller throws is conspicuous. The probable (mean) value of the throw of predicted faults is 29.41 m, that based on the data of the actual faults is 21.58 m. This significant discrepancy is the result of a dual effect. On the one hand, the throw of faults whose sites were accurately indicated during prospecting is, generally, 10 to 30 percent less than the value estimated during prospecting. On the other hand, prospecting predicts faults with a bigger throw with a probability of 60 to 100 percent, while faults with a smaller throw (0 to 10 m) are predicted only on a less part (0 to 20 percent). At the same time faults with a small throw appear in a large

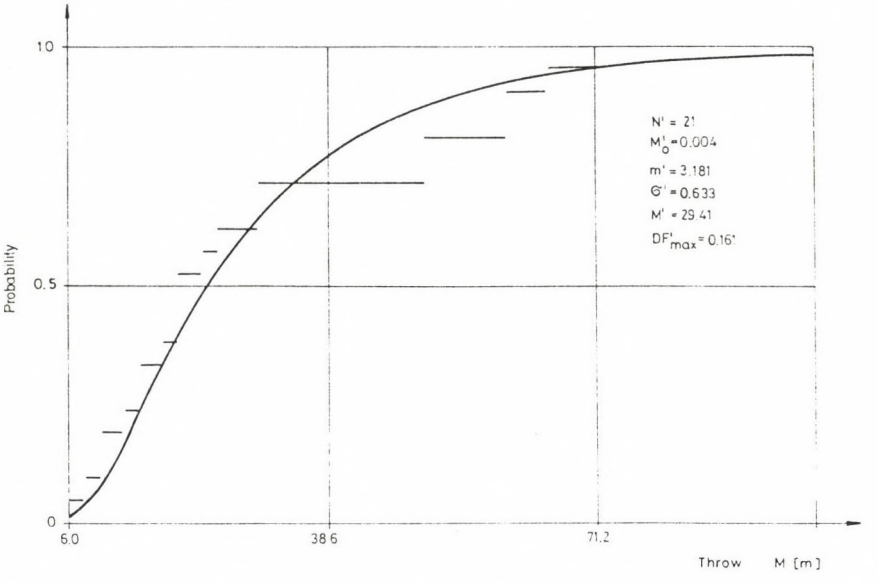

Fig. 1. The distribution function of throw data of predicted faults (Oroszlány, shaft No. 21)

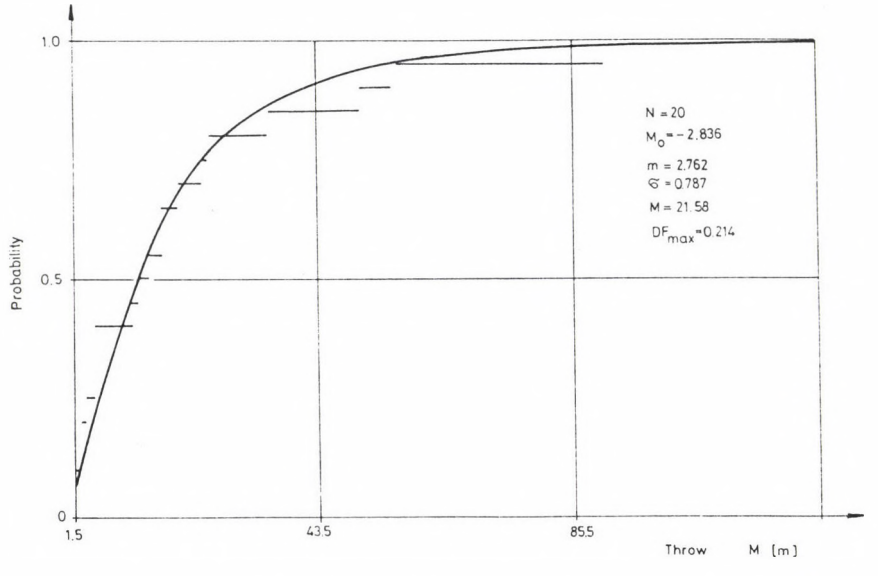

Fig. 2. The distribution function of throw data of actual faults (Oroszlány, shaft No. 21)

number during exploitation and decrease the mean throw of the actual faults.

Figure 3 presents results from data of Balinka. The average throw of predicted faults is 38.58 m, the value expected on the basis of data of actual faults being 11.26 m.

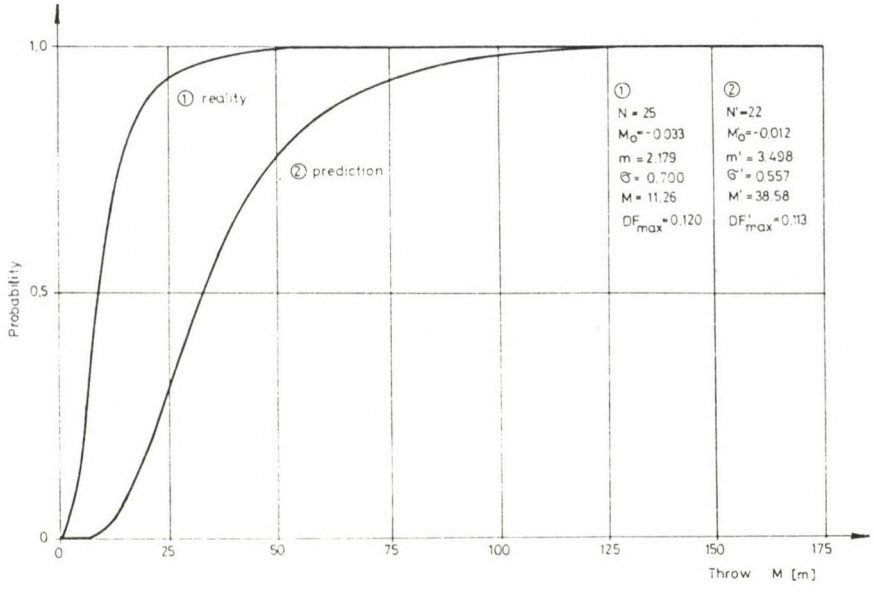

Fig. 3. The distribution function of throw data of predicted and actual faults (Balinka)

Figure 4 shows the data of mining works of Nagyegyháza. The predicted mean throw is 26.72 m, the probable value calculated on the basis of the data of actual faults 6.71 m. The mean throw of faults, the calculated parameters of the distribution functions are included in Table III.

The task is to give a method on the basis of the results of the present investigation for the determination of the probable parameters of the actual tectonic situation starting from the prediction made on the basis of the data of geological prospecting. The parameters of the predicted and the actual situation are supposed to develop in a new field of prospecting in the same way as in areas prospected earlier and already

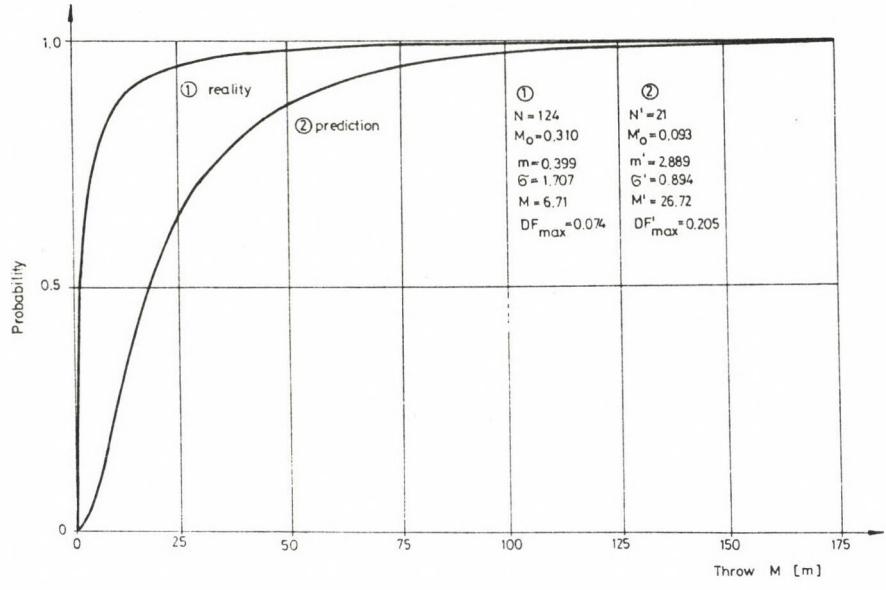

Fig. 4. The distribution function of throw data of predicted and actual faults (Nagyegyháza)

Table III. The parameters of throw data and distribution functions in the individual territories

Territory	Mean throw of faults		The calculated parameters of distribution functions			
	Prediction	Reality	Prediction		Reality	
	M'	M	m'	σ'	m	σ
Oroszlány, shaft No. 21	29.4	21.6	3.18	0.63	2.76	0.79
Balinka	38.6	11.3	3.50	0.56	2.18	0.70
Márkushegy	51.0	11.0	3.67	0.76	1.44	1.40
Nagyegyháza	26.7	6.1	2.89	0.89	0.40	1.71
Mány	33.0	12.9	2.84	0.88	1.14	1.92

exploited, if the methods of prospecting and their accuracy, respectively, do not change fundamentally.

The regression functions giving the relation between the predicted and actual data were calculated on the basis of data of five mining works. Figure 5 shows the function describing the relation between the probable values m' and m and Fig. 6 presents the function describing the relation between the standard deviations σ' and σ.

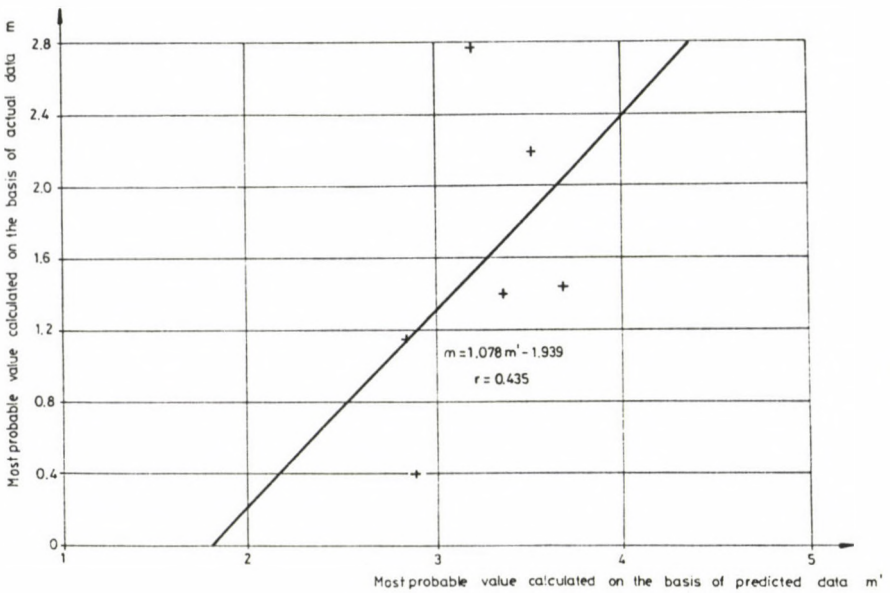

Fig. 5. The function describing the relation between most probable values

In the case of a new area of prospecting where the prediction of geological prospecting is known the parameters (m, σ) characterising the probable actual situation can be calculated on the basis of the predicted data (m' and σ'), using the equation of the regression functions. From the distribution parameters m and σ - knowing the character of distribution - the mean (probable) throw of faults (M) as well as the distribution (distribution function) can be calculated according to the throw of the probable number of faults (to be determined separately).

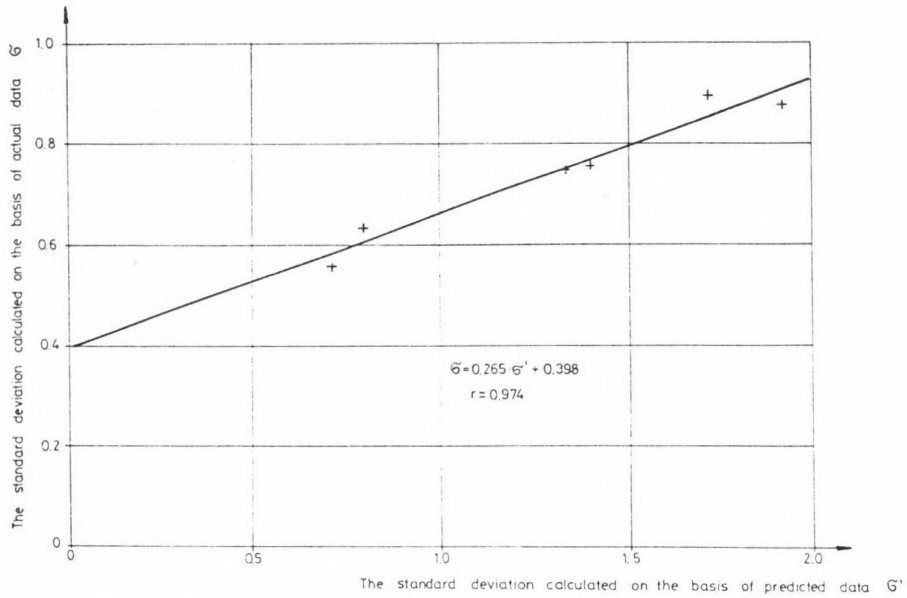

Fig. 6. The function describing the relation between standard deviations

DETERMINATION OF THE PROBABLE NUMBER AND STRIKE-LENGTH OF FAULTS

Table IV gives the ratio of the actual and predicted values of the number, the strike-length and fault plane area for the individual mining works.

The data of the individual territories show that the reliability of predicting faults with a small throw is lower and the probability of their preliminary detection is of a lower level. It follows from this that on territories with a large number of small faults the rate of actual and predicted faults is higher. In other words, there is some kind of relation between the throw of faults (the mean throw) and the preliminary detection rate. Considering this, the changes in the ratios N/N', L/L', T/T' vs. can be determined.

Figure 7 presents the prediction ratio of the number of faults (rate of discovering) as a function of the mean throw of faults. The rate of preliminary detection improves regularly with the increase in throw, the ratio N/N' decreases considerably.

Table IV. The predicted and actual tectonic characteristics in the individual territories

Territory	The rate of actual and predicted parameters		
	Number of faults N/N'	Strike-length of faults L/L'	Fault plane area T/T'
Lyukóbánya	16.00	3.61	1.28
Oroszlány, shaft No. 21	0.85	0.80	0.63
Balinka	2.95	2.17	0.82
Márkushegy	3.29	1.69	0.67
Nagyegyháza	5.90	2.79	1.12
Mány	2.89	1.49	0.92
Average	3.97	1.98	0.80

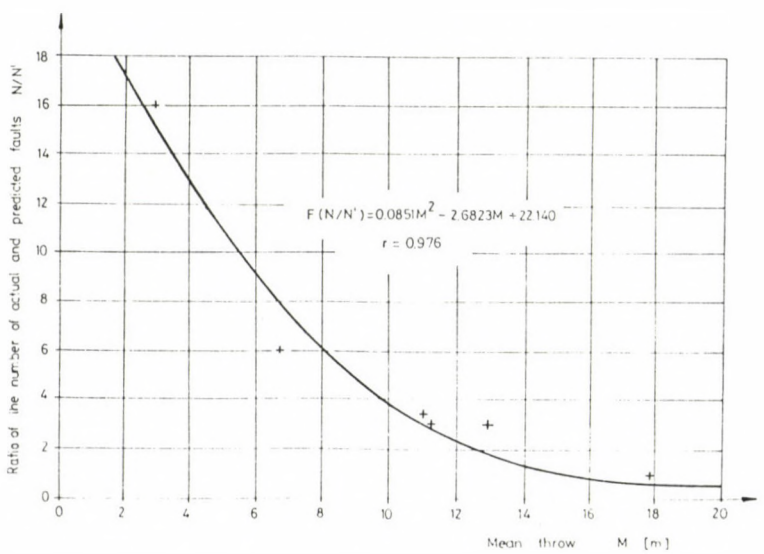

Fig. 7. Ratio of the number of actual and predicted faults vs. mean throw

By using the function determined above, e.g. if M = 6.5 m,

the ratio N/N' is 8.3. If the prediction indicated, say, 30 faults in an area of 20 km^2 of the given deposit, the probable actual number of faults is 250, and the probable density of faults is 12.5/km^2.

A similar method can be used in estimating the probable strike-length of faults. The regression function of Fig. 8 gives the ratio L/L' vs. mean throw. The correlation indicates a close connection, the reliability of the prediction improves with an increase in throw. If M = 6.5 m, the ratio L/L' is 2.813. If in the given case the prediction gives 80 km as total strike-length in a productive territory of 20 km^2, the probable value is 225 km, the specific strike-length of faults being 11.25 km/km^2.

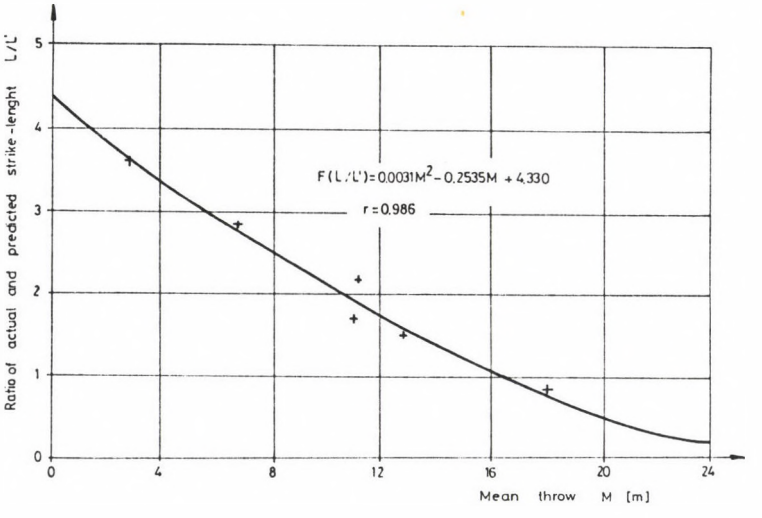

Fig. 8. Ratio of actual and predicted strike-lengths vs. mean throw

The relation between the prediction rate and mean throw in case of fault plane area is presented in Fig. 9. The regression relation is close, the reliability of the prediction improves with an increase in throw. An example to illustrate this: if M = 6.5 m, the ratio T/T' is 1.062. If T' = 1.8 km^2, T = = 1.91 km^2, for a productive area of 20 km^2 the specific fault

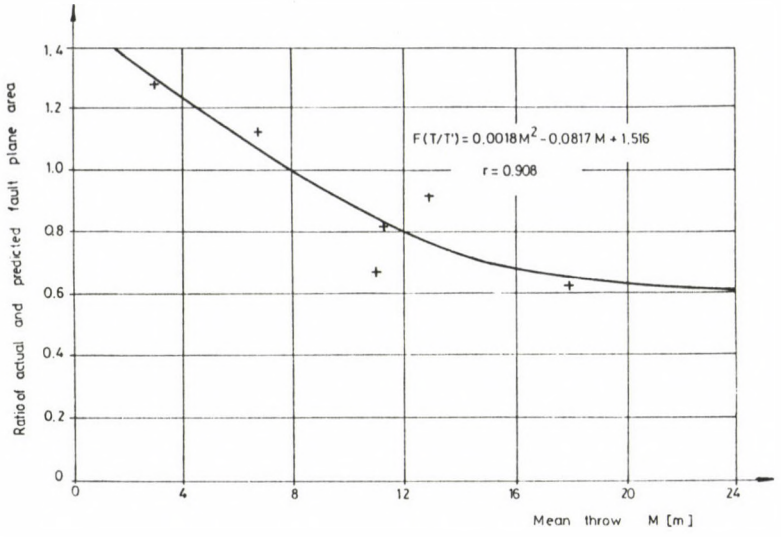

Fig. 9. Ratio of actual and predicted fault plane area vs. mean throw

plane area is 0.096 km^2/km^2.

This method makes it possible to calculate the probable tectonic parameters of a given deposit on the basis of the prediction data of geological prospecting. If the tectonic parameters are known, the technical implementation of prospecting and exploitation can be planned, the output and economic characteristics can be estimated.

REFERENCES

Jeneyné Jambrik R 1987: Bányászati és Kohászati Lapok, Bányászat,120, No. 2, 84-89.

Kovács F 1988: Földtani Kutatás, 31, 47-54.

Rényi A 1954: In: Probability computation (in Hungarian). Tankönyvkiadó, Budapest, 596-609.

Acta Geod. Geoph. Mont. Hung., Vol. 25 (1-2) pp. 25-38 (1990)

SPATIAL DEVELOPMENT OF OPTIMUM MINING SEQUENCE IN SOFT UPPER-SEAM AND BRITTLE LOWER-SEAM ROCK-ENVIRONMENT

M Petrássy

Central Institute for the Development of Mining, H-1037 Budapest, Mikoviny u. 2-4, Hungary

The study is dealing with tests and test results carried out and obtained respectively in the mine of Nagyegyháza to understand movement phenomena around faces surrounded by soft and brittle rocks of the Eocene period and to develop optimum mining sequence.

Keywords: brittle rocks; mining sequence; Nagyegyháza mine; soft rocks; support system; upper seam face operation

INTRODUCTION

The stratifical characteristics of the new coal basins of the Eocene period adjacent to the Tatabánya Coal Basin and among them the Nagyegyháza Coal Basin are very unadvantageous. Coal seams of this area are tectonically highly dissectioned, moderately folded and besides rock pressure increasing with depth, strength characteristics of the rocks are also declining in function of depth. The upper coal seam and surrounding rocks (Fig. 1) are very soft, but the surrounding rocks of the lower seam are brittle. Resulting from this characteristic feature of petrographical and stratigraphical conditions, the mining of coal occurrences in question has following essential problems:

- high degree and intensive plastic strata flow during upper-seam operations, further conservation of drift tunnels as well as main and tail gates originating from the problem above (Petrássy 1987);
- dynamic pressure phenomena appearing when undercutting brittle fresh water limestone with lower-seam faces and development of support structures for these dynamic loads (Petrássy 1987);

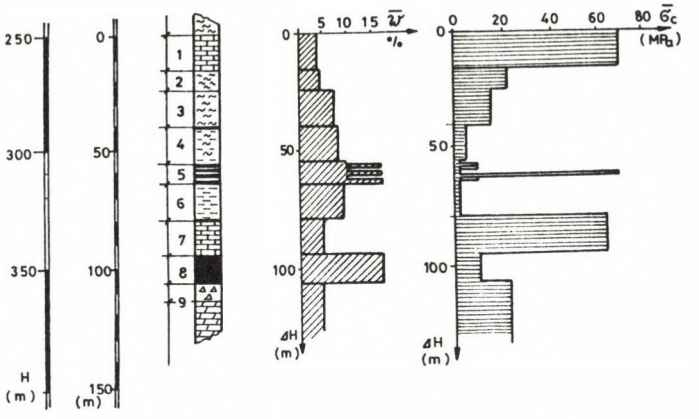

Fig. 1. Average water content and uniaxial compression strength of layers of the Eocene period in the coal basin of Nagyegyháza. 1 - limestone; 2 - marl; 3, 4 - clay, clayey marl; 5 - upper seam; 6 - fresh water clay; 7 - fresh water limestone; 8 - lower seam; 9 - redispositioned dolomite; 10 - stand-up dolomite

- assurance of the spatial system of optimum mining sequence between these two seams.

This study is disclosing how to determine the optimum mining sequence which is successful, if as a result of this mining sequence problems of supporting faces both in the upper and in the lower seams will be minimized.

PETROGRAPHICAL AND STRATIGRAPHICAL CONDITIONS OF PRODUCTIVE STRATA

The substratum of the coal basin of Nagyegyháza is the main dolomite of the Triassic period. This is the relatively rigid frame of the basin. Within this frame the basin sediments are located, with the lowest member redispositioned dolomite. The productive strata evolved on the repositioned dolomite (Fig. 1) with its lower part up to the adjacent roof of the upper seam, being marsh-sediments. This is followed by continuous sedimentation by some shallow-sea brackwater formations. The successive layers of the Eocene period are closed by salt-water sediments. The adjacent floor of the lower seam is a thin

marshy or continental clay of variable colour and redisposi-tioned dolomite.

The strata of the lower seam are composed of one or two benches, with an average uniaxial compressive strength of 10 MPa, the thickness is 5 to 15 m, the consistence of coal is good. The adjacent roof is fresh water limestone of 15 to 20 m thick-ness, with an uniaxial compressive strength of 60 to 100 MPa. Above the limestone a 5 to 10 m thick fresh water clayey marl layer follows of an uniaxial compressive strength of 1 to 2 MPa and of bad consistence. This is the adjacent roof of the upper seam. This rock is generally characterized by thin-benched, la-melled joints, rough lumpy fracturing and often by greasy joint planes. The upper-seam strata of 6 to 8 m thickness are devided into many benches, they contain 55 percent coal, 42 to 45 per-cent fresh water clay of very bad consistence and some percent fresh water limestone.

The adjacent roof of the upper-seam is of a variety of rocks, mostly globularian brackwater clay of very bad consis-tence having an average compression strength of 1.5 MPa and an average thickness of 16 m. This is followed with continuous sedimentation by consecutive layers (forming the high roof of the upper seam): globularian clay, clayey marl having an aver-age thickness of 15 m and a uniaxial compression strength of 15 MPa, nummulinar clayey marl of 9 to 10 m thickness and of 30 to 40 MPa uniaxial compression strength and a nummulinar, alveolinar limestone of 15 to 20 m thickness and very good consistence deposited over the foregoing layer. The average water content of the rocks in the successive layers is low. The uniaxial compression strength of the rocks downwards from the alveolinar, nummulinar limestone is exponencially decaying (Fig. 1) and its minimum value is in the upper seam and in its direct environment. According to petrographical potentialities from the point of view of conservation of upper-seam roadways and of plastic behaviour of rocks, the critical strata are the soft clay, clayey marl and coaly strata of 25 to 30 m thick-ness deposited above the fresh water limestone.

The upper-seam soft strata are abruptly followed by the thick-benched fresh water limestone of high strength which is the initial source of dynamic pressure phenomena of lower-seam faces.

SUPPORT SYSTEM OF MAIN AND TAIL GATES IN THE UPPER-SEAM

The essential problem of upper-seam operations is the conservation of drift tunnels and main and tail gates driven in plastic rock-environment. Experiences made it unambiguous that the support of upper-seam roadways is only adequate if support structures are applied in closed form simultaneously with the driving, the support resistance is sufficient, and the support structure has an adequate yield. In drift tunnels these requirements are met by (TH) arches of a specific mass of 33 kg/m. Based on these requirements a side dam support system of main and tail gates (Stuber and Petrássy 1986) has been developped; the basic idea has been taken from advantageous experiences of advancing faces of the British and German mining (Hunke 1976). Using these ideas the conception of the support system has been developped and it was investigated if a side dam (Fig. 2) built along a longwall gate supported with circular arches provides a protection for the gate which is suitable within a time interval to serve also the next face. In these experiments, pressure gauge boxes developed by the Institute of Water Engineering at the Technical University Budapest have been built into side dams (Halász 1984) and parallel with pressure detection the convergence of the roadways has also been measured.

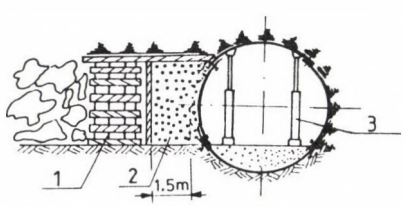

Fig. 2. Development of side dams. 1 - buttress; 2 - side dam; 3 - roadway with circular arch support system strengthened by hydraulic props

PRESSURE AND MOVEMENT PHENOMENA UNDER THE INFLUENCE OF UPPER--SEAM FACE OPERATION

According to the test results:

- the load acting on the side dam increases due to influence of the first face, with the moving-off of the face up to 40 to 60 m, then reaches the maximum value, and it starts to decrease;
- the second face causes only in the case a further increase of the load, if the common load bearing function of the gate and the side dam is not ensured;
- the convergence of longwall gates is monotonously increasing due to the influence of the first face. This process is not altered with decreasing load acting on the side dam;
- the speed of gate-convergence increases (due to the influence of the second face) but its rate is not depending on the extent of the load;
- the maximum value of the pressures measured in the side dams is 20 to 30 percent of the primary rock pressure.

An interpretation of the measured data resulted in the following:

- continuous and intensive plastic rock yield is taking place around the face, due to abutment transferred rock pressure and caving, the field of movement is devided in two parts (Fig. 3) in accordance with the current position of the face, i.e. in parts before and behind the face.
- Before the face and in the undisturbed rock bordering the gates, plastic rock yield is taking place following failing conditions: its maximum intensity is in a zone of 10 to 15 m width before the face.
- Based on load and convergence, three zones located besides each other can be distinguished in the space behind the face:
  a) a loosening zone,
  b) a solidifying zone and
  c) a zone of rocks of entirely plastic behaviour.

The loosening zone is an unloaded strip of 10 to 15 m width behind the face. Rocks of this area are caving and

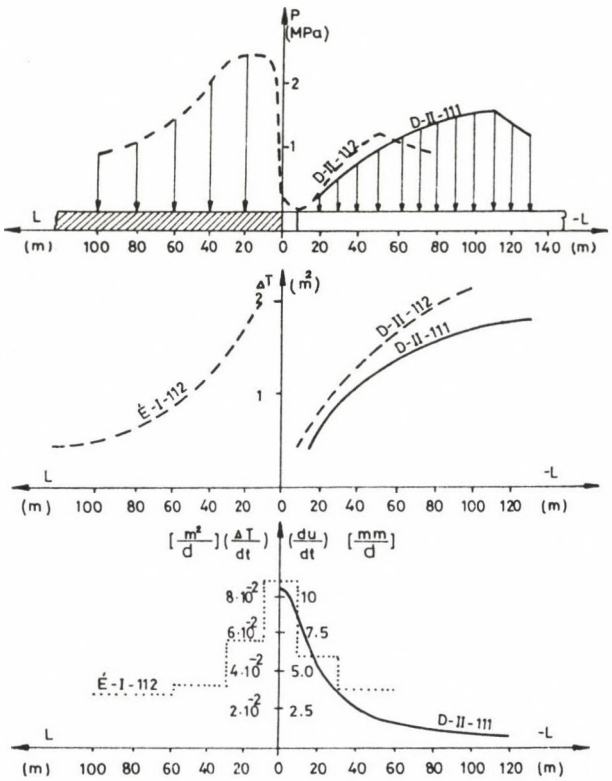

Fig. 3. Pressure p, section-contraction ΔT and rate of convergence in function of the distance L from the face

loosening, therefore the zone is unloaded. Since the loosened rocks of this zone are unloaded, the virgin rock adjacent to this zone gets the maximum transferred load what explains the maximum convergence-speed developed in a 10 to 15 m thick strip around the face.

The thickening rock zone (behind the first zone) extends to 50 to 60 m distance from the face. Due to the influence of thickening, the load is dynamically increasing in time and in proportion to time in function of the distance. With the increase of load, the transferred load is reduced and the rate of convergence is more intensively reduced.

Measurements have shown that in this zone the load is in

proportion to convergence and both the load and the convergence of roadways follow the logarithmic time variation of the plastic rock yield (Fig. 4). This relation is probably eliminated when pure plastic rock yield develops. The rheological function of load (Fig. 4a) breaks up when a maximum value is attained. Beginning at this point the load reduces, whilst the convergence of gates continues with unchanged trend and with plastic rock yield characteristics (Fig. 4b).

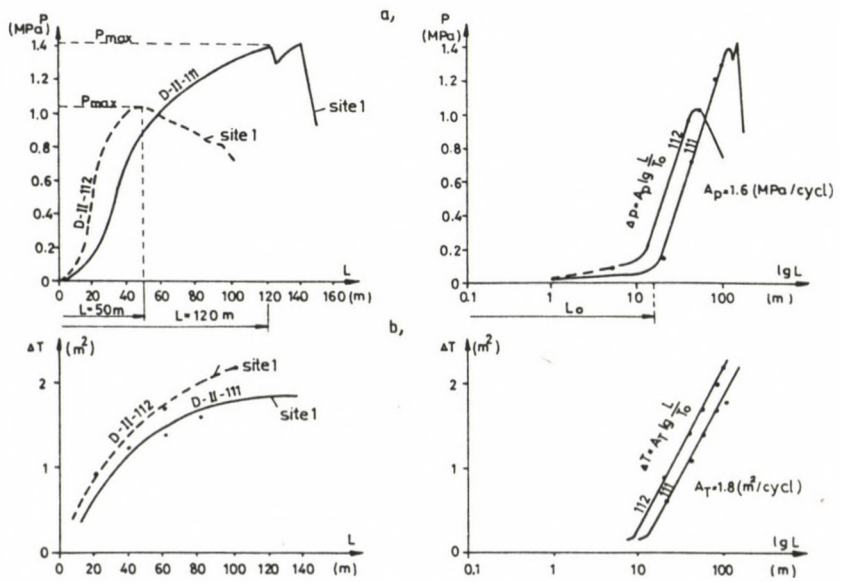

Fig. 4. Change of load on side dam (a) and of cross section-contraction of the roadway (b) in function of the distance L from the face

In consequence of the fact that the steepness of the rheological function of the measured convergence is in time constant, the dynamic character of the plastic rock yield is the same in the second and third zones. Since in the first and second zones an intensive plastic rock yield takes place as belonging to an unstable condition and in the third zone the character of movement is the same as that in second zone, the convergence phenomena developing around the face are in the

upper seam and in its soft rock environment of the same nature. The rock yield - at least within the investigated time interval - cannot be divided to dynamic and static sections resp., it is an uninterrupted process in time.

The pressure decrease in the third zone indicates plastic rock yield accompanied by stress-rearrangement, i.e. the development of a zone around the face poor in stress what lasts as long as the measurable movements of the surface subsidence, i.e. the consolidation comes to end. Experiences show that consolidation is a process of more years (Martos 1969), what indicates that a rock zone being poor in stress can develop even for several years both for overcut lower-seam and undercut upper-seam operations.

MOVEMENT PHENOMENA DURING EXTRACTION OF THE UPPER SLICE OF THE LOWER SEAM

Investigations regarding the movement phenomena of the lower seam were ensured by the roadway retained in the upper seam which remained in good condition after extraction of the upper 3 m slice of the lower seam (Fig. 5).

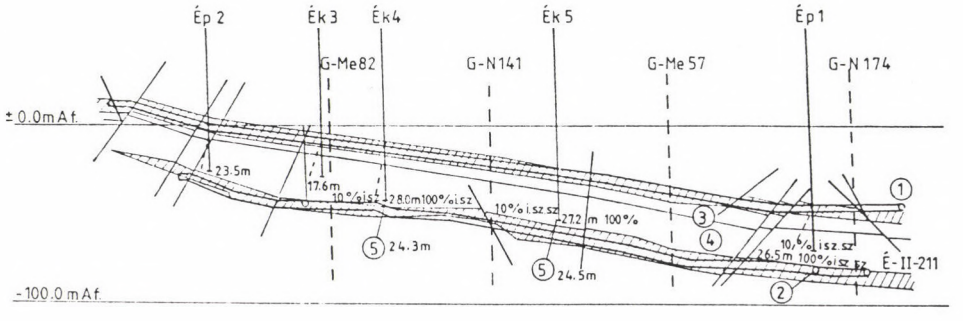

Fig. 5. Vertical section of the return gate of the upper seam. 1 - return gate; 2 - development tunnel of lower seam face; 3 - clayey marl; 4 - fresh water limestone; 5 - axis of borehole

Movements caused by the lower-seam face have been measured by levelling the roof-point of the roadway. Maximum values of

the movements were found to be 1.7 to 2.0 m. These values originate from the sum of sinking of roof-points and deformation of the roadway. In the sinking curve no sharp breaks were experienced what could refer to rigid break of large panels.

To reconcile compression waves with rock-sink, it has been decided to drill exploratory boreholes from the roadway. The lower-seam goaf was attained by four exploratory boreholes.

At one borehole the waterbearing marl could not be drilled. Before casing the borehole wall consecutively collapsed. But with the four productive drillings the fresh water limestone layer has been transversed after the marl layer, in 15 m length with a drilling speed referring to in-situ conditions, without observing any fissuring or deterioration. This was followed by a loosened zone of 2.0 to 2.5 m with partial loss of flushing fluid, then the borehole reached the goaf with full loss of flushing fluid.

Measurements and boreholes have proven that collapse of the fresh water limestine area in full extent of 150×300 m^2 did not take place above the face panel. The deflection of the fresh water limestone in a distance of 140 m was 1.5 to 2.0 m, the time process could be deduced from measurements of prop--pressures and subsidence. Surface subsidence movements have been measured above a return ventilation drift and perpendicularly to its direction parallel to underground sinking measurements. The maximum measured subsidence was 1 m on the surface. Its movement elements did not show any anomaly.

The sinking trough measured in the upper-seam return gate has a profile differring from that of the surface subsidence. The deflection is in the sections constant (Fig. 6) and the inverse of the radius of curvature is everywhere equal zero. The maximum sinking amounted to 2 m. The movement elements of the sinking trough prove neither deflection nor any load originating from this in the soft upper-seam strata forming adjacent roof of the fresh water limestone.

The movement of the upper-seam soft strata is governed by the plastic rock yield as proven by the change of sinking in function of distance (Fig. 6) and time (Fig. 7) measured in the

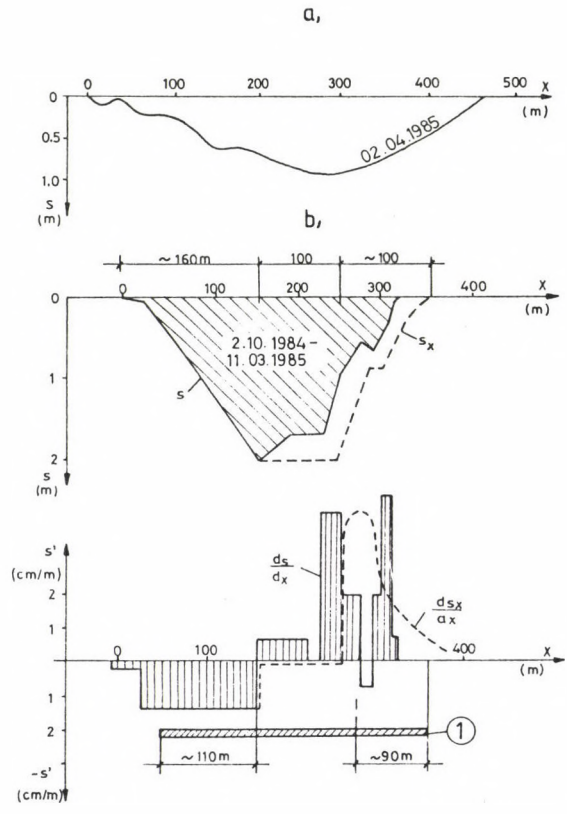

Fig. 6. Subsidence due to the influence of the face No. 1 of the lower seam developed along the longitudinal axis of the return gate on the surface (a) and in the return gate of the upper seam (b)

return gate.

The change of maximum subsidence in function of depth is characterized by a continuous curve between the roof of the face and the surface. The regression equation of the curve is:

$$s_o = M - \lg \frac{h}{M} ,$$

where M is the extracted slice thickness and h is the height measured from the roof of the face. According to this formula the roof of the face sunk in a rate complying with the slice thickness what contradicts results of direct observations and

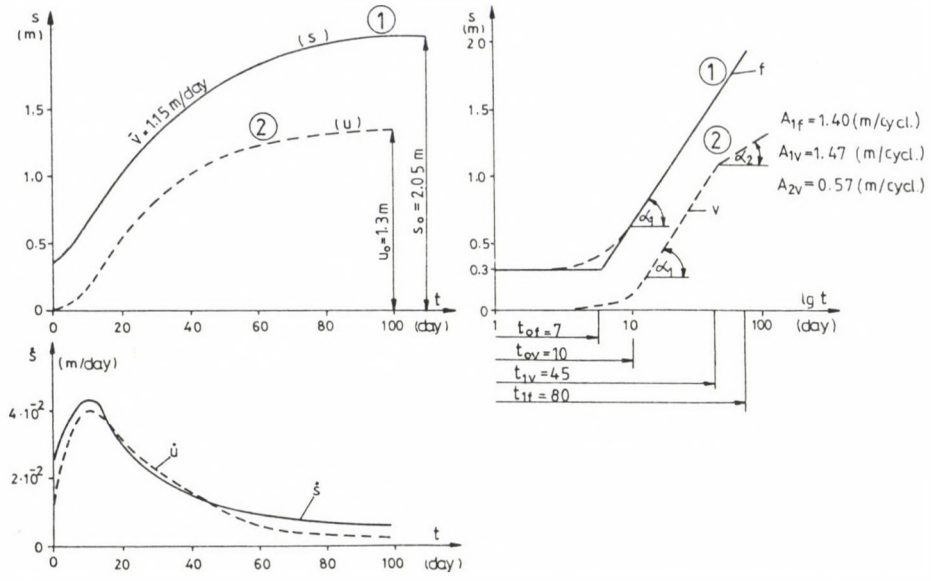

Fig. 7. Development of deflection in time of fresh water limestone and of the section contraction of upper-seam gates. 1 - fresh water clay above the face; 2 - upper-seam gate

measurements relating to caving of the fresh water limestone.

The changes of subsidence in function of distance (Fig. 6b) and time (Fig. 7) measured in the return gate are in accordance with the regularities of the plastic rock yield, the intensity is equal to that measured in drift tunnels and longwall gates (Fig. 4).

Since the nature and numerical value of characteristics of both curves correspond each other in the initial section of the movement-phase, it is quite sure that plastic yield of the fresh water clayey marl has taken place within the investigated time-interval without any difficulty; it was not hindered in its movement by the limestone beneath also moving. In this phase movements of the two strata are separated; and until the characteristic features measured in the return gate of the upper seam reflect the plastic movement of the fresh water clayey marl, the movement measured in the face is characteristic for in-time processes of the fresh water limestone.

The forced connection between fresh water limestone and

fresh water clay located above the former is temporarily interrupted due to caving, loosening and deflection occurring with the advance of the face. The fresh water limestone is temporarily relieved and the forced connection of the two layers develops again during the phase of consolidation. This transition condition is shown in Fig. 8.

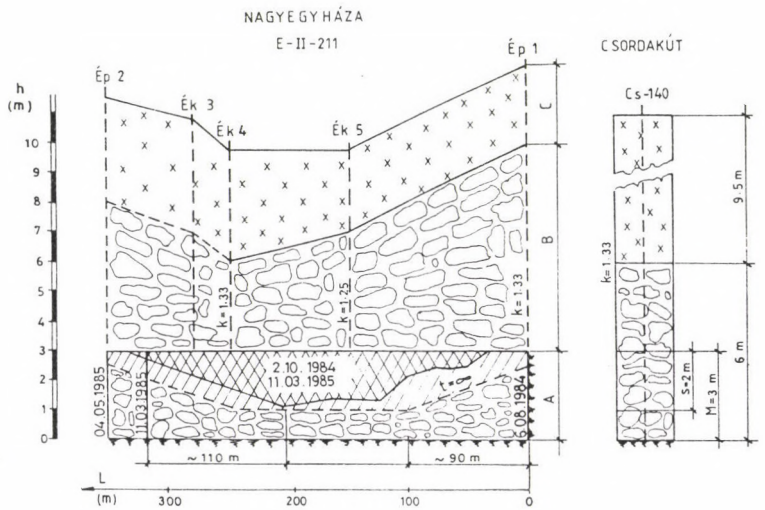

Fig. 8. Thickness of the broken and fissured rock zone in fresh water limestone. A - seam; B - broken rock zone; C - fissured rock zone

The position of the deflecting, fissured, and broken rock zone was defined by boreholes drilled from the return gate of the upper seam. Since the boreholes Ép2 and Ék3 have not attained the border of the broken rock zone, its position is shown in Fig. 8 (based on known data of adjacent boreholes) with dotted line.

The height of the broken rock zone is above the extracted slice of the seam:

$$x = \frac{M - s}{k - 1} \quad ,$$

where M is the extracted slice thickness, s is the deflection

of the fresh water limestone, and k is the loosening factor of the limestone.

The subsidence of limestone is equal to the subsidence measured in the return gate of the upper seam. Its measured value is indicated by double shading, its final state by dotted line.

Depending on the position of the face, the thickness of the broken rock zone as measured above the face is 3 to 7 m. Its loosening factor varies between 1.25 and 1.33. Data of the borehole Cs-140 drilled in Csordakut (Soki 1983) (see Fig. 8) show similar values, proving the mutual validity of experiences. In the undermined area three zones develop along the longwall face of the lower seam, during caving of the upper 3 m slice of the seam, depending on the face length; the two outside ones have a length of 90 to 110 m, the middle one has an approximately constant caving height.

With the development of the whole surface the deflecting fresh water limestone probably subsides on the goaf. By this means the stress of the fresh water limestone beam, the load on shield supports decreases, but the conditions for dynamic compression phenomena during extraction of the upper slice of the lower seam, mentioned in the introduction remain unchanged along the full width of the face.

OPTIMUM EXTRACTION SEQUENCE

According to investigations carried out an intensive plastic rock yield takes place in the soft strata of the upper seam due to the influence of both the upper and the lower faces, therefore parts overcut in the lower seam or undercut in the upper one get in a rock strip being poor in stress.

Since retainment of roadways in the stress-poor rock strip is essentially much easier and more economic in the upper seam, therefore the optimum sequence is represented by undercutting of the upper seam.

The reasonable mining sequence has been developed based on the experiences discussed, i.e. the upper slice of the lower

seam is first mined, then that of the upper seam follows. The undercutting of the upper seam is applicable - what is proven also by mining experiences in several years - as corroborated by the expertise of the University for Heavy Industry (1985) which shows that undercutting does not damage the upper seam.

Movements and plastic rock yield developed with undercutting of the upper seam in the soft rocks of the upper seam. The stress-poor zone provides on one hand an essential help to maintain galleries of the upper seam as a natural shield on the other hand it makes longwall face operations easier. This fact also proves that with the recognition of natural processes, these processes may utilized and even the very unadvantageous plastic rock yield can be to the service of the miner.

REFERENCES

Halász I 1984: Experimental Investigation of rock pressures Loading Roadway Supporting Structures of the Nagyegyháza Colliery (in Hungarian). Report of the Professorship of Reinforced Concrete Structures of the Technical University of Budapest, Budapest

Hunke H 1976: Betriebserfahrungen mit dem Dammbaustoff Anhydrit in Streb und Strecke. Glückauf, 3.

Martos F 1969: Studies on Mining Damages (in Hungarian). Tankönyvkiadó, Budapest

Petrássy M 1987: Pressure Phenomena of Rigid Limestone Roof of the Eocene Period and Tasks of Longwall Support Systems (in Hungarian). BKL Bányászat, 120, 303-308.

Petrássy M 1987: Investigation of Movement Phenomena and support requirements of Soft and Rigid Associated Rocks of the Eocene Period Based on Experiences of the Mines Nagyegyháza and Csordakut (in Hungarian). Ph.D. thesis, Budapest,

Soki I 1983 Report on the Borehole Cs-140, on Technical and Geological Data Obtained (in Hungarian). Manuscript, Tatabánya

Stuber Gy, Petrássy M 1986: BKL Bányászat, 119, No. 3,

University for Heavy Industry, Institute of Mining 1985: Investigations of Possibilitie of Undermining the Upper Seam of Nagyegyháza (in Hungarian). Research report. Miskolc

Acta Geod. Geoph. Mont. Hung., Vol. 25 (1-2), pp. 39-64 (1990)

IMPACT OF MARGINAL DRAINING CONDITIONS ON THE QUANTITATIVE VARIATIONS IN KARSTIC WATER INFLOW RATES

A Schmieder

Central Institute for the Development of Mining, H-1037 Budapest, Mikoviny u. 2-4, Hungary

Based on rheological laws, governing the migration of waters within the system of main karstic water reservoirs in the Transdanubian Midmountains, as well as on mechanic ones pertaining to the function of overlying protective layers, the author discusses the problem how the rate of karstic water inflow is quantitatively varying in function of the marginal conditions of drainage. A system of general hydraulic relationships is derived enabling the analytical description of equilibrium conditions, created in spontaneous way or established artificially within the system of water storing and protective layers. In addition, they are adapted to calculate reliably expected rate of total water inflow and waste water to be drained respectively.

Keywords: protective layers; splitting; throttling; water inflow rate; water inrush

INTRODUCTION

Processes in the nature take place in well defined conditions and within a given system any state of equilibrium is to be established but in specified conjunctures. Such conditions are in relationship with the presence or shortage of sealing strata and in mines under water hazard with the efficiency of natural or artificially constructed layers by which underground areas are separated from water reservoirs.

The total amount of karstic water Q(t) - to be drained for protecting the workings separated by protective layers from aquiferous strata, or inflowing into the area - is varying in broad limits, depending on the geometric character of drainage and the efficiency at which the protective layer can reduce the rate of water inflow. In an extreme case it may vary within the

range of $0 \lesssim Q(t) \lesssim Q_{max}$, which emphasizes the importance of reasonable selection of marginal conditions of drainage and their full exploitation, as well as their influence under aspects of both mining and environmental protection. In the present paper questions are discussed which are related to the effect of marginal draining conditions - pending on the method of hydraulic protection and the character of protecting layers - on the variations in the total amount of karstic water to be tapped for protecting the workings and on the rate of karstic water flowing into mine spaces from the floor side. The timeliness of this subject is linked to the increased requirement to use efficient water reserve preserving and proper karstic water protecting methods. In Hungary, the importance of this subject, both from social and economical points of view, is stressed by the fact that in the area of the Transdanubian Midmountains steps have been continuously taken to protect mines exposed to the hazard of karstic water inrushes and preserving available karstic water reserves, simultaneously. Based on experiences, acquired with working mines under karstic water hazard in the area of the Transdanubian Midmountains, as well as with the function of the system of main karstic water reservoirs, the author indicates the effect of the marginal conditions of drainage on the quantitative variations in the rate of karstic water inflow, on the one hand, and on the other hand as a synthesis of the relevant investigations, a system of relationships was established which enabled the anticipated rate of water inflow and its interval of confidence to be analytically estimated more generally and reliably as it was done earlier. Depending on marginal conditions these values are varying in very broad limits.

HYDRO-GEOLOGICAL CHARACTERISTICS OF KARSTIC WATER RESERVOIRS

In the Transdanubian Midmountains the system of main karstic water reservoirs is constituted of tectonically very disturbed limestone and dolomite formations karstified in a varying extent, their thickness is several hundred to several

thousand meters (Schmieder and Szilágyi 1988). Its territorial extension is near to 10 000 km^2 in the area being of importance from the point of view of mines supplying solid minerals, i.e. in that lying between Budapest and Keszthely Mts. Depending on the conditions of infiltration the average rate of water inflow is 600 to 900 m^3/min (Schmieder and Szilágyi 1988). Its water reserves amount to 40 to 50 km^3 from which the mines have drained in yearly average more than 600 m^3/min during past years. The average void volume for the hydro-dynamically coherent karstic water reservoir (Table I) varies from 1 to 4 %, depending on lithological characteristics, degree of tectonical load and karstification of the strata. The fissured character tends to diminish exponentially vs. the depth (Schmieder et al. 1975). A similar trend is valid for the average sickering factor $\bar{k}(z)$ vs. depth (Schmieder 1976), the integrated value of which, related to the total thickness of reservoir, in other words the lateral water supplying factor kM of the reservoir

Table I

Field	Dolomite		Limestone	
	kM	n	kM	n
	m^2/s	%	m^2/s	%
Nagyegyháza	$1.0 \cdot 10^{-2}$	2.5	-	-
Mány	$0.4 \cdot 10^{-2}$	1.5	-	-
Tatabánya XIV/a	$1.2 \cdot 10^{-2}$	2.5	-	-
Kincsesbánya	$0.6 \cdot 10^{-2}$	1.3	-	-
Nyirád	$7.0 \cdot 10^{-2}$	4.0	-	-
Tatabánya XV/c	-	-	$4.0 \cdot 10^{-2}$	1.5
Dorog	-	-	$5.0 \cdot 10^{-2}$	1.5

(Table I), varies considerably in each basin. The extent to which reservoir rocks are fractured is also highly divergent in each basin and moreover in parts of the same basin (Schmieder et al. 1975). At non-covered parts of reservoir, at surface outcrops or in lack of protective layer the extent of tectonic fracturation mapped underground, i.e. the specific value of

strike length per unit surface, is varying from 5 to 25 km/km^2 (Schmieder et al. 1975). Within the reservoir the process of water migration is decisively bound to these lines and takes place in tectonically fractured, more or less karstified fault zones. The local water supplying factor of fault zones varies by 5 to 6 orders of magnitude (Fig. 1a) and the empirical distribution of its values is logarithmic (Schmieder 1971, 1982b).

A similar distribution is shown by water inrushes in zones without protective layers (Fig. 1b), illustrating the close relation between the rate of water inrushes without any resistive effect and the local water supplying capacity of fault zones.

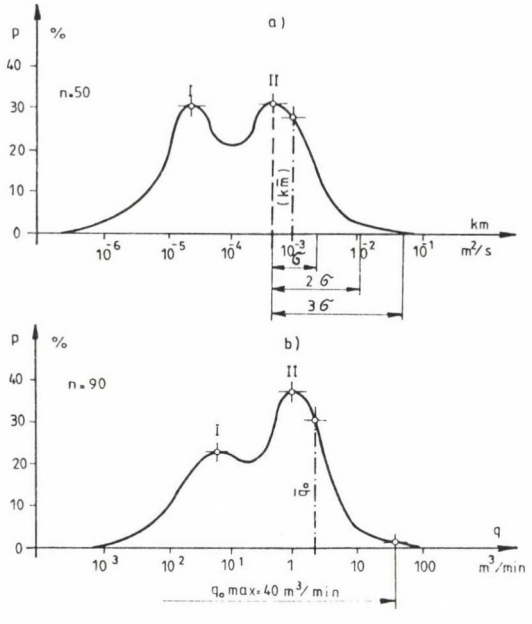

	kM	$(km)_{max}$	s_o	q_o max	(u σ)
	m²/s	m²/s	m	m³/min	—
E	$0.8 \cdot 10^{-2}$	$1.7 \cdot 10^{-2}$	240	30	2.2 σ
D	$1.0 \cdot 10^{-2}$	$1.3 \cdot 10^{-2}$	190	40	2.1 σ

Fig. 1. Empirical distribution functions for measured local water supplying factors of fault zones (a) and some values for water inrushes inflowed from fault zones consisting of dolomitic rocks (b)

DYNAMIC CHARACTER OF KARSTIC WATER MIGRATION

It could be concluded from investigations, based on extensive measurements and observations (Schmieder 1971, 1982b) that within karstic reservoirs, water migration takes place essentially in voids and follows Darcy's law of linear sickering in the outer belt of movement field around point like tappings (wells, water inrushes), i.e. in the zone outside of a circle with a radius $r \gtrsim x_o$ and in the case if sufficiently great amount of rocks are present. In this zone of movement the Dupuit-Thiem relationship

$$s_k = \frac{q}{2\pi kM} \ln \frac{R(t)}{r} \qquad (1)$$

valid for the cylinder symmetrical movement of stressed level water can be applied with good approximation for the variations in space of the depression (Schmieder 1971).

In the internal belt of movement the migration of water is no more of a potential character. Approaching the point of tapping the migration of water is more and more localized to a unique fault zone. The speed of water flowing increases and the dynamic character of its migration is effectively similar to the transitional water migration process described by Forchheimer (Schmieder 1971). In this zone - e.g. around a well of vertical axis with a radius r_o, a penetration depth l and a yield q, drilled into the water reservoir - the spatial variations of the depression are described by a Minski-type relation (Schmieder et al. 1975, Schmieder 1976)

$$s_b \approx \frac{q}{2\pi kl} \ln \frac{x_o}{r_o} + \frac{q^2}{(kl)^{3/2} r_o} \qquad (2)$$

The major part of formation energies is consumed in the internal belt of movement field. This part can reach 95 to 99 percent in some cases what indicates the importance of this range under karstic hydraulic aspect. Summing up the losses produced in the outer and internal belts of the movement, the equation of energy balance describing fully the depression created

around a well of vertical axis drilled into the water reservoir (Schmieder 1976) is:

$$s_o \approx \frac{q}{2\pi kM} \ln \frac{R(t)}{x_o} + \frac{q}{2\pi kl} \ln \frac{x_o}{r_o} + \frac{q^2}{(kl)^{3/2} r_o} . \qquad (3)$$

The total depression formed in the water reservoir around a karstic water inrush of a yield q, is similarly without any effect of a protective layer (Schmieder 1976):

$$s_o \approx \frac{q}{2\pi kM} \ln \frac{R(t)}{x_o} + \frac{q}{\pi km} \ln \frac{x_o}{\Delta_o} + \frac{q^o}{(km)^{3/2} \Delta_o} . \qquad (4)$$

In these relationships the full variation is s_o, in the water level related to the points of tapping while kM is the average lateral water supplying factor of the reservoir, kl is that of the rocks surrounding immediately the well penetrating in a lenght l into the water reservoir, km the local factor for the zone of fault, R(t) is the remote effect of depression, r_o the radius of well, Δ_o that of the water inrush and x_o that of the transitional range of movement. The lateral water supplying factor of the reservoir is determined using the first term on the right side of the equations. By means of their second and third terms on the right side the characteristics

$$s_o = a_o q + b_o q^2 \qquad (5)$$

is evaluated for the relevant wells and water inrushes (Fig. 2). If the depth of penetration l is reasonably selected, the local water supplying factor km for the zone of faults can be directly calculated. Its empirical distribution function can be obtained using 40 to 60 wells drilled in a nearly uniform territorial density and with nearly identical depth of penetration (Schmieder 1982b). The subsequent analyses in this paper are based on the presumption that the geometry of the water reservoir, its position in space, extension, degree of tectonic fracturation and pressure status are known, together with its permeability and water storing characteristics, as well as the empirical distribution in space and the equations of movement

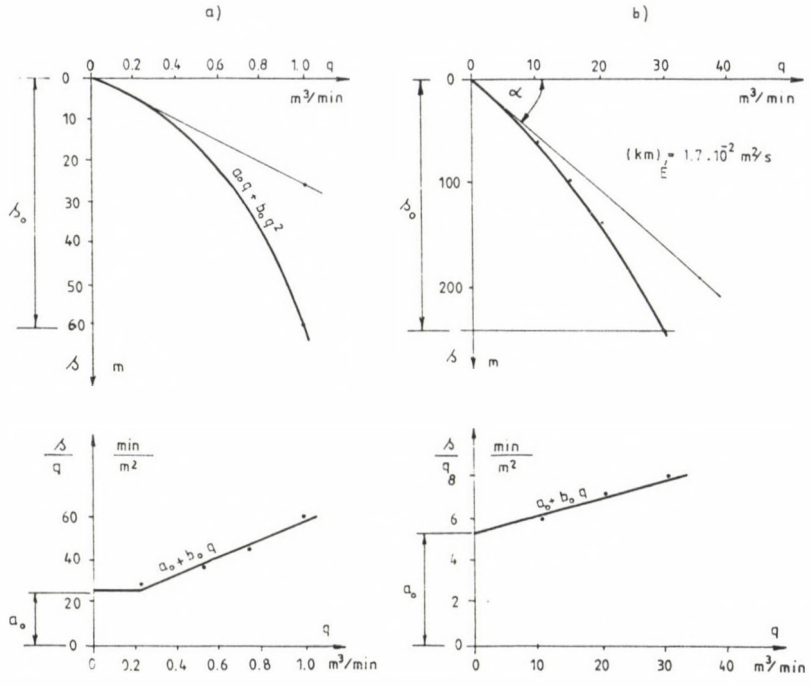

Fig. 2. Measured characteristics for wells (a) and water inrushes (b)

describing these processes are given. In other words, all the data, necessary to describe directly the equilibrium vs. the marginal conditions of drainage, are known about the reservoir. The simplest marginal conditions of drainage are characteristic for the areas without protective layer.

LACK OF PROTECTIVE LAYERS

In lack of protective layers the quantitative variations in karstic water yield are exclusively influenced by the geometry of drainage. Two types of characteristics are shown in Fig. 3.

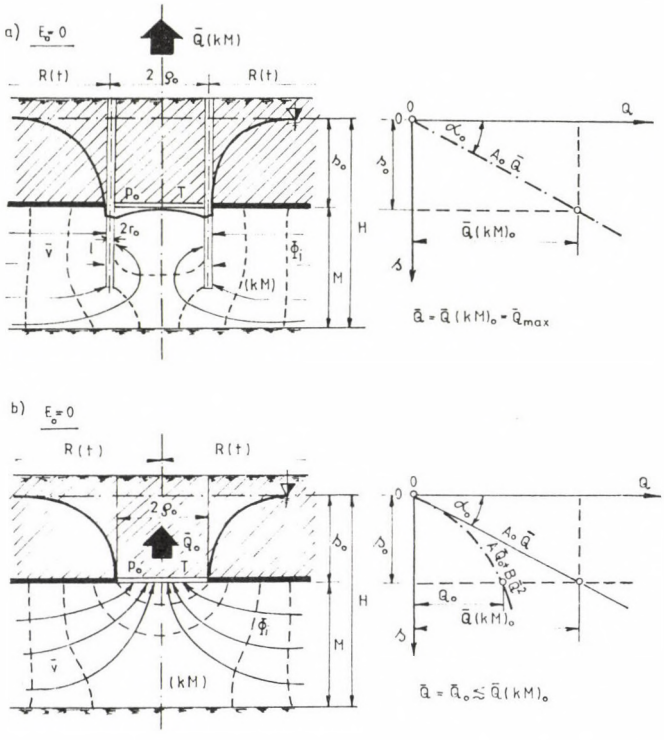

Fig. 3. Kinematic sketch of a karstic water reservoir drained on floor side through wells (a) and level mine openings (b)

The system for lateral drainage, outlined in Fig. 3a, corresponds to a one step method of karstic water table sinking by wells, i.e. the conventional passive mine water protection by tapping on surface. For both methods all the reservoir parameters, as well as the depth under water level of the operations and the area of simultaneously protected and open surfaces T, respectively, are identical.

For the wells the depth of penetration and the extent to which the water table is to be sunk, can be between certain limits freely selected. When draining is made from surface the suction is at any point bound to the value s_0.

By considering all these factors, the question should be replied: to which extent the differences in the geometric marginal conditions of draining do influence the quantitative

variations in the volume of karstic waters to be tapped for protecting mine workings and in the total yield of karstic water, respectively?

a) The operation of sinking the karstic water table is considered as convenient provided that the karstic water level is sunk by the draining system below that of workings at every point of the protected area. For a given well distribution this requirement is fulfilled if the karstic water table has been sunk in the centre of protected area to s_o, i.e.:

$$s_o = \frac{\bar{Q}}{2\pi kM} \ln \frac{R(t)}{\varrho_o} = A_o \bar{Q} \ , \qquad (6)$$

in which: $\bar{Q}$ is the expected value of water yield to be drained, necessary to establish dynamic equilibrium and ϱ_o is the equivalent radius of a great well. The water yield $\bar{Q}$ obtained is proportional to the depression (Fig. 3a). The maximum water desorption capacity of the reservoir is indicated by the straight line. In other words, the maximum value of the total karstic water yield to be drained for protecting underground operations is the same as the amount of water drained laterally from the reservoir. For distinction this water yield is designed by $Q(kM)_o$, its expected value is:

$$\bar{Q}(kM)_o = \frac{s_o}{A_o} \ . \qquad (7)$$

This expected water yield has a relative dispersion $\pm$ 20 to 25 percent if the effective water supplying factor kM is derived either from data obtained by measuring a group of wells or from a series of production data (Schmieder 1982b).

b) In the case if surface draining is performed, the dynamic equilibrium is established spontaneously due to water inflows occurring over the area T of the open surface. The values of water inflow are divergent over the open surface depending upon the degree of tectonic fracturation and on the local water supplying factor of the fault zones.

According to the experience the number of karstic water inflows over the area in a dispersed way is limited and its

average value is (Schmieder et al. 1975, Schmieder 1982b)

$$\bar{n}_o = \frac{\bar{k}L}{\bar{k}m} = \frac{\bar{k}L_o}{\bar{k}m} T \quad , \tag{8}$$

where $\bar{k}$ is the average sickering factor for the uppermost belt (30 to 40 m) of the karstic water reservoir, L_o is the degree of specific tectonic fracturation of the reservoir and $\bar{k}m$ is the average water supplying factor for the fault zones.

Be the average value of water yields for various water inrusches designated by $\bar{q}_o$, then the following equation of equilibrium is valid for the relationship between the total yield of inflows at the open surface and the maximum depression at the points of drainage

$$s_o \approx \frac{\bar{Q}_o}{2\pi\bar{k}m} \ln \frac{R(t)}{\varrho_o} + \frac{\bar{n}_o\bar{q}_o}{\pi\bar{n}_o\bar{k}m} \ln \frac{x_o}{\Delta_o} + \frac{n_o^2\,\bar{q}_o^2}{\bar{n}^2(\bar{k}m)^{3/2}\,\Delta_o} \quad . \tag{9}$$

By substituting $\bar{n}_o$ and $\bar{n}_o\bar{q}_o \approx \bar{Q}_o$ (Schmieder 1982b):

$$s_o \approx \frac{\bar{Q}_o}{2\pi\bar{k}M} \ln \frac{R(t)}{\varrho_o} + \frac{\bar{Q}_o}{\pi\bar{k}L} \ln \frac{x_o}{\Delta_o} + \frac{\bar{Q}_o^2}{(\bar{k}L)^{3/2}\sqrt{\bar{n}_o}\,\Delta_o} \quad . \tag{10}$$

A reduction of the constants yields:

$$s_o = A\bar{Q}_o + B\bar{Q}_o^2 \quad , \tag{11}$$

and solving the quadratic equation, the expected total volume of the inflowed surface water is:

$$\bar{Q}_o = \sqrt{\frac{s_o}{B}}\ \lambda_o \quad , \tag{12}$$

where λ_o is the factor of hydraulic interaction (Schmieder 1972). The main relative dispersion for the expected values of surface water yield does not exceed generally $\pm$ 30 to 40 percent as estimated from measured characteristics. Limits of confidence (reliability 1-p from the probability function (Fig. 4a)

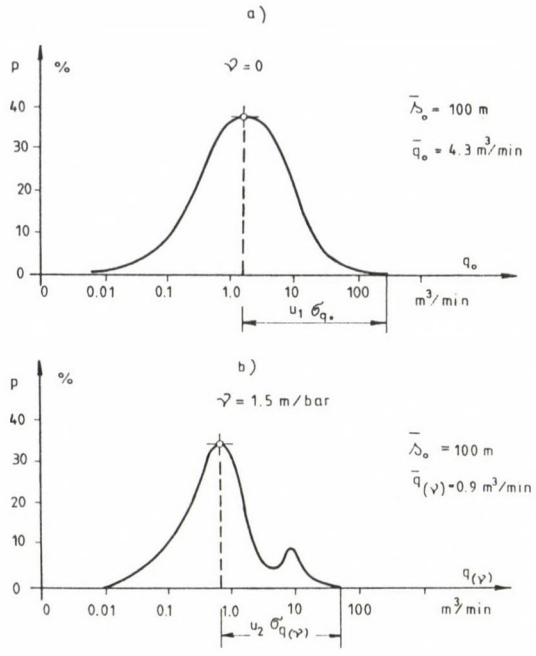

Fig. 4. Empirical distribution function for a partial set of water inrushes in the Dorog coalfiled, as related to mine panels without protective layer (a) and covered by a protective layer (b)

expressing the anticipated values for different water inrushes) are estimated from the following relationship:

$$\lg \frac{\bar{q}(p)}{\bar{q}_o} = \frac{u \sigma_q}{\sqrt{n_o}} \qquad (13)$$

$$\bar{Q}(p)_o = \bar{Q}_o \left(1 + 2.3 \frac{u \sigma_q}{\sqrt{\bar{n}_o}} \right) , \qquad (14)$$

where σ_q is the dispersion of water inrushes (σ_q = 0.8 - 1.1) (it is estimated by an empirical distribution function represented in the Briggsian logarithmic coordinate system and the average number of water inrushes in $\bar{n}_o$).

The extreme value of the interval of confidence is determined by the value of $Q(kM)_o$.

In general, the surface water yield is substantially lower than the maximum transmission capacity of the water reservoir.

Increases the area T of surface

$$s_o = A_o\bar{Q}_o + C_1\frac{\bar{Q}_o}{T} + C_2\frac{\bar{Q}_o^2}{T^{3/2}} \qquad (15)$$

due to variation according to T, the characteristic (11), shown in Fig. 3b is more and more shifted towards the tangent and in a limit case, the expected value of $\bar{Q}_o$ is $\bar{Q}(kM)_o$.

In the case of measured data illustrating the values of simultaneously inflowing total surface water volumes $Q(t)_o$ vs. the established laminar depression s_L, the straight line $A_o\bar{Q}$ characterizes the maximum water desorption capacity of the reservoir. At s = 0 it is the tangent of the characteristic curve of surface water yields.

In knowledge of measured and calculated data, respectively the reduction in water yield originating from the difference of geometrical random conditions of drainage the expected and real degree of water yield reduction can be defined by the water yield reduction factor:

$$\bar{\eta}_o = \frac{\bar{Q}_o}{\bar{Q}(kM)} \qquad (16)$$

being the ratio of yield values.

In Table II data are shown on some practical examples, where kM is the average lateral water supplying factor, characteristic of the basin, s_o is the average depth of workings under the water table, Q(t) is the total volume of effectively drained and inflowed water, s_L is the established average of laminar depression, $Q(kM)_o$ is the maximum water yield involved with full depression and the factor of water yield reduction is $\bar{\eta}$.

The three other columns in this table include data on the effective depression characterizing the water inrush of greatest yield, on the average of some values of drained and inflowed water volumes in the case of no productive layer and

Table II.

Designation of the field	kM	$\bar{s}_o$	Q(t)	$\bar{s}_L$	A_o	$\bar{Q}(kM)_o$	$\bar{\eta}$	$s(t)_{oi}$	$\bar{q}_o$	$q_{o\ max}$
	m^2/s	m	m^3/min	m	min/m^2	m^3/min	-	m	m^3/min	m^3/min
Nagyegyháza	$1 \cdot 10^{-2}$	190	120	85	0.7	270	0.45	190	2.2	40
Mány	$4 \cdot 10^{-3}$	200	40	120	3.0	65	0.60	170	0.8	15
Tatabánya XIV/a	$1.2 \cdot 10^{-2}$	110	65	70	1.1	100	0.65	100	2.2	15
Kincsesbánya	$6 \cdot 10^{-3}$	200	90	100	1.1	180	0.50	200	1.0	15
Nyirád*	$(7 \cdot 10^{-2})$	120	300	120	0.4	300	1.00	120	10.0	160
Dorog	$5 \cdot 10^{-2}$	250	150	25	0.17	1200	0.12	250	8.0	120

*Note: On account of the considerably lower permeability of surrounding strata the effective value of (kM) is $2.2 \cdot 10^{-2}$ m^2/s.

the maximum yield of effective water inrushes. In the Nyirád area, where the water table is sunk by shaft wells (Schmieder et al. 1975), no reduction in the water yield is observed.

In mines without protective layer, as at Mány, at the shaft XIV/a of Tatabánya and in the Kincsesbánya area, on account of draining operations the reduction in water yields reached 30 to 50 percent, depending on the extension of the relevant area and the underground method of drainage. For areas covered by protective layers, the effective extent of water yield reduction tends to increase further, what resulted for the Nagyegyháza coalfield in a reduction of the water yield by 55 percent and for Dorog field by 88 percent, spectacularly showing the importance of marginal conditions of draining.

FUNCTIONING OF PROTECTIVE LAYERS

According to Point 1, the water migration between reservoir and mine openings starts in lack of protective layers even at the smallest pressure difference. Thus, water inrushes without any resistive effect may occur in any point of acquiferous fault zones with equal probability, with maximum areal frequency and water yield.

With intercalation of protective layers the starting conditions of water movements change and both the number of water inflows $n(\nu)$ and their average yield $\bar{q}(\nu)$ are reduced, further on the empirical function of distribution for various values may be distorted (Fig. 4b).

According to massive mining experiences the average number of water inrushes/unit area $n(\nu)$ and their average yield diminish (Schmieder et al. 1975), if clayey-marly water barring layers of durable hydraulic resistance are intercalated, with increasing specific thickness of the protective layers. In basins or basin parts it can be characterized (Schmieder 1972) by the average resistance factor:

$$\mu(\nu)^{*} = \frac{n(\nu)}{\bar{n}_{o}} \qquad (17)$$

and by the average throttling:

$$\varphi(\nu)^{*} = \frac{\bar{q}(\nu)}{\bar{q}_0} \qquad (18)$$

derived empirically for given water storing and protective layer systems (Fig. 5). In Eqs (17) and (18) $\bar{n}_0$ and $\bar{q}_0$ mean average characteristics for the area without protective layer interpreted on empirical basis. According to experiences, no water inrush breaking through the protective layers should be reckoned with, provided that the specific thickness of protective layers is equal to or greater than the value of ν_0 (Fig. 5).

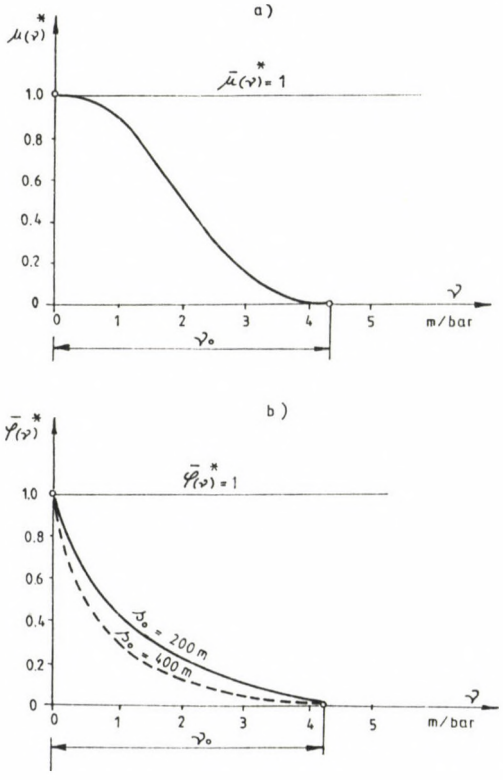

Fig. 5. Average sealing (a) and throttling factors (b) derived empirically for clayey-marly protection layers in the Dorog coalfield

In such conditions the expected values for the number of water inflows $\bar{n}(\nu)$ and for their yields $\bar{q}(\nu)$ are zero. Through water barring protective layers, water migration starts at points and in the case when the hydrostatic pressure difference s_o, related to the floor level of mining operations, is higher than the internal resistance (Schmieder 1976, 1989) to water migration of the protective layers:

$$E_o = \bar{I}_o m \tag{19}$$

i.e.:

$$s_o - E_o > 0, \tag{20}$$

where $\bar{I}_o$ is the reciprocal of ν_o and m the efficient thickness of protective layers. If the free formation energy (Schmieder 1982b), expressed by the difference $s_o - E_o$ is negative at all surface points of the system of cavities, i.e. E_o is everywhere higher than the formation energy s_o necessary for water migration, then no water movement takes place through the protective layers. For this reason the protective layers act in such conditions as a homogeneous sealing structure for reducing the yields of water. This situation is characterized by the sealing factor $\mu(\nu) = o$ and by the total volume of simultaneously inflowed water $\bar{Q}(\nu) = 0$.

If the free formation energy is at any point or over a larger surface positive or it becomes positive under the effect of changes in the stress or shearing resistance of rocks (Schmieder 1989), then water migration starts and a single water inrush, or a series of inrushes may occur the dynamic equilibrium is re-established between the water reservoir and protective layers. This occurs when the condition of equilibrium

$$s_o - E_o \lesssim 0 \tag{21}$$

necessary for a stable state, is created, i.e. in all points of the cavity system the effective value ν for the specific thickness of protective layers is at any point equal to, or

higher than, ν_0.

When the process of water migration is established the exclusive sealing action of protective layers is lost. From this moment on the water barring protective layers act - in addition to their sealing effect - as a flow resistance connected in series with the reservoir. Then, it has a significant part along the paths of motion in dissipating the energy causing the motion. This effect is called throttling of the protective layer, while the volume of water, inflowed against flow resistance of protective layer is called water inrush of throttled rates.

In basins or basin parts where the protective layer consist of strata with lasting hydraulic resistance and their function is characterized by throttling, the reduction in water inflow rates is the consequence of the combined effects of sealing and throttling.

In basins or basin parts where the protective layer is easily eroding detrital and soft rock resp. and the migrating water is able to widen out the passage created through the protective layers beyond all limits, or the passage is the consequence of hydraulic rock breaking forces, the throttling effect of protective layers cannot be any more exercised and water is inflowed without being throttled. This type of protective layers is characterized by an average throttling factor $\varphi(\nu) = 1$ and by an exclusive sealing effect. Since the dynamics of the water migration taking place within the reservoir as well as the function of water barring formations overlying it directly are known, it can be found how and to which extent the insulation does influence for a given geometry of drainage the variations in the total volume of simultaneously inflowed karstic waters to be tapped for protecting the operations underground further: what is the physical meaning of the average factors of sealing and throttling to be measured and interpreted empirically and to which extent they are characteristic for a given system of reservoir and protective layers?

DIMINISHING OF WATER INFLOW RATES BY PROTECTIVE LAYERS

The diminishing of the water inflow rates by protective layers depends, essentially, on three factors: on the character of protective layers, on the geometry and on the method of draining.

Protective layers may be without and with a throttling effect. The impact of diminishing the rates of water inflow varies in both cases according to the condition, if draining is made laterally or from the surface. In the latter case the throttling effect is only exercised by the protective layers if water is inflowed through them by overcoming the throttling action.

A) Protective layers without throttling exercise their action of diminishing the rates of water inflow like a sealing mechanism. The simplest possibility of representing this type is by the system of water table sinking shown in Fig. 3a.

a) Be between the underground workings, protected by water table sinking and the reservoir a protective layer of thickness m, without throttling (Fig. 6). In such layer conditions a proper protection for mine openings is offered against water inrushes, only if the specific thickness of protective layers is in every point of the protected area equal to or greater than ν_0. With the system of water table sinking shown in Fig. 3a, this condition can be fulfilled by annihilating within the protected area the free formation energy s_0-E_0 which induces water migration. In other words if for an arrangement of a given geometry the water table is sunk in the centre of the protected area by wells below

$$s_0 - E_0 = A_0 \bar{Q}(\nu) \tag{22}$$

By dividing the expected water yield $\bar{Q}(\nu)$ by the expected value $\bar{Q}(kM)_0$ of the yield due to a total water table sinking (7) one gets

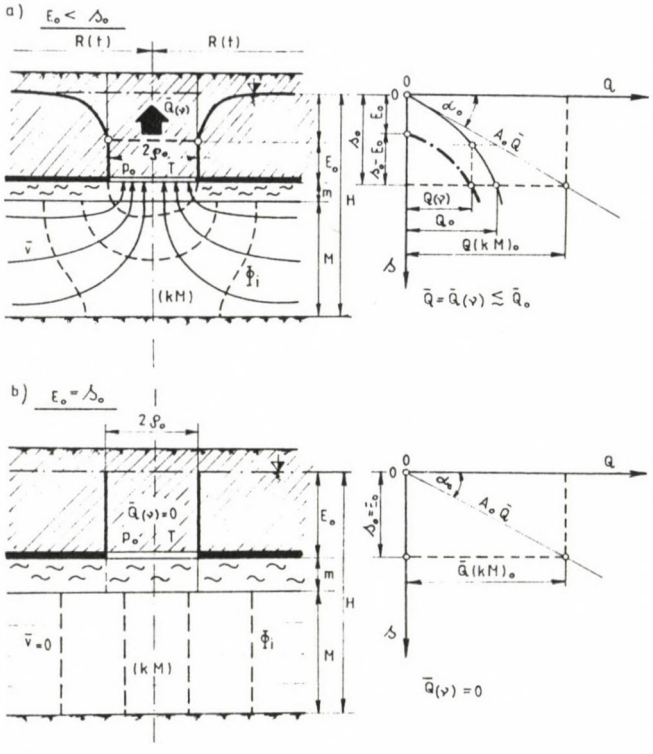

Fig. 6. Kinematic sketch for the underground draining of a karstic water reservoir on floor side, with the intercalation of a protective layer

$$\eta\,(\nu)_o = \frac{\bar{Q}(\nu)}{\bar{Q}(kM)_o} = \frac{s_o - E_o}{s_o} \,. \tag{23}$$

as the average, relative reduction in water yield, due to the utilization of intercalated protective layers.

By substituting the known value of E_o (19):

$$\eta\,(\nu)_o = 1 - \frac{\bar{I}_o m}{s_o} = 1 - \frac{\nu}{\nu_o} \,, \tag{24}$$

where ν is the specific thickness of the protective layer, prior to sinking the water table and ν_o is the value obtained after water table sinking. Supposing that the average yield $\bar{q}_o$

for water table sinking wells is the same in both cases without and with intercalated protective layers, the average relative factor of diminishing the water yield is expressed by the relative reduction in the number of wells, i.e. by:

$$\eta(\nu)_0 = \frac{n(\nu)}{n_0} \quad . \tag{25}$$

If the reservoir is drained laterally, the expected reduction of the water yield remains the same even if the throttling effect is due to intercalated water barring protective layers.

The variations in water yields of layer water reservoirs on the floor side, covered by water barring protective layers without throttling, are governed by the same laws irrespective whether draining is made by wells or the dynamic equilibrium is established by self regulation following water inrushes breaking through the protective layers (Schmieder 1982a).

b) When the method of drainage from the surface is applied (Fig. 6) the dynamic equilibrium between water reservoir and protective layer is established in accordance with the operation of water table sinking when in consequence of

- artificial draining operations carried out from underground openings, or
- water inrushes breaking through the protective layers the karstic water table is sunk in any point of the protected area or in the area opened by mining to such an extent as to annihilate everywhere the free formation energy. With the intercalation of protective layer without throttling the equilibrium is described by the following equation:

$$s_0 - E_0 = A\,\bar{Q}(\nu) + B\,\bar{Q}(\nu)^2 . \tag{26}$$

It can be expressed from the quadratic equation (26):

$$\bar{Q}(\nu) = \sqrt{\frac{s-E_0}{B}}\;\lambda(\nu) \quad . \tag{27}$$

By dividing the expected value Eq. (27) of the yield of water $\bar{Q}(\nu)$ by the expected value of $\bar{Q}_0$ Eq. (12), the average

relative reduction in the rate of water inflowed from intercalated protective layer without throttling is:

$$\bar{\eta}(\nu) = \sqrt{\frac{s_0 - E_0}{s_0}} \cdot \frac{\lambda(\nu)}{\lambda_0} \quad . \tag{28}$$

As the protective layer without throttling operates exclusively as sealing mechanism, their average water yield reduction factor corresponds to the average sealing factor of the system of reservoir protective layer

$$\bar{\mu}(\nu) = \sqrt{1 - \frac{\nu}{\nu_0}} \cdot \frac{\lambda(\nu)}{\lambda_0} \quad . \tag{29}$$

Its variations are represented in Fig. 7a by substituting $\lambda(\nu)/\lambda_0 = 1$ as compared to the average factor of sealing $\bar{\mu}(\nu)^*$, interpreted and derived on an empirical basis for clayey-marly protective layers with throttling effect in the Dorog coalfield. With the sealing factor the expected volume of simultaneously inflowed water is from strata with intercalated protective layer without throttling:

$$\bar{Q}(\nu) = \bar{Q}_0 \bar{\mu}(\nu) \quad . \tag{30}$$

The upper limit of the confidence interval of the expected value is $\bar{Q}_0$. If protective layers with throttling effect are intercalated then the reduction of the water yield is also the same, provided that the surface of reservoir is tapped through holes located underground. Water volumes inflowed through intercalated protective layer without throttling, or through holes traversing the protective layer, as well as the characteristics of the function of distribution are estimated in knowledge of the parameters of reservoir on the basis of Eq. (4).

B) Water yield reduction by protective layer is partly by sealing, partly by throttling mechanisms. This double action can be jointly effective only in a case if water from the reservoir is flowing into underground openings through protective layers and along the paths of movement therein. This condition

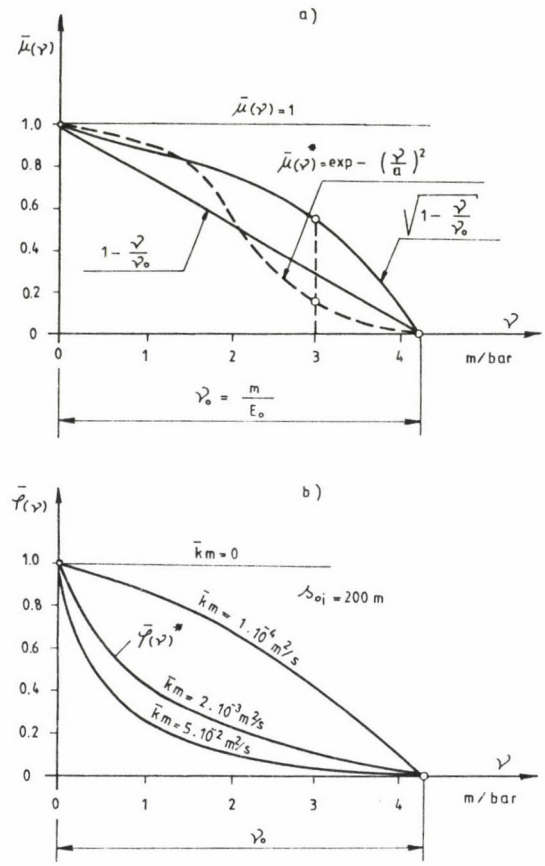

Fig. 7. Theoretical value of average sealing factor for a Dorog type clayey--marly protective layer (a) and variations in its average throttling factor in function of the average water supplying capacity for fault zones in the reservoir

can be fulfilled if tapping is made from the surface and the equilibrium between the water reservoir and the system of protective layers is established either by self-regulation or as the consequence of drainage using the "instantaneous" method (Schmieder 1982a).

Equation of regression for the average yield of water inrushes through protective layer with throttling effect (Schmieder 1976, 1982b) is:

$$s_o - \bar{I}_o m = a_o \bar{q}(\nu) + b_o \bar{q}(\nu)^2 + a_1 m \bar{q}(\nu) + b_1 m \bar{q}(\nu)^2 \ , \quad (31)$$

where a_o and b_o are factors depending on the water reservoir, while $a_1 m$ and $b_1 m$, respectively, depend on the protective layer.

The equation of regression, derived from data on more than 700 water inrushes is the essential point for the operation of a water barring protective layer on the one hand, and it illustrates the rheological importance of protective layer on the other hand. If a protective layer with throttling effect are intercalated, the free formation energy is consumed partly by the water reservoir, partly by the protective layer. It follows from this equation that similarly to protective layer without throttling effect, the protection of underground openings against water inrushes is only active if the free formation energy, which induces the migration of water, ceases in every point of the surface opened up by mining. This condition, and the related equilibrium are described by the following equation of equilibrium:

$$s_o - E_o = A\bar{Q}(\nu) + B\bar{Q}(\nu)^2 + A_1 m \bar{Q}(\nu) + B_1 m \bar{Q}(\nu)^2 \ . \quad (32)$$

By expressing $\bar{Q}(\nu)$ from Eq. (32), and dividing the water yields using Eq. (12), the average relative reduction is in the yield of surface waters traversing a water barring, intercalated protective layer with throttling:

$$\bar{\eta}(\nu) = \sqrt{\frac{s_o - E_o}{s_o}} \sqrt{\frac{B}{B+B_1 m}} \cdot \frac{\lambda(\nu)}{\lambda_o} \ , \quad (34)$$

respectively.

Comparing the water yield reduction factor for a protective layer with throttling effect to that without throttling effect Eqs (28), (29), it can be seen that water yield reducing effect of throttling protective layer is

$$\bar{\eta}(\nu) = \bar{\mu}(\nu) \sqrt{\frac{B}{B+B_1 m}} \quad (35)$$

i.e., more intensive than that of a protective layer without throttling. It depends on the hydraulic resistance $B_1 m$ of the protective layer, i.e. on their throttling characteristics, that is on the average throttling factor of the system reservoir-protective layer

$$\overline{\varphi}(\nu) = \frac{1}{\sqrt{1 + \frac{B_1}{B} m}} . \tag{36}$$

For a certain system of reservoir-protective layer the throttling factor expresses the relative reduction in water yield, due to the surplus flow resistance of the protective layer.

Substituting the values of B and B_1 into the Eq. (36), the average throttling factor (Schmieder 1975, 1982b) is:

$$\overline{\varphi}(\nu) = \frac{1}{\sqrt{1 + \frac{b_1}{b_o} \nu_o \, s_o \frac{\nu}{\nu_o - \nu}}} , \tag{37}$$

and

$$\overline{\varphi}(\nu) \quad \frac{1}{\sqrt{1 + \beta(\bar{k}m)^n \, s_o \frac{\nu}{\nu_o - \nu}}} , \tag{38}$$

respectively, where β is a characteristic factor of the protective layer and n is an exponent $1 \lesssim n \lesssim 1.5$.

For protective layers of the same type the variations in the throttling factor are primarily influenced by the changes in the characteristics of water reservoir and of the protective layer. Figure 7b shows the variations in the average throttling factor (Fig. 5b) of a Dorog type protective layer vs. the local water supplying factor $\bar{k}m$. For a given type the closest correlation existed between measured and calculated values if n = 1.

With the throttling factor the expected total yield of water inflowed through the protective layer with throttling

effect (Schmieder 1972, 1982a) is:

$$\bar{Q}(\nu) = \bar{Q}_o \bar{\mu}(\nu) \bar{\varphi}(\nu) \quad . \tag{39}$$

The upper limit of the confidence interval of the expected value is: $\bar{Q}_o \bar{\mu}(\nu)$.

The ratio of the value from Eq. (39), expected for the yield of surface water inflowed through an intercalated protective layer, and to the expected value of $\bar{Q}(kM)_o$ gives a relationship which completely expresses the joint effect of water yield reduction in marginal draining conditions. The factor of water yield reduction expressing the joint action of marginal draining conditions is:

$$\frac{\bar{Q}(\nu)}{\bar{Q}(kM)_o} = \bar{\mu}(\nu) \bar{\varphi}(\nu) \eta_o \quad , \tag{40}$$

where $\bar{\eta}_o$ is the factor of water yield reduction (16), due to differences in geometric marginal conditions.

CONCLUSIONS

- Starting from the dynamic laws governing the migration of water within a reservoir and the mechanical ones pertaining to the function of water barring protective layers, a system of relationships in closed form can be derived which in accordance with experiences enable the hydraulical description of dynamic conditions of equilibrium developing spontaneously or artificially.
- For the system of reservoir-protective layer, irrespective of the character of the protective layer, the unique condition of equilibrium is that the formation energy inducing water migration should be in every point of the opened surface equal to or lower than zero.
- The relative reduction in formation energy, necessary to establish equilibrium is expressed by the average throttling factor of the system reservoir-protective layer, and its mode of dissipation by the average throttling factor.
- The greatest amount of elevated water to protect workings

underground, is due to lateral draining of the reservoir, while the lowest water yield is in connection with the spontaneous equalization due to intercalation of throttling protective layers. The relationship between these two values is expressed by the product of the yield reduction factors - more exactly of the average sealing factors - of the average throttling and of the average water yield reduction factor derived from the differences in geometric marginal conditions.

- Depending on marginal draining conditions the total amount of simultaneously inflowed water varies in very broad limits, in an extreme case even within the range $0 \lesssim Q(t) \lesssim Q(kM)_0$ what stresses the importance of selecting, exploiting and influencing reasonably the marginal conditions of drainage under the aspects of both mining and environment protection. For the area of the Transdanubian Midmountains the importance of this is particularly emphasized.

REFERENCES

Schmieder A 1971: Acta Geod. Geoph. Mont. Hung., 6, 429-448.

Schmieder A 1972: Budapest, BKI Idegen nyelvű Közlemények, No. 15, 17-29.

Schmieder A 1975: Budapest, BKI Idegen nyelvű Közlemények, Martos F (ed.), No. 18, 115-120.

Schmieder A 1976: MTA X. Osztály Közleményei, 9, No. 3-4, 173-187.

Schmieder A 1982a: The effect and utilization of protection layers in mine water control (in Hungarian). IMWA I. International Conference, Budapest, Proceedings ABCD, 175-195. (BKL Bányászat, 117, 1984, No. 3, 157-165.)

Schmieder A 1982b: Study on the process of movement, taking place in voids breaking through soft protection layers on the floor side of mining operations, and on that of karstic water inrushes. Candidate dissertation, Budapest

Schmieder A 1989: Function of water-barring protective layers. Manuscript, Budapest

Schmieder A, Szilágyi G 1988: BKL Bányászat, 121 (Number special), K72-K89.

Schmieder A, Kesserű Zs, Juhász J, Willems T, Martos F (ed.) 1975: Water hazard and water management in the mining industry (in Hungarian). Műszaki Könyvkiadó, Budapest

Acta Geod. Geoph. Mont. Hung., Vol. 25 (1-2), pp. 65-94 (1990)

FUNCTION OF WATER-BARRING PROTECTIVE LAYERS

A Schmieder

Central Institute for the Development of Mining, H-1037 Budapest,
Mikoviny u. 2-4, Hungary

The problem of the function of protective layers built-up of clayey, marly rocks has existed for more than 30 years. Starting the differential equation for the process of hydraulic rupture of strata, problems of spontaneous splitting processes of water-barring protective layers are solved; these problems include the character of spontaneous processes developing among different initial and peripherical conditions, the conditions of equilibrium limits, the stability of equilibrium conditions, in entirety the function of water-barring protective layers, from the beginning of spontaneous splitting up to the development of water- and water- and rock--inrushes.

Keywords: hydrofracturing; mining safety; splitting of rock; water--barring layers; water inrush

1. INTRODUCTION

As the costs of pumping increase with depth and owing to more and more rigorous environmental limitations, the mining significance of water-barring protective layers increases, too. In consequence efforts are made to collect knowledge about the function of water-barring protective layers, processes of rock- and water movement developing within and breaking through them, further about conditions of equilibrium limits of developing processes.

In spite of all these efforts differring conceptions about protecting layers exist in Hungarian mining which are contradictory to each other and are a source of discussions (Kesserű 1984, 1986a b, Schmieder 1986 a b, Juhász 1987). They also cause smaller-larger uncertainties in the dayly practice of estimation of protective layers in dimensioning of water-

-barring pillars, further in mechanical interpretation of water- and rock-movements during mining operations.

The present conceptions existing in Hungarian mining about protective layers - the traditional one by Vigh and Szentes (1952), the micro-infiltration one by Schmieder (1970), the instantaneous one by Kapolyi (1975), the energodynamical one by Schmieder (1982, 1983) and the stress-theory by Kesserű (1984, 1986) - were developed with the increase of knowledge mostly due to the fact that experiences based on direct observations allow diverse interpretations lacking a concordant theoretical principle. This is the reason why different concepts explain the function of water-barring protective layers in different ways. The development of water- and rock-movement processes piercing protective layers, and limit conditions of impermeable protective layers are defined by equilibrium limit equations.

This study reports on results which allow an interpretation and description of the functional mechanism of water-barring protective layers in a more complete and valuable form than before. Its method is built up on mathematical deduction, the results are checked by experiences based on direct measurements and observations.

This study follows the logic of research. An interpretation of water-barring protective layers and the presentation of protective layer concepts is followed by the mathematical model based on conservation of energy. Last, some general conclusions are reached in mirror of experiences.

2. INTERPRETATION OF WATER-BARRING PROTECTIVE LAYERS

Rocks which are bad aquifers and have some internal resistance E_0 against water movement are called water-barring rocks, or water-barring protective layers if insulating layers are meant between water bearing layers and mine opening.

Sedimental formations have a prominent role among water-barring rocks (Fig. 1). Water-barring sedimental rocks can be ranked in two large groups.

Rocks of the first group are easily eroding, fragmented, of smaller cohesion, they are generally water-saturated and

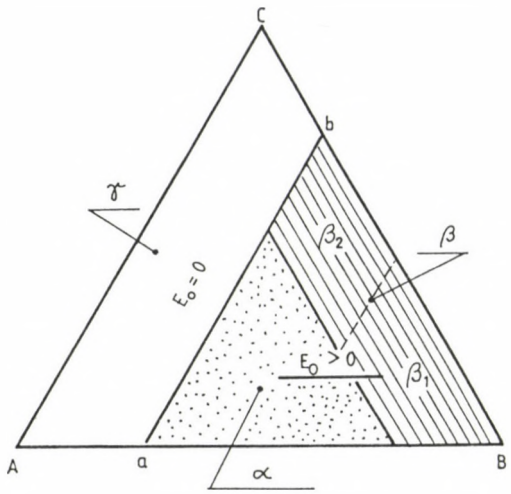

Fig. 1. Interpretation of water-barring sedimented rocks

have an interparticle threshold-gradient I_o (Juhász 1976) shown in the field α of Fig. 1. In these rocks water moves if the actual hydraulic gradient reaches or exceeds the threshold of infiltration, or if due to infiltration, the pressure transferred to the rock as a mass force, rock fracture occurs (Kézdi 1972). This study does not deal with sedimental rocks of group one.

The second group, as shown by field β in Fig. 1 is constituted by clayey, marly unsaturated sediments of more or less plastic behaviour. Rocks of this group are of high practical significance. They can be devided based on their behaviour against water to the subgroups:

- easily eroding soft materials (β_1) and
- hardly eroding clayey-marly sediments (β_2).

In these rocks fractures and splits developed in geological processes are in the natural stress condition generally closed against hydrostatic water pressure (Schmieder et al. 1975). A water movement between two water bearing layers or between a water bearing layer and a tapping opening starts through the zones traversed by joints only if joints formerly closed open

up due to
- a decrease of the rock-stress, or
- an increase of the water pressure

and conditions for water movement saturated with water develop. Laboratory tests of clayey-marly rocks traversed by joints (Kesserű 1976) indicate (in accordance with experiences of hydraulic rupture of strata (Lányi et al. 1983)) that joints in these rocks remain closed or the clayey-marly protective layer operates as water-barring structures as long as the rupturing pressure p_r affecting the surface of the rock traversed by joints is less than the minimum normal rock-stress σ_m closing the fissures. According to Kesserű (1976) a splitting of closed joints occurs at the limit if the condition of equilibrium is valid:

$$p_r = \sigma_m \quad . \tag{1}$$

One of the most disputed questions of clayey-marly protective layers is: why, at which pressure and to which extent do the closed joints of the rock split within the range $p_r \gtrsim \sigma_m$, if the limit condition of equilibrium is reached? What does govern the process of splitting and what does mining experience reflect?

Lacking adequate theoretical principles, the answers to these questions are naturally different. They are concisely expressed in diverse concepts of protective layers based on differring interpretation of experiences.

3. MINING EXPERIENCES

Most of the Hungarian experiences about water inrushes piercing clayey-marly protective layers were gathered in mines under carstic water hazard conditions in the Transdanubian Central Mountains. During the last 100 years nearly 2000 water inrushes were recorded which welled from carstic water reservoirs covered by water-barring protective layers located below the mining operations and connected to tectonically broken

zones of water-barring rocks (Ajtay 1962, Vigh and Szentes 1952).

70 to 80 percents of the water inrushes occurred directly along fault planes. 16 to 20 percents were in the fractured zone of faults and only in cases of a few percents it was impossible to find any connection between faults intersecting the protective layer and water inrush (Ajtay 1962). According to sporadic observations, the initial period of inrushes was indicated by swellings of smaller extent, in some cases by weak infiltrations. This situation lasted sometimes a few days, nay more weeks long. After a certain time the process accelerated. The water yield and its settlings content increased and a water inrush developed. During this period sound phenomena of variable intensity, cracking of support structures, intensive swelling, in some cases rapid destruction of adjacent mine openings could be observed, later water settled gradually and the dynamic equilibrium between rock and water phases set in. Large scale water inrushes prove beyond doubt that they developed there where the specific value of the so-called effective protective layer-thickness (the thickness reduced by the throw of the fault) referred to unit water-pressure difference, i.e. the specific protective layer-thickness was less than a certain limit value (Vigh and Szentes 1952). With increasing specific protective layer-thickness the areal frequency of water inrushes decreases (Fig. 2) and above a certain ν_o limit the danger of water inrushes ceases (Ajtay 1962, Vigh and Szentes 1952). This limit varies in case of soft materials between 0.5 and 1.0 m/bar, with harder clayey-marly rocks it reaches 3.0 to 4.0 m/bar (Schmieder et al. 1975, Schmieder 1983, Vigh and Szentes 1952).

The traditional concept of protective layers has been formulated based on these experiences: water inrushes penetrating floor-sided water-barring protective layers should not be expected if

$$\nu = \frac{m}{\Delta p_v} \gtrsim \nu_o \qquad (2)$$

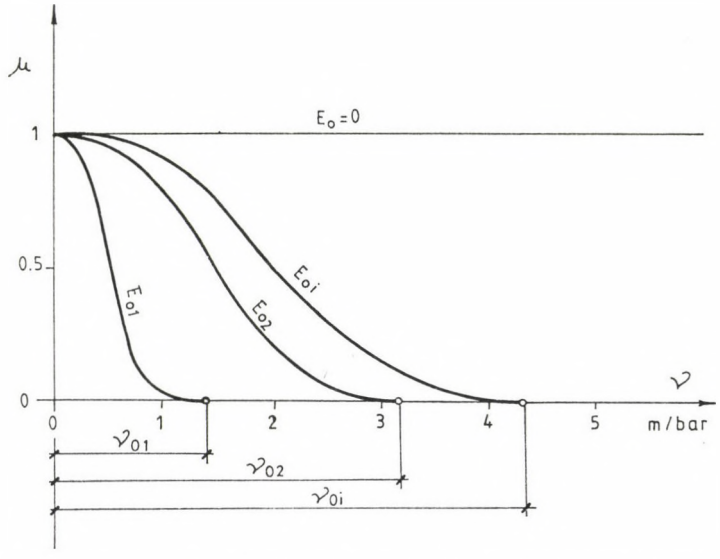

Fig. 2. Changes in relative frequency of water inrushes in function of the specific protective layer thickness

i.e. the specific protective layer-thickness is equal or higher than the limit ν_0 characteristic for a given protective layer (Vigh and Szentes 1952). In empirical formula (2) Δp_v is the hydrostatic pressure difference related to the floor level of the mining operations.

Water protecting pillar dimensioning was traditionally based in Hungary on these experiences, they were also used in the estimation of water inrush hazard and in official prescriptions. This practice is loaded with uncertainty because the physical interpretation of ν_0 and that of the equilibrium limit, Eq. (2) remain unexplained.

This problem has not been solved since more than 30 years (Vigh et al. 1961).

4. INTERPRETATION OF THE EXPERIENCES

The first interpretation of the equilibrium limit equation supported by physical facts was formulated on the basis of regularities of the micro-infiltration.

a) According to the microinfiltration concept of protective layers (Schmieder 1970) ν_o is the inverse of the average threshold gradient $\bar{I}_o^*$ belonging to the start of water movement and the equation of the related condition

$$\Delta p_v = \bar{I}_o^* \, m \qquad (3)$$

expresses the limit-equilibrium at the development of infiltration.

b) The concept of instantaneous protective layer (Kapolyi 1976) leaves open the characteristic conditions and the problem of related limit equilibrium. It investigates the function of the protective layer in the conditions preceding the development of water inrush. Departing from the traditional conception this concept supposes that in the initial phase of water inrush penetrating the protective layer, rock and water phases move simultaneously and permeate each other. These movements are described based on the macroscopic impulse-balance.

The differential equation which describes the common movement of both phases is:

$$\varrho_k \frac{d^2u}{dt^2} = - \text{grad} (\varrho_k gz) + \text{Div } F + k^* v \, , \qquad (4)$$

where ϱ_k is the mass-density of the rock,
u the field of movement of rock,
F the stress-tensor caused by the rock deformation,
k^* a factor depending on water-permeability of the infiltration field, and
v the current vector of water relative to rock.

Although the instantaneous concept of the protective layer leaves experimental problems unanswered, its up-to-date concept has contributed to the development of research.

c) The energodynamic concept of the protective layer (Schmieder 1982, 1983) interpretes a protective layer as a natural pressure equalizing valve which restores due to its self-regulating operation the equilibrium upset by mine cavities in accordance with the actual minimum energy level. It

starts to operate when the water-pressure difference between the aquifer and tapping cavities gets higher than the internal resistance E_o against movements in the protective strata. E_o is a function of the nature of the movement.

According to this idea in the case of argillaceous protective layers the necessary precondition of a water inrush penetrating the said protective layer is a fracture developing in that layer which might be caused by a hydraulic rockburst or the hydraulic rupture of rock.

As soon as the limit condition Eq. (1) has been reached, a smallest pressure difference starts the hydraulic rock-rupture. During this process microsized splitting of closed joints appears in the protective layer. Their development is controlled by the relief of rocks, its current equilibrium is described by the function

$$E_o = \sigma_\alpha + \bar{I}_o^* \, m \qquad (5)$$

and its limit condition by Eq. (3) where σ_α is the principal stress perpendicular to the joints. In this state the effective stress is in all points of the splitted and water-saturated rock-zone equal to zero. At the limit condition of water-inrushes a bifurcation may occur, one of the branches is the hydraulic rock-rupture, the other one is the infiltering water movement.

d) According to the stress-theoretical concept (Kesserű 1984, 1986a) - which is based on the experiences with hydraulic rupture of the hydrocarbon mining (Alliquander et al. 1975) of laboratory investigations (Kesserű 1976) and of operating experiments - both the traditional and the energodynamic methods are involving contradictions. Namely in these models the hydrorupturing pressure on the one hand is a linear function of the thickness m of the protective layer, on the other hand in Eq. (5), as in a hybrid model, both the stress and the infiltration resistance are included. According to the stress-theoretical concept of protective layers, in the protective layers of low strength which are in their original condition practically

water-barring, the process of water inrush starts by hydraulic rupturing. This occurs when in layers near the surface the hydraulic rupturing pressure

$$p_r = 1.1 - 1.5\sigma_m \qquad (6)$$

reaches or exceeds 1.1 to 1.5-times the value of the least normal principal stress.

In compliance with this concept:

- the splitting of the protective layer is analogous with the hydraulic rupturing; the process is controlled by the rock--stress zone being changed around the mine cavity and during the splitting macrosized splits of mm and cm widths resp., appearing;
- the so-called threshold-gradient $\bar{I}_o^x$ of the protective layer reflects the conditions of hydrorupturing in the environment of the mine cavity;
- the defined quantity of the specific protective layer-thickness may be only applied in the altered rock-stress zone around the mine cavity, both in lateral direction and in the footwall, but as a maximum only up to 40 to 50 m; beyond this distance it is no more valid;
- is the thickness of the protective layer less than 25 to 50 m, i.e. less than the rock zone of altered stress condition, there is no practical contradiction between the different evaluation methods of protective layers, the physical sense of this phenomenon is however, complying with that of the hydraulic rupturing.

In principle the energodynamical and stress-theoretical protective layer concepts are in contradiction with each other. Since any objective basis of evaluation is missing, their real respective merits cannot be specified.

This fact has justified theoretical investigation of the functional mechanism of water-barring protective layers in order to find answers to the following essential questions:

- Are the similarity conditions realized with regard of processes during hydraulic rupturing by external energy input

and spontaneous splitting of the protective layer?
- What does determine the size of the gap developing during spontaneous splitting of the protective layer and which is its range of size?
- What does determine the experimental limit of the specific protective layer thickness ν_o, what does it express and how far can it be considered stable?

The answers to these questions are built on similarity rules according to which the necessary, and satisfactory condition of the similarity of two systems is that the differential equations and conditions of agreement could be mutually and unambiguously converted into each other (Szücs 1972). In simpler terms, the similarity of two phenomena supposes that mathematical models describing the phenomena and all their constituting factors be respectively corresponding each other.

5. THE MATHEMATICAL MODEL DESCRIBING HYDRAULIC RUPTURING

The essential characteristics of the hydraulic rupturing are shown in Fig. 3. As a geotechnical procedure it acomplishes artificial quick rupturing of rocks (2) either from the surface, or through closed drilling holes (1) sunk from underground openings. The operation is successful when the splitting pressure p_r operated from an external energy source exeeds the lowest total normal principal stress of the rock (Kézdi 1972, Lányi et al. 1983), i.e.

$$p_r > \bar{\sigma}_m + p_v \,, \tag{7}$$

where $\bar{\sigma}_m$ is the lowest effective normal principal stress of the rock, and

p_v is the water pressure filling pores and splits of the rock.

During hydraulic rupturing, the stress-condition of the rock F(u,t) and its mechanical characteristics are constant in time. The developing split is perpendicular to the plane of the lowest normal principal stress. Breaking, splitting, propagation

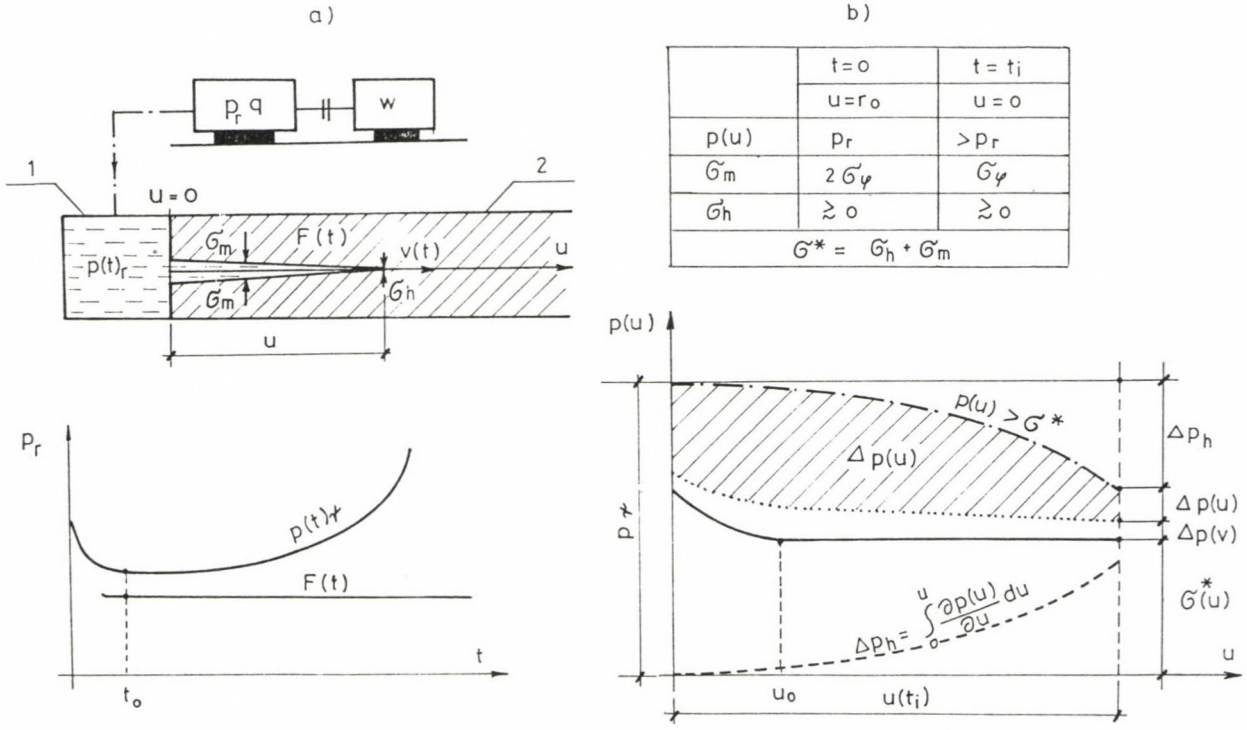

	t = o	t = t_i
	u = r_o	u = o
p(u)	p_r	> p_r
σ_m	2 σ_φ	σ_φ
σ_h	≳ o	≳ o
$\sigma^* = \sigma_h + \sigma_m$		

Fig. 3. Fundamental model of hydraulic rupturing

of splitting and split dilatation of the rock contacting the borehole are successively following each other in the process of hydraulic rupturing.

Breaking and splitting of the plane of rock bordering the borehole occur when a tensile stress appears in the rock. For example this is realized in the case of a borehole with vertical axis, due to the altered rock-stress-zone around the borehole functioning as a "potential barrier", if at a spot where $r = r_o$ (in Fig. 3, $u = 0$) the acting initial rupturing pressure is

$$p_{ro} \gtrsim \sigma_{mo} + \sigma_h \,, \tag{8}$$

where $\sigma_{mo} = 2\sigma\varphi$ and σ_h is the tensile strength of the rock. The tensile strength of the rock is interpreted in accordance with the deteriorating-condition by Griffith established for brittle materials (Brady and Brown 1985, Denby et al. 1982). It is zero or positive (depending on structure of the rock) during splitting of the rock and it can be taken as approximately constant both in time and space. With splitting of the bordering surface of the rock surrounding, the borehole rupturing pressure decreases (Fig. 3) and further process of rupturing will follow on a lower pressure level depending on the external energy led into the system

$$w = \int_{t=0}^{t} p_r q dt = \int_{V_2=0}^{V_2} p_r dV_2 \tag{9}$$

where q - is the volume rate of flow of rupturing fluid,
V_2 - the volume of the gap, and
t - the time.

After rupturing of the rock, a gap may develop only if the gauge pressure acting along the split (Fig. 3b) is

$$\Delta p(u) = p(u) - \sigma^* \tag{10}$$

in all points higher than zero, where $\sigma^* = \sigma_h + \sigma_m$.

The overpressure necessary to the development and support of the gap is, supposing elastic deformation

$$\Delta p(u) = cd \ , \tag{11}$$

where d - is the width of the gap, and
c - a factor depending on elasticity of the rock and water.

The rupturing pressure applied in the closed borehole space is used during hydraulic rupturing for rupturing, for the development of the gap, to overcome the pressure drop of flow and to replace losses due to changes in mass forces and kinetic energy.

The sum of all the pressure losses during energy--balance equation of the process for time $t = t_1$ yields

$$p_r = \sigma^* + cd + \int_{u=0}^{u} \frac{\partial p(u)}{\partial u} du + \varrho_v \int_{u=0}^{u} \frac{\partial v}{\partial t} du + \varrho_v \frac{v^2}{2} + \varrho_v gz. \tag{12}$$

The first derivate of the rupturing pressure gives the mathematical model describing the mechanical processes during hydraulic rupturing:

$$\frac{\partial p_r}{\partial t} = \left[\frac{\partial \sigma^*}{\partial u} + c \frac{\partial d}{\partial u} - \frac{\partial p(u)}{\partial u} + \varrho_v \left(a + v \frac{\partial v}{\partial u} + g \frac{\partial z}{\partial u} \right) \right] v \ , \tag{13}$$

where 'a' is the conductive part of acceleration, and
z the vertical height above the datum level.

For easier handling of the differential equation denoting the last terms on the right hand side of the equation as ε :

$$\frac{\partial p_r}{\partial t} = \left(\frac{\partial \sigma^*}{\partial u} + c \frac{\partial d}{\partial u} - \frac{\partial p(u)}{\partial u} + \varrho_v \varepsilon \right) v \ , \tag{14}$$

During hydraulic rupturing, the rupturing pressure is generally changing in time, it is characteristically increasing. Operating a rupturing pressure in time increasing, the process will go on as long as conditions for pressure increase

exist. Naturally the process of hydraulic rupturing goes on also in the case of a rupturing pressure artificially maintained constant i.e.

$$\frac{\partial p_r}{\partial t} = 0 \ , \tag{15}$$

and the initial conditions of the development of the gap (Eq. 8) are realized.

In the case of a simultaneous realization of all these conditions, the process starts and will go on as long as the conditions are all fulfilled. In this case the rate v(u,t) of the process is inevitably higher than zero, therefore the mathematical model of the process within constant rupturing pressure is:

$$\frac{\partial p(u)}{\partial u} = \frac{\partial \sigma^*}{\partial u} + c \frac{\partial d}{\partial u} + \varrho_v \varepsilon \ . \tag{16}$$

In accordance with Eq. (16) the process gets stopped in rocks in natural stress conditions, where the rupturing gradient in direction of splitting is zero, i.e.

$$\frac{\partial \sigma^*}{\partial u} = 0 \ , \tag{17}$$

in the case of a constant rupturing pressure, because sooner or later the full pressure difference $(p_r - \sigma^*)$ of rupturing is consumed by the presssure drops of flow. The full energy consumed during hydraulic rupturing, i.e.

$$w = w_Q + \frac{1}{2} \int_{V_2=0}^{V_2} \left[p(u) - \sigma_m \ dV_2 \right] \tag{18}$$

is partly dissipated as heat, partly it is accumulated in the rock as elastic energy. Energy function (18) shows that during hydraulic rupturing the internal energy of the ruptured rock system increases and the process varying around minimum gap

size is going on at the minimum potential. The gap size - due to $p(u) > \sigma^*$ - is in the macroscopic range. Having ceased the external energy input, the elastically stored energy performs further work, a stable condition of the system is achieved at equilibrium $p(u) = \sigma_m$.

6. MATHEMATICAL MODEL DESCRIBING SPONTANEOUS SPLITTING OF A WATER-BARRING PROTECTIVE LAYER

The spontaneous splitting of a water-barring protective layer - it differs from the process of hydraulic rupturing - takes place without external energy input (Fig. 4), with a pressure practically constant in time. In consequence of the constant nature of the water reservoir, an essential characteristic of spontaneous splitting is:

$$\frac{\partial p_v}{\partial t} \equiv 0 \ . \tag{19}$$

During these processes the stress condition of the rock is both in space and in time changing. Due to this another essential characteristic of spontaneous processes is that the rupturing gradient u

$$\frac{\partial \sigma^*}{\partial u} \neq 0 \tag{20}$$

is in its whole range differring from zero. The spatial range of the process is constituted by the broken, water-barring zone (Fig. 4a) between aquifer and tapping cavities. In initial state fractures starting at the contact surface between the water bearing and water-barring rocks and ending at the bordering surface of the tapping cavity are between the full range of the two limiting surfaces closed.

The normal rock stress which closes the cross fractures parallel to the axis u (e.g. σ_m) is monotonously decreasing towards the discharging cavity and reaches the minimum at its

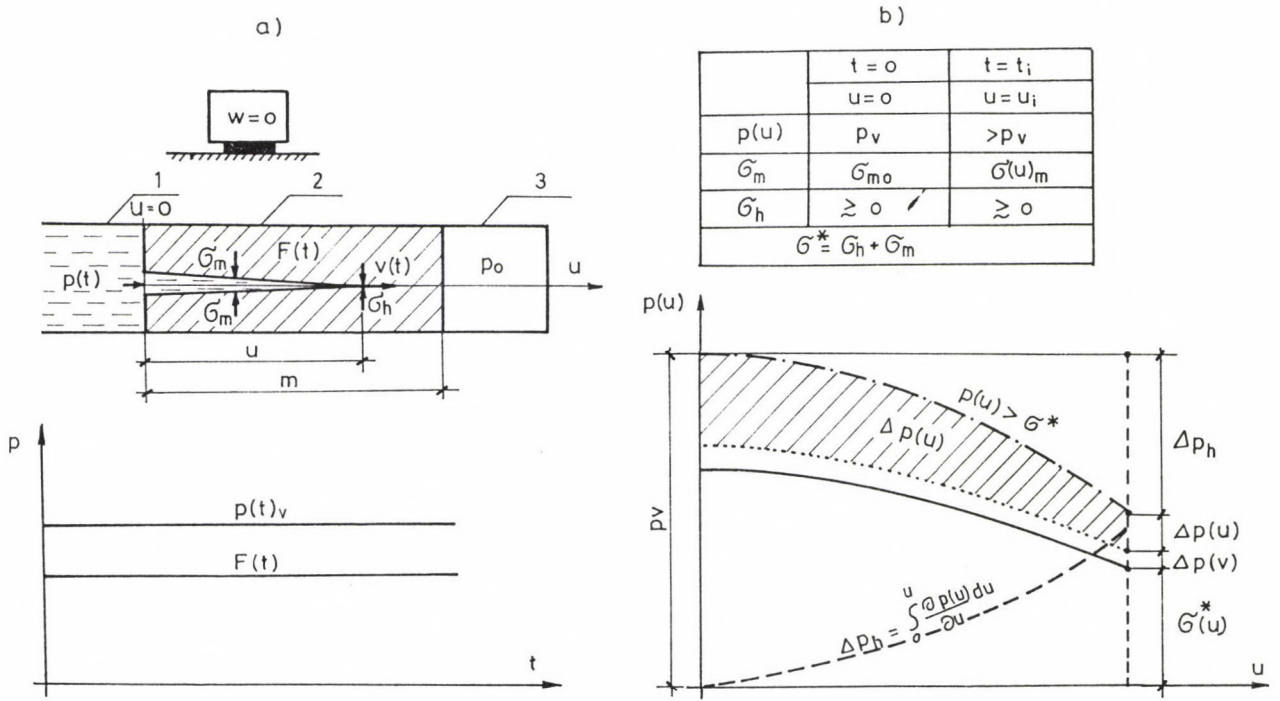

Fig. 4. Fundamental model of spontaneous splitting of argillaceous protective layers

limiting surface (Fig. 4b).

On the contact surface of the water bearing and water-barring rocks - in contrast to the bordering surface of rupturing borehole - no potential dam is acting and no tensile force appears from the water pressure. Therefore it can be only stated with certainty that the rock splits there where the initial rupturing pressure creating rupturing is a minimum, i.e.

$$p_v \gtrsim \sigma^*_{mo} \tag{21}$$

and if, due to rock pressure decrease the p_v pressure of the aquifer reaches or exceeds the former.

Depending on the initial conditions of splitting, spontaneous splitting may start

- as a process analogous to hydraulic rupturing, and
- as one differring from hydraulic rupturing.

Should the rupturing pressure belonging to the process be higher than σ^*_{mo}, and the process starts, i.e. $v > o$, then the mathematical model of the process is necessarily the same as that of the process of hydraulic rupturing (see differential equation (16)). Should $p_v > \sigma^*_{mo}$, then the spontaneous splitting of the water-barring protective layer can be described by the following mathematical model:

$$\frac{\partial p(u)}{\partial u} = \frac{\partial \sigma^*}{\partial u} + c\,\frac{\partial d}{\partial u} + \varrho_v\,\varepsilon. \tag{22}$$

According to this formula, spontaneous splitting of water-barring rock takes place as a process of hydraulic rupturing as far as the hydraulic pressure gradient is higher than the rupturing gradient. The limit equilibrium of this process is defined together with the limit of the similarity conditions of the process by

$$\frac{\partial p(u)}{\partial u} = \frac{\partial \sigma^*}{\partial u} \tag{23}$$

that is by equality of gradients and by $p(u) = \sigma^*$.

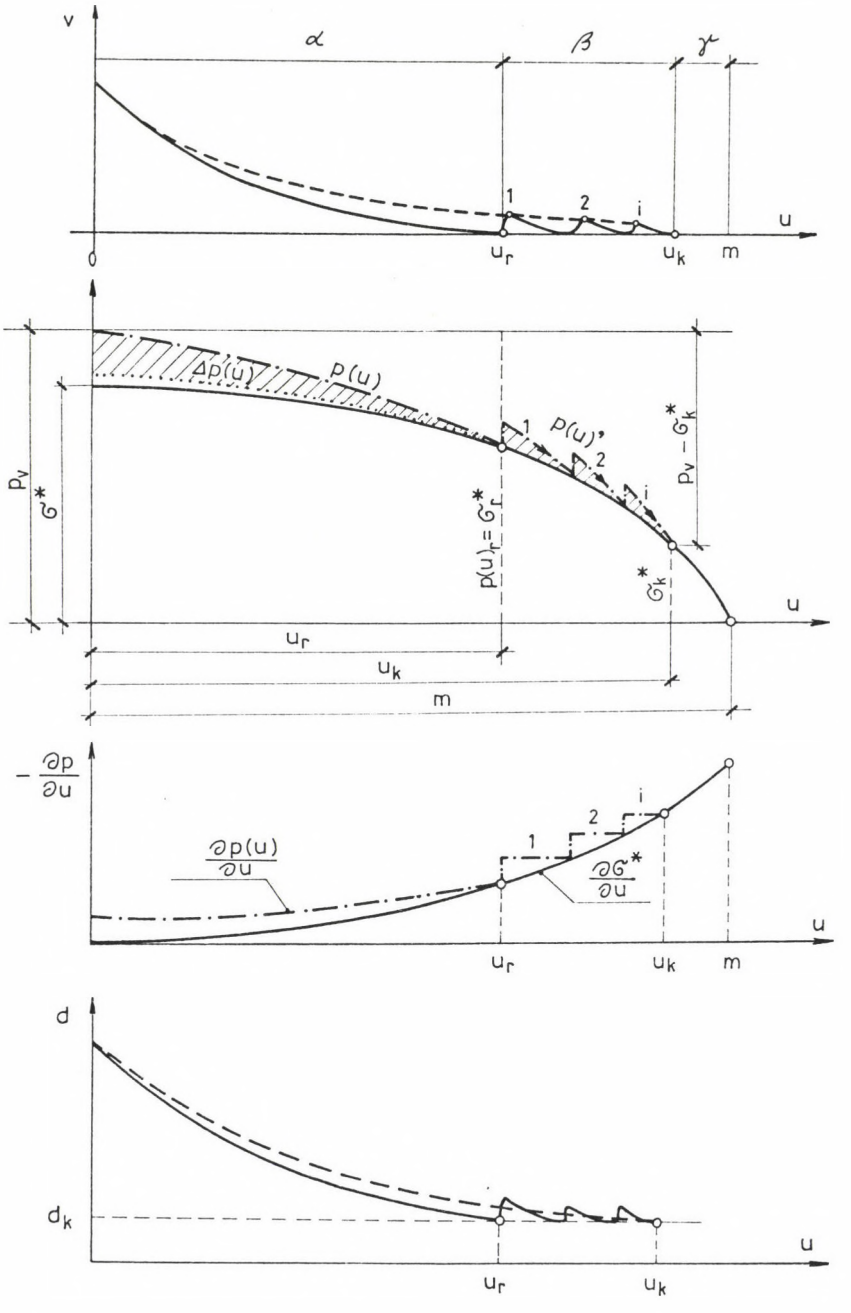

Fig. 5. Curves characterizing changes along the route of spontaneous splitting of protective layers

The characteristics of the process are shown in Fig. 5. During this process the speed of water flowing in the split and the rate of split-development decrease with increasing length of the split, and having reached the limit Eq. (23) the movement stops. The width of the gap is also decreasing with the distance of the aquifer, and at a distance, where $u = u_r$ it assumes a constant value. Within this distance, i.e. within the zone α, the basic features of the process assume the characteristics of the stress-theoretical concept of the protecting layer. In this range:

- the process starts at a pressure $p_v > \sigma^*_{mo}$,
- the process takes place similarly to hydraulic rupture,
- during the process macrosized joint develops due to overpressure acting in the split $[p(u) > \sigma^*(u)]$.

In contrast to the stress-theoretical concept of protecting layers, rupturing is controlled by the water pressure and not by the altered rock-stress zone.

The hydraulic threshold-gradient, the limit ν_0 of the specific protective layer thickness and the stress-theoretical criterion of the depth limit of the process cannot be interpreted based on the process of hydraulic rupturing discussed above.

The splitting depth is a function of the initial pressure difference $(p_v - \sigma^*_{mo})$. Should the pressure difference be high then a split of considerable depth may occur. Should the pressure difference be zero then no hydraulic rupturing will develop.

During the process, if the thickness m of the water-barring rock is less than the splitting depth or they are equal, the rock gets relatively quickly ruptured and water inrush develops, all at once thus confirming the stress-theoretical concept of protective layers.

Is u_r less than the thickness of the protective layer (Fig. 5), and get during the process water pressure p(u) and rupturing pressure σ^*_m equal, then the splitting developed analogously to hydraulic rupturing gets stopped and the process continues following other laws.

Should the equilibrium be attained, the rate $v(u_r)$ of split development tends to zero. This causes that in a distance u_r from the aquifer, the water pressure $p(u)$ increases in the split filled with water. Due to its effect

- the elastic energy of rock-zone in contact with the split and
- at the place, where $u = u_r$, the local value of the hydraulic pressure gradient

increase.

By a relative increase of the local hydraulic pressure gradient at $u = u_r$, the condition of splitting gets restored again and rock-splitting continues on a length of Δu, till the new equilibrium situation is attained. Within this phase of the movement, i.e. in the range β in Fig. 5, no change in elastic energy occurs during successively continuing pulsations. The change of the split is along the route in average zero. Supposing the validity of Darcy's infiltration-law, the sum of average pressure losses occurring during the process yields the energy-balance equation of the process:

$$p(u)_r = \sigma^*(u) + \int_{u=u_r}^{u} \frac{\bar{v}}{k^*}\,du + \varrho_v \int_{u=u_r}^{u} \varepsilon\,du \,. \qquad (24)$$

The derivative of Eq. (24) after u gives the mathematic model of the pulsation process:

$$\frac{\partial \sigma^*}{\partial u} + \frac{\bar{v}}{k^*} + \varrho_v \varepsilon = 0 \,. \qquad (25)$$

During the pulsation, the energy required for rupturing is covered by the elastic energy-change accumulated in the field α, while the flow pressure drops are covered by stress potential. The process will be stopped before full splitting of the rock if microforces appearing in the split of constant width, i.e. the impulse-change

$$I_o^* = \frac{2\tau_o}{d} \qquad (26)$$

originating from the shear resistance τ_o of resting water brings the water pressure

$$p(u)_r = \sigma^*(u)_k + \int_{u=u_r}^{u_k} I_o^* \, du + (z_u - z_r)\, \varrho_v g \qquad (27)$$

and the counteracting resistances into balance. In the above formulas

k^* - is the infiltration factor - expressed in bar/s - of the split of width d, being constant along the route,

z_u - the height of point u_r above datum,

z_k - the height of point u_k above datum, and

I_o^* - the hydraulic threshold-gradient.

Substituting the threshold-gradient in Eq. (27) with the average value $\bar{I}_o^*$, the state-function expressing the current equilibrium of the process is

$$\Delta p(u)_r = \sigma^*(u)_k + \bar{I}_o^* \, (u_k - u_r) \; . \qquad (28)$$

Equilibrium-equation (28) corresponds to the formula (5) of the energodynamic concept of protective layer. If $u_k = m$, i.e. $\sigma^*(u)_k = 0$ and $u_r = 0$, the limit-equilibrium interpreted on the basis of experiences of water inrushes is expressed by the following formula:

$$\Delta p_v = \bar{I}^* \, m \; . \qquad (29)$$

Equilibrium conditions (27-29) depending on the hydraulic threshold-gradient are - in contrast to the limit condition of hydraulic rupturing (23) - stable. In these conditions the dynamic balance is maintained by the shearing resistance of the rock between rock- and water-phases against the infiltration pressure transferred to the rock as a mass-force. This condition exists as far as no notable change takes place in the stress-condition or in the shearing resistance of the rock. This condition shows directly that the experimental limit of

the specific protective layer thickness ν_o interpreted as the reciprocal value of the average hydraulic threshold gradient in the limit-equilibrium, Eq. (29) expresses stable balance against water inrush, and as a material constant is a factor depending on the shearing resistance of water in rest and on the width of the gap. Multiplying the experimental limit ν_o of the specific protective layer thickness by the shearing resistance τ_o of the water in rest a value of a few microns is obtained for the width d of the gap (Schmieder 1983). The physical meaning of this characteristic also explains in some extent the experimental fact that ν_o is in softer rocks lower, in rigid rocks higher.

This characteristic value and the stability against water inrush of the condition corresponding to this characteristic value do not change, if in the split and water-filled gap due to e.g. a decrease of the rock-pressure, infiltration develops. With its development, the dynamic balance of the water phase is maintained in this case by the infiltration loss arising from movement

$$p(u)_r = \int_{u=u_r}^{m} \frac{\bar{v}}{k^*} du + (z_m - z_r)\, \varrho_v g \qquad (30)$$

the value of which is expressed for the full protective layer thickness in function of the hydraulic pressure-gradient by the relation

$$p_v = \bar{I}\, m \,. \qquad (31)$$

This condition, similarly to the rest one Eq. (29) exists as long as the rock is able to take the load due to infiltration pressure or as the flow resistance is considerably reduced by erosion.

In all cases if spontaneous splitting of the protective layer starts with the initial condition $p_v = \sigma^*_{mo}$, or if during hydraulic rupturing the water pressure p(u) and rupturing

pressure $\sigma^{*}(u)$ get equal in course of splitting, the entire or further process resp. takes place confirming the energodynamic concept of protective layers.

The mathematical model describing the spontaneous splitting of water-barring rocks in the pulsation period of the splitting fits - with exception of the term referring to the control of the process - directly the energodynamic concept of protective layers. The process starts and ends corresponding to this concept at the condition of equilibrium $p(u) = \sigma^{*}(u)$ and the gaps will be microsized ones. In the case of an adequate protective layer thickness, the process is stopped, the limit-balance condition belonging to rest is defined by the specific protective layer thickness ν_0 and by its reciprocal value and by the hydraulic threshold-gradient, resp. For a definition of the safe protective layer thickness this condition characterizing value can be only applied, if the spontaneous splitting is a determinative pulsation process.

Since the spontaneous splitting of water-barring rocks may take place equally either by hydraulic rupturing, or by pulsation successively, or independently, the question inevitably arises: does one or other of the processes predominate or not? An answer to this question is given by the determinative initial condition belonging to splitting.

7. EFFECT OF INITIAL AND CIRCUMFERENTIAL CONDITIONS ON THE DEVELOPMENT OF THE PROCESSES

The initial conditions have an essential influence on the nature of the process, while circumferential conditions have the same on the intensity.

As discussed in the previous section the process regularly starts with hydraulic rupturing if the initial value of rupturing pressure is less than the water pressure what is characteristic for the process, otherwise it is of a pulsation nature, when defining the determinative role, no considerable omission should be made supposing that splitting starts at the contacting boundary surface of aquifer and water-barring rocks.

This means that on a surface, on which no potential dam exists principally no tensile stress may arise due to water pressure. That means that in opening of closed joints , a factor or some factors being independent from water pressure may have a role. Such a role can be played by

- the different elastic behaviour of water bearing and water-barring rocks,
- the water intake of water-barring rocks,
- the existence of splits starting from the aquifer and ending at the boundary,
- the predominance of interfacial forces,
- the deformation-labour during relieving the rock.

All these factors are acting against the initial overpressure. Without a listing of factors it is worth mentioning that a shearing force appears due to the different elasticity of the water bearing and water-barring rocks, at the contacting boundary in consequence of a difference between the deformations. The maximum shearing force generally reaches the maximum either on one, or on the other side of the fault-zone, depending on the fact at which side of the fault-zone the relieving of rock is higher. This may explain the experience that most of water inrushes appeared along fault planes (Ajtay 1962).

The joints opened in such a way and the expansion of joints resp., also change - as reflected in the mathematical models - in function of labour necessary to expand opened joints. According to Denby et al.(1982) adsorption of water is notably reducing the surface energy needed to expand the joint, - i.e. σ_h in the mathematical models - which may considerably contribute in interaction with the deformation labour to the splitting of relieved joints.

Since no potential dam brakes, the spontaneous splitting of the protective layer and all other factors are acting against the development of overpressure, the determinative condition of splitting is identically with the energodynamic concept

$$p_v = \sigma^*_{mo} \quad , \tag{32}$$

In a limit case, if $\sigma_h = 0$, $p_v = \sigma_{mo}$.

The reality of the determinative limit conditions (32) is strengthened by mining experience which confirms that a stable equilibrium of the final condition of the processes belongs to the value ν_o of the specific protective layer-thickness.

The simplest circumferential condition of the process is shown in Fig. 4, as the spatial distribution of rock-stress. The lowest normal principal stress is perpendicular to the cross-breaks in u direction connecting the aquifer with the draining cavity. The principal stress decreases towards the draining cavity. Around mine cavities a real replica of this model occurs never or very seldom. A typical example is an aquifer with overpressure (Juhász 1976, Szalai 1983).

With such circumferential conditions closed breaks perpendicular or inclining to the plane of the principal stress are passive ones. During the process one or several breaks may have the opportunity to form microsized splits, therefore the volume-increase of the water-barring rock can be neglected.

A more considerable change of volume may appear when cross-directional splitting of the rock is not bound to the plane of the least, but e.g. to the highest rockstress (Fig. 6). According to this model cross-directional splitting of the rock occurs then and only then, when the water pressure is equal or higher than the rupturing pressure at the bordering surface, i.e.

$$p_v \gtrsim \sigma_h + \sigma_{o1} = \sigma^*_{1o}. \tag{33}$$

The character of the process is also in this case defined by the initial conditions which is as discussed in the plane of maximum principal stress determinatively of a pulsation character.

All closed breaks which are in contact with the splitted cross-directional break or breaks filled up with water of a pressure p(u) become active with the development of the process and an intensive cross-directional process starts.

Since σ_1 and σ_m are essentially different, the

	t = o	t = t_i
	u = o	u = u_i
p(u)	p_v	> p_v
σ_u	σ_{10}	$\sigma_{(u)_1}$
σ_m	< σ_{10}	< $\sigma_{(u)_1}$
σ_h	≳ o	≳ o

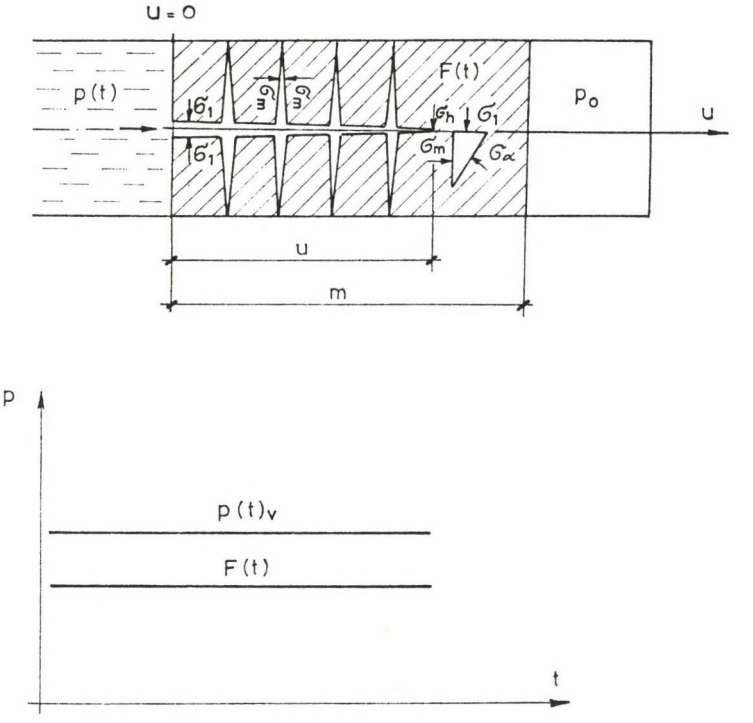

Fig. 6. Fundamental model of spontaneous splitting in the plane of the maximum principal stress

cross-directional splitting starts as a regular hydrorupturing process and macrosized joints are dominating.

If the rock is not hindered in deviation, a considerable change of volume may appear due to this cross-effect the lateral effect of which may reach larger distances in case of advantageous conditions.

In case of the circumferential conditions shown in Fig. 6 - pulsation as a primary process, and

- hydraulic rupturing, as a secondary process are taking place simultaneously.

The process - in contrast to the stress-theoretical concept of the protective layer - does not develop at the least, but depending on the given limit conditions at the maximum rock-stress; its course follows the laws discussed.

A real equivalent of the model shown in Fig. 6 is represented by a protective layer below the draining cavity.

At real bedding the boundary conditions are various. Therefore the general validity of the principle of least principal stress as splitting criterion cannot be accepted. But its application for splitting of the protective layers excludes on the entire mass of the boundary conditions. But as a dimensioning principle (Kesserű 1984, 1986a) it results in absolute safety. The principle of equal safety is satisfied in the case if the dimensioning is based on an up-to-date stress analysis and on measurements of rock-stresses (Kesserű 1986a).

Dimensioning using the limit ν_0 of the protective layer thickness provides lower safety. As a traditional method, it results in identical safety for the entire mass of boundary conditions in contrast to the development of water movement. It is reliable, if ν_0 is known at the place of application from identical or nearby identical petrographical and bedding situations.

A water protecting pillar based on these dimensioning principles is sensible to changes or rock-stress conditions in the case of applying the least principal stress, and in the case of applying ν_0 to the shearing resistance of the rock.

Changes of the parameters which cause in one case spliting of the rock, in another case the start of infiltration does not mean that the pillar is deteriorating. The splitted protective layer broken by water-filled joints still takes the full water pressure in this state. Local deterioration occurs only if the dynamic equilibrium between the rock- and the water-phase is upset and erosion or hydraulic rock-breaking penetrating the protecting layer results by means of mass transport in the equalization of the entire free energies related to a

given point of the aquifer (Schmieder 1982, 1983).

CONCLUSIONS

- The general mathematical model of spontaneous splitting process in water-barring argillaceous protective layers can be deduced and interpreted starting from the process of hydraulic rupturing and based on energy conservation. This allows us a more complete interpretation and description of the functioning of the protective layer.
- It can be proven based on the mathematical model describing the process and in conformity with experiences that both the energodynamic and the stress-theoretical concepts of protective layers are based partially or entirely on real processes.
- The character of the processes is defined by the relation between rupturing pressure and reservoir pressure during spontaneous splitting of the protective layer and changes in volume during the process are determined by the spatial distribution of rock-pressure and by the structure of the splitting rock.
- It could not be shown that the water pressure could be higher than the rupturing pressure at the boundary surface in contact with the aquifer and the water-barring protective layer, therefore processes corresponding to the energodynamic concept of the protecting layers play a defining role in the development of cross-breaks connecting aquifer and draining cavity.
- Microsized splitting operating with pulsation gets stupped during the development of cross-breaks, if the protecting layers are of adequate thicknesses, the limit condition of which is defined by the limit value ν_0 of the specific protecting layer thickness depending on the hydraulic threshold--gradient. This as a material-constant expresses uniformly the limit-equilibrium before the development of infiltration with any boundary condition.
- By processes according to the stress-theoretical concept of protective layers the value of ν could not be interpreted

and this could not be used for the indication of the limit equilibrium of the process.

- Spontaneous splitting of the water-barring rock develops in function of the prevailing circumferential conditions there, where the rupturing pressure belonging to the splitting is the lowest. Since this is not necessarily belonging to the plane of the least principal stress, the general validity of the least principal stress principle cannot be accepted as a splitting criterion.
- The splitting of the protective layers is for the entire set of boundary conditions excluded by the application of the principle of least principal stress. This method satisfies the requirement of equal safety, if it is based on stress--analysis and measurement of the rock-pressure.
- Dimensioning of the specific protective layer thickness with respect to the limit-value ν_0 is affording equal safety as a traditional method against the development of water pressure for the entire set of boundary conditions, without any limitation of the thickness.

REFERENCES

Ajtay Z ed. 1962: Protection against mine water. Műszaki Könyvkiadó, Budapest

Alliquander Ö, Gyulai Z, Szepesi J 1975: Rock rupturing by liquids. I. NIMDOK, Budapest

Asszonyi Cs, Kapolyi L 1976: Definition of mechanical characteristics of rocks. MTA VEAB Monograph, Volume II, No. 4, Veszprém

Brady B H G, Brown E T 1985: Rock Mechanics. London, George Allen Co., Unwin

Denby B, Hassani F P, Scoble M J 1982: Influence of water on shearing strength of coal strata and stratification faults in open pits. Transactions of the Ist Congress of IMWA, Volume A, Budapest

Juhász J 1976: Hydrogeology. Akadémiai Kiadó, Budapest

Juhász J 1987: Opponent's opinion on the study of dr. Schmieder A: Some remarks on novel valuation of initial processes of water inrushes penetrating a soft protecting layer. Manuscript, Miskolc

Kapolyi L 1975: BKL Bányászat, 109, 811-818.

Kesserű Zs 1976: MTA X. Oszt. Közl., 9, 189-199.

Kesserű Zs 1984: Int. Journ. of Mine Water, 3, 1-12.

Kesserű Zs 1986a: BKL Bányászat, 119, 9-16.

Kesserű Zs 1986b: Answers to the questions of dr. Schmieder A regarding the article: "Novel valuation of initial process of water inrush penetrating a soft water-barring protective layer". Manuscript, Budapest

Kesserű Zs, Bagdy I, Szűcs I 1980: Experiments on standpipe fastening in 1980. Research report. KBFI, Budapest

Kézdi Á 1972: Soil mechanics I. Tankönyvkiadó, Budapest

Kipko E Ya 1978: Vremennaya instruktsiya po tamponazhu treshinovatikh gornikh porod kompleksom metodom pri soaruzheniy stbolov shakht. M.U.P. SSSR, Voroshilovskaya pravda

Lányi T, Mucsányi J, Szabó M 1983: BKL Kőolaj és Földgáz, 6, 372-373.

Schmieder A 1972: BKL Bányászat, 105, 107-109.

Schmieder A 1982: The effect and utilization of protection layers in mine water control. IMWA Congress, Budapest, Proceedings ABCD, 175-195 (BKL Bányászat, 117, 1984, 157-165)

Schmieder A 1983: Investigation of movement processes of soft protective layers penetrating split and carstic water inrushes in footwall side of mining operations. Candidate's dissertation, Budapest

Schmieder A 1986a: Some remarks on novel valuation of initial processes of water inrush penetrating a soft protecting layer. Manuscript, Budapest

Schmieder A 1986b: Answers to the questions of dr. Kesserű regarding the article: "Novel valuation of initial processes of water inrush penetrating a soft protecting layer". Manuscript, Budapest

Schmieder A, Kesserű Zs, Juhász J, Willems T, Martos F (ed.) 1975: Water hazard and water management in mining. Műszaki Könyvkiadó, Budapest

Szalai Á 1983: BKL Kőolaj és Földgáz, 116, 363-371.

Szűcs E 1972: Similarity and model. Műszaki Könyvkiadó, Budapest

Vigh F, Szentes F 1952: Bányászati Lapok, 85, No. 11, 588-600; No. 12, 645-665.

Vigh F, Schmieder A, Darányi F 1961: Theoretical and methodological investigations to more exact definition of specific protective layer thickness. Research report. BKI, Budapest

Acta Geod. Geoph. Mont. Hung., Vol. 25 (1-2), pp. 95-105 (1990)

A MODELLING OF INTERRELATIONS BETWEEN SUBSURFACE WATER AND ITS STORING ROCK

R Jeney-Jambrik and L Balla

University for Heavy Industry, H-3515 Miskolc, Egyetemváros, Hungary

Accepting the systems approach as a basic principle in the control of the processes of exploration, exploitation, preparation, marketing, distribution and utilization of mineral resources further in the coordination of economic processes, the authors present the structure, the parameters of the systems model of mineral raw materials and water management, the physical laws describing natural processes as well as the possibilities of their mathematical approximation; the flow-related, hydrogeological, mathematical models are also studied describing the relation of water movement to mining activities.

Keywords: environmental effects of mining; hydrogeology; seeping water; subsurface; system model; water

1. INTRODUCTION

The higher demand on natural resources, the reduction of mineral reserves and the necessity to exploit mineral deposits in increasingly unfavourable natural conditions require the management of mineral raw materials in a system approximation (Kapolyi 1980).

The system approximation-type economic management of natural resources is based on a simultaneous evaluation of exploration, exploitation, distribution and utilization. Its system model is built up from subsystems; the most important ones of them are: the system of the geological survey of mineral raw materials, the system of exploitation, the system of processing of the mineral raw materials including, as auxiliary activities, transportation and storage as well; the system of the mineral utilization (Kapolyi 1981).

The subsystems contain further partial systems being in close connection with one another.

The aim of the paper is to review the general characteristics of the system model of environmental processes as well as principles and methods describing the simultaneous movement of the water seeping laminarly in the porous reservoir and of the rock being flexibly deformated (Exploration Report 1987).

2. CHARACTERISTICS OF THE SYSTEM MODEL

2.1 Parameters of the system model

The characterization of a zone of the Earth's crust is given - arranged according to the field of parameters being typical of the given range - as follows:

I. Geometric field: the geometry of the raw material deposit, the data typical of its micro- and macrostructure, the geometric data of the secondary rocks (depth, thickness and extension in space) and their structural properties, in case of typical hazard sources the geometric properties of the permeable and impermeable layers, the geometric data of the connection with the natural environment, i.e. of the boundary conditions in the nature, etc.

II. Density field: Material- and mass-parameters of the half--space, as porosity, permeability, transmissibility, body density, etc.

III. Property field: Different physical and technical parameters of the material of the half-space, as physical condition, physico-chemical properties, state-related properties, mineralogical-petrological properties, etc.

2.2 Physical laws describing the system model

The geometric field and the material system defined on it are in constant movement. If the geometric, property-related and density parameters of the system model are known, the time process of the effect of human intervention on the natural environment can be described by means of physical laws, as mass

balance equation, momentum balance equation, energy balance equation.

2.3 Mathematical approximation of the environmental processes

If the field parameters, the initial- and boundary-conditions are known, the general balance equations of the transport- and transformation-processes, i.e. the processes of the natural environment can be described by a mathematical model.

Depending on the dimensions and fullness of details of the field parameters discovered by mineral raw material exploration one-, two- or three-dimensional models can be formed, by means of which the effect of human intervention - in function of the reliability of the field parameters, given as random variables - can be determined and used at the preparation of decisions.

In the field of modelling the hazards for water inrush, for gasburst, fire and rock movements as well as in the modelling of environmental effects caused by mining activity, several scientific results have been achieved both in Hungary and abroad in the recent decades. In the present paper a possible mathematical model of the interaction between water and rock is outlined connected to the example of open-pit coal mining, whereby the rocks are regarded as elastic, i.e. as following Hooke's law.

3. MODEL OF RELATION BETWEEN WATER AND ROCK MOVEMENT

3.1 Description of the general flow model

The subsurface waters, being the subjects of the hazard-protection in open-pit coal mines, are simple formation waters stored in the coal-seam formation and in its porous secondary rocks (bearing rock) being under pressure and having fresh supply; they can be drained in a gravitational field. Their fresh supply comes through the ground water from the local precipitation, and by lateral water movement from the precipitation in the mountain edge area; their natural drainage takes place through evapotranspiration and lateral leakage.

The subsurface water-flow is in general case a time-dependent three-dimensional process taking place in a porous medium.

For the description of isothermal underground water-flow different mathematical models are known, since different authors consider different factors - in dependence of a given case - as negligible from the general model.

The steps of the forming of the general model are:

- to define the general model of the complex hydrogeological system composed from subsystems, which are in an internal boundary condition-type interrelation;
- to form the mathematical model describing the flow processes in the different subsystems;
- to determine the external boundary conditions concerning the different subsystems, the internal boundary conditions between the different subsystems, the initial conditions and the physical parameters; and finally
- to choose the numerical solution method of the mathematical model.

3.2 Description of the hydrogeological model

The subsystems of a hydrogeological system are in a general case: porous subsurface aquifers (permeable layers), separating or impermeable layers of lower or higher water permeability between the aquifers, water-production or water-injection wells of the aquifers, rivers and lakes on the surface, natural atmospheric effects, the artificial water-management-interventions on the surface, and mining technologies.

The subsystems are very complicated in themselves, thus it is necessary to simplify the system on the basis of different assumptions.

The processes of the subsystems are three-dimensional, time-dependent processes, thus the handling of the relations between the subsystems is complicated, the computer capacity necessary for the numerical solution and the computer technology time increase exponentially with the number of dimensions. Thus it is advisable to reduce the number of dimensions, if allowed by the character of the task.

The horizontal dimension of regional aquifers under the surface is generally by several orders of magnitude greater than their thickness, therefore in the aquiferous layers the vertical component of water flow can be in most cases neglected with respect to the horizontal component. Thus the practical requirements can be fulfilled by the study of the water-bearing subsystems in a two-dimensional field.

In the separating layers of lower or higher permeability the water is not modelled in itself, but the process taking place in them is considered as the internal boundary condition of the hydrogeological system as a one-dimensional vertical flow determined by the potential difference between the subsystems and the hydrodynamical parameters of the separating layer.

Water-production and water-injection wells can be taken into consideration in regional analyses as surface sources or surface sinks, respectively. The water level or water yield of the wells depend on the regional potential and the boundary conditions concerning the wells, what means the recording either of the yield or of the potential of the well.

The subsystems of the processes resulting from surface rivers, lakes, natural atmospherical effects, precipitation, evaporation, underground capillary zones, interferences of artificial surface water management, and mining technology are not modelled. Temporal and spatial changes of the parameters of the subsystems are taken as known, thus, with regard to the total hydrogeological system, they are treated as the external boundary conditions of the system.

The geological model of the hydrogeological system will be modified by opencast mining activity, which should be taken in the mathematical model as a boundary condition changing in time. In practice the mining technology can be divided into phases in which the hydrogeological model can be considered as constant with regard to the modelling of water flow.

The general hydrogeological model is presented in Fig. 1, the connection graph of the corresponding hydrogeological model in Fig. 2.

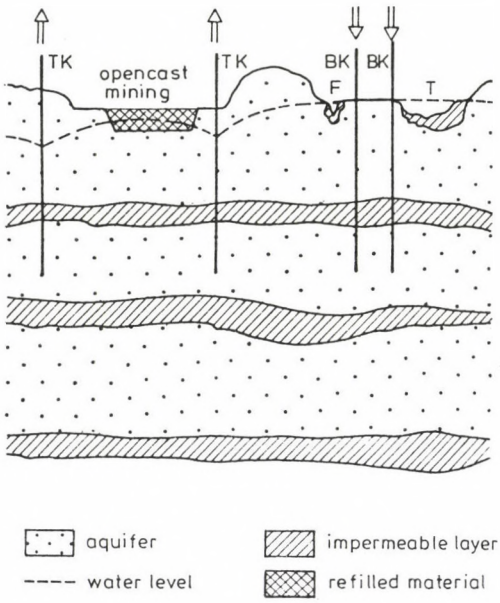

Fig. 1. Scheme of the hydrogeological model

The elements of the hydrogeological system are, according to Székely (1973) and Kovács (1984), the following: aquifer (porous rock of relatively high permeability with respect to its surroundings and having either a free water surface (SR) or a tense water surface (FR)); impermeable layer (rock with relatively low permeability with respect to its surrounding (ZR)); surface water reservoirs (rivers (F), lakes (T)); wells (drilled from the surface (K) which can be in connection with permeable or impermeable layers as well as with surface water reservoirs separately or simultaneously; depending on the flowing direction of the water they are either production wells (TK), or injection wells (BK)).

The boundary conditions of the system are: yield or potential of the wells; potential of surface water reservoirs; intensity of atmospheric phenomena (infiltration or evaporation of precipitation on the surface); intensity and technical characteristics of technologies on the surface (irrigation,

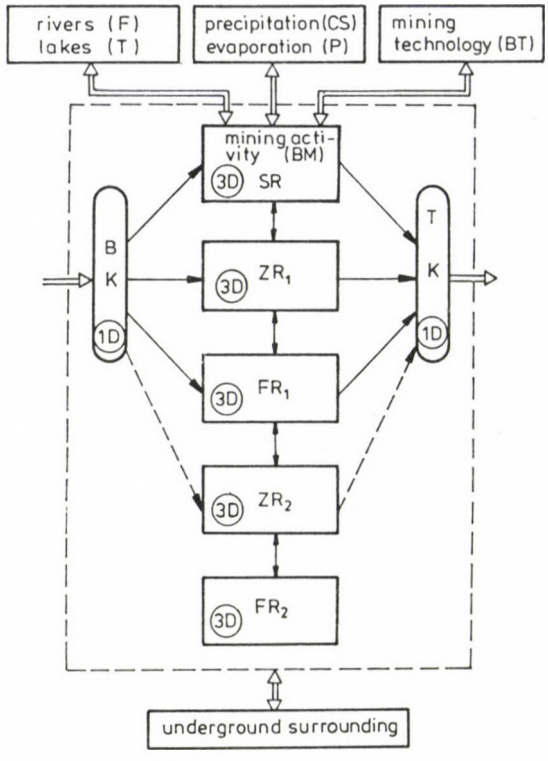

Fig. 2. Connection graph of the hydrogeological model

opencast mining activity); characteristics of water flow in the layers or of water yield; characteristics of rock displacement.

3.3 Description of the mathematical model

In the macroscopic elementary part of the hydrogeological model shown in Fig. 1, the isothermal water flow is described for a general case by the law of conservation of mass (Bear 1982, Aziz and Settari 1979):

$$\frac{\partial(\phi \varrho)}{\partial t} + \operatorname{div}(\varrho v) + q = 0 \qquad (1)$$

where ϱ = water density; ϕ = porosity; t = time; v = seeping velocity; q = intensity of volumetric water mass of source/swallower.

Assuming that the porous system is completely filled up with water and that Darcy's flow conditions are fulfilled, the velocity v is:

$$v = \frac{k}{\mu} \operatorname{grad} (p + \varrho g h) \tag{2}$$

where k = rock permeability; μ = dynamic viscosity of water; p = water pressure of pore; g = gravitational acceleration; h = height potential.

Water density and porosity are in an isothermal case functions of water pressure and effective rock stress, respectively, hence the first term of relation (1) can be expressed as follows:

$$\frac{\partial(\phi \varrho)}{\partial t} = \phi \frac{d\varrho}{dp} \frac{\partial p}{\partial t} + \varrho \cdot \frac{d\phi}{d\sigma_2} \frac{\partial \sigma_2}{\partial t} . \tag{3}$$

Connection $\varrho(p)$ is known or can be determined for the given water quality.

It is assumed that the vertical stress distribution σ_z^o is unidirectional and that under the effective rock stress σ_z the following conditions are fulfilled:

$$\begin{aligned} \sigma_z^o (x,y,z) &= \sigma_z + p(x,y,z,t) \\ \sigma_z^o &= \int_0^z \varrho_s (x,y,z) \cdot g \cdot dz \end{aligned} \tag{4}$$

where ϱ_s = rock density (density of the water-saturated rock); z = depth measured from the surface.

Assumed that ϱ_s and σ_z^o are constant in a given place, one gets:

$$\begin{aligned} \frac{\partial \sigma_z^o}{\partial t} &= 0 \\ \frac{\partial \sigma_z}{\partial t} &= -\frac{\partial p}{\partial t} \end{aligned} \tag{5}$$

by means of which connection (3) can be written in the form:

$$\frac{\partial(\phi\,\varrho)}{\partial t} = \left(\phi\,\frac{d\varrho}{dp} + \varrho\cdot\frac{d\phi}{dp}\right)\frac{\partial p}{\partial t} \qquad (6)$$

The compressibility of the water is:

$$\frac{1}{\varrho}\,\frac{d\varrho}{dp} = \beta \qquad (7)$$

the vertical compressibility of the porous rock is:

$$\frac{d\phi}{dp} = \alpha \qquad (8)$$

Using these expressions relation (6) can be written in the form:

$$\frac{\partial(\phi\,\varrho)}{\partial t} = \varrho\,(\phi\cdot\beta + \alpha)\,\frac{\partial p}{\partial t} \qquad (9)$$

where α and β can be determined in case of a given sample system by measurement or calculation, and the results can be rendered probable with higher or lower accuracy for real regional systems, too.

Relation (5) does not hold in cases where σ^{o}_{z} cannot be assumed to be constant due to larger rearrangements of stresses caused by rock movements, which occur at different mining operations in a more or less negligible degree. In such cases it is necessary to calculate the spatial porous rock displacements by means of Kapolyi's equation (1981) for small, quasi-statical deformation:

$$\operatorname{div}\,\underline{\underline{\sigma}}^{o} + f = 0, \qquad (10)$$

where f is the volumetric force density.

In the most cases of the practice the total stress tensor $\underline{\underline{\sigma}}^{o}$ can be determined by assuming the validity of Hooke's law:

$$\underline{\underline{\sigma}}^{o} = 2\cdot G\cdot\underline{\underline{E}} + 3K\cdot\underline{\underline{E}}_{o} \qquad (11)$$

where G = tangential modulus of elasticity; K = modulus of

compressibility; $\underline{\underline{E}}$, $\underline{\underline{E}}_0$ = deformation tensors.
The average deformation e is:

$$e = \frac{1}{3} \operatorname{div} u \tag{12}$$

where $u = \{ u_x, u_y, u_z \}$ is the displacement vector. The connection between the average deformation and the porosity is:

$$\phi - \phi_0 = 3e \tag{13}$$

where the initial porosity of the system is ϕ_0. By using the relations (12) and (13) one gets:

$$\frac{\partial(\phi \varrho)}{\partial t} = \varrho \left(\phi \beta \frac{\partial p}{\partial t} + \frac{\partial \operatorname{div} u}{\partial t} \right). \tag{14}$$

The solution of the equation set consisting of Eqs (1), (2), (10) (11-14) provides in case of small, quasi-static deformations, the distribution of water pressure and rock displacement of the individual layers, which represents in case of the uppermost layer the surface rock movements (surface subsidences).

The analytical solution of the equation set is not known for the general case, but approximating solutions of required accuracy can be obtained by means of different methods of finite elements or finite differences.

In the most cases of practice there is anyway no real demand on the solution of the general model, since in case of a given problem approximations and simplifications can be made, the accuracy of which meets the demands of practice.

It was not the aim of this paper to analyze the numerical solution possibilities of the mathematical model which describes the water and rock movement phenomena taking place in the hydrogeological model.

REFERENCES

Aziz K, Settari A 1979: Petroleum Reservoir Simulation. Applied Science Publishers LTD, London

Bear J 1972: Dynamics of Fluids in Porous Media. American Elsevier Publ. Co., New York

Exploration Report 1987: Environmental effects of 'Thorez' opencast mine; II. Mine Working Department of the Technical University of Miskolc

Kapolyi L 1980: Journ. of Mining and Metallurgy - Mining, 113, 658-664.

Kapolyi L 1981: Systems- and functional approach of natural resources of mineral origin. Publication of the Academy, Budapest

Kovács Gy 1984: Importance and principle characteristics of groundwater systems. VITUKI (The Research Center for Water Resources Development), Manuscript, Budapest

Székely F 1973: Hydrological Review, No. 5, 229-234.

Acta Geod. Geoph. Mont. Hung., Vol. 25 (1-2), pp. 107-126 (1990)

NUMERICAL SIMULATION OF SEEPAGE OF TWO FLUIDS IN HARD RESERVOIR ROCKS AND SOME APPLICATIONS

Zs Kesserű[1], T Vincze[2], I Havasy[1]

[1]Central Institute for Development of Mining, H-1037 Budapest, Mikoviny u. 2-4, Hungary

[2]Hungarian Hydrocarbon Institute, H-2443 Százhalombatta, Hungary

In order to find new ways of process control in mine water engineering, a finite difference seepage model of two fluids in the reservoir rocks used in the oil industry was modified to match the underground mining conditions.

One of the versions was tailored to simulate the dewatering of underground reservoirs aided by gas injection.

The simulation model of dewatering aided by gas injection was applied first to determine the possible ways/fields of applicating this method to accelerate the dewatering process in low permeability reservoirs.

As a result of investigation the most characteristic situations appeared and proved that the dewatering aided by compressed air is able to accelerate the process under special conditions or by applying this method in special new ways.

The simulation model of grouting was applied first for determining the role of the density of the grouting fluids. This model also shows new ways for process control.

Keywords: air injection; dewatering; finite difference model; mine water; seepage; simulation

1. PRESENTATION OF THE MODEL

A short description of the special and unique solutions of the applied model is given below.

The governing equations of the model are the Darcy-law, the principle of the mass continuity and the equation of state for fluid systems. The applied differential equations are suitable to solve any kind of isotherm problems in reservoir engineering. The number of phases, the dimensions of nodes and the boundary conditions can be specified arbitrarily.

1.1 Governing equations

The equation of a fluid system can be written as

$$\Delta U_x + U_o + U_g + Q = C \cdot \frac{\partial P}{\partial t} \tag{1}$$

where U_x - intrinsic velocity of phase x (vol/time)
Q - intensity of source and/or sink (vol/time)
C - compressibility (vol/pressure)
P - pressure
t - time.

The phase state at the end of the time-step is calculated by using the pressure distribution obtained from Eq. (1) (Coats 1967).

For each (i) liquid phase

$$\Delta\left(\frac{U_i}{B_i}\right) + Q_{in} = \frac{\partial}{\partial t}\,\phi\,\frac{S_i}{B_i} \tag{2}$$

for the gas phase

$$\Delta\left(\frac{U_g}{B_g} + \frac{R_{sw} \cdot U_w}{B_w}\right) + Q_{gn} = -\frac{\partial}{\partial t}\,\frac{S_g}{B_g} + \frac{S_w \cdot R_{sw}}{B_w}\,\phi \tag{3}$$

are valid, where

B_i, B_g - formation volume factor
R_{sw} - gas volume dissolved in fluid (water)
S_i, S_g - degree of saturation for water and gas
Q_{in}, Q_{gn} - fluid and gas flow rate for nodes under normal conditions
ϕ - porosity.

For modeling the process of dewatering aided by compressed air (by gas injection) the pressure of water phase is calculated implicitly and the terms depending on the degree of saturation (as relative permeability, capillary pressure, etc.) are determined explicitly (IMPES method). Significant stability and time-step increment are reached by the implicit calculation of the production from wells.

When discretising equation (1), the mass transport, the

source and sink terms and the right-hand side can be handled separately from each other throughout the simulation procedure.

The flow filtrating through the interface of nodes within time-step Δt is calculated as

$$Q_x = A_x \cdot (P_{rswz} - P_{rswl} + B_x) \cdot t \qquad (4)$$

where $A_x = T \frac{k_r}{\mu}$

T - specific absolute transmissibility

k - relative hydraulic conductivity

μ - viscosity

$B_x = f(P_c, \varrho)$ formation volume factor

P_c - initial capillary pressure of time-step

ϱ - mean initial density of time-step (depth-dependent).

The flow rate in sink nodes (production wells) is computed by using the formation volume factor and the rate of dissolved gas content of the adjacent nodes. The source term (injection) depends on the PVP behaviour of the injected medium.

The volume change within the time-step is:

$$\Delta V = V \cdot C \cdot \Delta P \qquad (5)$$

where the compressibility C is phase- and pressure dependent, therefore it can be calculated in an explicit way. The exponential functions of the fluid parameters and the changes of phases are also considered in the calculations.

The difference equation of the mass equibalance of nodes is written as:

$$P_{rswz} \cdot \Sigma A_x - P_{rswz} \Sigma A_x - \frac{V \cdot C}{t} = -Q - \frac{V \cdot C}{t} P_{rswl} - \Sigma A_x \cdot B_x \qquad (6)$$

where x is the phase of water and gas.

The dependent variables of the differential equations referring to the nodes which cover the area to be modelled, are the final pressures P_{rsw} of the time-step. Then the mass equibalance equations are written for each phase and the degree of saturation is calculated by means of parameters PVT determined

from pressure values.

For modelling the grouting process two liquids of different μ and ϱ should be applied. In this case $p_c = 0$ and the viscosities of the two fluids are regarded as constants.

1.2 The simulation programs

The modified version of the numerical model presented above was used for the simulation of dewatering by gas injection. The program code called EASY matches the requirements arising in the design and management of oil production for everyday. An error of less than 1 percent in the calculation of the mass equibalance is reached by means of modified IMPES method. Full scale projects can be solved by computer IBM-PC. As a result of extensions the components of yield (implicitly) and the timestep Δt (automatically) are determined.

The evaluation of the results is simplified by the addition of postprocessor codes.

The following modifications of the program used in the oil industry were applied to match the conditions of the given tasks:

- The water production at maximum depression is advantageous from the very beginning of dewatering. The calculation is fairly sensibile in determining the time-step.
- The non-linearity induced by the relatively low water head is to be considered. The limits of saturation and pressure changes were restricted to 1 percent.

The initial input parameters required for running are as follow:

- geometric structure of the network
- pore volume, porosity
- relative depth
- specific, absolute hydraulic conductivity
- degree of gas saturation (only for dewatering with compressed air)
- hydraulic pressure
- capillary pressure (only for dewatering with compressed air)
- viscosity

- density
- formation volume factor.

The output list consists of data in tabulated form at the desired simulation time. These are:

- separated and total yields of the production and injection wells, the gas-water proportions,
- maps and profiles of isobars (water head) and degree of gas saturation,
- collected data of the reservoir,
- lists of pressure and saturation data for arbitrary slices and profiles of the network.

2. THE FIRST APPLICATIONS OF THE MODEL OF DEWATERING AIDED BY COMPRESSED AIR

2.1 Reasons of using numerical simulations

New short-term dewatering technologies should be applied to protect mining openings endangered by aquifers of low permeability. In many aquifers a considerable volume of pore water cannot be discharged in the roof of extractions by using either some of the effective methods or the gravitational one because of the energy level decrease induced by dewatering.

Dewatering by compressed air is a technique applied in the civil engineering practice for a long time where underground workplaces are open in aquifers with special conditions. Hopeful attempts and semi-pilot operations were carried on in underground mining to extend the application of this method over a larger field (Pera 1982).

Considering the widespread method of simulation for modelling physical phenomena, the preparation of a feasibility study seemed to be useful by applying mathematical methods.

The question was whether the well-known technology could be used economically under the circumstances of Hungarian deep mining endangered by water inflows from roof-side aquifers. The oil production by gas or water injection which method is widespread and applied usefully, is prepared for a given reservoir on the basis of mathematical modelling. These experiences

provided the possibility of applying this program to the conditions characterised by underground mining.

The question to be answered was: under what conditions is the dewatering method combined with gas injection applicable and economic.

2.2 Task to be simulated

A simplified model of dewatering the porous aquifer in the roof of a longwall face was developed to illustrate the main features of the dewatering method based on compressed air injection. The filters are installed in the productive developments and the injection is carried on in the longitudinal axis of the strip.

The aquifer situated horizontally was covered by simulation grid of nodes of different size. A quarter of the network is illustrated in Fig. 1. The aquifer with thickness of 15 m consists of three slices. The total area (400 × 140 m) is dewatered by means of 24 production wells. The initial water yield of the production well is assumed as 300 m^3/day which decreases in a linear way in function of the depression increment.

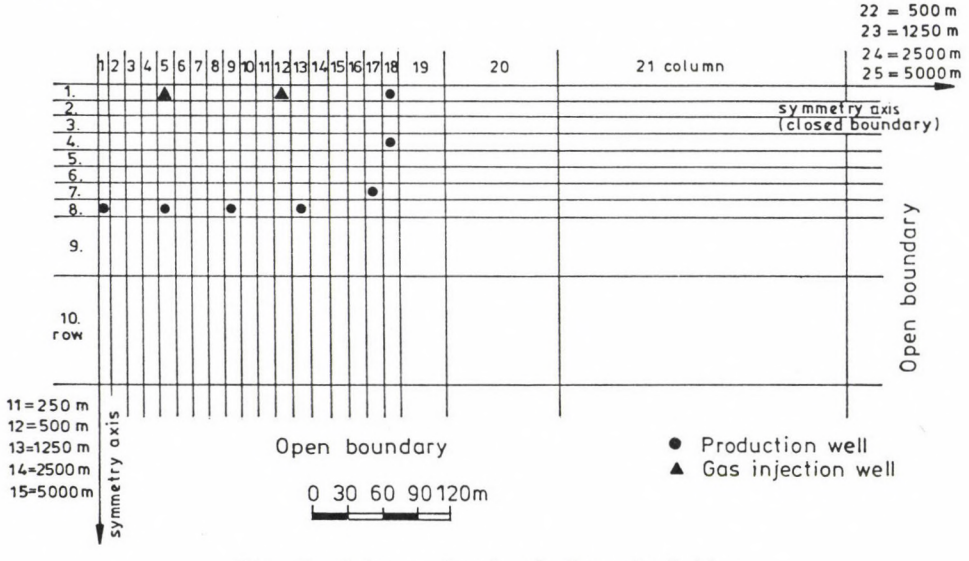

Fig. 1. Scheme of network for simulation

The parameters of the basic variant are listed in Table I. Several variants with some altered parameters and boundary conditions different from the basic variant were investigated and their results were compared with each other.

Table I. Initial parameters for variant No. 1 of modelling the drainage accelerated by compressed air

Simulated area:	10 × 10 km
Size of network (due of symmetry):	25 × 25 × 3 = 1125 nodes
Thickness of aquifer:	15 m
Closed boundary at symmetry axes	

Parameters of reservoir	
porosity	0.1
permeability horizontal	100 mD
permeability-vertical	50 mD
compressibility of rock	$6.8 \cdot 10^{-5}$ (1/bar)
initial water head	17 bar

Parameters of phases	water	gas
normal density (kg/m^3)	1012.0	1.0155
viscosity under pressure (cP)	0.95	0.0132
formation volume factor (B_w)	$1.022-3.15 \cdot 10^{-5} \cdot P$	$0.9693 \cdot P$
degree of gas saturation	$0.0468 \cdot P$	-

2.3 Discussion and comparison of variants

The main features of the different variants are listed below:

Variant No. 1: Basic version. Inhomogeneous sandy aquifer. (Parameters in Table I.) Horizontal position. 5 production wells with total yield and 2 with half of the production are supposed over the simulated area (it is a quarter of the total

area to be dewatered) (see Fig. 1). Water discharge without compressed air. Degree of gas saturation is 100 percents.

Variant No. 2: Gas injection through four wells with a yield of 100 m^3/day each. The injection is started on the 50th day of the dewatering operation. Fully saturated water.

Variant No. 3: Inhomogeneous 3-layered stratum (horizontal permeability values downwards from above are: 1, 10, 100 mD). The ratio between the vertical permeability values is the same. Fully saturated water.

Variant No. 4: Same as variant No. 3 but the initial gas saturation of the water is specified as zero.

Variant No. 5: Inclined aquifer with an angle of 20^o. Closed boundary along three sides. Single layer with permeability of 100 mD (Fig. 2). Production wells without gas injection.

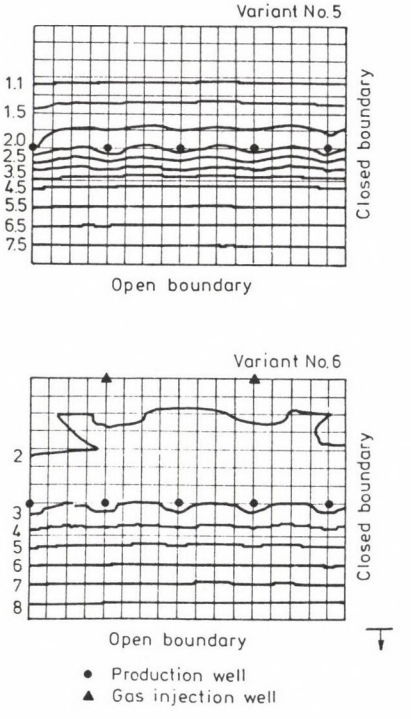

Fig. 2. Water head maps of inclined variants at a simulation time of 220 days in bars

Variant No. 6: Same as variant No. 5 but compressed air injection through 2 wells at the upper symmetry axis.

The displayed and printed maps of the results of the different variants show the trends of the simulated processes. The simulation of the aquifer with water saturated fully by gas (Variants 1 and 2) hides the differences between the method of dewatering by gravity and that of the production completed by gas injection. The version with zero degree of saturation is more suitable for comparison.

Comparing the variants the following conclusions can be drawn:

- Some increment of water production occurs when gas injection is applied. The rate of increment compared to the gravitational method is less by 5 percents. (Comparable variants: 1-2 and 5-6, see Fig. 3.)
- The areal distribution maps of gas saturation curves prove that the injected gas "escapes" at the upper part of the horizontal layer and the compressed air is exhausted in the water production wells.

  Although a gas-front can be recognised in the lower slice of the inhomogeneous multi-layered system, a permanent water yield increase cannot be reached (Variant No. 3, see Fig. 4).
- The vertical distribution of gas saturation is better in case of Variant 4, where the gas front spreads towards the production wells more slowly.
- The comparison of the pressure-time diagrams of Variants 3 and 4 illustrates the differences of the reaction of the system to gas-injection. The pressure stabilizing effect of the gas released by pressure increase is higher than the pressure increment induced by gas injection. Therefore no significant change can be seen on the pressure curve of the regular node 1.1 from the 50th day of production. The pressure change curve of the sink node (production well) shows gas exhaust phenomena. The water not saturated with gas is less compressible at the given low pressures and the start of injection occurs significantly in the nodes near the gas

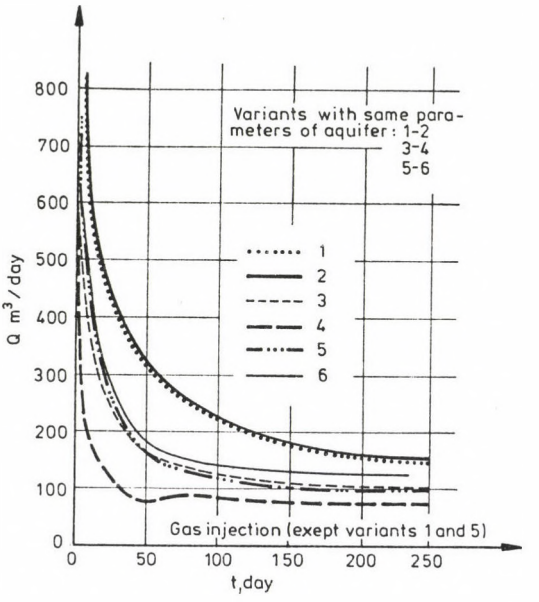

Fig. 3. Change of water yield in different variants

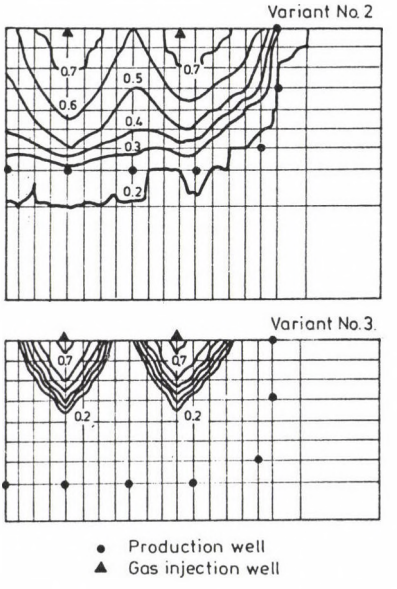

Fig. 4. Degree of gas saturation of the upper slice after 200 days of gas injection

injection well (Fig. 5).

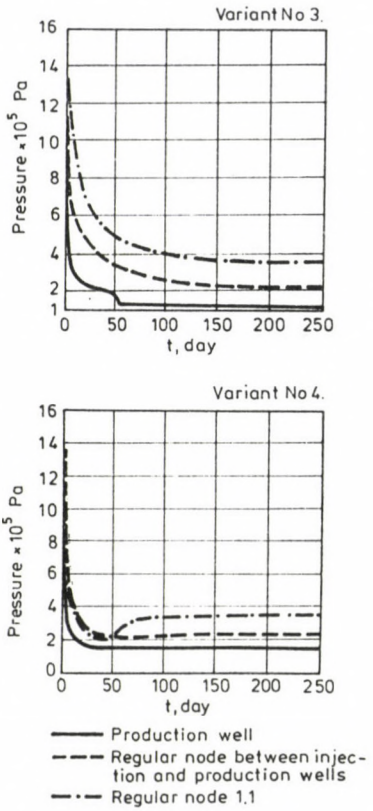

Fig. 5. Pressure in different nodes

As a result of simulation of Variants 1-4, one can conclude that dewatering by gas injection has not been proved to be an effective technology in case of special stratification of horizontal layers either. The injected gas is exhausted towards the production well in the upper part of the aquifer to be dewatered. The phenomenon takes place because under low pressure conditions the parameters for the water and gas components are different in order of magnitude. This phenomenon is proved by the experience according to which the compressed air outburst in the water production well is not caused by the improper

realization of the technology, but it can be derived from basic physical principles.

On the basis of the mentioned consideration an inclined part of the aquifer without water recharge was investigated (Variant No. 5). Gas injection at the top of the layer increased the velocity of dewatering, however, a characteristic yield increment did not occur. These boundary conditions are most similar to the problems of hydrocarbon reservoirs. In the Hungarian coal mining practice, however, special geological conditions like this exist very rarely. Moreover, the detection of the tectonic blocks without recharge requires more expensive exploration to make decision on the proper dewatering technology (i.e. with or without gas injection).

2.4 Conclusions on the applicability of dewatering aided by compressed air injection

On the basis of the results of simulation modelling and on that of the experiences we can conclude that the numerical model applied is suitable for the simulation of dewatering by gas injection. The phenomena observed in the practice could be matched qualitatively by simulation. However, the model verification of the actual data measured on the site has not been carried out. A model calibrated to the data observed is a suitable tool for the practical design tasks with acceptable accuracy.

The application of the conventional way of dewatering by gas injection seems to be realistic even under advantageous hydrogeological conditions. This is the possible utilization of the spontaneous and local liquefraction of the sandy reservoir due to air intrusions through the water drainage wells, because these spontaneous air intrusions may form channels which serve as extended drainage tools in the low permeability reservoir (Pera et al. 1986). This spontaneous process should be regulated and utilized to accelerate the dewatering process. This will be the next step of our research in order to find new ways of the process control by utilizing the regulated interactions between the gas phase and the liquid one.

3. FIRST APPLICATIONS OF THE GROUTING MODEL

3.1 Tasks to be solved and the model

The applicability of the model was checked qualitatively first by modelling well-known conventional situations of grouting by injection wells. The next task was to analyse the influence of the density of the grouting slurries/fluids and that of the extension of the grouted zones under different reservoir rock conditions.

Taking into consideration the tasks outlined above the model and the proper node-network were created as presented in Fig. 6.

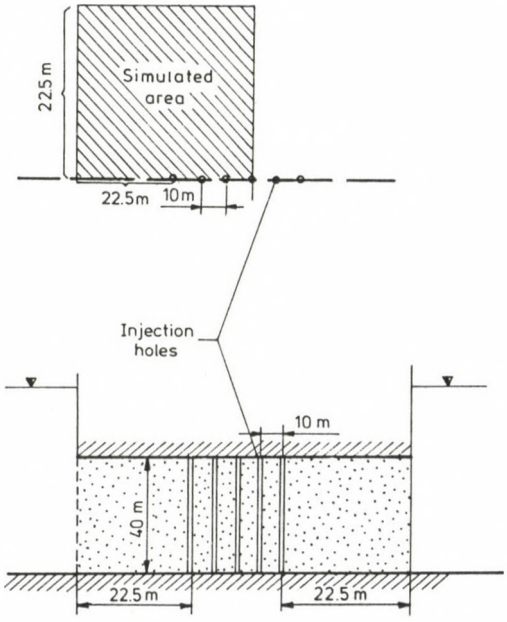

Fig. 6a. The model

The 3D network of 1800 nodes allows us to match even quasirealistic situations.

The following situations were modelled:

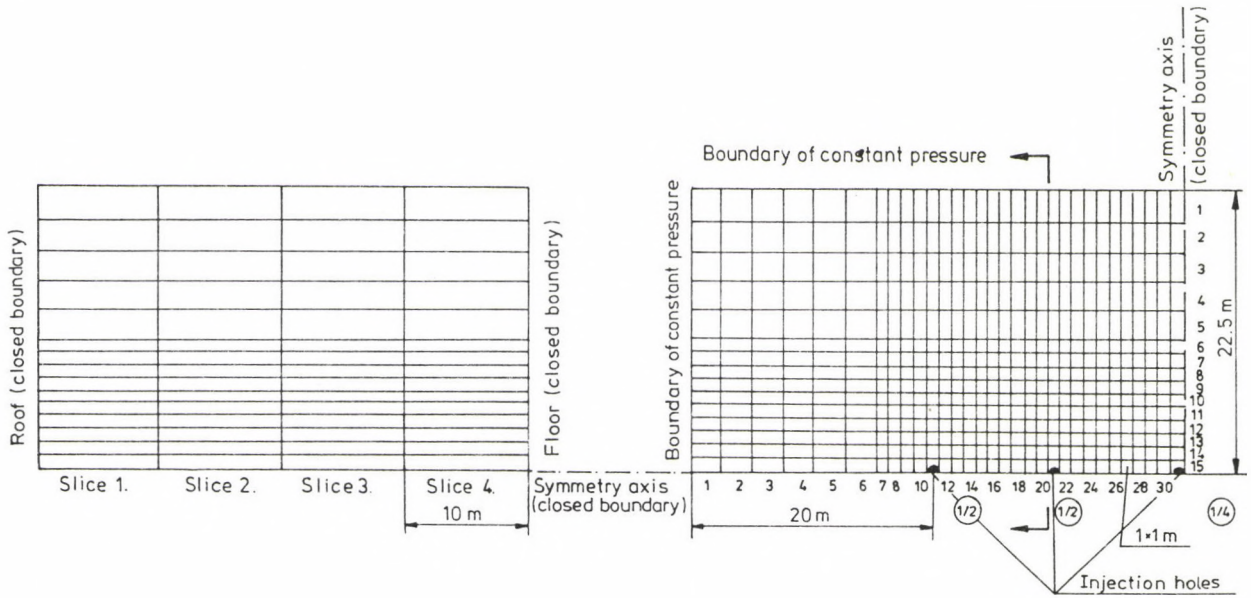

Fig. 6b. The node network

- Injection into a homogeneous reservoir through all of the wells by using conventional cement slurry of constant viscosity. This fits real situations when the solidification of the grouting slurry is retarded by using proper additives. This well known process can be compared with the experience and with additional solutions (Fig. 7).

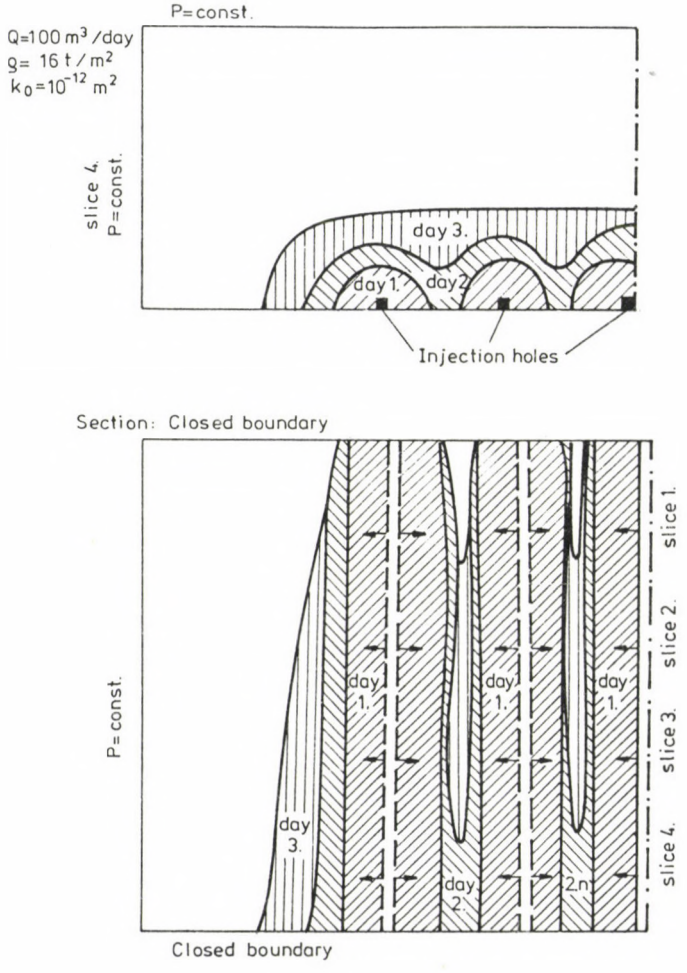

Fig. 7. The propagation of the grouting slurry (Variant 1.)

- The next group of situations were related to the possibilities of process control by the regulation of grouting slurry

densities.

Light slurry (ϱ = 800 kg/m^3) injections into the lowest layer (for four days) were modelled and after stopping the injection the slurry was let to filtrate freely (by gravity) under different reservoir properties, namely:

- homogeneous reservoir of medium conductivity (Fig. 8)

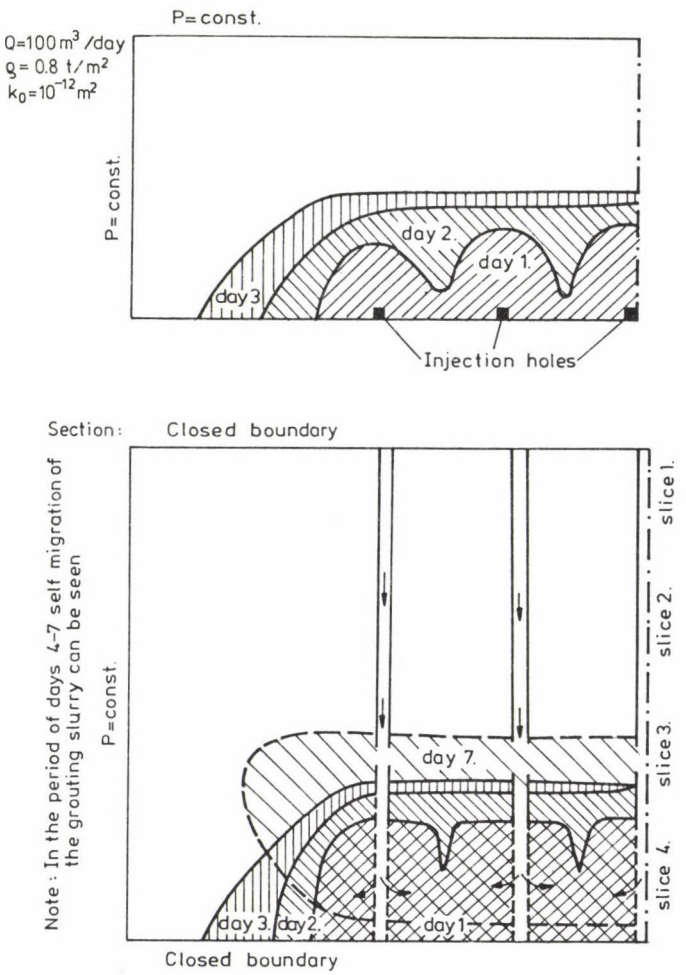

Fig. 8. The extension of the grouting slurry (Variant 2.)

- homogeneous reservoir of high conductivity (Fig. 9)
- extra-high conductivity zone (faulted zone) in a medium conductive homogeneous reservoir (Fig. 10).

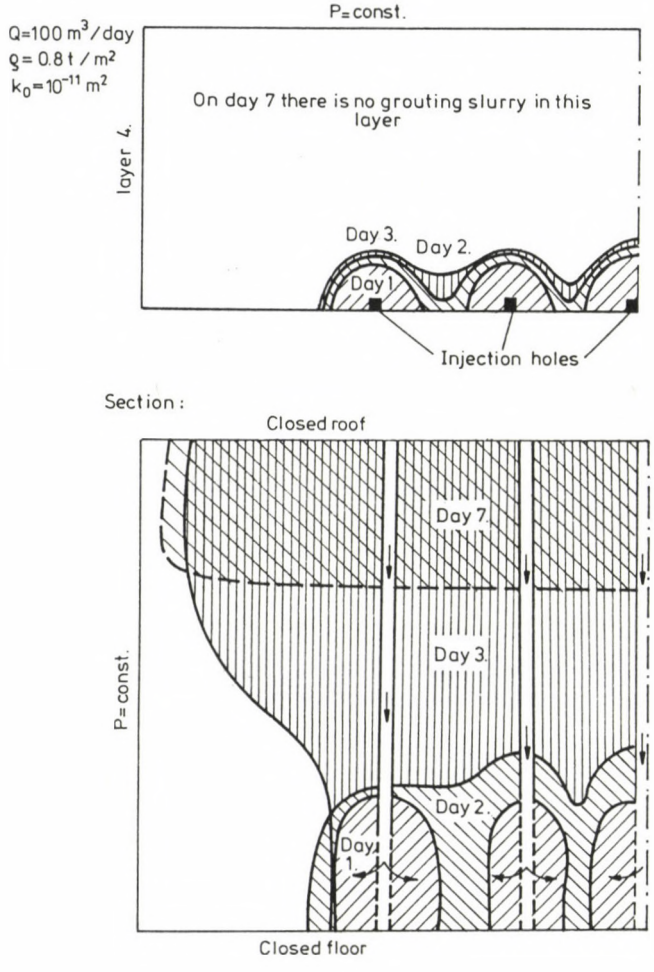

Fig. 9. The extension of the grouting slurry (Variant 3.)

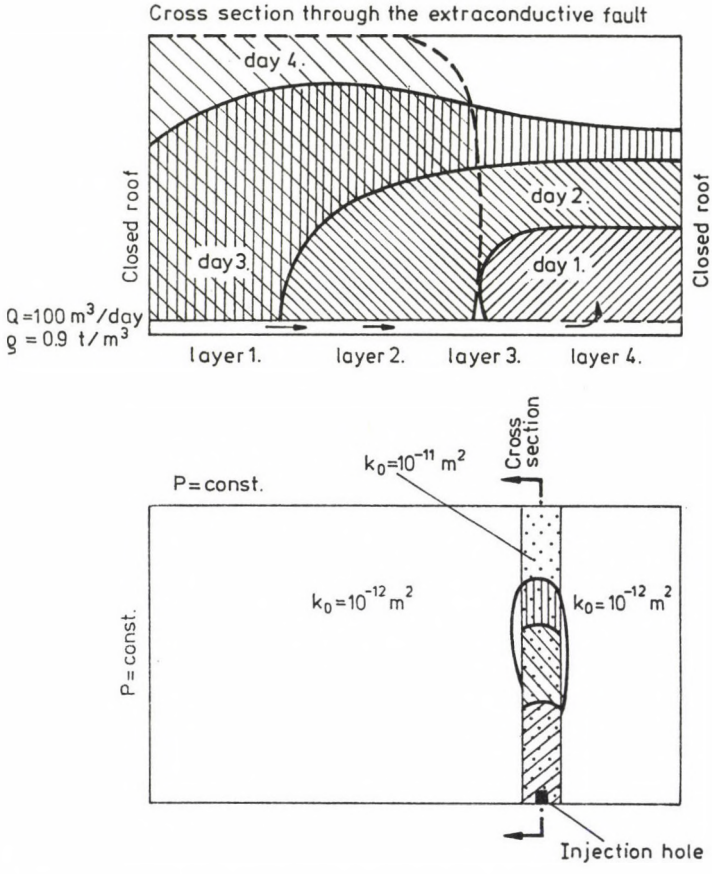

Fig. 10. The extension of the grouting slurry (Variant 4.)

3.2 Discussion and comparison of the grouting variants

Only one of the output parameters, the propagation of the grouting slurry is presented in Figs 7, 8, 9 and 10. The isolines represent those stages where 80 percents of the whole pore volume is filled with grouting slurry.

The most important comments are only listed below:

- In cases of medium permeable (and quasi-homogeneous) reservoirs the role of the grouting slurry densities may be considered negligible (Figs 7 and 8).

Consequently, the well-known analytical solutions can

also be utilized for the simplest boundary conditions.
- The role of the density of the grouting slurries is not negligible in case of reservoirs of high permeability.
- The self-movement of the slurry governed by the density difference can be utilized practically for process control in karstified reservoirs where extra high conductive zones exist.
- Based on the results of some modelled situations the model seems to be applicable even in a wider area, namely
  - for back analyses of the recorded parameters of grouting operations to determine the qualitative features of the reservoir in the grouted zone,
  - for the selection of the proper grouting strategy under different situations.

As the first practical result of the model studies some new ways of grouting were found which should be patented.

The model is planned to be developed for the simulation of grouting under changed viscosity of the grouting slurry.

4. SOME FINAL CONCLUSIONS

By adopting the numerical simulation technique EASY for modelling the seepage of two different fluids in hard reservoir rocks some useful tools have been realized matching two kinds of processes, namely

. preventive drainage of the reservoir rocks aided by compressed air and

.. grouting the pores/fissures of the reservoir rocks by injection of slurries.

The first versions of the models were applied for "parametric studies". As a result of these studies some important practical conclusions were obtained. The most important ones are:
- The applicability of compressed air to accelerate the drainage of a water reservoir is limited to the inclined reservoirs of closed upper boundaries.
- The governing forces of the grouting process strongly depend

on the rock permeability parameters; namely

- in the reservoirs of low or medium permeability the main force is the injection pressure,
- in the reservoirs of high permeability two governing forces should be taken into consideration, namely the injection pressure and the density difference between the grouting slurry and the water.

By utilizing these two governing parameters new patentable ways of groutings were developed.

ACKNOWLEDGEMENTS

This project is supported simultaneously by a Grant No. 1580 of the National Founds for Science of Hungary and by the Hungarian National Commission for Technical Development.

REFERENCES

Asiz K, Settari A X 1983: Petroleum Reservoir Simulation. Elsevier Applied Science Publishers Ltd.

Coats K H 1967: SPEI, 377-388.

Fanchi I R X 1987: Geobyte, 2, No. 2, 22-25.

Kershow D S 1978: Journ. of Computational Physics, 26, 43-65.

Pera F 1982: Special Control Methods of Underground Water and Sediment in the Veszprém Coal Mining Company. Proceedings of 1st IMWA Congress, Volume B, Budapest

Pera F, Szentai Gy, Szepessy A 1986: Mining experiences on the application of compressed air for accelerating the drainage of underground reservoirs, and the feasibility of its further application in Dubicsány coal mine. Report of a Working Commission of the Hungarian Mining and Metallurgical Soc. (in Hungarian)

Acta Geod. Geoph. Mont. Hung., Vol. 25 (1-2), pp. 127-152 (1990)

LIMIT CONDITIONS OF ROCK-PLASTICITY AND -DETERIORATION

Zs Somosvári

University for Heavy Industry, H-3515 Miskolc, Egyetemváros, Hungary

Changes of rock-strength are determined in this study pending on art and kind of stresses, showing results of triaxial-compression, extension and triaxial-tensile, further of polyaxial and biaxial compression tests of rocks. It is many-sidedly and convincingly proven that neither the Tresca nor the Huber-Mises-Hencky limit-conditions can be applied on rocks, even approximately not.

The study treats criteria of deterioration by Murrel and Drucker-Prager and points out the limited scope of their application. The Drucker-Prager criterium can be applied only in the case of rocks having an angle of internal friction $\phi \cong 20^{\circ}$, i.e. in the case of some types of soils.

It is also emphasized that the deterioration criteria by Mohr and Mohr-Coulomb respectively are only partially adequate. Limit conditions of deterioration and plasticity, modifying the original Mohr and Mohr-Coulomb ones are formulated which are describing limit conditions of conglomerates complying with the measured results.

Keywords: HMH limit; Mohr's condition; Mohr-Coulomb limit; rock mechanics; Tresca's condition; triaxial test

From the point of view of mechanical behaviour limit conditions of rock-plasticity and -deterioration are of special importance, since without exception with regard of all stability problems (stability of slopes, cavities, pillars, etc.) the primary question is at which safety factor the condition of rock environment will near plasticity or deterioration limit conditions.

In the case of a quasistatic load, the plastic limit condition represents at a general stress condition the initial stage of plastic flow and the end of elastic response, respectively. The limit condition of deterioration means the initial stage of deterioration and the end of plastic flow. The mechanism of evolution of both limit conditions is similar,

therefore it is practical to treat them jointly. In the case of loose, grained rocks, the limit conditions of deterioration and plasticity cannot be separated, because they coincide.

1. LABORATORY INVESTIGATIONS

The different triaxial tests allow a comprehensive cognition of rock-characteristics. Those laboratory tests are called triaxial compression tests in which rock specimens are exposed to principal stress loads with $\sigma_1 \neq 0 > \sigma_2 \neq 0 > \sigma_3 \neq 0$. During laboratory tests stress conditions can be approximately adjusted which have loaded the rock in the earth's crust in its in-situ condition which allows us to study the characteristics of the rock nearly in the same conditions as the natural state. This emphasizes the special importance of these tests.

The first triaxial tests were carried out by T Kármán in the year 1911 on cylindrical marble specimens of Carrara with axial-symmetrical principal stresses where $\sigma_1 \neq 0 > \sigma_2 = \sigma_3 > 0$. These tests carried out under axial-symmetrical load have got the name: "triaxial test"; they are called today traditional (conventional) triaxial tests. Tests carried out with principal stresses, where $\sigma_1 \neq 0 > \sigma_2 \neq 0 > \sigma_3 \neq 0$, i.e. the most universal tests are called polyaxial tests, with principal stresses and those with principal stresses $\sigma_1 \neq 0 > \sigma_2 \neq 0 > \sigma_3 = 0$ are called biaxial ones (Bieniawski 1969, Cook 1967, Crough 1971, Denkhaus and Bieniawski 1968a, b, 1970, Vutukuri et al. 1974).

Triaxial tests of proper sense have developed also is several methods; these are tests

- with axial and mantle compression (σ_1, $\sigma_2 = \sigma_3$) loads (conventional tests);
- with axial and mantle compression plus pore-pressure (σ_1, $\sigma_2 = \sigma_3$, p) loads, and
- with axial tension and mantle compression loads ($\sigma_3 > 0$; $\sigma_2 = \sigma_1 > 0$).

Tests carried out under pore-pressure have contributed in a high degree to a more profound knowledge of internal resistances of the rocks. Tests carried out with mantle compression

and axial tension, called triaxial tension tests, have contributed as well in a high degree to the more accurate determination of limit conditions (Somosvári 1986, 1987, Somosvári et al. 1984, 1985).

A conventional triaxial test characterized by the stress condition $\sigma_2 = \sigma_3$, σ_1 can be more accurately specified as a triaxial compression test, because after adjustment of a smaller mantle compression $\sigma_2 = \sigma_3 = \text{const.}$ the test will be continued with increasing axial compression stress σ_1 up to the fracture, while the specimen is continuously exposed to compression.

A triaxial test can be carried out also in such a way that after adjustment of a high mantle compression $\sigma_2 = \sigma_1 = \text{const.}$ the axial compression stress σ_3 is reduced, till deterioration ensues. While reducing the axial compression stress, the specimen is exposed to extension, therefore this type of test is called triaxial extension test (Jaeger and Cokk 1969, Somosvári 1986, Vutukuri et al. 1974).

Thus four different kinds of triaxial tests of proper sense can be defined. But all of them have one common characteristics namely the axial symmetry of the stress condition.

A test with extension ($\sigma_1 = \sigma_2$) means a triaxial tensile test when $\sigma_3 < 0$.

Results of conventional triaxial compression tests ($\sigma_2 = \sigma_3$) yield only one section of the deterioration stress surface in the plane where $\sigma_2 = \sigma_3$. More generally situated points of surface are still unknown. The cognition of these unknown factors is assisted by biaxial and poliaxial compression tests.

In polyaxial and biaxial compression tests cubiform, or prismatic specimens are exposed to loads where $\sigma_1 \neq \sigma_2 \neq \sigma_3 > 0$ and $\sigma_1 \neq \sigma_2 > 0$, $\sigma_3 = 0$ respectively. Polyaxial and biaxial compression tests are carried out mostly to determine relations of principal stresses causing deterioration.

A triaxial tension test can be made by a triaxial cell where there is a possibility to axial tensioning of the specimen. In the case of a test with mantle compression

$\sigma_1 = \sigma_2$ = const. the axial tensile stress ($\sigma_3 > 0$) is increased up to the fracture of the specimen. Results of these tests show that in the case where the mantle compression is not high $\sigma_1 = \sigma_2 \leq \sim |3\sigma_t|$, a specimen made of solid rock fracture at the tensile stress $\sigma_3 = -\sigma_t$ obtained in a uniaxial tensile test (Jaeger and Cokk 1969, Schwartz 1964, Vutukuri et al. 1974).

Using results of triaxial extension tests in the system σ_1, σ_3, the relation of the principal stresses at the time of deterioration is described by the curve shown in Fig. 1a. Here σ_{cb} means the biaxial compression strength belonging to the stress condition of $\sigma_3 = 0$, $\sigma_1 = \sigma_2$. The same compression strength appears in extension-compression tests and in biaxial tests too.

Characteristic curves and lines resp., of triaxial tensile, triaxial compression and extension, and biaxial tests for sake

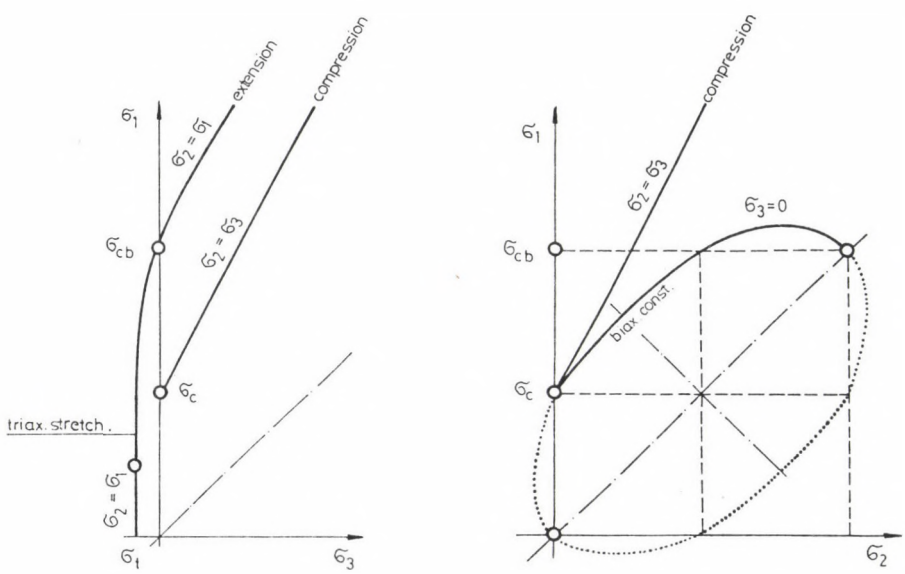

Fig. 1. Characteristic stress conditions of rocks causing deterioration, obtained by triaxial and biaxial tests

of comparison are shown together in Fig. 1. In this figure σ_t represents the tensile strength, σ_c the uniaxial compression strength and σ_{cb} the biaxial compression strength. Important facts are $\sigma_{cb} > \sigma_c$ and for the directional tangents of extension and compression lines $\tan \beta > 1$.

Polyaxial, triaxial and biaxial load-tests prove unambiguously that the compression strength of rocks is essentially determined by σ_1 and σ_3, i.e. by the maximum and minimum principal stresses, but at the same time the middle principal test σ_2 has also a not negligible role in the evolution of the actual strength and deterioration, respectively.

2. PLASTICITY AND DETERIORATION LIMIT CONDITIONS NOT APPLICABLE TO ROCKS

In this section generally accepted limit conditions shall be dealt with which are in use nowadays in mechanics.

In the case of bodies of an elastic-plastic nature it is very important to determine at which threshold value plastic yield begins in general stress conditions. This is described by the plasticity or yield condition. In a uniaxial stress condition this is

$$\Psi = \sigma - \sigma_Y = 0 .$$

If $\varphi < 0$, the material is in elastic condition.

In the marginal case at the moment when plastic yield begins, the Hooke-rule is still valid, thus deformations can be unambiguously expressed by the stresses. It follows that the yield-condition may be also expressed by means of the six stress components characterizing the stress condition. These components are the elements of the stress tensor

$$\varphi(\sigma_x, \sigma_y, \sigma_z, \tau_{xy}, \tau_{yz}, \tau_{zx}) = 0 .$$

The yield condition must be independent (invariant) of the situation of the coordinate system, thus the function φ must

be a function of the invariants of the stress-tensor.

In the case of uniaxial compression and tension of structural metals, yield points are to be taken as equal $\sigma_{Yc} = \sigma_{Yt}$. But tests prove that no plastic deformation occurs in hydrostatic stress condition ($\sigma_1 = \sigma_2 = \sigma_3$) howsoever high the stresses may be. This means that the spherical stress tensor expressing the hydrostatic stress condition has a negligible role, i.e. the yield condition is pending on the invariants of the deviator-tensor.

According to Huber-Mises, the plasticity condition can be expressed with the second deviator invariant as below

$$\varphi = I_2 - \tau_Y^2 = 0$$

where τ_Y is the yield point in the case of pure shear load.

In a system of coordinates with its axes coinciding with the principal stress directions

$$\psi = \frac{1}{6}\left[(\sigma_1 - \sigma_2)^2 + (\sigma_2 - \sigma_3)^2 + (\sigma_1 - \sigma_3)^2\right] - \tau_Y^2 = 0 \ .$$

In accordance with Hubert-Mises the plastic state occurs at a point being in a general stress condition when the second invariant of the deviator-tensor of the stress-tensor attains a certain limit value.

Hencky has shown (Jaeger and Cokk 1969, Kaliszky 1975) that in a point being in a general stress condition the specific value of labour expended for deformation is equal to

$$\frac{I_2}{2G}$$

where G is the modulus of rigidity. Therefore the plasticity condition mentioned above may be also interpreted so that the plasticity condition arise, when the specific deformation labour attains a certain limit value. This is the reason why the above plasticity condition is called also as Huber-Mises--Hencky (HMH) plasticity condition.

The HMH-plasticity condition is determined in Fig. 2 by a

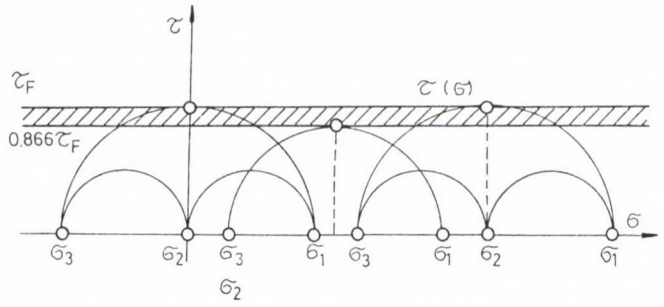

Fig. 2. HMH-deterioration-condition on the plane $\sigma - \tau$

band in the plane σ, τ the width of which is 0.13 τ_Y. Material is in plastic condition when the standard Mohr-circle $(\sigma_1 - \sigma_3)$ characterizing the stress condition is tangential to the straight line parallel to the axis σ in the band mentioned. The straight line is defined by σ_2.

Thus the HMH-plasticity condition is to be applied with materials (e.g. with steel) for which the yield point is the same at uniaxial compression and tension.

In accordance with Tresca's plasticity condition the plastic condition of material occurs when the maximum shearing stress attains a value where pure shear load yield takes place (Fig. 3). Tresca's plasticity condition is (Jaeger and Cokk 1969, Kaliszky 1975)

$$\Psi = (\sigma_1 - \sigma_3) - 2\tau_F = \tau 0 \ .$$

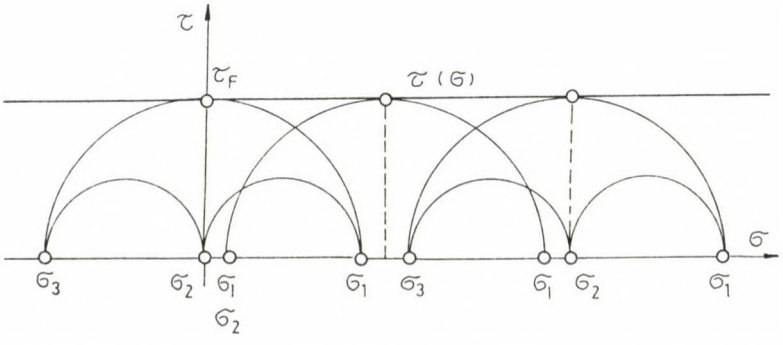

Fig. 3. Tresca's deterioration condition on the plane $\sigma - \tau$

In the cases of uniaxial compression and tension plasticity conditions are the same what means that the Tresca's plasticity condition can be only applied with materials, for which the yield point is the same at uniaxial compression and tension. Tresca's condition does not take into account the effect of the middle principal stress (σ_2). Due to the fact that the middle principal stress has in the HMH-condition no significant effect (13 percent), therefore the HMH-condition does frequently substitute Tresca's one. In the case of

$$\sigma_2 = 0.5\ (\sigma_1 + \sigma_3)$$

HMH and Tresca's conditions are the same.

With materials where the yield stress of compression and tension are essentially different, neither HMH nor Tresca's condition can be applied.

Naturally, the HMH and Tresca's conditions show not only in the plane σ, τ essential differences against measured results of rocks, but also in conditions of triaxial compression, triaxial extension and in biaxial state, too.

The HMH limit condition results both at compression (σ_1, $\sigma_2 = \sigma_3$) and at extension ($\sigma_1 = \sigma_2$, σ_3) in

$$\sigma_1 = \sigma_3 + \sqrt{3}\,\tau_Y\ .$$

In a biaxial stress condition (σ_1, σ_2, $\sigma_3 = 0$) the result is

$$(\sigma_1 - \sigma_2)^2 + \sigma_1\,\sigma_2 = 3\,\tau_Y^2$$

which formula is the equation of an ellipse having its centrum in the origin, the axes of which encompass angles of 45^o with the axes σ_1, σ_2 and its half-axes have a size of $\sqrt{6}\ \tau_Y$ and $\sqrt{2}\ \tau_Y$, resp.

Significant differences of the HMH condition against measured results of rocks are shown in Fig. 4.

Tresca's limit condition leads both at compression

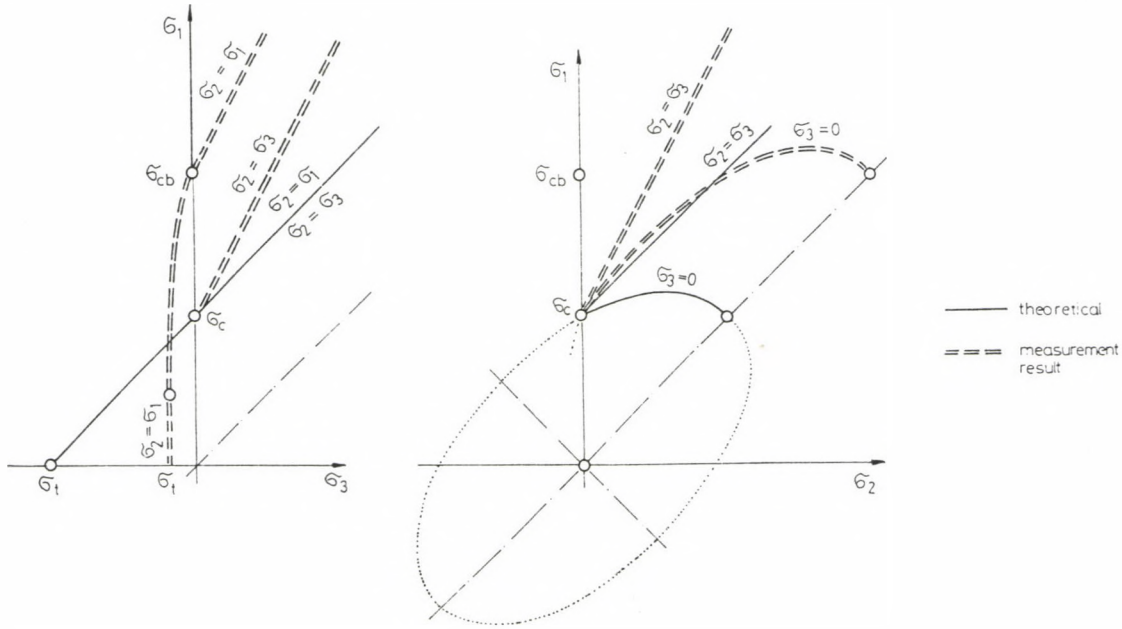

Fig. 4. Comparison of measured results obtained in deterioration-stress condition of rocks and HMH-plasticity condition

(σ_1, $\sigma_2 = \sigma_3$) and at extension ($\sigma_1 = \sigma_2$, σ_3) to the result

$$\sigma_1 = \sigma_3 + 2\tau_Y .$$

In a biaxial stress condition (σ_1, σ_2, $\sigma_3 = 0$) the result is

$$\sigma_1 = 2\tau_Y .$$

Essential differences of Tresca's condition against measured results of rocks are shown in Fig. 5.

Measured values prove that limit conditions according to HMH and Tresca are even approximately not applicable to describe limit conditions of rocks.

In the case of the HMH-condition misunderstanding may arise as it can be formulated that the plastic limit condition occurs when the specific deformation labour cumulated in the body attains the value $\tau_Y^2/2G$. In this formulation it seems entirely clear that the plasticity condition dealt with would be valid for all elastic-plastic materials alike. This is the reason why researchers standing on the basis of an energetic view recommend to apply this plasticity condition in the case of rocks, too. But exactly the above comparative investigations show that this point of view is incorrect.

3. APPLICABILITY OF CRITERIA BY MOHR AND BY MOHR-COULOMB TO ROCKS

Granular materials, as loose, grained rocks can transfer only compression and friction forces to each other on contacting points of the grains. Grains may glide as compared to each other when the friction force attains a certain limit value. The friction force is in relation - in accordance with the Coulomb-law - with the compressive force perpendicular to the surface. Therefore the connection between the shear-stress and the normal stress in the grained heap is in the plastic yield condition as below

$$|\tau| = \sigma \tan\phi$$

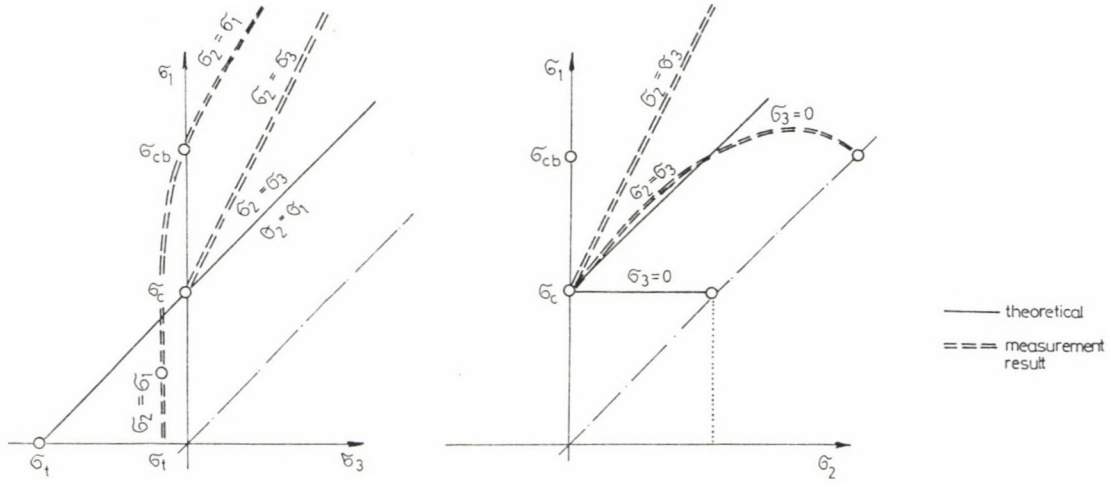

Fig. 5. Comparison of measured results obtained in deterioration-stress condition of rocks and Tresca's plasticity condition

where ϕ is the internal friction angle of the granular heap.

Plasticity and deterioration conditions are as follows (Kaliszky 1975, Kézdi 1972):

$$\Psi = \sigma_1 - \sigma_3 \frac{1 + \sin\phi}{1 - \sin\phi} = \sigma_1 - \sigma_3 \tan^2 (45^o + \frac{\phi}{2}) = 0 \ .$$

In accordance with the plasticity condition by Mohr--Coulomb, the grained heap is in plastic condition when the maximum shear-stress attains a definite fraction of the average of maximum and minimum principal stresses. According to Mohr's theory the middle principal stress (σ_2) has no influence on the plasticity threshold.

In the case of granular materials, where small cohesive forces are also acting at contact points of the grains, i.e. with loose, cohesive rocks, the connection between shear stresses and normal stresses in the yield condition is approximately

$$|\tau| = c_Y + \sigma\tan \quad ; \qquad \sigma \geqq 0$$

where c_Y is the yielding cohesion. The above condition can be represented in the coordinate system σ, τ with two straight lines inclining at an angle of ϕ, which cross the axis τ at a distance $-c_Y$ and the axis σ at a distance $c_Y \cot \phi$. But the above equation is only valid, when $\sigma \geqq 0$.

At loose, granular rocks plastic and deteriorated conditions coincide as neither cohesion nor a yield point exists, and the relation $\tau - \sigma$ is described by the limiting straight line $\tau = \sigma \tan \phi$. This limiting straight line is derived by deduction, has a concrete physical content, thus it is a physical law. But the plasticity limit straight line

$$\tau = c_F + \sigma\tan \phi$$

which is valid for loose cohesive rocks is no law, but a good approximation to it.

Mohr's deterioration theory states that if on the plane σ, τ stress-circles of maximum and minimum principal stresses

are plotted which belong to different stress conditions causing fractures, then these circles have a common enveloping curve, the form of which depends on the material. But a common envelop is possible only in the case when the middle principal stress (σ_2) has no influence on the two extremal principal stresses causing fracture (σ_1, σ_3). Thus an essential supposition of Mohr's limit condition is that the value of the middle principal stress has no influence on the fracture.

However on the contrary results of triaxial compression, triaxial extension and of biaxial and triaxial compression tests prove unambiguously that in many cases the middle principal stress has an essential role in deterioration, although deterioration is basically determined by the two extremal principal stresses. Therefore it is obvious that Mohr's deterioration hypothesis may be used for rocks only in a rather rough approximation.

The approximation can be essentially improved when Mohr's deterioration condition is modified as follows. If the middle principal stress $\sigma_2 = \sigma_1 - a(\sigma_1 - \sigma_3)$ is located at the same place (i.e. a = const.) within the interval $\sigma_1 - \sigma_3$, with $0 \leq a \leq 1$, the stress circles determined by the maximum and minimum principal stresses of the stress condition causing deterioration have a common envelop. This envelop is varying with changes of σ_2.

In compliance with the statements above, the Mohr-Coulomb deterioration hypothesis may also correctly determine only in a modified form the deterioration condition of rocks. Notably at $\sigma \geq 0$

$$\psi = \sigma_1 - \sigma_3 \tan^2 (45^\circ + \tfrac{\phi}{2}) - \bar{\sigma}_c (\sigma_2) = 0$$

If $\sigma_2 = \sigma_3$, i.e. a = 1, then $\bar{\sigma}_c (\sigma_2) = \sigma_c$

$$\psi = \sigma_1 - \sigma_3 \tan^2 (45^\circ + \tfrac{\phi}{2}) - \sigma_c = 0 ,$$

if $\sigma_2 = \sigma_1$, i.e. a = 0, then $\bar{\sigma}_c (\sigma_2) = \sigma_{cb} > \sigma_c$

$$\Psi = \sigma_1 - \sigma_3 \tan^2 (45^o + \frac{\phi}{2}) - \sigma_{cb} = 0 .$$

The above relations are supported by results of measurements of triaxial compression and triaxial extension tests.

Thus if a linear deterioration or plasticity limit curve is used, then it is not for the reason which is found frequently in the literature - that this is the most simple limit curve, but in the range of compression loads results of triaxial (compression and extension) measurements yield frequently such a character.

The minimum strength is obviously determined by conventional triaxial compression tests and it is a neglection on the side of safety if the condition (which is only valid when $\sigma_2 = \sigma_3$)

$$\Psi = \sigma_1 - \sigma_3 \tan^2 (45^o + \frac{\phi}{2}) - \sigma_c = 0$$

is used also in cases when $\sigma_2 \neq \sigma_3$.

4. SPATIAL DEPICTION OF LIMIT CONDITIONS OF PLASTICITY AND DETERIORATION; CONCLUSIONS

From the point of view of computer-technics it is more expedient to formulate limit conditions in the spatial system of σ_1, σ_2, σ_3. Tresca's limit condition is depicted in space by a cylindrical surface of symmetrical hexagonal meridian with axes $\sigma_1 = \sigma_2 = \sigma_3$. The limit condition by Huber-Mises-Hencky is depicted by a circular cylinder surface with axes $\sigma_1 = \sigma_2 = \sigma_3$. The limit condition by Mohr-Coulomb is depicted as a conic surface with hexagonal meridian. All the three surfaces are shown in Fig. 6 (Jaeger and Cokk 1969, Kaliszky 1975).

In the following some general limit condition are dealt with which may be brought up in case of certain rocks.

Griffith's deterioration criterium has been improved by Murrel extending the two-dimension investigations to three dimensions (Jaeger and Cokk 1969). In the space system of σ_1, σ_2, σ_3 the deterioration is depicted by a paraboloid having a

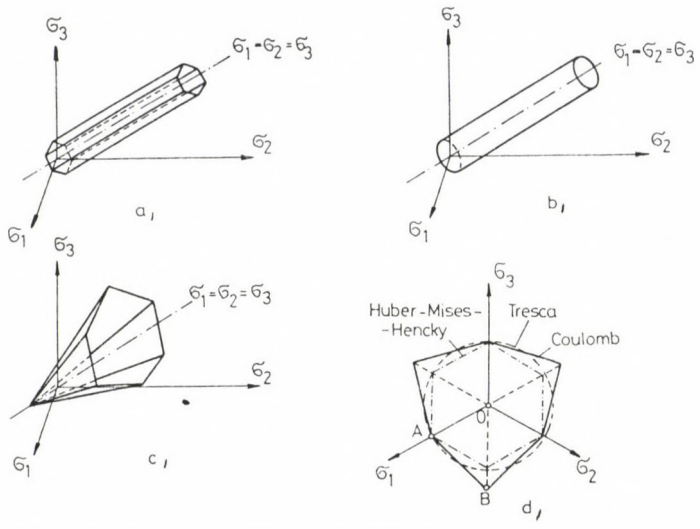

Fig. 6. Spatial representation of plasticity and deterioration conditions

straight axis of ($\sigma_1 = \sigma_2 = \sigma_3$) and it is enveloped by a pyramid developed of respectively perpendicular planes with

$$\sigma_1 = -\sigma_t, \qquad \sigma_2 = -\sigma_t, \qquad \sigma_3 = -\sigma_t .$$

Edges of the pyramid $\sigma_2 = \sigma_3 = -\sigma_t$ are tangential to the paraboloid. The equation of this paraboloid, i.e. Murrel's deterioration condition or let us say Griffith's improved one is as follows (Jaeger and Cokk 1969):

$$(\sigma_1 - \sigma_3)^3 + (\sigma_2 - \sigma_3)^2 + (\sigma_1 - \sigma_2)^2 - 24\,\sigma_t\,(\sigma_1 + \sigma_2 + \sigma_3) = 0 .$$

It is worth studying this deterioration condition in remarkable stress conditions. In traditional triaxial tests by substituting $\sigma_2 = \sigma_3$ the deterioration condition is:

$$(\sigma_1 - \sigma_3)^2 - 12\,\sigma_t\,(\sigma_1 + 2\sigma_3) = 0$$

i.e. a parabola, the tangent of which has a directional tangent at $\sigma_3 = 0$

$$d\sigma_1/d\sigma_3 = 4, \qquad \sigma_1 = \sigma_c = 12\,\sigma_t .$$

In triaxial extension tests with substituting $\sigma_1 = \sigma_2$ the deterioration condition is

$$(\sigma_1 - \sigma_3)^2 - 12\,\sigma_t\,(2\sigma_1 + \sigma_3) = 0$$

i.e. a parabola, its tangent has a directional tangent at $\sigma_3 = 0$

$$d\,\sigma_1/d\,\sigma_3 = 2.5; \qquad \sigma_1 = 24\,\sigma_t .$$

In a biaxial stress condition after substitution $\sigma_3 = 0$, the deterioration condition is

$$(\sigma_1^2 - \sigma_1\,\sigma_2 + \sigma_2^2) - 12\,\sigma_t\,(\sigma_1 + \sigma_2) = 0$$

i.e. an ellipse, the tangent of which has a directional tangent at $\sigma_2 = 0$, $d\,\sigma_1/d\sigma_2 = 2$. The ellipse crosses the straight line $\sigma_1 = \sigma_2$ in the point $\sigma_1 = \sigma_2 = 24\,\sigma_t$, if $\sigma_2 = 0$, $\sigma_1 = \sigma_c = 12\,\sigma_t$.

Finally, if $\sigma_2 = 0.5\,(\sigma_1 + \sigma_3)$, the deterioration condition is

$$(\sigma_1 - \sigma_3)^2 - 24\,\sigma_t\,(\sigma_1 + \sigma_3) = 0$$

i.e. a parabola, which gives a value of $\sigma_1 = 24\,\sigma_t$ at $\sigma_3 = 0$, i.e. in biaxial stress condition.

Curves complying with Murrel's deterioration criterion are shown in Fig. 7. Murrel's criterion approaches the discussed measured results at notable stress conditions

$$\sigma_2 = \sigma_3,\ \sigma_1; \qquad \sigma_1 = \sigma_2,\ \sigma_3; \qquad \sigma_3 = 0,\ \sigma_1,\ \sigma_2$$

and by this the conditions of deterioration in the spatial system of σ_1, σ_2, σ_3, but its applicability is very limited due to the quotient of compression strength to tensile strength fixed by the value 12.

In Fig. 7 are presented also the three remarkable plane positions enumerated above which are sectioning the three remarkable curves.

Murrel's condition in the spatial system of σ_1, σ_2, σ_3 is depicted in Fig. 8.

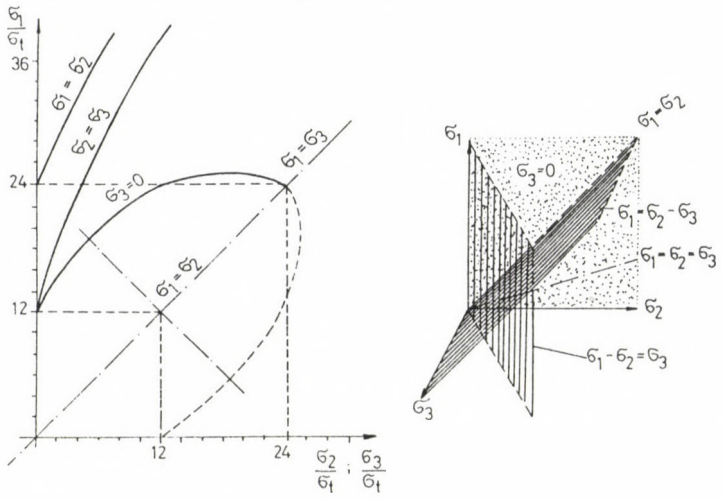

Fig. 7. Characteristic curves of Murrel's deterioration condition

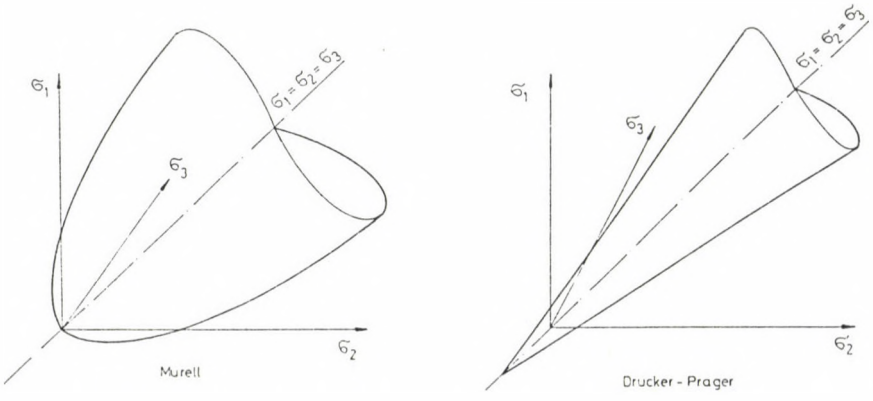

Fig. 8. Spatial representation of deterioration conditions by Murrel and by Drucker-Prager

A generalized form of the limit condition by Mohr-Coulomb in the spatial system of σ_1, σ_2, σ_3 is the condition by Drucker-Prager which is depicted as a circular cone in the system σ_1, σ_2, σ_3 (Fig. 8) (Desai and Abel 1975).

The limit condition by Drucker-Prager is (Desai and Abel 1975):

$$\psi = \alpha_1 I_1 + \sqrt{I_{D2}} - \alpha_2 = 0$$

where I_1 - is the first invariant of the stress tensor,
I_{D2} - is the second invariant of the stress-deviator tensor,
α_1, α_2 - are constants.

It is to be noted that in the case of $\alpha_1 = 0$, the Drucker-Prager condition is corresponding to the HMH one.

The Drucker-Prager condition expanded in the system of principal stresses is

$$\psi = \alpha_1 (\sigma_1 + \sigma_2 + \sigma_3) +$$
$$+\left\{ \frac{1}{6} \left[(\sigma_1 - \sigma_2)^2 + (\sigma_2 - \sigma_3)^2 + (\sigma_3 - \sigma_1)^2 \right] \right\}^{\frac{1}{2}} - \alpha_2 = 0.$$

The parameters α_1 and α_2 can be determined using measurement results of triaxial compression and extension tests.

In the case $\sigma_2 = \sigma_3$, i.e. in triaxial compression tests:

$$\sigma_1 \left(\alpha_1 + \frac{1}{\sqrt{3}} \right) - \sigma_3 \left(\frac{1}{\sqrt{3}} - 2\alpha_1 \right) = \alpha_2 .$$

Further at $\sigma_3 = 0$, $\sigma_1 = \sigma_c$, thus

$$\alpha_2 = \left(\alpha_1 + \frac{1}{\sqrt{3}} \right) \sigma_c .$$

Thus the Drucker-Prager condition is

$$\psi = \alpha_1 I_1 + \sqrt{I_{D2}} - \sigma_c \left(\alpha_1 + \frac{1}{\sqrt{3}} \right) = 0 .$$

Expanding after reduction

$$\psi = \sigma_1 - \frac{\sqrt{3} - 6\alpha_1}{\sqrt{3} + 6\alpha_1}\ \sigma_3 - \sigma_c = 0$$

the above result is obtained. The directional tangent of the straight line is:

$$\frac{\sqrt{3} - 6\alpha_1}{\sqrt{3} + 3\alpha_1} = B\phi \ .$$

From where

$$\alpha_1 = -\frac{\sqrt{3}\ (B\phi - 1)}{3\ (B\phi + 2)} = -\frac{(B\phi - 1)}{\sqrt{3}\ (B\phi + 2)} \ .$$

With this substitution the Drucker-Prager condition is

$$\psi = -\ (B\phi - 1)\ I_1 + \sqrt{3}\ (B\phi + 2)\ \sqrt{I_{D2}} - 3\ \sigma_c = 0 \ ,$$

or after expansion

$$\psi = -(B\phi - 1)\ (\sigma_1 + \sigma_2 + \sigma_3) +$$

$$+ (B\phi + 2)\ \frac{1}{\sqrt{2}} \left[(\sigma_1 - \sigma_2)^2 + (\sigma_2 - \sigma_3)^2 + (\sigma_3 - \sigma_1)^2 \right]^{\frac{1}{2}} - 3\ \sigma_c = 0$$

if $\sigma_2 = \sigma_1$, i.e. in a triaxial stress condition of extension

$$\psi = -(B\phi - 1)\ (2\sigma_1 + \sigma_3) + (B\phi + 2)\ (\sigma_1 - \sigma_3) - 3\ \sigma_c = 0$$

where $$\sigma_1 = \frac{3}{4 - B\phi}\ \sigma_c + \frac{2B\phi + 1}{4 - B\phi}\ \sigma_3 \ .$$

The above equation could be interpreted theoretically in case of $1 \leq B\phi < 4$. Practically the area of interpretation is narrow or because

at $B\phi = 1$ ($\phi = 0^o$) $\quad \sigma_1 = \sigma_c + \sigma_3 = \sigma_{cb} - \sigma_3$

at $B\phi = 2$ ($\phi = 19.5^o$) $\quad \sigma_1 = 1.5\sigma_c + 2.5\sigma_3 = \sigma_{cb} + 2.5\ \sigma_3$

at $B\phi = 3$ ($\phi = 30^o$) $\quad \sigma_1 = 3\sigma_c + 7\sigma_3 = \sigma_{cb} + 7\sigma_3$

At $B\phi = 3$, the Drucker-Prager condition can be never applied,

because on the one hand the biaxial compression strength is $\sigma_{cb} = 3\sigma_c$, on the other hand the 7 directional tangents are too high and their values are not confirmed by results of measurements.

Thus the deterioration condition by Drucker-Prager can be applied in the interval where $1 \leqq B_\phi \leqq 2$ ($0^o = \phi = 20^o$), that is in the case of loose rocks and soils.

The narrow area of applicability is supported by the arrangement belonging to the Drucker-Prager condition on the plane σ_1, σ_2 in biaxial test condition of σ_1, σ_2, $\sigma_3 = 0$ shown in Fig. 9. The plane section of the circular cone is an ellipse at $B\phi = 1$; 2 or 3, a parabola at $B_\phi = 4$ or 5, and a hyperbola at $B\phi = 6$. Only at $B\phi \cong 2$ ($\phi \cong 20^o$) the Drucker-Prager condition yields a result complying with the measurements, therefore its applicability is very restricted.

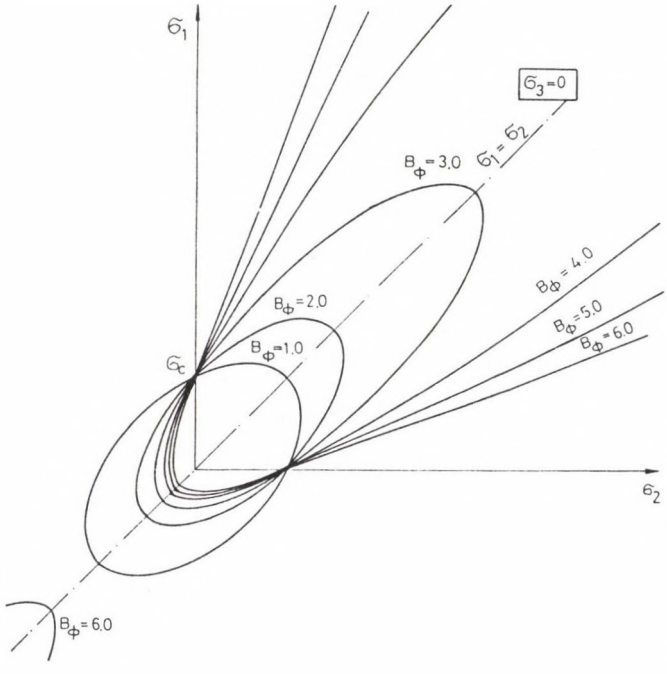

Fig. 9. Characteristic curves of deterioration condition by Drucker-Prager in biaxial stress condition

5. PROPOSAL FOR A PLASTICITY AND DETERIORATION CRITERIUM OF ROCKS SUITED FOR EXTENDED USE

Based on measurement results and theoretical investigations demonstrated above the following facts can be stated:

- criteria perfectly describing plasticity and deterioration limit conditions of rocks for wide ranging use are not available in the literature,
- however with adequate modification of the Mohr-criterium, a criterium closely approximating measured results can be developed.

It is useful to introduce besides the hitherto current quotient $B = \sigma_c/\sigma_t$ (Brinke-number) an another quotient $\sigma_{cb}/\sigma_t = B_b > B$ too, since these quotients can be easily determined by measurements.

The results of measurement and theoretical investigations show that in the range of tensile load ($\sigma < 0$) the limit curve is a parabola on the plane σ, τ , therefore the Richter's parabola (Mészáros 1986) is generalized as follows. In the case of $\sigma_2 = \sigma_3$, the deterioration limit curve can be described as

$$\tau^2 = \sigma_t \left(\sqrt{B + 1} - 1\right)^2 (\sigma_t + \sigma) .$$

In the case of $\sigma_2 = \sigma_1$ the deterioration limit curve is

$$\tau^2 = \sigma_t \left(\sqrt{B_b + 1} - 1\right)^2 (\sigma_t + \sigma) .$$

The limit condition of deterioration based on the above develop on the plane $\sigma_1 - \sigma_3$ as below:

at $\sigma_2 = \sigma_3$, $\sigma_3 = -\sigma_t$ if $\sigma_1 < \sigma_3$ $\left[1 + 0.5 \left(\sqrt{B + 1} - 1\right)^2\right]$.

In the case of $B = 8$, the deterioration condition by Griffith is the result.

At $\sigma_2 = \sigma_1$, $\sigma_3 = -\sigma_t$ if $\sigma_1 < \sigma_3$ $\left[1 + 0.5 \left(\sqrt{B_b + 1} - 1\right)^2\right]$.

Consequently, this description is based on the fact that the tensile strength (σ_t) does not depend on the middle princi-

pal stress (σ_2), since in the case of a tensile load, the internal friction mechanism which might cause a deviation, does not work.

In the range of compression stresses ($\sigma > 0$), the limit curve is by the evidence of measurements in most cases nearly linear. On the σ, τ plane for the limit line of deterioration it is dictated, to tangent the fitting circle of the apex of the parabolic limit curve and the Mohr-circle of biaxial compression strength.

In the case of $\sigma_2 = \sigma_3$ fitting circles at the apex of the parabolic limit curve is the Mohr-circle determined by principal stresses

$$\sigma_3 = -\sigma_t \quad \text{and} \quad \sigma_1 = 0.5\,\sigma_t\,(\sqrt{B + 1} - 1)^2 .$$

With the Mohr-circle of the uniaxial compression strength $\sigma_3 = 0$, $\sigma_1 = \sigma_c$. A tangent straight line to both circles has the form

$$\sigma_1 = \sigma_c + B_\phi\,\sigma_3 .$$

This straight line is tangent to the two Mohr-circles if

$$B_\phi = \tan^2\left(45^o + \frac{\phi}{2}\right) = B - 0.5\,(\sqrt{B + 1} - 1)^2 .$$

Thus the condition of deterioration is, if

$$\sigma_1 > \sigma_3\left[1 + 0.5\,(\sqrt{B + 1} - 1)^2\right]$$

then

$$\varphi = \sigma_1 - \left[B - 0.5\,(\sqrt{B + 1} - 1)^2\right]\sigma_3 - \sigma_c = 0 .$$

In the case of $\sigma_2 = \sigma_1$ on analogy of the above

$$\sigma_1 > \sigma_3\left[1 + 0.5(\sqrt{B_b + 1} - 1)^2\right]$$

then

$$\varphi = \sigma_1 - \left[B_b - 0.5(\sqrt{B_b + 1} - 1)^2\right]\sigma_3 - \sigma_{cb} = 0 .$$

If the diagrams indicating the results of biaxial tests, or those of Murrel's deterioration conditions regarding biaxial stress condition are observed, it is experienced that the strength in a biaxial stress condition ($\sigma_3 = 0$) changes approximately according to Fig. 10. When $\sigma_2 = 0$, $\sigma_1 = \sigma_c$, then the strength is linearly increasing up to σ_{cb}, which is reached at the value $0.5\ (\sigma_2 + \sigma_3)$. In the interval $0.5\ (\sigma_1 + \sigma_3) \leq \sigma_2 = \sigma_1$ the strength σ_{cb} remains constant. Thus the deterioration condition being valid at $\sigma_2 = \sigma_1$ may be extended also for this interval.

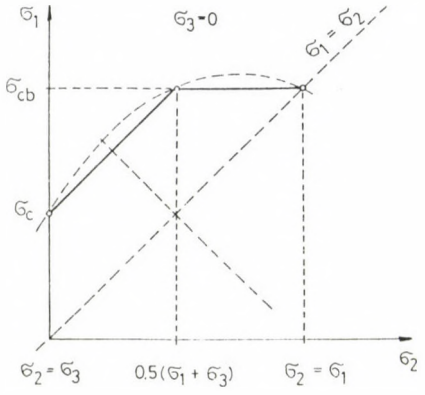

Fig. 10. Deterioration stresses characterizing rocks in biaxial stress condition

Further the deterioration limit condition valid in the interval of

$$\sigma_3 \leq \sigma_2 = 0.5\ (\sigma_1 + \sigma_3)$$

if $\sigma_3 = -\sigma_t$ $\quad \sigma_1 > \sigma_3 \left[1 + 0.5(\sqrt{B_b' + 1} - 1)^2\right]$, then

$$\Psi = \sigma_1 - \frac{(\sigma_{cb} - \sigma_c)\ (\sigma_2 - \sigma_3)}{0.5\ (\sigma_1 - \sigma_3)} - \left[B_b' - 0.5\ (\sqrt{B_b' + 1} - 1)^2\right] \sigma_3 - \sigma_c = 0$$

where, following from the proportionality

$$B' = B \left[1 + \frac{(B_b - 1)\ (\sigma_2 - \sigma_3)}{0.5\ (\sigma_1 - \sigma_3)}\right]$$

at $\sigma_2 = \sigma_3$ $B_b' = B$ and at $\sigma_2 = 0.5\,(\sigma_1 + \sigma_3)$ $B_b' = B_b$.

In accordance with that on the σ, τ plane the zone shown in Fig. 11 describes the limit curves of rocks. Within this zone, the limit curve is determined by the middle principal stress σ_2. To this corresponds the limit curve on the plane $\sigma_1 - \sigma_3$.

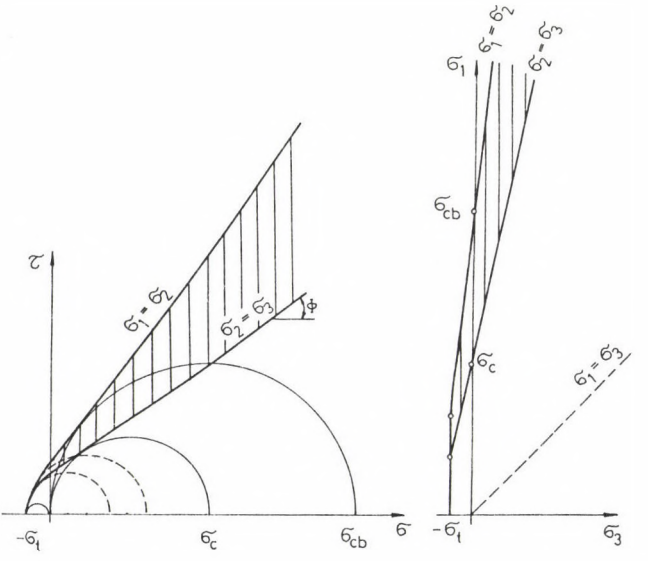

Fig. 11. Deterioration limit curves according to Mohr's modified deterioration condition

REFERENCES

Bieniawski Z T, Denkhaus H G, Vogler U W 1969: J. Rock Mechanics Min. Sci., Pergamon Press, 6, 323-341.

Cokk N G W, Denkhaus H G, Rapson W S 1967: Deep Level Mining Research in South Africa. International Mining Conference, Moscow

Crough S L 1971: The Post-Failure Behaviour of Norite in Triaxial Compression. Engineering Geology, Elsevier Publishing Company, Amsterdam

Denkhaus H G, Bieniawski Z T 1968a: Scientific Development of

Rock Mechanics During the Past Ten Years. National Mechanical Engineering Research Institite. Council for Scientific and Industrial Research, Pretoria

Denkhaus H G, Bieniawski Z T 1968b: Festigkeit von Gestein und Gebirge. 10. Ländertreff. Internat. Gebirgsmech. Leipzig, Akademie-Verlag, Berlin

Denkhaus H G, Bieniawski Z T 1970: The Significance of Rock Mechanics in Safe and Efficient Mining. VI. International Mining Congress, South Africa

Desai C S, Abel J F 1975: Introduction to the Finite Element Method. Von Nostrand Reinhold Company

Jaeger J C, Cokk N G W 1969: Fundamentals of Rock Mechanics. Methuen 8. Co. Ltd.

Kaliszky S 1975: Science of Plasticity (in Hungarian). Akadémiai Kiadó, Budapest

Kézdi Á 1972: Soil Mechanics I (in Hungarian). Tankönyvkiadó, Budapest

Lang T A 1964: Rock Mechanics Consideration on Design and Construction. Proceedings on the Sixth Symposium on Rock Mechanics. Rolla

Mészáros Z 1986: Generalization of hyperbolic limit curve of fractures (in Hungarian). OMBKE Egyetemi Osztályának Jubileumi Közös Kiadványa, Miskolc

Nayak G C, Zienkiewicz O C 1972: Int. Journ. for Numerical Methods in Engineering, 5, 113-135.

Obert L 1964: Deformational Behavior of Model Pillars Made from Salt, Trona, and Potash Ore. Proceedings of the Sixth Symposium on Rock Mechanics, Rolla

Peng S 1978: Coal Mine Ground Control. John Wiley Sons. New York, Chichester, Brisbane, Toronto

Schwartz E 1964: Failure of Rock in the Triaxial Shear Test. Proceedings of the Sixth Symposium on Rock Mechanics. Rolla, Missouri

Sokholovski V V 1953: Theory of Plasticity (in Hungarian). Akadémiai Kiadó, Budapest

Somosvári Zs 1986: In: NME Közleményei, I. Series, Bányászat, 34, No. 1-4, 181-204.

Somosvári Zs 1987: Geomechanics I (in Hungarian). Tankönyvkiadó, Budapest

Somosvári Zs, Németh A, Mészáros Z 1984: BKL, Bányászat, 117, 585-591.

Somosvári Zs, Bodonyi J, Németh A, Mészáros Z 1985: In: Központi Bányászati Fejlesztési Intézet és a Szovjetunió Tudományos Akadémiája Szibériai Tagozata Bányászati Intézetének közös közleményei, Budapest, 104-121.

Stagg K G, Zienkiewicz O C 1968: Rock Mechanics in Engineering Practice. John Wiley Sons, London, New York, Sidney

Vutukuri V S, Lama R K, Saluja S S 1974: Handbook on Mechanical Properties of Rock. Trans Techn. Publication, Clausthal

Acta Geod. Geoph. Mont. Hung., Vol. 25 (1-2), pp. 153-178 (1990)

ROADWAY STABILITY INVESTIGATIONS BY PHYSICAL AND MATHEMATICAL MODELING

Gy Gajári

Veszprém Coal Mines, H-8201 Veszprém, Budapesti u. 2, Hungary

The possibility of supporting roadways by dowels driven in low-strength, plastic rock (bauxite) was investigated. Notwithstanding that the investigations served practical purposes, the theoretical problems of stability came more and more into prominence. This paper presents the results of physical model experiments and sums up the aspects which are important regarding a numerical model to be developed.

Keywords: Bakony Bauxite Mines; dowel support; mathematical modeling; physical modeling; steel arch support

1. THE SUBJECT OF INVESTIGATIONS

The stopes of bauxite are located at the depth of about 300 m in the mines of Bakony Bauxite Mining Company (Bakonyi Bauxitbánya Vállalat, Tapolca). A typical roadway is supported by steel arches (TH-arches) as shown in Fig. 1a. The mechanical contact between the rock and a Swellex type dowel is provided

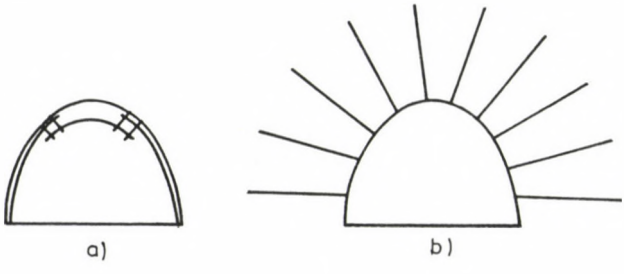

Fig. 1.

by friction along its entire length. The length of dowels is 3 m. The uniaxial compressive strength (σ_c) of the bauxite is between 3 and 5 MPa, the angle of internal friction (φ) is 20^o. The costs of floor dinting and reparation are high, because the roadways are located mostly in the zone of shifted pressure caused by stopes. The magnitude of vertical and horizontal convergence varies between 1 and 2 m. Preliminary investigations by Everling-type digital modeling showed that the pressure (around the roadways located close enough to stopes) is three or four times higher than the pressure prior to mining. The Mining Company wants to apply dowels as main supports and partly as additional ones, thus the study of the following problems was decided as investigation target:

1. Comparing the dowel support with the steel arch support applied previously in order to clarify which support is more advantageous in respect of roadway stability.
2. How the two types of support operate?
3. Do the low strength and the plasticity of bauxite limit the applicability of dowels for supporting independently the roadways?
4. What are the most important aspects for developing a numerical model for sizing a system of dowels?

2. THE IMPORTANCE OF PHYSICAL MODELING WITH RESPECT TO THE GIVEN PROBLEMS

The method of physical modeling seemed the best for starting the investigations in every respect. The success of solving the problems depends on the cognizability of the nature of mechanical processes around the strongly loaded roadway. The best for this purpose is the physical modeling, because the constitutive laws of a physical model with the same physical nature as the real object are automatically valid, and so it can be considered equivalent to the studied real object, at least qualitatively, from the viewpoint of observation. At the same time the laboratory conditions enable the reproduction of tests and give an easy way of observation as well. Neither in

situ measurements and observations nor other models (e.g. photoelastic or numerical models) can give possibilities of these kinds.

3. PRINCIPAL PARAMETERS OF THE PHYSICAL MODEL

Figure 2 shows the scheme of modeling in the plane perpendicular to the longitudinal axis of the roadway. Pressures, of magnitude determined as boundary conditions, act normal to the boundaries in directions Y and Z. Displacements and strains are limited in X direction. Thus a planar state of strain and a 3D state of stress can be obtained. The scale of the model related to geometry and strength is 1:20. The requested conformity referring to several physical properties provides the scales:

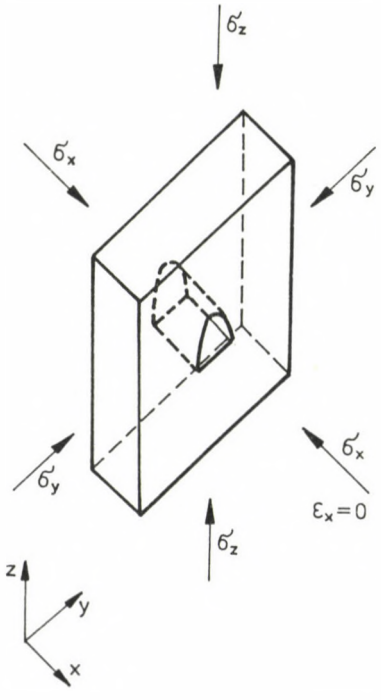

Fig. 2.

Length	1:20
Strain	1:1
Pressure, strength, Young's modulus	1:20
Force	1:8000
Bending moment of steel arches	1:160000
Coefficient of friction	1:1

The basic data of the built model are the following:

Front face area of the model	1.2 m × 1.2 m
Thickness of the model block	0.2 m
Height of roadway modeled	0.19 m
Width of roadway floor	0.26 m
Length of dowels modeled	0.15 m
Diameter of dowels	2.0 mm
Angle of dowel friction	$5\text{-}17^{o}$
Uniaxial compressive strength of rock modeled	0.15 MPa
Angle of internal friction of the rock	20^{o}
Young's modulus of the rock	15-20 MPa
Resistance against yielding of arches modeled	30-50 N
Resistance against bending of arches	0.19-0.23 Nm
Maximum boundary pressures in directions Y and Z	1.3 MPa

Ratio of boundary pressures in directions Y and Z:

$$\frac{\sigma_H}{\sigma_V} = 1.0 \ .$$

Figure 3 shows the photo of the modeling equipment. The boundary pressures are provided by 12 hydraulic cylinders. The hydraulic pressure of the cylinders is provided by an automatically controled hydraulic unit. During the tests the convergence of the roadway is recorded by an X-Y writer in function of the boundary pressure.

Figure 4 shows the sticks of the convergence indicator inserted in the roadway modeled, the displacement of which is converted to electric signals by strain gauges. The construction of the loading equipment allowed to cover the front side of the model by plexiglass in spite of the relatively large pressures (1.3 MPa) acting inside the model. The plexiglass is supported by solid steel ribs with a cross-section of

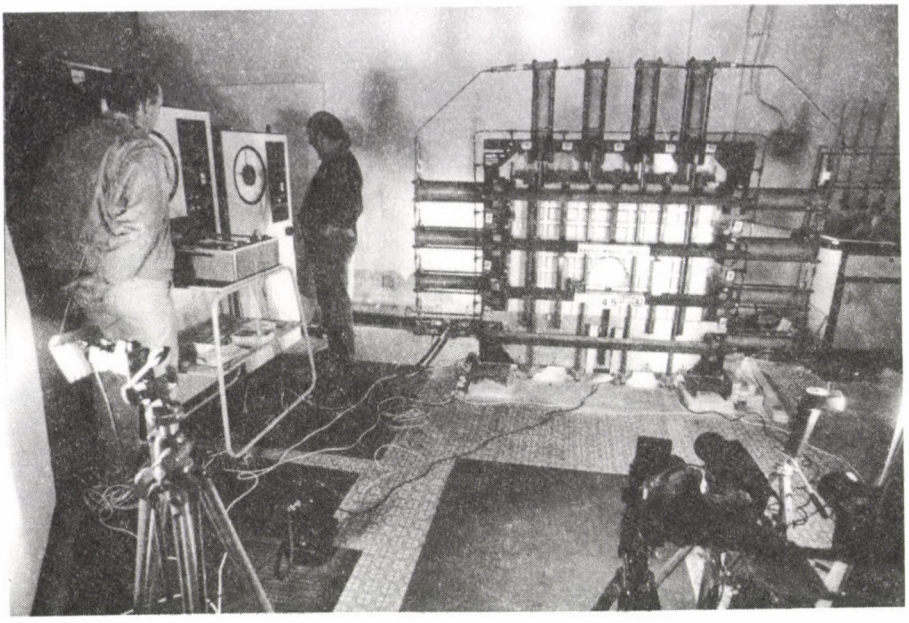

Fig. 3.

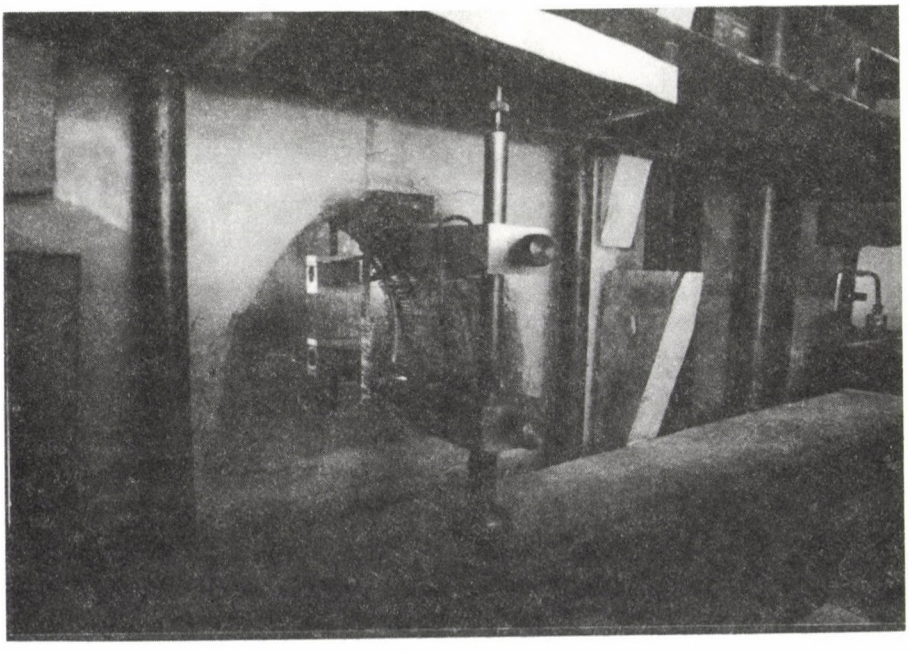

Fig. 4.

100 mm × 50 mm. Thus, the roadway modeled can be observed visually during the whole loading process. The quantitative evaluation of the strain of the rock modeled is possible by measuring the relative displacements of a square net with a scale of 100 mm × 100 mm and fixed on the plexiglass and another one with the same scale painted on the front side of the modeled rock. Figure 5 shows the front side of the model in the immediate surrounding of the roadway modeled.

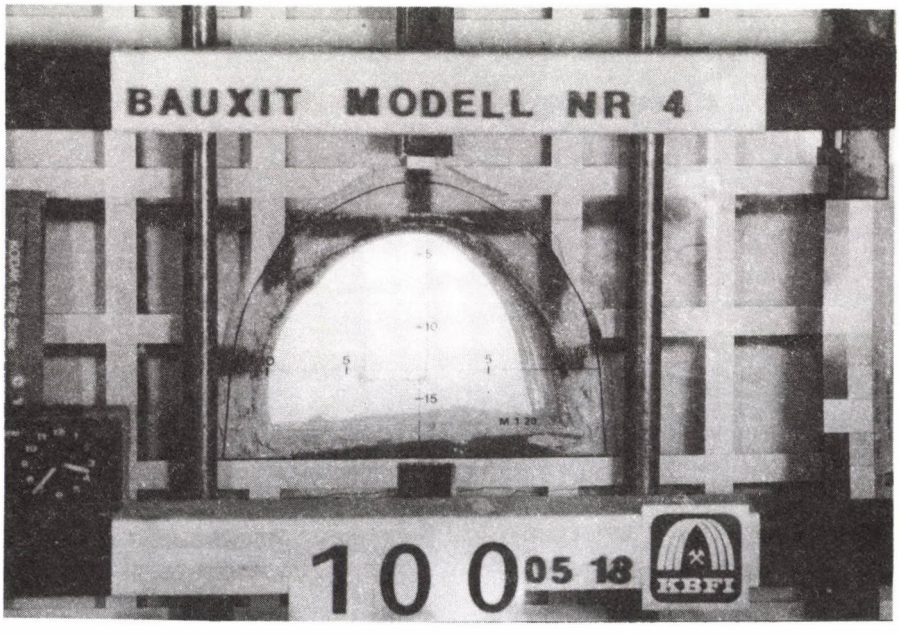

Fig. 5.

4. DISCUSSION OF TWO TEST RESULTS

Two test results are presented as follows. The two tests differred from each other only by the type of the roadway support. All the other circumstances were the same. In the first case the roadway was supported by steel arches, and in the second case by dowels. The comparison of the results of the two tests serves the clarification of problems No. 1, 2 and 3 described in Section 1.

4.1 Steel arch support

The distance between two built-in arches is 40 mm which is equal to 0.8 m in a real case. From the viewpoint of equilibrium the roadway worked in two different ways during the test. The two stages can be described by a convergence vs. boundary pressure curve (Fig. 6). The sections of the curve with positive slope represent states of stable equilibrium, while the

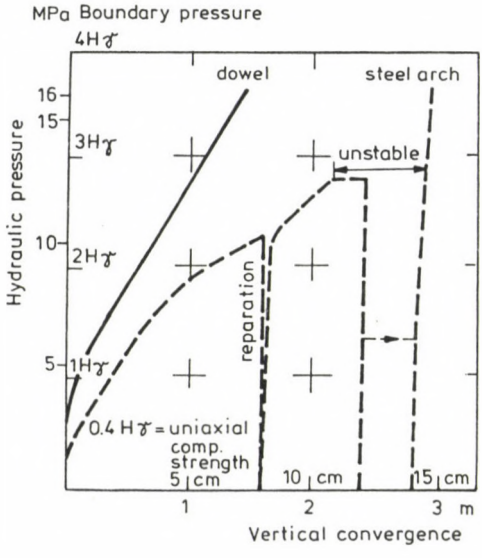

Fig. 6.

sections with negative slope indicate the state of unstable equilibrium. The curve related to the steel arch support is not monotonic. It has a relative maximum at the boundary pressure of 2.8 $H\gamma$ and a relative minimum at 1.3 $H\gamma$. Every point of the curve between these two extreme values has a negative slope, and therefore this section is unstable in respect of the equilibrium. The instability during the test can be observed in such a way that the convergence is increasing continuously at constant boundary pressure, whereas in stable state a certain value of convergence is attached to a given boundary pressure.

In an unstable state not only the walls of the roadway are moving, but the surrounding rock masses as well. In this test the unstable displacement spreads up to the boundaries. This involves that instability means the unstable equilibrium of the surrounding rock mass. This observation is very important indicating that in the state of unstable equilibrium a considerable, precipituous extension of discrete faults can be seen in the immediate vicinity of the roadway.

In the stable stage with positive slope before reaching the relative maximum of the convergence curve, when the boundary pressure was 2.2 $H\gamma$, the roadway was widened and the folded arches were replaced by new ones. This state, just before the reparation is shown in Figs 5, 7, 8. The convergence curve shows that during reparation the value of the boundary pressure was zero (0). It can be stated that the roadway and the surrounding rock mass is strain-hardening in stable state and the magnitude of elastic deformations in negligible.

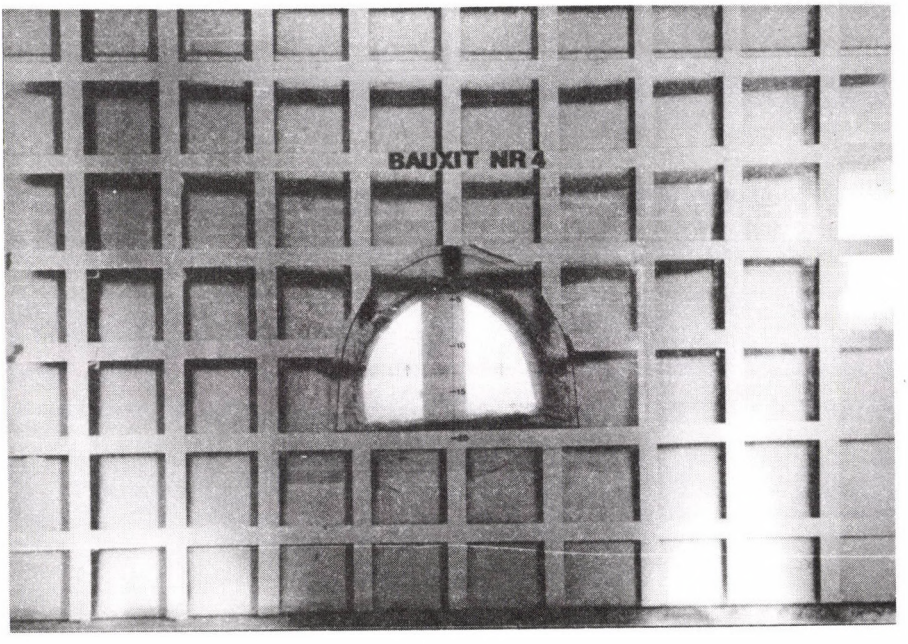

Fig. 7.

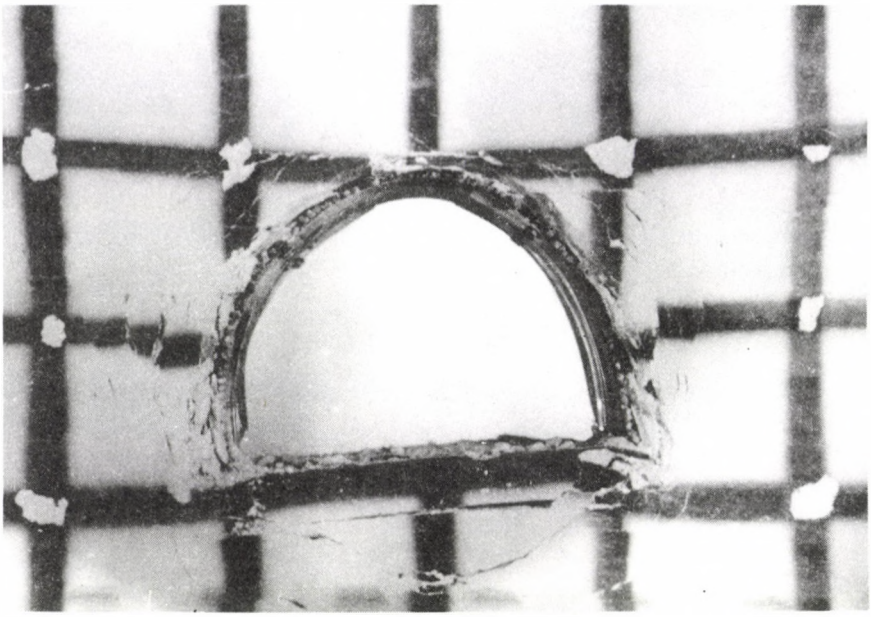

Fig. 8.

Figure 9 shows the state corresponding to the relative minimum point of the convergence curve. During the final period of the test (after the relative minimum point), the model had a stable behaviour again until reaching the maximum of the boundary pressure (3.6 $H\gamma$). The increase of the convergence was not significant. Figures 10, 11 and 12 show the final state. The differences between the final state and the state of reparation occurred in the intermediate unstable stage. Thus the unstable equilibrium is the result of the failure of the immediate surroundings (mostly the unsupported floor) along the discrete faults.

4.2 Support by dowels

The dowel-supported roadway showed unexpectedly advantageous results in respect of both convergence and stability.

The scheme of dowel support is shown in Fig. 1b. The distance between two sets of dowels was 50 mm which is equal to

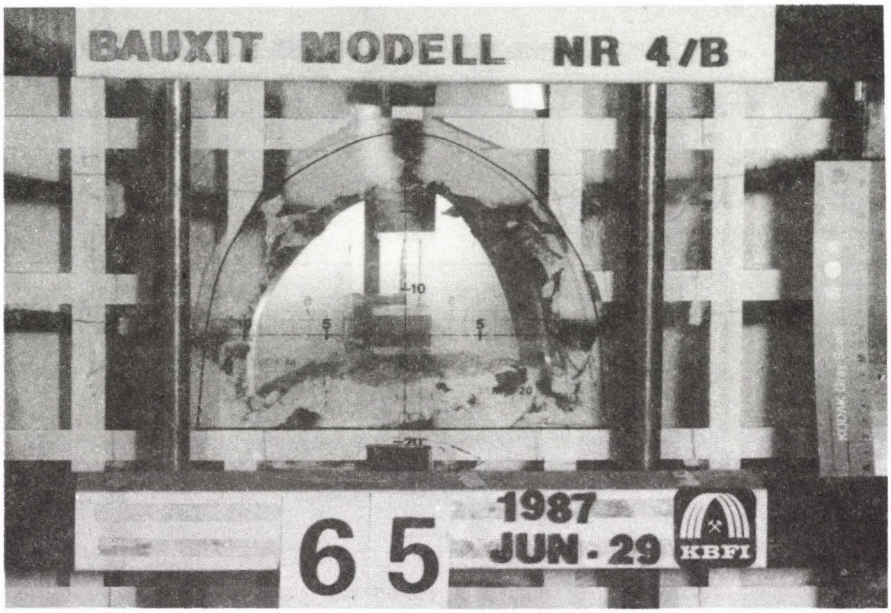

Fig. 9.

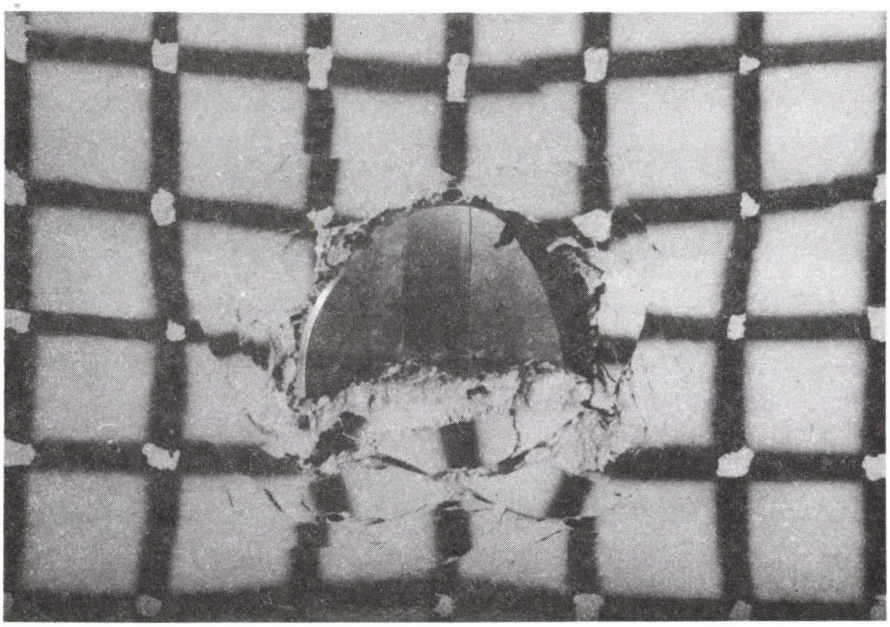

Fig. 10.

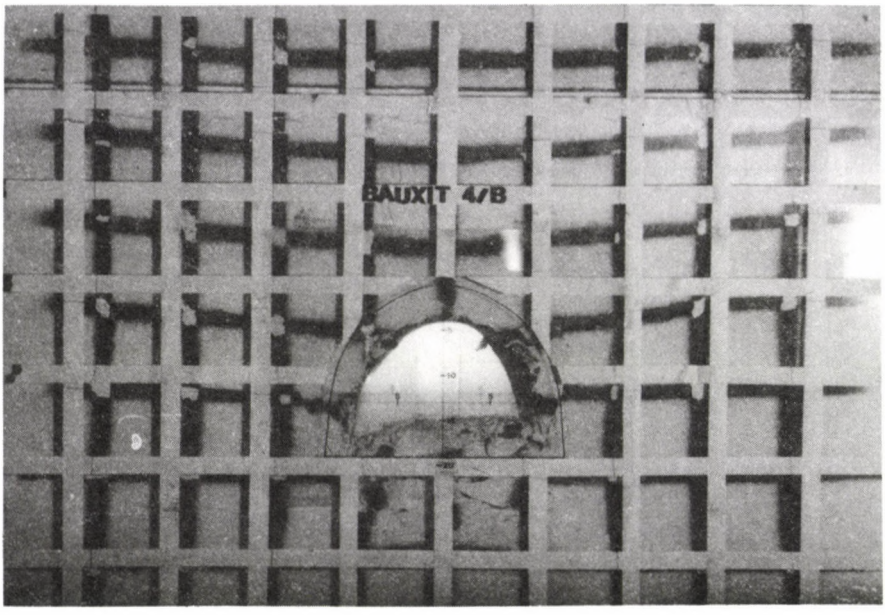

Fig. 11.

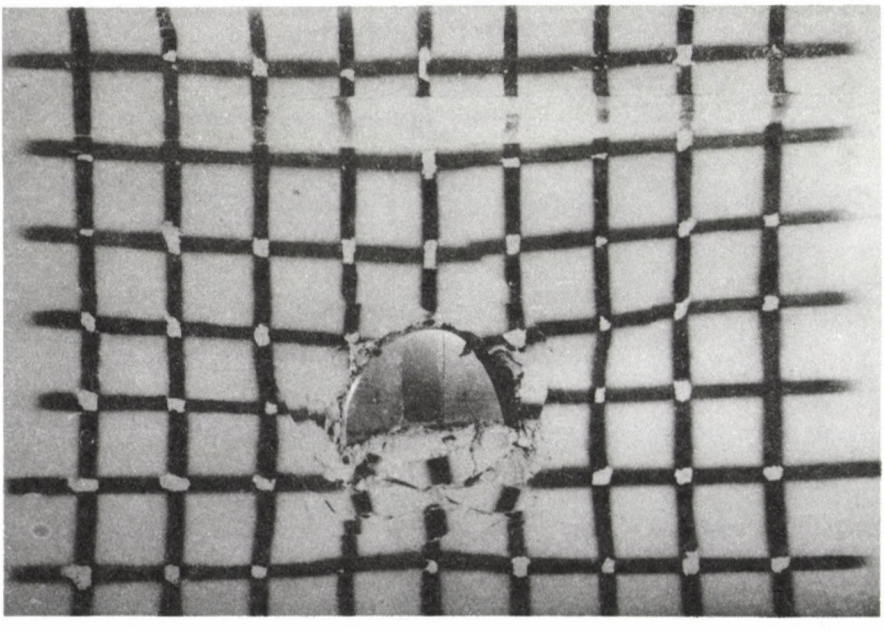

Fig. 12.

1 m in a real case. The dowels were not pasted, thus only the friction kept them in the holes bored previously. A small spring was located between the face plate of a dowel and the wall of the roadway. Therefore the yield of dowels increased.

The convergence vs. boundary pressure curve is shown in Fig. 6. The slope of the curve was positive from beginning to end and it was larger than in case of steel arch support, thus the total convergence was significantly less than in the previous test. Widening of the roadway was not neccessary.

Figures 13 to 15 show the final state. Though discrete faults occurred in the surrounding rock mass, the deformation field seems to be more homogeneous than in the previous case. It is remarkable that the loosening of the undoubtedly mostly broken floor is less extensive than in case of steel arch support.

Two of the problems described in Section 1 can be answered directly comparing the two tests:

- the dowel support is more advantageous than the steel arch

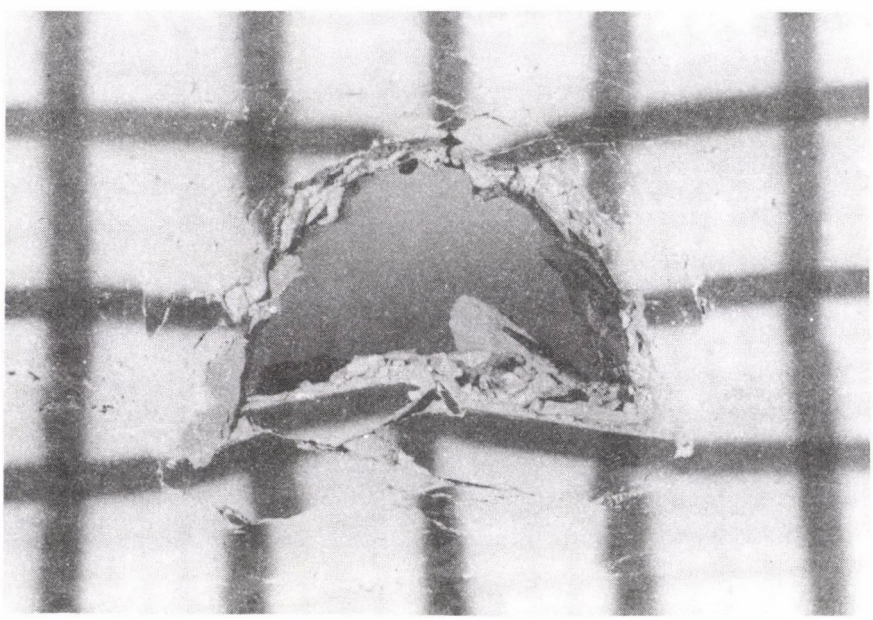

Fig. 13.

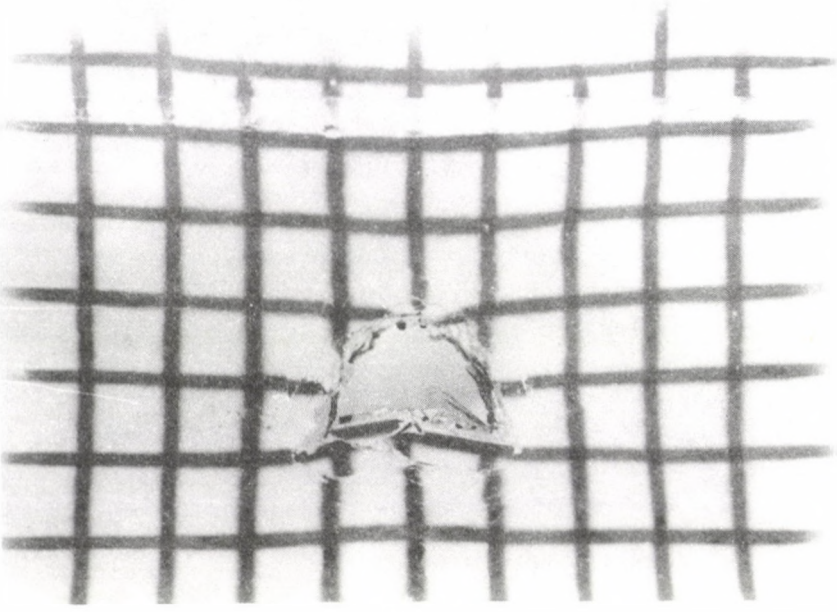

Fig. 14.

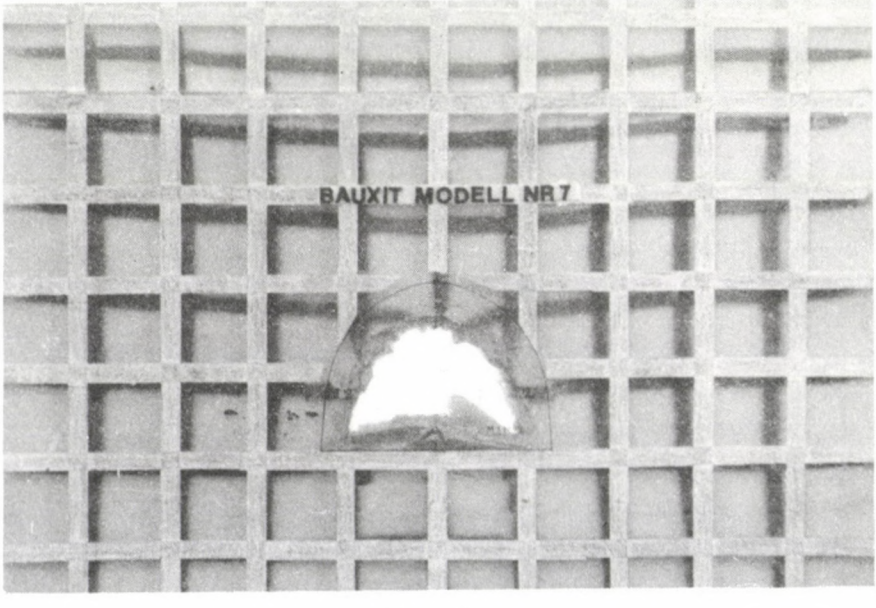

Fig. 15.

support with respect both to convergence and stability
- the low strength and the plasticity do not limit the applicability of dowels for supporting roadways.

5. CALCULATION OF ROCK MASS STRAINS IN ROADWAY SURROUNDING

By means of the square net mentioned previously and shown by the photos, the displacement components u_y, u_z of the discrete points - corresponding to the nodes of the net - parallel to axes Y and Z can be measured. Replacing the partial derivates by the proper finite differences the volumetric strain (dilatation) can be calculated.

$$\Theta = \varepsilon_{yy} + \varepsilon_{zz} = \frac{\partial u_y}{\partial y} + \frac{\partial u_z}{\partial z}$$

and the shear strain is:

$$\gamma_{yz} = \frac{\partial u_y}{\partial z} + \frac{\partial u_z}{\partial y}$$

Tha maximum shear strain γ (y,z) can be obtained by the proper transformation:

$$\gamma = \left[(\varepsilon_{yy} - \varepsilon_{zz})^2 + \gamma_{yz}^2 \right]^{1/2} .$$

Figure 16 shows the isolines of the dilatation (volumetric strain) corresponding to the stable state of roadway supported by steel arches. The negative sign shows the places of expansion and the positive sign shows the places of compression. Above the roof and under the floor two, independent zones of rock are loosened. The maximum dilatation is 10 percents. The side walls of the roadway are compressed, the maximum value of compression is 35 percents. Farther from the roadway compression is typical with the mean value of 5 percents.

Figure 17 shows the volumetric strain at the final state after instability. Even the side walls compressed originally are loosened. The roadway is surrounded by a continuous,

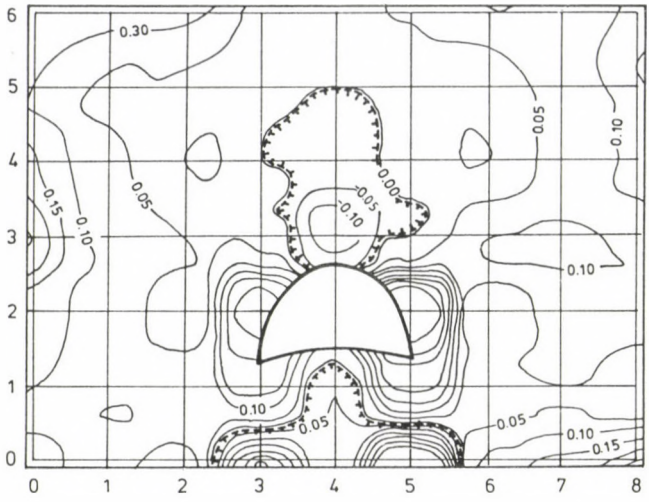
0.30
0.05
0.10
0.15
0.10
0.05
0.00
-0.05
-0.10
0.10
0.10
0.05
0.05
0.10
0.15
0 1 2 3 4 5 6 7 8
0 1 2 3 4 5 6

Fig. 16.

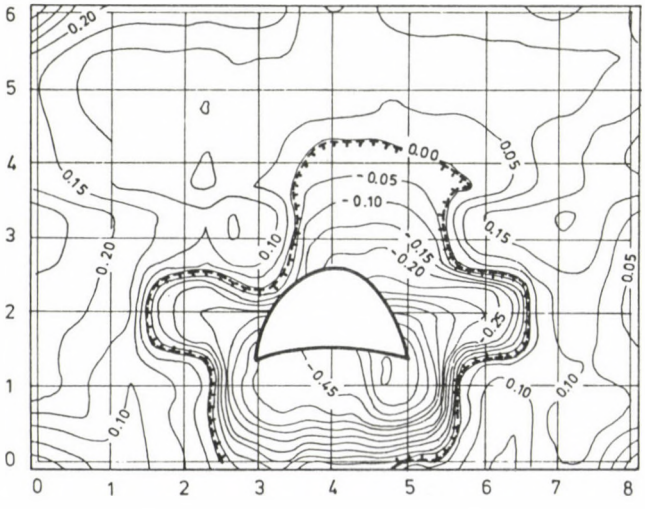
-0.20
0.00
0.05
-0.05
-0.10
0.15
0.15
0.20
0.10
-0.15
-0.20
0.05
-0.45
-0.45
0.10
0.10
0.10
0 1 2 3 4 5 6 7 8
0 1 2 3 4 5 6

Fig. 17.

loosened zone of rock, with an external contour around the region, inside of which discrete fractures can be seen. The maximum of the dilatation is at the lower right corner with the value over 60 percents. On the right side of the roadway the peak of compression moved away farther from the side wall than on the left side. The maximum value of compression is 20 percents on the right side, and 25 percents on the left side. It is interesting that the loosened region above the roadway does not extend upward, quite the contrary, its upper boundary comes somewhat closer to the roadway.

Figures 18 and 19 show the isolines of the maximum angular distortion (γ) in the state before instability and after that in the final state. The maximum distortion of the immediate surroundings of the roadway is 20^{o} ($\gamma = 0.35$), and located at the place of the maximum peak of compression close to the right side wall. The distortion of the roof is 9^{o} ($\gamma = 0.15$) and that of the floor is 6^{o} ($\gamma = 0.1$). The values of the distortion in the final state (Fig. 19) are considerably bigger than before instability. The rock zones with the same distortion are similar to concentric rings around the centre of the roadway floor,

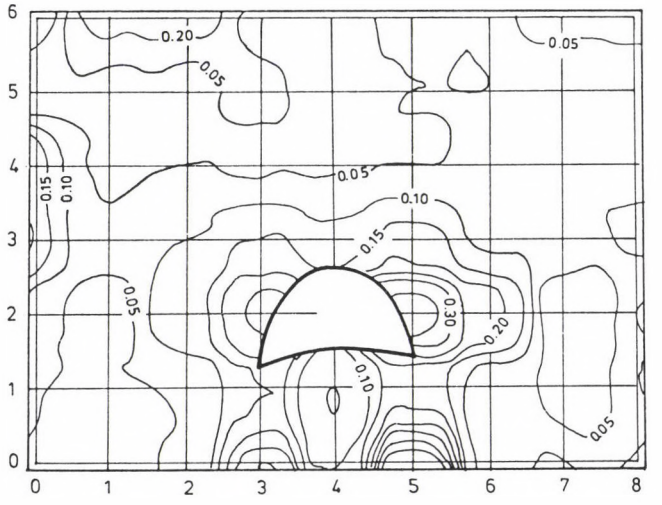

Fig. 18.

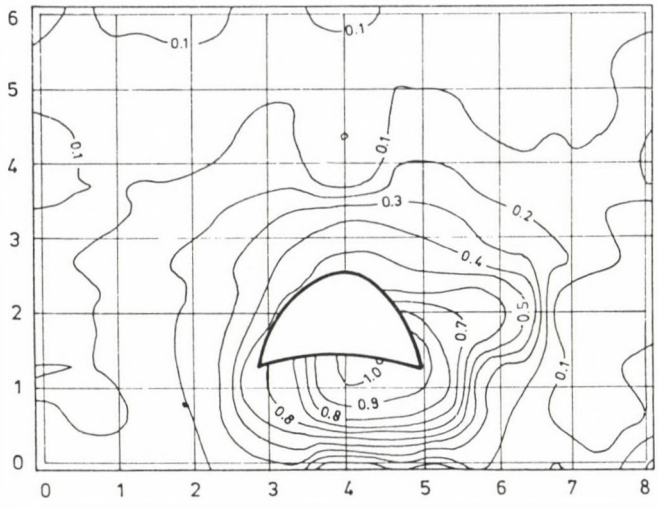

Fig. 19.

the angular distortion of which is 45^{o} ($\gamma = 1.0$). The minimum distortion of the roadway wall is at the upper right area with a value of 26^{o} ($\gamma = 0.5$).

Figure 20 shows the isolines of the volumetric strain referring to the final state of the dowel-supported roadway. The maximum dilatation is at the floor with a value of 45 percents. The minimum dilatation is at the roof (15 percents) and on the left side (10 percents). On the right side the dilatation is 20 percents. The outer contour of the loosened zone reaches the end of the dowels in the roof only (two dowels) while all the other dowels overlap this zone. The peak values of volumetric dilatation listed above cover very small rock regions only. In this case the outer contour of the loosened zone is significantly closer to the roadway wall than in the final state of the arch support.

Figure 21 shows the distortion of the surroundings of a dowel supported roadway. Comparing it with the final state of steel arch support test one can find that the distortions of the immediate surroundings are less (17^{o} i.e. $\gamma = 0.3$) and the maximum distortions of the side walls (30^{o}, i.e. $\gamma = 0.6$) are

valid for very small regions only.

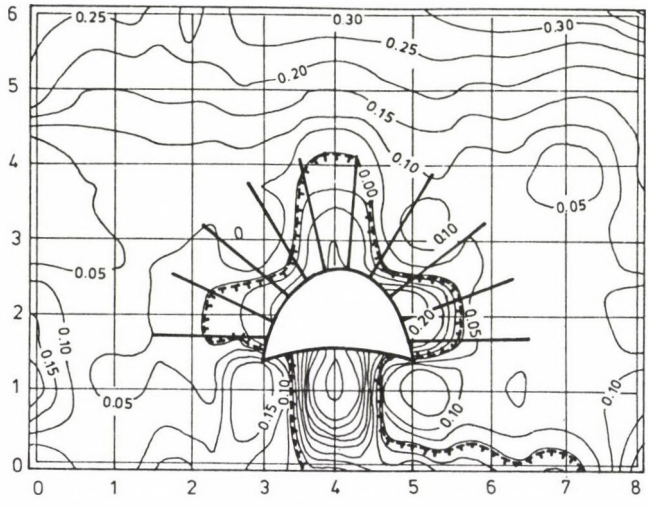

Fig. 20.

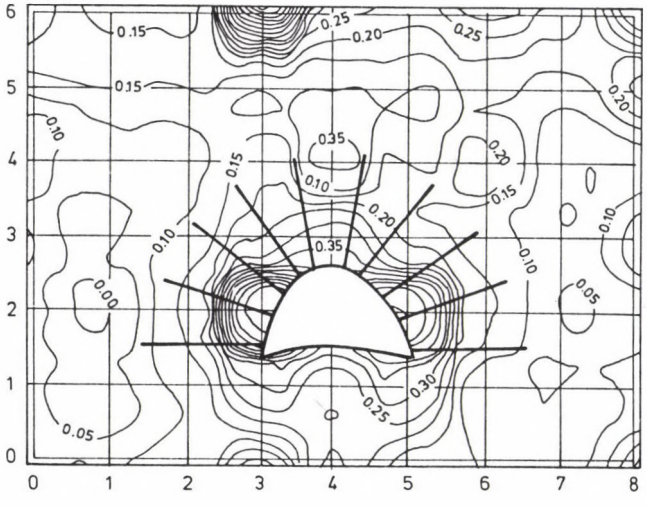

Fig. 21.

It is to be remarked that the strong disturbance which can be seen on the upper part of Figs 20 and 21 is caused by a layer which was not compressed satisfactorily before the test. It has no importance from the viewpoint of evaluation.

6. CONCLUSIONS FROM THE TEST RESULTS

Further investigations aim at coming closer to the solution of problems No. 2 and 4 described in Section 1. It is to be mentioned in advance that the results obtained up to now are insufficient to clear these problems completely.

On the basis of two experiments, the instability of the roadway is related to the propagation of discrete cracks and this kind of crack propagation is related to the dilatation of the surrounding rock masses. The close relationship between the unstable state of a roadway and the discrete cracks can be regarded from a theoretical viewpoint as the most important result of the experiments. The discrete fractures can be observed as opening cracks or as a discontinuous displacement field. According to St. Venant's strain compatibility principle - which declares that the strains of a body can be calculated from a continuous displacement field - blocks bounded by discrete cracks cannot be jointed with each other continuously after the decrease of the stresses. The discontinuous displacement field indicating the discrete fractures involves the dilatation of the surrounding rock mass if the dilatation is calculated such a way as given in the previous section. This is illustrated in Fig. 22 which shows the isolines of the dilatation caused by the discrete fractures producing instability. Comparing the outer contour of the asymmetrical zone of rock surrounding the roadway with Fig. 10 and 11 there is a good coincidence with the boundary of the zone of discrete fractures. The magnitude of loosening is proportional to the widening of cracks among the individual blocks and to the frequency of discrete fractures.

The great angular distortion does not indicate a discrete fracture by all means. This is illustrated in Fig. 21 which

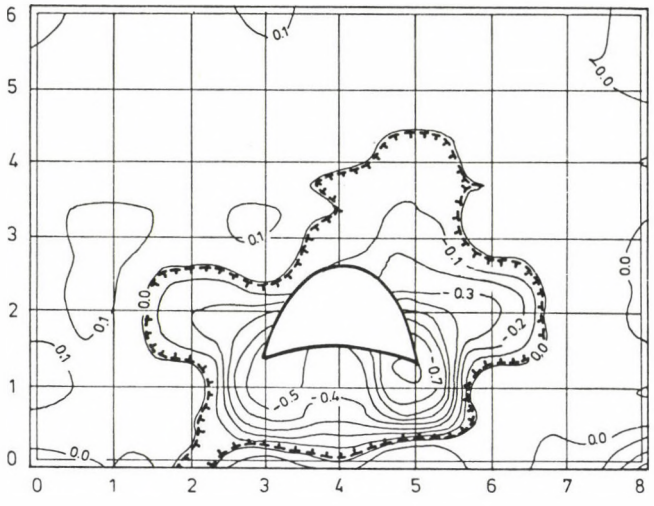

Fig. 22.

shows the dowel supported roadway and in Fig. 19 as well, which shows that the closed concentric curves corresponding to a γ = constant value come out of the zone of discrete fractures and go through the area of compression (mostly in the upper and left part of the roadway) where the displacement field is continuous. The state of strain can be described by a co-ordinate system the horizontal axis of which means the dilatation (Θ) and the vertical axis means the maximum distortion (γ). Then an angle α can be determined:

$$\alpha = \operatorname{atan} \frac{\Theta}{\gamma} \qquad \text{(see Fig. 23).}$$

The special cases for value α are

$\alpha = 90^{\circ}$ - pure compression,

$\alpha = 0^{\circ}$ - pure distortion,

$\alpha = -90^{\circ}$ - pure dilatation.

It is known that the failure criterion can be satisfied by small shearing load, if the principal stresses decrease at the same time. This type of load is indicated by a range of α between -90° and 0°. This disadvantageous load is characteristic

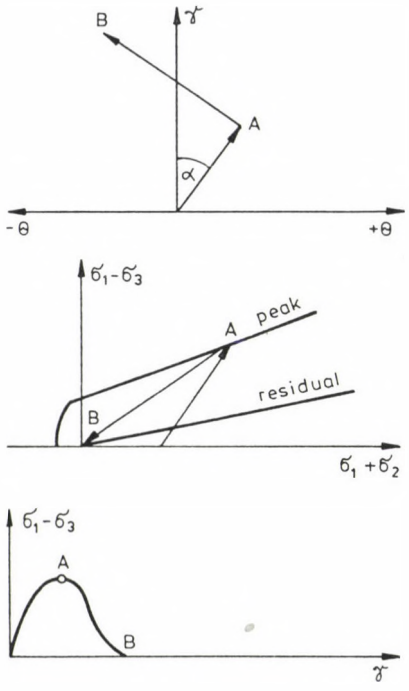

Fig. 23.

of steel arch support which leads to instability (see Fig. 24). Failure is the state when the shear resistance of rock is maximum. The failure is indicated by the maximum point of the curve τ vs. ε determined experimentally. The section of this curve preceding the failure is usually strain-hardening and the section following the failure is strain-softening. The resistance corresponding to a significant strain (i.e. ideal plastic behaviour) is termed residual strength. This is proportional to the normal stress similarly to the peak strength:

$$\tau_r = \operatorname{tg} \varphi_r \cdot \sigma$$

where φ_r is the residual angle of internal friction. (The residual cohesion is usually zero.)

In case of discrete fractures the strength decreases considerably, because $\sigma = 0$ at the boundaries of incompatible rock blocks. The decrease of the principal stresses i.e. the

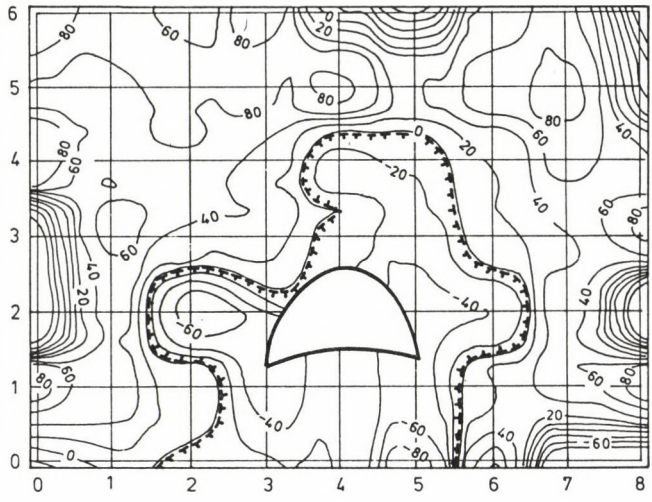

Fig. 24.

dilatation has a disadvantageous effect on the mechanical resistance of the surrounding rock mass both before failure and after failure states. The advantageous effect of dowels is above all that they impede rock loosening i.e. the decrease of the principal stresses. This effect, however, is slighter in case of small internal friction.

The several types of failures observed in physical model tests and the close connection between instability and discrete fractures indicates that beyond the well-known effect based on internal friction - as described above - the dowel support has a more essential effect - in contrast to the steel arch support - which tends to increase the stability of the surrounding rock mass. The effect described above does not explain satisfactorily from a mechanical viewpoint, why an unstable state occurs in case of steel arches providing a surface support, and why does not occur in case of dowel support. The author has made an attempt in forming a theoretical mechanical model which is in accordance with the results of the model tests. In the subsequent part of the study this conception is presented briefly.

7. BRIEF DESCRIPTION OF THE THEORETICAL MODEL

In case of planar deformation of an elastic body owing to the equilibrium and compatibility condition the displacement field $(u_y(y,z), u_z(y,z))$ has to satisfy the following differential equations:

$$\Delta \Delta u_y = 0$$
$$\Delta \Delta u_z = 0$$

where

$$\Delta = \frac{\partial^2}{\partial y^2} + \frac{\partial^2}{\partial z^2} .$$

Furthermore the boundary conditions have to be satisfied. In the model tests the surroundings of the roadway is not a simply connected domain. Let us disregard this fact now. Let us cut the model by its vertical symmetry axis in thought and consider the surface of cutting as a boundary. Thus one half of the model becomes a simply connected domain. The boundary conditions are the following:

- along the symmetry axis: $u_y = 0, \quad \frac{\partial u_z}{\partial y} = 0$
- along the lower boundary: $u_z = 0, \quad \frac{\partial u_y}{\partial z} = 0$
- along the upper boundary: $\sigma_{zz} = p, \quad \sigma_{zy} = \tau_{zy} = 0$
- along the lateral boundary: $\sigma_{yy} = p, \quad \sigma_{yz} = \tau_{yz} = 0$
- along the roadway countour;
  - stress proportional to the displacement in case of steel arch support
  - no stress or load acting on the contour in case of dowel support.

An approximate solution of the problem can be obtained by the finite element method which leads to a system of inhomogeneous linear equations (Zienkiewicz 1983):

$$K_t u = r - f$$

where K_t = the coefficient matrix of the system of equations
u = the unknown displacement vector
r = the vector of the loads acting on the boundaries
f = the vector of external loads or of loads equivalent to the initial stresses.

The stiffness matrix K_t has to satisfy certain requirements e.g. the compatibility condition. Stable resolution can be obtained if the stiffness matrix

$$K_t = \frac{\partial^2 \Pi}{\partial u_i \, \partial u_j}$$

is positive definite, where Π is the total potential. Then the eigenvalues of the problem:

$$\lambda_1, \lambda_2, \cdots, \lambda_n$$

are positive real numbers (Frank and Mises 1966).

The tangential stiffness matrix K_t changes if the restrictive compatibility condition is neglected between certain jointed elements, and infinitely large strain (i.e. discontinuous displacement field or discrete fault in previous terms) is allowed. Obviously, the stiffness of the system decreases. According to the results of the variational analysis the eigenvalues changes continuously with the propagation of faults and the minimum eigenvalue decreases (Frank and Mises 1966). If it is equal to zero, the system of equations cannot be solved. This involves that the total potential has no minimum i.e.:

$$\frac{\partial \Pi}{\partial u} \neq 0 \ .$$

However large are the supporting reactions of the steel arch support the roadway and the surroundings will not be stable anyway.

However, the Griffith type crack propagation theory according to Rice is just satisfied:

$$G \leq \frac{\partial \Pi}{\partial u} \cdot \frac{\partial u}{\partial x}$$

where G is the energy which is neccessary to move the peak of the fault in direction X by a unit distance (Zienkiewicz 1983).

According to Rice (1968) the energy available from the surroundings for the propagation of a fault can be calculated by a line integral:

$$\frac{\partial \Pi}{\partial x} = \int_{\Gamma} (W\, dy - T_i \frac{\partial u_i}{\partial x}\, ds)$$

where Γ = is an arbitrary curve surrounding the peak of the fault, beginning and ending at the fracture walls,

$W = 1/2 \cdot \sigma_{ij} \cdot \varepsilon_{ij}$

$T_i = \sigma_{ij} \cdot n$

n = outward normal to an elementary range (ds) of the curve Γ

x = direction of crack propagation

y = direction perpendicular to x.

In case of shear failure - according to Rice - G is equal to the integral of the shear resistance, raised between the peak strength and the residual strength, with respect to the displacement. In case of dowel support the following effects can be considered that improve the stability:

- Every constraint relating to the displacements increases the eigenvalues (Frank and Mises 1966), however the dowels obviously decrease the degree of freedom of the system, thus the solution of the boundary value problem is always stable.
- The value of the Rice integral - i.e. the force available to drive the crack peak - will be reduced.
- The magnitude of G - i.e. the force necessary to drive the crack peak - will be enlarged by the compression of the cracks.

From the foregoing it follows that in certain insecure situation the stability cannot be assured even theoretically by a steel arch support acting as a boundary condition, however, it can be by a dowel support. The dowel support cannot be compared with the steel arch support in respect of pull-out

resistance and support reaction.

ACKNOWLEDGEMENTS

The author should like to thank the Bakony Bauxite Mining Company (Bakonyi Bauxitbánya Vállalat) for financing the experiments and Mr Machalek, member of VVUU, Ostrava for placing the prescription of the modeled rock at the author's disposal.

REFERENCES

Frank Ph and Mises R 1966: The differential and integral equations of mechanics and physics (in Hungarian). Műszaki Könyvkiadó, Budapest

Rice J R 1968: Journ. of Applied Mechanics, 90, 379-385.

Zienkiewicz O C 1983: Methode der finiten Elemente. VEB Fachbuchverlag, Leipzig

Acta Geod. Geoph. Mont. Hung., Vol. 25 (1-2), pp. 179-190 (1990)

MODELLING OF AIR LEAKAGES IN MINES

Z Buócz and J Janositz

University for Heavy Industry, Mining Department, H-3515 Miskolc, Egyetemváros, Hungary

Based on functions relating to underground water leakages the authors are presenting an air current (leakages) model in the goaf of mine workings. The program (software) run on IBM PC-s is modelling direction and magnitude based on parameters of the goaf and neighbouring headings. The method provides assistance for protection against endogenous mine fires both in the phase of prevention and elimination.

Keywords: air leakage; endogenous fire; modelling; self-ignition

1. INTRODUCTION

One of the main coal mining hazards is endogenous mine fire. This source of hazard is equal in age with coal mining and except for firedamp explosions, it caused the largest mine catastrophes. These depressing statistics present a still more frightening picture when taking into account that among the causes of ignition initiating firedamp explosions there are more than 20 percent due to mine fires.

In Hungary the collieries belonging to the Mecsek Coal Mines are qualified as seriously exposed to fire hazards and except of few collieries all of our coal mines are endangered by fire hazard. It is a specific feature of the Hungarian geological conditions that our bauxite mines are partly qualified as fire hazardous ones due to coal strips and coaly, bituminous shale layers above the bauxite.

In the last two to three decades considerable material and mental power has been used to prevent endogenous fires and for quick elimination of fires occurred, resp. These efforts

resulted in a considerable decrease of fire cases, but 4 to 10 endogenous fires of greater significance, as well as a much higher number of warming-up cases call the attention to the necessity of further research work to be carried out.

The importance of this research work is increased by the fact that endogenous fires generate considerable material damage in faces, since it is very often impossible to save the equipment from the area under fire. In other cases the existence of mine fields becomes uncertain and a considerable amount of developed coal reserve becomes unexploitable.

2. CONDITIONS ORIGINATING ENDOGENOUS FIRES

Self-ignition is an oxidization process which is slow at low temperatures and accelerates around $80^{o}C$. From the point of view of our investigations the characteristics and amount of oxygen flow and air flow resp. necessary to the self-ignition are of essential importance as preconditions of self-ignition.

Formulating in a simple way, one of the conditions of self-ignition is the presence of a weak air flow with no cooling effect. The weak air flow contacting the coal mass is ensuring the oxygen necessary to oxidization, but it removes only a part of the oxidization heat as a result of which the temperature get raised.

Due to the weak air flow described as condition, the self-ignition of coal occurs in the goaf of faces, in the environment of road ways, and in coal pillars resp.

In the rock environment of roadways and in coal pillars self-ignition takes place if the coal is fractured, loosened and air can penetrate into it. In case of faces the precondition of self-ignition is in the goaf a coal loss which must exceed 10 to 15 percent (Kovács 1972). Another precondition is in this case the relatively weak compression of the goaf which allows air flow to pass through.

The resistance against air flow in goafs and loosened pillars is generally high therefore the development of flow requires higher pressure differences.

The object of our investigations is to develop an air flow model applicable for modelling air leakages through goafs and loosened pillars. The model allows the detection of air escapes, air leakages in the goaf of faces of different types and this way it reveals protection possibilities in a wider scale as well as the possibility of reducing air leakages to the minimum when developing faces and designing ventillation.

3. MODELLING AIR FLOWS IN ABANDONED AREAS OF FACES

The definition of resistance against air flow in goafs can be deduced from the functions of water seepage.

The most frequently used function of fluid seepage or leakage is in the case of gases the Darcy-law:

$$V_l = \frac{Q}{F} = k \cdot I \qquad (1)$$

where V_l - is the leakage speed (m/s), i.e. the ratio of the flowing volume $Q(m^3/s)$ and the cross section $F(m^2)$

k - leakage ratio factor (m/s)

I - hydraulic jump (without dimension).

According to Darcy's investigations, the leakage factor k does not depend on speed or on hydraulic jump. Its value is influenced only by the space of flow filled up with particles and by the characteristics of the fluid material.

The relation between leakage factor and material characteristics of the flowing medium and the space of flow resp. is as follows (Kovács 1972):

$$k = \frac{1}{5} \cdot \frac{\varrho \cdot g}{\eta} \cdot \frac{n^3}{(1-n)^2} \cdot \left(\frac{D_h}{\alpha}\right)^2 , \qquad (2)$$

where k - leakage factor (m/s),

ϱ - density of flowing medium (kg/m^3),

η - dynamic viscosity factor of the flowing medium (Pas),

g - gravitational acceleration,

n - the ratio of void section f (m^2) and the total section F (m^2) in a given cross section dimensionless

quantity,

D_h - active diameter of particles according to Kozeny (m).

Consequently the leakage factor can be related with three groups of variables:

- characteristic parameter of the flowing medium $\frac{\varrho \cdot g}{\eta}$, or g/ν, where the kinematic viscosity is

$$\nu = \eta / \varrho \tag{3}$$

- characteristic parameter of solidity of the layer

$$n^3/(1-n)^2 ,$$

- characteristic parameter of particle size and particle shape D_h/α.

The characteristic parameter of the flowing medium depends on the temperature, thus in the case of warming up, the flowing characteristics of the air will be improved in the abandoned space.

The variable to characterize solidity was first applied by Kozeny in the following form:

$$N_k = \frac{n^3}{(1-n)^2} = \frac{e^3}{1+e} \tag{4}$$

where N_k - characteristic value of layer solidity in function of voids volume (without dimension),

e - void factor (without dimension)

$$e = \frac{V_h}{V_t} \tag{5}$$

V_h - voids volume (m^3)

V_t - volume of solid particles (m^3).

Based on Eq. (4),

$$e = \frac{n}{1-n} . \tag{6}$$

To characterize solidity N, another function based on

measurement results has also been defined which is slightly different from Eq. (4):

$$N = e^{a} \quad . \tag{7}$$

The measurement results show that $2 \leq a \leq 3$.

The magnitude of friction of the flowing medium is characterized by the ratio D_h/α of the particle size and particle shape. Among the forces braking the air flow the most significant one is friction. The influence of adhering force and inertia is of less importance. Two of these three forces - the friction and the adhering force - may be in connection with the size of contact surface between the flowing medium and the solid phase, while the accelerating force is related to the mass of the flowing medium. The latter is proportional to the difference of the total volume and the volume of the particles, and thus it can also be characterized by the volume of the particles. Therefore, the shape factor which is best corresponding to the physical character, can be calculated for the purpose of leakage investigations as the ratio of surface (F) and volume (V) of the particles. This ratio has the dimension of 1/m what means that it is the ratio of the dimensionless factor and of a characteristic diameter:

$$\frac{F}{V} = \frac{\alpha}{D_h} \quad . \tag{8}$$

The shape factor α depends as shown by function (8) on the diameter selected to characterize the particles. According to Kovács (1972) the shape factor depends in a high degree on the mineralogical character of the particle what is related in its turn to the diameter of the particle. In the case of gravel - where the primary material is quartz - the particles are generally stubby, i.e. their principal axes are not too much different from each other in their sizes. Thus their shape factor α is varying between 7 and 11. Particles of laminar rocks (as sandstones, shales) are of different nature, their shape factor may grow up to $\alpha = 20$.

The active diameter (D_h) of particles, according to Kozeny can be determined from the grain-size distribution curves.

Since in the goaf of faces rock pieces of considerable volume may also be found in great number in addition to small grain sizes, the active diameter belonging to the 10 percent value of the grain-size distribution curve (D_{10}) must be corrected. Based on investigations by Kovács (1972), if the degree of irregularity $\frac{D_{60}}{D_{10}}$ exceeds 10, the active diameter is 2.5 to 3 times higher than D_{10}.

The Darcy law is valid only in the case of laminar flow. But the air flow in the goaf is not always laminar. Therefore the characteristics of turbulent and transient air flows should also be investigated.

The transient range between laminar and turbulent flow is divided into two parts in the technical literature. The division is made in accordance with the Reynolds-number used for the hydraulic investigation of pipes. This can be calculated from the characteristics of the bulk material as follows:

$$Re_{pipe} = \frac{4}{1-n} \cdot \frac{D_h}{\alpha} \cdot \frac{V_1}{\nu} .$$

Using this formula, the following limit values are valid:

	Re_{pipe}	< 10	laminar range (Darcy),
10 <	Re_{pipe}	< 100	first transient range (Lindquist),
100 <	Re_{pipe}	< 1000	second transient range,
1000 <	Re_{pipe}	-	turbulent range (Froude).

Flows of different ranges are described by the flowing functions (Kovács 1972):

$$I = a_1 v_1^2 + b_1 v_1 \qquad (10)$$

where

$$a_1 = \frac{0.4}{g} \cdot \frac{\alpha}{D} \cdot \frac{1-n}{n^3} \qquad (11)$$

$$b_1 = 4 \frac{\nu}{g} \cdot \left(\frac{\alpha}{D}\right)^2 \cdot \frac{(1-n)^2}{n^3} . \qquad (12)$$

In the second transient range

$$I = a_2 v_1^2 + b_2 v_1 , \tag{13}$$

where

$$a_2 = \frac{0.16}{g} \cdot \frac{\alpha}{D} \cdot \frac{1-n}{n^3} = 0.4 \cdot a_1 \tag{14}$$

$$b_2 = 10 \frac{\nu}{g} \cdot \left(\frac{\alpha}{D}\right)^2 \cdot \frac{(1-n)^2}{n^3} = 2.5\ b_1 . \tag{15}$$

In the turbulent range

$$I = a_3 \cdot v_1^2 \tag{16}$$

where

$$a_3 = \frac{0.2}{g} \cdot \frac{\alpha}{D} \frac{1-n}{n^3} = 0.5 \cdot a_1 . \tag{17}$$

In the functions of water leakage I is the ratio of the flow inducing water level difference ΔZ to the leakage route length L. In the case of water head ΔZ the water pressure is:

$$\Delta p = \Delta Z \cdot \varrho \cdot g . \tag{18}$$

Thus the depression h used in ventillation can be calculated in function of I as follows:

$$h = \Delta p = I \cdot \varrho \cdot g \cdot l . \tag{19}$$

Consequently, functions of the air flow in the goaf are: In the case of laminar streams, based on Eqs (1) and (19)

$$h = \frac{v \cdot \varrho \cdot g \cdot l}{k} = \frac{\varrho \cdot g \cdot l}{F \cdot k} \cdot Q \tag{20}$$

where k is the leakage factor.

In the first transient range

$$h = \varrho \cdot g \cdot l \cdot (a_1 v^2 + b_1 v) = \frac{\varrho \cdot g \cdot l \cdot b_1}{F} Q + \frac{\varrho \cdot g \cdot l \cdot a_1}{F^2} Q^2 , \quad (21)$$

where

$$h = R_1' Q + R_1'' Q^2 . \quad (22)$$

In the second transient range

$$h = \varrho \cdot g \cdot l \ (a_2 v^2 + b_2 v) = \frac{\varrho \cdot g \cdot l \cdot b_2}{F} Q + \frac{\varrho \cdot g \cdot l \cdot a_2}{F^2} Q^2 , \quad (23)$$

$$h = R_2' Q + R_2'' Q^2 . \quad (24)$$

In the turbulent range

$$h = \varrho \cdot l \cdot 0.2 \cdot \frac{\alpha}{D} \cdot \frac{1-n}{n^3} \cdot \frac{Q^2}{F^2} = R Q^2 . \quad (25)$$

For the purpose of calculation, the value of Re_{pipe} defines the formula valid in a definite case.

Soviet authors (Ushakov 1977) deal with leakage in goafs on a similar basis but dividing the flow ranges into three parts only. Based on several empirical observations, resistance functions have been determined for goafs.

The basic relationship between the pressure difference and the flowing quantity is:

$$h = R' \cdot Q + R'' \cdot Q^2 \quad (26)$$

where h - depression arising in streaming (Pa)
R' - linear aerodynamical resistance (Ns/m^5),
R" - quadratic aerodynamical resistance (kg/m^7),
Q - mass flow of air leakage (m^3/s).

Resistance values can be calculated by applying formulae as below:

$$R' = \frac{\eta \cdot l}{k \cdot F} \quad (27)$$

$$R'' = \frac{\varrho \cdot l}{sF^2} \quad . \tag{28}$$

Here η - dynamic viscosity of air (Pa·s)
k - permeability factor (m^2),
l - length of leakage route (m),
F - cross section of filtration flow (m^2),
ϱ - density of air (kg/m^3),
s - macro-roughness coefficient (m).

The nature of air movement is defined by a Reynolds number differring from Eq. (9):

$$Re = \frac{v \cdot k}{\nu \cdot s} \tag{29}$$

where

$$\nu = \eta / \varrho$$

is the kinematic viscosity factor (m^2/s).

In the case of Re values calculated as above, leakage is laminar, if $Re \leq 0.25$;
if $0.25 \leq Re \leq 2.5$ it is of transient nature and
if $Re \geq 2.5$ it belongs to the turbulent range.

The value of the air friction factor in the three ranges is as follows

$$\lambda_{la} = \frac{1.14}{Re} \quad , \qquad \lambda_{tr} = \frac{1.14}{Re} + 0.86 \quad , \qquad \lambda_{ta} = 1.18 \quad .$$

To determine values R' and R", first the values of the specific resistances r' and r" are to be defined based on Eqs (27) and (28):

$$r' = \frac{\eta}{k} \tag{30}$$

and

$$r'' = \frac{\varrho}{s} \quad . \tag{31}$$

In the case of medium seam inclinations, these values can be calculated in function of the distance x measured from the

face:

$$r' = ax^{c} , \qquad r'' = bx^{c/2} \tag{32}$$

where a and b are empirical coefficients which depend on the characteristics of the caved rock.

x - is the distance measured from the working (m),

c - is a coefficient depending on the compression in the caved rock.

Coefficient c is a function of the rate of face progress v_f :

$$c = \exp (0.5 - 0.10\ v_f) . \tag{33}$$

Values of coefficient a and b

Type of caved rock	a	b
Dunn bass, loose	0.6 - 1	100 - 200
Dunn bass of medium strength	0.2 - 0.5	71 - 100
Hard clayey and sandy slate	0.06 - 0.1	51 - 70
Sandstone and limestone	0.03 - 1.15	35 - 50

4. MODELLING OF LEAKAGE ROUTES

In most cases the exploited areas, caved zones of workings are of rectangular shape. The solidity characteristic for the goaf is changing most markedly in the directions embordering the caving. Behind the face of the working, the solidity of the goaf is increasing with the distance as expressed by Eq. (32). The goaf characteristics are changing parallel to the working face as well, since along the intact coal wall and in one part of the cases in the line of the abandoned face headings resp. the resistance of the goaf is less than in the environment of face middle line.

Based on the direction of the change of goaf characteristics, as well as on the shape of abandoned areas leakage routes are modelled by a square net, the lines of which are parallel

to the border lines of the abandoned face area (Fig. 1). The distances of net lines are u and v resp., thus the air flow is always moving through a prism with a base area of $u \times w$ and with the same height as the height of the goaf. The mesh of the square net depends on the required accuracy of modelling, on the dimensions of caving and partly on the capacity of the computer applied. Dimensions may vary between 2 and 20 m.

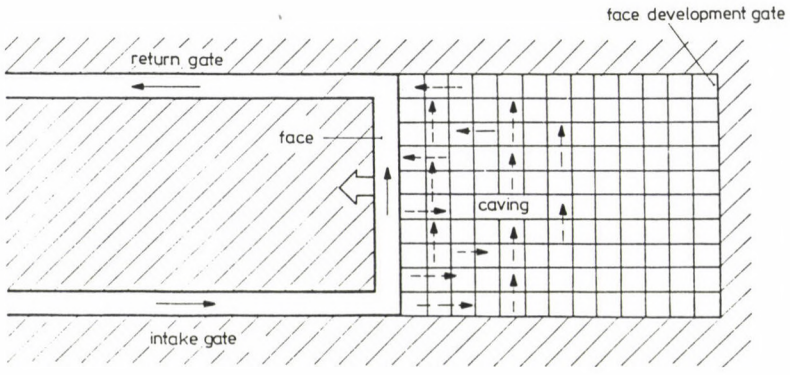

Fig. 1.

In knowledge of the dimensions of caving and of mesh of net, the computer program generates the connection model of air routes, in which each prism represents one section of air route parallel and perpendicular to the face.

The bordering drifts of cavings are divided into sections corresponding to the mesh and are applied to the net model in this form.

The quantity of air leakage is determined by the software using the Newton-Raphson method. In the calculation the leakage ranges are followed up successively and resistances are modified consequently. The software has been developed in FORTRAN for IBM PC/XT-AT compatible computers.

The resistances evolved among faces, cavings and bordering drifts are modified in accordance with the prevailing conditions, as essential deviations are possible in the case of

shield supports, single props, bordering barriers and perhaps in the case of establishing pillars.

The model has been applied successfully for modelling a face with Z-type ventillation and to simulate air resistance of an endogenous fire occurred in an abandoned face of a more complicated ventillation system resp., and to take measures necessary to its elimination.

REFERENCES

Kovács Gy 1972: Hydraulics of leakages. Publishing House of the Hungarian Academy of Sciences, Budapest

Ushakov K Z 1977: Spravochnik po rudnichnoy ventilatsii. Nedra, Moscow

Acta Geod. Geoph. Mont. Hung., Vol. 25 (1-2), pp. 191-202 (1990)

SOLUTIONS OF BLASTING TECHNOLOGY LESS HARMFUL FOR THE STABILITY OF SECONDARY ROCKS

G Bohus and J Földesi

Mine Working Department of the Technical University for Heavy Industry,
H-3515 Miskolc, Egyetemváros, Hungary

The authors describe a seismic method which is suitable for the determination of weathering, fractures around the drift. Weathering changes the properties of rock, the field stress around the drift and thus the support requirements, too.

A practical example is given to compare the rock stabilities and support demands in the cases of carelessly designed vs. rock protecting blastings.

Keywords: blasting; Dorog Coal Mines; mine headings; ripped rock mantle; seismic method; weathering

The stability, support requirement of mine headings (tunnels) are basically affected in addition to the known rock--mechanical conditions (depth, rock density, section and shape), by the method of breaking out the heading. Other important rock parameters (strength and flexibility) may also considerably change depending upon the method of heading. Regarding the conditions of drift-driving, a lot of investigations have already dealt with the function of the time factor but there is still relatively little information on the harmful effects of the destruction of rock surroundings during cutting. The aim of the present paper is to deal with this problem.

The adjectives "collapsible" or "non-collapsible" are often used for stand-up formations as well. In fact the rock becomes, in the majority of the cases, easily collapsible when improper breaking methods are applied. The descriptions on rock engineering generally disregard the technical conditions of drift driving (tunnelling) and the uneven surface area of the drift; although even in case of a shield type heading,

ruptures of at least 30 cm depth are formed in the remnant rock environment which can be as deep as 60 cm in case of cutting--headed shearers. The uneven surface results, on the other hand, in an uneven distribution of stress according to the law of physics, resulting finally in the formation of additional ruptures.

This is all the more true for drift driving made with the blasting method. Although by accurate drilling and by using rock-saving blasting technology, a contour well approximating the one that can be achieved by mechanical heading (sometimes even exceeding it) and fractures shorter than 60 cm are formed; in most of the cases, the blastings are performed without particular caution and planning. In such cases, an extensive destruction zone will be formed around the heading.

THE PRINCIPLE OF ROCK-PROTECTING BLASTING

Effects of blasting are intended to concentrate into a given volume of the rock to be broken, thus increasing working efficiency and reducing the non-desirable effects on the environment. When smaller rock parts are separated, the charges located inside the rock will effect, in the first approximation, the rock-parts to be cut off, although, on the basis of the well-known law of effect - counter effect, they produce fractures on the remnant rock wall that are exactly as deep as those in the displaced block. The only difference is that, proceeding backwards, the external destruction zone cannot be formed and that there is no space for loosening of the rock. Thus the ruptures resulting from blasting will be closed.

As a result of the backward effect of blasting, the stability of the newly formed rock surface will be reduced and this will result in rock spin, unexpected collapse and a shorter service life of the support structures located underground.

The simplest way of reducing the degree of backward effect, that is, reducing the length of the ruptures is to reduce the diameter of the charge. Decreasing the charge diameter does

not necessarily mean that the diameter of the blasting hole will be smaller. The peak pressure of the shock-wave resulting from blasting will be considerably lower if an empty annular space remains around the blast hole and the charge (Fig. 1). After the blasting thus performed, half of the hole mantle will remain undamaged, the new surface area of the rock will become even and relatively smooth. For the borehole location, the ratio between the front-piece (W) and the borehole interval (A) is:

$$\frac{A}{W} \approx 0.8 \ .$$

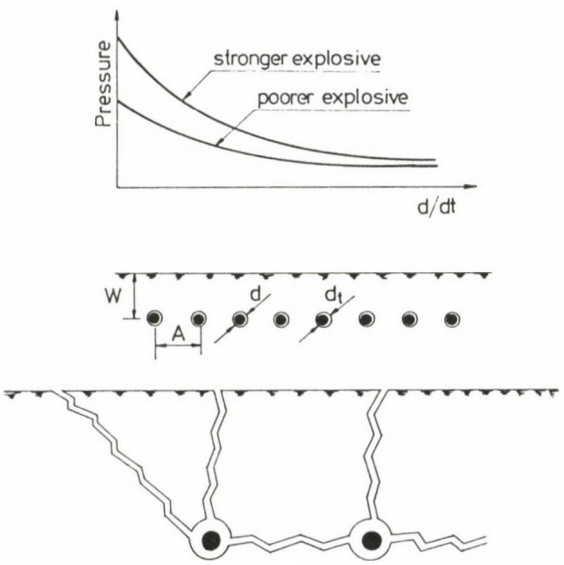

Fig. 1. Practice of rock-protective blasting

The small-diameter charges applied for blasting are designed to be expandable fitted with centralizing plastic holders (Fig. 2). An important preliminary condition of obtaining a surface of the technically necessary smoothness is an accurate drilling. With the up-to-date drilling machines it is possible to perform drilling in any direction with a

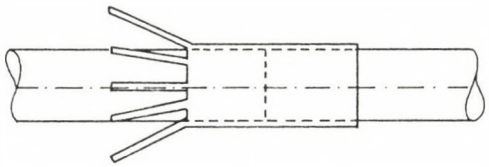

Fig. 2. Special charge for rock-protecting blasting

directional deviation less than 1^{o}. The nearer the moments of time when the charges explode are, the easier the shearing of the rock-parts between the charges will be.

The ratio between the borehole interval and the front-part is also important since, if $A/W < 1$, the front-piece of the rock will be displaced without larger deformation generating only lower stresses inside (except, of course, for the environment of the plane passing the charges). What happens then is that the rock-part between the two adjacent charges is very quickly broken through, the energy accumulated in the rock on the shearing surfaces of the separated rock blocks converts into heat and the explosion will only affect the rock parts by the expansion of the blast products remaining in the plane of fracture. In the increasingly expanding plane of fracture, the blasting gases will quickly loose power and thus their backward effect will also be lower (Bohus et al. 1983).

THE ENVIRONMENT OF A HEADING DESTRUCTED BY BLASTING

By way of an example; the water drift of 'Lencsehegy II' Mine Plant of the Dorog Coal Mines was driven with blasting technology; Swellex type anchors were used as primary support, shotcrete as final support. After the blasting, the drift section remained highly uneven, a lot of deep fractures were formed visibly in the dacite rock. To detect these fractures, a seismic method was applied.

The velocity of the elastic wave propagating in the rock depends on the type, density, porosity, texture and on the degree of weathering of the rock. In a given rock, with a given

depth of location and structure, the velocity of elasting waves depends only on how weathered the rock is and on the properties of the materials filling up the fractures. Consequently, the degree of loosening of the drift mantle can be determined on the basis of the velocity of elastic waves.

The ruptures can be of two types: original ruptures resulting from the geological effects and those formed during mining activities (mostly during cutting work). When opening cavities, fractures can, of course, be formed as a result of the increasing stresses or the fracture system can be changed. While moving away from the drift surface, the ruptures resulting from both cutting and cavity opening will become incresingly rare and at certain intervals, the original fracture system will be found.

The rock fractures prevent the propagation of elastic waves. The effect of this obstacle can be observed in the absorption and reflection of waves, as a joint result of which, the average linear velocity of propagation will be lower. To detect this, a Vibroguard 1207 type instrument by the Swiss firm Geotest was used by means of two borehole-contained, 3-component type geophones with a measuring accuracy of $\pm$ 5 percent. The results are recorded, together with the calibration signals, on paper sensitive to ultraviolet light.

Boreholes of 56 mm diameter, 4.0 $\pm$ 0.2 m lengths were drilled into the heading side to locate the geophones and holes of 40 mm diameter and 2.0 $\pm$ 0.3 m length, to locate the explosive serving to generate vibrations (Fig. 3). For generating vibration, small charge was used (0.05 kg Paxite) in order that the same hole could be used several times.

The propagation velocity of the elastic waves can be determined by the relation

$$C_l = \frac{l}{\Delta t}$$

where

l - distance between the two geophones, m;

Δt - time difference between the arrival of the two signals, s.

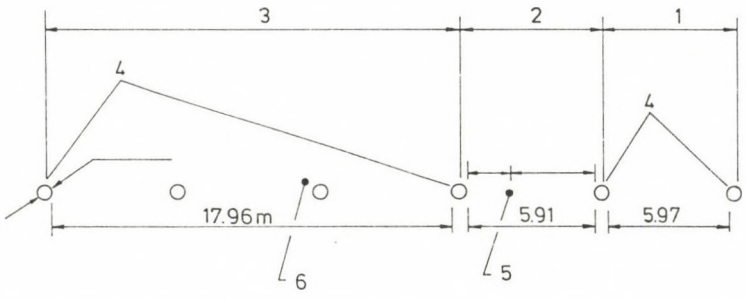

Fig. 3. Scheme of seismic measurement performed in the water heading of 'Lencsehegy II', Dorog Coal Mines. 1 - 1st measuring section, 2 - 2nd measuring section, 3 - 3rd measuring section, 4 - measuring holes, 5 - blasting hole for the 1st and 3rd measuring sections, 6 - blasting hole for the 2nd measuring section

The temporal difference between the arrivals of the seismic waves was determined as shown in Fig. 4.

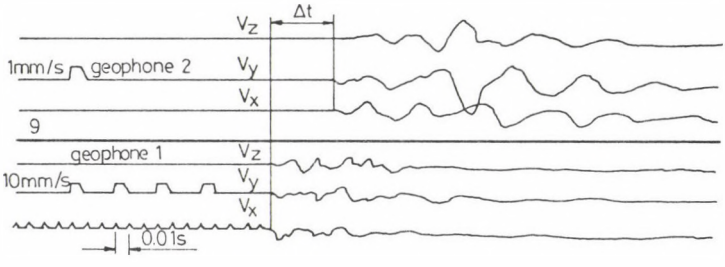

Fig. 4. Determination of time differences Δt

The geophones were located in 0.5 m intervals moving away from the drift wall to perform measurements, the result of which have been summarized in Table I. As the values of C_1 obtained do not show a difference greater than $\pm$ 10 percent in the same depth calculated from the surface of the drift which can result in an error of $\pm$ 5 percent in the record, the same when Δt is determined, $\pm$ 2 percent in the actual 1 interval between the geophones due to the inclination of the holes, therefore an arithmetical averaging of the data can be made.

Table I. Measuring results for the determination of the propagation velocity of sound

No. of measurement	l m	Δt s	C_l m/s	Distance of geophones from drift surface m
1.1	5.97	0.0020	2980	0.5
1.2		0.0017	3510	1.0
1.3		0.0015	3980	1.5
1.4		0.0012	4970	2.0
1.5		0.0012	4970	3.0
1.6		0.0012	4970	4.0
2.1	5.91	0.0020	2960	0.5
2.2		0.0019	3110	1.0
2.3		0.0017	3480	1.5
2.4		0.0013	4550	2.0
2.5		0.0013	4550	3.0
2.6		0.0013	4550	4.0
3.1	17.96	0.0060	2990	0.5
3.2		0.0056	3210	1.0
3.3		0.0042	4280	1.5
3.4		0.0040	4490	2.0
3.5		0.0040	4490	3.0
3.6		0.0040	4490	4.0

These data are found in Table II.

Both the measuring data and Fig. 5 clearly show that, as a result of blasting and cavity opening the rock mantle will be fractured in a thickness above 1.5 m but not exceeding 2.0 m, and the original ruptures will also open up and expand. The most probable value is:

$$l_{rep} = \frac{1.5 + 2.0}{2} = 1.75 \text{ m.}$$

Table II. The average sound velocities and the factor of rupturing

Distance of geophones from drift surface m	C_l, m/s	R
0.5	2980	2.46
1.0	3230	2.09
1.5	3910	1.43
2.0	4670	1.00
3.0	4670	1.00
4.0	4670	1.00

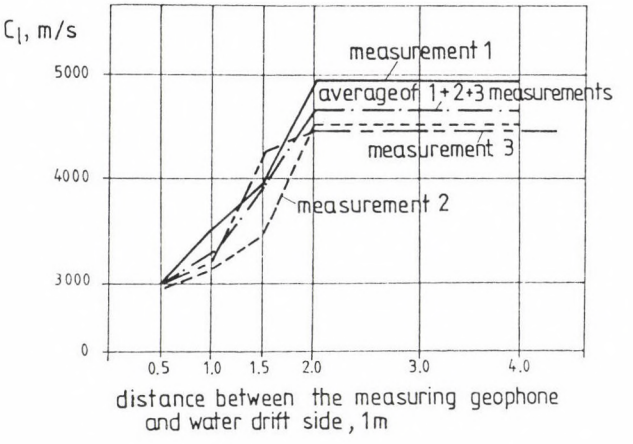

Fig. 5. Propagation velocity of the elastic wave vs. distance calculated from the drift surface

For the explosion, charges of 30 mm diameter are used (r_o = 0.015 m) and thus

$$l_{rep} = \frac{1.75}{0.015} = 117\ r_o\ .$$

New ruptures cannot expand to cover such a distance, the

expansion of the existing ones is only possible.

EFFECTS OF A RIPPED ROCK MANTLE

A change of the original fractures of the rock has a direct effect on the selection of support structures. In the present case, it is only reasonable to build in rock bolts of an active length of above 1.75 m.

The rock parameters affecting dimensioning of the support will also change as a result of rupturing. Let us study some of them.

The modulus of elasticity of the rock (E) will change according to the following formula:

$$\frac{E_o}{E_1} = \left(\frac{C_{1_o}}{C_{1_1}} \right)^2 ,$$

where index o is valid for the rock range of the original ruptures, index 1 for that ripped with blasting. The expression

$$\left(\frac{C_{1_o}}{C_{1_1}} \right)^2 = R$$

can be regarded as the factor typical of the ruptures, the values of which can also be found in Table II (Rzhevsky et al. 1970).

Figure 6 shows the change of the values of C_1 and R extrapolating the curves up to the rock surface, where

$$C_1 = 2850 \text{ m/s} \quad \text{and}$$
$$R = 2.70 .$$

The value of C_1 was also determined under laboratory conditions and it was found to be

$$C_{1,\ \text{labor}} = 4040 \text{ m/s} .$$

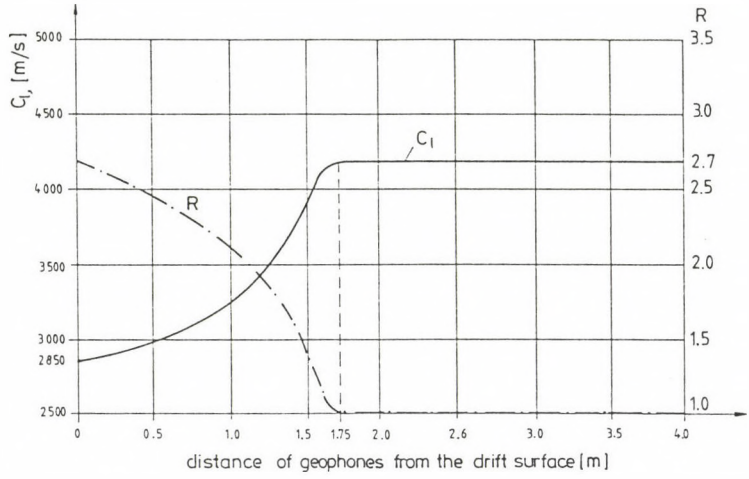

Fig. 6. Change of the propagation velocity of sound (C_l) and the rupturing factor of the rock (R) as moving away from the drift surface

This velocity of propagation indicates that the sample taken from the blasted reserve was more destructed than the original rock material (where C_l = 4670 m/s). The rupturing factor typical of the rock sample is:

$$R_{labor} = \left(\frac{4670}{4040}\right)^2 = 1.\bar{3}4 \ .$$

It is somewhat more complicated to determine the propagation velocity of the transversal (shearing) waves but it can be taken from a sufficiently characteristic seismogramme. The propagation velocity of transversal waves is in an elastic, isotropic medium:

$$C_t = \frac{E_{din} \cdot m_{din}}{2\varrho(m_{din}+1)} \ ,$$

the dynamic Poisson's number:

$$m_{din} = \frac{2(C_l^2 - C_t^2)}{C_l^2 - 2C_t^2}$$

and the dynamic modulus of elasticity:

$$E_{din} = \varrho \cdot C_t^2 \frac{3C_l^2 - 4C_t^2}{C_l^2 - C_t^2}.$$

By determining the value of C_t from the seismogramme, knowing the rock density (ϱ) from laboratory measurements, the dynamic parameters have been included in Table III (Research Report 1987).

Table III. The transversal wave velocity with dynamic rock parameters

Distance of geophones from drift surface m	C_t m/s	m_{din}	E_{din} MPa
0.5	1800	4.7	32 665
1.0	2100	7.2	44 098
1.5	2450	5.7	61 557
2.0	2980	3.3	88 964
3.0	2980	3.3	88 964
4.0	2980	3.3	88 964

Thus in the fractured rock, the modulus of elasticity will considerably decrease, nearly linearly with the increase of the rupturing factor R. Poisson's number slightly increases and changes rhapsodically but the increase at the surface of the drift is not too high. It follows logically from all the above that the ruptures in the environment of the drift in the elastic range have an effect on the rock stresses as well: in the drift mantle of lower modulus of elasticity, lower stresses will be generated. The smaller the thickness of the destroyed mantle and the greater the destruction of the rock mantle of V thickness is, the greater the above reduction will be.

The aim of the above example is to demonstrate the effect of the blasting technology applied for heading on the rupturing

of the drift environment as well as on its other properties and finally the support requirement.

REFERENCES

Bohus G, Horváth L, Papp J 1983: Industrial Blasting Technology. Technical Publisher, Budapest

Research Report by the Mine Working Department of the Technical University for Heavy Industries 1987: Qualification of the support of main water drift driven in dacite, support requirement of the escaping drift to be driven in Mine Plant 'Lencsehegy II'. Miskolc

Rzhevsky V V et al. 1970: Metodika seismicheskogo opredeleniya treshchinovatosti massivov gornikh porod na karerakh s tselyu otsenki ikh vzrivaemosti. Moskva

Acta Geod. Geoph. Mont. Hung., Vol. 25 (1-2), pp. 203-219 (1990)

PRELIMINARY ESTIMATE OF THE ENVIRONMENTAL EFFECTS OF MINING BLASTINGS AND TECHNOLOGICAL SOLUTIONS FOR THEIR REDUCTION

G Bohus and J Földesi

Mine Working Department of the Technical University for Heavy Industry,
H-3515 Miskolc, Egyetemváros, Hungary

When mining solid rocks by blasting undesirable environmental effects (seismic and fragmentation effects, air blasts, toxic gas und dust development) are to be taken into account. In case of a given blasting technology efforts should be made to minimize damaging environmental effects or to keep their values under a given level. All these measures, however necessitate the pre-estimate of damaging effects.

In the present article the results of investigations carried out in the Mining Department of the University for Heavy Industry are disclosed, on the basis of which the seismic effect and air blast of surface blastings, as well as degree of fragmentation effect may be estimated. Attention is called by the authors to the technological parameters also by the modification of which the degree of damaging effects can be reduced.

Keywords: air blast; blasting; length of stemming; seismic effect; vibrational velocity

1. INTRODUCTION

In Hungary like in any other part of the world, cutting of high-strength rocks is performed with blasting. Blasting works often involve adverse environmental effects (seismic-, air--blast-, fragmentation effects, toxic gas and dust formation). The effects of blasting are particularly harmful in the surroundings of surface mines. A human body feels e.g. vibrations of very low intensity to be of high intensity.

Therefore it is important that in the vicinity of the faces where blasting technologies are applied, the vibration, air-blast and fragmentation effects be accurately and realiably calculated.

The present paper reports on results of blasting research performed at the Mine Working Department of the Technical

University for Heavy Industry which are important for the protection of the environment of blasting spots.

The expected velocity of vibrations generated by the blastings, the length and composition of the stemming affecting the air-blast as well as the conditions of the fragmentation are studied. Relations are presented which enable a reliable calculation of the expected non-desirable effects.

2. PRELIMINARY ESTIMATE OF THE SEISMIC EFFECTS RESULTING FROM BLASTING

It can be decided on the basis of the velocity of vibrations generated by blastings whether a blasting may be damaging for the environment. In the international practice, the velocity of the vibration is determined from Koch's relation:

$$V = a(l/\sqrt{Q})^{-b}, \qquad \text{mm/s} \qquad (1)$$

where:

a - depends on the conditions of blasting and the geological build of the vicinity of the quarry;

l - the distance between the blasting and the object to be protected, m;

Q - mass of the charge exploded (in some countries, it means the mass exploded in one firing, in Hungary it means that exploded in 100 ms, in other places, that exploded in one delay phase), kg;

b - is in the range from 1.0 to 1.4.

In practice, the values of a and b are determined for each individual mine on the basis of several measurements by regression analysis.

The values a and b determined in some surface mines of Hungary are shown in Table I together with quality parameters of regression. The data have been studied in three versions. First, the change of the distance dependent vibration velocity was studied vs. mass of the charge exploded simultaneously (Q_o), in the second step, vs. the mass exploded during 100 ms

Table I. Parameters of the regression functions determined by Koch's-formula and their quality indices

$1/\sqrt{Q}_i$	Parameters	Plants				
		Bélapátfalva	Nagyharsány	Tarcal	Beremend	Keszeg
$1/\sqrt{Q}_o$	a	31.4	85.57	68.04	26.99	33.92
	b	-1.12	-1.29	-1.16	-1.23	-0.85
	r	0.9178	0.8143	0.7513	0.9469	0.6757
	DV	1.30	2.58	1.27	1.51	3.62
	DV %	60.28	47.77	42.97	37.35	71.83
$1/\sqrt{Q}_{100}$	a	78.47	77.18	43.09	45.44	55.90
	b	-1.20	-1.14	-0.85	-1.24	-0.84
	r	0.8897	0.7935	0.6589	0.9575	0.6457
	DV	1.49	2.70	1.45	1.35	3.75
	DV %	69.31	50.08	48.98	33.50	74.41
$1/\sqrt{Q}_{deg}$	a	70.15	175.37	139.25	45.44	209.92
	b	-1.12	-1.16	-1.05	-1.24	-1.19
	r	0.9121	0.9471	0.9259	0.9575	0.851
	DV	1.34	1.43	0.72	1.35	2.58
	DV %	66.23	26.42	24.60	33.50	51.19

(Q_{100}) and in the third step, vs. the mass of charge per one delay phase (Q_{deg}). On the basis of the quality parameters, the most reliable way of determining the vibration velocity is vs. the mass of charge per one delay phase, when the correlation coefficient r is the highest. The preliminary estimate of the velocity of vibration is the least reliable from Q_{100}.

By plotting the results in a coordinate system V – $1/\sqrt{Q}_i$ with Q_i being Q_o, Q_{100} or Q_{deg} – it is evident that a relation better than Koch's formula can be found. For the next test, the parameters and quality indices of the relation

$$V = a\, e^{-b(1/\sqrt{Q}_i)}, \quad mm/s \qquad (2)$$

have been determined from the data (Table II).

Table II. Parameters of regression functions determined by the exponential function and the quality indices

		Plants				
$1/\sqrt{Q_i}$	Parameters	Bélapátfalva	Nagyharsány	Tarcal	Beremend	Keszeg
$1/\sqrt{Q_o}$	a	15.07	32.91	11.41	24.15	15.74
	b	-0.17	-0.20	-0.08	-0.34	-0.10
	r	0.9465	0.8518	0.7339	0.9449	0.7272
	DV	1.08	2.35	1.29	1.53	3.39
	DV %	49.96	43.54	43.85	37.99	67.39
$1/\sqrt{Q_{100}}$	a	19.61	29.68	8.04	25.48	14.39
	b	-0.12	-0.16	-0.04	-0.24	-0.05
	r	0.9255	0.8414	0.5571	0.9591	0.6874
	DV	1.26	2.42	1.60	1.32	3.59
	DV %	58.62	44.91	54.08	32.87	71.30
$1/\sqrt{Q_{deg}}$	a	16.81	28.47	10.09	25.48	25.72
	b	-0.09	-0.08	-0.03	-0.24	-0.07
	r	0.9590	0.9568	0.9338	0.9591	0.8757
	DV	0.95	1.30	0.69	1.32	2.39
	DV %	43.90	24.16	23.30	32.87	47.41

A comparison of the data in Tables I and II shows that an exponential function gives a better and more reliable relation. The value of the correlation index is here the highest vs. the mass of the charge for one delay phase, too. In a plot of the functions $V = f(1/\sqrt{Q_i})$ the curves calculated from Q_{deg} run on the top (Fig. 1). That means that for a given value of $1/\sqrt{Q_i}$ the highest vibration velocity is expected from the relation determined vs. $1/\sqrt{Q_{deg}}$ but this gives the expected vibration velocity with the lowest scatter.

From the point of view of the environmental effect of

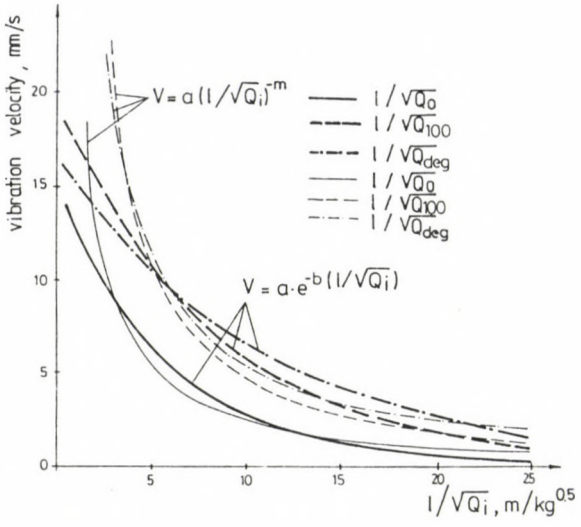

Fig. 1. Velocity of vibrations generated by blastings vs. specific distance

blastings, an important question is how the frequency of the vibrations modifies the velocity of the expected vibrations. The effect of the frequency has been examined with a multivariable-type regression analysis.

2.1 The multivariable vibrational velocity function and its partial correlation indices

It is possible by using the partial correlation coefficients to clarify the effect of all the data recorded with seismic measurements on the vibration velocity. For the most important parameter the partial correlation coefficient is nearest to General Blasting Safety Regulations (1987).

The multivariable function has the form

$$V = a_1 + b_1 x_1^{C_1} + b_2 x_2^{C_2} + \ldots + b_n x_n^{C_n} \qquad (3)$$

where:

- a_1, b_1, b_2, ... b_n and c_1, c_2, ... c_n are constants;
- x_1, x_2, ... x_n are variables.

Relation 3 is e.g. for the mine of Beremend the following:

$$V = -1.17 + \frac{41.68\sqrt{Q_{deg}}}{l} - 0.0031\ f^2 + 0.036\ f \qquad (4)$$

where f - is the vibration frequency, Hz
r - 0.9730 (total correlation coefficient)
DV = 1.13 mm/s
DV% = 28.17

$r(1/\sqrt{Q_{deg}}) = 0.9702$
r(f) = 0.5500. (partial correlation indices)

Relation (4) shows that with the increase of f, V decreases i.e. in case of higher frequencies the mass of charge per one delay phase can be higher or a relatively large charge can be exploded even at a shorter distance. On the basis of the partial correlation coefficients the vibration velocity is a function of $1/\sqrt{Q_{deg}}$ and of the vibration frequency.

2.2 Effect of the distance on the vibration velocity

There are both domestic and foreign observations showing that moving away from the location of blasting, the seismic effects got stronger. The relation of the distance on the vibration velocity was studied at Bélapátfalva mine. The form of the function used was:

$$V = al^2 + bl + c\ . \qquad (5)$$

The regression function and its quality parameters are

$$V = 4 \cdot 10^{-6}\ l^2 - 1.36 \cdot 10^{2}\ l + 11.91 \quad mm/s \qquad (6)$$

$$r = 0.9369;\quad DV = 1.16\ mm/s;\quad DV\% = 54.13\ .$$

The measured points and the regression function are shown in Fig. 2. At the plant examined, the vibration velocity with l = 1300 ... 1400 m is the same as at a distance of 2300 ... ... 2400 m in spite of the fact that the vibration velocity

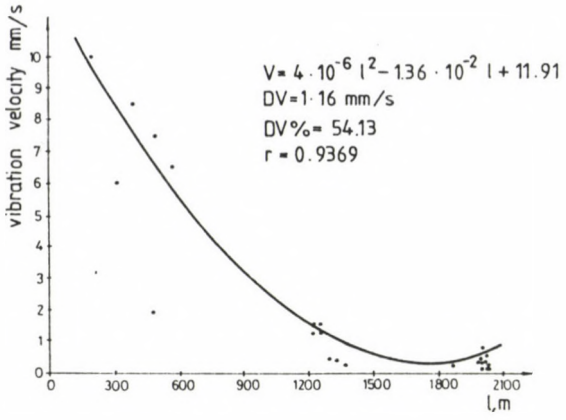

Fig. 2. Vibration velocity vs. distance in case of blastings performed in the Bélapátfalva quarries

generally decreases with increasing distance, due to energy scattering. Figure 2 also shows that $V < 1$ mm/s. But after all, how can it be explained that this low velocity causes sometimes problems? The explanation is that the frequency of the vibration is reduced as a result of the frequency-filtering effect of the soil, into the eigen frequency band of a human body and thus a resonance is obtained even in case of vibrations of low intensity. The attenuation time of the low-frequency signals is longer and the long period vibration reduces the threshold of the uncomfort feeling.

2.3 Conclusions from the measurement results

The following major consequences can be drawn from these investigations:

- the expected value of the seismic velocity can be reliably determined in function of the mass of the charge for one delay phase;
- at higher frequencies, the expected vibration velocity is lower, thus, as far as possible, vibrations of high frequency should be generated (high-frequency vibrations require small charges and accurate blasting caps of a large number of

stages and of the millisecond type);
- the expected velocity of the vibration can be estimated with a simple exponential relation more accurately than with Koch's formula;
- at a long distance from the location of blasting, the vibration velocity may increase again in certain conditions but in the majority of the cases it is of a very low intensity.
- no common seismic relation can be given for all the quarries operating under different geological conditions. For blasting spots at unfavourable places, the locally valid seismic relation should be found on the basis of measurements;
- in case of $1/\sqrt{Q_{deg}} \geq 40$, the velocity of the vibration is ≤ 2 mm/s. It means that there is no need for seismic measurements since the vibration velocity of 2 mm/s is harmless for buildings and other structures as well as for living organisms.

3. DEPENDENCE OF AIR-BLASTS ACCOMPANYING CUTTING EXPLOSIONS ON STEMMING PARAMETERS

One of the non-desirable effects resulting from the blastings applied in the mining cutting methods is air-blast. In order to reduce the effect of air-blast, the blasting holes are stemmed. In the surface and underground blastings, a great number of stemming methods are applied (sand, clay, drill flour and breakstone, sand in foil-hose or water etc.) which seal the blasting holes to a different degree. Air pressure measurements are the simplest way of deciding which of the stems of different structure and length makes the blasting chambers closed and to what degree. A practical benefit of these air pressure measurements is that they allow a qualification of the blasting technologies, since if the harmful environmental effects of the blasting are low, a larger portion of the explosive filled in the blasting holes ruptures the rock. In case of improperly stemmed charge chambers, almost 20 percent of the energy applied for useful work generates a shock-wave in the air which can be observed in the form of sound-blast.

When heading is performed with the blasting method the volume of toxic gas content is also higher if improperly stemmed charges are exploded, in addition to air-blast and to damaging of the support structures.

The air-blast effect of explosions was studied for individual blast holes and for industrially applied technologies. (Air-blasts were measured with a Vibroguard 1207 D type instrument manufactured by the Swiss firm Geotest and procured with the support of the State Office for Technical Development. A channel of the two-channel device is connected to the microphone of the American firm Sinco which measures static and dynamic air-pressure in a range of 2 ... 1000 Pa, with an accuracy of 5 percent in the frequency range of 1 ... 360 Hz.)

3.1 Properties of air-blasts accompanying explosions

In case of charges freely exploded in the air, the propagating shock-wave has a supersonic velocity up to a distance corresponding to 20 ... 30 charge diameters. If the distance is more than 20 ... 30 charge diameters the propagation velocity of the shock-wave is about 330 m/s depending on the humidity and temperature of the air. This shock-wave is of a very steeply rising front and has a very short decay time (Fig. 3). In the vicinity of blastings, the shock-wave is observed in the form of noise. The intensity and the value of overpressure formed in the air largely depends on the conditions of blasting. In case of cutting-type blastings, the air-pressure value is largely affected by the closedness of the charge chamber (Fig. 4). In case of charges exploded without stemming, much higher values of the air-pressure can be expected than in case if the charges are fitted with the proper stemming.

3.2 Dependence of air-pressure during blastings on the specific length of stemming

Figure 3 shows that in case of blastings, blast of a very steep wave front propagates in the air. This overpressure with a steep wave-front has a very short decay time.

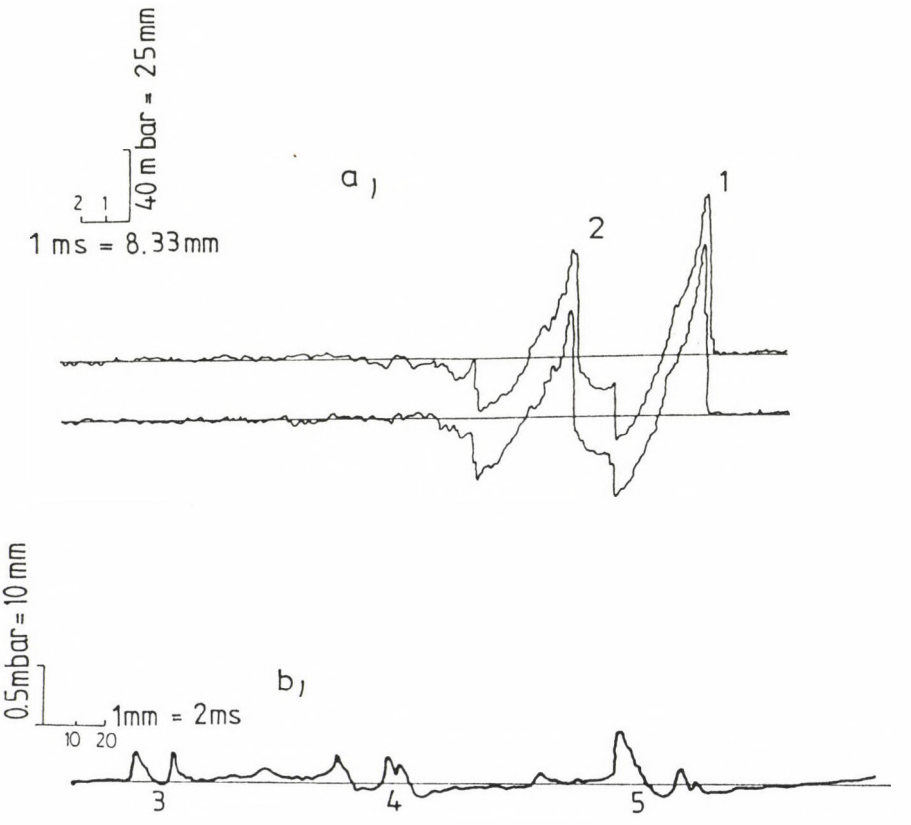

Fig. 3. a) Shape of the air-pressure curve in case of blasting 200 g ANDO at a height of 2 m from ground level (Distance between the location of blasting and that of the measurement is 5 m. For the air-pressure measurement, a Kistler 4041 A type instrument was applied with a measuring range of 0 ... 2 bar). 1 - peak value of the air-blast; 2 - wave reflected on ground,
b) Diagram of one of the blastings performed at the Nagykőmázsa Plant of the Cement and Lime Works. (Charge diameter: 90 mm; No. of hole series: on the roof 3, on the bottom 1, explosive applied ANDO and Paxite, length of stem: 3.0 ... 3.5 m borings and breakstone; on the bottom 1.2 m foil-contained borings; interval between the sites of blasting and measurement: 430 m). 3 - 1st and 2nd hole series; 4 - 3rd hole series; 5 - bottom holes (MS 1 ... 5 blasting cap, RK-3 blasting cap, RK-4 blasting cap)

The specific peak pressure ($p = \Delta p/l$) changes has been analyzed vs. specific stemming length ($l_f = L_f/d_r$). (Δp is the peak value of the air pressure measured in Pa; L - distance

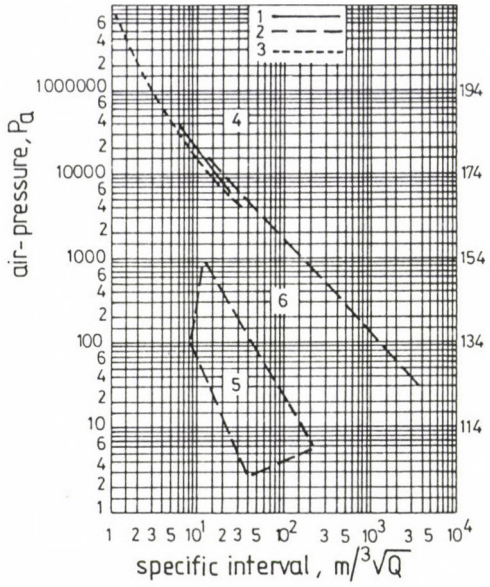

Fig. 4. Value of the air-pressure generated by blasting vs. specific interval. 1 - CERCHAR measurement result; 2- measurement results obtained by the Bureau of Mines; 3 - measurement result obtained by Berger--Viard (Tolite); 4 - blasting without stem; 5 - result of air-blast due to explosion performed on a plant-scale in surface mine, according to the measurement by the Bureau of Mines; 6 - stem-provided blasting

between the locations of blasting and measurement, m; L_f - length of stemming, m; d_r - diameter of the blasting hole, m). It was necessary to use the specific peak pressure and specific stemming length because the measurements were made at different distances, in different rocks and using different blasting technologies.

If the air-blast results from surface mines are plotted in a coordinate system p - L_f/d_r (Fig. 5), then the specific regression function has the form

$$p = a\,(L_f/d_r)^b + c\,, \qquad Pa/m\,. \tag{7}$$

The parameters and quality indices of relation (7) are in case of blastings performed in surface mines in Hungary: a = 6.457;

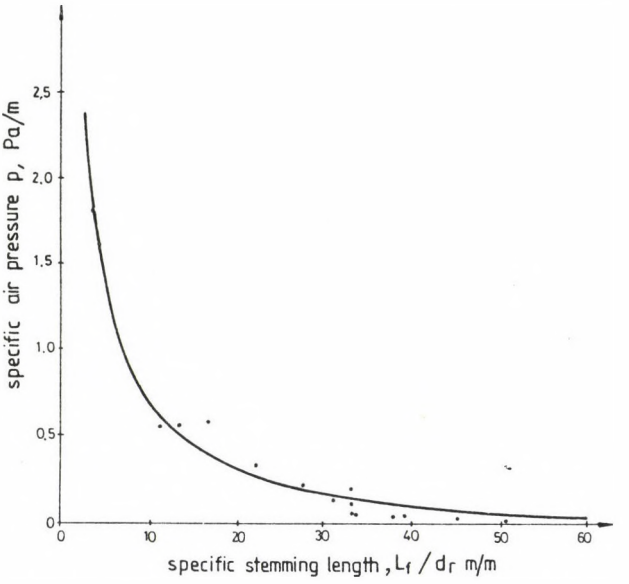

Fig. 5. Change of specific air pressure in the function of specific length of stemming

b = -0.899; c = -0.132; r = 0.9894; D_p = 0.077 Pa/m; D_p% = 22.17.

The quality parameters of the correlation show that the specific pressure can be accurately calculated in the function of the specific stemming length. If $L_f/d_r \geqq 20$, there is no air-blast of a dangerous intensity.

In surface mines it is of course important to know the stemming lengths which ensure air-blasts of harmless intensity. Depending on the explosive, the rock and the density of the stemming applied no harmful air-blast should be expected if the length of stemming is

$$L_f \geqq 1.12 \frac{W \cdot D}{C_l} \cdot \sqrt{\frac{\varrho_{ra}}{\varrho_f}} \quad , \quad m \qquad (8)$$

where W - the length of the front-piece, m; D = detonation velocity of the explosive, m/s; C_l - the velocity of sound propagating in the rock, m/s; ϱ_{ra} - density of explosive, kg/m^3; ϱ_f - stemming density, kg/m^3.

The stemming lengths from the analytical relation (8) and from the regression relation (7) are almost the same.

In addition to the determination of the stemming length, the selection of the stemming material is also important. The laboratory and pilot-plant tests conducted in Hungary and abroad clearly prove that it is practicable to apply stemming formed from breakstone of different grain sizes and borings. The stemming has the greatest internal angle of friction if 60 ... 65 percent breakstone and 35 ... 40 percent borings is in the stemming. The maximum grain size of the breakstone should not exceed 20 percent of the borehole diameter. Grain size of borings should range from 0 to 5 mm.

The investigations pointed out that the water-content of the stemming reduces the resistivity of stemming. In case of sand-stemmings filled in plastic foil for bottom holes, the air-blast expected is twice as strong as in case of stemmings without foils.

In case of underground blastings, the air-blast can considerably be reduced if sand stemming filled up with compressed air is applied instead of clay. The effect of the air blast can be further reduced by the application of parallel-cut holes instead of key-cut ones.

4. THE FRAGMENTATION EFFECT IN ROCK CUTTING WITH BLASTING METHOD

With a properly planned and carefully implemented blasting, the mined deposit does not move away too far from the location of blasting. As the structure of the rock is not always known, it is inhomogeneous, the front-part changes and errors are made during the drilling and blasting work, the distance of throw of the rock pieces may be very large. The great fragmentation effect is particularly dangerous in the vicinity of surface mines. We consider now how the conditions for a non-desirable degree of fragmentation can be obtained in surface mines.

The most likely locations of fragmentation are the places

in front of the stemming and in the front-piece reduction zones (places of collapse).

The conditions for fragmentation can be summarized on the basis of Fig. 6 as follows:

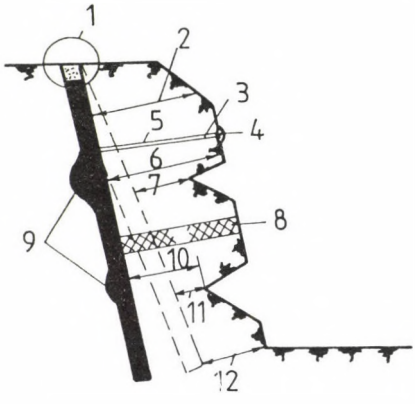

Fig. 6. Conditions of formation of the fragmentation effect in surface mines. 1 - L_{fi} small, 2 - W_i small, 3 - air, 4 - loose lump of rock, 5 - open fracture, 6 - large charge diameter, 7 - small front-piece, 8 - rock of low strength, 9 - cavity, d_r - large, 10 - small front-piece, 11 - small front piece and rock slide-out, 12 - inaccurate drilling

1. $L_{fi}/L_f \ll 1$; $d_i = d$ (the stem is too short);
2. $W_i/W \ll 1$; $d_i = d$ (the so-called local front-piece is small);
3. $E_i/E \ll 1$; $d_i = d$ (due to inaccurate drilling, the charge is $W_i = W$ concentrated);
4. $d_i/d \gg 1$; $W_i = W$ (charge diameter increases);
5. $d_i/d \gg 1$; $W_i < W$ (charge diameter increases, the local front-piece is smaller);
6. $x/W \ll 1$; $W_i = W_{air}$ (loose lump of rock in front of an open rupture in the face);
7. $W_i/W = 1$; $d_i/d = 1$; $\sigma_{ki} \ll \sigma_k$ (strength of rock reduced);

where L_{fi}, W_i, E_i, σ_{ki} - length of stemming at the rupture formation, the front-piece, borehole interval, value of charge diameter and the breaking strength of rock; L_f, W, E, D, x, σ_k - according to the technology scheduled: stemming,

front-piece, borehole interval, value of charge diameter, size of the loose lump of rock in the face, breaking strength of the rock.

Thus the distance of fragmentation is basically determined by the relation of the front-piece to the charge diameter. If the requirements found in practice are met, the quotient W/d ranges from 25 to 60. The fragmentation becomes dangerous if $W/d < 20$.

If the above conditions are not present, the distance of the fragmentation of blastings performed in Hungarian surface mines can be calculated with the following relation:

$$R = 13.57 \frac{d^{1.33}}{W} \sqrt{\frac{\varrho_{re} Q}{m}}, \quad m \tag{9}$$

where d - diameter of the blasting hole, m; W - size of front-piece, m; ϱ_{ra} - density of filling of explosive, kg/m^3; Q - specific energy content of the explosive J/kg; m - factor of proximity.

A dangerous fragmentation can be avoided with the following measures:

- before planning the blasting, the face to be blasted should be measured with instruments in order to gain information on possible under-collapses and front-piece reduction;
- the blasting holes should be drilled accurately since a deviation of 1 ... 2^o from the drilling direction results in a change of 1 ... 2 m in the front-piece in case of high mine walls (30 ... 40 m);
- the weak points of the rock should be found (in order to recognize the cavities, open ruptures before filling, the drilling record should be kept accurately; the rupture system of the rock should be measured and the direction of mine working as well as the slope of the front should be adjusted acorrdingly);
- the length and composition of stemming should be determined according to the previous chapter;
- in case of a delayed blasting, millisecond-type blasting caps

should be applied if possible, in order to avoid great splinter effect of the charges exploded later due to the cut-off resulting from the previously exploded charges.

5. SUMMARY

From the point of view of environmental effects resulting from rock cutting with the blasting method, the preliminary estimation of the intensity of seismic vibrations, of the air--blast and of the fragmentation effect is an important task for environmental protection. The present paper provides relations suitable for preliminary calculation of these parameters and it also deals with the way of limiting the non-desirable effects.

ACKNOWLEDGEMENTS

Hereby we express our thanks to our colleagues dr. Z Buócz and L Mészáros, members of the Mine Working Department, for the computer processing of the measured data. Parts of the data have been provided by the Instrumentation and Measuring Technology Service of the Hungarian Academy of Sciences, the Central Mining Development Institute and the Research Department of the Mecsek Coal Mines. We should like to express our thanks for their assistance.

REFERENCES

Anderson D A, Ritter A P, Winzer S R 19 : A Method for Site--Specific Prediction and Control of Ground Vibration from Elasting (Martin Marietta Laboratories, 1450 South Rolling Road, Baltimore, MD 21227)

Chironis, Nicholas P 1983: Back Yard Blasting on the Quict. Coal Age/June

Dangreaux J, Gagniere C 1981: Quelques aspects des methodes d'exploitation des carriéres. Annales des Mines, Mars--avril

Földesi J 1988: Blasting Technology for Mining II. (Manuscript) Educational Publishers, Budapest

Investigation report on the regression analysis of seismic effect of blastings performed in the quarries of the Cement-

and Lime Works 1988. Technical University for Heavy Industry, Miskolc, Mine Working Department

Report by Mining Supervision 1987: General Blasting Safety Regulations. Issue 3, Vol. 2.

Tseytlin Ya I, Smolin N I 1981: Seizmicheskie i udernie vozdushnie volni promishlennikh vzrivov, Moscow, "Nedra"

Ferenc Martos

1918-1989

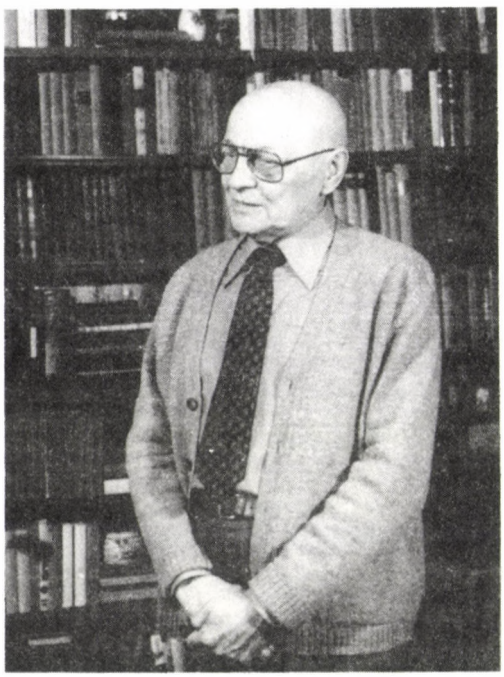

At the time when we celebrated his 70th birthday, and in the last volume of Acta we published his short curriculum vitae we did not expect that in a very short time we have to return to his person again to commemorate his activity as editor-in--chief of the journal. He spent a few years in this position, but did his best to increase the scientific level and to ensure continuous publication. One of his greatest efforts is just the present issue in which investigations on mine hazards and environmental damages are summarized. He followed with interest the publication till the very last days, organized future authors, gave advices for better presentation, could be rough upon too lengthy texts - so all authors in this issue owe him somewhat

for the merits of the papers. His activity, however, was not restricted to this: he looked for support, organized future issues, made connections with the European Association of Scientific Editors closer, and was open-minded for all ideas which aimed at an improvement of Acta.

One of his last publications deals with natural sciences during the French Revolution. In this essay he has shown the effects of the developments in France on science in Hungary, but he did not forget to mention that influences were mutual: the Mining Academy in Selmec-Schemnitz-Banska Stiavnica was taken as example when the similar French institution was established. This is characteristic for his activity: he was a European humanist, but at the same time he lived in the reality of a Central European country (as symbolized by the name of the site of the Academy in three different languages) and spared no time to emphasize the importance of a better knowledge of its mineral resources and generally, of the geologic-tectonic construction of the area.

We think that his best monument is on the pages of this issue for which he worked till his last days.

J Somogyi and J Verő

F P AGTERBERG and C N RAO eds: Recent Advances in Quantitative Stratigraphic Correlation Techniques. International Symposium Papers. Hindustan Publishing Corporation, Delhi, 1988, 192 pp.

This is the proceedings of a meeting held at Kharagpur, India as a formal terminating event of IGCP Project 148 in 1983. The meeting rose the interest and played an important role in dissemination of quantitative stratigraphy.

The book consists of four parts.

Part I deals with statistical methods and their application to stratigraphy. Agterberg F P developed a maximum likelihood method for estimating the age of chronostratigraphic boundaries expressed on the "absolute" scale. A Jurassic time-scale is given as an example. Watson G S discussed the methods required to display and analyse two- and three-dimensional unit vectors. He wanted to show users of statistical methods how they can conduct in their computer numerical experiments which will give them real insight into their data and the methods. I am afraid that this elegant introduction will prove to be too high for beginners and few for graduates. Qirui Zhang reviewed Fischer's and Zhang's segmentation methods. The methods don't meet traditional phylosophy of stratigraphic classification and their value in practical geological problem solving has not yet been proved. Rao S V L et al. after giving a short inventory of some geostatistical terms compiled several tables and figures to portray uni- and two--dimensional variability of Landsat imagery.

In the second part Metzger E P and Brower J C employed cluster analysis and lateral tracing to quantify assemblage zones for Lower Cretaceous microfossils. The isochrones crossing each other are a terrorist's action against geologists' and even human mind and clearly indicate the measure these methods can be applied in real problems. However biostratigraphic fidelity introduced by the authors equalling the percent of occurrences of a species i within a zone j may be a useful indicator.

Ghose B K and Jaiprakash B C analysed twelve DSDP holes from the Indian Ocean. He transformed the autocovariance function of some Foraminifera abundances and detected 4.5 cycles and reconstructed paleoclimatical (temperature) curve of the area. van Hinte J E and Wise S W in a very informative communication summarized the objectives and main findings of Leg 93 of DSDP. Rubel M using his quantitative method was able to reconstruct datum planes in Edwards' hypothetical data set. Westermann G E G estimated the duration of Jurassic stages based on averaged and scaled subzones and compared the results to previous estimations. In some points Brower's J C informations on quantitative biostratigraphy need correction. For example the reader may believe that in one of my 1977 papers I advocate multidimensional integer kriegeing (MIK) for sequencing. Being the author, I am sure MIK is suitable for plotting vertical lithoprofiles.

Part III is for quantitative lithostratigraphy. Casshyap S M et al. gave a detailed statistical analysis of interrelationships of stratigraphic and lithologic variables in Permian fluviatile coal measures. They detected differences in net subsidence, fluvial regime and stream channel pattern. Griffiths C M worked on recognition of hand specimen lithology using acoustic, gamma and neutron porosity logs measured in North Sea wells. The numerical lithologies had only rough correspondence to hand specimen lithology and depositional environment. In a well founded paper, Niichi Nishiwaki succeded in explaining Pleistocene Osaka Bay sedimentation by a two factor model of which the first is climate and the second is block tilting of the area. Rao C N et al. studied hidden periodicities of the energy index in the middle proterozoic Vempalle Formation, India. A Markov process

or a second order autoregressive process can be fitted to the data and the study of the spectrum revealed two periodicities of different wavelength. Schwarzacher W's paper is on possible causes of complex cycles in carbonate sequences. The 100 k.a. periodicity found was related to Milankovich-Bacsák cycle and an extraterrestrial cause. Mukherjea A et al. analysed graphic plots of depth versus percentages of heavy mineral assemblages using concepts of heavy mineral stability order and energy sequence. In a study by Syed H Akhter et al., carbonate formations from two different and widely separated basins have been taken for termoluminescence analysis. Each lithounit was found to have a characteristic TL glow pattern.

Part IV is devoted to traditional biostratigraphy. Tapaswi P M made an attempt to subdivide Upper Cretaceous rocks on the basis of their serpulids by the traditional assemblage zones. Tripathi A identified some sporogenera from Indian formations.

The book is heterogenous. In a number of papers quantitative stratigraphic correlation techniques are not involved. Some papers can be considered as a fruitless effort to solve a problem that has not been defined. The reviewer believes that quantitativity assumes proof. Validity and correctness of "solutions" suggested cannot be assessed without having the problem defined. As a consequence of the rapid development on the area, the four years passed were obviously too much for the majority of papers. In 1988, this cannot be considered as recent advances, particularly because meanwhile many ideas (Brower's, Agterberg's, Schwarzacher's) have even been published elsewhere. The book is well edited but printing is under the international standards.

I Dienes

M ERDÉLYI and J GÁLFI: Surface and subsurface mapping in hydrogeology. Akadémiai Kiadó, Budapest, 1988, 384 pp, 251 figs

This very comprehensive, interdisciplinary book is really a hydrogeological manual which can be recommended to everybody interested in any aspect of hydrogeology. Its subject is the exploration of the GROUNDWATER, one of the most important earth material for the mankind and for the whole life in the earth. The mapping techniques of water resources treated in the book, are uptodate from the geological ones to their detection by remote sensing, by different geophysical methods, by borehole logging, etc. The book is based mainly on the great experience of the authors in Hungary and outside its borders, too. It is very strong in the description of geophysical methods (longest chapter) among them geoelectric ones most frequently used as water bearing formations are electrically well indicable.

Excellent case histories and their figures illustrate the application of the exploration techniques in very different hydrogeological conditions such as in sedimentary basins, volcanic rock areas, karstic terrain, etc. The quality of the water, the engineering aspects got also special chapters. To show the complexity of the book and its subject we cite at the end of this short review the titles of 15 chapters.

1. Introduction
2. Preparation of hydrogeological field surveys
3. Hydrogeological maps and cross-sections
4. Hydrogeological mapping and prospecting
5. The application of remote sensing in hydrogeological mapping
6. The application of geophysical prospecting methods in hydrogeological mapping

7. Exploratory drilling and borehole geophysics
8. Mapping of the quality of groundwater
9. Hydrogeological mapping of crystalline and metamorphic rocks
10. Hydrogeological mapping of volcanic rock areas
11. Hydrogeological characteristics and mapping of sedimentary areas
12. Hydrogeological mapping of carbonate rock terrains
13. Hydrogeological mapping of river valleys
14. Hydrogeological mapping of sedimentary lowlands
15. Hydrogeological mapping for engineering purposes

The book is especially recommended to hydrogeologists water autorities, industrial companies and academic institutions.

A Ádám

S J GIBOWICZ ed.: Seismicity in Mines. Basel-Boston-Berlin, Birkhäuser, 1989, 680 pp.

The book is reprint from Pure & Applied Geophysics (PAGEOPH), Volume 129 (1989), No. 3/4. It contains 22 papers from 8 countries where substantial research is conducted in the field of mine-induced seismicity. Out of 22 papers in total, 8 papers have been presented at the Fred Leighton Memorial Workshop on Mining Induced Seismicity, held in Montreal on August 30, 1987.

The papers in the book are divided into four groups. The first group contains 10 papers describing seismicity patterns in various mines in general and seismic source mechanisms in particular. The second group of 4 papers deal with coda waves, source model proposed to interpret mine tremors, correlation between the deposit extraction and seismic hazard, microgravimetric anomalies. The four papers in the third group are devoted to the methods based on travel times and velocities of seismic waves. The papers deal with location methods of mine tremors for which an accuracy of the order of a few tens of meters is required. The last group contains papers which are of informative rather than research character.

L Tóth

PRINTED IN HUNGARY

Akadémiai Kiadó és Nyomda Vállalat, Budapest

— treble underlining: bold-face italics
— red underlining: Greek letters
— green underlining: script letters.

Rules for mathematical-physical notations:

— trigonometric, logarithmic, analytic symbols, symbols for units and functions are in roman type (not underlined)
— letter symbols in mathematical and physical formulas, scalars, and subscripts of algebraic and physical quantities are in italics (underlined)
— vectors, matrices, operators in probability theory are in bold-face roman type (double underlining)
— tensors, operators and some special functions are in script letters (green underlining). These cannot be bold.
— Greek letters (red underlining) cannot be bold or extra bold type (thus they cannot be used for vectors or tensors)
— void upper lines e.g. for vectors
— avoid possible confusion between o (letter) and 0 (zero), l (letter) and 1 (one), ν (Greek nu) and v, u (letters) etc.
— explain ambiguous or uncommon symbols by making marginal notes in pencil
— be careful about superscripts and subscripts
— formulae must be numbered consecutively with the number in parentheses to the right of the formula. References in text to the equations may then usually be made by the number in parenthesis. When the word equation is used with a number, it is to be abbreviated, Eq. or Eqs in the plural
— the International System of Units (SI) should be used.

Authors are liable for the cost of alteration in the *proofs*. It is, therefore, the responsibility of the author to check the text for errors of facts before submitting the paper for publication.

3. *References* are accepted only in the Harvard system. Citations in the text should be as:

...(Bomford 1971)...or Bomford (1971)

...(Brosche and Sündermann 1976)...

...(Gibbs et al. 1976b)...

The list of references should contain names and initials of all authors (the abbreviation et al. is not accepted here); for *journal articles* year of publication, the title of the paper, title of the journal abbreviated, volume number, first and last page.

For *books* or *chapters in books,* the title is followed by the publisher and place of publication.

All items must appear both in the text and references.

Examples:

Bomford G 1971: Geodesy. Clarendon Press, Oxford

Brosche P, Sündermann J 1976: Effects of oceanic tides on the rotation of the earth. Manuscript. Univ. of Bonn

Buntebarth G 1976: Temperature calculations on the Hungarian seismic profile-section NP-2. In: *Geoelectric and Geothermal Studies (East-Central Europe, Soviet Asia), KAPG Geophysical Monograph.* Akadémiai Kiadó, Budapest, 561–566.

Gibbs N E, Poole W G, Stockmeyer P K 1976a: An algorithm for reducing the bandwidth and profile of a sparse matrix. *SIAM J. Number. Anal.,* 13, 236–250.

Gibbs N E, Poole W G, Stockmeyer P K 1976b: A comparison of several bandwidth and profile reduction algorithms. *ACM Trans. on Math. Software,* 2, 322–330.

Szarka L 1980: Potenciáltérképezés analóg modellezéssel (Analogue modeling of potential mapping). *Magyar Geofizika,* 21, 193–200.

4. *Footnotes* should be typed on separate sheets.

5. *Legends* should be short and clear. The place of the tables and figures should be indicated in the text, on the margin.

6. *Tables* should be numbered serially with Roman numerals. Vertical lines are not used.

All the illustrations should contain the figure number and author's name in pencil on the reverse.

Figures will be redrawn. Therefore the most important point is clearness of the figures, even pencil-drawings are accepted (with a duplicate).

Photographs and *half-tone* illustrations should be sharp and well contrasted.

If a specific reduction or enlargement is required, please indicate this in blue pencil on the figure.

The editors will send information to the first author about the *arrival* and acceptance of the papers. A galley proof is also sent to the first author for *correction.* Hundred *offprints* are supplied free of charge.

Periodicals of the Hungarian Academy of Sciences are obtainable at the following addresses:

AUSTRALIA
C.B.D. LIBRARY AND SUBSCRIPTION SERVICE
Box 4886, G.P.O., *Sydney N.S.W. 2001*
COSMOS BOOKSHOP, 145 Ackland Street
St. Kilda (Melbourne), Victoria 3182

AUSTRIA
GLOBUS, Hochstadtplatz 3, *1206 Wien XX*

BELGIUM
OFFICE INTERNATIONAL DE LIBRAIRIE
30 Avenue Marnix, *1050 Bruxelles*
LIBRAIRIE DU MONDE ENTIER
162 rue du Midi, *1000 Bruxelles*

BULGARIA
HEMUS, Bulvar Ruszki 6, *Sofia*

CANADA
PANNONIA BOOKS, P.O. Box 1017
Postal Station "**B**", *Toronto, Ontario M5T 2T8*

CHINA
CNPICOR, Periodical Department, P.O. Box 50
Peking

CZECHOSLOVAKIA
MAD'ARSKÁ KULTURA, Národní třida 22
115 66 Praha
PNS DOVOZ TISKU, Vinohradská 46, *Praha 2*
PNS DOVOZ TLAČE, *Bratislava 2*

DENMARK
EJNAR MUNKSGAARD, Norregade 6
1165 Copenhagen K

FEDERAL REPUBLIC OF GERMANY
KUNST UND WISSEN ERICH BIEBER
Postfach 46, *7000 Stuttgart 1*

FINLAND
AKATEEMINEN KIRJAKAUPPA, P.O. Box 128 *SF- 00101 Helsinki 10*

FRANCE
DAWSON-FRANCE S.A., B.P. 40, *91121 Palaiseau*
EUROPÉRIODIQUES S.A., 31 Avenue de Versailles, *78170 La Celle St. Cloud*
OFFICE INTERNATIONAL DE DOCUMENTATION ET LIBRAIRIE, 48 rue Gay-Lussac
75240 Paris Cedex 05

GERMAN DEMOCRATIC REPUBLIC
HAUS DER UNGARISCHEN KULTUR
Karl Liebknecht-Straße 9, *DDR-102 Berlin*
DEUTSCHE POST ZEITUNGSVERTRIEBSAMT Straße der Pariser Kommune 3-4, *DDR-104 Berlin*

GREAT BRITAIN
BLACKWELL'S PERIODICALS DIVISION
Hythe Bridge Street, *Oxford OX1 2ET*
BUMPUS, HALDANE AND MAXWELL LTD.
Cowper Works, *Olney, Bucks MK46 4BN*
COLLET'S HOLDINGS LTD., Denington Estate *Wellingborough, Northants NN8 2QT*
WM. DAWSON AND SONS LTD., Cannon House *Folkstone, Kent CT19 5EE*
H. K. LEWIS AND CO., 136 Gower Street
London WC1E 6BS

GREECE
KOSTARAKIS BROTHERS INTERNATIONAL BOOKSELLERS, 2 Hippokratous Street, *Athens-143*

HOLLAND
MEULENHOFF-BRUNA B.V., Beulingstraat 2, *Amsterdam*
MARTINUS NIJHOFF B.V.
Lange Voorhout 9-11, *Den Haag*
SWETS SUBSCRIPTION SERVICE
347b Heereweg, *Lisse*

INDIA
ALLIED PUBLISHING PRIVATE LTD., 13/14
Asaf Ali Road, *New Delhi 110001*
150 B-6 Mount Road, *Madras 600002*
INTERNATIONAL BOOK HOUSE PVT. LTD.
Madame Cama Road, *Bombay 400039*
THE STATE TRADING CORPORATION OF INDIA LTD., Books Import Division, Chandralok 36 Janpath, *New Delhi 110001*

ITALY
INTERSCIENTIA, Via Mazzé 28, *10149 Torino*
LIBRERIA COMMISSIONARIA SANSONI, Via Lamarmora 45, *50121 Firenze*
SANTO VANASIA, Via M. Macchi 58
20124 Milano
D. E. A., Via Lima 28, *00198 Roma*

JAPAN
KINOKUNIYA BOOK-STORE CO. LTD.
17-7 Shinjuku 3 chome, Shinjuku-ku, *Tokyo 160-91*
MARUZEN COMPANY LTD., Book Department, P.O. Box 5050 Tokyo International, *Tokyo 100-31*
NAUKA LTD. IMPORT DEPARTMENT
2-30-19 Minami Ikebukuro, Toshima-ku, *Tokyo 171*

KOREA
CHULPANMUL, *Phenjan*

NORWAY
TANUM-TIDSKRIFT-SENTRALEN A.S., Karl Johansgatan 41-43, *1000 Oslo*

POLAND
WĘGIERSKI INSTYTUT KULTURY, Marszalkowska 80, *00-517 Warszawa*
CKP-I W, ul. Towarowa 28, *00-958 Warszawa*

ROUMANIA
D. E. P., *Bucuresti*
ILEXIM, Calea Grivitei 64-66, *Bucuresti*

SOVIET UNION
SOJUZPECHAT — IMPORT, *Moscow*
and the post offices in each town
MEZHDUNARODNAYA KNIGA, *Moscow G-200*

SPAIN
DIAZ DE SANTOS, Lagasca 95, *Madrid 6*

SWEDEN
GUMPERTS UNIVERSITETSBOKHANDEL AB
Box 346, *401 25 Goteborg 1*

SWITZERLAND
KARGER LIBRI AG, Petersgraben 31, *4011 Basel*

USA
EBSCO SUBSCRIPTION SERVICES
P.O. Box 1943, *Birmingham, Alabama 35201*
F. W. FAXON COMPANY, INC.
15 Southwest Park, *Westwood Mass. 02090*
READ-MORE PUBLICATIONS, INC.
140 Cedar Street, *New York, N.Y. 10006*

YUGOSLAVIA
JUGOSLOVENSKA KNJIGA, Terazije 27, *Beograd*
FORUM, Vojvode Mišića 1, *21000 Novi Sad*

Index: 26.031

Acta Geodaetica, Geophysica et Montanistica Hungarica

VOLUME 25, NUMBERS 3–4, 1990

INCLUDING REPORT OF THE INTERNATIONAL LITHOSPHERE PROGRAM

Akadémiai Kiadó, Budapest
AGGM 25 (3–4) 227–472 (1990) HU ISSN 0236-5758

ACTA GEODAETICA, GEOPHYSICA et MONTANISTICA HUNGARICA
A Quarterly Journal of the Hungarian Academy of Sciences

Acta Geodaetica, Geophysica et Montanistica (AGGM) publishes original reports on geodesy, geophysics and minings in English.

AGGM is published in yearly volumes of four numbers by

AKADÉMIAI KIADÓ
Publishing House of the Hungarian Academy of Sciences
H-1117 Budapest, Prielle K. u. 19–35.

Manuscripts and editorial correspondence should be addressed to

AGGM Editorial Office
H-9401 Sopron P.O. Box 5

Subscription information

Orders should be addressed to

KULTURA Foreign Trading Company
H-1389 Budapest P.O. Box 149

INSTRUCTIONS TO AUTHORS

Manuscripts should be sent to the editors (MTA Geodéziai és Geofizikai Kutató Intézete, AGGM Editorial Office, H-9401 Sopron, P.O.Box 5, HUNGARY). Only articles not submitted for publication elsewhere are accepted.

Manuscripts should be typewritten in duplicate, double-spaced, 25 lines with 50 letters each. The papers generally include the following components, which should be presented in the order listed.

1. Title, name of author(s), affiliation, dateline, abstract, keywords
2. Text, acknowledgements
3. References
4. Footnotes
5. Legends
6. Tables and illustrations

1. The *affiliation* should be as concise as possible and should include the complete mailing address of the authors. The *date of receipt* of the manuscript will be supplied by the editors. The abstract should not exceed 250 words and should clearly and simply summarize the most important methods and results. 5–10 significant expressions describing the content are used as *keywords*. Authors may recommend these keywords.

2. The *text* should be generally in English and as short and clear as possible. From Hungarian authors papers are also accepted in Hungarian.

The section heading should *not* be underlined or in capitals.

Please note that underlining denotes special types:

— single underlining: italics
— double underlining: bold-face roman

CONTENTS

Report for the International Lithosphere Program

General Section

Book Reviews

FINAL REPORT

OF THE HUNGARIAN NATIONAL COMMITTEE FOR THE INTERNATIONAL LITHOSPHERE PROGRAM

Edited by:

A Ádám and F Horváth

1990

PREFACE

The International Lithosphere Program was one of the most important international ventures in Earth sciences during the past decade (1981-90). The Hungarian National Committee was formed to organize the Hungarian contribution to the scientific activity of the Inter-Union Commission on the Lithosphere. Our research in the Pannonian basin of Hungary was planned to concentrate on four major topics:

i) Recent tectonic movements and deformations
ii) Neogene-Quaternary basin development
iii) Structure of the lithosphere and asthenosphere
iv) History of evolution of the Tethys as reflected by the geological formations of Hungary.

The results obtained in the Pannonian basin during the first half of the Program were summarized in Acta Geologica Hungarica (1984-85, Vol. 27(3-4) and 28(1-2)) with the title "Tectonic significance of the Hungarian Mountains in the Alpine edifice". This volume presents the Final Report and contains eleven review papers.

The paper by Joó et al. describes the main features of an improved map of "Recent vertical movements in the Carpatho--Balkan region". It has become clear that there are quite a few methodological problems associated with the reliable determination of vertical movement velocities, and the geodynamic interpretation of the results is still in a preliminary stage.

The paper by Horváth illustrates that there has been a remarkable progress in understanding the Neogene-Quaternary evolution of the Pannonian basin, especially in depicting the kinematic pattern of the region during basin formation. However, recent geodynamics is poorly known, but stress determination initiated by Dövényi and Horváth will contribute to the solution of the problem.

Important information about the Alpine evolution of the Pannonian region is found in the structure of the lithosphere. Posgay et al. review the first results of deep seismic soundings along the Pannonian Geotraverse and attempt to give an

interpretation of reflecting horizons in the lower lithosphere and asthenosphere.

The two papers by Ádám et al. present a more reliable and detailed imaging of the shallow asthenosphere below the Pannonian basin and show the relationship with the high heat flow of the area. Another manifestation of the anomalous thermal state of the basin is the finding in a shallow position of the lower crustal conducting layer which may be connected to free fluids released by dehydration process. Ádám et al. and Pápa et al. demonstrate that there are linear conducting structures in the upper crust associated with major tectonic lineaments (e.g. Periadriatic and Balaton line). Geoelectric features suggest that these conductors are most probably graphite schists associated with zones of major tectonic dislocations.

Further progress in the understanding of the kinematics of the Pannonian basin can only be achieved by better knowledge of the pre-Neogene geologic history. Haas et al's and Kubovics et al's contributions give a comprehensive summary on the recent results about the evolution of the western Tethyan realm and the related Mesozoic magmatism. The transition from the Tethys to Paratethys during the Paleogene is reviewed by Nagymarosy's paper. These papers show clearly the significant mobility of units comprising the present lithosphere of this area. Márton's paper summarizes the possibilities of paleomagnetism to give constraints for the description of the complex motion of different crustal units in the Pannonian basin.

At the end of these 10 years of coordinated research we feel only appropriate to arrive at the conclusions that joint works should be continued and we see more problems now than when we started.

A Ádám and F Horváth

Acta Geod. Geoph. Mont. Hung., Vol. 25 (3-4), pp. 231-242 (1990)

ON RECENT CRUSTAL MOVEMENTS IN THE PANNONIAN BASIN

I Joó[1], Á Czobor[2], M Gazsó[2], Zs Németh[2]

[1]College of Surveying (EFE FFFK), H-8000 Székesfehérvár, Pirosalma u. 1-3., Hungary

[2]Satellite Geodetic Observatory Penc, H-1373 Budapest, Pf. 546, Hungary

During the last fifteen years intensive investigations have been carried out in the Carpatho-Balkan Region for revealing recent crustal movements, by means of repeated geodetic measurements. These investigations aimed mostly at the detection the vertical components of the movements, but preparations have been made to carry out investigations of the horizontal movements at certain areas.

Within this program the levelling network for crustal movements have been completed in the Pannonian Basin, on the area of Hungary. This net is suitable for the investigation of the movements' on a long time base. Recently precise levellings are carried out which help a more detailed investigation. Moreover regional nets for the investigation of the horizontal movements, and for the complex investigation of movements, are partly functioning, partly they are being constructed.

The investigation of the movements is promoted on the area of Hungary by the fact that Hungary co-ordinates these investigations in the Carpathian Basin and its surroundings. Within the international co-operation the map of the recent vertical crustal movements in the Carpatho-Balkan Region has been published twice (1979, 1985).

For the time being a map is compiled on the horizontal gradients of the vertical movements of the Carpatho-Balkan Region and information is derived from repeated geodetic measurements.

In the present paper geodetic investigating methods are discussed and results of investigations on the vertical movements are presented.

Keywords: Carpatho-Balkan region; Hungary; levelling; recent crustal movements

1. INTRODUCTION

For the geodetic investigation of recent crustal movements, the results of repeated measurements are utilized practically in all cases. The vertical and horizontal components of crustal movements are usually dealt with separately in accordance with the old practice of geodetic measurements.

This fact is important as horizontal and vertical determinations are different regarding both reliability and other conditions of the measurements.

Vertical determinations are carried out easier than horizontal ones. Accordingly, vertical determinations require less investment and therefore it is easier to repeat them.

The situation is quite the same with the reliability. The reliability of height difference (ΔH) obtained from precise height measurement is generally:

$$\mu_{\Delta H} < \pm 1 \text{ mm}/\sqrt{\text{km}} .$$

The reliability in the case of horizontal determinations is worse by an order of magnitude.

We present here the investigation of the vertical movements and in Hungary respecting the applicability of the conclusions for the investigation of horizontal movements.

2. GEODETIC INVESTIGATION OF VERTICAL MOVEMENTS

First a general remark is given on these investigations. Geoscientists are mainly interested in movements of the Earth's crust.

A geodesist puts his control points on the surface of the Earth and carries out measurements there. Thus movements of the Earth's surface are revealed by means of geodetic investigations. Movements of the surface involve both the impacts of crustal movements and of compaction and other technogenous activities, too.

Another problem is if the derived movements are to be considered as absolute or as relative ones.

Earlier data representing the changes in height of a given point relative to the sea level were considered as absolute vertical movements. At the same time (both then and now) a relative movement is a change in height between two points relative to each other.

Theoretical investigations consider vertical movements as

absolute ones, if besides the geometric transfer of masses, the change of level surfaces is taken into account thus the geoid changes, too. The latter idea has not been utilized concretely according to our knowledge.

In this paper the traditional interpretation will be utilized considering these conditions and the fact that the change of position of level surfaces is small.

In accordance with the traditional interpretation, the absolute vertical surface movements are interpreted as related to a chosen sea level; i.e. "geometrically absolute movements" will be introduced in this article.

2.1 Methods of the geodetic investigation of vertical movements

It is a quite common geodetic practice that velocities of the surface movements are deduced for their characterization (in mm/a). These velocities can be (in a geometric sense) either absolute velocities V_{abs}, or relative ones ΔV.

Vertical velocities are generally deduced as follows. The same line is precisely levelled twice (T_1 and T_2 epochs). The results of the two levellings are differences of height ΔH_1 and ΔH_2. From these data the velocity of the relative movement is between the end points of the section:

$$\Delta V = \frac{\Delta H_2 - \Delta H_1}{T_2 - T_1} = \frac{\Delta(\Delta H)}{\Delta T} \quad (mm/a) .$$

The followings are supposed:

- the points were not affected by any other effects
- during the period between the two measurements the vertical movements were continuous and smooth.

As geodetic control networks for vertical movements consist normally of systems of closed polygons, ΔV data deduced from raw ΔH_1 and ΔH_2 data can be adjusted. As results ΔV_{adj} values and a reliability index ($\mu_{\Delta V}$) are obtained for each levelling section (i.e. line).

When (geometrically) absolute velocities are to be

obtained a connection to mareographs should be established. Then absolute velocities and their mean square errors (V_{abs}, $\mu_{V_{abs}}$) can be deduced from the known absolute vertical velocities deduced for the mareographs and from the relative velocity values for all nodal points (or even for all points).

The absolute velocities of mareographs should be considered as a separate problem which is not discussed here in detail. We only mention that the absolute velocities of mareographs placed at the coast of the same sea are to be determined by precise levelling. A further problem is if the sea level may be considered unchanged or not (eustatic effect). This question is very important if mareographs at coasts of various seas are utilized in the same investigation.

For deducing absolute velocities conditions related to the temporal stability of the spatial position of mean sea levels should also be taken into account.

The results of vertical movement studies by means of geodetic methods can be presented in various forms. One traditional method is by charts which can be completed by graphs.

For larger areas, it is a more advantageous method to compile a map of crustal movements. It contains - besides the usual geographic information - the following: the lines of investigation, the adjusted absolute velocities, a detailed description of movements (by means of isolines) and other geologic, tectonic informations.

2.2 The most important vertical movement investigations

In the last decades attempts were made in many countries to deduce vertical movements by means of the available results of repeated levellings in certain areas. These attempts were generally occasional and involved smaller areas (sometimes only one specified line).

There were some additional insufficiencies as:

- the reliabilities of the utilized levellings were different,
- the motion free character of the geodetic control points was disputable in many cases,
- the planning of the lines was determined by the practical

form of the vertical control net
- geologic (tectonic) information was not considered, or it was considered in a late phase.

This practice was transgressed by an investigation program, which aimed to find vertical movements of larger areas, utilizing available geologic, later on seismologic information, too.

Such programmes were organized twice by the Soviet Geodetic Service (with co-operation of the Academy of Sciences of the Soviet Union) for Eastern Europe on the one hand, and on the other hand by the Hungarian Geodetic Service for the area of the Carpatho-Balkan Region (CBR).

Experts and institutes of several countries took part in both investigations. Both the East European and the CBR investigations were organized twice following each other and the results were presented on maps. In the second investigation the experience of the first one were considered. Meantime more up-to-date levelling networks have been established in the East European countries (they are connected at the borders). By this way the reliability of the data of repeated levellings was improved in the second case.

Some characteristics of the East European and CBR investigations are:

a) The first contiguous investigation of vertical movements in Eastern Europe:
   - the investigation was carried out between 1966-1971,
   - it was co-ordinated by the Soviet Geodetic Service,
   - the scale of the map of movements is 1:2.5 million,
   - the map was presented in 1971 at Moscow at the plenary meeting of the International Union of Geodesy and Geophysics (IUGG).

b) The first investigation of vertical movements in the Carpatho-Balkan Region (CBR_I)
   - the programme was based on a Hungarian proposal,
   - it was carried out between 1974 and 1979,
   - it was co-ordinated by the Hungarian Geodetic Service,
   - scale of the map is 1:1 million,
   - the results were presented at the plenary meeting of IUGG

at Canberra, Australia in 1979.

c) Second CBR investigation (CBR_{II}):
   - it was carried out between 1980 and 1985,
   - co-ordinator: the Hungarian Geodetic Service,
   - scale of the map: 1:1 million,
   - presented at Budapest, at an international symposium (within the framework of the International Association of Geodesy - IAG).

d) The second investigation in Eastern Europe:
   - it was carried out between 1980 and 1986,
   - co-ordinator: the Soviet Geodetic Service,
   - scale of the map: 1:2.5 million.

3. RECENT VERTICAL MOVEMENTS IN THE PANNONIAN BASIN

The Pannonian Basin which includes Hungary, is situated at the centre of Europe and is surrounded by the Carpathian Mountains.

As the Pannonian Basin is to be interpreted together with the Carpathian Mountains from a geological point of view, in discussing the vertical movements of the Basin, the recent movements of the Carpathians - and the Transylvanian Basin located within them - should be dealt with, too.

For the description of vertical surface movements of the area, the results of the second CBR investigation (CBR_{II}) will be utilized.

The total length of lines in the network is 35 046 km, with 432 levelling lines forming 127 closed polygons.

The Hungarian part of the net has the following characteristic data:

- 44 levelling lines,
- 11 closed polygons,
- total length of lines: 3 858 km,
- the first measurements were carried out between 1949 and 1962,
- the second series of measurements were carried out between 1975 and 1979, so $\Delta T \simeq 13\text{-}27$ years,

- the reliability of the measurements:

$$\mu_I = \pm (0.73 - 1.00) \quad mm/\sqrt{km}$$

and

$$\mu_{II} = \pm (0.27 - 0.34) \quad mm/\sqrt{km} .$$

The original CBR_{II} map on the vertical surface movements contains isolines of real vertical movements and the values of movements by means of colour codes for the whole area of the Carpatho-Balkan Region. The sketch (see Fig. 1) was made on the basis of the CBR_{II} map, and shows vertical movements of the area surrounded by the belt of the Carpathians (Pannonian Basin, Transylvanian Basin).

Figure 1 shows the following:

- the Carpathians are uplifting from their North-Eastern part to the Southern-Carpathians,
- the Transylvanian Ore Mountains and Bihar Mountains are uplifting,
- the Pannonian Basin is not uniform. West of Danube it is generally uplifting, while East of the Danube a subsiding tendency is observed.

A detailed description of vertical movements of the area is the following:

a) Transdanubia is mostly uplifting in the South-Western part (Fig. 2).
   From South-West to North-East the uplift decreases.
   The maximum value of the uplift: +1.3 mm/a in the county Zala.

b) A subsiding tendency is characteristic for the Little Hungarian Plain and for Western Slovakia, but it is of changing value. The greatest velocity is -2.2 mm/a.

c) Central Slovakia is characterized by a slight subsidence, i.e. the tendencies are somewhat uncertain, but the High Tatras show uplift.

d) The area of Western Rumania (Transylvania) shows sharp uplift. The uplift in the Eastern Carpathians is remarkable ($V_{max} \geq + 7$ mm/a). Other parts of the Carpathians uplift at

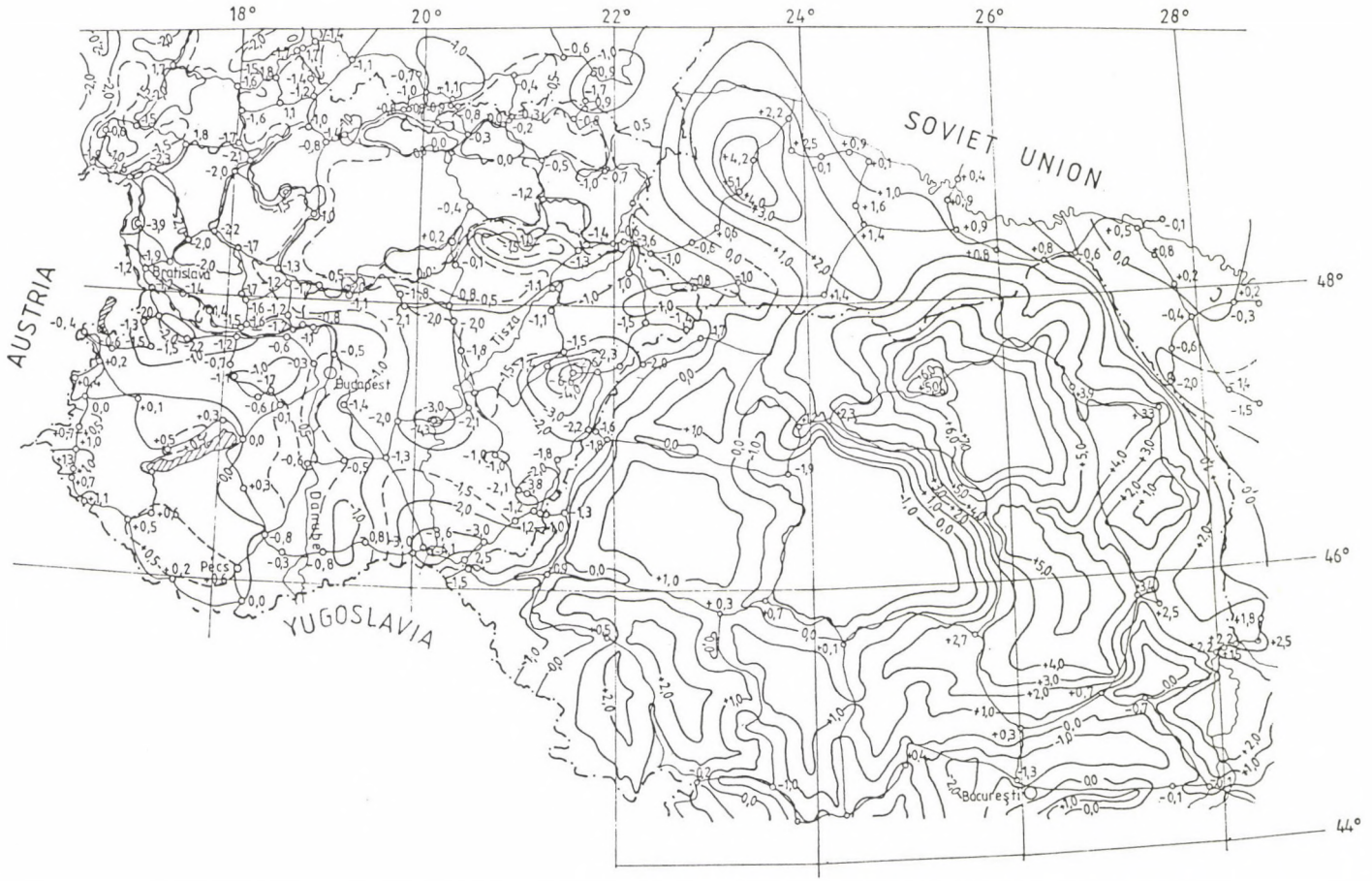

Fig. 1. The recent vertical movements in the Carpathians and in the Carpathian Basin

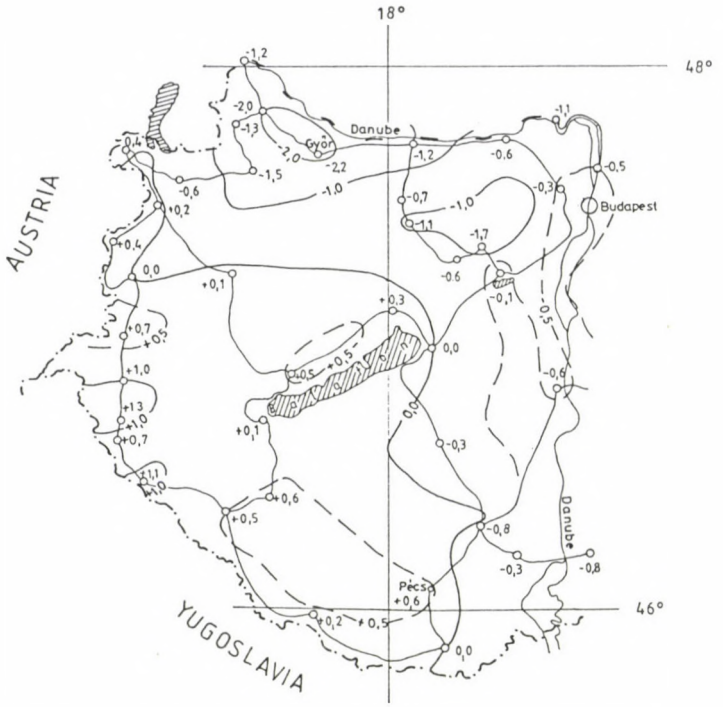

Fig. 2. The vertical movements of Transdanubia (Western Hungary)

a velocity of +2 mm/a, and +(4-5) mm/a, respectively. The Transylvanian Basin is subsiding (up-to -1.9 mm/a).

e) In the Pannonian Basin east of the Danube (including Eastern Slovakia, the territory East of the river Tisza, and the North-Western part of Transylvania) subsidence is the general tendency (Fig. 3).

Definitely sharp subsidence is witnessed

- around Debrecen where the maximum of subsidence is -6.6 mm/a
- at Szolnok -4.3 mm/a
- at Szeged -4.1 mm/a
- at Békéscsaba -3.8 mm/a.

4. INTERPRETATION OF THE RESULTS

It was proven on the basis of CBR_{II} that the Carpathians

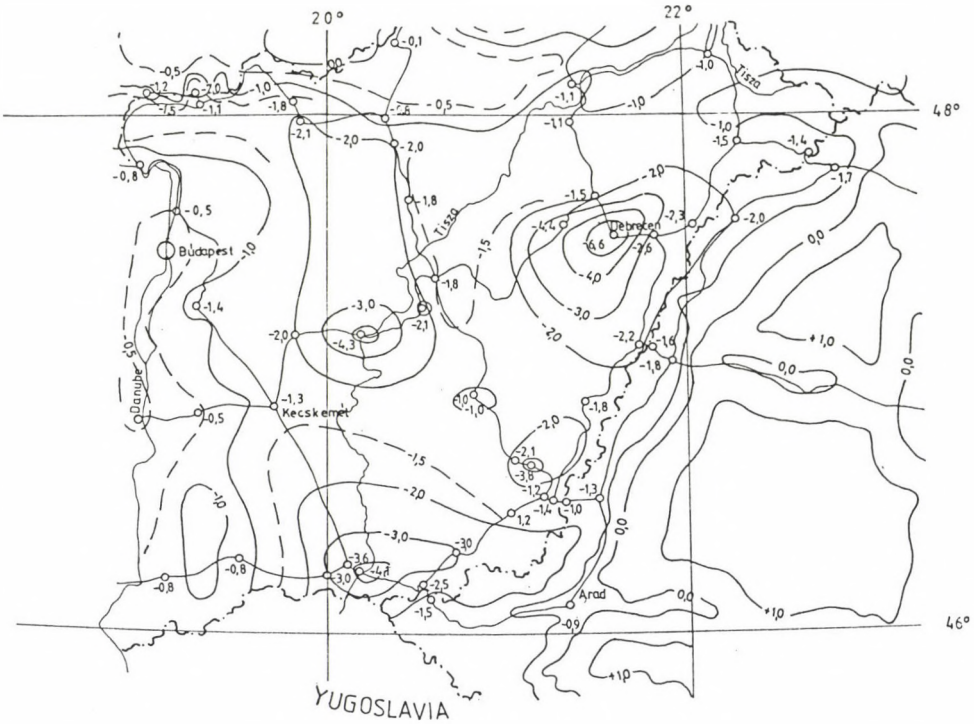

Fig. 3. Vertical movements in the Pannonian Basin to the east of river Danube

are generally uplifting. The Eastern Carpathians are significantly uplifting. For the territory of North-Western Slovakia there is no unambiguous evidence for an uplift.

The Great Hungarian Plain and the Little Hungarian Plain are subsiding. The areas of the Great Hungarian Plain where strong subsidence was found (Debrecen, Szolnok, Szeged, Békéscsaba) coincide with regions where sedimentary cover on the pre-Tertiary basement rocks are thickest (i.e. the compaction is also most significant). It is further characteristic that there are significant fluidum and water mining activities in the same areas.

The reliability of the derived velocity values was dealt with in Chapter 2.1. The original CBR_{II} map of motion includes reliability of the derived velocities, too (as an inset).

Accordingly the value of $\Delta v_{V\text{-}CBR} = \pm(0.75\text{-}2.5)$ mm/a. The

greater mean square errors of velocities are found in the adjacent areas of the Soviet Union and Rumania. In Hungary and in Czechoslovakia, the mean square errors are slighter (μ_V $\pm$ 1.0 mm/a).

The derived velocities are significant, where $|V_{abs}| \gg \mu_V$. Such areas are the Great Hungarian Plain, the Little Hungarian Plain, Western Slovakia, the Carpathians. The velocities in other parts of the Pannonian Basin are only suitable for the determination of movements tendencies. In these regions, more reliable results will be obtained from new precise levellings in the next years, and from other methods.

New more detailed measurements have been carried out in the Eastern part of Hungary, and they are being started in Transdanubia. Having finished the new measurements, the investigation will be continued. About a study of the vertical surface movements by other methods, the following can be said.

The method described in Chapter 2 is suitable to derive results at zones showing characteristic movements. Nevertheless it is more useful to use relative methods instead of absolute ones and their adjustment in zones of smaller movements. In the case of relative methods, relative velocities (ΔV) are produced for each levelling section, they are matched to the absolute velocities derived for the nodal points of the lines, and detailed information results along the whole length of the lines.

The application of this new method has been started (including derivation of the horizontal gradients along the lines with the vertical velocities). Having finished the new step of the investigation it will be possible to describe movements in areas of smaller vertical velocities.

REFERENCES

Joó I 1988: Investigation of recent surface movements in the country of Hungary and in the Carpatho-Balkan region. 6th International Symposium on "Geodesy and Physics of the Earth", GDR, Potsdam

Joó I 1988: Status report on investigation of recent crustal movements in the country of Hungary and in the Carpatho-

-Balkan region. KAPG Symposium on the Investigation of Recent Earth's Crust Movements, Sochi, Soviet Union

Joó I 1989: Earthquakes' impact on changes in height. Geophysical Monograph 49, IUGG series 4, Washington D.C. USA, 87-95.

Joó I, Arabadzijski D, Mladenovski M M, Vanko J, Füry M, Thury J, Wyrzykowski T, Mihaila M, Mescerskij I M, Semic V, Csáti E 1985: Map of recent vertical movements in the Carpatho-Balkan region. Budapest, scale: 1:1 000 000

Joó I, Czobor Á, Németh Zs, Gazsó M 1988a: RCM investigation by horizontal velocity-gradients. 6th International Symposium on "Geodesy and Physics of the Earth", GDR, Potsdam

Joó I, Czobor Á, Gazsó M, Németh Zs 1988b: Scientific report on the investigation of vertical crust movements in Hungary and in the Carpatho-Balkan region and their co-ordination (in Hungarian). Székesfehérvár

Joó I, Czobor Á, Németh Zs, Gazsó M 1989: National map of horizontal gradients of the Hungarian vertical surface movements. Székesfehérvár

Acta Geod. Geoph. Mont. Hung., Vol. 25 (3-4), pp. 243-255 (1990)

STRUCTURAL EVOLUTION OF THE PANNONIAN BASIN: A PROGRESS REPORT

F Horváth

Geophysical Department, Eötvös University, H-1083 Budapest, Kun Béla tér 2, Hungary

An evaluation of the recent progress in understanding the structural evolution of the Pannonian basin is presented. The model of transtensional origin of the Pannonian basin is supported by independent tectonic studies in outcrops of the basement (e.g. Hungarian "mountains"). A most remarkable new concept about the extrusion tectonics of the Eastern Alps presents a new perspective to derive a three-dimensional geodynamic model for extensional collapse of orogens.

One alternative model is discussed. It is argued that the model which suggests major clockwise rotation of a large part of the Pannonian basement during basin formation is unjustified. Finally a few real problems are lined up and suggestions for promising areas of future research are put forward.

Keywords: block rotation; geodynamics; Pannonian basin; transtensional tectonics

INTRODUCTION

Study of the formation of the Pannonian basin has been one of the focal points of the activity of the Hungarian National Committee for the International Lithosphere Program. The reason for this was not only the fact that nearly the whole territory of the country belongs to this basin. More important was, however, our conviction that the formation of the basin on an Alpine orogenic terrain could be of general interest because of potential contribution to better understanding of the dynamics of the lithosphere/asthenosphere system.

The half-term report of the Hungarian National Committee (Contribution 1984-85) dealt mainly with the relationship of Mesozoic through Paleogene rocks in the Alpine-Carpathian--Dinaric mountains and those inside (and mostly below) the

Pannonian basin, and with the pre-Neogene structural evolution. The Pannonian basin proper was not considered in detail, but one paper illustrated by a few seismic sections the characteristic Neogene structural styles and their possible connections to earlier tectonic features (Horváth and Rumpler 1984). Moreover, the first attempt was reported here to decipher the Neogene structural evolution of the area by microtectonic studies, i.e. statistical analysis of all observable fault striation and related features in outcrops (Bergerat et al. 1984).

Our recent understanding of the Pannonian basin has been summarized in a comprehensive volume edited by Royden and Horváth (1988) as Memoir 45 of the American Association of Petroleum Geologists. This volume represents the end-results of an eight-years' research project between the Eötvös University (Budapest) and the Massachusetts Institute of Technology (Cambridge), and also included other participants both from academies and industry. The Memoir contains chapters on the Cenozoic tectonic evolution of the Pannonian basin system, and covers subjects from theoretical basin models to implications for more reliable assesment of hydrocarbon prospects in the Neogene sedimentary rocks.

The purpose of this brief report is to present my personal view on the progress we have made in the last couple of years in understanding the structural evolution of the Pannonian basin. I shall review a few important new results of other investigators which support our view and may open new perspectives for future research. In addition, I shall discuss the most remarkable alternative view on the formation of the Pannonian basin, and attempt to arrive at an objective summary about the most important open problems.

RECENT RESULTS

New deep reflection seismic soundings (Posgay et al. 1986) support earlier observations that the Pannonian basin is characterized by an attenuated continental crust, with a depth to Moho of 25 to 29 km. The only important exception is the Transdanubian Central Range to the North of Lake Balaton (Fig.

1). This is the largest fairly continuous area inside the Pannonian basin where Mesozoic rocks crop out. This Range was never below water level during the formation of the Pannonian basin, but the recent topographic elevation is the consequence of Quaternary uplift. The Moho discontinuity is not a sharp reflector below the Range, rather a transitional layer in a depth of 30 to 35 km. This increased crustal thickness is not reflected by the shape of the lithosphere/asthenosphere boundary. New magnetotelluric soundings combined with inversion of seismic travel-time residuals clearly delineate a large asthenospheric dome associated with the basin. The minimum lithospheric thickness is about 50 km in a central and elongate stripe (Ádám et al. 1982, 1989, Babuska et al. 1987).

The Pannonian basin was one of the first test areas where the quantitative model of McKenzie (1978) for extensional basin evolution proved to be applicable (Sclater et al. 1980). At that time, however, we had no idea at all about the style, space and time distribution of lithospheric extension. A number of papers document the progress of our understanding which culminated in the Memoir. I briefly summarize our main points here.

Subsidence of the Alpine orogenic terrain in the future Pannonian basin started in the early Miocene and the region became part of the epicontinental Central Paratethys sea. Clastic material derived from the neighbouring mountainous areas of the Alps, Carpathians and Dinarides, and were transported to the sea mostly by rivers. Clastic influx significantly increased towards the end of the middle Miocene when rapid uplift of the mountains around the Pannonian basin occurred. These rising mountains separated the basin from the world seas and led to the development of a large lake characterized by evolution of endemic fauna. The lake has been filled up progressively since the late Miocene and the area became a dryland during the Quaternary.

A typical sedimentary succession in the Pannonian basin consists of (from bottom to top) basal conglomerates passing into shallow marine sediments. This is followed by deep water deposits, usually of black shales with turbiditic

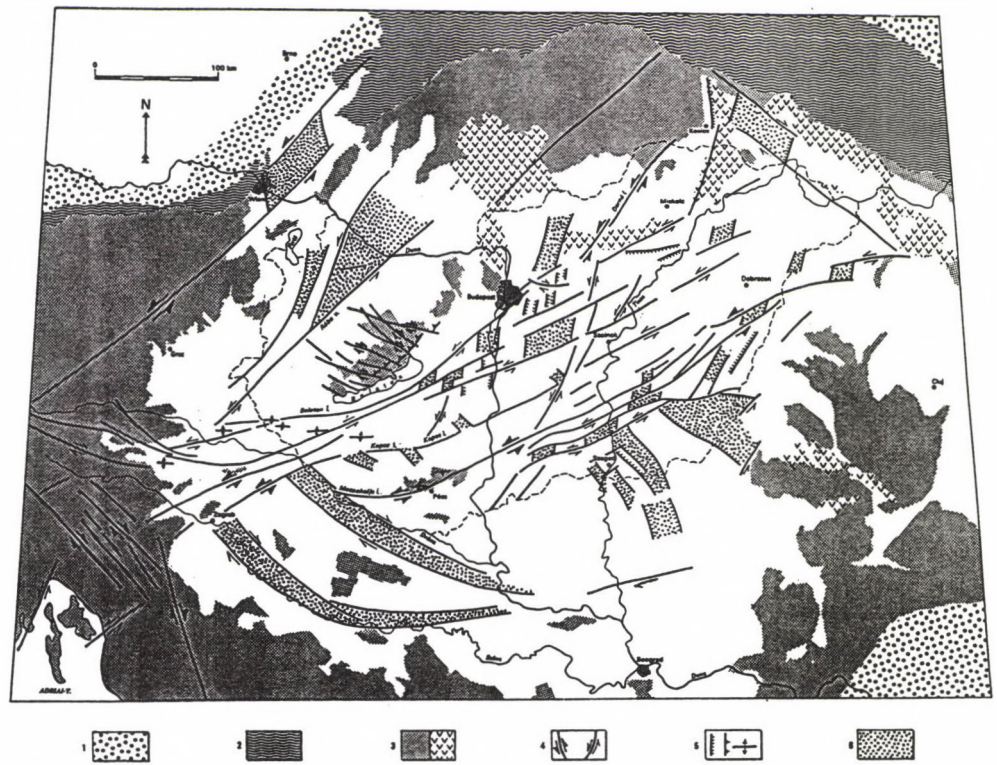

Fig. 1. Tectonic sketch of the Pannonian basin and surrounding regions showing the main faults and folds of Neogene age. Note that the sketch outside of Hungary is extremly oversimplified and mainly conceptual. Legend: 1. Molasse foredeep, 2. Alpine-Carpathian flysch belt, 3a. Inner Alpine-Carpathian Mountain belt and the Dinarides, 3b. outcrops of Neogene calcalkaline volcanic rocks, 4. strike-slip faults, the sense (and usually the amount) of displacement is well constrained (thick arrows) or unconstrained (thin arrows), 5. normal fault, thrust fault, and fold, 6. areas of major crustal extension and subsidence

intercalations. It is overlain by prodelta to delta-slope sediments, and eventually by a thick complex of delta-plain deposits. Two megasequences can be distinguished. The middle Miocene strata represent the syn-rift deposits and they locally contain a significant amount of volcanic materials. This is usually unconformably overlain by the late Miocene to Quaternary post-rift deposits.

Interpretation of reflection seismic sections combined with other geological data has led to a tectonic scheme of the Pannonian basin (Fig. 1). The Pannonian basin is a result of crustal extension which culminated during the middle Miocene and, locally, has continued with greatly reduced intensity until recent times.

The tectonic scheme shows two principal sets of conjugate strike-slip faults. All of the faults that strike East-Northeast or Northeast are left lateral. All of the faults that strike Northwest are right lateral. Curvature, splaying and side-stepping of strike-slip fault segments occur frequently. Areas of extension and normal faulting are associated with discontinuous or divergent strike-slip faults, and with fragmentation in zones bounded by two major strike-slip faults (transtension). Locally thrust faults and folds with East-West trending fold axes are present (transpression).

This kinematic pattern can be explained by a simple regional stress field. The Pannonian region was characterized during the middle Miocene by a North-South maximum principal stress (σ_1), an East-West minimum principal stress (σ_3), and a vertical intermediate stress (σ_2), where:

$$\sigma_1 = \sigma_{N\text{-}S} > = \sigma_2 = \sigma_{vertical} > \sigma_3 = \sigma_{E\text{-}W} .$$

This stress field is compatible with two conjugate sets of strike-slip faults (if $\sigma_1 = \sigma_{N\text{-}S}$) and it provides the conditions for oblique slip along these faults (if $\sigma_1 \cong \sigma_2$) and for pure normal faulting elsewhere (if $\sigma_1 = \sigma_{vertical}$).

Plate tectonic evolution of the Alpine-Mediterranean region during the Miocene can explain the formation of this stress field. A roughly North-South largest principal stress

was generated probably by the African plate, which exerted a push on the Pannonian through the Adriatic promontory. An East--West least principal stress is thought to be related to the retreat of the subducted slab along the Eastern Carpathians.

In other words, the Pannonian basin is an escape structure characterized mostly by transtension and subordinately transpression. Crustal blocks extruded from the main Alpine collision front towards the "free boundary" in the Eastern Carpathians where they overrode the subductible crust of the molasse foredeep. Accordingly, strike-slip faulting and extension in the Pannonian area was compensated by coeval folding and thrusting in the outer arc of the Eastern Carpathians. In this model the total amount of Pannonian extension relative to stable Europe (100 $\pm$ 50 km) should be the same as the coeval crustal shortening in the Outer Eastern Carpathians.

Our model received important independent support from continuing microtectonic observations in the Pannonian basin (Bergerat 1989, Bergerat and Csontos 1989, Csontos et al. 1990). These observations have been performed in the Hungarian mountains which are actually emergent blocks of the Pannonian basement. Hence, basement tectonics can be well studied, but the time constraints are often poor due to the lack of abundant young sedimentary rocks. Anyhow, these studies demonstrate that the tectonic activity during the Neogene (particularly the Miocene) were very intensive and predominated by strike-slip faults. The orientation and offset of these faults are generally in concert with what were inferred from seismic and drillhole data in the basin. On the other hand, it has become obvious that the model for the formation of the Pannonian basin as illustrated in Fig. 1 is a general scheme and cannot describe all the complexity of the structural evolution. For example, observations at distant localities in and around the Pannonian basin show a systematic temporal change of the orientation of strike--slip faults. This implies a significant rotation of the maximum horizontal stress from the North (middle Miocene) towards the Northeast (late Miocene) and then counterclockwise towards West-Northwest (Pliocene). Csontos et al. (1990) argue that part of this rotation is apparent and is caused by internal

block rotations within two major boundary wrench faults. The rest of the inferred rotation can be a real change of the regional stress field due to change of the boundary conditions and interaction of the European and African plates. From this point it is also interesting to determine the recent stress field in the Pannonian basin (Dövényi and Horváth, this volume) and to see how much it is under the control of forces acting on the boundary of the European plate.

Major breakthrough has occurred recently in understanding the uplift history of high-pressure metamorphic core complexes in Phanerozoic origenic belts. It can be shown that these complexes were initially deeply buried (30 to 50 km) as a consequence of subduction during plate convergence. Then, they were detached from the lower plate and brought back to the Earth's surface strikingly fast. It has been suggested that this rapid exhumation and unroofing is an extensional collapse within compressional orogenic belts (Platt 1986, Dewey 1988). This can happen by gravitational spreading of decoupled crustal flakes away from topographic highs caused by uplift of thickened orogenic wedge.

One of the test areas where this model has been most successfully applied is the Eastern Alps. Studies of uplift and deformation history of Penninic rocks in the Tauern and Rechnitz windows show that the overlying Austroalpine nappes were removed during the Oligocene and Miocene along low-angle normal faults and the general direction of extension was East--West (Selverstone 1988, Ratschbacher et al. 1989). Ratschbacher et al. (1990) have remapped and reinterpreted the Tertiary faults and other deformations and defined in detail the kinematics of the Eastern Alps. This clearly suggests that extrusion of the Eastern Alps occurred parallel to their main strike and took place by brittle deformation of the upper crust and ductile flow of the lower crust and lithosphere. The fault pattern is shown to be intimately related to the basin formation in the intra-Carpathian area. They argue convincingly that extrusion of the Eastern Alps and formation of the Pannonian basin is one, integral process which was driven by gravitational

instability of the orogenic wedge and boundary forces due to the indenting South Alpine/Apulian plate. The fact that the Eastern Alps remained mountains and the Pannonian area became basin can be explained in terms of different amount of extension which was probably controlled by the changing boundary conditions from the West towards the East (e.g. the stiffnes of the European foreland and the distance from the Apulian indenter). I think these outstanding results if combined with further data and interpretations from the Pannonian basin may open new perspectives in understanding the evolution of complex geodynamic systems.

I would like to emphasize that we really need a lot of new data and interpretations from the Pannonian basin, because I am aware that quite a few elements of our model are speculative or oversimplified, and can be the subject of debate. Fortunately, there are alternative models available which may stimulate further progress. I shall briefly discuss only one remarkable concept which received wide publicity in the recent years (Balla 1985, 1986a, b, 1987, 1988). This concept is markedly different basically because the author assigns a fundamental role to rotation kinematics in the Tertiary evolution of the Alpine-Carpathian-Pannonian domain. He has arrived at that conclusion on the basis of studying paleomagnetic data. Indeed, anomalous paleodeclinations can readily be interpreted in terms of rotation of the sampled rock units. In a complex orogenic belt, however, it is very difficult to make a sound judgement about the tectonic unit this rotation refers to, and to decipher the actual displacement history.

A mid-Hungarian mobile belt divides the intra-Carpathian domain into two contrasting megatectonic units: the Pelso unit on the NW and the Tisza unit on the SE. The differences are reflected by the late Paleozoic to Paleogene geologic history of the two units (see a recent review by Fülöp et al. 1987). It is well established that the two units were quite far away during the Jurassic and located to the South (Pelso unit) and the North (Tisza unit) of the spreading axis of the Tethys (e.g. Vörös 1987). As a consequence of Europe/Africa convergence the Tethyan oceanic domain was consumed until the end of Cretaceous

and a complex nappe structure developed in both units. Eocene to early Miocene structural evolution was controlled by strike--slip faulting and, eventually, juxtaposition of the Pelso and Tisza units occurred (Báldi and Báldi-Beke 1985). Formation of the Pannonian basin took place on this continental assemblage which accordingly was strongly influenced by earlier deformations.

Paleomagnetic data from the Mecsek Mts (SW Hungary), however, led Balla (1986b) to suppose that this was not the case. He suggests that the Tisza unit was in a significantly twisted position throughout the Oligocene which leads to the postulation of a large, westward widening bay characterized by subductible crust (see Fig. 7 of Balla 1987). Clockwise rotation of the Tisza unit by an angle of about 100^{o} back to its present position has taken place since the early Miocene around a proximate rotation pole (western Moesia). Rotation rate was seemingly larger initially, but about 30^{o} of the rotation has occurred during the last 11 million years. Balla's main point is that all the Neogene tectonics (i.e. strike-slip faulting, rifting and graben formation) during the evolution of the Pannonian basin are secondary features and were induced by this primary rotation (Balla 1987, 1988). I think, however, that serious objections can be raised against his idea. Some of them are as follow:

i) The Mecsek Mts constitute a push-up structure associated with a major Neogene left-lateral wrench fault (Némedi Varga 1983). Their structure is strongly influenced by the activity of the master fault, secondary thrust faults and Riedel shears. It seems to me, therefore unreasonable to suppose that paleomagnetically detected rotations in these mountains can be extrapolated for the whole Tisza unit.

ii) The postulated bay which was a few hundred kilometer wide at the West, and characterized by subductible crust is a "terra incognita", as not any remnants have been found so far.

iii) To avoid this discrepancy Balla (1986) suggests an alternative possibility. He speculates that the gap between the two units were filled by other known crustal blocks. These

blocks moved politely aside when it was necessary to give way to the clockwise rotating Tisza unit. In other words, this alternative leads to a hopeless jigsaw puzzle.

iv) To make reasonable the rotation of the Tisza unit Balla (1986, 1988) attempts to offer a driving mechanism. He suggests that the western tip of the Tisza unit was pushed towards the North by counterclockwise rotation of a northern Adriatic microplate. This microplate, in turn, was separated from southern Adria and rotated counterclockwise as a consequence of the opening of the Ligurian sea. I think, however, that this mechanism does not work because of three reasons. First, counterclockwise rotation of a northern Adriatic microplate would lock rather than drive rotation of the Tisza unit, because of simple geometrical reasons (compare Figs. 7 and 11 of Balla 1986). Second, opening of the Ligurian sea (late Oligocene to early Miocene, Jemsek et al. 1985) finished when the supposed rotation of the Tisza unit started (early Miocene through Pliocene, Balla 1986). Third, opening of the Ligurian sea resulted in about 30^{o} counterclockwise rotation of the Corsica-Sardinia block, which was compensated by crustal shortening in the internal Appeninic nappe front (Rehault et al. 1984). In other words, opening of the Ligurian sea has nothing to do with the movement of the Tisza unit.

All in all, I think that the idea of major rotation of the southeastern unit of the Pannonian basement during basin formation is unjustified both geologically and kinematically. However, this is just one, though fundamental element of Balla's concept. There are quite a few other elements I accept and appreciate. One example is given by studies in western Hungary along the contact zone of the Pelso and Tisza units (Balla et al. 1987). They have shown that to the North of the contact zone, along the Balaton line (see Fig. 1) a 200 km or perhaps 300 km long belt can be found which was remarkably influenced by middle Miocene compression. We have also recognized this belt and interpreted as en echelon folds and the consequence of transpression during oblique convergence. We may be still right but we never analyzed the relationship of Tertiary wrench

faults to earlier thrust faults. From a mechanical point of view it is reasonable to suppose that wrench faults flatten at depth and root in deep detachment planes associated with Alpine nappe emplacement. There are ample evidence from the North American Cordillera that regional strike-slips and thrust faults share a common decollement (Oldow et al. 1989). If this is the case, then significant thrusting may have occurred during oblique convergence along the Balaton line and elsewhere in the Pannonian basin during the Neogene.

CONCLUDING REMARKS

One can observe a remarkable progress in the understanding of the structural evolution of the Pannonian basin during the Neogene. The good level of knowledge can help to define the main open problems and promising areas for future research. My preferences are as follow:

1. It is very important to have a better understanding of the basement (pre-Tertiary) tectonics. There is no more further doubt that the basement is made up from a stack of Alpine--Carpathian nappes, but their geometry, areal extent and correlation is unknown at all. Such kind of research can rely on proper interpretation of deep reflection seismic profiles and borehole data. I am convinced that, in addition to good data, we need to learn more from Alpine geologists and experts on seismic interpretation in orogenic belts.

2. Reactivation of earlier thrust faults should have occurred during the Tertiary strike-slip dominated tectonic history. Presumably, flower-structures are only superficial manifestations of wrench faults which root at depth in detachment planes. Future research in this field can elucidate the role of tectonic heritage and lead to a good idea about the changing style of deformation with depth.

3. It appears to be vital to continue modern structural geological studies in outcrops of the Pannonian basement to map all the indications of Tertiary kinematics. I think the most

interesting areas are at the periphery of the Pannonian basin, particularly in the internal Dinarides and Southern Carpathians. Equally important is to study the coeval deformations of the Outer Carpathian arc.

4. The Tertiary kinematics of the Carpathian-Pannonian region should be combined with the results of extrusion tectonics in the Alps. From a general geodynamic point of view it has a great promise to arrive at an improved 3D model of the evolution of the lithosphere in a collisional orogenic belt.

5. There are some indications that Quaternary tectonics may be somewhat different from the pattern of Neogene structural evolution. We need to study the neotectonic processes to understand recent geodynamics and have a reliable ground for protection of the environment.

Naturally, we need time and money to carry on these researches. Last but not least, I believe in better chances for constructive cooperation between scientists in this part of the world.

REFERENCES

Ádám A, Vanyan L L, Varlamov D A, Yegorov I V, Shilovsky A P, Shilovsky P P 1982: Phys. Earth Planet. Inter., 28, 251-260.

Ádám A, Landy K, Nagy Z 1989: Tectonophysics, 164, 361-368.

Babuska V, Plomerova J, Sileny J 1987: In: K Fuchs and J Froidevaux eds, Composition, Structure and Dynamics of the Lithosphere-Asthenosphere System. Am. Geophys. Union. Geodyn. Ser., 16, 239-251.

Báldi T, Báldi-Beke M 1985: Acta Geol. Hung., 28, 5-28.

Balla Z 1985: Geophys. Transact., 30, 313-353.

Balla Z 1986a: Tectonophysics, 127, 213-243.

Balla Z 1986b: Geophys. Transact., 32, 147-181.

Balla Z 1987: Tectonophysics, 139, 67-98.

Balla Z 1988: Acta Geol. Hung., 31, 63-63.

Balla Z, Tátrai M, Dudko A 1987: In: Annual Report of the Eötvös Loránd Geophysical Institute of Hungary for 1986, 74-91.

Bergerat F 1989: Tectonophysics, 157, 271-280.

Bergerat F, Csontos L 1989: Acta Geol. Hung., 31, 81-100.

Bergerat F, Geyssant J, Lepvrier C 1984: Acta Geol. Hung., 27, 237-249.

Contribution to the International Lithosphere Program, Publ. No. 0113, 1984-85: Acta Geol. Hung., 27, 205-459 and 28, 1-117.

Csontos L, Tari G, Bergerat F, Fodor L 1990: Structural evolution of the Carpatho-Pannonian area during the Neogene. Tectonophysics, in press

Dewey J F 1988: Tectonics, 7, 1123-1139.

Fülöp J, Brezsnyánszky K, Haas J 1987: Acta Geol. Hung., 30, 3-20.

Horváth F, Rumpler J 1984: Acta Geol. Hung., 27, 229-235.

Jemsek J, Von Herzen R, Rehault J-P, Williams D L, Sclater J 1985: Geophys. Res. Letters, 12, 693-696.

McKenzie D 1978: Earth Planet. Sci. Lett., 40, 25-32.

Némedi Varga Z 1983: In: Ann. Rep. Hung. Geol. Inst. from the year of 1981, 467-484.

Oldow J S, Bally A W, Ave Lallemant H G, Leeman W P 1989: In: A W Bally and A R Palmer eds, The geology of North America; An overview. Geol. Soc. of America, Boulder, Colorado, 139-232.

Platt J P 1986: Geol. Soc. Am. Bull., 97, 1037-1053.

Posgay K, Albu I, Ráner G, Varga G 1986: In: M Barayangi, L Brown eds, Reflection seismology: A global perspective. Am. Geophys. Union. Geodyn. Ser., 13, 55-65.

Ratschbacher L, Frisch W, Neubauer F, Schmid S M, Neugebauer J 1989: Geology, 17, 404-407.

Ratschbacher L, Behrmann, Pahr A 1990: Tectonophysics, 173, in press

Rehault J-P, Boillot G, Mauffret A 1984: Marine Geol., 55, 447-477.

Royden L H, Horváth F eds 1988: Am. Ass. Petrol. Geol. Memoir 45, Tulsa, Okl., 1-394.

Sclater J G, Royden L, Horváth F, Burchfiel B C, Semken S, Stegena L 1980: Earth Planet. Sci. Lett., 51, 139-162.

Selverstone J 1988: Tectonics, 7, 87-105.

Vörös A 1987: Acta Geol. Hung., 30, 59-80.

Acta Geod. Geoph. Mont. Hung., Vol. 25 (3-4), pp. 257-266 (1990)

DETERMINATION OF CONTEMPORARY CRUSTAL STRESS REGIME IN HUNGARY

P Dövényi and F Horváth

Geophysical Department of Eötvös University, H-1083 Budapest, Kun B. tér 2, Hungary

This report presents an overview of the first results of stress determinations in the Pannonian basin, Hungary. In cooperation with experts from the University of Karlsruhe we analyzed borehole breakout data in ten hydrocarbon exploration wells. Furthermore, in situ stress determinations have been carried out at three sites in the Hungarian mountains. We conclude that both methods give good results but further data are required to understand the regional stress pattern.

Keywords: breakout; Hungary; overcoring; Pannonian basin; stress determination

INTRODUCTION

Motivation for crustal stress determinations is multifold. The patterns of the intraplate tectonic stress field can be used to determine the direction and relative magnitude of the various forces controlling plate motion. Stress data provide critical input for assessing the origin of tectonic movements and seismicity and evaluation of earthquake hazard in intraplate region. These data are useful for a variety of problems in mining, petroleum exploration and production, and civil engineering as well.

The understanding of the causal connection between the most common tectonic phenomenon i.e. the faulting and the three principal stress directions in the earth's upper crust was grounded by Anderson (1951) in his classical study. Many data support his theory that the three principal stress directions lie in approximately horizontal and vertical planes. Thus, in areas of deviatoric extension (normal faulting) the maximum

principal stress is vertical, in areas of deviatoric compression (thrust faulting) the minimum principal stress is vertical, and in areas of strike-slip faulting the vertical stress is the intermediate one. Seismological studies showed that most of the earthquakes are the consequences of such faulting taken place somewhere in the brittle regions of the crust (Brune 1974). The stress regime plays an important role in the initiation of hydrocarbon (Du Rouchet 1981, Tissot and Welte 1987). The idea of primary migration originated from the mechanics of hydrofracturing (Hubbert and Willis 1957).

Early investigations of regional stress patterns in North America and in Europe indicated that uniform horizontal stress orientation and relative stress magnitudes existed over broad regions of the earth's crust (Sykes 1974, Haimson 1977). Further data collection and data acquisition have been organized in the World Stress Map project of the International Lithosphere Program. Preliminary results of the project indicate that most intraplate regions are characterized by uniformly-oriented compression; intraplate extension is limited almost entirely to thermally uplifted areas. In several plates the maximum horizontal stress direction is approximately parallel to the direction of absolute plate motion. This suggests that regional tectonic stresses are primarily related to plate driving forces, although crustal structure and rheology have important effects on the stress field (Zoback et al. 1988).

TECTONIC STRESS INDICATORS

In the description and grouping of reliable stress indicators we follow the recommendations of the World Stress Map project (Zoback et al. 1988).

Four different categories of geophysical and geological data are being used to indicate stress orientations:

i) earthquake focal mechanisms;

ii) in situ stress measurements at depth, including hydraulic fracturing and overcoring;

iii) measurement of young geologic deformation and features,

including both fault slip and volcanic alignments;

iv) stress-induced well bore enlargements or "breakouts".

The elastic waves generated by earthquakes and recorded at seismological stations can be used for the analysis of the seismic source. The orientation of the fault plane and the direction of slip on the fault determine the first motion directions of the recorded wave pulses at the stations. Only the focal mechanism give reliable information about the state of stress in the deeper regions of the crust; more and more, well constrained focal mechanisms are available in the last decade using waveform modeling with data collection from digital seismic networks. However, the inherent difficulty in estimating principal stress directions from focal mechanisms remains. Most crustal earthquakes are presumed to occur on pre-existing faults, in which case the orientation of two nodal planes is a function of both the orientation of the fault and orientations and relative magnitudes of the principal stresses.

In Hungary there are only three reliable focal mechanism determinations (Tóth et al. 1989, Tóth, personal communication) because of the insufficient seismic network and relatively low seismic activity. Results of the Hungarian focal mechanism determinations are shown in Fig. 1.

Using the hydraulic fracturing technique in vertical boreholes, one principal stress is assumed to be parallel to the borehole and equal in magnitude to the overburden pressure. In this case a vertical hydraulic fracture should initiate at the borehole wall along an azimuth perpendicular to the minimum horizontal principal stress. Measurements of breakdown pressure and shut-in pressure can be used to evaluate the magnitude of principal stresses lying in horizontal plane. The principal stress direction can be determined by the examination of well bore cross-section along the fractured interval using borehole televiewer or four-arm caliper log data.

Our experience shows that data acquired during routine hydraulic fracturing in hydrocarbon exploration are not satisfactory for stress determination. Hydraulic fracturing for crustal stress measurements has not been carried out in Hungary, so far.

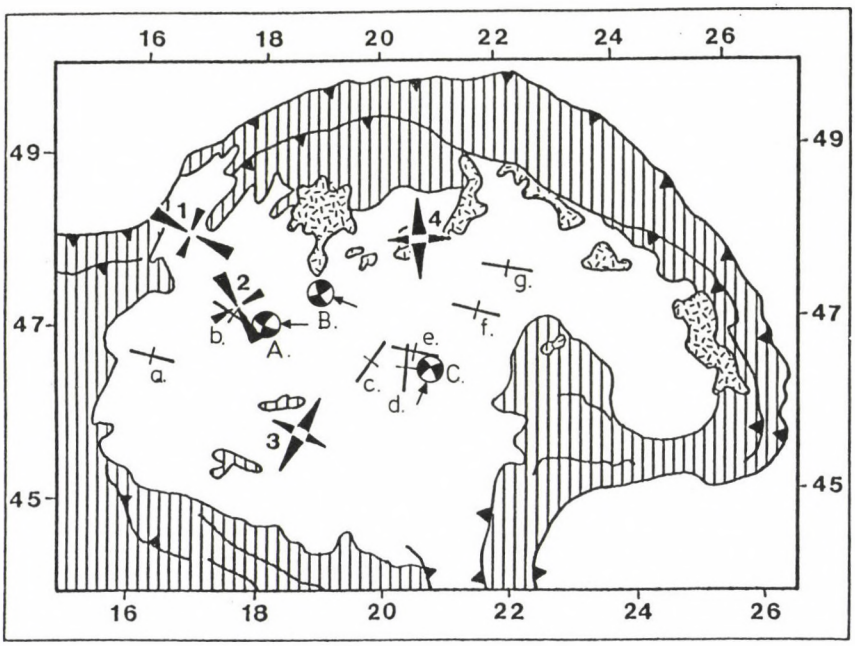

Fig. 1. Contemporary stress data in the Pannonian basin indicated by the analysis of borehole breakouts (a-g), by overcoring measurements (1-4) and by focal mechanisms (A-C). (Modified after Becker 1989.) The longer axis (arrow) shows the direction of maximum horizontal stress. Note that localities no. 3 and 4 are characterized by tensional stresses. Localities are: a = Bajánsenye, b = Bakonyszűcs, c = Gátér, d = Fábiánsebestyén, e = Szarvas, f = Sáránd, g = Baktalórántháza, 1 = Hainburg (Austria), 2 = Ugod, 3 = Beremend, 4 = Miskolc, A = Berhida, B = Dunaharaszti, C = Békés

One of the earliest and best studied techniques for investigating the state of stress in the earth's crust are stress or strain relief measurements commonly referred to as "overcoring" measurements. This technique generally involves determination of the natural, 3-D deformation relieved in a body of rock in situ when separated from the surrounding rock volume. It is the only technique which measures the complete stress tensor. The primary drawbacks of this method are that the measurements usually must be made near the surface and the measured stress is subject to effects of local topography, rock anisotropy and natural fracturing.

In situ stress measurements were carried out in Hungary

for the first time during the summer of 1989 in cooperation with experts from the University of Karlsruhe (FRG). Three test locations were carefully selected: one near the village Ugod in the Bakony (northwest Hungary), another one near Beremend, south to the Villany Mountains (southern Hungary) and the third one at the margin of the Bükk Plateau (northeastern Hungary). Alltogether 44 single stress measurements by two different overcoring techniques - the doorstopper and the triaxial strain cell method - were done using the equipments of the Karlsruhe University. Preliminary results of the measurements are shown in Fig. 1 (Becker 1989).

The basic idea of the fault slip technique is that striations (slip vectors) observed on small fault planes of a variety of altitudes along active fault zones can be inverted to yield a single deviatoric stress tensor. The validity of this method has been established by numerous studies which have demonstrated that the match between predicted and observed slip vectors is quite good (Angelier 1984).

In Hungary this technique can be used mostly for determination of the paleo-stress field during Miocene and Pliocene (Bergerat and Csontos 1989).

Volcanic feeder vents (i.e. dikes) propagate as natural hydraulic fractures perpendicular to the minimum principal stress. Thus, the mean strike of volcanic alignments corresponds to the maximum horizontal stress (Nakamura et al. 1977). In Hungary there are no volcanic rocks younger then Pliocene in age therefore this technique could only be useful for paleo--stress studies.

The analysis of well bore breakouts have been established in the last decade. The theoretical and experimental outlines of this new technique are summarised in the next chapter.

THE THEORY OF BREAKOUT ANALYSIS

Cox (1970) and Babcock (1978) were the first to investigate borehole breakouts in deep drillings. They observed that zones of elongated cross section over a great depth interval of

a drillhole show a constant preferential elongation direction which is independent from the stratigraphy. Bell and Gough (1979) concluded that these elongations of borehole cross section are breakouts of well bore wall. Well bore breakouts are natural phenomena resulting from shear fracturing in the region of maximum compressive hoop stress. According to elastic analysis (Tomoshenko and Goodier 1951), the maximum compressive hoop stress developed around a vertical borehole is concentrated on the azimuth of the least horizontal stress. If the stresses exceeded the shearing strength of the rocks the fractured material can break out of the borehole wall and a new free surface develops inducing a change in stress concentration which will lead to further failure.

Numerous investigations have established that breakouts form with consistent orientations within an individual well and in wells within a given field. Moreover, comparison of stress directions derived by earthquake fault plane solution and by hydraulic fracturing with those determined by breakout analysis also verified the method. There are exceptions too, i.e. as some interpretation of borehole breakouts showed (Plumb and Hickman 1985), the breakout direction within a well is not necessarily consistent and in zones near the surface the direction might be perpendicular to those in deeper zones. Above all, variations in breakout direction are the result of the influence of formation fluid pressure and of the drilling mud pressure. Micro fractures or anisotropic elastic characteristics of the rocks might be another reason for abnormally oriented breakouts (Blümling 1986).

BREAKOUT DATA AQUISITION AND DATA PROCESSING

Elongations of the well bore wall can be measured by optical (borehole camera), acoustic (seismo-acoustic televiewer) and mechanical (four-arm caliper log) methods. The caliper tool as a part of the dipmeter is the most commonly used of the three methods. The dipmeter determines the strike and dip of bedding planes by registration of formation resistivity on

four orthogonal pads. The pads are hydraulically extended to the borehole wall and therefore monitor the hole geometry as the tool is drawn up the well. Moreover, all the data to orient the tool are also recorded. As the tool is drawn up it is rotating because of the tension and twisting of the cable. The full shape of the borehole is recorded over a depth interval of 90^{o} rotation. Close to the surface the cable torque decreases, the rotation slows down and increases the depth interval while the tool rotate 90^{o}.

The measured caliper and orientation data should be displayed in a special way creating so-called contour plot. This plot gives an impression of the mean contour in a given interval along the borehole. To select breakout intervals strictly and determine the corresponding breakout directions precisely it must be considered some criteria established by Plumb and Hickman (1985):

- The tool is rotating beyond and below a borehole breakout.
- The rotation stops over the breakout zone. The required breakout depth is about 0.6 cm which means a diameter difference of 12 mm.
- The borehole elongation is clearly seen in the log. In contrast to the so-called washouts only one pair of pads show a relatively sharp ascent and descent of the borehole diameter.
- The smaller borehole diameter is nearly equal to the bit size. If both caliper values are higher than the bit size, the shorter pad distance must show a smaller variation of the borehole diameter.
- The elongation direction should not correspond to the hole azimuth for a longer time if the drilling deviates from the vertical. (At non vertical drillings borehole elongation can be induced by the weight effects of the drilling bars.)

BREAKOUT STUDIES IN HUNGARY

Dipmeter soundings as a part of routine well-logging have been carried out for 3-4 years in Hungar. 10 boreholes were

selected for experimental breakout analysis: Algyő-836, Bajánsenye-4, Bakonyszűcs-I, Baktalórántháza-I, Fábiánsebestyén-4, Földes-3, Gátér-M-1, Kiskundorozsma-16, Sáránd-S-1 and Szarvas-25.

The breakout analysis was carried out using a computer programme developed. This programme displays the different components of the caliper log and computes the breakout direction taking interactively into account the criteria listed above. At the same time and with the same data set a similar analysis was made by the experts of the Karlsruhe University (Müller and Heinemann 1988). The results of the two independent analyses are similar. In seven boreholes there was possible to calculate valuable breakout orientations. The discrepancies between the calculations of the two teams were less then 10 % in every case. In three boreholes the calculation was impossible either because of lack of breakouts or because of the bad quality of data.

The directions of maximum horizontal stress derived from mean breakout orientations is shown in Fig. 1. The results of earthquake fault plane solutions and of overcoring stress measurements are also shown. It is only a very preliminary interpretation (rather an impression) that the Pannonian basin can be divided into three stress provinces. The north-western part of the basin is characterized by W-NW compression, the middle and southern part by W-NW extension and the eastern part by W-NW compression (??) again. It must be emphasized, however, that distribution and number of stress determinations are not enough to give reliable information about the regional stress pattern of the Pannonian basin. It is our immediate objective to make further breakout analyses and in situ stress determination in Hungary.

ACKNOWLEDGEMENTS

Cooperation in stress determinations in Hungary was initiated by Prof. K Fuchs (University of Karlsruhe) and gladly accepted by Prof. A Meskó (Eötvös University, Budapest) and

dr. P Varga (Central Office for Geology, Hungary). We are grateful for financial support to the University of Karlsruhe and the Central Office for Geology, Hungary. The German group we work with is headed by Birgit Müller and dr. Arnfried Becker.

REFERENCES

Anderson E M 1951: The dynamics of faulting. 2nd edit., Oliver and Boyd, Edinburgh

Angelier J 1984: J. Geophys. Res., 89, 5835-5848.

Babcock E A 1978: AAPG Bull., 62, 1111-1126.

Becker A 1989: In situ stress measurements in Hungary. Manuscript

Bell J S, Gough D I 1979: Earth Planet. Sci. Lett., 45, 475-482.

Bergerat F, Csontos L 1989: Brittle tectonics and palaeo-stressfields in the Mecsek and Villány mts (Hungary). Correlation with the opening mechanisms of the Pannonian basin. Acta Geol. Hung. (in press)

Blümling P 1986: In situ Spannungsmessungen in Tiefbohrungen mit Hilfe von Bohrlochrandausbrüchen und die Spannungsverteilung in der Kruste Mitteleuropas und Australiens. Dissertation, Universität Karlsruhe, 1-135.

Brune J N 1974: Trans. Am. Geoph. Union, 55, 820-827.

Cox J W 1970: The high resolution dipmeter reveals dip-related borehole and formation characteristics. 11th Ann. Logging Symp. Soc. Prof. Well Log Analysis, 1-25.

Du Rouchet J 1981: AAPG Bull., 65, 74-85.

Haimson B C 1977: In: The earth crust, Geophysical Monograph Series. American Geophysical Union, Washington, D.C., 20, 575-592.

Hubbert M K, Willis D G 1957: Trans. Am. Inst. Mech. Engrs., 210, 153-168.

Müller B, Heinemann B 1988: Borehole breakout analysis in boreholes in the Pannonian basin. Manuscript

Nakamura K, Jacob K H, Davies J N 1977: Pageoph, 115, 87-112.

Plumb R A, Hickman S H 1985: J. Geoph. Res., 90(B7), 5513-5521.

Sykes L R 1974: Geodynamics of Iceland and the North Atlantic. D. Reidel, Dordrecht. Holland, 207-224.

Timoshenko S, Goodier J N 1951: Theory of Elasticity. 2nd ed. McGraw-Hill, New York, 506.

Tissot B, Welte D H 1978: Petroleum formation and occurrence.

Springer-Verlag, New York, 1-521.

Tóth L, Mónus P, Zsíros T 1989: The Berhida (Hungary) Earthquake of 1985. Gerlands Beiträge zur Geoph. (in press)

Zoback M L, Zoback M D, Adams J, Assumpcao M, Bell S, Bergman E A, Blümling P, Denham D, Ding J, Fuchs K, Gregersen S, Gupta H K, Jacob K, Knoll P, Magee M, Mercier J L, Müller B C, Paquin C, Rajendran K, Stephansson O, Suter M, Udias A, Xu Z H 1988: Global Patterns of Intraplate Stress: A Status Report on the World Stress Map Project of the International Lithosphere Program. Manuscript

Acta Geod. Geoph. Mont. Hung., Vol. 25 (3-4), pp. 267-277 (1990)

DEEP SEISMIC INVESTIGATIONS ALONG THE PANNONIAN GEOTRAVERSE

K Posgay, I Albu, E Hegedűs, Z Tímár

Eötvös Loránd Geophysical Institute of Hungary, H-1145 Budapest,
Columbus u. 17-23, Hungary

The investigation of the Earth's crust and upper mantle by seismic reflection methods has significant history in Hungary. Researchers of the "Eötvös" Institute observed reflections from the crust-mantle boundary as early as at the beginning of the 1950-s (Gálfi and Stegena 1955) and in the 1970-s characteristic arrivals were determined from the time range of the upper mantle by multiple coverage seismic reflection techniques. They were interpreted as reflections (Posgay et al. 1981). Conspicuous arrivals from the time range of the asthenosphere (15-20 s) were also received along the Pannonian Geotraverse in 1987.

In the bulk of sections published in other countries the upper mantle seems to be transparent. In the present paper investigations are discussed which lead to the conclusion that this apparent transparency is due to the frequency range below 10 Hz being neglected in both signal generation and observation in the overwhelming part of reflection deep soundings carried out on continents. The correctness of the assumption that arrivals from the time range of the asthenosphere are primary reflections is subjected to further investigation and conclusions are made concerning the structure of the asthenosphere.

Keywords: asthenosphere; deep seismic reflection method; Pannonian Basin

FOREWORD

In the course of 1986 an operative commission was established for investigating the structure of the lithosphere-asthenosphere in the Pannonian basin within the framework of the ICL National Committee. The task of this commission is to coordinate related geophysical studies.

The duration of investigations initiated on the basis of experiences obtained in past decades is planned for several years. The bulk of work is made with seismic reflection method. We intended to perform thoroughful investigations also with

magnetotelluric, geothermal and paleomagnetic methods. We also reinterpreted earlier gravity and geomagnetic results.

From the investigations that belong in the space of the ICL commission we shall give account in this paper of the seismic studies of the lithosphere and asthenosphere.

DATA ACQUISITION, PROCESSING AND RESULTS

The field work along the Pannonian Geotraverse was started in 1987; it joins the regional profile of Czechoslovakia marked 2T (Fig. 1) and crosses the Hungarian Central Range (HCR) and a part of the Pannonian Basin which comprises the Great Hungarian Plain. The Tertiary Pannonian Basin encircled by the Alps, Carpathian Mountains and Dinarides is bisected by the Hungarian Central Range into two parts: the Little Hungarian Plain and the Great Hungarian Plain.

Seismic measurements were carried out on the greatest part of the Pannonian Geotraverse. In this paper we review the results of a 50 km long profile section, measured in 1987, marked by a thick continuous line in Fig. 1. Along this section, observation was made using asymmetric split spreads, 48 channels on one side of the shot hole and 144 on the other. Five seismometers with 4.5 Hz eigenfrequency were grouped for each channel. Spacing between seismometer groups was 50 m. No low-cut filter was used during data acquisition. The 3 dB point of the amplifier was at 3 Hz. Coverage over a great part of the profile was 48-fold. Recording time was 30 s. In reflection deep seismic sounding along the Pannonian Geotraverse, shots were used for signal generation instead of vibrators, the former being more advantageous for generating low frequency seismic signals. To optimize the signal to noise ratio, charges of 50 kg were put in shotholes 50 m deep. For bigger charges more holes were used, but the size of the charge in a single hole was never increased.

Steps used in processing the present version of the Pannonian Geotraverse are as follows: true amplitude recovery, static and NMO corrections, 48-fold CDP stack, coherency enhancement. Filtering methods according to apparent velocities

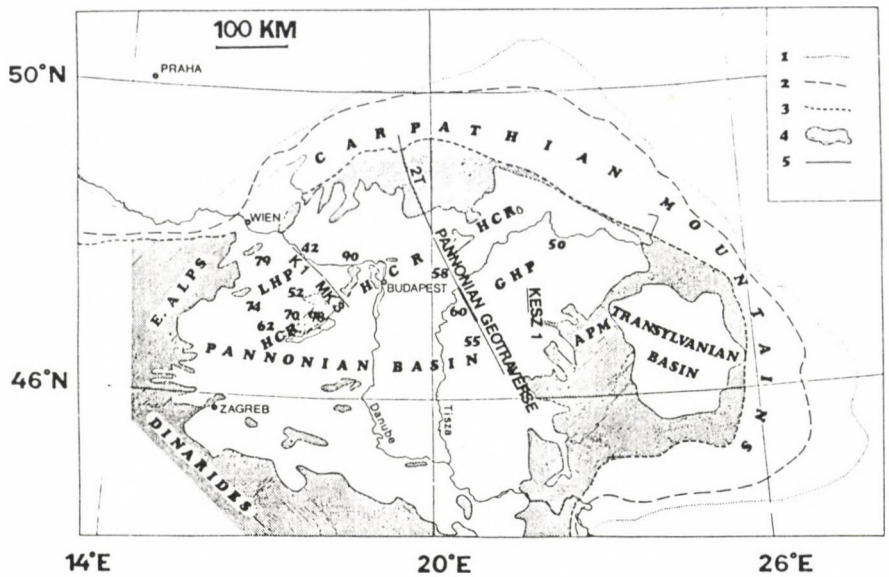

Fig. 1. Tectonic sketch map of the Pannonian basin and its environment; location of deep reflection profiles. 1 - foredeep contour; 2 - Carpathian front; 3 - boundary of the Outer and Central Carpathians; 4 - Pre-neogene formations within the Alpine fold belts; 5 - deep reflection lines. Part of the profile discussed in the paper is marked with thick line. Numbers in the figure indicate the depth of the asthenosphere in km's at the site of magnetotelluric measurements (MTS). HCR - Hungarian Central Range, LHP - Little Hungarian Plane, GHP - Great Hungarian Plane, APM - Apuseni Mountains

applied to the seismograms led to a substantial improvement of the signal to noise ratio. Narrow band filtering and migration were not used in the preliminary processing of the Geotraverse.

The importance of careful trace editing should be emphasized in the improvement of the signal to noise ratio for low energy arrivals coming from the time range of the lower crust and the asthenosphere. In the recent processing a 24 sec two-way travel time section has been prepared with 48-fold coverage.

Figure 2 shows a line drawing prepared on the basis of a processed profile section. The following figures illustrate details selected from typical places along the profile.

Figure 3 shows a part of the section from the upper crust. The time range is 1 to 6 s. The Neogene sediments are good

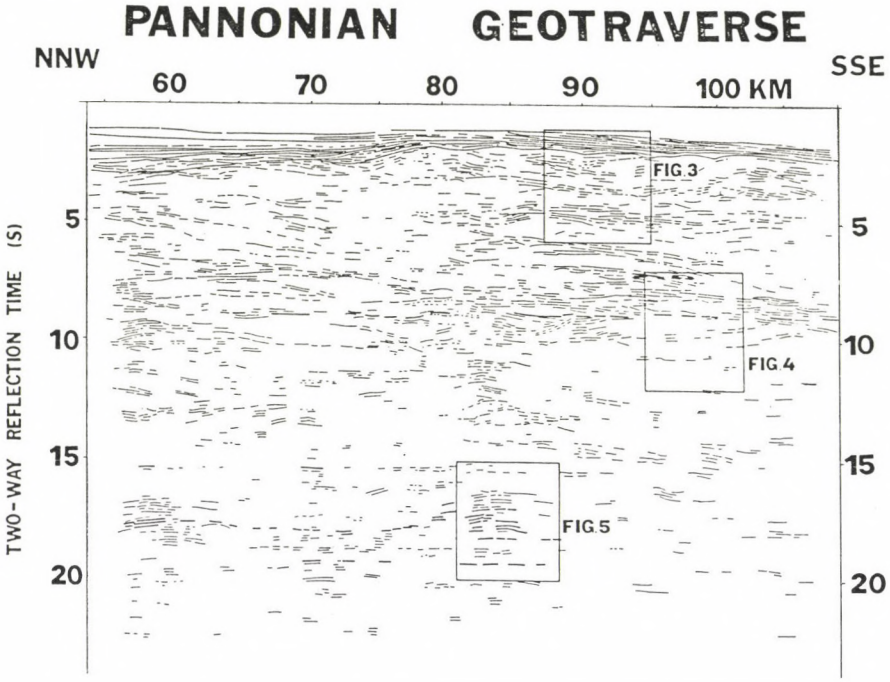

Fig. 2. Line drawing of a preliminarily processed part of the Pannonian Geotraverse. Squares indicate parts of sections referred to in further figures

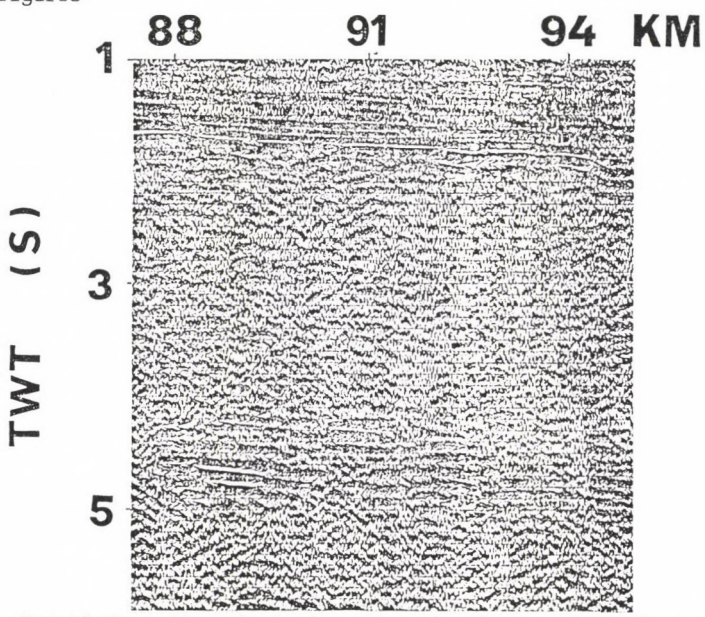

Fig. 3. Detail from the stacked section showing part of the upper crust

reflectors. They differ from the underlying Paleogene and Mesozoic sediments. The bottom of the Neogene basin can be inferred from the weakening of reflections at 1.6-2.0 s TWT. The so called transparent zone of the upper crust seems to appear only prior to 4.5 s (about 10 km depth). This is in agreement with the correlation revealed by Klemperer (1987), according to which the reflecting zone has a shallow position within the crust if the heat flow is high.

Figure 4 shows the depth range of the lower crust and upper mantle. Strongly marked horizons can be found within the whole lower crust. At the bottom of the crust an increase of shorter reflecting regions is observed. Below the Moho (at 8.8 s TWT) a decrease in their number is conspicuous.

Figure 5 shows the time range of the asthenosphere. Around 15 s there is a zone characterized by weak reflections,

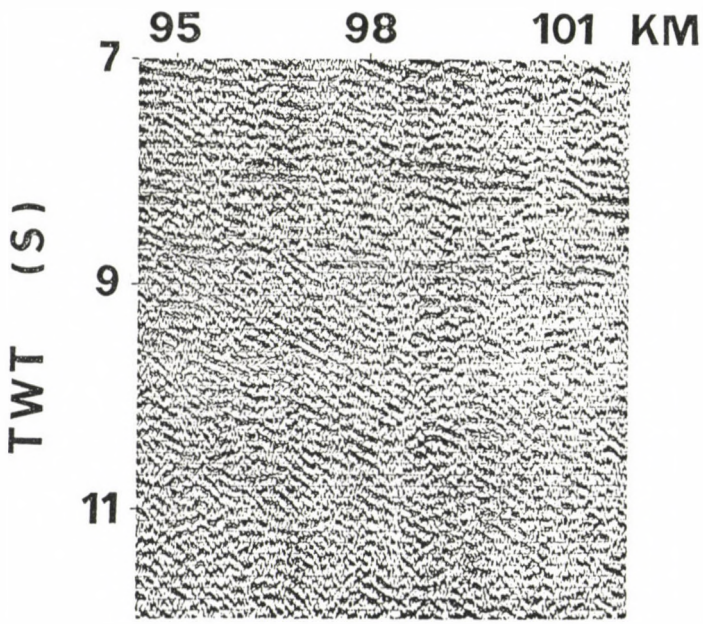

Fig. 4. Detail from the stacked section showing part of the lower crust and upper mantle

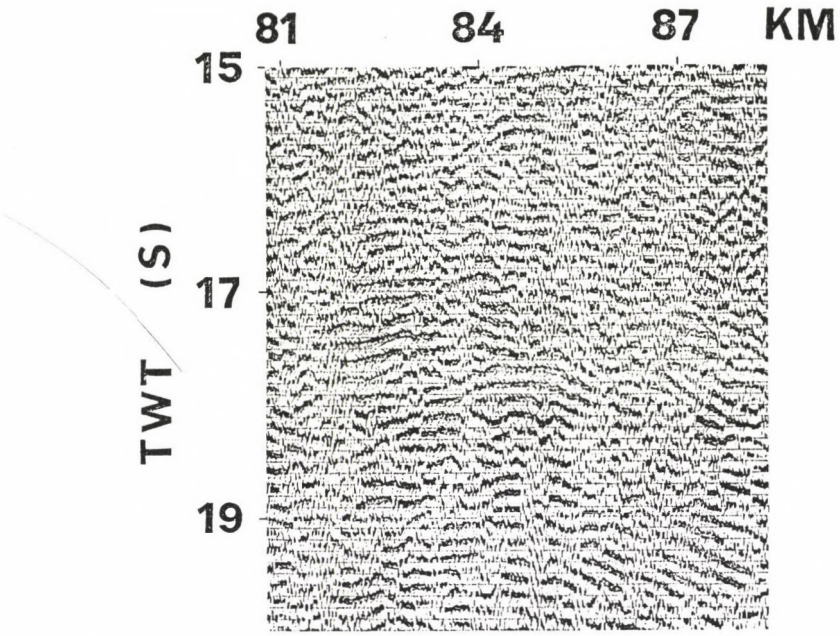

Fig. 5. Detail from the stacked section showing part from the time range of the asthenosphere

but between 17 and 19 s both amplitudes and traceability of reflections have significantly increased.

When interpreting arrivals observed within the time range of the asthenosphere, one has to weigh the pros and cons as to their reflected character. In planning, conducting, processing and interpreting such measurements one has always to choose from several possibilities. Through an analysis of results obtained so far and by the means of subsequent complementary investigations we continue to study the possibility of arrivals other than single reflections (multiples, lateral arrivals, converted waves), the reality of reflection (signal to noise ratio, true amplitudes, reflection coefficients) and the particular features of the Pannonian basin. Though these are only the preliminary results of our investigations, certain considerations may be of interest.

The bulk of investigations of the continental lithosphere by seismic reflection methods has been performed with vibrators

as signal sources. According to our experiences the base plate of the vibrator and the resonating ground mass perform oscillations with an attenuation substantially less than the critical (Bodoky et al. 1979). In related studies relative attenuation values between 0.3-0.4 were determined, letting the authors infer that for generating frequencies less than resonance frequencies a low cut taper of at least 12 dB/oct should be used. (At the time of the experiment no force control was yet used.) The energy transmission into the earth below the resonance frequency is extraordinarily unfavourable.

In the Pannonian basin the apparent frequency of arrivals observed within the time range of the mantle was below 8 Hz. Thus the question arises whether signal generation by vibrators in continental measurements may have caused the absence of arrivals in the time-range of the mantle? Such an explanation is supported by crustal studies carried out in Hungary with vibrator source, too. In the western part of the Pannonian basin, in the Little Hungarian Plain, a crustal investigation profile (Fig. 1, line K 1) was recorded with vibrator source (Pápa et al. 1987), a part of which is presented in Fig. 6. The upper mantle, similar to the results of other vibroseis measurements, seems to be transparent.

The application of a low cut filter to the Pannonian Geotraverse produces remarkable results. A detail of the section - selected from the time range of the asthenosphere - is shown in Fig. 7 with band pass filters 4-32 and 12-32 cps. The arrivals disappeared when the frequency of the low-cut filter was increased.

On the basis of the foregoing it is assumed that equipment and methodology may also be influential in obtaining arrivals from the range of the upper mantle. The generally accepted methodology was established for studying crustal structure, and the depth of investigation did not reach in most cases the asthenosphere.

Nevertheless results can be found in the literature, obtained with pulsed type sources that render probable reflection arrivals from the upper mantle. For example Dohr (1970)

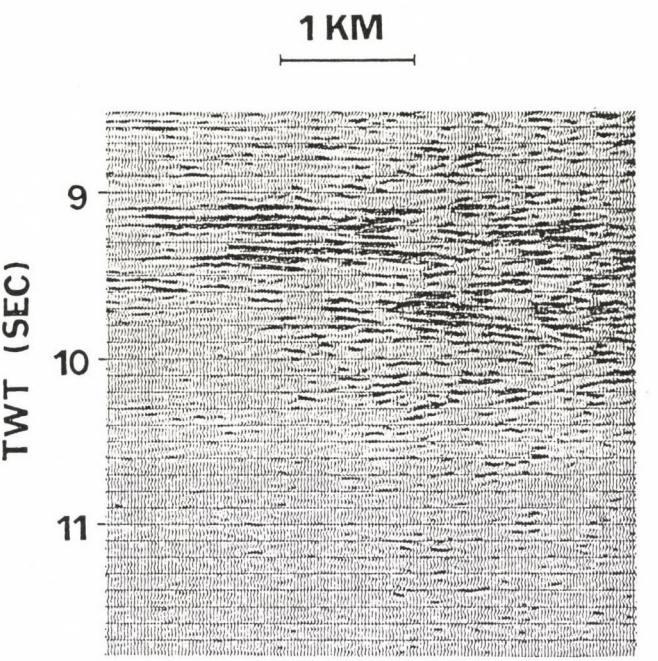

Fig. 6. Part of a section measured in the western part of the Pannonian basin by vibroseis method. The upper mantle is apparently transparent

received deep reflections in his pioneering work. In this reflection survey conducted in the Upper Rhine valley he received arrivals from below the Moho up to a total recording time of 18 s.

In the marine deep soundings of BIRPS, arrivals of excellent quality were received from the range of the upper mantle (Brewer et al. 1983). In the Pamir-Himalayan Project, reflections from the upper mantle were also observed when big charges were used for shots (Kaila 1988). They were interpreted to have come from the top and bottom of the asthenosphere, respectively.

When weighing the possibilities it should also be considered that the heat flow in the measured section of the Pannonian Geotraverse is between 80-100 mW/m^2 (Dövényi et al. 1983). In accordance with this, the conductive layer of the upper mantle was determined at a relatively shallow depth by

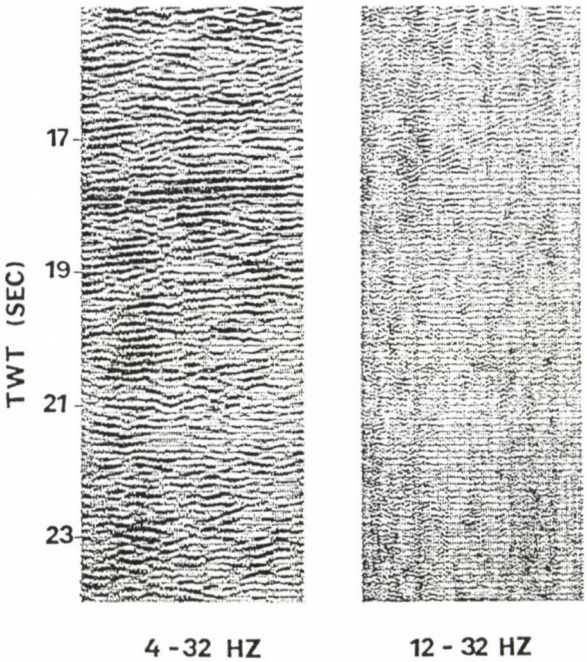

Fig. 7. Detail of the Pannonian Geotraverse selected from the time range of the asthenosphere. Band filter on the left side is 4-32 Hz, on the right 12-32 Hz. On the latter part the upper mantle seems to be transparent!

magnetotelluric measurements (Ádám et al. 1982).

Magnetotelluric Sounding (MTS) points with apparent depth values of the asthenosphere are indicated in Fig. 1. The depth of the conductive layer of the upper mantle is expected at about 50-60 km over the presented section of the Pannonian Geotraverse. The relatively shallow depth of the asthenosphere may provide sufficient conditions for defining lithospheric properties and thickness by seismic methods, since arrivals from this depth range are expected at relatively short arrival times, i.e. along a shorter wavepath with smaller energy loss through absorption.

CONCLUSIONS

In the reviewed part of the Pannonian Geotraverse arrivals

in the time range of the asthenosphere appeared in bundles. Assuming reflection arrivals we may infer a new laminated complex. Laminated structure of the lower crust is interpreted by Meissner and Kusznir (1987) since the decrease of viscosity below a critical value (1023 poise) in the hot lower crust may play a significant role in the formation of laminae. The rheologic model was determined to be q = 50 mW/m^2 for shields, q = 70 mW/m^2 for postorogenic Paleozoic types, q = 90 mW/m^2 for extensional Cainozoic types. It is assumed that in the multimineral crust the conditions for the formation of laminae are more favourable than in the upper mantle that can be regarded as relatively homogeneous.

A viscosity decrease in the case of shear stress may promote lamination. Lamination is also possible for an upper mantle composed largely of olivine due to the following causes:

1. According to Fuchs (1986), in the horizontal shear strain of the subcrustal lithosphere "a preferred orientation of olivine crystals is probable". Such a regime is regarded by him as suitable for the formation of laminae.

2. Alternation of partially molten and solid laminae of intrusive bodies.

3. Sheet-like arrangement of volatiles similar to that suggested for the lower crust (Posgay et al. 1986).

It is interesting that groups of arrivals from laminae appear only in certain parts of the profile. They may be due to problems of data acquisition and methodology, to the intermediate state of processing, but also to tectonic or perhaps petrographic conditions affecting the stress field of the asthenosphere.

ACKNOWLEDGEMENTS

The authors are deeply obliged to the Hungarian Academy of Sciences and the Central Geological Office of Hungary for their moral and financial support, as well as to the "Eötvös Loránd" Geophysical Institute of Hungary for permission to publish the results.

REFERENCES

Ádám A, Vanyan L L, Varlamov D A, Yegorov I V, Shilovski P P 1982: Physics of the Earth and Planetary Interiors, 28, 251-260.

Bodoky T, Rumpler J, Halmos P, Apor L 1979: Magyar Geofizika, 20, 201-210.

Brewer J A, Matthews D H, Warner M R, Hall J, Smythe D K, Whittington R J 1983: Nature, 305, 206-210.

Dohr G 1970: In: Graben Problems. Schweizerbart, Stuttgart, 207-218.

Dövényi P, Horváth F, Liebe P, Gálfi J, Erki I 1983: Geophysical Transactions, 29, No. 1, 3-114.

Fuchs K 1986: In: Reflection Seismology: The Continental Crust Geodynamics Series (Barazangi M and Brown L eds), Vol 14, Am. Geophys. Un. Washington, D.C., 67-76.

Gálfi J, Stegena L 1955: Geophysical Transactions, 4, No. 2, 37-40.

Kaila K L 1988: In: Deep Seismic Reflection Studies Newsletter (Blundell D J and Wright C eds), No. 2, University of London, U.K., 36-46.

Klemperer S L 1987: J. of Geophysics, 61, 1-11.

Meissner R, Kusznir N J 1987: Annales Geophysicae, 5, No. 4, 365-374.

Pápa A, Nemesi L, Hobot J, Pintér A, Ráner G, Redlerné T M, Varga G 1987: Several aspects of the deep structure in a complex study of the Northwestern Plain of Hungary. Lecture on the Geological and Geophysical Itinerary Meeting. Balatonszemes, Hung. Geophys. Soc., Budapest, Spec. Publ.

Posgay K 1975: Geophysical Transactions, 23, 13-18.

Posgay K, Albu I, Petrovics I, Ráner G 1981: Character of the earth's crust and upper mantle on the basis of seismic reflection measurements in Hungary. Earth Evolution Sciences, Vieweg, Wiesbaden, 1, No. 3-4, 272-279.

Posgay K, Albu I, Ráner G, Varga G 1986: In: Reflection Seismology: Global Perspective Geodynamics Series (Barazangi M and Brown L eds), Vol. 13, Am. Geophys. Un., Washington, D.C., 55-65.

Acta Geod. Geoph. Mont. Hung., Vol. 25 (3-4), pp. 279-290 (1990)

CRUSTAL CONDUCTIVITY ANOMALIES IN THE PANNONIAN BASIN

A Ádám[1], Z Nagy[2], L Nemesi[3], G Varga[3]

[1]Geodetic and Geophysical Research Institute of the Hungarian Academy of Sciences, H-9401 Sopron, POB 5, Hungary

[2]Geophysical Exploration Company (GKV), H-1062 Budapest, Népköztársaság u. 59, Hungary

[3]L Eötvös Geophysical Institute, H-1145 Budapest, Columbus u. 17-23, Hungary

Different types of electrical conducting formations or conductivity anomalies (CA) were found at different depths in the Pannonian basin by magnetotelluric deep soundings. They are presented here with characteristic examples.

The main types of CA's are as follows:
- Conducting formations embedded into the basement directly under the sedimentary cover (e.g. CA at Magyarmecske)
- CA within the resistive basement at a depth of some km (e.g. Transdanubian CA)
- CA in the lower crust (at a depth of about 18 km)
- CA connected to a tectonic line or zone (e.g. along the Balaton line).

Physical or material causes of these conductivity anomalies are illuminated by borehole samples or/and by other geological-geophysical information or hypotheses.

The depth distribution of the crustal conductivity anomalies is shown on a map for a part of Hungary.

Keywords: crustal conducting formations; electrical resistivity; fluids in the crust; graphitic schists; Pannonian basin

1. INTRODUCTION

The electrical resistivity distribution in the Earth's crust can be determined by electromagnetic induction methods, first of all by telluric (TT) and magnetotelluric (MT) deep soundings using a wide spectrum of natural electromagnetic variations. These methods have great resolving power for the conducting formations with metallic (electronic) or ionic conduction. The temperature effect on the conductivity of the rocks increases with depth due to electric semiconduction.

In the Pannonian basin the crustal conducting formations

are represented by strongly carbonized graphitic schists or shales, ore bodies, loose tectonic fracture zones in which a high pore volume fraction is filled by fluids or fluids in the lower crust originating from metamorphosis, etc. In the following different CA types are described between surface and lower crust which are characteristic for the geological tectonic feature of the Pannonian basin. In 1987 a map has been constructed on the depth of CA's in Hungary based on a telluric and magnetotelluric data set collected by different Hungarian institutions. A part of this map is shown in Fig. 1 (NW Transdanubia). It is to be noted that the Pannonian geotraverse has been measured after construction of this map.

2. CONDUCTING FORMATIONS UNDER TERTIARY SEDIMENTS

Subsidence and sedimentation or filling up of the Pannonian basin took place in the Tertiary, mainly in the Pliocene. The thickness of the Neogene sediments reaches in the deepest basin parts 6-8 kms. These sediments consist mainly of clay, then of sand, gravel, marl, sandstone. Their resistivity is between 2 and 10 Ωm, though rarely, first of all, in case of coarse fluvial sediments and Miocene conglomerates it reaches 30-40 Ωm. Therefore, the resistivity (as well as density and seismic velocity) of the basement under these Tertiary sediments, i.e. of the Mesozoic carbonates or Paleozoic crystalline rocks is generally higher than that of the young sediments. Hence, the Pretertiary basement is a first order geophysical horizon. There are small areas in the Great Hungarian Plain (SE part of the Pannonian basin) where Upper Cretaceous sediments of 20-40 Ωm cannot be separated from the Miocene sediments so the geoelectric basement starts at the bottom of the Cretaceous clastic sediments. In other small areas very conductive formations (Rho $\leqslant 1$ Ωm) are embedded into the Paleozoic formations. In NE Hungary (Szendrő, Alsóvadász) Devonian graphitic schists occur with some pyrite content in the basement. In the Magyarmecske-Bogádmindszent area (SW Hungary) Carboniferous carbonized sediments have been detected under Pliocene sediments

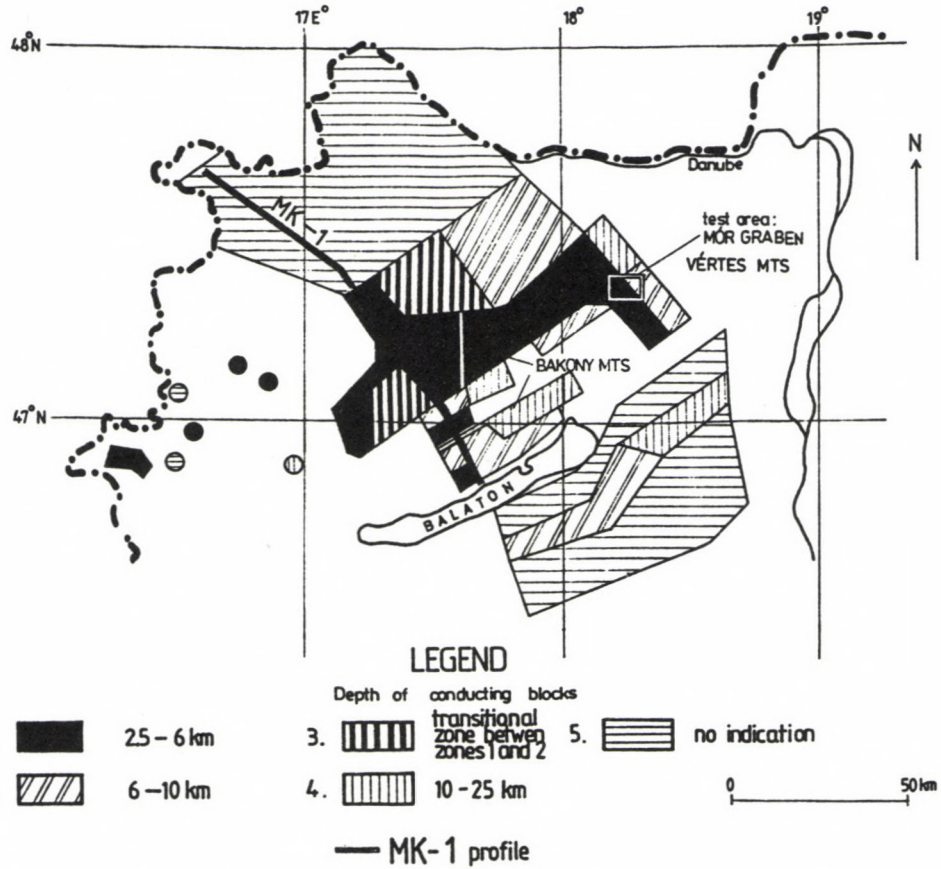

Fig. 1. Highly conductive formations within the Pre-Austrian basement in different depth ranges (see Legend) in the Northern part of Transdanubia. A part of the map constructed by Ádám et al., 1987

(Nemesi et al. 1985). The resistivity of some strongly carbonized borehole samples is less than 0.1-0.002 Ωm. The average resistivity of the whole Carboniferous sedimentary sequence is about 1 Ωm. Geological and geophysical results from this area are shown in Fig. 2.

The Bouguer gravity map (Fig. 2a) has been constructed using measurements made with a station density of 1 station/1 km^2. This map reflects qualitatively the basement depth of the Tertiary basin not deeper than 2-3 km. If the basin is deeper, the correlation between Bouguer anomalies and basement depth gets worse. A gravity maximum may even correspond to very deep parts of the basin due to the mantle material intruded into the thinning crust.

Since the mid-fifties we have experienced in Hungary that the telluric method images the basement relief of the deep basins essentially better than gravimetry. Therefore telluric profiling has been made in the greatest part of the country including the mentioned area (Fig. 2b). The telluric isoline map significantly differs here from the gravimetric one in consequence of the Magyarmecske CA of a conductance of 1000 Siemens. As the telluric anomaly is influenced - besides the basement relief - by the lateral inhomogeneity (variation) of the average resistivity of the sedimentary cover, this effect has been taken into account. For determination of the average resistivity of the sedimentary cover, D.C. Schlumberger or dipole equatorial soundings were used initially but from the mid sixties they have been substituted by magnetotelluric deep soundings. On the basis of these measurements, an isoohm map of the sediments was constructed and used for the transformation of the telluric map to a basement relief map.

In Fig. 2c the difference is shown between the geoelectric (telluric) (H_s) and seismic (H_s) basement depths. The geoelectric basement is in the syncline (minimum) about 2000 m deeper than the seismic one and the latter is well correlated with the gravimetric values.

This difference has been illuminated by the borehole samples and magnetotelluric soundings (see in Fig. 2d). The

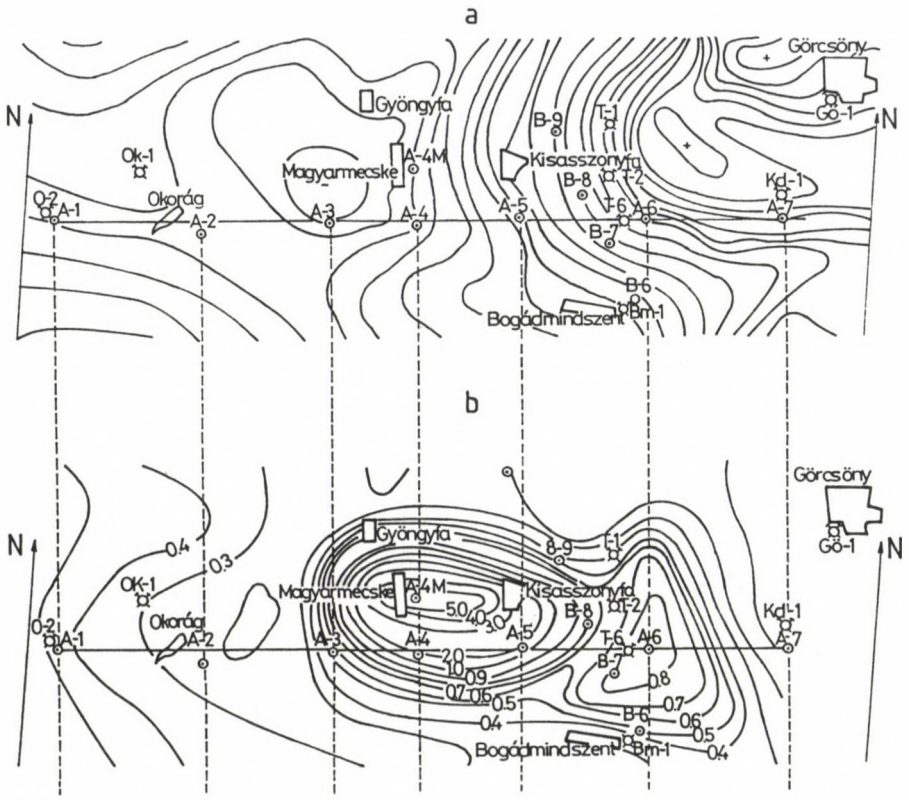

Fig. 2a. Gravimetry Bouguer map with the MT profile

Fig. 2b. Telluric isoarea map with the MT profile

derived geoelectric cross-section is given in Fig. 2e.

At borehole O-2, in the western part of the magnetotelluric profile, Lower Paleozoic crystalline rocks underlie the Pliocene sediments. Here the results of different geophysical techniques agree. Eastwards the Pliocene and younger sediments are thinning out according to gravimetric and seismic measurements. At the eastern end of the profile (borehole Kd-1) the depth of the Paleozoic basement does not reach 100 m.

In the intermediate boreholes there are Carboniferous sediments under the Pliocene one. In Bm-1 in a depth of 1200 m a Carboniferous carbonized formation of a very low resistivity

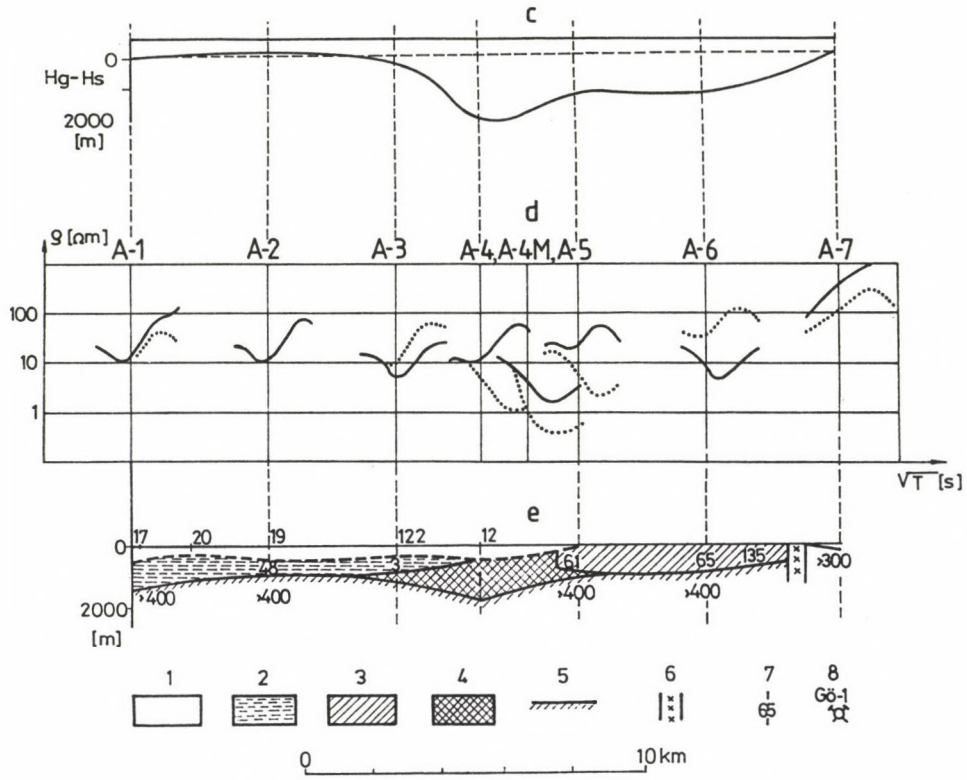

Fig. 2c. Difference between the depth of the basement of high resistivity (geoelectric) and that of high velocity (seismic) calculated prior to the detailed MT measurements along the line A-1 and A-7

Fig. 2d. MTS curves of E and H polarization at measuring sites between A-1 and A-7

Fig. 2e. Geological cross section based on the A-1 — A-7 MT profile 1. Upper Pliocene and Pleistocene formations (12-20 Ωm); 2. Lower Pliocene formations (4.8 Ωm); 3. Carboniferous formations of high resistivity (61-135 Ωm); 4. Carboniferous formations of low resistivity (1 Ωm); 5. Early Paleozoic crystalline basement (>400 Ωm); 6. Tectonic zone; 7. Resistivity of geoelectric layer calculated by 1-D MT inversion; 8. Borehole

lies under sandstone and conglomerate. The low resistivity is witnessed by the electric logging. The greatest thickness (>1000 m) was found at the MT site A-4M with an average

resistivity of 1 Ωm.

3. TRANSDANUBIAN CRUSTAL CONDUCTIVITY ANOMALY

The most characteristic crustal anomaly in Hungary (Fig. 1) is in Transdanubia between the Balaton- and Rába-lines under Mesozoic dolomites at a depth of a few kms. It was first indicated by relative telluric frequency soundings (Ádám and Verő 1964). Using magnetotelluric methods the main features of this extraordinary CA have been determined in the seventies as follows:

a) The anomaly consists of 10-20 km wide stripes of high conductivity at different depths. Stripes lie parallel to the longitudinal (NE-SW) fractures of the area. The impedance maximum directions (Z_{xymax}) are perpendicular to these stripes. The shallowest anomaly stripe lies about 25 km NW of Lake Balaton.

b) The ratio of the extreme resistivity values ($\varrho_{max}/\varrho_{min}$) i.e. the simple anisotropy is high (e.g. at station Zánka $\varrho_{min} < 1$ Ωm; $\varrho_{max} > 1000$ Ωm).

c) As the E polarization is connected in a vast area of the anomaly to the Rhomin curves according to the static shift EM distortion (Ádám and Varga 1990), it should be supposed on the basis of numerical model calculation that the anomaly consists of parallel and isolated conducting blocks (dikes).

These features initiated different explanations for the origin of the anomaly laying the emphasis on one or the other characteristic : graphite-model (Ádám 1971), electrolyte in the high porosity fractures (Ádám 1984), or their combination (Ádám 1985) .

A graphitic block structure seems to be at present the most probable cause of the Transdanubian CA as it is also supported by its coincidence with seismic reflexion horizons (Ádám O et al. 1984).

An indirect proof for this model was yielded by audio-magnetotelluric measurements in the western part of the Bakony-Drauzug independent geological unit (BDU) (Fig. 3),

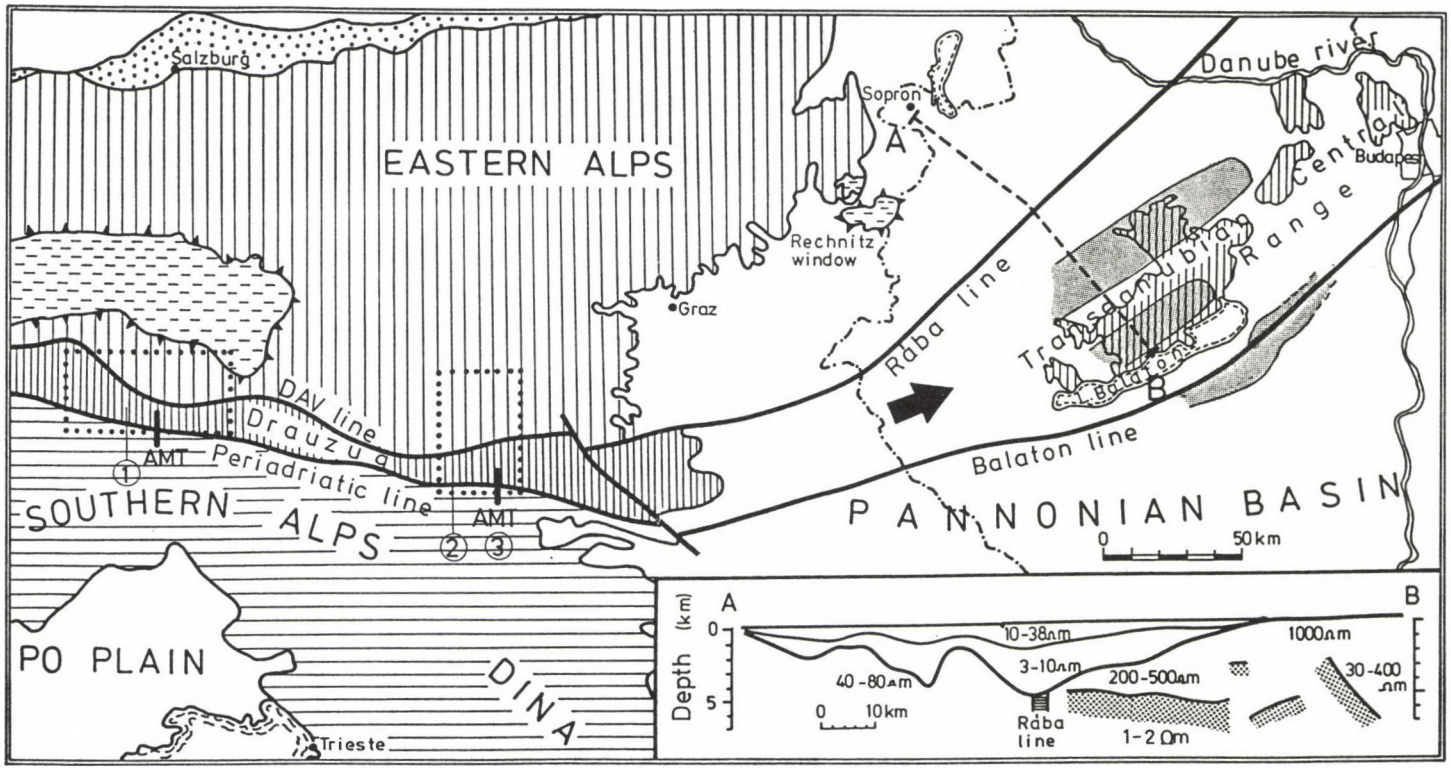

Fig. 3. Tectonic setting of the Bakony-Drauzug Unit (BDU) and the most characteristic conducting zones in the Transdanubian Central Range (Bakony) (stippled). Dotted squares indicate the magnetotelluric measuring sites in the Eastern Alps. 1. Gail-valley, MT, AMT (profile); 2. Zell Pfarre MT; 3. Karawanken MT, AMT (profile). The inset shows the electric structure along the profile A-B after Ádám O et al. (1984) Stippled lines give the position of good conductor. (The whole figure is redrawn after Horváth et al. 1987)

in the Gail-valley where the parallel E-W directed graphitic schist blocks were traced from below the dolomites of the Carnic Alps to the surface in the Gail-valley Alps (Ádám et al. 1986, 1988). These formations show the characteristic features in a, b and c.

We suggest that both the Transdanubian and Gail-valley anomalies are caused by similar Paleozoic graphitic shale or schist blocks beneath thick Mesozoic dolomites. The shales rotated due to a continent-continent collision (between Africa and Eurasia) around a horizontal axis into an almost vertical position. Thus shales have great horizontal electrical anisotropy in narrow elongated dikes (stripes) along the Balaton line and in parallel zones (see Fig. 1).

According to paleomagnetic data (Balla and Szalay 1980) the Transdanubian Central Range with the originally E-W directed conducting stripes suffered a counterclockwise rotation of 35^{o}. The graphite formations, a material of low viscosity, could play a role in motions during the Alpine orogeny (Horváth et al. 1987). Their hydrocarbon perspectives as a former source material are worth studying (see recent laboratory investigation of Duba and Will 1988).

4. CONDUCTING ZONE IN THE LOWER CRUST

On the basis of the empirical relation between the depth of the lower crustal conducting layer and the surface heat flow (Ádám 1987, Fig. 4), a CA is supposed in the depth range between 10 and 20 km according to the extremely hot Pannonian basin. Recently, this conducting layer is assumed to be a consequence of a dehydration process at temperatures higher than 300^{o}C (Hyndman 1988). Klemperer (1987) found similar relations between the reflectivity of the lower crust and the heat flow in agreement with Ádám (1987).

Our map (Fig. 1) shows some CA indications in this depth range. Nevertheless, the different EM distortion effects of near surface conductivity anomalies cannot be neglegted in interpreting these anomalies. The induction side effect of the much

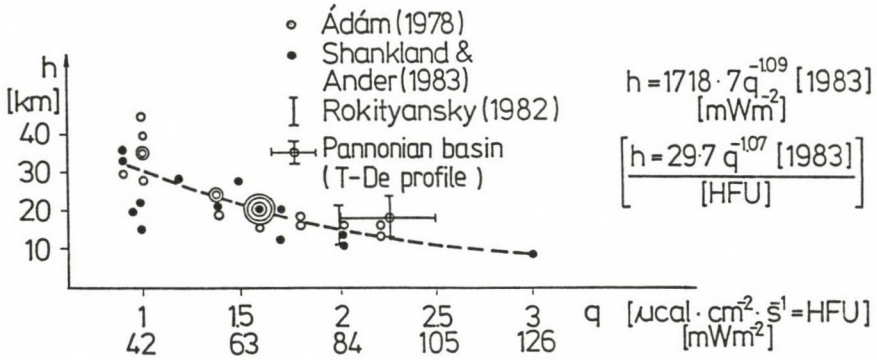

Fig. 4. Depth of the crustal conducting layer vs. surface heat flow (Ádám 1987)

shallower Transdanubian anomaly generates e.g. an indication of apparent deep conducting layers in the vicinity of the conducting body. It should also be noted that a conducting layer of some hundred Siemens can hardly be detected under a thick sedimentary cover. Ádám et al. (1982) subtracted the effect of the sediments with a correction method from the MT admittances measured in covered areas and on such a way the existence of this crustal conducting layer could be proved. The statistical treatment of a large MT data set measured by the high precision Phoenix MT instrument along a 60 km long MT profile with a station distance of 750 m hinted at the existance of this layer. The Bostick 1-D inversion of the Phoenix data drew our attention to this layer which was checked by 1-D layer inversion of MT data of longer period measured by another instrument (Ádám et al. 1989). Its most probable depth is 17-18 km and its conductance is some hundred Siemens. The depth value with its standard deviation is shown in Fig. 4 in function of the heat flow. As the depth values fit to the empirical relation, the lower crustal anomaly in the Pannonian basin represents the same dehydration phenomenon. (The referred MT profile is shown in Ádám et al. 1989.)

5. TECTONICS AND CONDUCTIVITY ANOMALIES

Tectonic implications of the graphitic block structure of

the Transdanubian crustal conductivity anomaly have been used in its interpretation. The Transdanubian CA relates unambiguously to the Balaton line (Figs 1 and 3). It is very probable that the Balaton anomaly forms only a parallel stripe of the Transdanubian anomaly having the same material composition.

The role of loose fracture zones with water circulation and the connected geothermal anomalies (Oelsner 1989) in the formation of CA's has not yet been studied sufficiently although the knowledge of these factors is needed for the geoelectric exploration of hydrocarbon reservoirs in the basement, too. For this latter purpose the resolving power of the EM sounding is to be increased.

6. CONCLUSION

In this study a few characteristic crustal conductivity anomalies in the Pannonian basin have been presented from the surface to the lower crust. The conductivity increase has been basically attributed to two material causes: strongly carbonized, graphitic formations and fluids (electrolytes). In the spatial distribution of these anomalies geological-tectonical factors, state parameters (temperature, pressure) play decisive roles. Consequently, they can indirectly be studied in the Earth by the parameters of the crustal conductivity anomalies.

REFERENCES

Ádám A 1971: Geonómia és Bányászat, 4, 297-308.

Ádám A 1984: Geophys. Prospecting, 32, 543-554.

Ádám A 1985: Acta Geod. Geoph. Mont. Hung., 20, 173-182.

Ádám A 1987: Phys. Earth Planet. Inter., 45, 209-215.

Ádám A, Varga G 1990: Phys. of the Earth and Planet. Int., 60, 80-88.

Ádám A, Verő J 1964: Acta Techn. Hung., 47, 63-77.

Ádám A, Vanyan L L, Varlamov D A, Yegorov I V, Shilovski A P, Shilovski P P 1982: Phys. of the Earth and Planet. Int., 28, 251-260.

Ádám A, Duma G, Gutdeutsch R, Verő J, Wallner Á 1986: J. of Geophysics, 59, 103-111.

Ádám A, Nagy Z, Varga G 1987: Map "Presence of highly conductive formations within the Preaustrian basement"

Ádám A, Duma G, Horváth J 1988: Magyar Geofizika, 29, 27-43.

Ádám A, Landy K, Nagy Z 1989: Tectonophysics, 164, 361-368.

Ádám O, Haas J, Nemesi L, Redlerné Tátrai M, Ráner G, Varga G 1984: An. Rep. Eötvös L. Geophys. Inst. Hung. for 1983, 37-44.

Balla Z, Márton-Szalay E 1980: Geophys. Transactions, 26, 57-77.

Duba A, Will G 1988: Electrical conductivity of black shale: implications for crustal conductivity anomalies. Lecture at the IX EM Induction Workshop, Dagomys, Oct. 1988.

Horváth F, Ádám A, Stanley W D 1987: Rendiconti della Societa Geol. Italiana, 9, 123-130.

Hyndman R D 1988: J. Geophys. Res., 93, 13.391-13.405.

Kázmér M, Kovács S 1985: Acta Geol. Hung., 28, 71-84.

Klemperer S L 1987: J. of Geophysics, 38, 279-296.

Nemesi L, Hobot I, Varga G 1985: Acta Geod. Geoph. Mont. Hung., 20, 135-150.

Oelsner Chr 1989: Tectonophysics, 164, 369-374.

Acta Geod. Geoph. Mont. Hung., Vol. 25 (3-4), pp. 291-307 (1990)

ELECTRICAL CONDUCTIVITY ANOMALIES ALONG THE PANNONIAN GEOTRAVERSE AND THEIR GEOTHERMAL RELATION

A Ádám[1], Z Nagy[2], L Nemesi[3], G Varga[3]

[1]Geodetic and Geophysical Research Institute of the Hungarian Academy of Sciences, H-9401 Sopron, POB 5, Hungary

[2]Geophysical Exploration Company (GKV), H-1062 Budapest, Népköztársaság u. 59, Hungary

[3]L Eötvös Geophysical Institute, H-1145 Budapest, Columbus u. 17-23, Hungary

Electrical conductivity anomalies (CA) detected by deep magnetotelluric (MT) soundings along the Pannonian geotraverse - crossing Hungary from the Northern Hungarian Central Range to the Great Hungarian Plain in NW-SE direction - are presented. After discussing some important methodical aspects of the indication of the anomalies, geoelectric parameters of the lower crustal and the asthenospheric conductivity increase are described with their spatial variation. While the crustal conductivity anomaly of some hundred Siemens is hardly detectable under low resistivity sediments the conducting asthenosphere unambiguously appears on the MTS curves. All of these anomalies are related to the exceptionally high heat flow of the Pannonian basin.

Keywords: asthenosphere; electrical conductivity anomaly; heat flow; lower crust; magnetotellurics; Pannonian basin

1. INTRODUCTION

One of the first results of magnetotelluric research in Hungary was that the conducting asthenosphere, corresponding to the Gutenberg low velocity channel in the upper mantle under the lithospheric lid lies much shallower in the young Pannonian basin than in the surrounding old platforms in accordance with the difference in their geothermal conditions (Ádám 1963). This result helped to explain the physical state of the asthenosphere by its partial melting and at the same time to understand the kinematics of the plates.

In the case of the magnetotelluric deep soundings, the shallower anomalies weaken and distort or even fully cover the deeper ones similarly to other geophysical methods. Therefore, many experiments have been made in Hungary for a more precise

determination of the parameters of the conducting asthenosphere, the MT measuring and data processing techniques and not least the theoretical basis were successively improved. (From our experiments only the two latest ones are referred here: Ádám et al. 1982 and Ádám et al. 1989.)

Along the Pannonian geotraverse (see in Fig. 1 on the

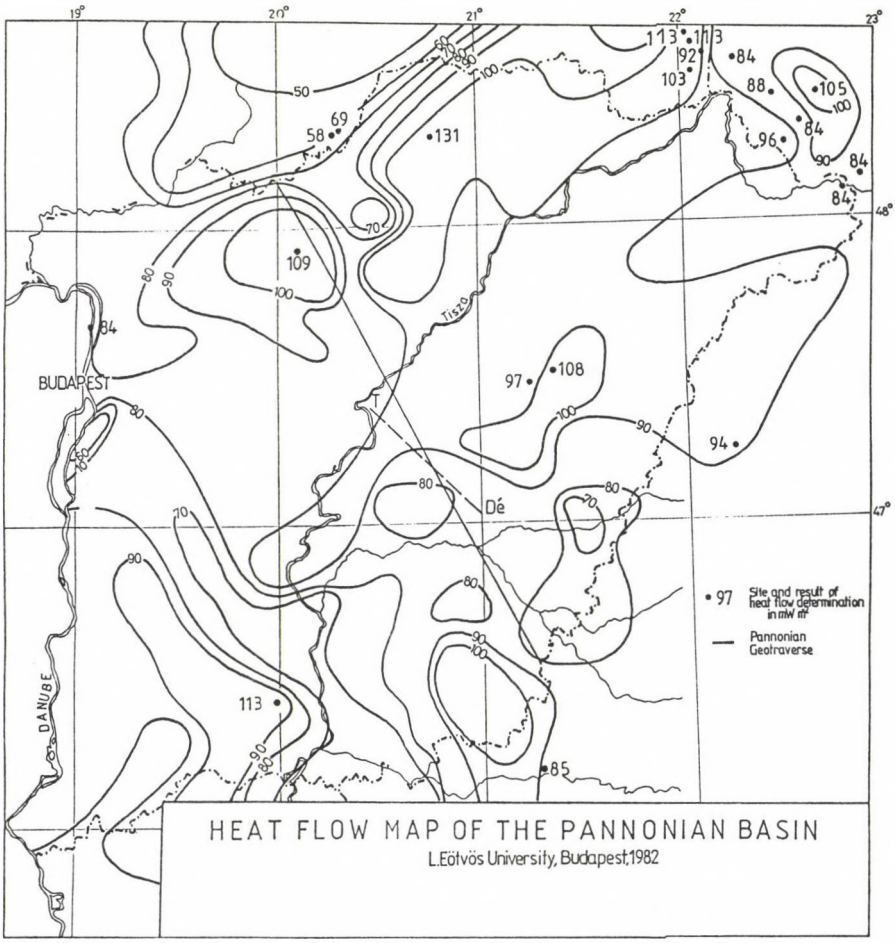

Fig. 1. The position of the Pannonian geotraverse and of the T-De MT profile on the heat flow map of Dövényi et al. (1983)

redrawn heat flow map of Dövényi et al. 1983) 3 Hungarian institutions (GGKI, ELGI, GKV) made MT soundings with different techniques, data processing and inversion methods. Their results are presented in this paper for the whole lithosphere and the geothermal relation of the conducting formations is also shown.

2. METHODICAL DIFFICULTIES

Some basic methodical difficulties are to be mentioned here and illustrated by examples to inform about the reliability of the geoelectric results.

a) The Pannonian geotraverse starts in the Northern Central Range and ends in the 7 km deep Békés trench. Thin sediments in the mountains make not only the industrial noises stronger but increase the distortion effect of surface (topography) and near surface inhomogeneities so that the reliability of the deep MT data gets doubtful (Ádám et al. 1986). A narrow trench with steep walls such as the Békés one, is also a source of very different electromagnetic field distortions (static shift, edge effect, induction effect variable, anisotropy etc.).

According to Berdichevsky and Dmitriev's (1976) theory the E polarized sounding curves give more reliable data about parameters of conductivity anomalies in the case of 2-D structures. The determination of the E pol. direction is promoted by geological data (isopach map) and by the tipper, or induction vector calculated from records of the three geomagnetic components.

The reliability of the determination of the asthenosphere is questioned in the mentioned complicated geological situation.

MT data of the station ELEK (No. 7) in the Békés trench are shown to illustrate the difficulties.

Disturbing factors in the interpretation:

- Extreme values of impedance (Z) change by 90^{o} in direction at periods shorter than 60 s then they reach a constant value (Fig. 2.).

(Fig. 2).

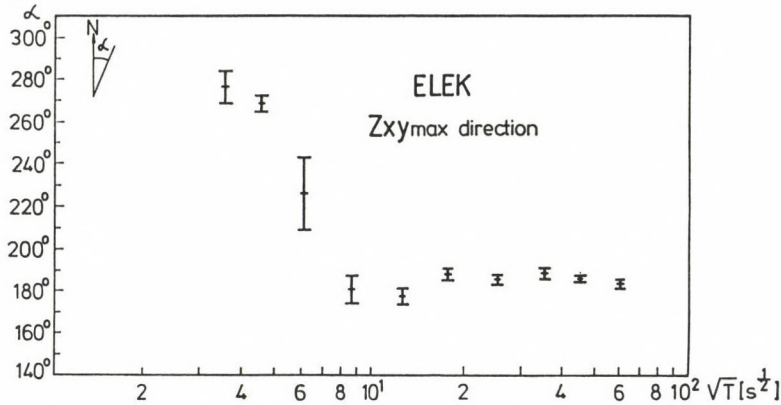

Fig. 2. The change of the direction of the impedance maximum (Z_{xymax}) vs. period at the MT sation ELEK (Békés trench)

- The induction vector is only at periods less than 60 s perpendicular to the Z_{xymax} direction.
- Due to the great anisotropy, the inversion of the Rho_{max} and Rho_{min} curves as well as their phase curves, resp. results in different layer sequences (Figs 3, 4).

Choice of the direction of the E polarization

- The direction Z_{xymax} is constant as mentioned at periods longer than 60 s, i.e. at periods which correspond to the indication of crustal and asthenospheric conducting layers. The direction Z_{xymax} is N-S.
- The strike of the steep trench wall is on the isopach map also N-S (see in Fig. 5 the MT point Elek (No. 7)).

According to these aspects the E polarization is represented by the N-S directed Z_{xymax} values. Therefore, the layer sequence derived from Rho_{max} is more reliable than that from Rho_{min} as the different distortions (static shift, edge effect) appear in the latter one being the H polarized sounding curve.

There is no explanation at present for the clockwise

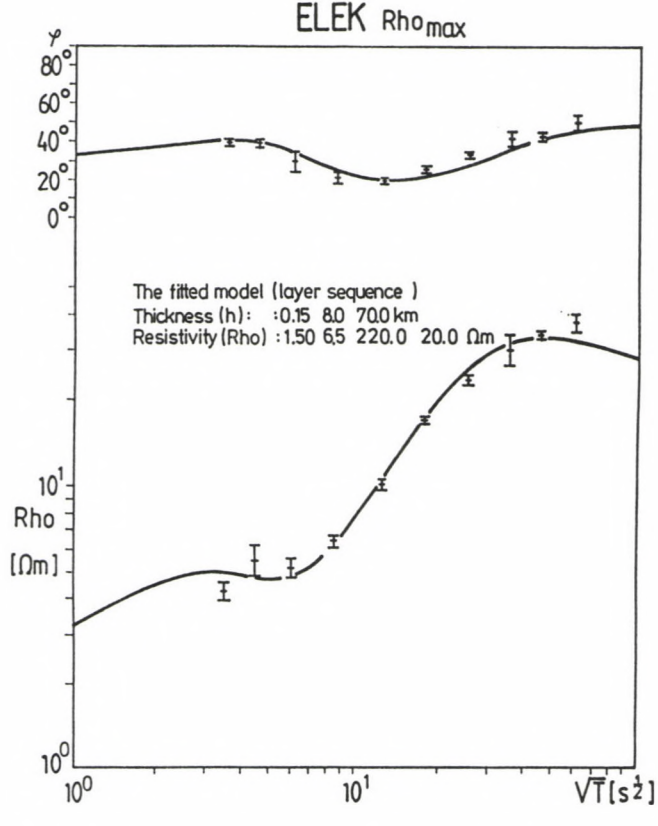

Fig. 3. 1-D model curves fitted to the Rho_{max} and φ_{max} data at Elek and the corresponding layer sequence

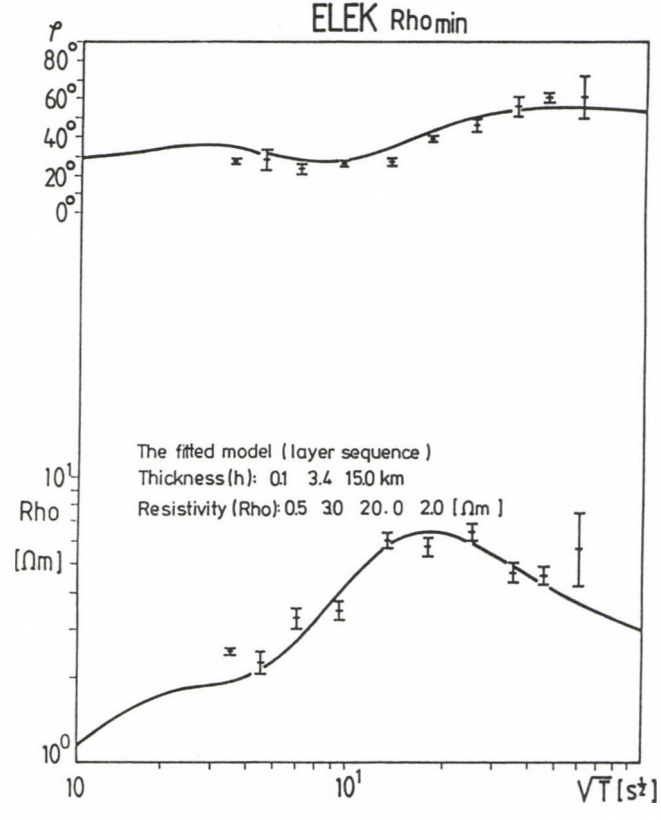

Fig. 4. 1-D model curves fitted to the Rho_{min} and φ_{min} data at Elek and the corresponding layer sequence

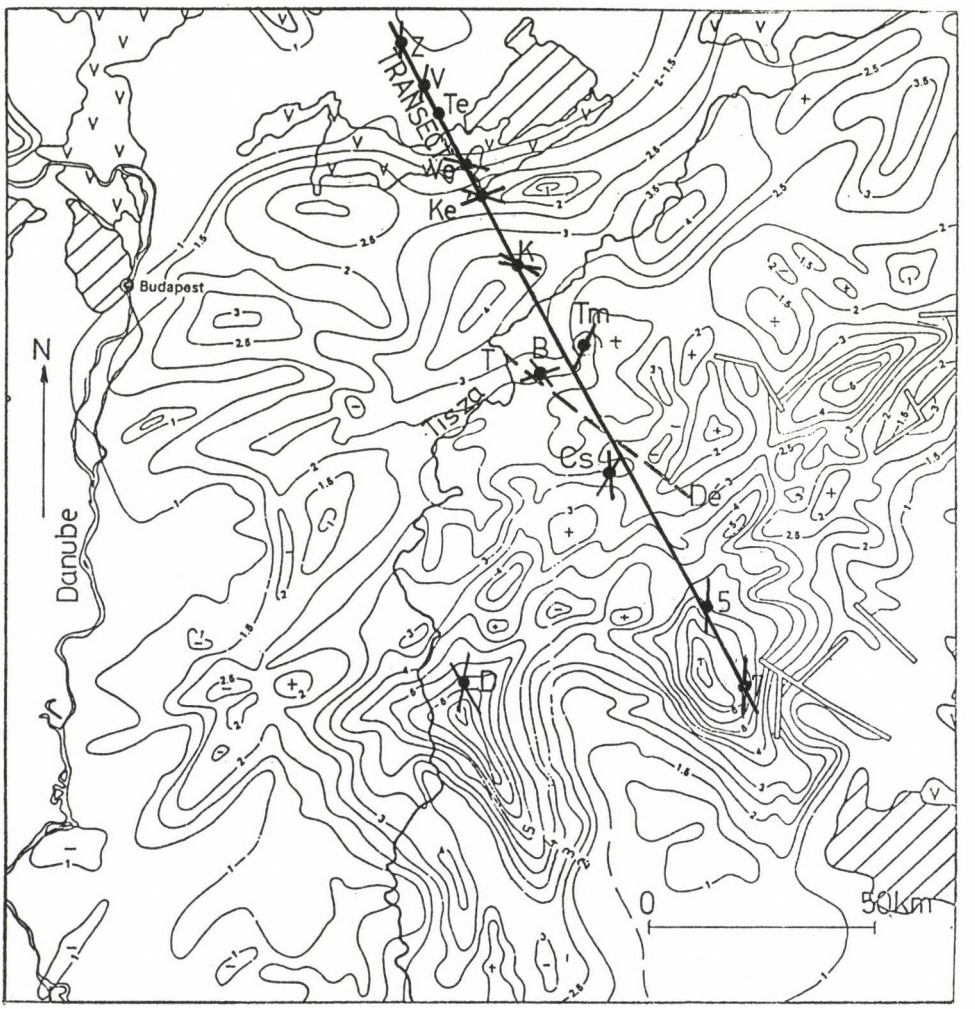

Fig. 5. Isopach map on the basement of the Great Hungarian Plain (after Horváth and Royden 1981) and Z_{xymax} directions with their variation vs. period

rotation of the induction vector from the dip to the strike of the structure at longer periods, in agreement with the Wiese arrows measured earlier (Ádám et al. 1972). Some lateral inhomogeneity e.g. a mantle intrusion detected by gravimetry could generate this phenomenon.

b) MT sounding curves have been inverted by 1-D layer or

by 1-D Bostick transformation. The latter supposes a continuously varying resistivity - depth function. For a comparison of the results of these two processes, layer boundaries on the continuous Bostick transforms should be identified. If the upper boundary of a conducting layer is taken at the maximum preceeding the decreasing branch of the Bostick resistivity curve, its depth value is generally somewhat less than that supplied by the 1-D layer inversion.

According to the comparison, the deviation is minimum in the case of the CA in the lower crust (in the Pannonian basin between 15 and 20 km) and somewhat greater in the asthenosphere as it will be shown later on.

c) If there is no great difference between the depths of the crustal and upper mantle CA-s the success of their separation is questionable in the case of any inversion techniques. The effects of the two CA-s merge into each other and this is promoted by smoothing techniques with different polynomials. As an example the Bostick transform of the MT site No. 113 is shown (Fig. 6). In Fig. 6a the two CA-s are clearly separated but in Fig. 6b they run into each other. This latter case explains the high occurrence frequency of the depth of about 30 km - being an intermediate one between the real depths of the crustal and upper mantle anomalies - along the T-De profile (Fig. 10).

d) Using Steiner's 1-D layer inversion programme we studied if a crustal conducting layer with a conductance of 200-300 Siemens could be detected under thick sediments. The sensibility of the H polarized sounding curves is much less for a conducting layer than that of the E polarized one. This is confirmed by the very small deviation in the H pol. impedances of a 3- and a 5-layer model with the latter including a crustal conductor, too. This small difference appears similarly in the deviation (DEV) between the measured (m) and calculated (c) impedance values (Z) when a 3- and a 5-layer model is fitted to the measured H pol. curve of Tomajmonostor

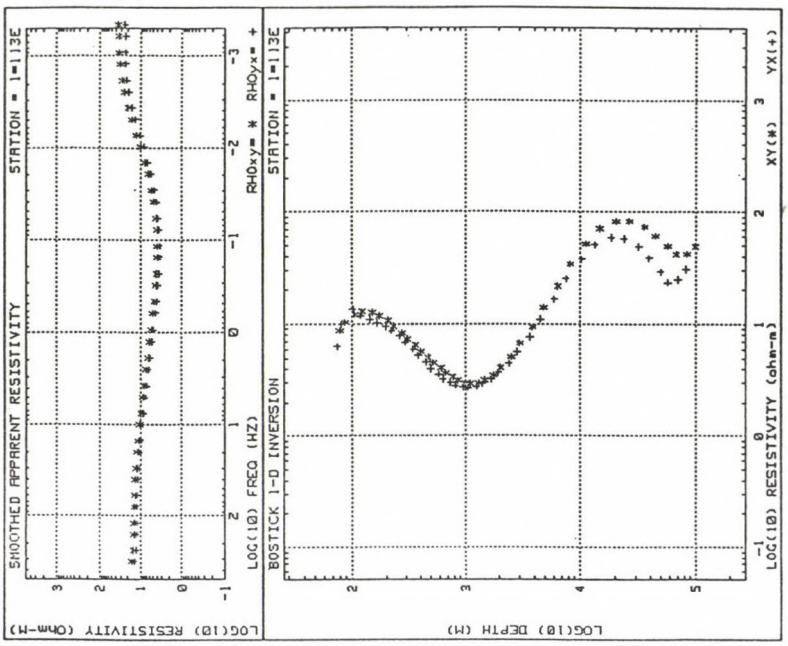

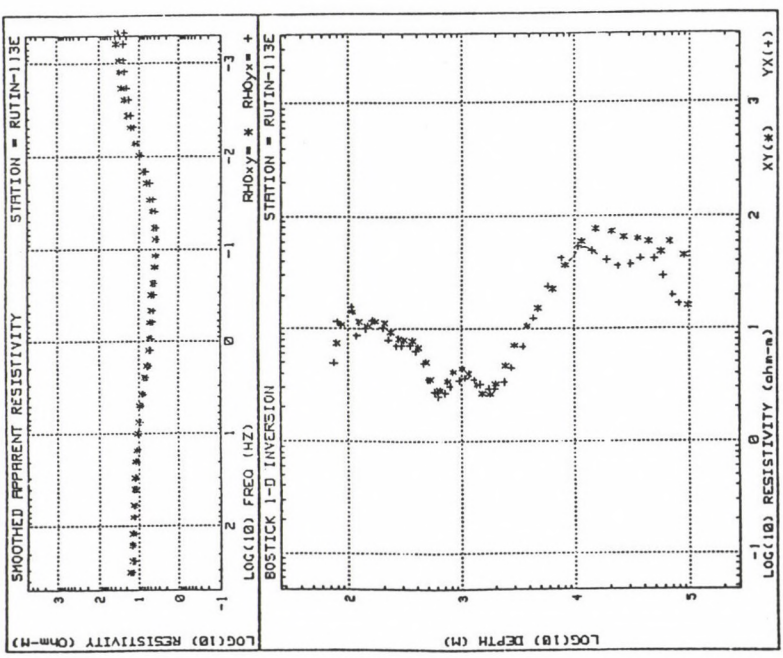

Fig. 6. A comparison of the Bostick transforms of differently smoothed MT curves

$$\text{L2DEV (3 layers)} = \frac{1}{n}\sqrt{\sum_{1}^{n} |Z_c - Z_m|^2} = 0.61$$

L2DEV (5 layers) = 0.059.

The deviations for the E pol. Rho_{min} curve:

L2DEV (3 layers) = 0.081

L2DEV (5 layers) = 0.075.

Omitting the less reliable phase value from the inversion:

APPDEV (3 layers) = 0.065

APPDEV (5 layers) = 0.0076

i.e. this latter 5-layer-model fits better to the measured curve, confirming the existence of conducting layer in the lower crust (see Fig. 7).

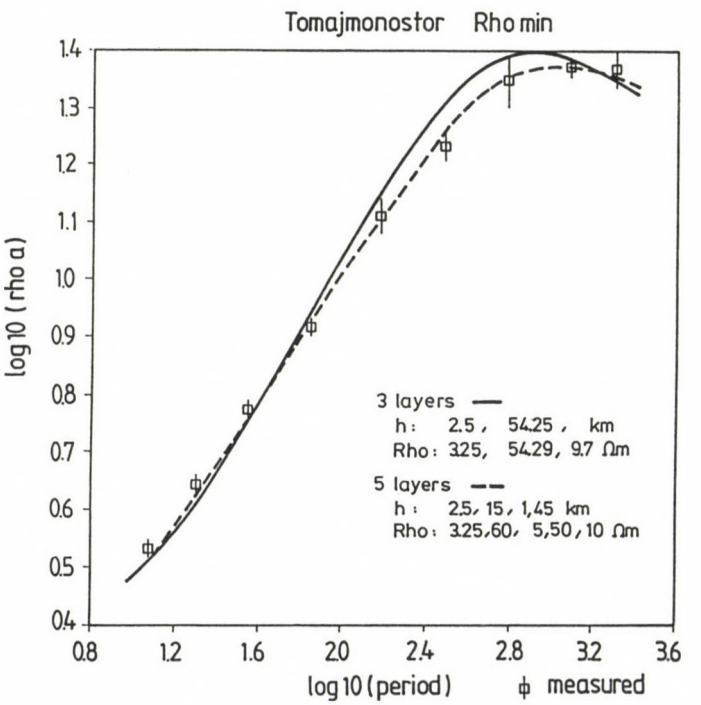

Fig. 7. 3- and 5-layer models fitted to the Rhomin curve of Tomajmonostor (In the case of the 3-layer model the phase is also taken into consideration; see in detail in the text.)

Nevertheless, all these calculations hint at the weakness of the determination of a low conductance crustal CA under thick sediments in the Great Hungarian Plain.

3. CONDUCTING ANOMALIES ALONG THE PANNONIAN GEOTRAVERSE

Depths of the conducting anomalies in the lower crust as well as in the upper mantle resp. are shown by three profiles. Figure 8 displays the whole transect from the Czechoslovakian border to the Rumanian one with depths calculated by 1-D layer inversion. This profile includes the data of six Phoenix MT measurements between Tiszaroff (T) and Dévaványa (De) by Geophysical Exploration Company (GKV). The layer sequence of these MT points is given in Fig. 9 irrespective to real distances between the points. For the same 60 km long profile (T-De) along which at every 750 m a MT sounding was measured, depths derived from Bostick transforms are presented both for the crustal and asthenospheric CA-s. The average depth values and their error bars are also shown (Fig. 10).

Conclusions drawn from these data concerning the resistivity distribution in the crust and upper mantle are as follows:

a) In the lower crust the average depth of the CA is 17-18 km. The data of the profiles (Fig. 8 and 10) are in good agreement. Nevertheless, the layer sequences of the 6 GKV points show significant changes in depth and anisotropy for the crustal CA.

The average depth of the asthenosphere is 65 km according to the 1-D layer inversion and between 47 and 52.6 km from the Bostick transforms. The difference between the average values of the two inversions are due to the different techniques (see Point 2b).

b) The depths of the asthenosphere scatter at the measurement sites between 45 and 88 km. In this range two systematic variations are observed:

α) The asthenosphere deepens from the Northern Central Range towards the Békés trench (in the south) in agreement with decreasing heat flow as shown in Fig. 1.

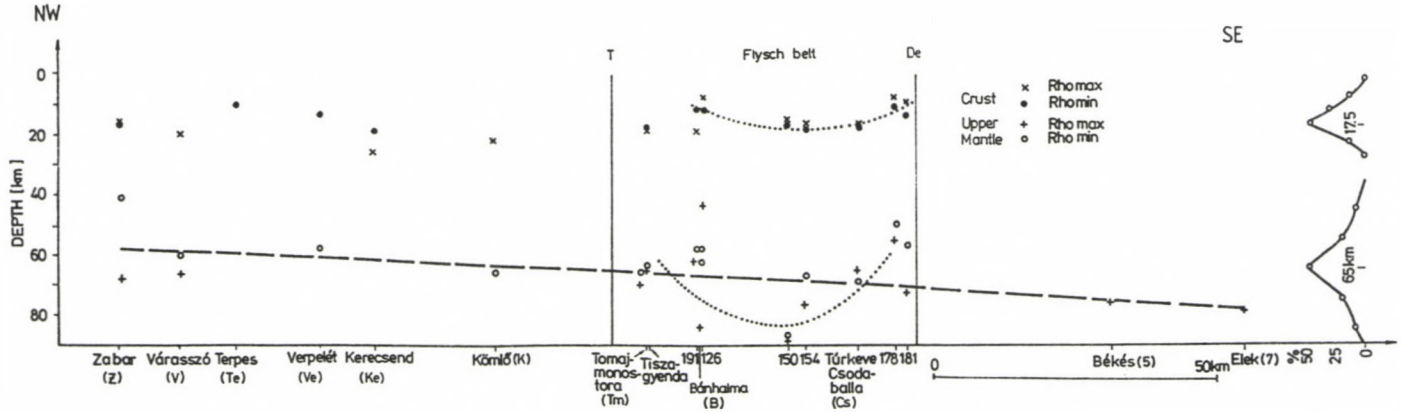

Fig. 8. Depth of the crustal and upper mantle (asthenosphere) conducting layers calculated by 1-D layer inversion along the Pannonian geotraverse

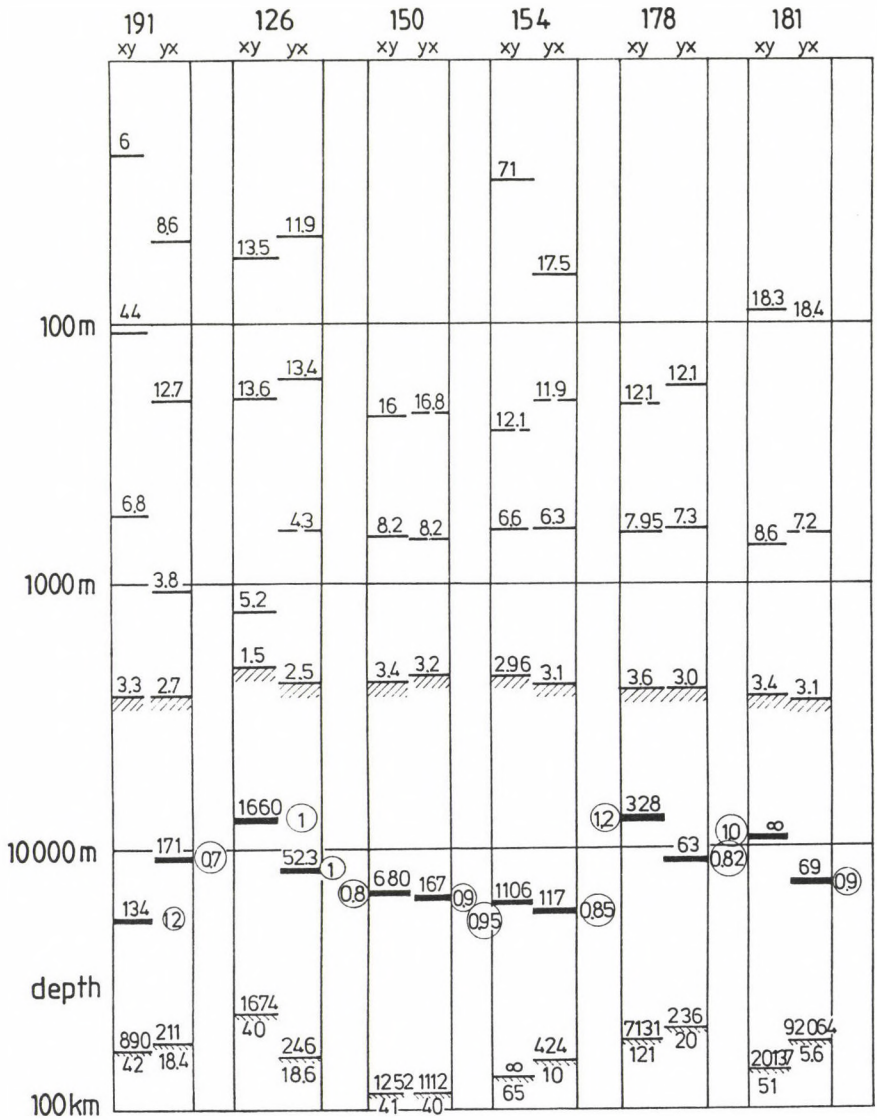

Fig. 9. The 1-D layer sequence of 6 MT soundings measured by the Phoenix MT instrument with remote reference station along the T-De profile

β) The middle part of the MT profile Tiszaroff-Dévaványa crosses the Szolnok flysch belt (see Balla's (1988) tectonic map, Fig. 11). Both the crustal and upper mantle conducting layers are deeper in the flysch belt than to NW and to SE

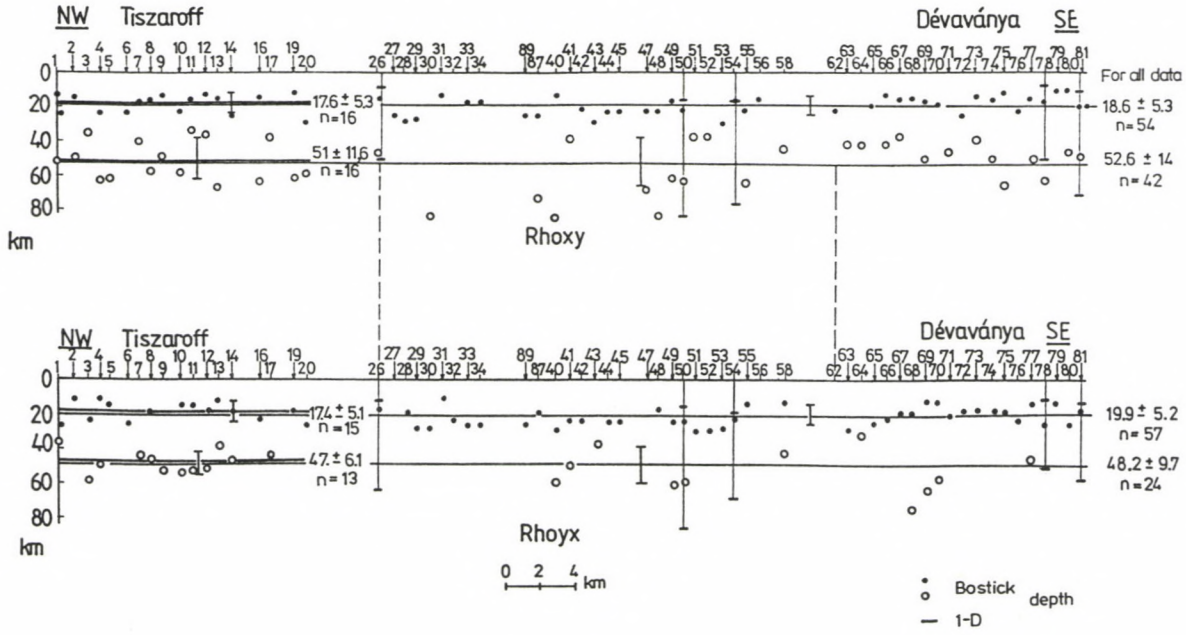

Fig. 10. Depths of the crustal and asthenospheric conducting layers calculated on the basis of the Bostick transforms along the T-De profile (Ádám et al. 1989)

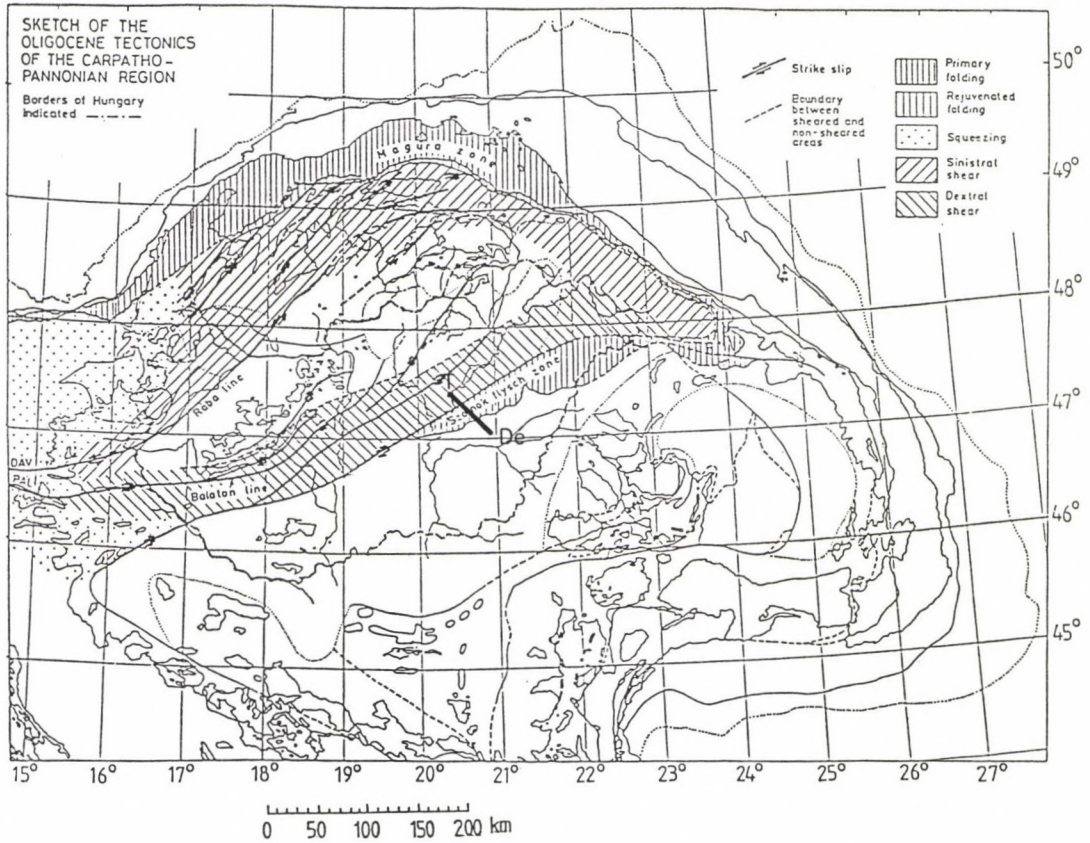

Fig. 11. Oligocene tectonics of the Carpathian basin after Balla (1988); the T-De profile is also indicated

of it (Fig. 9). MT sites 150 and 154 represent this deeper zone on the 6 point profile (Fig. 10). According to a statistical (two-sided T) test the crustal conducting layer is deeper in the flysch zone at a level of significance 99.8 percent than in the surrounding area.

Of course, in the case of such a great variation, the possible effect of lateral inhomogeneities (geological noise) cannot be neglected.

4. PHYSICAL INTERPRETATION OF THE CONDUCTING ANOMALIES

The weak conducting anomaly in the lower crust, observed along the Pannonian geotraverse may be attributed to free water generated at about 400^{o}C during the metamorphic dehydration process in the greenschist facies according to Klemperer (1987) and Hyndman (1988). The seismic reflectors in the lower crust probably represent the local zones of the same high fluid pore-pressures (Klemperer 1987). As the dehydration is temperature dependent, a relation exists between the depth of the crustal conducting layer and the surface heat flow (Ádám 1976, 1978, 1987). The depth of the CA in the lower crust of the Pannonian basin fits well to this empirical relation (Ádám et al. 1989).

The depth of the conducting asthenosphere is determined by the solidus temperature of peridotite at which its (partial) melting starts. This physical connection is expressed by the empirical relation derived between the depth of the conducting asthenosphere and the surface heat flow of the area (Ádám 1978). The depth values measured recently along the Pannonian geotraverse fit well to Ádám's empirical relation. In Fig. 12 the depths corresponding to the highest and lowest heat flows as well as those measured along the T-De profile confirm the shallowness of the asthenosphere in the "hot" Pannonian basin. The electromagnetic data are in agreement with Posgay et al's (1990) recent reflexion seismic data and Babuska et al's (1984) conclusion based on the delay of the seismic waves in the mantle of the Pannonian basin due its lower density as a

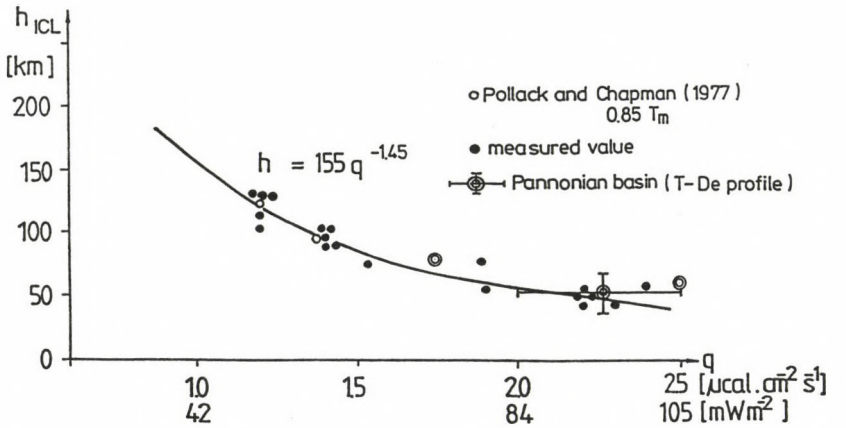

Fig. 12. Empirical relation between the depth of the conducting asthenosphere and the regional surface heat flow (Ádám 1978)

thermal effect.

The deepening of the crustal and asthenospheric conducting layer in the flysch zone may be explained on the basis of the heat flow map (Fig. 1). The northern border of the flysch zone lies along the isoline 90 mWm^2 which separates the northern part of the Great Hungarian Plain of higher heat flow and the southern one of lower heat flow. Within the southern area of 80-90 mWm^{-2} there are small patches of lower heat flow just in the flysch zone crossed by the T-De profile. In the opinion of some authors (e.g. Channel and Horváth 1976, Haas et al. this volume) this flysch zone is at the contact of two megatectonic units (Tisza and Pelso) in the Carpathian basin and some parts of it are still active (Kapos line). The collision could also rearrange similarly to a subduction the temperature distribution down to the asthenosphere. Of course, this idea is a first rough hypothesis about this curious phenomenon which should be studied further and confirmed by other MT profiles crossing this zone excluding the effect of geological noises.

5. CONCLUSIONS

The study of the conducting zones in the crust and the

upper mantle by magnetotelluric deep soundings supplied new information about the deep structure of the Pannonian basin, about the variation of the state parameters, first of all of the temperature and about physical changes (dehydration, partial melting) at the depth. A new hypothesis could be formulated about the position of the collision zone between microplates in the Carpathian basin on the basis of the physical changes affecting the whole lithosphere.

REFERENCES

Ádám A 1963: Study of the electrical conductivity of the Earth's crust and upper mantle: Methodology and results. Dissertation (in Hungarian), 111 pp. Sopron

Ádám A 1976: Acta Geod. Geoph. Mont. Hung., 11, 503-509.

Ádám A 1978: Phys. of the Earth and Planet. Int., 17, P21-P28.

Ádám A 1987: Phys. of the Earth and Planet. Int., 45, 209-215.

Ádám A, Verő J, Wallner Á 1972: Acta Geod. Geoph. Mont. Hung., 7, 251-287.

Ádám A, Vanyan L L, Varlamov D A, Yegorov I V, Shilovski A P, Shilovski P P 1982: Phys. of the Earth and Planet. Int., 28, 251-260.

Ádám A, Szarka L, Verő J, Wallner Á, Gutdeutsch R 1986: Phys. of the Earth and Planet. Int., 42, 165-177.

Ádám A, Landy K, Nagy Z 1989: Tectonophysics, 164, 361-368.

Babuska V, Plomerova J, Sileny J 1984: Geophys. J. R.A.Soc., 79, 363-383.

Balla Z 1988: Acta Geol. Hung., 31,

Berdichevsky M N, Dmitriev V I 1976: Acta Geod. Geoph. Mont. Hung., 11, 447-485.

Channel J E T, Horváth F 1976: Tectonophysics, 35, 71-101.

Dövényi P, Horváth F, Liebe P, Gálfi J, Erki I 1983: Geophys. Transactions, 29.

Haas J, Császár G, Kovács S, Vörös A 1990: Acta Geod. Geoph. Mont. Hung., 25 (present issue)

Horváth F, Royden L 1981: Earth Evolution Sciences, 1, 307-317.

Hyndman R D 1988: J. of Geophysical Res., 93, 13391-13405.

Klemperer S L 1987: J. of Geophysics, 38, 279-296.

Posgay K, Albu I, Hegedüs E, Timár Z 1990: Acta Geod. Geoph. Mont. Hung., 25 (present issue)

Steiner T 1989: Magyar Geofizika, 30, 1-8.

Acta Geod. Geoph. Mont. Hung., Vol. 25 (3-4), pp. 309-323 (1990)

SEISMIC AND MAGNETOTELLURIC INVESTIGATION ON A NETWORK OF BASE LINES

A Pápa, G Ráner, M Tátrai, G Varga

Eötvös Loránd Geophysical Institute of Hungary, H-1440 Budapest, POB 35, Hungary

Regional studies carried out within the framework of geophysical investigations along Geological and Geophysical Base Lines and of the Preliminary Complex Geophysical Investigation of the Little Hungarian Plain furnished new clues to the examination of mountain areas and their foreland, contributed to the contouring of tectonic units and helped to find prospective targets of exploration for mineral resources.

The paper presents the distribution of conductive formations in the crust on the basis of the latest electromagnetic, mainly magnetotelluric results obtained by ELGI. Seismic regional profiles recorded up to 10-12 s furnished data about the middle and lower parts of the crust. The examples shown permit in particular instances to separate greater tectonic units and to illustrate changes of the Mohorovicic zone in time.

Keywords: electrical conductivity anomaly; geophysical base lines; Little Hungarian Plain; magnetotelluric sounding; Mohorovicic discontinuity; seismics

In the series of maps "The Geological Atlas of Hungary" the map of conductivity anomalies of the crust in the Pre-Austrian basement was compiled in 1987 in cooperation by researchers of the "Eötvös Loránd" Geophysical Institute of Hungary, of the Geophysical Exploration Company and of the Geodetical and Geophysical Research Institute of the Hungarian Academy of Sciences. This map which is in press for the time being was partly presented by Ádám et al. (present issue 1990). They discuss in detail the spatial distribution of conductivity anomalies in the crust determined by means of telluric and magnetotelluric measurements and offer possible explanations for their existence.

Since the construction of this map further work has been done in the scope of the Pannonian Geotraverse, the Geophysical

Base Line and the Little Hungarian Plain and Mátra Mountain Projects and the interpretation of new areas has been completed. Making use of latest data we have summarized the distribution of conductivity anomalies in the crust on the basis of measurements performed by ELGI (Fig. 1). (Preparation of an up-to--date map-similarly to the 1987 edition - would take more time owing to the differences in methodology and processing of the participant institutions.)

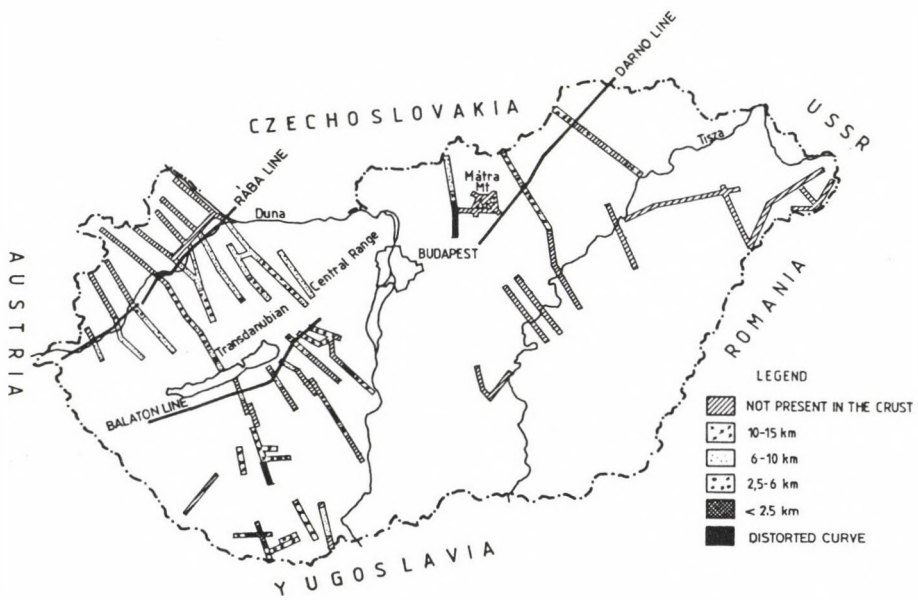

Fig. 1. Occurrence of conductive formations below the Pre-Austrian basement. According to ELGI's data

An investigation of conductivity anomalies within the crust contributes substantially to the determination of geophysical parameters over tectonic units, and renders their contours more accurate. Such a possibility is illustrated through the magnetotelluric investigation of the Rába line (Figs 2 and 3). In the area to NW of the Rába line where there are formations belonging to the lower and upper stages of the East--Alpine cover and to the Penninic unit, conductivity anomalies

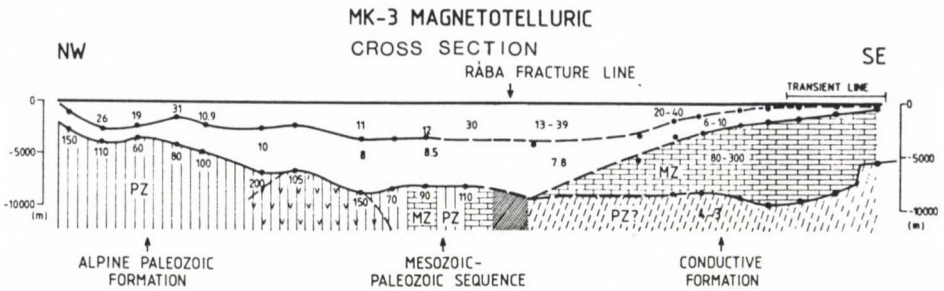

Fig. 2. Resistivity-depth section along the line MK-3

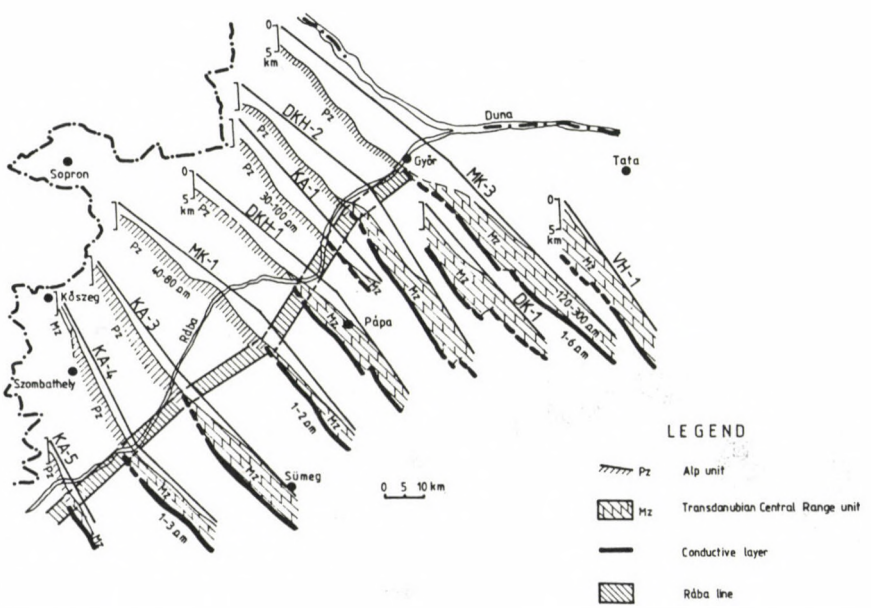

Fig. 3. Tracing the Rába-line on the basis of the distribution of conductive formations

could not be detected in the crust. The Transdanubian Central Range is characterized by conductive formations (Transdanubian conductivity anomaly).

The conductivity anomaly detected in the Transdanubian

Central Range and its NW foreland by magnetotelluric measurements in the depth interval of 5 to 10 km was examined in 1987 in cooperation with VNIIGeofizika (USSR) using the method of deep electromagnetic transient sounding.

Transient measurements were performed in the SE part of line MK-3 (Fig. 2). Interpretation and results of measurements are shown in the transformed differential conductivity - depth cross - section of transient curves (Fig. 4). The detailed transient measurements (distance between stations was 400 m) confirmed the existence of the crustal conductivity anomaly; depth data for the conductive formation agree with those obtained from MT soundings.

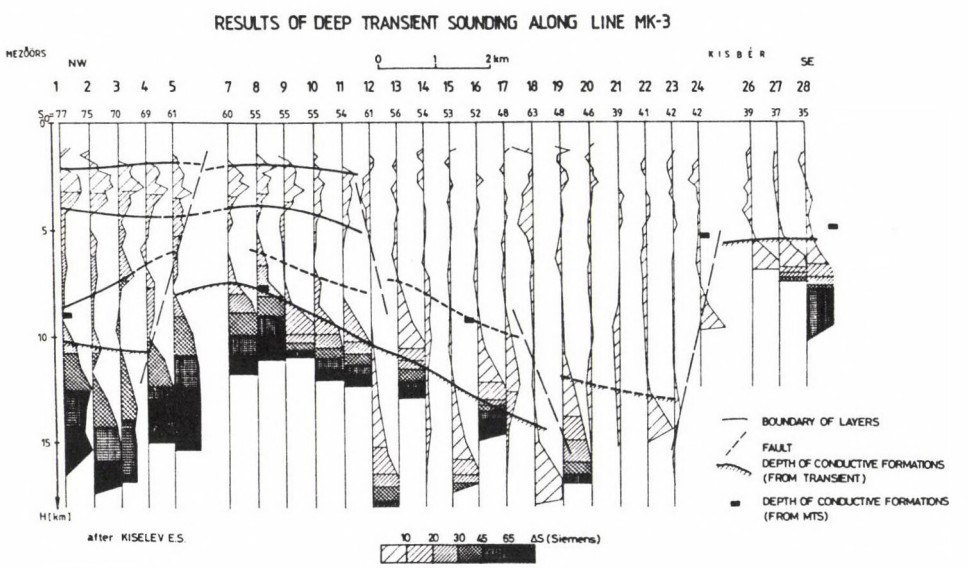

Fig. 4. Detection of conductive formations by deep transient measurements

The map of conductivity anomalies in the crust does not allow us a synthesis for the whole territory of Hungary due to differences in point density and reliability. In addition to new measurements the map should be expanded in international cooperation, too (e.g. tracing the Rába-line in Czechoslovakian

territory by magnetotelluric method).

In the scope of Earth's crust and upper mantle studies, measurements along the Geophysical Base Line and regional investigations on the Little Hungarian Plain, seismic and magnetotelluric measurements have been performed since 1971 (Figs 1 and 5). Seismic data are recorded and processed up to 10-12 s. This permits to study the environment of the Mohorovicic discontinuity and the overlying complex of the crust. Results of these measurements are mainly published in the Annual Reports of ELGI.

These measurements resulted in typically differing sections from the middle and lower parts of the crust. Their correlation is still uncertain because of the rare network, but the following examples illustrate their contribution to be expected in detecting tectonic lines.

Further on we are going to discuss results measured to NW of the Rába-line (Fig. 5). The thick section of seismic lines in Fig. 5 indicate the reflection seismic profiles shown in Figs 6 to 10. In the NW section of MK-1 line (Fig. 6) in the lower part of the crust around the Mohorovicic discontinuity comparatively quiet, slightly dipping reflections were found while the middle part of the crust is ruptured and characterized by reflections of high energy. A similar character is shown by the western part of the section K-1 (Fig. 7).

In the figure we have to remark that crust domain of 4 to 7 s arrival times is dissected by reflection bundles slightly dipping to NW; these bundles may be interpreted as seismic characteristics of folded structures as well.

In the western and northwestern part of the Little Hungarian Plain these reflection features of the crustal sequence cover the area marked by I in Fig. 5. The basement of the Neogene formations is identified as the metamorphite sequence along the Rába river (it is a part of the Upper Eastern Alpine thrust system) as well the Sopron sequence of crystalline shales (a part of the Lower Eastern Alpine thrust system) in the northwestern part of the profiles shown in Figs 6 and 7. On the basis of the identification of pre-Neogene

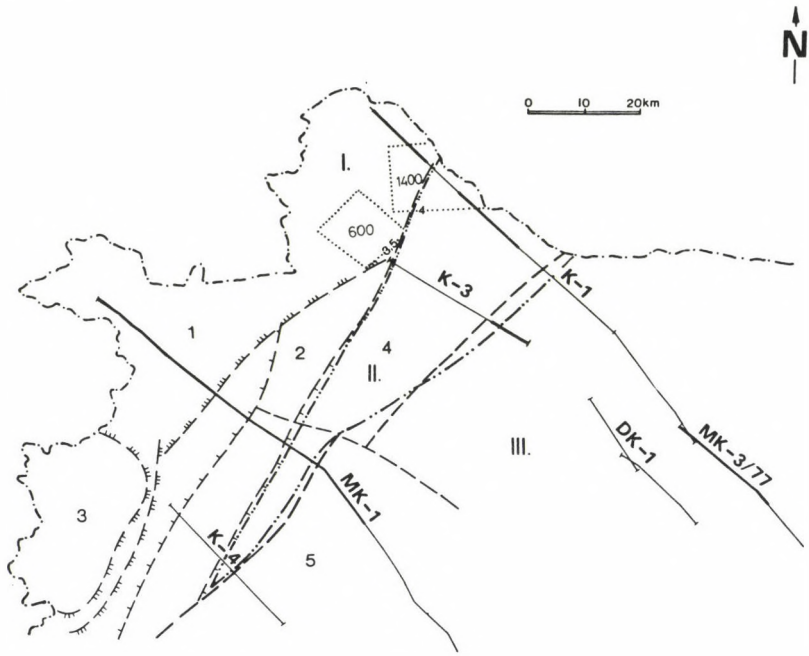

Fig. 5. Plan of reflection seismic measurements with observation time up to 10-12 s in the environment of the Rába-line in the North-Western part of Hungary

Legends:

——— reflection seismic line

thick parts of the line indicate the location of sections significant of the seismic parameters of the crust

Geological units according to the Geological Atlas of Hungary (1987): 1. Lower East-Alpine cover, schist series of Sopron; 2. Upper East-Alpine cover, metamorphite complex along the Rába-river; 3. Penninic unit, metamorphite complex of Kőszeg; 4. Basement of uncertain or unknown age and facies; 5. Individual formations in the Transdanubian Central Range in general

— — tectonic line of the first order

— — older tectonic line of the second order

┬ ┬ Tertiary fault of the second order

┬┬┬ ┬┬┬ older upthrust of the second order or cover boundary

.. — .. — boundary of reflection units in the crust

600 / 3.5 magnetic bodies (according to Posgay 1967) with magnetic susceptibility ($\times 10^{-6}$ CGS) calculated depth of the magnetic body

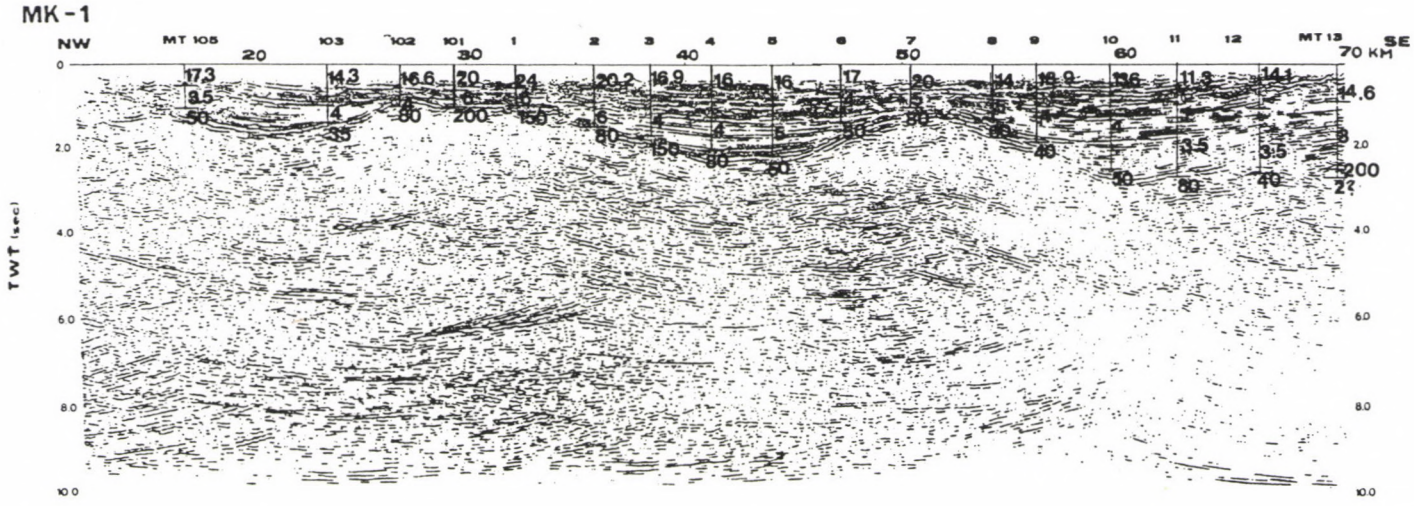

Fig. 6. Seismic reflection time section MK-1 with geoelectric layers

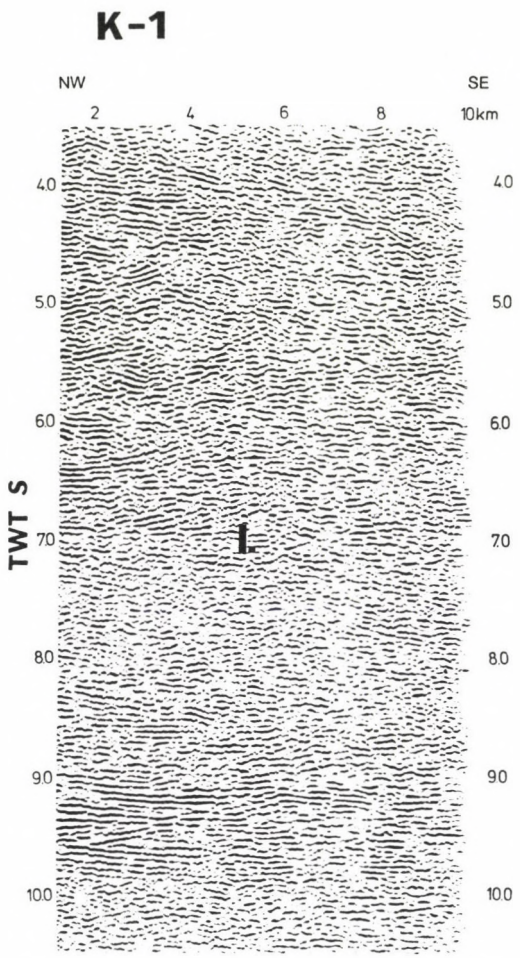

Fig. 7. Seismic reflection time section K-1

formations and of their uniform crustal structural characteristics, the E, SE boundary of area I may indicate the spreading of covered formations of the Lower and Upper Alpine thrust system.

The following part of the profiles in the area of the Rába-line seems to be transparent both in the upper crust and in the vicinity of the Mohorovicic discontinuity (Fig. 8). The transparent part of the crust is marked by II in Fig. 5. The lack of reflection bundles may be caused by thick Lower Miocene

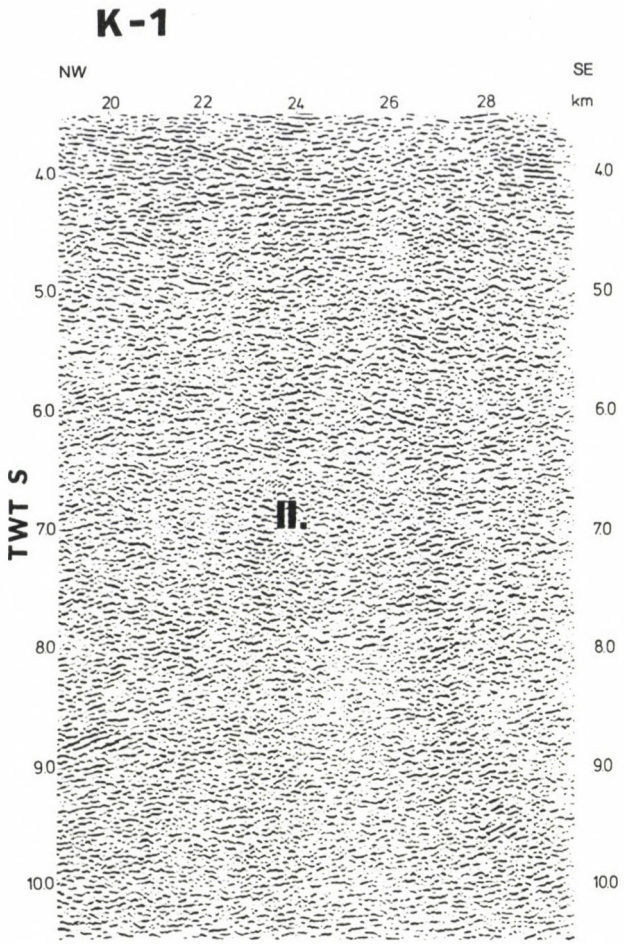

Fig. 8. Seismic reflection time section K-1

volcanic sequences with high energy absorption values detected in deep drillholes.

In the area marked by III in Fig. 5 no characteristic reflected signals were received from the lower part of the crust (with exceeds 7 s), in connection with the deepening of the Mohorovicic discontinuity below the Transdanubian Central Range (Figs 9 and 10). At the same time, high energy reflections were detected from the upper part of the crust (3-6 s arrival times, Fig. 9). This part of the crust is dissected by reflection

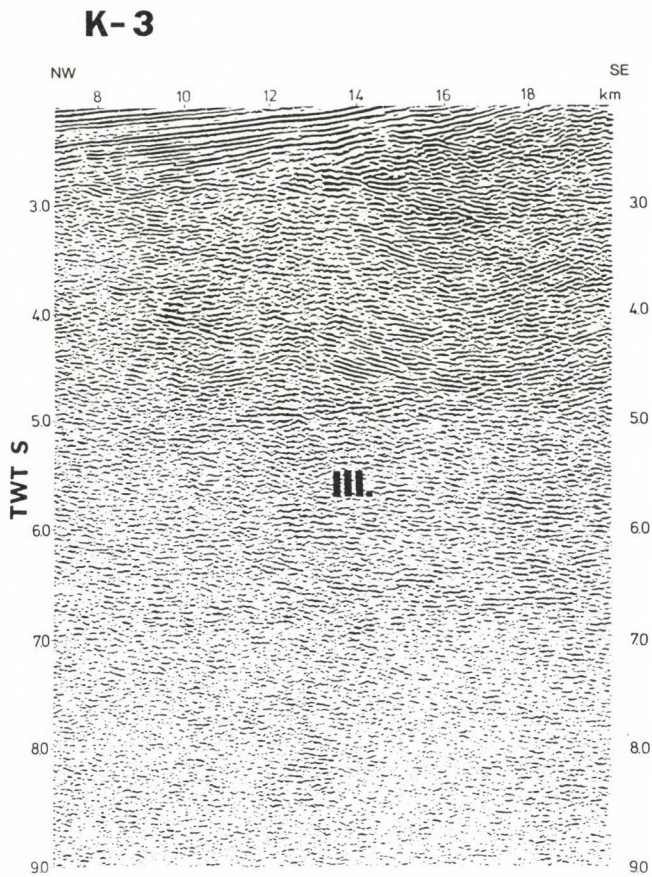

Fig. 9. Seismic reflection time section K-3

bundles slightly dipping to SE. According to the most probable interpretation they indicate the boundary of units of a folded thrust system. This seismic picture characterizes the western margin of the Transdanubian Central Range unit.

In a part of reflection profiles measured in the Transdanubian Central Range reflection boundaries of high energy coincide with the surface of conductive formations. This is most conspicuous in a detail of section MK-3 (Fig. 10). In 1990 methodological investigations are planned to interpret this anomaly. We intend to examine the eventual fluid content by P-A

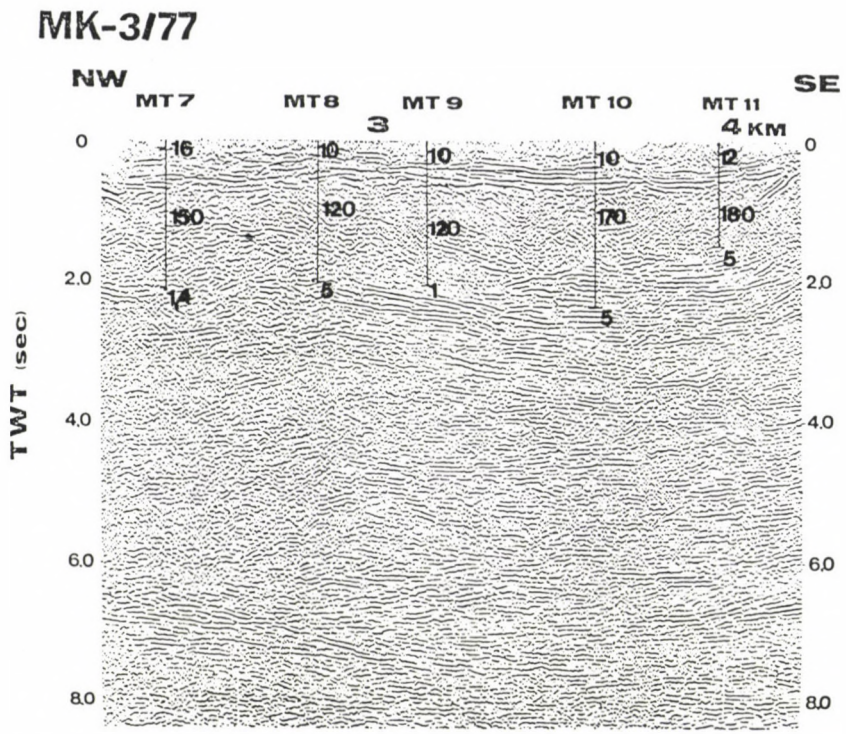

Fig. 10. Seismic reflection time section MK-3/77 with geoelectric layers

waves.

Exploration of an unknown area is a fascinating task, results are being often achieved there where they have not been expected.

In section MK-3/85 measured in 1985 (Fig. 11) the bottom of the basin could be traced but at certain places and even there poorly. This holds particularly for the area of Miocene volcanic formations. About the environment of the Mohorovicic discontinuity, however, a most interesting feature was obtained.

Reflection arrivals with high energy start between about 7 to 8 s in the first part of the section (Fig. 12). The Mohorovicic discontinuity does not significantly emerge of this laminated complex.

In the top zone of the Miocene volcanic series a deep dome (diffraction?) can be observed at 6.5 and 8.4 s (Fig. 13).

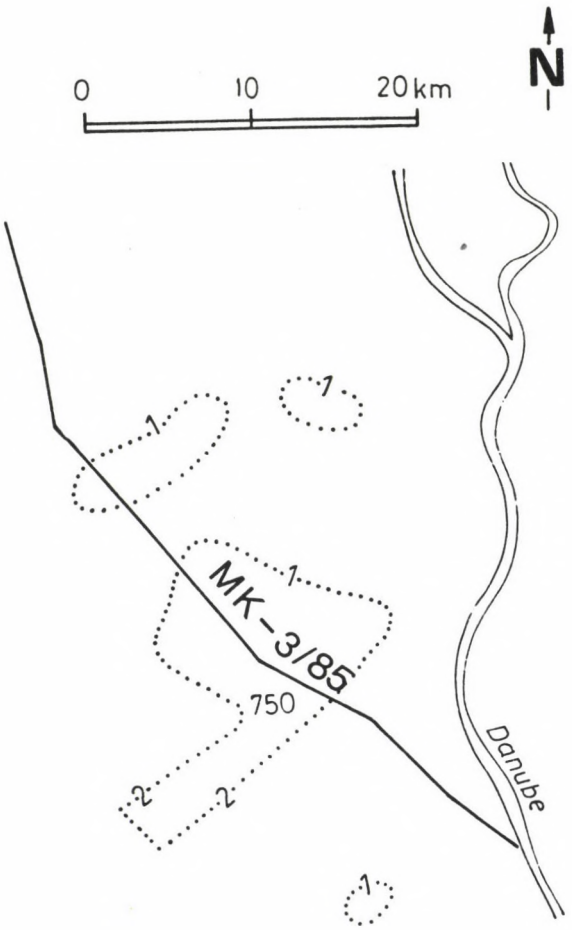

Fig. 11. Location of the section MK-3/85 with Miocene magnetic bodies indicated (according to Posgay 1967)

750 magnetic susceptibility ($*10^{-6}$ CGS)

1 km calculated depth of the magnetic body

In the third part of the section (Fig. 14) the Mohorovicic complex is characterized by arrivals of various dips. Comparing arrivals inceding with different dips to horizons within the sedimentary cover they can be taken for elements of the Mohorovicic discontinuity which were formed at varius ages.

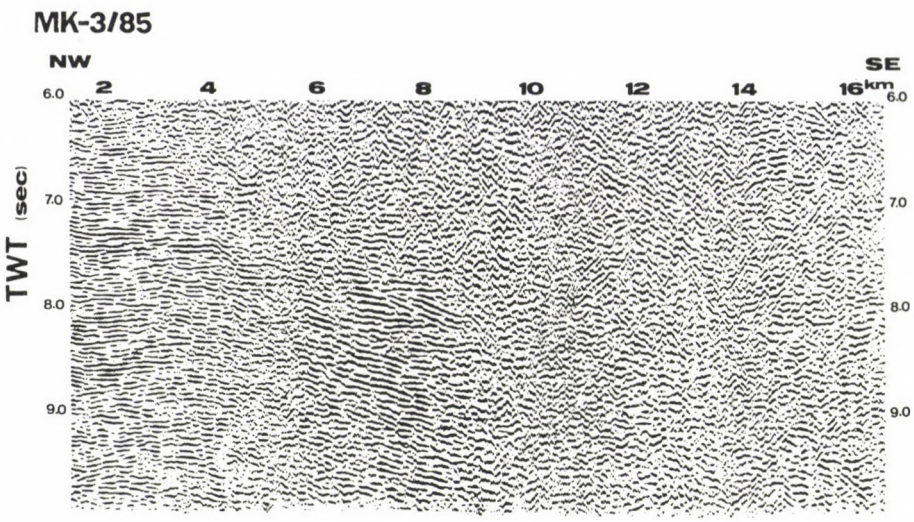

Fig. 12. Seismic reflection time section MK-3/85

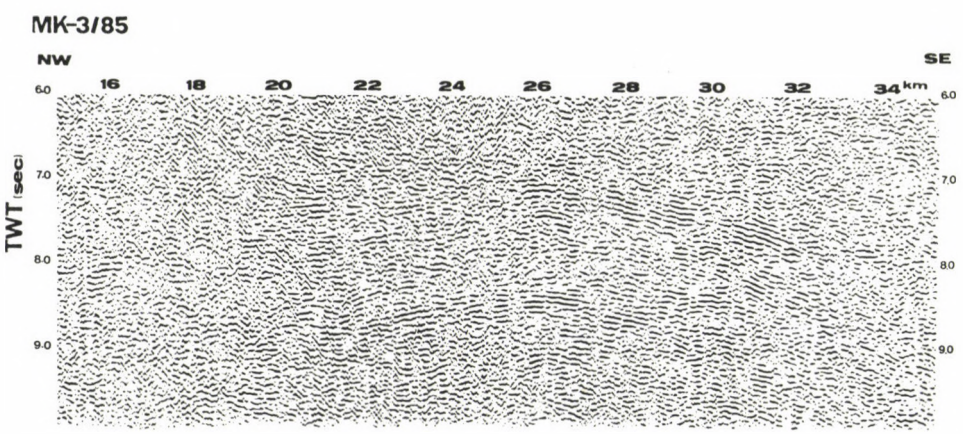

Fig. 13. Seismic reflection time section MK-3/85

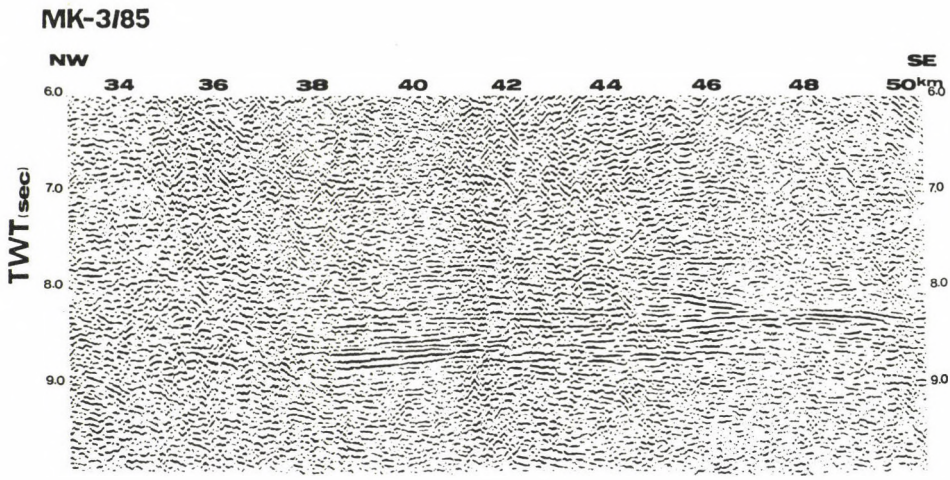

Fig. 14. Seismic reflection time section MK-3/85

CONCLUSIONS

The reflection measurements searching for deep structures of the Little Hungarian Plain indicate the main structural units possessing independent and characteristic crustal reflection behaviour both in the upper part of the crust and in the vicinity of the Mohorovicic discontinuity.

In the upper part of the crust the general dip directions of the folded thrust units are different from each other. The dip of the Eastern Alpine thrust system is northwestern in the Little Hungarian Plain, while in the area of the Transdanubian Central Range it is southeastern. Crustal areas without reflection make impossible to determine exactly the contact zone between the two regional structural units. At the same time, volcanic rocks appearing in areas without reflections may indicate the tectonic activity of the contacting crustal parts.

Comparing the reflection features obtained in profile MK-3/85 (Figs 12, 13, 14) with geological data one can establish that differences between the middle and lower parts of the crust can be brought into connection with the boundaries of great structural units.

In addition to the changes of the seismic character the existence of crustal conductive formations and their locations may considerably help to build up a more exact regional structural view.

REFERENCES

Ádám A, Nagy Z, Nemesi L, Varga G 1990: Crustal conductivity anomalies in the Pannonian basin. Acta Geod. Geoph. Mont. Hung. (present issue)

Nemesi L, Hobot J, Varga G 1985: Acta Geod. Geoph. Mont. Hung., 20, 135-150.

Posgay K, Albu I, Ráner G, Varga G 1986: In: Reflection seismology: A global perspective, Geodynamics Series, Washington, Vol. 13, 55-56.

Posgay K 1967: Geophysical Transactions, 26, No. 4, 23-118.

Acta Geod. Geoph. Mont. Hung., Vol. 25 (3-4), pp. 325-344 (1990)

EVOLUTION OF THE WESTERN PART OF THE TETHYS AS REFLECTED BY THE GEOLOGICAL FORMATIONS OF HUNGARY

J Haas[1], G Császár[2], S Kovács[3], A Vörös[4]

[1]Central Office of Geology, H-1051 Budapest, Arany J. u. 25, Hungary

[2]Hungarian Geological Institute, H-1143 Budapest, Népstadion u. 14, Hungary

[3]Geological Research Group of Hung. Acad. Sci., H-1088 Budapest, Múzeum krt. 4/a, Hungary

[4]Museum of Natural Science, H-1088 Budapest, Múzeum krt. 14/16, Hungary

The aim of this paper is to outline the evolution of some parts of the Western Tethys as it can be deciphered from the geology of Hungary.

During the Late Paleozoic and most of the Mesozoic time lithospheric fragments which build up the basement of Hungary were situated relatively far from each other in different parts of the Tethys. The present-day setting formed by plate-tectonic movements from the Cretaceous to the Miocene including large-scale strike-slip faulting, microplate rotation and overthrusting.

Keywords: geohistorical phases; megatectonic units; Mesozoic; Paleogene; paleogeographic reconstruction; Pelso Unit; Permian; Tethys; Tisza Unit

INTRODUCTION

Investigations of geological and structural features of the Hungarian mountains and the basement of the large basins revealed the key-role of the Pannonian basin for the geodynamic reconstruction of the Western Tethys. Without fitting of the Hungarian lithospheric blocks into the Alpine-Carpathian--Dinaric framework it would be impossible to compile any realistic reconstruction about the region where both the Triassic--Jurassic Vardar rift system and the Jurassic-Cretaceous Penninic rift system played important roles.

In the last decades and particularly since the appearance of the plate-tectonic concept a lot of interpretations were elaborated (Balla 1982, 1988, Báldi et al. 1985, Brezsnyánszky and Haas 1986, Császár et al. 1987, Fülöp et al. 1987, Géczy 1983, Haas 1987, Channel and Horváth 1976, Kázmér 1984, Kázmér and Kovács 1985, 1989, Royden and Báldi 1988). However, due to

the uncompleteness of our knowledge and the complexity of the processes, the problem has not yet been solved.

Works for understanding of the Alpine geohistory and compilation of the data were carried out in the framework of different national and international projects. Among them the National Key Section Project, the Hungarian Geological Atlas program, and the IGCP Project No 198 (Northern Margin of the Tethys) are particularly important in this context.

In the present paper we try to outline the evolution of some parts of the Western Tethys as deciphered from the geology of the lithospheric fragments which build up the basement of Hungary.

The final phase of the evolution of the Tethys as well as some arguments of crucial importance like paleomagnetic evidences and the tectonic interpretation of the magmatites are reviewed in this volume by other papers but their results are incorporated into our summary.

GEOHISTORICAL PHASES AND STRUCTURAL UNITS

Three major geohistorical periods are reflected in the geology of Hungary:

- A pre-Alpine evolutionary stage. It is difficult to reconstruct, but should have connected with the Precambrian--Paleozoic history of Central Europe.
- The Alpine stage including the Late Paleozoic, Mesozoic and Paleogene evolution of the Tethys. It is characterized by orogenic events (Eoalpine, Paleoalpine, Mesoalpine) manifested in nappe tectonics, folding and large scale strike-slip movement.
- The Pannonian (Neoalpine) evolutionary stage, which lasts from the Early Miocene up to the present. This period is characterized by the formation of small pull-apart basins and that of the Pannonian basin by high-amplitude subsidence.

According to the development patterns of pre-Tertiary formations, the territory of Hungary can be divided into the following megatectonic units (Fig. 1).

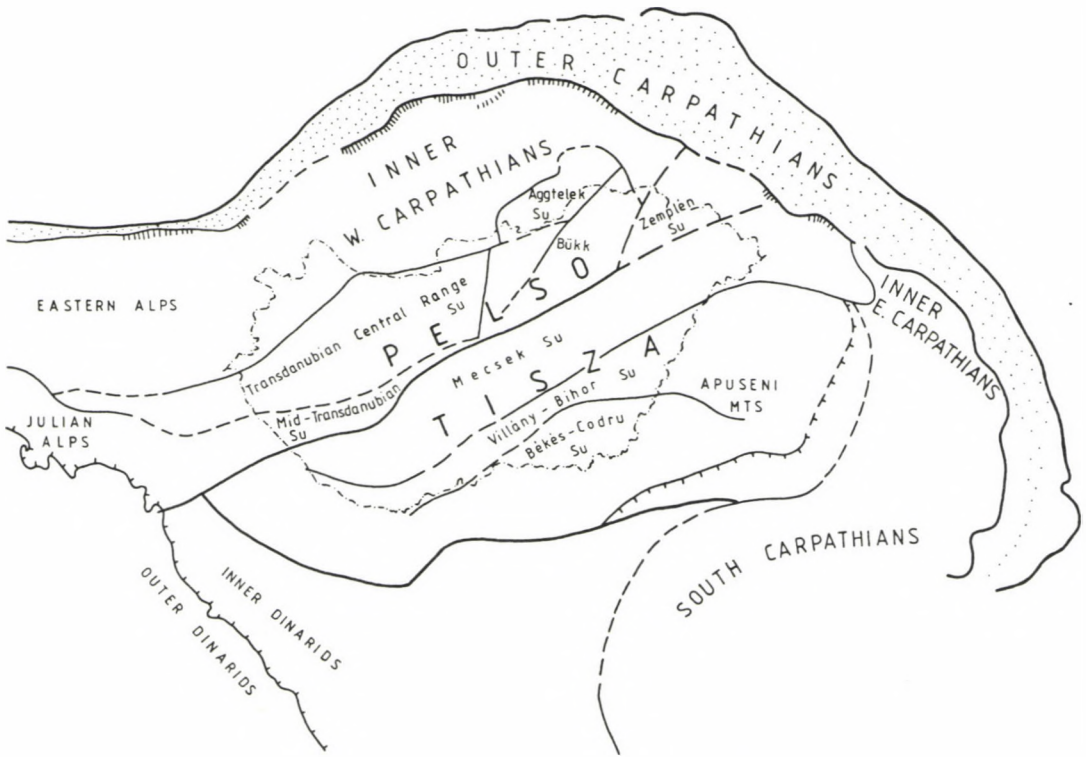

Fig. 1. Setting of the Hungarian megatectonic units within the Alp-Carpathian-Dinaric framework

1. The Tisza Unit

To the south of the Mid-Hungarian Fault Zone the Tisza Unit includes the Mecsek and Villány Mountains and their subsurface extension in the basement of the Great Hungarian Plain (Alföld). This unit shows affinities with the Apuseni Mountains, Romania.

The high-grade polymetamorphic pre-Alpine basement is covered by a Germano-type Permo-Triassic of continent foreland origin (in the Mecsek Subunit) which progresses to Alpine-type successions (in the Upper Codru nappes and in the basement of Vojvodina). Development of the Jurassic and Cretaceous series are more diversified and these differences enabled us to distinguish the Mecsek, Villány and Békés Subunit within the Hungarian part of the Tisza Unit.

The Mecsek Subunits is characterized by a Germano-type continental-shallow marine Permo-Triassic sequence, Upper Triassic of fluvial to delta facies, Grestein-type Liassic, deep-water facies from the Late Dogger and an intensive Early Cretaceous alkali submarine rift volcanism.

Triassic of the Villány Subunit shows some Germano-type characters but to a less extent than the Mecsek Subunit. The Jurassic sequence is characterized by a great number of stratigraphic gaps. The Lower Cretaceous Urgon facies shows connections to the Bihor "autochthonous unit" in the Apuseni Mts.

The Békés Subunit contains Upper Jurassic to Lower Cretaceous dark shales similar to the higher nappes of the Codru nappe system of the Apuseni Mts.

Upper Cretaceous formations of predominantly marine clastic facies lie on older rocks with unconformity. Paleogene is known only in the subsurface range of the Mecsek Subunit (Szolnok Flysch Zone).

2. The Pelso Unit

Situated between the Rába-Hurbanovo Lines and the Mid-Hungarian Fault Zone, the Pelso Unit is characterized by very

low-grade and low-grade metamorphic marine Early Paleozoic formations, continental and marine Late Paleozoic sequences. In the Mesozoic, formations accumulated on the passive continental margin of the Tethys are dominant. In certain subunits, remnants of the oceanic basement are known, too. Their development indicates Alpine-Dinaric relationship.

Large-scale island-arc volcanism in the Eocene is an important feature of the unit which is unknown in the Tisza Unit.

The Pelso Unit can be divided into the following subunits:

The Transdanubian Central Range is characterized by terrestrial to marine Upper Permian, slow transgression from the Early Triassic, intrashelf rifting in the Middle Triassic, thick peritidal carbonate sequence in the Upper Triassic, intrashelf rifting with general trend of subsidence in the Jurassic, and tectonically controlled trans-regressive cycles in the Middle and Upper Cretaceous and in the Eocene.

The Mid-Transdanubian Subunit is known only from boreholes. Most important features are the marine Upper Permian and the shallow carbonate platform formations in the Middle and Upper Triassic.

Very low grade metamorphic Triassic formations and ophiolitic rocks are known from some boreholes which may belong to a deeper structural unit.

The Bükk Subunit is constituted by a Late Paleozoic marine sequence from which the Lower Triassic evolved without break in sedimentation, followed by a Middle and Upper Triassic carbonate platform facies and island-arc volcanites and by Jurassic formation of "schistes lustres" facies deposited in a deeper-water slope and basin, as well as in ocenic type crust.

The Meliata Subunit is a deep-water facies from the Middle Triassic with magmatic rocks of oceanic basement origin.

The Aggtelek-Bodva Subunit. The Upper (Silica) nappe includes Triassic of carbonate platform facies and deeper-water Jurassic showing affinity to the Northern Calcareous Alps. The deeper nappes (e.g. the Bódva Nappe) are composed of Middle and Upper Triassic deep-water facies, and of Jurassic "schistes lustres" facies which is similar to its counterpart in the

Bükk Mts.

3. Inner West-Carpathian Units

North of the Hurbanovo Line a crystalline complex of the Vepor Unit extends into the country's territory. It is known only from boreholes.

4. Austroalpine Units

The Penninic Unit: Jurassic to Lower Cretaceous metamorphic rocks of greenschist facies in the Hungarian part of the Rechnitz Window (Kőszeg Mts and its subsurface extension in the basement of the Little Hungarian Plain (Kisalföld).

Lower Austro-Alpine Unit: Paleozoic mesometamorphic formations known from the Sopron Mts.

Upper Austro-Alpine Unit: very low to low grade metamorphites known from the basin substratum between the Répce and Rába rivers, representing an extension of the Graz Paleozoic series.

In terms of a present-day interpretation, the above-mentioned megatectonic units approached each other only in the Early Tertiary, by sizeable plate tectonic reorganization processes that had initiated probably in the Cretaceous in connection with the late phase of the Tethys subduction and the subsequent collision.

CHARACTERISTICS OF THE EVOLUTION OF THE STRUCTURAL UNITS

The main geohistorical features of the Pelso and the Tisza Units are shown in Fig. 2 comparing them with the main events of the evolution of the Alps (Trümpy 1982).

Pecularities of the structural units and their affinity with the units of the surrounding Alpine-Carpathian-Dinaric system can be summarized as follows:

1. There are significant differences between the pre-Alpine basement and the Alpine history of the Pelso and the

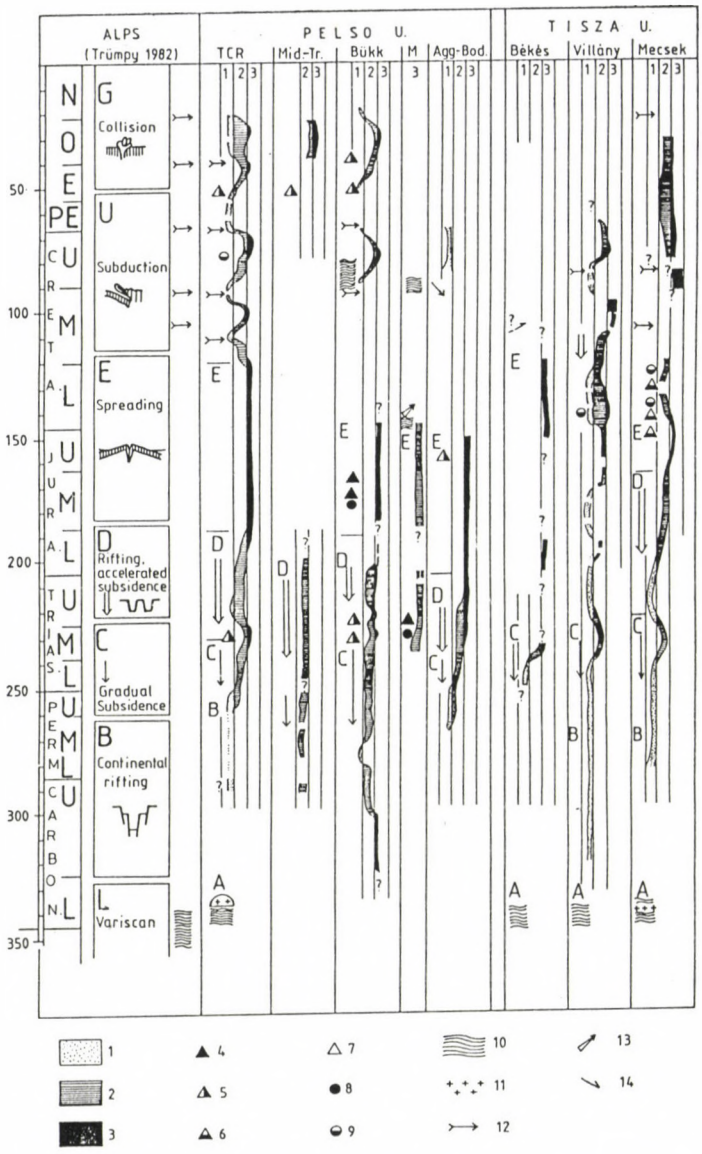

Fig. 2. Geohistory of the Pelso and the Tisza Units compared them with the Alpine evolution (after Trümpy 1982). Legend: Sedimentation: 1. continental; 2. shallow marine; 3. deep marine; magmatism: 4. mid--oceanic rift basalt (MORB) volcanism; 5. island-arc volcanism (IAV); 6. rift volcanism; 7. volcanism of unknown origin; 8. MORB--type intrusions; 9. rift-type intrusions; 10. metamorphism; 11. granites; 12. orogenic events; 13. obduction; 14. nappe formation (overthrusting as well as sliding)

Tisza Units although the basic characters of the Tethys evolution are observable in both units.

2. Evolutionary trend of the Pelso Unit is fairly similar to the Alpine one in the case of the Transdanubian Midmountains. The Middle Triassic rifting with volcanic activity, the Upper Triassic carbonate platform evolution and the disintegration of the platform in the Liassic suggest the original position of the Transdanubian Midmountains somewhere between the Southern and the Northern Limestone Alps on the southern passive margin of the Tethys. The periods of the subduction and the collision are manifested in the phases of the deformations and uplifts.

3. The Permian-Triassic shallow-water carbonate rocks of the Mid-Transdanubian Subunit show Dinaric-Slovenian affinity.

4. The North Hungarian - South Slovakian subunits (Bükk--Meliata-Aggtelek-Bódva) represent the inner zones of the Tethys: the shelf margin, the slope and the oceanic basement. The Bükk subunit of Dinaric affinity may have been a sector of the southern margin, with carbonate platforms in the Triassic, slope sediments and oceanic basalts in the Jurassic. The Meliata subunit represents the axial zone of the Vardar oceanic branch of the Middle Triassic. The Triassic platform carbonates and the deep water Jurassic sediments of the Aggtelek Subunit can originate from the northern margin, neither its southern origin can be excluded.

5. The history of the Tisza Unit fits into the general trend of the Tethys evolution upto the Mid-Triassic. In the Middle Triassic there is not any trace of the volcanic activity. The Mecsek Subunit is characterized by terrestrial siliciclastic sedimentation from the Upper Triassic to the Liassic (Gresten facies). The Upper Triassic is of Carpathian Keuper type in the Villány Subunit, while in the Békés Subunit dolomites of shallow shelf facies were formed.
These features suggest the position of the Tisza Unit in the Northern (European) shelf of the Tethys upto the late Jurassic - Early Cretaceous. The significant Early Cretaceous rift volcanism in the Mecsek (and subordinately in the Villány) Subunit may indicate the separation of the Tisza Unit from the

European plate. This process could be interrupted by the compressive Mid-Cretaceous tectonism caused overthrusting and nappe formation in every subunits of the Tisza Unit.
The dominantly siliciclastic Upper Cretaceous sediments were accumulated in the syn- or postorogenic grabens or basins.

PALEOGEOGRAPHIC RECONSTRUCTIONS

The original positions of the Hungarian megatectonic units as well as subunits during the Tethys evolution are shown in Fig. 3 to 8.

We have to emphasize that these reconstructions are drafts without real scale, and they demonstrate first of all the relations of the units (subunits) to each other.

Some comments on the position of the Hungarian lithospheric fragments during the Tethys evolution:

1. Upper Permian (Fig. 3)

After the Hercinian tectogenesis the fragments of the present-day Hungarian basement were situated around the northwestern termination of the Panthalassa embayment (epicontinental sea) that can be traced from Eastern Asia to the Alps.

In the Upper Permian the lateral transition of the continental-alluvial sedimentation environment (rift-grabens), the continental and the coastal sabkha and the shallow-marine shelf is well observable in the Southern Alps, and a very similar facies distribution is recognized in the Transdanubian Central Range.

The Permian successions of the Julian Alps - Slovenia, the Mid-Transdanubian and the Bükk subunits represent the inner belt of the Permian epicontinental sea.

Evaporites of the Aggtelek Subunit (similarly to those of the "Haselgebirge" in the North Alpine Juvavicum) can be fitted into the marginal belt of this sea.

In the Tisza Unit fluvial-lacustrine sediments accumulated in rift grabens due to the post-Hercynian erosion.

Transgression near to the Permian/Triassic boundary can be traced in the Southern Alps, in the Transdanubian Central Range

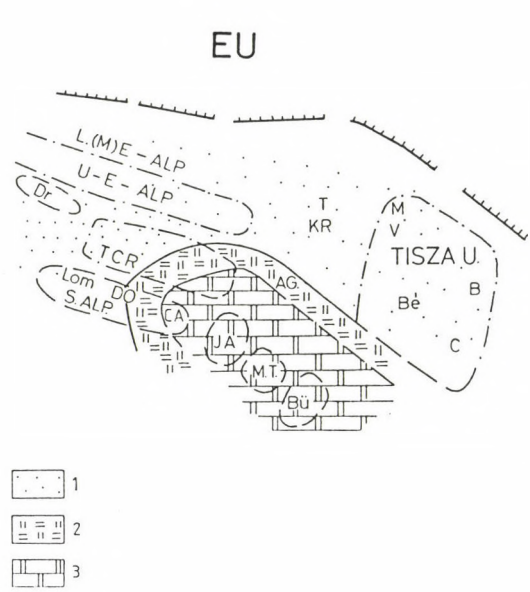

Fig. 3. Late Permian palaeogeography. L(M)E-ALP — Lower (and Middle) East Alpine; U-E.ALP — Upper East Alpine; Dr — Drauzug; TRC — Transdanubian Midmountains (= Central Range); S.ALP — South Alpine; Lom — Lombardia; DO — Dolomites; CA — Carnic Alps; JA — Julian Alps; MT — Mid-Transdanubian Subunit; Bü — Bükk Subunit, AG — Aggtelek Subunit; T — Tatra Unit; Kr — Križna Unit; M — Mecsek Mts; V — Villány Mts; Bé — Békés Subunit; B — Bihor Mts; C — Codru Mts. Legend: 1. continental; 2. evaporitic lagoon-sabkha; 3. shallow marine facies

while in the northern zones of the Tisza Unit it started only at the Scythian/Anisian boundary with evaporite-bearing formations (similarly to the German "Röt" facies). In the Middle Triassic carbonate platform formation started on a wide shelf which was followed by a process of disintegration of the platform as a consequence of the spreading in the Vardar zone. In the northern zones of the Tisza Unit vermicular limestones (similar to the German "Wellenkalk"), then ultra-back-reef lagoonal dolomites were deposited. The rifting was interrupted at the end of the Middle Triassic or in the early Upper Triassic in the Transdanubian Central Range and in the Southern Alps.

In Northern Hungary the rifting continued (with probable intervals of quiescence) throughout the rest of the Triassic.

It leads to the formation of deep-water, partly oceanic (Meliaticum) basin between a northern (Silice Nappe of Aggtelek-Rudabánya Subunit) and a southern (Bükk Subunit) outer shelf domains. It was situated in the continuation of the Vardar Oceanic Branch and was connected with the Euhallstatt basin in the Alps (Kovács 1984, 1989).

2. Upper Triassic (Fig. 4)

In the Carnian the process of disintegration was followed by nivellation due to terrigenous upfilling of the basins and an extremely wide carbonate platform began to form on the quickly subsiding shelf. Only the central Euhallstatt and Rudabánya-Meliata basins were not filled up; this event is also missing, in some outer shelf carbonate platforms (e.g. in the Mürztal Alps: Lein (1987) and in the Silice Nappe: Kovács (1984)).

Facies belts of the pelagic basin (Hallstatt basin), the reef (Dachstein reefs), the outer and inner shelf (Dachstein platform) and the ultra-back platform lagoon and tidal flat (Hauptdolomit) can be traced in the Northern Limestone Alps (Upper East-Alpine Unit). In the Transdanubian Central Range and in the Southern Alps most of these facies zones can be recognized as well (Haas 1987). The carbonate platform of the Julian Alps could be formed between the intrashelf Slovenian trough and the pelagic Hallstatt basin. Platform carbonates of the Mid-Transdanubian and the Bükk Subunits are regarded as the continuation of the Outer Dinaric outer shelf platform. Disintegration of the carbonate platforms is observed in the latest Triassic up to the early Jurassic in the Transdanubian Central Range and in the Bükk Subunits. Deep-water, pelagic sedimentation continued in the Aggtelek-Rudabánya Subunit. By this time the shelf margin platform of the southern part of the Silice Nappe (Aggtelek facies) had also subsided and became part of the Hallstatt limestone facies belt.

Within the Tisza Unit the Upper Triassic formations of the Mecsek Subunit represent a quickly subsiding basin filled up by fluvial as well as delta sediments.

In the Villány and in the northern nappes of the Codru

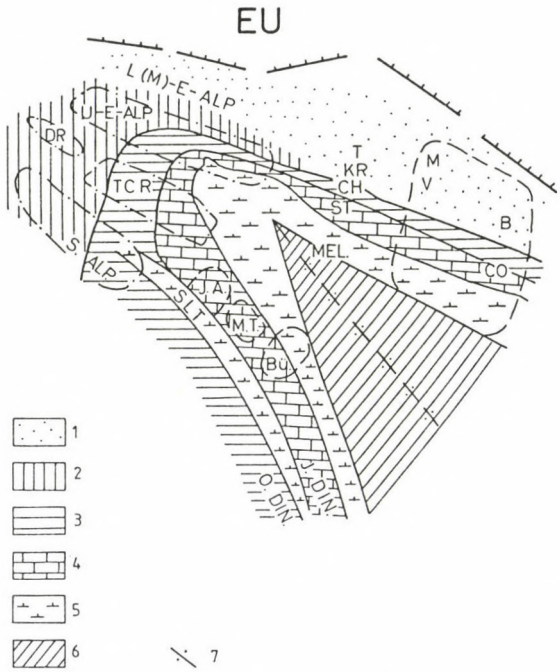

Fig. 4. Late Triassic Palaeogeography. I.DIN — Inner Dinaric units; O.DIN — — Outer Dinaric units; SLT — Slovenian Trough; MEL — Meliaticum; ST — Strážov nappe; CH — Choč nappe. Legend: 1. continental-shallow marine (Keuper facies); 2. ultra-back platform (Hauptdolomite facies); 3. inner platform (Dachstein Dolomite-Dolomia Principale); 4. outer platform (Dachstein Limestone facies); 5. pelagic sedimentation (Hallstatt facies); 6. oceanic basement; 7. mid-oceanic ridge

nappe system, Carpathian Keuper-type formations are characteristic.

In the Békés Subunit as well as in the Papuk Mts and in the Arieseni Nappe of the Codru nappe system dolomitic Upper Triassic occurs.

In the southern part of the Tisza Unit in the higher nappe units of the Codru nappe system and in Vojvodina carbonate platform formations (Dachstein Limestone) appear, locally with pelagic influence.

In the Inner West-Carpathian units the facies-distribution is more or less similar to above mentioned one.

This suggests the Early Mesozoic position of the Tisza block beside the reconstructed place of the Inner West Carpathian units (Kovács 1980).

3. Middle Jurassic (Fig. 5)

Disintegration and spreading continued during the Jurassic but while formerly the ruptures came from the east, now a new spreading system evolved from the west, from the Central Atlantic. The newly formed Brianconnais - South Penninic belt (which apparently joined the Vardar zone) separated the southern and northern margins of Tethys.

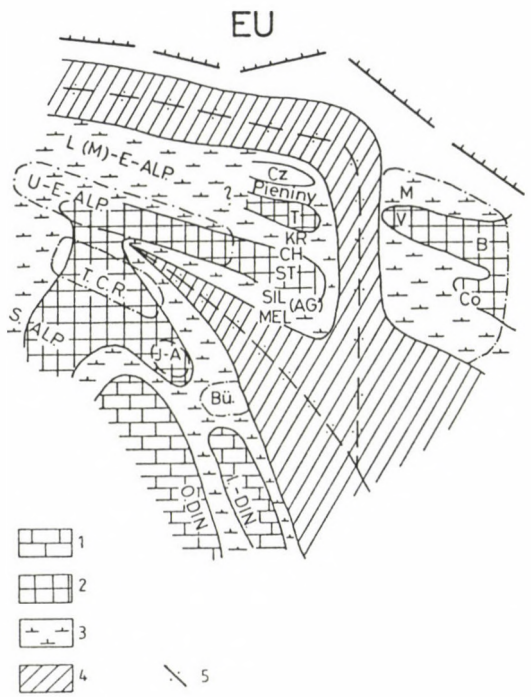

Fig. 5. Middle Jurassic palaeogeography. SIL — Silicium (Aggtelek Subunite); Cz — Czorsztyn unit. Legend: 1. carbonate platform; 2. submarine graben and horst system (disintegrated platform); 3. pelagic sedimentation; 4. oceanic basement; 5. mid-oceanic ridge

Differential subsidence, block-faulting and formation of basins was characteristic to the northern part of the southern

margin (West Carpathians, Northern Limestone Alps, Southern Alps). In the Early Jurassic, thick marly ("Fleckenmergel") and siliceous ("Moltrasio") sediments accumulated in the basins, while the elevated areas (submarine plateaus or seamounts) were characterized by non-deposition (hardgrounds) or by very condensed carbonate sedimentation. The Transdanubian Midmountains and the Aggtelek Subunit show these general characters. In detail, the thick basinal sequence known in the Zala area can be compared with that of the Lombardian basin, whereas the condensed biogenic carbonates ("Hierlatz" limestones, calcarenites) found in the rest of the Transdanubian Central Range have close analogies in the northern part of the Trento plateau and in the Northern Limestone Alps (e.g. Hallstatt area). The Middle Jurassic radiolarites and the Upper Jurassic ammonitico rosso and biancone are almost uniformly widespread in the whole area.

In the more southern zones (Inner and Outer Dinarides) evolution of the shallow water carbonate platforms was uninterrupted from the Triassic and through the Jurassic. The Bükk area might be in the proximity of these areas and its deep water sedimentary basin received platform-derived, redeposited carbonate material from time to time.

The northern margin of Tethys was characterized by predominantly terrigenous detrital sedimentation in the Early Jurassic and by more and more pure carbonate accumulation in the Middle and Late Jurassic. The Tisza Unit shows similar development. The enormous, graben-like depressions in the Mecsek Subunit, locally with more than 1000 m clastic sediments and thick coal measures in the earliest Jurassic might be a continuation of the Danish-Polish Trough. The Villány Subunit was an elevated ridge area with thin and episodic sedimentation in the Early and Middle Jurassic.

Due to progressive rifting and spreading, in the Mecsek basin thin, pelagic, cherty limestones were formed in the Late Jurassic with traces of submarine volcanism. At the same time, the Villány Subunit became a "pelagic platform" with shallow water biogenic buildups in the Bihor and with "pelagic oolites" in the Villány area.

4. Early Cretaceous (Fig. 6)

The beginning of the closure of the Vardar and the opening of the Penninic oceanic branch are the main events of the Early Cretaceous. As a consequence of this opening the Tisza Unit separated from the European platform and at the first time during Mesozoic history its position in latitude coincides with that of the Transdanubian Central Range. The rift type alkaline basaltic volcanism in the Mecsek Subunit can be connected with this process too. The Villány Subunit is characterized by carbonate platform formation where a transgressive type Urgon facies proceeded toward the North from the Hauterivian to Albian ages after an emersion at the beginning of the Cretaceous. At the northern margin of the zone the Upper Jurassic limestone is directly covered by an Albian-Cenomanian flysch--like sequence.

In the Békés Subunit the open marine, deep water sedimentation is supposed to be continuous.

Due to the closing of NW branch of the Vardar ocean slices of ophiolite complexes were uplifted in the suture zone and trenches were formed in which terrigenous sedimentary sequences, containing ultrabasic detritus were accumulated.

Ultrabasic detritus of similar origin appear in the flysch-like succession of the Gerecse Mts in the Transdanubian Central Range too. On the contrary Early Cretaceous basin sediments of the Bakony Mts (SW-ern part of the Transdanubian Midmountains) show close similarity with the Maolica facies of the deep basins of the Southern Alps in the northern foreland of the Apulian platform.

The major part of the Transdanubian Central Range was elevated, eroded and gently folded during the Austrian phase. Its syncline shape is also a result of this phase. During the Albian the lacustrine environment was followed by the evolution of a carbonate platform (Urgonian facies). In Late Albian time the platform suddenly drowned and was covered by deeper water glauconitic sediments.

In the Outer Dinarides the evolution of the carbonate platform continued from the Jurassic while in the Inner

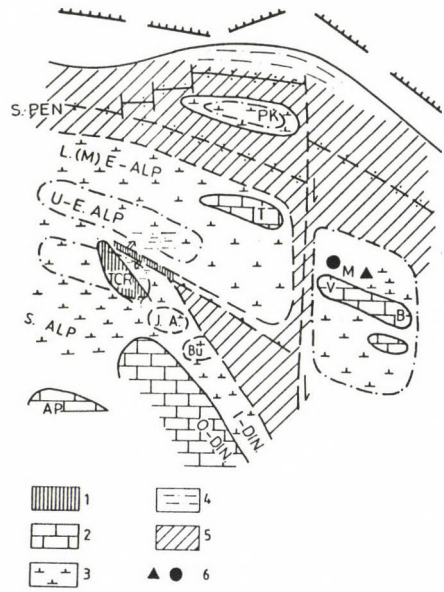

Fig. 6. Early Cretaceous palaeogeography. S.PEN — South Penninic, PK — Pieniny Klippen Belt, AP — Apulian platform. Legend: 1. elevated area; 2. carbonate platform; 3. pelagic sedimentation; 4. flysch sedimentation; 5. oceanic basement; 6. alcali basaltic rift volcanism

Dinarides deep water sedimentation started.

5. Late Cretaceous (Fig. 7)

During the Mid-Cretaceous subduction of the Tethys, subbasins significantly progressed. This period was the main phase of the nappe formation all over the Alpine - Inner Carpathian region. Contemporaneously deep troughs and basins formed in the subduction zones along the southern margin of the European plate (Rhenodanubian and Carpathian Flysch zones) and around the Apulian (-Adriatic microplate).

The block-faulting during the early part of the Late cretaceous resulted in the formation of separated subbasins (Gosau basins) above the nappe-systems. In the outer zones north to the Austroalpine-Inner Carpathian folded belts flysch sedimentation continued, while to the South, deep basins and large shallow carbonate platforms evolved.

In this framework the setting of the Transdanubian Central

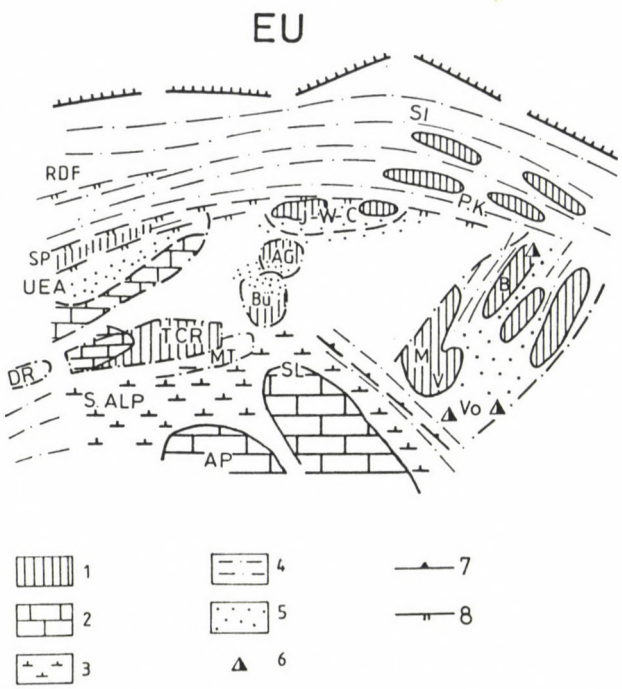

Fig. 7. Late Cretaceous. RDF — Rhänodanubian Flysch Zone, Sl — Silizean Flysch, I-W-C — Inner West Carpathian Units, SL — Slovenian area, Vo — Vojvodina. Legend: 1. elevated areas; 2. carbonate platforms; 3. pelagic sedimentation; 4. flysch sedimentation; 5. dominantly clastic sedimentation (Gosau facies); 6. island-arc volcanism; 7. subduction zone; 8. overthrusting zone

Range between the Southern Alps and the Austroalpine units did not change significantly, but its paleogeographic relations with them became looser (island position) and its motion towards northeast started.

The paleogeographic setting of the Bükk Subunit is uncertain, but the material of the gravels in the Senonian submarine fan deposites indicate its close connection to the Aggtelek Subunit.

There was a significant change in the position of the Tisza Unit during and after the Early Cretaceous volcanic activity, when the Tisza block separated and removed from the northern Tethys margin (anti-clockwise rotation $\sim 70^{o}$). The Mid-Cretaceous compressional period was manifested in thusting,

nappe formation and folding. It was followed by emersion, intense denudation then by block-faulting prior to a Senonian graben and basin formation. The trough in the Mecsek Subunit (Szolnok flysch zone) could be in connection with the Carpathian flysch zone.

6. Middle Eocene (Fig. 8)

During the latest Senonian and the Paleocene flysch-sedimentation continued in the outer flysch belts and the deep-marine clastic sedimentation extended into the area of the Northern Limestone Alps (Faupl et al. 1987). In the Transdanubian Central Range an emersion and a significant denudation is inferred at the end of the Cretaceous, and there is not any trace of the Paleocene sedimentation.

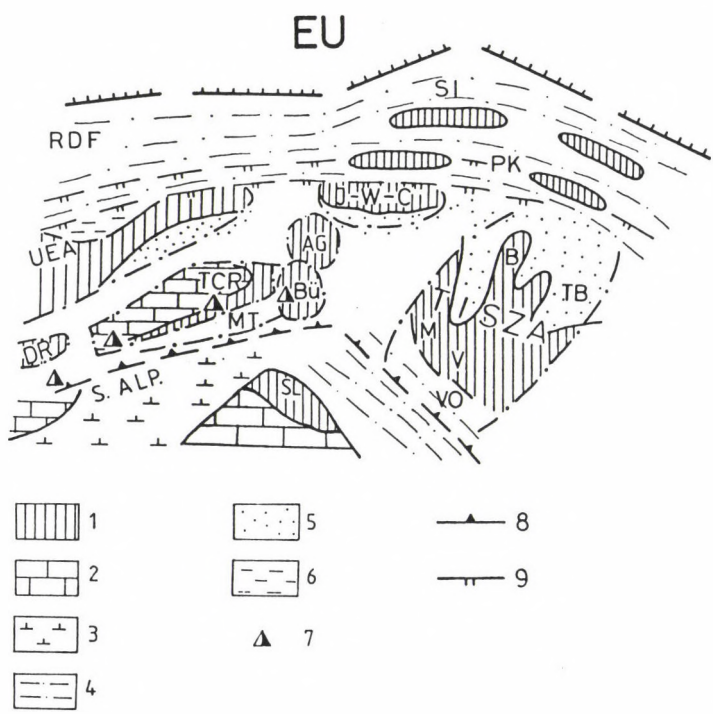

Fig. 8. Middle Eocene palaeogeography. Legend: 1. elevated area; 2. carbonate platform; 3. pelagic sedimentation; 4. flysch sedimentation; 5. dominantly clastic sedimentation; 6. argillaceous sedimentation; 7. island-arc volcanism; 8. subduction zone; 9. overthrusting zone

The North-eastward motion of the Transdanubian Central Range and together with it of the Mid-Transdanubian Subunit continued, and it can be supposed that the Bükk Subunit came into direct contact with the afore-mentioned subunits.

Thus we can say that this is the time of the establishment of the Pelso Unit. Juxtapositon of the Transdanubian Central Range, the Mid-Transdanubian and the Bükk Subunits are indicated by island-arc type volcanism which can be observed in each unit. The position of the Tisza Unit had not changed significantly since the Cretaceous, but its major part emerged due to the post-Cretaceous tectonic activity. During the Middle Eocene the "Szolnok flysch" basin and the Transylvanian subbasins were the sites of the accumulation of the dominantly terrigenous siliciclastic sediments.

Lateral movement of the Pelso Unit went on during the Oligocene and even in the Early Miocene as it was manifested in the formation of the North Hungarian Paleogene and Early Miocene Basins of transtensional origin (Báldi and Báldiné-Beke 1985, Royden and Báldi 1988, Nagymarosy, this volume).

It is an important fact that already the Paleogene Basin extended over the boundary of the Pelso Unit onto the Inner West Carpathian Units.

The Tisza Unit came into its present-day position by a 90^{o} rotation during the Tertiary prior to the Middle Miocene (see a discussion in Márton, Horváth, this volume).

The next phase is already the evolution of the Pannonian Basin iniciated by the formation of the transtensional proto--basins in the Middle Miocene which was followed by an extended subsidence in the Late Miocene-Pliocene.

REFERENCES

Balla Z 1982: Tectonophysics, 88.

Balla Z 1988: Acta Geol. Hung., 31, 53-63.

Báldi T, Báldiné-Beke M 1985: Acta Geol. Hung., 28, 5-28.

Brezsnyánszky K, Haas J 1986: Geol. Zbornik - Geol. Carpath., 37, 297-303.

Channel J E T, Horváth F 1976: Tectonophysics, 35, 71-102.

Császár G, Haas J, Halmai J, Hámor G, Korpás L 1987: In: Global Correlation of Tectonic Movement (Leonov Yu G and Khain V E eds). IGCP Project 107. John Wiley and Sons Ltd., 173-186.

Decker K, Faupl P, Müller A 1987: In: Geodynamics of the Eastern Alps (Flügel H W and Faupl P eds), 126-141.

Faupl P, Pober E, Wagreich M 1987: In: Geodynamics of the Eastern Alps, Deutiche - Vienna, 142-155.

Fülöp J, Brezsnyánszky K, Haas J 1987: Acta Geol. Hung., 30, 3-20.

Géczy B 1983: Ann. Univ. Sci., Budapest, Sec. Geol., 16, 99-114.

Haas J 1987: Acta Geol. Hung., 30, 243-256.

Kázmér M, Kovács S 1985: Acta Geol. Hung., 28, 71-84.

Kázmér M, Kovács S 1989: In: Tectonic Evolution of the Tethyan Region (Sengör A M C ed.), Kluwer Academic Publisher, Doodrecht, 77-92.

Kovács S 1980: Földt. Közl., 110, 360-381.

Kovács S 1984: Acta Geol. Hung., 27, 251-264.

Kovács S 1989: In: Tectonic Evolution of the Tethyan Region (Sengör A M C ed.), Kluwer Academic Publisher, Doodrecht, 93-108.

Márton E 1990: Kinematics of the principal tectonic units of Hungary from paleomagnetic observations (present issue)

Lein R 1987: In: Geodynamics of the Eastern Alps (Flügel W and Faupl P eds), Wien, Franz Dentiche, 85-102.

Pober E, Faupl P 1988: Geol. Rundschau, 77, 641-670.

Royden L H, Báldi T 1988: In: The Pannonian basin (Royden L H and Horváth F eds), AAPG Memoir, 45, 1-16.

Trümpy R 1982: In: Mountain building processes (Hsü K J ed.), Academic Press, London, 149-156.

Zupanic J, Babic L, Crnjakovic M 1981: Acta Geol., Zagreb, 11, 1-44.

Acta Geod. Geoph. Mont. Hung., Vol. 25 (3-4), pp. 345-371 (1990)

PETROLOGY AND PETROCHEMISTRY OF MESOZOIC MAGMATIC SUITES IN HUNGARY AND ADJACENT AREAS - AN OVERVIEW

I Kubovics, Cs Szabó, Sz Harangi, S Józsa

Department of Petrology and Geochemistry, Eötvös University,
H-1088 Budapest, Múzeum krt. 4/A, Hungary

In this paper the authors review the tectonic affinities and petrogenesis of Mesozoic magmatites in the main tectonic units of Hungary and the adjacent areas. Formations of these magmatic series are in close relationship with the evolution of the northwestern part of Tethys.

The Rechnitz (Rohonc) Series of Penninic Unit includes a typical ophiolitic sequence with N-type MORB character.

In the Pelso unit Middle Triassic, dominantly intermediate-acidic magmatites (lava flows, dykes and pyroclastites) are found in the Transdanubian Central Range and in the Eastern Bükk. Based on the petrographical and geochemical features of these volcanic suites they are related to convergent plate magmatism which can be found in the Outer Dinarides and Southern Alps, too. In the same tectonic unit the Middle Triassic-Jurassic (Meliate (Melléte)) and the Jurassic (Szarvaskő) incomplete ophiolite sequences appear in different nappes. Petrochemical studies and tectonic reconstructions led the authors to the conclusion that the Szarvaskő magmatites represent a back-arc basin-, the Meliata series an ocean floor magmatism and between them the Telekes-oldal (Rudabánya Mts) rhyolite represents an island-arc-type volcanic product in the northern part of the Triassic--Jurassic Vardar ocean.

During the Late Cretaceous a lamprophyre-picrite-carbonatite association, derived from a deep mantle source, intruded into the extensional zone of the Alpine collision.

In the Mecsek-Alföld zone (Tisza unit) the dominantly Early Cretaceous volcanic rocks belong to a basalt-tephrite-phonolite differentiation sequence. This volcanic suite is the product of a continental rifting initiated by the opening of the Penninic branch of the Tethys ocean.

Keywords: island-arc; magmatism; ophiolite; Pelso unit; Penninicum; petrochemistry; rift; Tisza unit

INTRODUCTION

In the last years extensive investigations were carried out on the Mesozoic magmatites of Hungary and of the adjacent areas by the Department of Petrology and Geochemistry (Eötvös

University). Previous studies have been focused on the petrology and origin of ultrabasic-basic magmatic assemblages of certain areas (Kubovics 1983, Bilik 1983, Kubovics 1984, Kubovics and Bilik 1984). In this paper we attempt to give a review about the petrogenesis, the original tectonic settings and areal relationships of the Mesozoic magmatic suites in connection with the evolution of the northwestern part of the Tethys.

Mesozoic magmatic rocks appear in different tectonic units in the central area of the Carpathian-Pannonian region (Fig. 1).

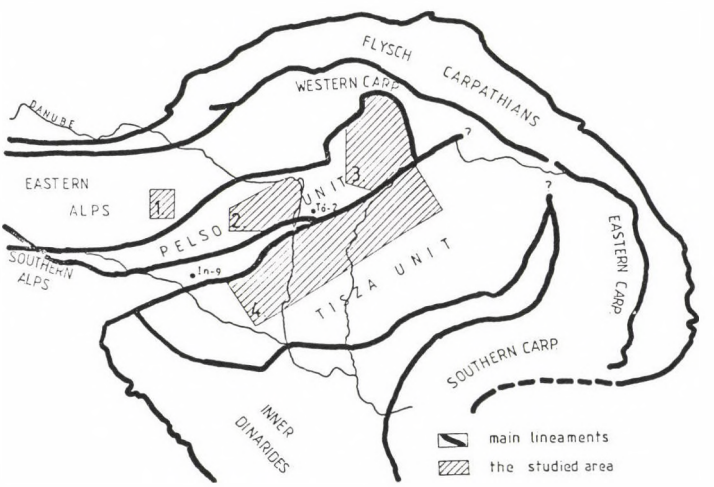

Fig. 1. Distribution of the studied magmatic areas in the central part of the Alp-Carpathian region. 1. Kőszeg-Rechnitz (Rohonc) Mts, 2. NE--Transdanubian, 3. NE-Hungary and S-Slovakia, 4. Mecsek-Alföld zone

The Rechnitz (Rohonc) Series, belonging to the Penninicum, crops out in four tectonic windows at the foot of the Eastern Alps. In the Pelso unit various magmatic formations can be found: i) Triassic volcanites in the Transdanubian Central Range and in the Eastern Bükk Mts, ii) sporadic occurrences of Middle Triassic-Jurassic magmatic rocks from Tóalmás (Northern part of the Great Hungarian Plain) through Darnó hill to Southern Slovakia, iii) Jurassic magmatic complex near Szarvaskő and

iv) Late Cretaceous lamprophyre-picrite-carbonatite dike rocks in NE-Transdanubia. In the Tisza unit the studied area included the Mecsek zone comprised Early Cretaceous volcanic sequence.

In this paper a large volume of published and unpublished major-, trace- and rare-earth element data (Table I) were evaluated by means of several geochemical and geomathematical methods. The petrochemical evolution of the magmatic series is demonstrated by the principal component variation diagrams (Le Maitre 1968, Harangi 1989a, 1989b).

THE RECHNITZ (ROHONC) SERIES (PENNINIC UNIT)

The Rechnitz (Rohonc) Series, which is correlated with Penninic units (Schmidt 1950, Pahr 1960, 1977), appears in four tectonic windows from below the Austroalpine nappes in the area of Burgenland (Eastern Austria) and Western Hungary (Koller and Pahr 1980, Kubovics 1983). They comprise greenschist facies metasediments (phyllite, calcareous phyllite, quartzite) and ophiolitic rocks. The ophiolite sequence includes large bodies of greenschist, slightly serpentinized ultramafics, metagabbros and blueschists (Schmidt 1950, Erich 1953, Koller and Pahr 1980, Koller and Wiesender 1981, Kubovics 1983, Koller 1985). The ophiolite complex suffered an oceanic metamorphism during the submarine eruptions and then a high-pressure Eoalpine- (65 Ma) and Tertiary (19-22 Ma) regional metamorphism (Koller 1985).

Serpentinite blocks, originally harzburgites (Koller 1985, Kubovics and Szabó 1988) and lherzolites (Evren 1972) could be found in each tectonic window and were interpreted as tectonic slices by Evren (1972). These rocks consist of talcs, tremolites and magnetites in addition to the serpentine minerals. The chlorite-rich precious serpentinite ("Edelserpentinite") may have been formed by Al-metasomatism from the ultramafic cumulates of the ophiolite suite (Koller and Pahr 1980, Koller 1985).

A geochemical study on the magmatic relicts preserved in the plutonic bodies - i.e. metagabbros and blueschists - provides information to the recognition of the metamorphic history

Table I. Sources of analytical data

Rechnitz (Rohonc) Series	Kubovics 1983
	Koller 1985
	Kotsis 1986
	unpublished data (ELTE, Dept. Petr.-Geochem.)
Meliata (Melléte) magmatites	Kiss 1958
	Pantó and Földvári 1950
	Pantó 1961
	Varga et al. 1975
	Juhász and Vass 1974
	Kubovics 1983
	Balla 1984
	Réti 1985
	Hovorka and Spisiak 1988
	unpublished data (ELTE, Dept. Petr.-Geochem.)
Szarvaskő magmatites	Szentpétery 1953
	Lengyel 1957
	Kubovics 1983
	Balla et al. 1983
	Balla and Dobretsov 1984
	Réti 1985
	unpublished data (ELTE, Dept. Petr.-Geochem.)
Transdanubian mafic-ultramafic dyke-rocks	Horváth et al. 1983
	Kubovics 1984
	Horváth and Ódor 1984
	Kubovics and Szabó 1988
	Dobosi and Horváth 1988
	Kubovics et al. 1989a
	Embey-Isztin et al. 1989
	unpublished data (ELTE, dept. Petr.-Geochem.)
Mecsek-Alföld zone volcanics	Mauritz 1913
	Viczián 1971
	Molnár 1985b
	Lentai 1987
	Molnár 1990
	unpublished data (ELTE, Dept. Petr.-Geochem.)

of this area (Koller and Wieseneder 1981, Lelkes-Felvári 1982, Kubovics 1983, Koller 1985). The petrochemical evolution of the Rechnitz (Rohonc) magmatic complex is displayed by means of a principal component variation diagram (Fig. 2). Normal gabbro (pumpellyitic metagabbro) is regarded as the most primitive

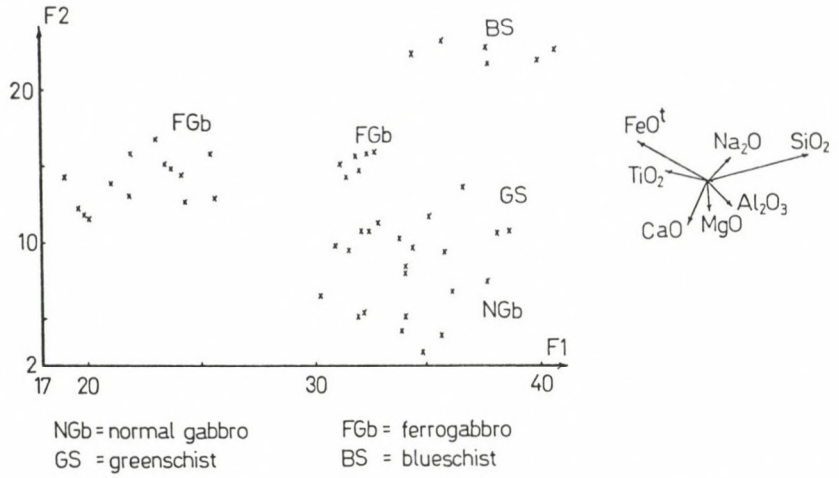

Fig. 2. Major element chemical evolution of Rechnitz (Rohonc) Series in the principal component variation diagram

member of this sequence. Fe-Ti-rich mineral separation from the gabbroic magma resulted in the formation of the ferrogabbros (melagabbros, crossitite), whereby the silica- and sodium-content of the residual magma increased and led to the plagiogranites (blueschists). Koller (1985) pointed out that the differentiation process was accompanied by a progressive REE-enrichment in good agreement with our observations.

The greenschist bodies comprise predominantly tholeiitic basalts with N-type MORB-composition, minor ferrobasalts, which may represent the original "sheeted-dyke" complex and unfractioned Cr- and Mg-rich picritic basalts (Koller 1985). He revealed the appearance of oceanic island-type alkali basalts within this area as well.

The Rechnitz (Rohonc) ophiolite complex shows clear correlation to the other units of Penninic Series representing the oceanic crust of the Jurassic-Cretaceous Penninic Ocean.

THE MELIATA (MELLÉTE) MAGMATITES

Formations of the Meliata (Melléte) series (Kozur and Mock 1973) appear sporadically in an elongated area from Tóalmás (boreholes Tó-2 and Tó-3) through Darnó hill (Földessy 1975,

Balla et al. 1980, Kubovics 1984, Balla (1984) and Bódva valley (Réti 1987) to Jaklovce (Jekelfalva, Southern Slovakia; Hovorka 1985, Hovorka and Spisiak 1988) (Fig. 3). From the Middle Triassic deep water sediments were accumulated which include basic submarine lava flows and submarine bodies considered as parts of an incomplete ophiolite sequence (Hovorka 1985). Basalt, gabbro and serpentinitized spinel peridotite - the latter occurs as tectonic slices - constitute this magmatic sequence which suffered a slight prehnite-pumpellyite facies metamorphism. According to Hovorka and Spisiak (1988) blueschist facies metamorphism took place at some sites as well.

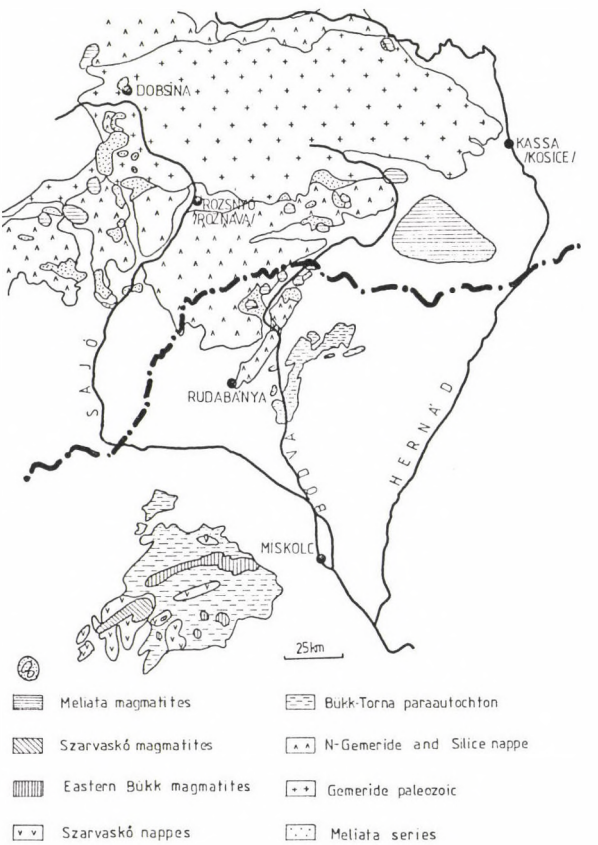

Fig. 3. Occurrences of Mesozoic magmatites in NE-Hungary and S-Slovakia (after Hovorka 1985 and Csontos 1988)

Most of the ultramafics are strongly serpentinitized and contain only small amounts of relicts (Hovorka 1985, Réti 1987).

Basalts are found as massive lava flows with intersertal to intergranular texture or as spherolitic, variolitic to hyalopilitic pillow lavas. Clinopyroxene, basic plagioclase and volcanic glass are the main components, albite, chlorite, epidote appear as secondary minerals. The "sheeted dyke" complex is represented by various gabbros with ophitic to intergranular texture and mineral content similar to the basaltic rocks.

Salic rocks belonging to this sequence are known only at one location, near Jaklovce (Jekelfalva, Southern Slovakia; Hovorka and Spisiak 1988). The felsitic, glomeroporphyriritic keratophyre consists of albite, actinolite, quartz, chlorite, titanite and epidote.

The major element chemical variation of the Meliata (Melléte) magmatites is typical of oceanic tholeiite assemblages (Fig. 4). Starting from a basaltic magma, the accumulation of femic minerals resulted in the formation of ferrogabbros, whereas CaO-enrichment in "normal gabbro" can be regarded as a basic plagioclase separation. As a working hypothesis we suppose that keratophyre may be the residual product of the differentiation process. The scatter of data-points in the variation diagram is explained as the result of secondary alterations.

There are several discrimination factors to distinguish oceanic tholeiites (Wood et al. 1979, Saunders et al. 1980 etc.). Plotting the Meliata (Melléte) magmatites onto the Th-Hf/3-Ta triangular diagram (Wood et al. 1979, Wood 1980) a great part of data-points falls in the E-type MORB-field (Fig. 5). Other incompatible trace element ratios (Zr/Nb, Hf/Ta, Nb/La, Ce/Nb) indicate both E-type and N-type MORB characters.

Based on the petrological and petrochemical features as well as the stratigraphic and tectonic observations (Réti 1985, Kozur 1989, Kovács 1982, 1989) the Meliata magmatic complex represents the remnants of the northern part of the Triassic--Jurassic Vardar ocean with dominantly anomalous (E-type)

MORB character.

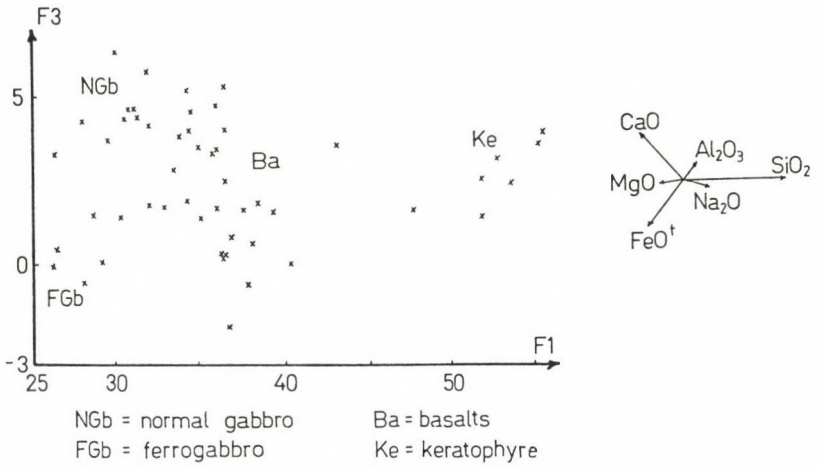

Fig. 4. Major element chemical evolution of Meliata (Melléte) magmatites in the principal component variation diagram

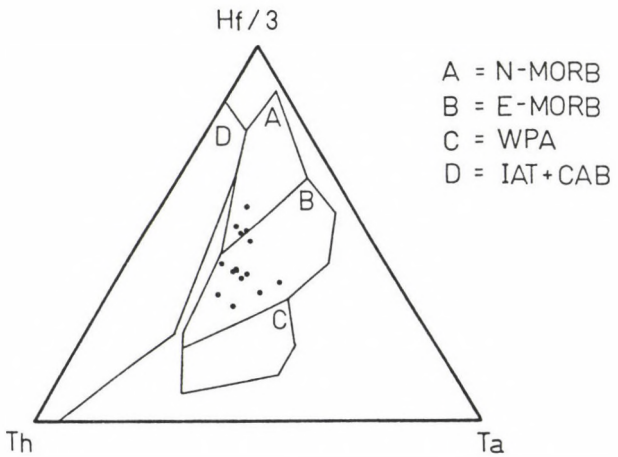

Fig. 5. Th-Hf/3-Ta discrimination diagram (Wood et al. 1979) for Meliata (Melléte) basalts and gabbros

THE SZARVASKŐ MAGMATIC COMPLEX

The Lower Jurassic (Balogh et al. 1984) dominantly mafic--ultramafic magmatic complex belongs to the Mónosbél-Szarvaskő nappe underlain by the Bükk-Torna paraautochton (Csontos 1988) (Fig. 3). The magmatic complex represents the upper part of an ophiolitic sequence (Balla and Dobretsov 1984). Massive lava flows with ophitic to intersertal texture and variolitic pillow lavas are found among the 300-500 m thick effusives (Szentpétery 1953, Balla and Dobretsov 1984). Based on the small sizes of pillows and the low volatile-content these lava flows may have erupted on the surface of a few thousand meter deep sea (Balla and Pelikán 1983). Pesudomorphs after olivine, augite, plagioclase and altered volcanic glass are the main components of the basalt.

The intrusive complex formed after the effusive rocks appears mainly as sills with 100-150 m thickness and comprises dominantly gabbros, as well as ultramafics (peridotite, pyroxenite, hornblendite), intermediate (diorite) and acidic (plagiogranite, albitite) differentiates. In the basic-ultrabasic rocks olivine, ilmenite and titanomagnetite occur as cumulate minerals (Balla et al. 1983, Kubovics 1984), while orthopyroxenes, clinopyroxenes, plagioclases and brown hornblende represent the post-cumulate mineral-assemblage. The crystallization of the intrusive bodies took place in high oxygen-fugacity which increased in the middle stages of the crystallization due to an in situ transvaporization from the argillaceous sediments (Balla et al. 1983, Kubovics 1984).

The magmatic series and the sedimentary wall-rocks suffered a low-grade pumpellyite- prehnite-quartz facies regional metamorphism (Árkai 1973).

The major element chemical evolution of this magmatic sequence is illustrated by a principal component variation diagram (Fig. 6). Two main trends are observed: separation of FeO-, TiO_2- and MgO-bearing minerals resulted in the formation of various ultramafics, while intermediate and acidic rocks were formed by alkali feldspar differentiation from a SiO_2- and

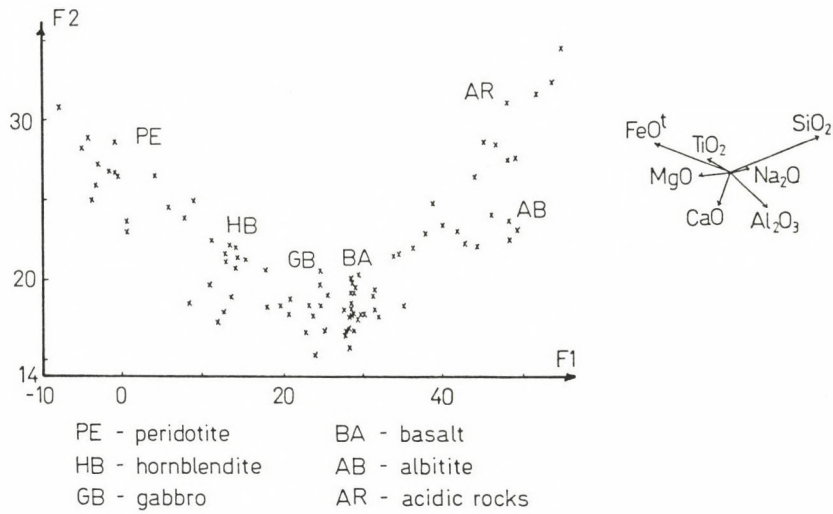

Fig. 6. Major element chemical evolution of Szarvaskő magmatic complex in the principal component variation diagram

Na_2O-rich evolved magma. Within these trends further specific rock-types were developed due to the accumulation of TiO_2 (peridotites), as well as Na_2O (albitite).

The REE patterns of different rock types reflect the differentiation characters (Fig. 7): gabbros and peridotites are LREE-depleted rocks, differing from each other only in the plagioclase-content caused the Eu-anomalies. The REE-abundances of hornblendites are high due to the REE accumulation in amphiboles. Formation of plagiogranite was accompanied with LREE--enrichment.

Based on the petrological and geochemical studies of the Szarvaskő magmatic rocks and the tectonic, stratigraphic observations this unit may represent a marginal basin of the Vardar oceanic branch (Balla et al. 1983, Kázmér and Kovács 1989).

Figure 8 shows some specific incompatible trace element ratios which are diagnostic for ocean basalts (Wood et al. 1979, Saunders et al. 1980). Comparing the above mentioned three tholeiitic magmatic series there are some differences. The Rechnitz (Rohonc) Series (Penninicum) represents the

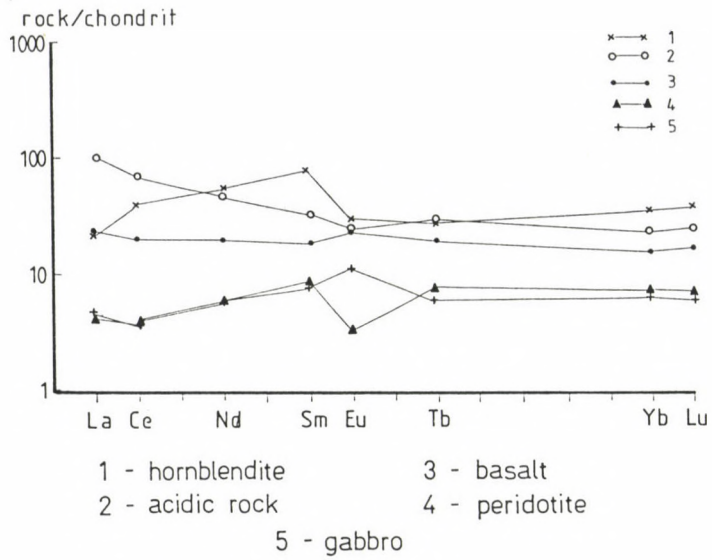

Fig. 7. Average REE pattern of the main rock-types found in the Szarvaskő ophiolite sequence

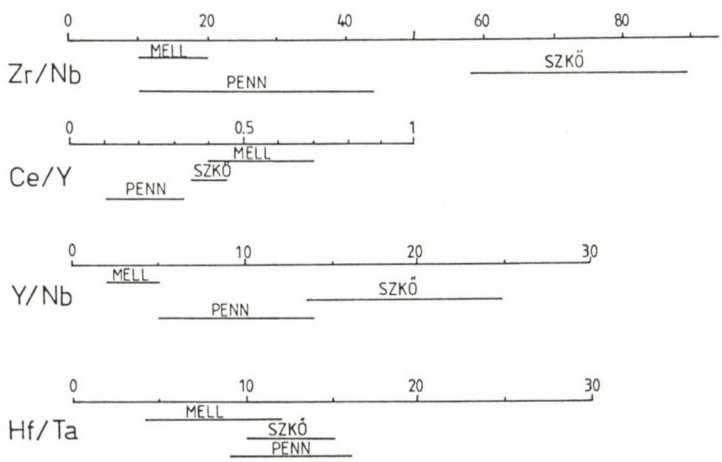

Fig. 8. Some specific incompatible trace element ratios for 3 oceanic tholeiitic series: MELL - Meliata (Melléte) magmatites; SZKő - Szarvaskő magmatites; PENN - Rechnitz (Rohonc) Series (Penninicum)

typical N-type MORB (Koller 1985), while the Meliata (Melléte) magmatites tend to have rather E-type MORB characters. The Szarvaskő magmatic complex has different discriminant factors, except the Hf/Ta ratio.

We suppose spatial and temporal relationship between the Szarvaskő and Meliata (Melléte) magmatites. Meliaticum represents the oceanic part of the Vardar oceanic branch formed from the Middle Triassic to Jurassic, while Szarvaskő represents its Jurassic marginal sea. The question is where the volcanic arc should be searched? In the Rudabánya Mts (Telekes-oldal Series) (Fig. 3) Jurassic (Grill et al. 1984, Grill and Kozur 1986) volcanites (rhyolite, Máté and Szakmány unpublished data) and Szarvaskő-Mónosbél-type sediments - are found. Since the petrochemistry of the rhyolite indicates island arc affinity, we suggest that this area may represent the volcanic arc between the back-arc basin (Szarvaskő) and the Meliata (Melléte) ocean (Fig. 9). This assumption is supported by the interpretations of Balla et al. (1983) and Kázmér and Kovács (1989) as well.

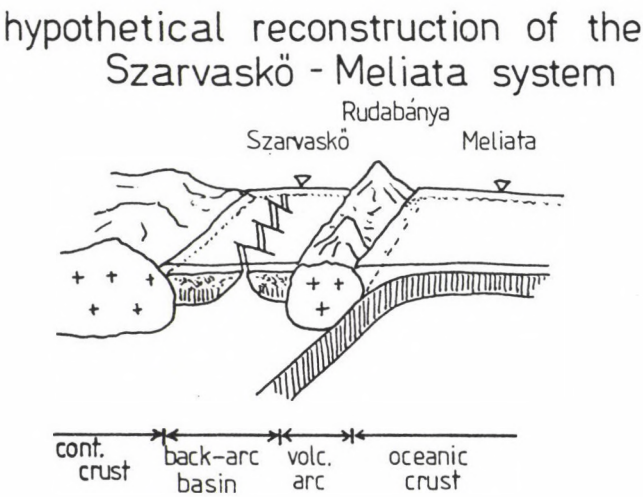

Fig. 9. Hypothetical reconstruction of the Szarvaskő-Meliata (Melléte) system

EASTERN BÜKK VOLCANICS

In the eastern part of Bükk Mts (Fig. 3) slightly metamorphosed (Árkai 1973) submarine lava flows and pyroclastics appear in several stratigraphical levels of Bükk-Torna paraautochton (Csontos 1988). Previous studies suggested two volcanic suites (Szentpétery 1953, Pantó 1961, Balogh 1964, Balogh et al. 1984): the Ladinian magmatites are characterized by mainly basic and intermediate composition, while the younger bimodal volcanism produced basic and acidic rock types. Lacking sufficient amount of rare-earth and trace element data we set up a preliminary working hypothesis that this volcanic assemblage belonged to a single magmatic sequence.

The Eastern Bükk magmatic rocks proved to be dominantly trachyandesite, andesite and trachyte plotted in the TAS diagram. The slight alkali-enrichment accompanied by high Al_2O_3-content is considered to be the effect of metamorphic alteration. The major element chemical characters indicate island-arc affinities. Based on several geodynamic reconstructions (Balogh et al. 1984, Kovács 1982) the stratigraphical correlation between the Bükk-Torna paraautochton (Csontos 1988) and the Southern Alps-Outer Dinaride zone is widely accepted. We think that a detailed geochemical study will reveal a relationship between the Eastern Bükk magmatites and other Triassic volcanic areas, like Southern Alps (Dolomites Mts, Carnic Alps, Karavanken) (Leonardi 1967, Pisa et al. 1980, Castellarin et al. 1980), the Transdanubian Central Range (in this paper) and the Outer Dinarides (Bébien 1980, Pamic 1982) characterized by magmatic rocks with similar petrographical characters and interpreted rather as an island-arc (Pisa et al. 1980, Castellarin et al. 1980) than of rift-origin (Pamic 1982).

TRIASSIC INTERMEDIATE-ACIDIC MAGMATITES IN TRANSDANUBIA

In the Transdanubian Central Range, belonging to the Pelso unit, Middle Triassic intermediate-acidic magmatites (lava flows, dykes and pyroclastics) appear (Fig. 1). The wide-spread

tufites ("pietra verde") (Szabó and Ravasz 1970, Ravasz 1973) indicate close relationship (Cros and Szabó 1984) to those of Northern Calcareous Alps (Bechstadt et al. 1978) and those of Southern Alps (Cros 1980, Bauer 1978). Kubovics (1983), Horváth and Tari (1987) pointed out that the source rock of a part of andesite- and rhyolite pebbles in the Middle to Upper Eocene basal-conglomerate (Buda Mts) (Széky-Fux and Barabás 1953, Wein 1977) can be traced back to the Triassic magmatites penetrated by the boreholes of Budaőrs-1 (Nagy et al. 1967) and Budafok-1 as well as to the trachyte- and rhyolite pebbles which appeared near Inota (Raincsák 1980). Based on the age (236 Ma, Dunkl 1983) of the andesite from the Szárhegy-Szabadbattyán area (Kiss 1954) and the radiometric age (Bagdasarjan 1989, pers. comm.) of andesites revealed by the borehole Ságvár-2 these occurrences belong to the Middle Triassic magmatism.

Most of the mentioned magmatites are andesites with porphyritic texture, large amount of plagioclase and dominantly altered pyroxene phenocrysts. Rhyolites and ignimbrites are common rock types among the pebbles. Some biotite flakes and weathered plagioclase phenocrysts have been observed in the silica-rich groundmass. In addition trachyte, latite and siliceous tufite appear in this area (Kubovics 1983, Horváth and Tari 1987).

Basic-intermediate-acidic lava flows and pyroclastics of Middle Triassic age have been reported in the Southern Alps (Leonardi 1967, Bechstadt et al. 1978, Calanchi et al. 1978, Castellarin et al. 1980, Pisa et al. 1980, Castellarin and Rossi 1981), dike-rocks and various intrusive bodies also occur (Del Monte et al. 1967, Lucchini et al. 1969). Based on the geodynamic tectonic model (Fig. 10) proposed by Kázmér and Kovács (1985), Horváth and Tari (1987) established a possible genetic relation between the Middle Triassic magmatites found in Transdanubia and in the Southern Alps. Based on our petrographical investigations and recent major-, trace- and rare-earth element studies we suggest that there is a spatial and temporal relationship between the Transdanubian Middle Triassic calc-alkaline andesite-rhyolite series and the magmatic

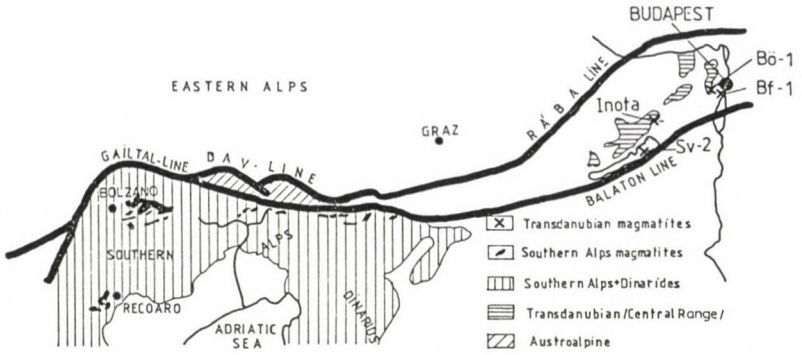

Fig. 10. Distribution of Middle Triassic magmatites in Southern Alps and Transdanubian (after Horváth and Tari 1987, modified)

assemblage found in the Dolomites Mts (Castellarin et al. 1980, Pisa et al. 1980, Castellarin and Rossi 1981). On the basis of geochemical characters these magmatites may have been formed at a convergent plate margin.

LATE CRETACEOUS ALKALINE MAFIC-ULTRAMAFIC DIKE-ROCKS

A new association of igneous rocks was found in NE Transdanubia some years ago which usually formed dykes or dyke swarms with the thickness range 5 cm to several m in N-S and NW-SE direction. Some more than 100 m long dikes can be traced below the Quaternary debris (Dudkó 1984, Kubovics et al. 1989a). Some occurrences (borehole AD-2, Remetehegy) contain a large amount of xenoliths derived from different depth (Szabó 1984, Kubovics et al. 1985, Szabó 1985, Kubovics et al. 1989a). The petrography, petrology and geochemistry of these formations, discovered in several boreholes and in two outcrops (Fig. 11) was reviewed by Kubovics (1984), Szabó (1984), Kubovics (1985), Szabó (1985), Kubovics and Szabó (1988), Kubovics et al. (1989a) as well as Horváth et al. (1983), Dudkó (1984), Horváth and Ódor (1984). Our study pointed out that the alkaline magmatites described by Wéber (1962) and the Buda basalt (Embey-Isztin et al. 1989) belong to this association. The K/Ar (Balogh Kadosa,

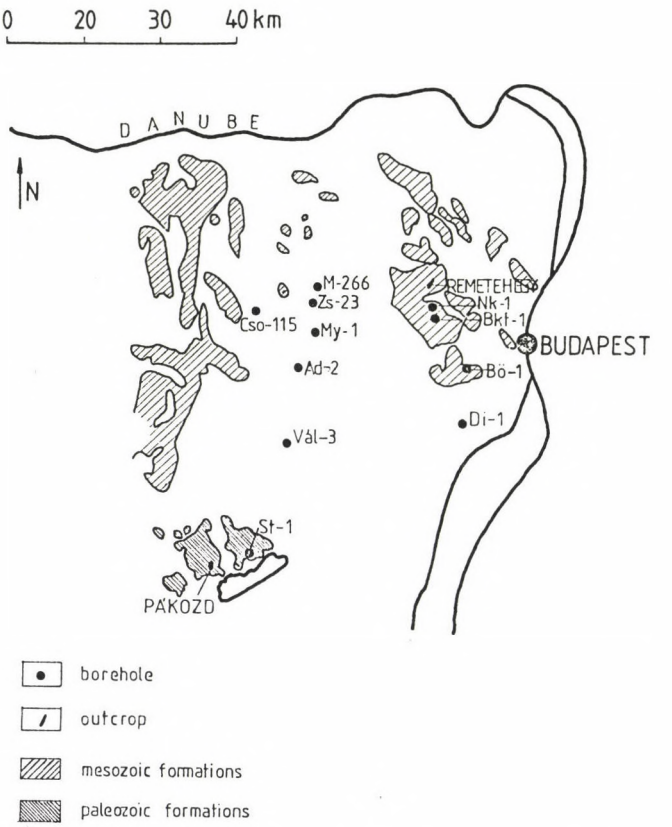

Fig. 11. Localities of the Late Cretaceous mafic-ultramafic dyke-rocks

Insitute of Nuclear Research, Debrecen, Hungary) and fission track (Dunkl 1989) measurements indicate Late Cretaceous age.

The texture of the dike-rocks is porphyritic-panidiomorphic with olivine and rarely clinopyroxene phenocrysts, but so-called felsic globular structure occur as well. The mesostases is made up of clinopyroxenes, micas, rarely feldspathoids and very minor patches of glass. Based on the modal analyses the dike--rocks are divided into two groups: i) the carbonate-poor variant contains mostly clinopyroxene, mica, olivine or its pseudomorphs and a small amount of carbonates, feldspar, feldspathoids and glass, whereas, ii) the carbonate-rich rock-type is characterized by a large amount of carbonates and the lack

of feldspar, feldspathoids and glass. Similar texture and mineral assemblage is typical of alkaline lamprophyres, especially of monchiquite (Rock 1977, 1987, Streckeisen 1979).

The major element chemical composition of the carbonate-rich rocks (Horváth et al. 1983, Kubovics and Szabó 1988) show carbonatitic character (extremely high volatile content, up to 20-30 %), while the other rock-type (Kubovics 1983, Horváth and Ódor 1984, Dobosi and Horváth 1988, Kubovics and Szabó 1988, Kubovics et al. 1989a, Embey-Isztin et al. 1989) displays ultramafic and alkaline lamprophyre properties, although the Hungarian samples contain more volatiles and less Ti and Fe.

The above mentioned differences disappear in Fig. 12, where Hungarian samples fall between the average alkaline and ultramafic lamprophyre-point (Rock 1987), most of them are in the alnöitic field and few of them display kimberlitic character. The mg-values ($100 * Mg/+Fe^{2+}+Fe^{3+}$) of dike-rocks are generally high (53 to 79) being characteristic for the undifferentiated, primitive melts.

The Hungarian lamprophyres are enriched in highly and

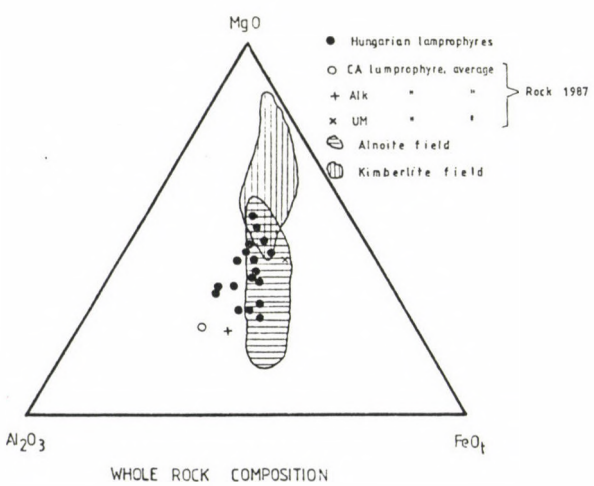

Fig. 12. Al_2O_3-MgO-FeO_t triangular diagram with the alnoite and kimberlite field for Hungarian lamprophyres

moderately incompatible trace elements (Fig. 13) compared to typical within continental plate magmatites (Bergman 1987, Wilson 1989).

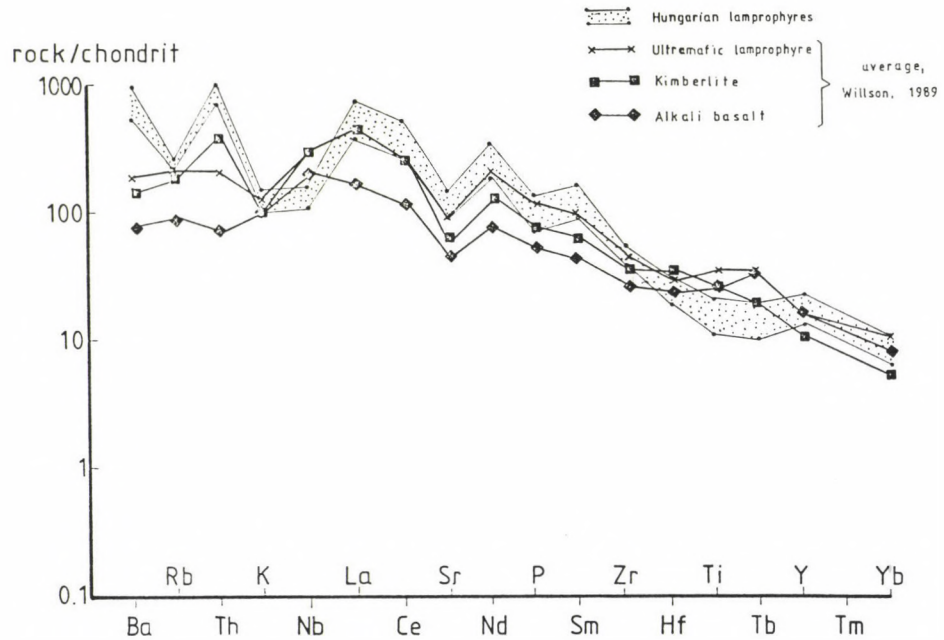

Fig. 13. Trace element distribution for Hungarian lamprophyres (the data are normalized according to Thompson et al. 1984)

The trace- and rare-earth element pattern of the Hungarian lamprophyres indicate partly kimberlitic and partly ultramafic affinity (Kubovics and Szabó 1988, Kubovics et al. 1989a) due to the high volatile content of the magma produced by minor partial melting of the metasomatized upper mantle (Kubovics et al. 1989b).

The Late Cretaceous lamprophyre-picrite-carbonatite assemblage can be intruded into an extensional zone perpendicular to the tectonic front of the Alpine collision (Kázmér and Szabó 1989a, 1989b).

THE MECSEK VOLCANIC ZONE

Volcanic rocks of the Mecsek-Alföld area (Tisza unit; Fig. 1) appear with the greatest volume and the most variable rock--types in the eastern part of the Mecsek Mts (Bilik 1983, Harangi 1988). Numerous boreholes in the Great Hungarian Plain have exposed basaltic rocks along the Kiskőrös-Ebes SW-NE line in a depth varying between 1100 and 3100 m (Szepesházy 1977, Molnár 1985a). Dike-like subvolcanic magmatites occur in the Western Mecsek Mts (Lantai 1987) and three boreholes penetrated basic-intermediate rocks to the north of the Mecsek Mts at Kurd and Döbrököz.

Volcanism already began in the Upper Jurassic (Főzy et al. 1985, Velledits et al. 1986), it only culminated, however, in Valangian (Bilik 1974, 1983).

The Western Mecsek magmatites include basalts (pseudomorphs after olivine, amphibole (Ca-rich kearsutite), clinopyroxene (salite), plagioclase (An50-60), Fe-Ti opaques) and trachytes (plagioclase, potash feldspar, analcime, amphibole, pyroxene, opaques), with a great part of them suffered alkali metasomatism (Lantai 1987). REE distribution patterns indicate light REE-enriched fractionated rock types.

In the Eastern Mecsek Mts bimodal volcanism took place producing a basalt-tephrite-phonolite sequence (Harangi 1989b), but potash-rich trachytes occur as well (Fig. 14). Occurrences of pillow lavas, lava breccias and hyaloclastites indicate submarine volcanism (Bilik 1983), whereas the majority of more evolved rock types appear as dikes or subvolcanic bodies. Bilik (1974, 1983) classified the basaltic rocks as alkali basalts, the geochemistry of these rocks, however, indicate greater diversity and transitional-slightly alkaline nature (Harangi 1988, 1989b). The pyroxene-rich olivine-bearing basalt with M-values of 65-70 can be regarded as the most primitive member of this volcanic suite. Among the slightly q-normative basalts several subgroups can be distinguished: ferrobasalt, plagioclase-basalt and basalt. Plagioclase (An_{50-60}), clinopyroxene, magnetite and ilmenite are the main components. The aphyric

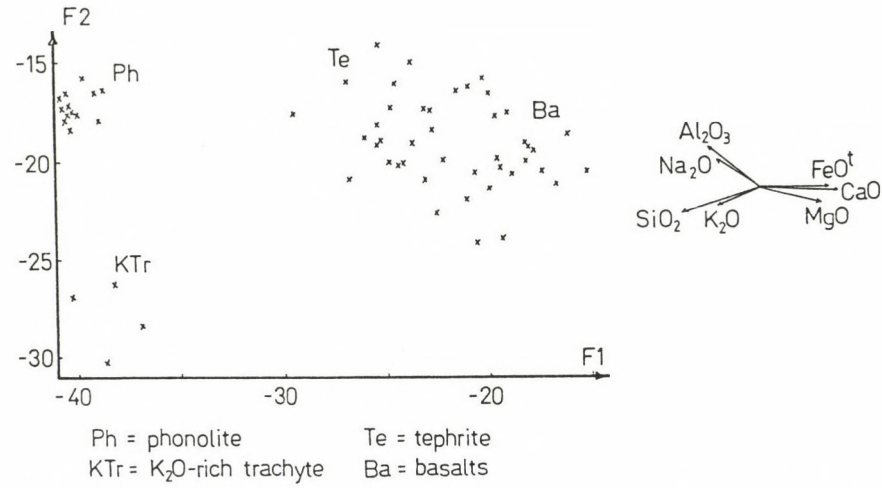

Fig. 14. Major element chemical evolution of the Late Cretaceous volcanic assemblage (Eastern Mecsek) in the principal component variation diagram

tephrite appears mainly as dikes and contains plagioclase, clinopyroxene, alkali amphibole apatite magnetite and analcime. The most differentiated endmember of this volcanic suite is the phonolite which forms two subvolcanic bodies (Viczián 1971). Its petrochemical features resemble the Kenya rift phonolites (Harangi 1989b). Formation of potash-rich trachyte is debated: Bilik (1983) suggested fractional crystallization origin, whereas Harangi (1989b) regarded its specific major element characters as a result of subsequent alteration.

Clinopyroxenes are common minerals in the Mecsek volcanics. Variation of pyroxene chemistry from diopside through hedenbergite to aegirine indicates low-pressure alkaline fractional crystallization (Fig. 15) (Dobosi 1987), which was corroborated by the major element chemical evolution of this volcanic assemblage (Fig. 14).

Linear correlation between the highly-incompatible elements supports the basalt-tephrite-phonolite differentiation model (Harangi 1989b). The REE and trace element distribution in basalts indicate transitional-slightly alkaline nature.

The Early Cretaceous volcanics revealed by boreholes in

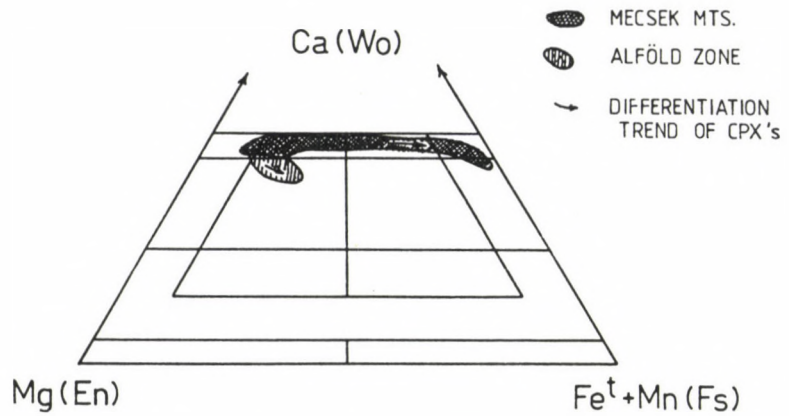

Fig. 15. Pyroxene fractionation trands in the Mecsek- (Dobosi 1987) and in the Alföld volcanites (Molnár 1990) in the En-Wo-Fs triangular diagram

the Kiskőrös-Ebes zone (Great Hungarian Plain Fig. 1) were originally feldspar-rich basalts (Szepesházy 1977, Molnár 1985a) which suffered different alteration processes. The original petrographical characters were highly concealed by spilitization, Mg-metasomatism and carbonatization (Molnár 1990). Only a few fresh clinopyroxene relicts were found in these rocks (Molnár 1990) that have augitic composition and show slightly alkaline affinities (Fig. 15). The REE distribution patterns of the Alföld volcanics indicate less-differentiated tholeiitic to slightly alkaline basalts.

The magmatic rock types, the mineralogical and petrochemical characters of the Mecsek-Alföld volcanics all suggested continental rift-type volcanism (Embey-Isztin 1981, Bilik 1983, Lantai 1987, Harangi 1988) which is corroborated by the Ta-Hf/3-Th discrimination diagram (Fig. 16). The continental rifting was initiated by the opening of the Penninic ocean. This opening resulted in several extensional basins underlain partly by oceanic- (Valais, Severin), partly by continental crust (Moravian-Silesian Beskidy, Mecsek zone, Black flysch, Ceahlau, Nis-Trojan) (Kázmér and Kovács 1989).

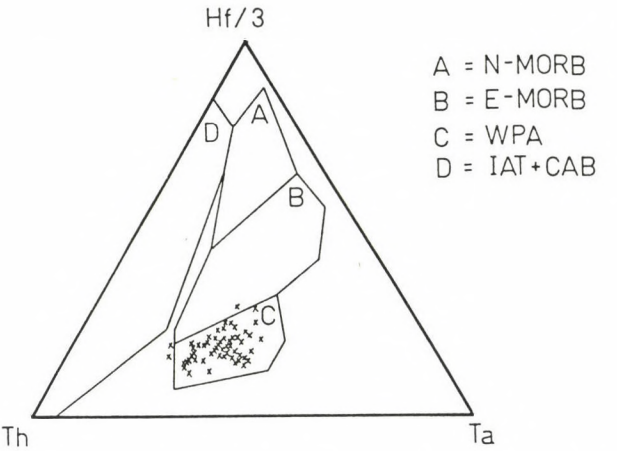

Fig. 16. Th-Hf/3-Ta discrimination diagram (Wood et al. 1979) for the volcanic associations of the Mecsek-Alföld zone

CONCLUSION

The formation of magmatic series, found in several tectonic units in Hungary, is in close relationship with the evolution of the northeastern branch of Tethys. The Meliata magmatites represent the axial zone of the Triassic-Jurassic Vardar-Ocean, whereas the Szarvaskő incomplete ophiolite sequence was formed in a marginal basin of this ocean. The remnants of the island-arc between them can be traced in the Telekes-oldal (Rudabánya Mts, rhyolites). The Middle Triassic intermediate-acidic magmatites in Transdanubia and Eastern Bükk can be related to convergent plate magmatism occurred in both the Southern Alps and Outer Dinarides. Ophiolites of the Rechnitz Series represent the remnant of the Jurassic-Early Cretaceous Penninic oceanic crust. The predominantly Early Cretaceous Mecsek-Alföld volcanic-subvolcanic sequences are the products of a continental rifting initiated by the opening of the Penninic ocean. The Late Cretaceous lamprophyre-picrite--carbonatite association intruded into the extensional zone perpendicular to the tectonic front of Alpine collision.

REFERENCES

Árkai P 1973: Acta Geol. Hung., 17, 67-83.

Balla Z 1984: Acta Geol. Hung., 27, 341-357.

Balla Z, Dobretsov N L 1984: Ofioliti, 9, 107-122.

Balla Z, Pelikán P 1983: Ophiolites and related rocks of the Bükk Mountain. Manuscript, Guide to Excursion of Hung.--Slov. Geol. Coop., Budapest

Balla Z, Baksa Cs, Földessy J, Szabó I 1980: Geol. Zborn. Geol. Carpath., 31, 485-493.

Balla Z, Hovorka D, Kuzmin M, Vinogradov V 1983: Ofioliti, 8, 5-46.

Balogh K 1964: Ann. Hung. Geol. Inst., 48, 555-705.

Balogh K, Kozur H, Pelikán P 1984: Geol. Paleont. Mitt., 13, 89-96.

Bauer F K 1978: Bericht 1977 über Aufnahmen in der Mitteltrias des Südkarawanken auf Blatt 211, Windisch Bleiberg. Verh. Geol. B.A., 52-153.

Bébien J 1980: J. Volc.Geoth. Res., 8, 337-342.

Bechstadt T, Brandner R, Mostler H 1978: Geol. Rundschau, 65, 616-648.

Bergman S C 1987: In: Alkaline igneous rocks (Fitton J G, Upton B G J eds). Geol. Soc. Spec. Publ., Oxford-London--Edinburgh-Boston-Palo Alto-Melbourne, 103-190.

Bilik I 1974: Acta Geol. Hung., 18, 315-325.

Bilik I 1983: Lower Cretaceous submarine (rift) volcanism in South Transdanubia (South Hungary). Proc. 17th Assembly of the ESC, 569-576.

Castellarin A, Rossi P M L 1981: Eclogae Geol. Helv., 74, 313-316.

Castellarin A, Lucchini F, Rossi P L, Simboli G, Bosellini A, Sommavilla E 1980: Riv. Ital. Paleont., 85, 1111-1124.

Cros P 1980: Riv. Ital. Paleont., 85, 953-982.

Cros P, Houel P 1983: Geol. Paleont. Mitt., 11, 415-452.

Cros P, Szabó I 1984: Acta Geol. Hung., 27, 265-276.

Csontos L 1988: Étude géologique d'une portion des Carpathes internes: le massif du Bükk (NE de la Hongrie) (Stratigraphie, structures, métamorphisme et géodynamique). Manuscript, PhD Thesis, Lille

Del Monte M, Paganelli L, Simboli G 1967: Miner. Petrogr. Acta, 13, 75-118.

Dobosi G 1987: N. Jb. Miner. Abh., 156, 281-301.

Dobosi G, Horváth I 1988: N. Jb. Miner. Abh., 158, 241-256.

Dudko A 1984: Magnetic research on igneous rocks near Nagykovácsi (in Hungarian). MÁFI évi jel. 1982-ről, 263-269.

Dunkl I 1983: Skarn-bearing and argillitized magmatic rocks in two boreholes at Szárhegy and Polgárdi, Hungary (in Hungarian). Manuscript, B.Sc. Thesis, Budapest

Dunkl I 1989: Application of fission track method for solution of geochronological problems (in Hungarian). Manuscript, Doct. Thesis, Budapest

Embey-Isztin A 1981: Acta Geol. Hung., 24, 351-368.

Embey-Isztin A, Dobosi G, Noske-Fazekas G, Árva-Sós E 1989: Min. Petr., 40, 183-196.

Erich A 1953: Die Grauwackenzone von Bernstein. Manuscript. Doct. Thesis, Wien

Evren I 1972: Tschermaks Min. Petr. Mitt., 17, 101-122.

Földessy J 1975: In: Proc. 10th Congr. CBGA Sect. VI GUDS Bratislava, 55-64.

Főzy I, Lantai Cs, Schlemmer K 1985: Annls. Univ. Sci. Budapest. Sect. Geol., 25, 97-115.

Grill J, Kozur H 1986: Geol. Paleont. Mitt., 13, 239-275.

Grill J, Kovács S, Less Gy, Réti Zs, Róth L, Szentpétery I 1984: Földt. Kut., 27, 49-56.

Harangi Sz 1988: Annls. hist.-nat. Mus. natn. hung., 80, 11-24.

Harangi Sz 1989a: Multivariate mathematical methods in the study of a single volcanic suite. Fragmenta Paleont. Miner. (in press)

Harangi Sz 1989b: Geochemistry of Early Cretaceous volcanic rocks of Mecsek Mts, Southern Hungary. (Application of multivariate mathematical methods in the petrochemical studies). Manuscript, Doct. Thesis, Budapest

Horváth I, Ódor L 1984: Min. Slov., 16, 115-119.

Horváth E, Tari G 1987: Ann. Univ. Sci. Geol. ELTE Budapest, 27, 3-16.

Horváth I, Darida-Tichy M, Ódor L 1983: Magnesitiferous dolomitic carbonatite (beforsite) dyke rock from Velence Mountains (in Hungarian). MÁFI évi jel. 1981-ről, 369-389.

Hovorka D 1985: Ultramafic rocks of the Western Carpathians, Czechoslovakia. Geol. Ustav. Dion. Stura Bratislava

Hovorka D, Spisiak J 1988: Vulkanizmus mezozoika Zapadnych Karpat. VEDA Bratislava

Juhász A, Vass G 1974: Acta Geol. Hung., 18, 349-358.

Kázmér M, Kovács S 1985: Acta Geol. Hung., 28, 71-84.

Kázmér M, Kovács S 1989: In: Tectonic evolution of the Tethyan Region (Sengör A M C ed.). Kluwer Acad. Publ., Amsterdam, 77-92.

Kázmér M, Szabó Cs 1989a: Late Cretaceous lamprophyre dykes in

the hinterland of the Alpine deformation front. EUG-V, Strasbourg, Terra abstract, 177.

Kázmér M, Szabó Cs 1989b: Apulian plate margin geometry: Contrains neptunian and plutonic dykes. 28th IGC abstract, 2, Washington, 167.

Kiss J 1954: Földt. Közl., 84, 183-188.

Kiss J 1958: Földt. Közl., 88, 27-41.

Koller F 1985: Jb. Geol. Bundesanst., 128, 83-150.

Koller F and Pahr A 1980: Ofioliti, 5, 65-72.

Koller F and Wiesender H 1981: Fortschr. Min., 59, 167-178.

Kotsis T 1986: Acta Min. Petr., 27, 5-9.

Kovács S 1982: Geol. Rundschau, 71, 617-640.

Kovács S 1989: In: Tectonic evolution of the Tethyan Region (Sengör A M C ed.). Kluwer Acad. Publ., Amsterdam, 93-108.

Kozur H 1989: Evolution of Meliata-Hallstatt rift and its significance for early evolution of Alps and Western Carpathians. 28th IGC Abstract 2, 200.

Kozur H, Mock R 1973: Geol. Zbor. Geol. Carpath., 24, 365-374.

Kubovics I 1983: Földt. Közlöny, 113, 207-224.
Kubovics I 1984: Acta Geol. Hung., 27, 163-189.

Kubovics I 1985: Acta Geol. Hung., 28, 141-164.

Kubovics I, Bilik I 1984: Acta Geol. Hung., 27, 321-339.

Kubovics I, Szabó Cs 1988: Mineralogical, petrological and geochemical investigation on alkali mafic and ultramafic dykes from AD-2 borehole (in Hungarian). MÁFI évkönyv, 65, 335-356.

Kubovics I, Szabó Cs 1989: Acta Geol. Hung., 32, 169-181.

Kubovics I, Gál-Sólymos K, Szabó Cs 1985: Geol. Carpathica, 36, 433-450.

Kubovics I, Szabó Cs, Sólymos K 1989a: N. Jb. Miner. Abh. (in press)

Kubovics I, Szabó Cs, Gál-Sólymos K 1989b: Acta Geol. Hung., 32, 149-168.

Lantai Cs 1987: Acta Geol. Hung., 30, 339-356.

Lelkes-Felvári Gy 1982: N. Jb. Geol. Paleont. Mh., 5, 297-305.

Le Maitre R W 1968: J. Petrol., 9, 220/252.

Lengyel E 1957: Ann. Hung. Geol. Inst., 46, 251-368.

Leonardi P 1967: Le Dolomiti Vol. 1, 2, Arti Grafiche Manfrini, Rovereto

Lucchini F, Mezzetti R, Simboli G 1969: Miner. Petrogr. Acta, 15, 109-145.

Mauritz B 1913: Jahr. kgl. ung. Reichan., 21, 171-213.

Molnár S 1985a: Acta Miner. Petrogr. Szeged, 27, 33-38.

Molnár S 1985b: Investigation of the Lower Cretaceous magmatism in the Great Hungarian Plain (in Hungarian). Manuscript, MÁFI, Budapest

Molnár S 1990: Acta Geol. Hung. (in press)

Nagy E, Nagy G, Széky F 1967: The Budaőrs-1 borehole (in Hungarian). MÁFI évi jel. 1965-ről, 289-303.

Pahr A 1960: Ein Beitrag zur Geologie des nordöstlichen Sporns der Zentralalpen. Verh. Geol. Bundesanst. Wien, Jg. 1960, 274-282.

Pahr A 1977: Ein neuer Beitrag zur Geologie des Nordostsporns der Zentralalpen. Verh. Geol. Bundesanst. Wien, Jg. 1977, 23-33.

Pamic J 1982: Tijaski magmatizam Dinarida. Nafta, Zagreb

Pantó G 1961: Ann. Hung. Geol. Inst., 49, 979-995.

Pantó G, Földváry-Vogl M 1950: Na-gabbro in the Bódva valley (in Hungarian). MÁFI évkönyv, 39, 3-11.

Pisa G, Castellarin A, Lucchini F, Rossi P L, Simboli G, Bosellini A, Sommavilla E 1980: Riv. Ital. Paleont., 85, 1093-1110.

Raincsák Gy 1980: Geological makeup and structure of a Triassic range between Várpalota and Iszkaszentgyörgy (in Hungarian). MÁFI évi jel. 1978-ról, 187-196.

Ravasz Cs 1973: Acta Miner. Petrogr. Szeged, 21, 123-139.

Réti Zs 1985: Ofioliti, 10, 411-422.

Réti Zs 1987: Ofioliti, 12, 43-52.

Rock N M S 1977: Earth Sci. Rev., 13, 123-169.

Rock N M S 1987: In: Alkaline igneous rocks (Fitton J G, Upton B G J eds). Geol. Soc. Spec. Publ., Oxford-London--Edinburgh-Boston-Palo Alto-Melbourne, 191-226.

Saunders A D, Tarney J, Marsh N G, Wood D A 1980: In: Ophiolites (Panayiotou A ed.). Proc. Int. Ophiolite Symp. Cyprus, 193-204.

Schmidt W 1950: Z. Deutsch. Geol. Ges., 102, 311-316.

Streckeisen A 1979: Geology, 7, 331-335.

Szabó Cs 1984: Mineralogy, petrology and geochemistry of nodules in lamprophyre dykes of Alcsutdoboz-2 (AD-2) borehole (Bakonyicum, Hungary): Their origin and genetic implications. Doct. Thesis, Budapest

Szabó Cs 1985: Acta Miner. Petrogr., 27, 39-50.

Szabó I, Ravasz Cs 1970: Ann. Mus. Nat. Hung. min. geol. pal., 62, 31-51.

Széky-Fux V, Barabás A 1953: Földt. Közl. 83, 217-229.

Szentpétery Zs 1923: Acta Litt. Sci. Univ. Szeged, 1, 113-124.

Szentpétery Zs 1953: Diabase and gabbro bodies in Southern

Bükk (in Hungarian). MÁFI Évkönyv, 41, 3-102.

Szepesházy K 1977: Földt. Közl., 107, 384-397.

Thompson R N, Morrison M A, Hendry G L, Parry S J 1984: An assessment of the relative roles of a crust and mantle in magma genesis: an elemental approach. Phil. Trans. R. Soc. Lond. A310, 549-590.

Varga Gy, Csillag-Teplánszky E, Félegyházi Zs 1975: Geology of the Mátra Mountains (in Hungarian). MÁFI Évkönyv, 57, 9-300.

Velledits F, Híves T, Bársony E 1986: Annls. Univ. Sci. Budapest. Sect. Geol., 26, 159-175.

Viczián I 1971: Petrographical study on the Mecsek phonolite (in Hungarian). MÁFI évi jel. 1969-ről, 327-345.

Wéber B 1962: Földt. Közl., 92, 455-457.

Wein Gy 1977: The tectonics of the Buda Mountains (in Hungarian). MÁFI special edition, Budapest

Wilson M 1989: Igneous petrogenesis. London, Hyman

Wood D A 1980: Earth Planet. Sci. Lett., 50, 11-30.

Wood D A, Joron J-L, Treuil M 1979: Earth Planet. Sci. Lett., 45, 326-336.

Acta Geod. Geoph. Mont. Hung., Vol. 25 (3-4), pp. 373-385 (1990)

FROM TETHYS TO PARATETHYS, A WAY OF SURVIVAL

A Nagymarosy

Eötvös University, Department of General and Historical Geology,
H-1088 Budapest, Múzeum krt. 4/A, Hungary

The closing of the Tethys ocean resulted in the formation of two large basin systems in Europe: the Mediterranean and the Paratethys. The "Paratethys" may be a pure paleogeographical concept according to its recent position, i.e. a row of sedimentary basins in the Late Tertiary, North of the Alps, Dinarids, Hellenids and Pontids. Due to its specific endemism through the Oligocene and Miocene it can be regarded as a biogeographic concept, though in this sense a separated, individual Paratethys existed only in the periods of endemism (Kiscellian, Ottnangian and from the Sarmatian through the Pliocene). From a geodynamic point of view the Paratethys is a complex of flysch, foreland molasse and intramontan basins.

Keywords: endemism; Late Paleogene; Neogene; paleogeography; Paratethys

1. INTRODUCTION

The closing of the Tethys ocean along the Alpine collisional zone terminated around the Eocene/Oligocene boundary. At about the same time the formation of the flysch sediments has been finished along the northern front of the Alpine chain, but proceeded in the Carpathian trough. This fact permits the assumption that the subduction in the Carpathian region did not finish at the Eocene/Oligocene boundary, but went on possibly until the Lower Miocene (in the Eastern Carpathians).

The beginning of the collision between the European and African plates led to the uplift of the Alpine-Dinaric orogenic belt. The Alpine-Carpathian chain thrust over the margin of the European plate, and the Dinarids thrust onto the African/Apulian plate. This orogenic belt on the former place of the Tethys separated two large basin systems, the Mediterranean in the

South and the Paratethys in the North (Fig. 1).

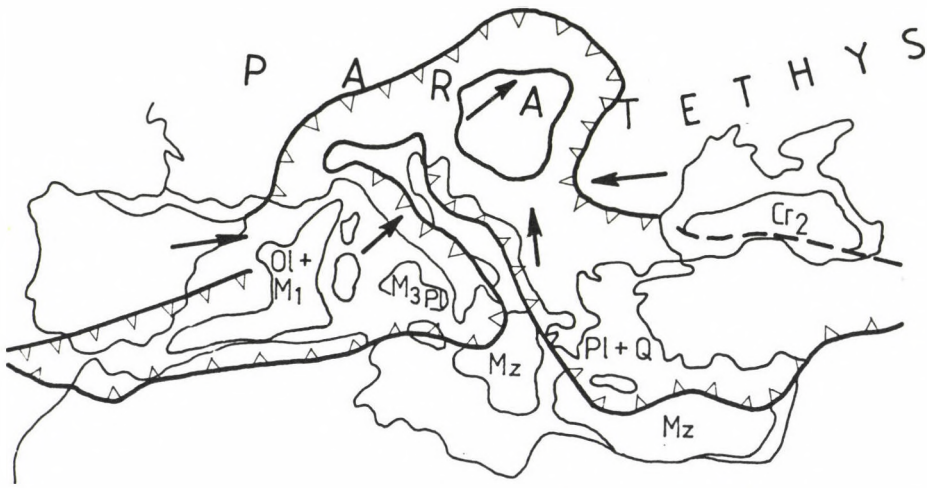

Fig. 1. Sketch of the Mediterranean basins (after Biju-Duval 1978, Sandulescu 1988 and Sartorio et al. 1988). Arrows show the directions of the plate movements

2. THE MEDITERRANEAN

The Mediterranean region is no "descendant" of the Tethys in a geodynamic sense. It consists of basins of different origin and if there is any remnant of the former Tethys oceanic crust, it can be in the Ionian and Levantine basins.

Biju-Duval et al. (1978) distinguished two types of the Mediterranean basins:

- Type a) is characterized by a thin lithosphere, shallow Moho, high heat flow and thin sedimentary sequence of Tertiary and Quaternary age. These basins are located between young orogenic belts as the Balearic-Ligurian basin, the Tyrrhenian

basin or the Aegean sea. Their age is rather young taking into consideration that the Balearic basin began its rapid subsidence in the Late Oligocene, the Tyrrhenian sea in the Late Miocene and the Aegean region as late as in the Pliocene.

- Type b) shows a different character with its thick lithosphere, deep Moho, low heat flow and thick sedimentary column. Their sedimentation history extends from the Late Mesozoic to the Quaternary. The Levantinian, Ionian basins and the Herodotos and Strabon trenches belong to this type.

The depositional environment in the Mediterranean region had a marine character through the whole Late Paleogene, Neogene and Quaternary. Permanent sea connections existed toward the Atlantic and the Indian oceans supplying normal salinity water for the Mediterranean basins all the time. Only a "momentary" (some 100,000 years long) event has broken the continuous marine sedimentation during the Messinian, when a short separation of the Mediterranean from the world sea system resulted in the formation of the huge latest Miocene evaporitic sequence.

3. THE PARATETHYS

North from the Alps-Dinarids-Pontids-Anticaucasus-Kopet Dag line a heterogenous basin system began to be formed from the Early Oligocene: the Paratethys. This term was introduced originally by Lashkarev (1924), who used the name Paratethys for the regions, where an endemic mollusc fauna lived during the Late Miocene and Pliocene, thus including a large area from the Vienna basin to the Caspian sea. Later, the term "Paratethys" has changed its original meaning and has got a wider sense both in time and space. Báldi (1989) distinguished two basic views:

1. Many of the specialists (most recently Cicha and Krystek 1987) use the term Paratethys for the molasse sedimentation which occurred from the Rhône valley through the Alpine and Carpathian molasse areas to the Russian platform and Central Asia. The existence of this kind of Paratethys would include a time interval from the Late Oligocene (stage Egerian)

until the Pliocene (stage Rumanian).

2. Báldi (1983, 1984a, b, 1986, 1989) pointed out that since the establishing of the term Paratethys was due to the Late Miocene and Pliocene endemism which occurred in the mentioned area, the dimension of the Paratethys can be defined better by the distribution of fossils than by similar sedimentation patterns. He suggested to extend the validity of the term also in time until the first large-scale endemism in the Tertiary (i.e. until the Early Oligocene). According to his concept the Paratethys is a bioprovince and "its sea covered very different crustal structures" (Báldi 1989).

This paper defines the Paratethys from two points of view:

3a. From a geodynamic point of view the Paratethys comprises the foredeep molasse areas of the Alps, Carpathians, Caucasus, etc., the basins between orogenic belts (as the Vienna, Pannonian, Transylvanian, etc. basins), the adjacent troughs of the flysch oceans and the epicontinental seas on the Russian platform. These geodynamically very different areas were covered by the same water mass which caused many similarities in the biogeography of these areas, uniform features in their sedimentation, and a similar history in their relation to the world sea system (considering periods of marine connections and periods of separation). All the characteristics above can be explained by supposing a continuous, connected water mass in the Paratethys. Its existence can be supported by many facts considering the planktonic organisms. Nannoplankton and planktonic foraminifera show strikingly similar distributional patterns in time from the Alps to the Caucasus. This could have led Rögl (1985) to the idea of setting up a special planktonic foraminifera zonation for the Central Paratethys. Also endemic nannoplankton (Transversopontis fibula GHETA, Reticulofenestra ornata MÜLLER see Nagymarosy and Voronina (1989) (and planktonic foraminifera) genus Velapertina Rögl (1985) evolved in the Paratethys region.

3b. From a strict biogeographical point of view the Paratethys can be considered as a unit independent from the world sea

system only during the time epochs of its endemism. In this sense the first Paratethys endemism developed in the Early Oligocene as Báldi proposed. After the Late Oligocene restoration of the marine connections the degree of the endemism decreased and only by the Late Ottnangian evolved a new endemic fauna in the Paratethys due to the more or less complete separation from the oceans. After a short "cosmopolitan" interval in the Middle Miocene the final separation of the Paratethys resulted in the evolution of the endemic Sarmatian, Pannonian, Pontian, etc. mollusc faunas.
This explanation gets a special emphasis if we have a look at the composition of the Oligocene mollusc faunas in Hungary (Table I after Báldi 1983).

Table I.

Mollusc faunas from	Mediterranean	boreal	Alpine--Carpathian--Caucasian	endemic (only in Hungary)	cosmopolitan
			percent		
Tard Clay (Early Kiscellian)	-	-	100	-	-
Kiscell Clay (Late Kiscellian)	29	18	24	16	13
Szécsény, Eger, Törökbálint Formations (Egerian)	22	20	11	26	19
Putnok Schlier (Eggenburgian)	40	6	20	2	32

Following this kind of philosophy, the Paratethys in a strict biogeographical sense existed only during the periods of endemism. In the intermediate intervals the Paratethys can be considered as a part of the world seas differing not very much from the other marine basins (Fig. 2).

The different biostratigraphical features of the

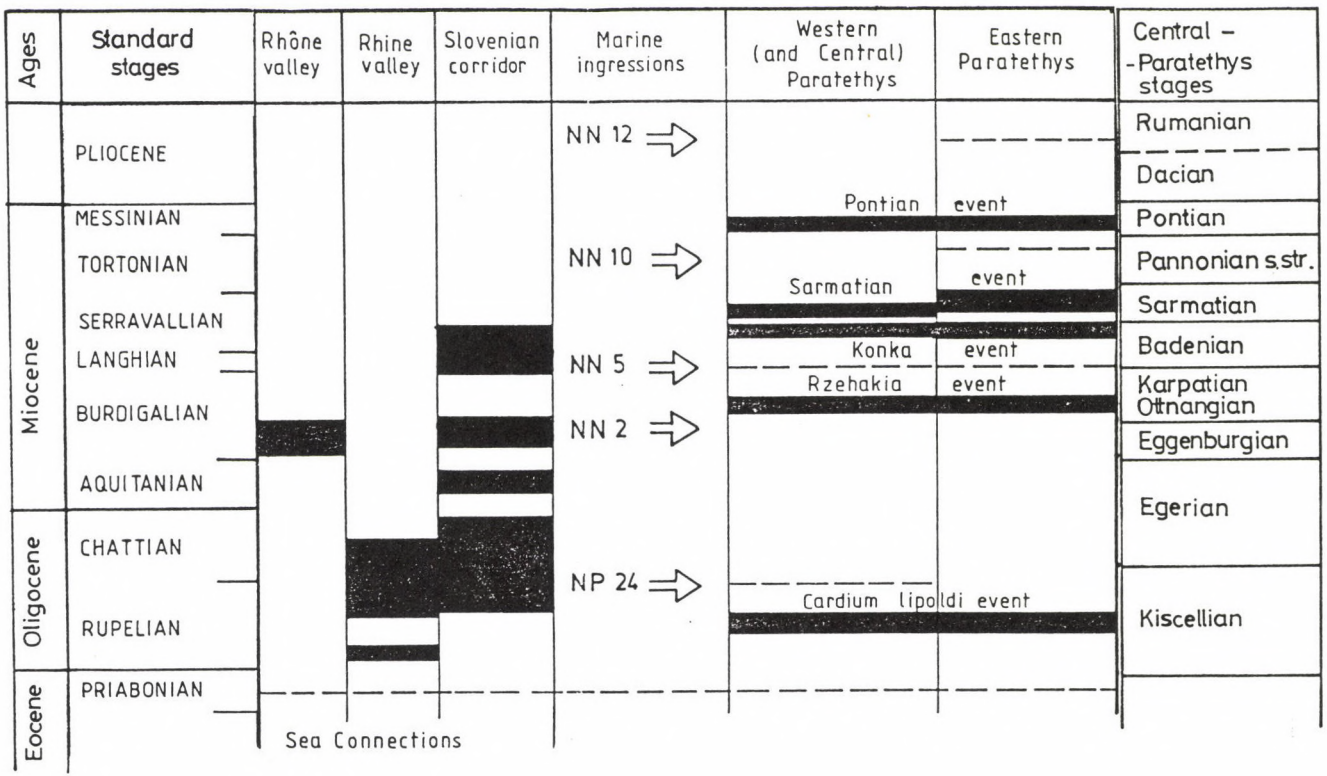

Fig. 2. Correlation between the active and inactive seaways and the events of endemism in the Paratethys

Paratethys, however, gave a ground for establishing a distinct chronostratigraphic scale with regional stages (see Steininger et al. 1988). Since a number of differences exist between the biostratigraphy of the eastern and western basins of the Paratethys, different stage systems are used for both. An imaginary line at the eastern edge of the Carpathians separates the Eastern and Western Paratethys.

4. THE PARATETHYS: RISE AND FALL

This chapter gives a very short review on the main features of the history of the Paratethys. More detailed descriptions have been published by Rögl and Steininger (1983), Báldi (1983, 1986), Nagymarosy (1981), Nagymarosy and Müller (1988). A mass of basic data has been collected in Steininger et al. (1985).

The prograding tectonism in the Alps caused the gradual wandering of the flysch belts from the inner to the outer zones during the Paleocene and Eocene. From the Helvetic and Ultrahelvetic units through the Carpathian flysch troughs a rather continuous sedimentary belt existed until the Eocene/Oligocene boundary with seaconnections toward the South (Alps Maritimes, Slovenia) and to the North (Turgay gate, "Polish connection"). From the Early Oligocene the uplift and folding of the Helvetic, Ultrahelvetic units and Dinarids cut the seaways to the South and also the northern sea connections came to an end. The load of the nappe pile initiated the formation of the Alpine foredeep which spread slowly northward during the Oligocene and Early Miocene. Due to these nappe movements and a strong global eustatic regression the first isolation of the Paratethys has been completed by the end of the NP 22 nannoplankton zone (Fig. 3). The first endemic mollusc fauna and also some endemic nannoplankton species developed in the Paratethys this time. The period of endemism was combined by an anoxic event extending from the Rhine graben to the Aral sea. The Late Oligocene (NP 24 nannoplankton zone) global eustatic transgression reached the Paratethys basins through the Rhine graben (supplying a number of boreal organisms) and through the Slovenian corridor

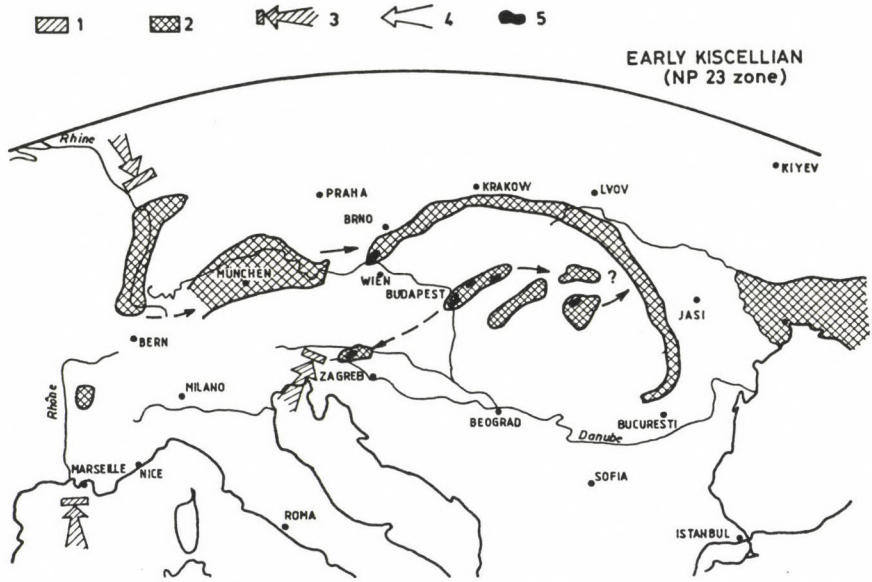

Fig. 3. Recent distribution of the anoxic sediments of the NP 23 nannoplankton zone (Early Oligocene) during the first isolation of the Paratethys. Key: 1 - non-anoxic marine sedimentation, 2 - anoxic marine and slightly brackish sedimentation, 3 - inactive seaway, 4 - active seaway, 5 - endemic mollusc fauna

whose Mediterranean influence can be traced among the Late Oligocene shallow water molluscs of Hungary (Fig. 4). By the end of the Oligocene the Rhine graben seaway has been closed and a non-marine sedimentation followed in the Alpine molasse areas.

The formation of the flysch in the Carpathians gradually came to an end from the West to the East. It terminated for example in the Magura unit (Polish part) in the Early Oligocene, while it proceeded until the Late Eggenburgian in the East Carpathians (Tarcău unit). The uplift of the Carpathian flysch belts also began during the Late Oligocene and shifted from the West to the East, from the inner zones to the outer zones.

The Carpathian structures formed the Carpathian foredeep, whose first basin began to subside in the Late Eggenburgian. The great Eggenburgian transgression (Fig. 5) reached the

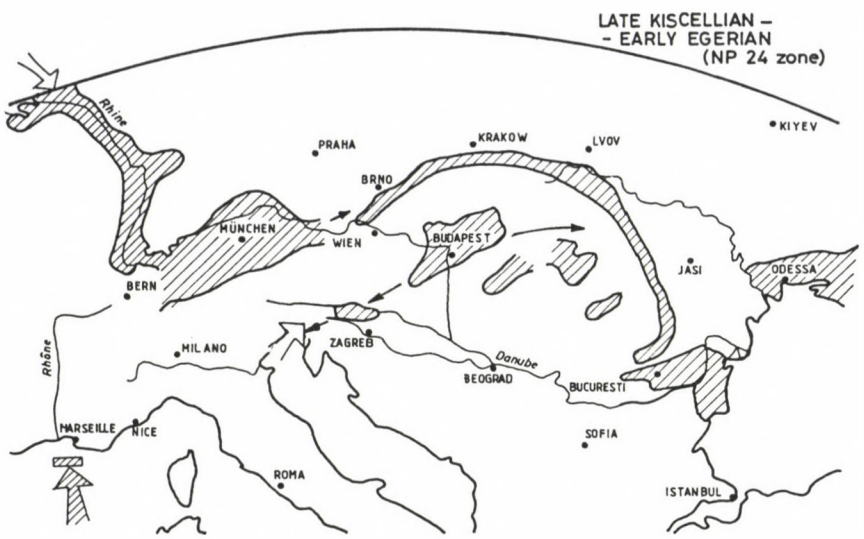

Fig. 4. Recent distribution of the marine sediments of the NP 24 nannoplankton zone (Late Oligocene) in the Paratethys (for key see Fig. 3)

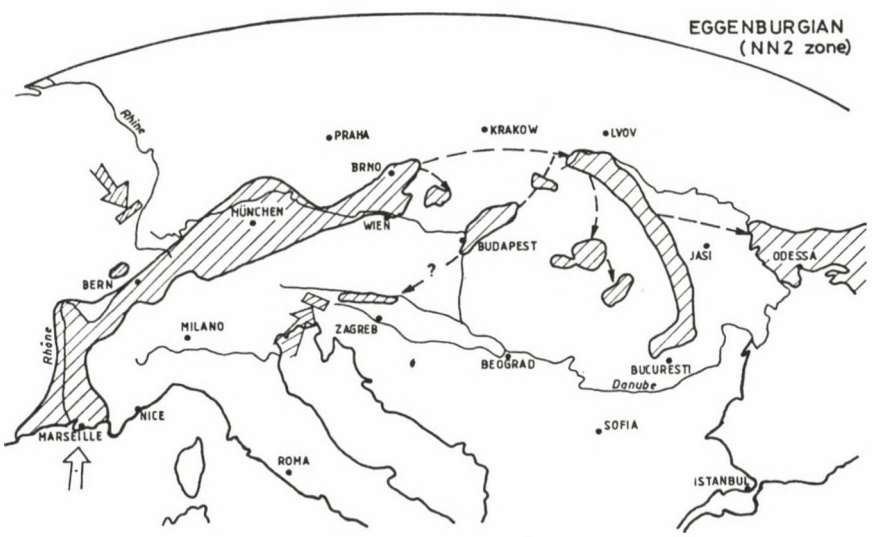

Fig. 5. Recent distribution of the marine sediments of the nannoplankton zone NN 3 (Early Miocene) in the Paratethys (for key see Fig. 3)

Paratethys from the Mediterranean through the Rhône valley and (probably) through the Slovenian corridor (Fig. 2). Thrusting and folding of the Northern Calcareous Alps, the Waschberg zone and the Zdanice unit closed the sea connections toward the Alpine molasse areas and also cut the Carpathian-Pannonian realm from the Rhône valley. The activity of the barriers caused a second, almost complete isolation of the Paratethys (Fig. 6) in the Late Ottnangian-Early Karpatian producing the endemic Rzehakia fauna.

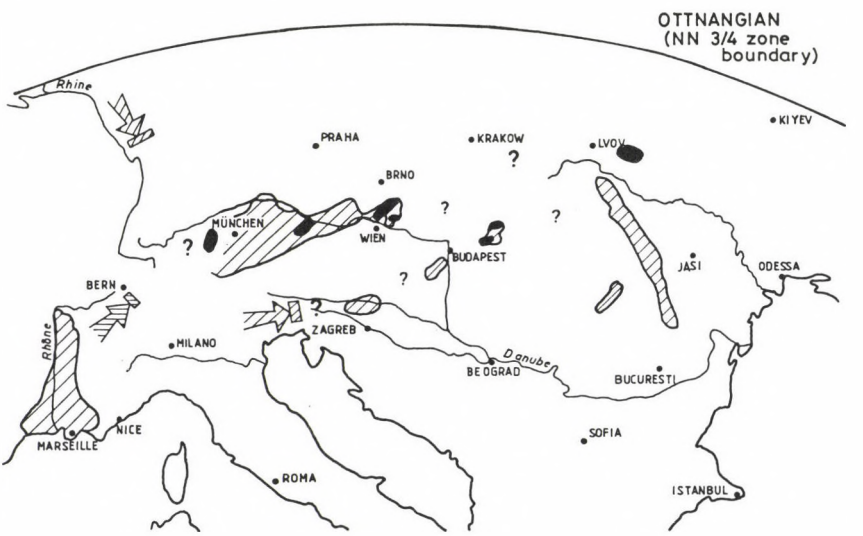

Fig. 6. Recent distribution of the marine sediments and the brackish Rzehakia beds around the NN 3/4 nannoplankton zone boundary (Early Miocene) before and during the seconds isolation of the Paratethys

The disappearing of the marine environment can be observed North of the Alps during the Miocene. The marine sedimentation ended in the Rhine graben during the Late Oligocene. For the Alpine molasse the Eggenburgian-Early Ottnangian transgression was the last marine "moment", however, the non-marine sedimentation persisted in this area.

East of the Alps the folding of the Carpathians was

accompanied by the formation of extensional basins, like the Vienna, Transylvanian, Pannonian, etc. basins. Their rapid subsidence began in the Karpatian and Badenian times.

Strong Mediterranean influence characterizes the fossil faunas and floras of the Paratethys during the Karpatian and Badenian. The activity of the Mediterranean seaway (presumably in Slovenia) decreased only in the Late Badenian. This is the time of the invasion of the endemic Konka fauna from the Eastern Paratethys, as it has been pointed out by Kókay (1985). The Eastern Paratethys namely, due to its paleogeographic situation was not very near to the ancient seaways and thus its faunas show more endemic features during the whole Oligocene and Miocene.

The movements of the Late Badenian orogenic phase already definitely isolated the Paratethys from the world seas and the endemic Sarmatian fauna developed (Fig. 7). The Late Miocene--Pliocene history of the Paratethys is characterized by the gradual decrease of the salinity and the slow wandering of the terrestric-freshwater environment toward the East. Highly endemic Pannonian and Pontian faunas render not only the extrabasinal but also the interbasinal correlation. Some paleogeographical and paleobiological interpretations may suggest that the Caspian and Aral seas are the only relicts of the former huge Paratethys.

REFERENCES

Báldi T 1983: Oligocene and Lower Miocene formations in Hungary (in Hungarian). Akadémiai Kiadó, Budapest

Báldi T 1984: Eclo. Geol. Helv., 77, 1-27.

Báldi T 1986: Mid-Tertiary stratigraphy and paleogeographic evolution of Hungary. Akadémiai Kiadó, Budapest

Báldi T 1989: Geologicky zbornik 40, No. 1, 85-100.

Báldi T, Horváth M, Nagymarosy A, Varga P 1984: Acta Geol. Hung., 27, 41-65.

Biju-Duval B, Letouzey J, Montadert L 1978: In: Initial Reports of the Deep Sea Drilling Project (Hsü K and Montadert L eds). Washington, 42, part 1, 951-984.

Cicha I and Krystek I 1987: Comments on the early history of

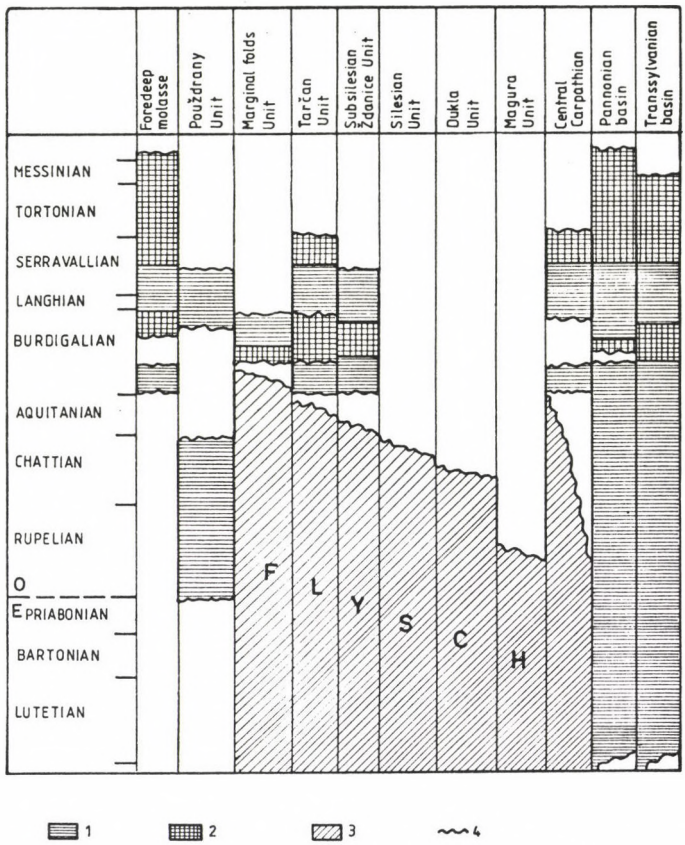

Fig. 7. Distribution of the sedimentation types in the Carpathian-Pannonian region from the Middle Eocene to the Late Miocene. Key: 1 - marine molasse sedimentation, 2 - non-marine molasse sedimentation, 3 - flysch sedimentation, 4 - unconformity

the Paratethys. Proc. 8th Congr. RCMNS, Ann. Inst. Geol. Hung., Budapest, 70, 323-328.

Kókay J 1985: Geol. Hung. Ser. Paleont., 48, 3-95.

Lashkarev V N 1924: Sur les equivalents du Sarmatien superieur an Serbie. Zbornik Cvijic, 1-5, Beograd

Nagymarosy A 1981: Earth Evol. Sci., 1, 183-194.

Nagymarosy A and Müller P 1988: Some Aspects of Neogene Biostratigraphy in the Pannonian Basin (Royden and Horváth eds), 69-78.

Nagymarosy A and Voronina A A 1989: Nannoplankton from the Solenovian Horizon (Lower Oligocene, South Soviet Union). Memorie di Scienze Geologiche, Padova (in press)

Rögl F 1985: In: Plankton stratigraphy (Bolli H M, Saunders J B, Perch-Nielsen K eds). Cambridge University Press, 315-328.

Rögl F and Steininger F 1983: Ann. Naturhis. Museums Wien, 85/A, 135-163.

Royden L H and Horváth F eds 1988: AAPG Memoir, 45, 394.

Sandulescu M 1988: Cenozoic Tectonic History of the Carpathians (Royden and Horváth eds), 17-26.

Sartorio D and Venturini S 1988: Agip S.p.A., 236.

Steininger F, Senes J, Kleemann K, Rögl F eds 1985: Neogene of the Mediterranean Tethys and Paratethys. Vol. 1-2, Inst. of Paleontology, Vienna

Steininger F, Müller C, Rögl F 1988: Correlation of Central Paratethys, Eastern Paratethys and Mediterranean Neogene Stages (Royden and Horváth eds), 79-88.

Acta Geod. Geoph. Mont. Hung., Vol. 25 (3-4), pp. 387-397 (1990)

KINEMATICS OF THE PRINCIPAL TECTONIC UNITS OF HUNGARY FROM PALEOMAGNETIC OBSERVATIONS

E Márton

Eötvös Loránd Geophysical Institute of Hungary, H-1440 Budapest, POB 35, Hungary

Distribution of paleomagnetic elements in time and between tectonic units is analyzed. As a result, periods of great mobility are recognized and significant differences between tectonic units pointed out.

In addition to referring the characteristic paleomagnetic elements of each unit to the present geographical system and to one another, a comparison is made occasionally with stable Europe, Africa and other units from the Central Mediterranean region.

Keywords: Hungary; mobility; paleomagnetism; tectonic units

INTRODUCTION

Paleomagnetic data of tectonic significance are known from all principal tectonic units of Hungary, except the Lower and Upper East Alpine, the Mid-Transdanubian and the Békés units (Fig. 1). Some of the observations, namely those made on the products of mid-late Miocene calc-alcaline volcanism and on younger rocks (both igneous and sedimentary) suggest that the tectonic regime responsible for the present arrangement of the tectonic units of Fig. 1 was over by that time. In contrast, great mobility is indicated by older data, representing the Transdanubian Central range, the Bükk, the Rudabánya-Aggtelek, the Gömör, the Pennin, the Mecsek and the Villány units (Fig. 1).

PALEOMAGNETIC ELEMENTS AS INDICATORS OF RELATIVE MOTION

A paleomagnetic vector characterizing a tectonic unit for a certain geological time interval may coincide with, or depart from, the direction expected for the sampling area in the

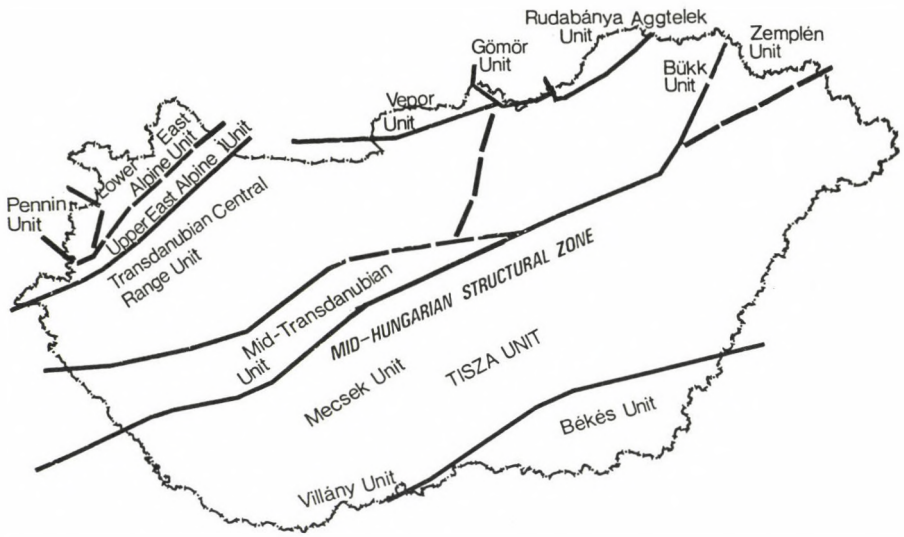

Fig. 1. Principal tectonic units of Hungary after Brezsnyánszky and Haas (1985)

actual geocentric dipole field. The departure is attributed to past motions, while coincidence in declination may be accidental. Similarly, relative movements between two or more tectonic units are recognized when coeval paleomagnetic directions of tectonic value are significantly different.

Of the paleomagnetic elements, inclination refers straightforwardly to the latitude at which the remanence was acquired. In contrast, a paleodeclination may be the result of complex tectonic rotations, taking place after the acquisition of remanence.

It follows that the two angular values of a single observed paleomagnetic vector are of different origins. This justifies the general practice which treats the paleomagnetic elements separately in tectonic interpretation.

Nevertheless, the crucial importance of paleoinclinations should be remembered when paleodeclinations are interpreted in terms of tectonic rotation. One is that even large declination deviations may be insignificant when inclinations are steep. The second is that tight grouping of coeval inclinations within

a tectonic unit for localities not far from one another is perhaps the most important criterion of high-quality paleomagnetic results. Therefore, it is their scatter that sets the real limit to the resolution power of paleomagnetic data when the significance of declination differences within a unit is considered.

PALEOMAGNETIC EVIDENCES OF RELATIVE MOVEMENTS FOR THE PRINCIPAL TECTONIC UNITS

In this section the time-dependence of paleomagnetic elements will be discussed, periods of great mobility identified, and patterns characteristic of each unit compared.

Regional consistency within a unit will be illustrated occasionally. These illustrations are intended to demonstrate the variability in tightness of grouping and in the character of scatter from unit to unit and depending on time within a unit.

Concerning the relationship of the principal tectonic units of Hungary to others in the Central Mediterranean Region, references will be only given. However, African and European paleomagnetic poles (Westphal et al. 1986) will appear in some figures, representing reference systems other than the present geographical one.

Figure 2 in which paleomagnetic elements are plotted against geological time for different tectonic units, north and south of the Mid-Hungarian Structural Zone reveals that the last period of great mobility is in fact very young. Declinations observed on Tertiary rocks suggest post-early Miocene rotations, in CCW sense north, in CW sense south of the zone. Indications for Miocene rotations others than shown in Fig. 2 were also found for the Pennin Unit (Márton et al. 1987: CCW) and for the Gömör Unit (Márton P, pers. comm.: CCW). All these movements must have been coeval, fast and independent of the motion of Africa and stable Europe, respectively (Fig. 3).

Paleomagnetic elements for the Mesozoic suggest that the Transdanubian Central Range Unit moved in coordination with the African plate (Márton and Márton 1983). The movement is reflected in both declination and inclination: CW rotation accompanied by southward shift started in the mid-Jurassic; the

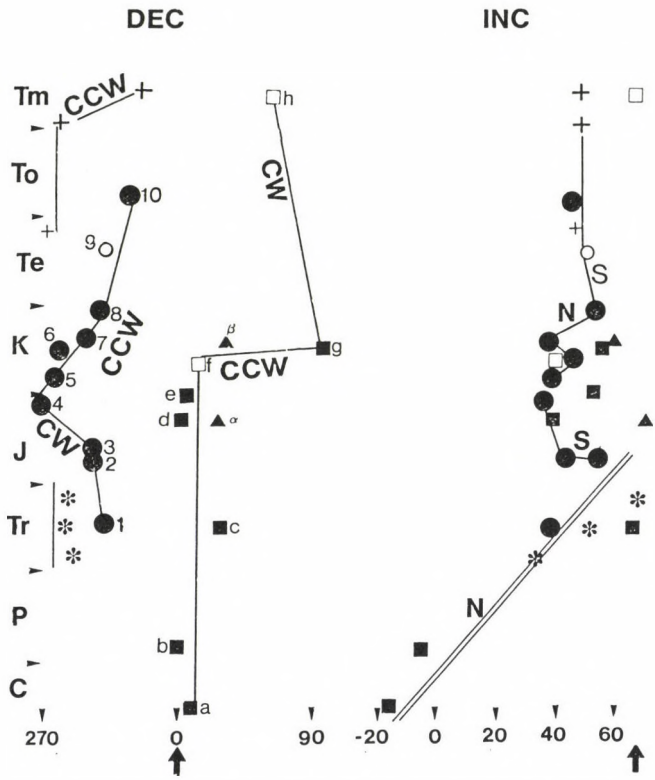

Fig. 2. Time-dependence of paleomagnetic elements for different tectonic units. Abbreviations: C - Carboniferous; P - Permian; Tr - Triassic; J - Jurassic; K - Cretaceous; Te - Eocene; To - Oligocene; Tm - Miocene; CW - clockwise rotation; CCW - counterclockwise rotation; N - shift to north; S - shift to south. Key: full or large symbols: directions based on more than two localities; light or small symbols: directions based on less than three localities; heavy arrows indicate the position of the magnetic elements in the present geographical system;
- circle, Transdanubian Central Range Unit (1, 9-10: Márton E 1988, 2-8: Márton and Márton 1983)
- square, Mecsek Unit (a, b, g, h: Márton E 1986, c-f: Márton E, unpublished)
- triangle, Villány Unit (Márton E 1988 and unpublished)
- asterisks, Rudabánya-Aggtelek Unit (Márton et al. 1988)
- cross, Bükk Unit (Márton E 1989)

the direction of the motion changed in the early Cretaceous so that by the end of Cretaceous both the net rotation and the latitude of the Unit was the same as in the early Jurassic (Fig. 2). The features of the Mesozoic declination - inclination

Fig. 3. The position of Miocene poles predating the calc-alcaline volcanism (calculated from measured paleomagnetic elements). Abbreviations: CW - clockwise; CCW - counterclockwise rotation with respect to the present orientation; Tm - the common Miocene pole for Africa and stable Europe; Eu Te - Eocene pole for stable Europe; Afr Te - Eocene pole for Africa. Key: full circle, paleomagnetic poles for the Bükk Unit (1: average pole for Eocene to Egerian sediments and lower ignimbrite horizon; 2: average pole for Ottnangian sediments and upper ignimbrite horizon)
- empty circle, paleomagnetic pole for the Gömör Unit (a single sedimentary locality of Ottnangian age)
- squares, poles for the Transdanubian Central Range Unit (1. a single sedimentary locality of Eocene age, 2. average pole for andesites of 30 Ma and remagnetized Carboniferous granite)
- triangle, pole for the Mecsek Unit (average for the Komló andesite of 21 Ma)

Pole for the Pennin Unit is not shown, for the locality mean directions are too scattered to give an overall mean with satisfactory statistical parameters

pattern for the Transdanubian Central Range Unit can be regarded as diagnostic of Southern Tethyan origin, for coeval paleomagnetic elements for this unit and for the Umbrian Apennines agree closely (Márton and Márton 1985, Márton et al. 1987).

Within the Transdanubian Central Range Unit regional consistency characterized the period of Mesozoic mobility (e.g. Tithonian poles in Fig. 4 are clustered while the Tithonian sampling localities are spread over an area shown by Fig. 5).

Fig. 4. Triassic and Tithonian paleomagnetic poles for the Transdanubian Central Range Unit. Triassic poles (numbered triangles) fall on a great circle (dashed line) drawn around the studied area (heavy arrow), joining African and European Triassic poles; this circle represents points of equal polar distance, i.e. the inclinations determined for the Transdanubian Central Range Unit correspond to the value expected either in a European or in an African system. The spread is due to differing degree of CCW rotation with respect to Africa. Tithonian poles, on the other hand, are clustered

In contrast, smeared distribution due to differences in declination was observed for ages predating the opening of the

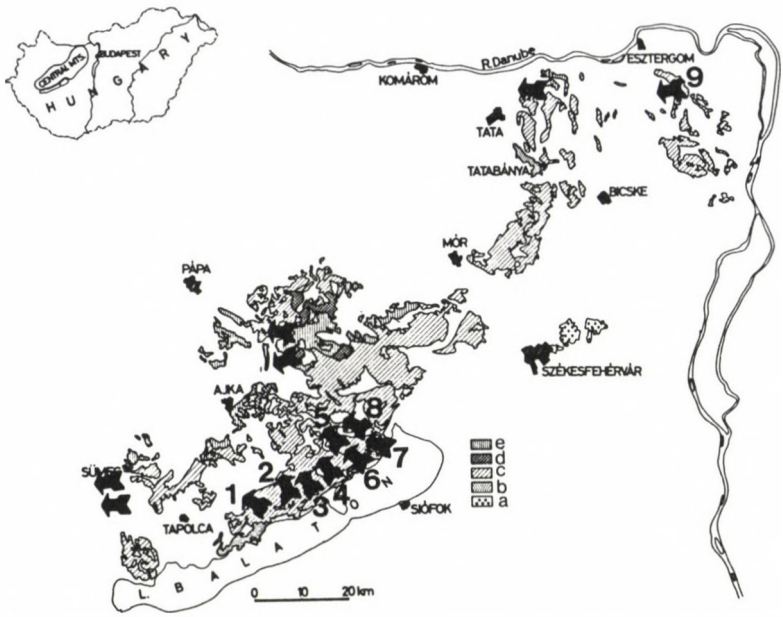

Fig. 5. Simplified geological map of the Transdanubian Central Range Unit showing Tithonian and Triassic sampling localities and paleomagnetic declinations as arrows. Triassic localities are numbered. The numbers correspond to those in Fig. 4. Key to the geological map: a - Carboniferous; b - Permian; c - Triassic; d - Jurassic; e - Cretaceous

Tethys (e.g. Triassic poles in Fig. 4 determined for localities plotted in Fig. 5). This situation is probably the result of block rotations that may have accompanied the disintegration of the Triassic carbonate platform, since the regional distribution of the more and less rotated declinations is not systematic.

Of the tectonic units situated today NE of the Transdanubian Central Range Unit the Triassic for the Rudabánya-Aggtelek, and the Tertiary of the Bükk Unit were studied so far systematically and succesfully. Compared to the first, the latter exhibit excess CCW rotation (Fig. 2).

The Tertiary rotation was shown to have affected the whole southern margin of the Bükk (Fig. 6). Its maximum amplitude which was observed in the Bükk on Paleogene sediments and

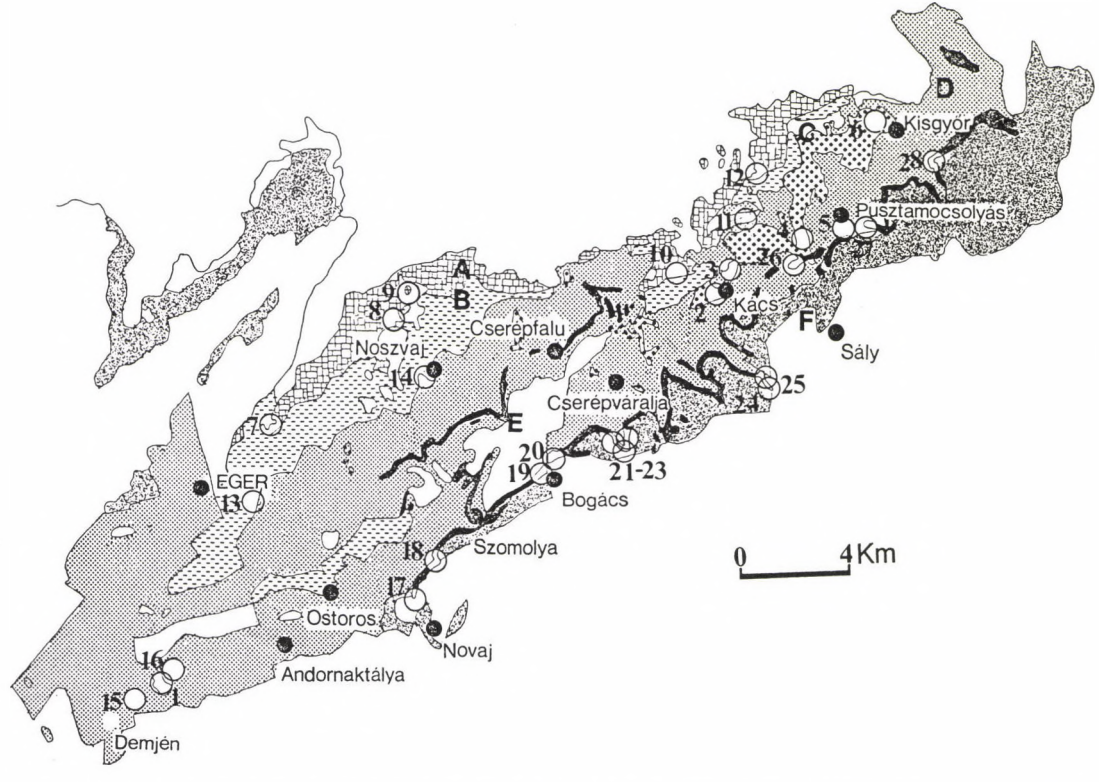

Fig. 6. Paleomagnetic sampling area at the southern margin of the Bükk. Localities 1-6 are in lower ignimbrite (and tuff) horizon; 7-12 are late Eocene, 13-14 late Oligocene sediments; 15-18 belong to the upper ignimbrite (and tuff) horizon. Geological map is modified after Balogh (1963). Key to the geological map: A - Eocene sediments; B - Oligocene-Ottnangian sediments; C - lower ignimbrite horizon; D - lower tuff horizon; E - upper ignimbrite horizon; F - upper tuff horizon

volcanics belonging to the lower ignimbrite horizon and also in the Mátra for Eocene andesite (Márton P, pers. comm.), is larger than the declination rotation of the Transdanubian Central Range Unit. The rotation must have been fast, for CCW rotation is less pronounced for the upper ignimbrite horizon in the Bükk. Moderate CCW rotation for Miocene sediments north of the Bükk and in the Gömör Unit (Márton P, pers. comm.) matches in angle that of the upper ignimbrite horizon. Though directly not proven, the Rudabánya-Aggtelek Unit may also have participated in the rotation that can fully account for the declinations observed on Triassic rocks (Fig. 2).

South of the Mid-Hungarian Structural Zone, paleomagnetic elements show less variation. Declination data available from and characteristic of the Mecsek Unit are consistent from the Carboniferous through the Valanginian-Hauterivian, with insignificant net rotation relative to the present orientation. Observations for the Villány Unit are similar including those obtained on Albian sediments. The lack of significant rotations suggests that this time-interval was uneventful for the Tisza Unit. Moreover, it implies that the post-Cretaceous CW rotation must have been common to the whole Tisza Unit, otherwise the agreement in declination between the Mórágy area, the Eastern and Western Mecsek and the Villány Hills would be too much of coincidence. Recent studies on late Cretaceous for the Apuseni Mts support this argument as a large CW rotation was observed (Patrascu et al., pers. comm.). This reasoning tacitly implies that intrusives showing CW rotation in the Mecsek Unit must be of post-Albian age, and the upper age limit of the CCW rotation is not constrained paleomagnetically.

While declinations are fairly consistent, inclinations are problematic in the Tisza Unit, for different reasons. Some of them are simply higher than expected: e.g. mid-Triassic for the Mecsek Unit which, according to the general trend of northward shift of all tectonic units in the Mediterranean region and that of all major plates (Carboniferous-Mid-Jurassic, Fig. 2 double line) would be more satisfactory for late, than mid-Triassic. Others are too high to be accomodated by the space

between two large plates (Fig. 7). Moreover, average inclinations determined for the same age for the Mecsek and the Villány, respectively, differ significantly. These are problems to be solved either by finding the source of inclination error or error in dating. In the case if these "anomalies" prove to be correct, tectonic models must be modified.

Fig. 7. Late Jurassic - Early Cretaceous paleomagnetic poles for the Mecsek (square), Villány (triangle) and Transdanubian Central Range (dot) Units compared to African and European reference systems. Circles of equal angular distance are drawn in dashed line. Poles situated along a circle reflect differences in inclination, different circles differences in the latitude of magnetization. Numbers, Latin and Greek letters refer to Fig. 2

CONCLUSIONS

1. A Neogene period of great mobility is common to all principal tectonic elements of Hungary. This period must have

been short, movements rapid and probably signifying the final welding of the tectonic units of Hungary to stable Europe.

2. Not only units north and south of the Mid-Hungarian Structural Zone moved in different manners in the course of this event; north of the zone differential rotations took place between the Pennin, the Transdanubian Central Range and the Bükk Units, respectively.

3. The Mesozoic pattern of declination and inclination dependence on time, diagnostic of tectonic units originated from the southern margin of the Tethys (e.g. Transdanubian Central Range Unit) is not recognized in the paleomagnetic data for the Tisza Unit.

4. Mesozoic and Tertiary inclinations for the Tisza Unit, with the exception of Oxfordian inclination for the Mecsek (point d in Fig. 2) are higher than those for other units. This suggest that the Tisza Unit was situated closer to stable Europe than the others.

REFERENCES

Brezsnyánszky K, Haas J 1985: In: Proceeding reports of the 13th Congress of KGBA, Part I, 174-177.

Márton E 1986: Geophysical Transactions, 32, 83-145.

Márton E 1988: In: Evolution of the northern margin of Tethys: the results of IGCP Project 198. Memoires de le Societe Geologique de France, Paris, Nouvelle Serie 154, 223-244.

Márton E 1989: Terra abstracts, 1, 86.

Márton E, Márton P 1983: Tectonophysics, 98, 43-57.

Márton E, Márton P 1985: Acta Geologica, 28, 59-70.

Márton E, Márton P, D'Andrea M 1987a: Rend. Soc. Geol. It., 9 (1986), 137-142.

Márton E, Mauritsch H J, Pahr A 1987b: Mitt. Österr. geol. Ges., 80, 185-225.

Márton E, Márton P, Less Gy 1988: Physics of the Earth and Planet. Inter., 52, 256-266.

Westphal M, Bazhenov M L, Lauer J P, Pechersky D M, Sibuet J C 1986: In: Evolution of the Tethys (Aubouin J, LePichon X, Monin A S eds). Tectonophysics, 123, 37-82.

Acta Geod. Geoph. Mont. Hung., Vol. 25 (3-4), pp. 399-413 (1990)

GENERAL ISSUE

A DOPPLER SATELLITE-DERIVED DATUM FOR NIGERIA

C U Ezeigbo

Dept. of Surveying, Faculty of Engineering, University of Lagos,
Akoka, Yaba, Lagos, Nigeria

[Manuscript received March 23, 1987, revised January 13, 1988]

The Doppler satellite technique is extensively used in the local datum determination. In this paper, preliminary results of the African Doppler Satellite (ADOS) program are used to determine a datum for Nigeria. The following conclusions, based on our investigations are arrived at:

a) The inclusion of a scale parameter in the datum determination leads to a large distortion of the results.
b) The use of different sets of the estimable parameters (shift and/or rotation) leads to results of comparable discrepancies. The following values: $X_0 = -76.2 \pm 0.9$ m; $Y_0 = -107.7 \pm 2.6$ m; $Z_0 = 56.1 \pm 4.2$ m; $\varepsilon_X = 0.1 \pm 0.1$ sec; $\varepsilon_Y = 2.0 \pm 0.1$ sec; $\varepsilon_Z = 0.3 \pm 0.1$ sec are the best estimates of the parameters based on the available observations.
c) More observations are needed to determine a reliable datum for the country.

Keywords: datum; Doppler-satellite observation; Nigeria

INTRODUCTION

Geodetic datums are basic frameworks for the geodetic operations. Only well-defined datums are adequate for such operations. Moreover, modern geodetic operations demand compatibility between geodetic reference systems for the improvement of the geodetic networks through the ever increasing accuracies of the space techniques. Compatibility between datums is also needed in the execution of global projects (Nagy 1974).

The African Doppler Surveys (ADOS) program which is intended to provide a unified datum for the African continent (Mueller 1982), will also provide member countries a unique opportunity to assess and improve their own individual local datums.

Obviously, the use of the Doppler satellite observations

in a geodetic datum determination or rectification presupposes that the satellite system coincides with the Average Terrestrial System (ATS) to within acceptable limit.

A number of attempts have been made to determine a geodetic datum for Nigeria using Doppler satellite observations. Table I shows the results of a few such determinations. The results are based on the comparison of coordinates of a number of stations on both the WGS 72 reference system and the local reference system in use in Nigeria. Very large discrepancies exist between the results. All the determinations have utilized different network points, as well as different number of observations. The discrepancies in these results are mainly a direct consequence of these differences. However, the inherent instability in the datum determination problems accounts for a substantial part of the discrepancies. How best to resolve these discrepancies is a subject of critical studies in the datum determination.

Table I. Different estimations of datum for Nigeria

Investigator	Parameters						
	X_o (m)	Y_o (m)	Z_o (m)	ε_x (sec)	ε_y (sec)	ε_z (sec)	K
Obenson and Fajemirokun (1979)	-73	-113	-8	-	-	-	-
Oyeneye (1985)	-90.3 $\pm$1.2	-107.9 $\pm$1.2	115.6 $\pm$1.2	-	-	-	-
Fajemirokun and Orupabo (1986)	-160.4 $\pm$0.1	-67.4 $\pm$0.0	144.0 $\pm$0.0	0.4 $\pm$3.0	1.2 $\pm$4.6	1.7 $\pm$3.7	1.0×10^{-6} $\pm14.0\times10^{-6}$

The objective of this study is therefore to consider a number of modelling techniques with a view to derive a datum of a best fit. We shall investigate the type and the number of parameters that may be reasonably determined, using the available observations. The effects of varying the number and the

configuration of the observation points are also investigated. We shall also vary the weighting procedures.

1. BASIC MATHEMATICAL FORMULATION

1.1 The transformation parameters

Let a point P in space be referred to two coordinate systems. Let X, Y, Z be the space rectangular coordinates of P in a satellite reference system while x, y, z are the coordinates of P in the local reference system. X, Y, Z and x, y, z are related by the following equations (Ezeigbo 1986):

$$\begin{aligned} X_i &= X_o + Kx_i + K\,\varepsilon_z y_i - K\,\varepsilon_y z_i \\ Y_i &= Y_o + Ky_i - K\,\varepsilon_z x_i + K\,\varepsilon_x z_i \\ Z_i &= Z_o + Kz_i + K\,\varepsilon_y x_i - K\,\varepsilon_x y_i \ , \end{aligned} \tag{1}$$

where the translation (X_o, Y_o, Z_o), the rotation, $(\varepsilon_x, \varepsilon_y, \varepsilon_z)$ and the scale K are the transformation parameters (Fig. 1). A linearized form of (1) is given by

$$\begin{aligned} dX_i &= dX_o - K^a z_i d\varepsilon_y + K^a y_i d\varepsilon_z + (x_i + \varepsilon_z^a y_i - \varepsilon_y^a z_i)\, dK + \\ &\quad + K^a (x_i + \varepsilon_z^a y_i - \varepsilon_y^a z_i) + X_o^a - X_i^b \\ dY_i &= dY_o + K^a z_i d\varepsilon_x - K^a x_i d\varepsilon_z + (y_i - \varepsilon_z^a x_i + \varepsilon_x^a z_i)\, dK + \\ &\quad + K^a (y_i - \varepsilon_z^a x_i + \varepsilon_x^a z_i) + Y_o^a - Y_i^b \\ dZ_i &= dZ_o - K^a y_i d\varepsilon_x + K^a x_i d\varepsilon_y + (z_i + \varepsilon_y^a x_i - \varepsilon_x^a y_i)\, dK + \\ &\quad + K^a (z_i + \varepsilon_y^a x_i - \varepsilon_x^a y_i) + Z_o^a - Z_i^b \ , \end{aligned} \tag{2}$$

where the superscripts "a" and "b" refer to the approximate and observed values respectively.

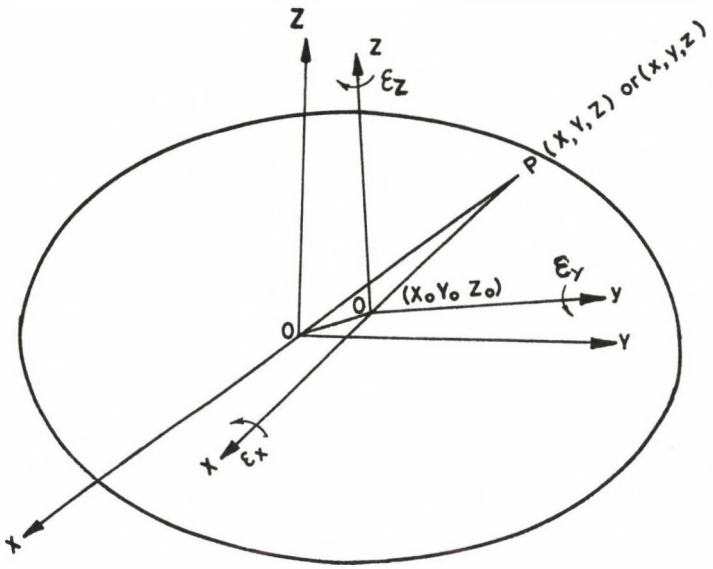

Fig. 1. Transformation from Doppler coordinate system to local coordinate system

We define the terms in equation (2) as follows:

$$x^T = (dX_o,\ dY_o,\ dZ_o,\ d\varepsilon_x,\ d\varepsilon_y,\ d\varepsilon_z,\ dK) \tag{3}$$

$$V^T = (dX_1,\ dY_1,\ dZ_1,\ dX_2,\ dY_2,\ dZ_2,\ \ldots) \tag{4}$$

$$l = \begin{bmatrix} X_o^a - X_1^b + K^a(x_1 + \varepsilon_z^a y_1 - \varepsilon_y^a z_1) \\ Y_o^a - Y_1^b + K^a(y_1 - \varepsilon_z^a x_1 + \varepsilon_x^a z_1) \\ Z_o^a - Z_1^b + K^a(z_1 + \varepsilon_y^a x_1 - \varepsilon_x^a y_1) \\ X_o^a - X_2^b + K^a(x_2 + \varepsilon_z^a y_2 - \varepsilon_y^a z_2) \\ Y_o^a - Y_2^b + K^a(y_2 - \varepsilon_z^a x_2 + \varepsilon_x^a z_2) \\ Z_o^a - Z_2^b + K^a(z_2 + \varepsilon_y^a x_2 - \varepsilon_x^a y_2) \\ \vdots \qquad\qquad\qquad\qquad\qquad\qquad \vdots \end{bmatrix} \tag{5}$$

$$A = \begin{bmatrix} 1 & 0 & 0 & 0 & -K^a z_1 & K^a y_1 & (x_1 + \varepsilon_z^a y_1 - \varepsilon_y^a z_1) \\ 0 & 1 & 0 & K^a z_1 & 0 & -K^a x_1 & (y_1 - \varepsilon_z^a x_1 + \varepsilon_x^a z_1) \\ 0 & 0 & 1 & -K^a y_1 & K^a x_1 & 0 & (z_1 + \varepsilon_y^a x_1 - \varepsilon_x^a y_1) \\ 1 & 0 & 0 & 0 & -K^a z_2 & K^a y_2 & (x_2 + \varepsilon_z^a y_2 - \varepsilon_y^a z_2) \\ 0 & 1 & 0 & K^a z_2 & 0 & -K^a x_2 & (y_2 - \varepsilon_z^a x_2 + \varepsilon_x^a z_2) \\ 0 & 0 & 1 & -K^a y_2 & K^a x_2 & 0 & (z_2 + \varepsilon_y^a x_2 - \varepsilon_x^a y_2) \\ \vdots & \vdots & \vdots & \vdots & & & \vdots \end{bmatrix}, \qquad (6)$$

where dX, dY, dZ, dX_o, dY_o, dZ_o, $d\varepsilon_x$, $d\varepsilon_y$, $d\varepsilon_z$, and dK are the corrections to X^b, Y^b, Z^b, X_o^a, Y_o^a, Z_o^a, ε_x^a, ε_y^a, ε_z^a and K^a.

A matrix form of Eq. (2), making use of Eqs (3-6), is given by:

$$V = Ax + l \ . \qquad (7)$$

The least squares solution of Eq. (7) is given by Ezeigbo (1986):

$$\tilde{x} = -(A^T P A)^{-1} A^T P l \ . \qquad (8)$$

The error covariance matrix of $\tilde{x}$ is also given by:

$$\Sigma_{\tilde{x}} = (A^T P A)^{-1} \sigma_o^2 \ , \qquad (9)$$

where σ_o^2 is the a posteriori variance of unit weight, and P is the weight matrix of the observations. If the a priori weight matrix (P_x) of the parameters is included in the modelling process, as indeed we shall do, Eqs (8) and (9) become:

$$\tilde{x} = -(A^T P A + P_x)^{-1} A^T P l \qquad (10)$$

$$\Sigma_{\tilde{x}} = (A^T P A + P_x)^{-1} \sigma_o^2 \ . \qquad (11)$$

1.2 Weighting of the observations

The observed coordinate differences in equation (2) or (4)

are functions of X, Y, Z and x, y, z. x, y, z are themselves functions of the geodetic coordinates ϕ, λ, h. If we consider the transformation parameters fixed, the rotation parameters small and the scale parameter K equal to unity, the variances dX, dY and dZ will be derived from Eq. (2) as follows:

$$\begin{aligned} \sigma^2_{V_X} &= \sigma^2_X + \sigma^2_X \\ \sigma^2_{V_Y} &= \sigma^2_Y + \sigma^2_Y \\ \sigma^2_{V_Z} &= \sigma^2_Z + \sigma^2_Z \,. \end{aligned} \tag{12}$$

Based on the available information on the Nigerian geodetic network (Field 1977, Omoigui 1973), the following values of σ_ϕ, and σ_h are adopted for the weight estimations: $\sigma_\phi = \sigma_\lambda = 1"$; $\sigma_h = 6$ m. The precision of the satellite observation is given by $\sigma^2_X = \sigma^2_Y = \sigma^2_Z = \sigma^2 = 2.25\ m^2$. The values of $\sigma^2_{V_X}$, $\sigma^2_{V_Y}$ and $\sigma^2_{V_Z}$ for a number of points are shown in Table II.

Table II. Variances of observed coordinate differences at different positions

Points			$\sigma^2_{V_X}$	$\sigma^2_{V_Y}$	$\sigma^2_{V_Z}$
ϕ	λ	h	(m^2)	(m^2)	(m^2)
4^o	4^o	500 m	47.7	947.7	952.3
8^o	7^o	500 m	69.2	942.9	940.8
14^o	14^o	500 m	486.1	855.2	904.7
14^o	14^o	0 m	483.1	855.2	903.1
14^o	4^o	0 m	96.1	928.3	904.4
4^o	14^o	0 m	97.2	900.5	954.0

2. NUMERICAL INVESTIGATIONS

The estimation of the transformation parameters in the geodetic datum determination is in a certain sense an ill-posed problem. Some of the parameters are correlated. Consequently, a unique determination of the individual components may be difficult to achieve. The solution is in general not stable. Different modelling techniques to achieve a reasonable degree of stability will be attempted here. In determining the transformation parameters, Eq. (8) or Eq. (10) is solved for the corrections to the approximate parameters. The application of the estimated corrections to the approximate values yields the desired parameters. A number of iterative steps are taken to arrive at any particular solution.

In arriving at a specific choice of the parameters, the following models are considered.

a) Observations are considered to be of equal weight.
b) Observations are weighted on the basis of Eq. (12) with the functions evaluated at the mean position of the observation area.
c) Observations are weighted on the basis of Eq. (12), but the functions are evaluated at the exact positions.
d) The a priori variances of the parameters which are derived from preliminary adjustment are incorporated into solution (c).
e) The configuration and the number of observations are varied.
f) The number and type of parameters in the transformation equations are also varied.
g) The convergence of the iterated solutions in all the cases above is investigated.

In all, except a), the a priori variances of the parameters are incorporated.

3. RESULTS AND ANALYSIS OF RESULTS

3.1 Results

In Table III to VII, the estimated parameters for the

various models considered in Section 2.1 are presented. Table III shows the estimates using uniform weight for the observations as well as the results obtained when the weight functions of Eq. (12) are evaluated at the mean position of the area. Table IV compares the estimates when: a) the weight functions are evaluated at the mean position, and b) when they are evaluated at the exact positions.

Table III. Estimation of seven parameters using different weighting systems

Parameters / Weighting	X_o (m)	Y_o (m)	Z_o (m)	ε_x (sec)	ε_y (sec)	ε_z (sec)	K
Uniform	-345.8	-51.6	-73.0	2.1	5.1	3.6	1.00004
Weight	$\pm$6.3	$\pm$7.6	$\pm$10.5	$\pm$0.2	$\pm$0.3	$\pm$0.2	$\pm 0.96 \times 10^{-6}$
Non-uniform	-167.2	-88.7	43.8	0.1	1.9	1.3	1.00001
Weight	$\pm$2.7	$\pm$2.8	$\pm$4.4	$\pm$0.1	$\pm$0.1	$\pm$0.1	$\pm 0.4 \times 10^{-6}$

Table IV. Estimates using seven observations (weight is evaluated): a) at mean position, b) at exact position

Parameters / Weighting system		X_o (m)	Y_o (m)	Z_o (m)	ε_x (sec)	ε_y (sec)	ε_z (sec)
a		-79.5	-96.6	65.1	0.1	1.7	0.7
		$\pm$0.9	$\pm$2.7	$\pm$4.3	$\pm$0.1	$\pm$0.1	$\pm$0.1
b		-76.2	-107.7	56.1	0.1	2.0	0.3
		$\pm$0.9	$\pm$2.6	$\pm$4.2	$\pm$0.1	$\pm$0.1	$\pm$0.1

Table V. Variation of precision of ϕ and λ . Six parameters are estimated and weight function evaluated at individual points ($\sigma_H^2 = 36\ m^2$, $\sigma^2 = 2.25\ m^2$)

Precision of ϕ and λ \ Parameters	X_o (m)	Y_o (m)	Z_o (m)	ε_x (sec)	ε_y (sec)	ε_z (sec)
$\phi = \lambda = 1''$	-80.6	-77.7	55.7	-0.1	2.0	1.3
	$\pm$1.0	$\pm$3.2	$\pm$5.0	$\pm$0.1	$\pm$0.2	$\pm$0.1
$\phi = \lambda = 2''$	-76.2	-107.7	56.1	-0.1	2.0	0.3
	$\pm$0.9	$\pm$2.6	$\pm$4.2	$\pm$0.1	$\pm$0.1	$\pm$0.1

Table VI. Observations varied (weight function evaluated at mean position)

No. of	X_o (m)	Y_o (m)	Z_o (m)	ε_x (sec)	ε_y (sec)	ε_z (sec)
4	-89.3	-60.5	113.2	0.4	0.3	1.8
	$\pm$17.8	$\pm$138.8	$\pm$58.0	$\pm$2.3	$\pm$1.8	$\pm$4.5
5	-82.0	-60.0	67.6	0.2	1.6	1.9
	$\pm$2.7	$\pm$0.6	$\pm$0.6	$\pm$2.6	$\pm$0.3	$\pm$0.4
6	-98.3	-32.6	113.7	0.0	0.1	2.7
	$\pm$0.8	$\pm$2.4	$\pm$3.4	$\pm$0.1	$\pm$0.1	$\pm$0.1
7	-79.5	-96.6	65.1	0.1	1.7	0.7
	$\pm$0.9	$\pm$2.7	$\pm$4.3	$\pm$0.1	$\pm$0.1	$\pm$0.1
8	-81.7	-69.0	51.9	2.9	2.6	1.7
	$\pm$1.2	$\pm$3.4	$\pm$5.5	$\pm$0.1	$\pm$0.2	$\pm$0.1

The results of the investigations show that the error

introduced in the estimates by the neglection of the undulation values in the computation of the geodetic height affects mainly the x-component of the shift parameters. The values of the x--component changed by approximately the same amount (6.0 m), while the values of the other components did not change appreciably. These results agree with those obtained by Ezeigbo (1984). There it was stated that the variations in the undulations affect the x-component more than any other components of the shift parameters when datums in a low latitude region are determined.

From the astrogeodetic geoid computed by Nwilo (1980), a maximum undulation of 6.0 m is estimated. Since we do not know the undulations at the observation points, we adopted the orthometric heights at those points as their geodetic heights and assigned an a priori variance of 36 m^2 to them.

In Table VII, the estimated parameters, when variances of 1 sec^2 and 4 sec^2 are assigned to the derived geodetic latitude and longitude, are presented. It is observed that a reduction

Table VII. Varying configurations of four observation points: a) four corner points, b) west located points, c) east located points, d) south located points

Configuration	X_o (m)	Y_o (m)	Z_o (m)	ε_x (sec)	ε_y (sec)	ε_z (sec)
a	-108.6	-180.6	-8.1	-1.8	3.8	9.5
	±2.0	±0.6	±0.8	±1.3	±0.2	±0.2
b	-11.9	-111.7	-321.5	-1.4	14.3	0.0
	±0.8	±0.3	±0.2	±0.6	±0.1	±0.1
c	-82.2	-99.8	111.3	0.1	0.2	0.5
	±3.0	±9.4	±14.4	±0.3	±0.5	±0.3
d	-87.0	-47.9	70.0	0.5	1.4	2.2
	±1.0	±3.8	±4.9	±0.1	±0.2	±0.1

in the weight assigned to the geodetic coordinates (ϕ , λ)

affects the estimated values of the x- and y-components of the shift parameters as well as the z-components of the rotation parameters appreciably. On the contrary, there are no appreciable changes in the estimated values of the Z-component of the shift parameter as well as of the X- and Y-components of the rotation parameters. The results also show that if the shift parameters alone are estimated, the variation in the weights of the geodetic coordinates (ϕ, λ) does not affect the estimates. In Table VII, the estimates for different configurations (Fig. 2) are presented.

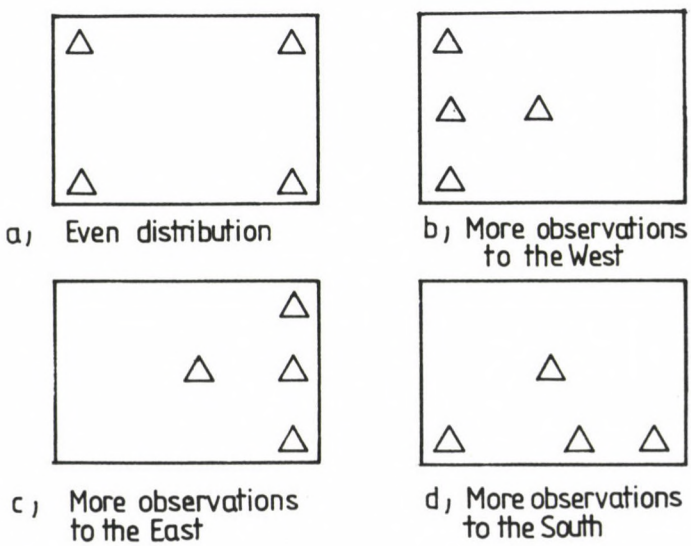

Fig. 2. Variation in configurations of four observation points

Table VIII shows the estimates for four different models: a) the original estimates of the shift and rotation parameters as in Tables IV and V, b) the estimates with the rotations obtained in a) deduced from the geodetic coordinates (ϕ, λ) of the local system.

The deduction of the estimated rotation from the latitudes and longitudes of the observation points seems to have reduced the discrepancies between the estimated shift components

Table VIII. Comparison of estimates with and without computed rotation deducted (σ_H^2 = 36 m^2, σ^2 = 2.25 m^2, $\sigma_\phi = \sigma_\lambda$ = 2")

Parameters	X_o (m)	Y_o (m)	Z_o (m)	ε_x (sec)	ε_y (sec)	ε_z (sec)
Initial estimates of six parameters	-76.2 ±0.9	-107.7 ±2.6	56.1 ±4.1	0.1 ±0.1	2.0 ±0.1	0.3 ±0.1
Estimates of six parameters after the deduction	-76.1 ±0.9	-108.1 ±2.6	56.2 ±4.2	0.4 ±0.1	0.0 ±0.1	0.6 ±0.1
Initial estimates of three parameters	-85.3 ±0.5	-116.2 ±0.5	116.0 ±0.6	-	-	-
Estimates of three parameters after the deduction	-73.7 ±0.4	-123.7 ±0.5	55.3 ±0.5	-	-	-

obtained when either six or three parameters are estimated. The estimation of the shift and rotation parameters, exhibits greater stability than the estimation of the shift parameters alone, when the estimated rotation is deduced. In the validation Cartesian coordinates of the seventh satellite station are compared with the transformed Cartesian coordinates of the same station on the satellite (geocentric) datum, using the estimated parameters. The results obtained show deviations of 4.1 m, 2.1 m in the x-, y- and z-coordinates, respectively. When five observation points are used, the corresponding deviations are 0.6 m, 3.1 m and 2.1 m. Considering the accuracies of the estimates, the general instability inherent in datum determination problems and the large separation between the points, the agreement can be considered reasonable. In fact the large discrepancies between the estimated parameters when six and five observations are used do not show up sufficiently in the estimated coordinates. This indicates that different sets of estimates may be utilized to obtain comparable results.

3.2 Analysis of the results

In Table III, the estimation of seven parameters, irrespective of the weighting procedure, leads to large distorion. The results differ greatly from any other estimates. The iteration steps do not converge to any specific values. The distortion and instability are more noticeable with uniform weights, than with the non-uniform weights. However, the estimation of the shift parameters alone is not sensitive to the weighting system. In fact, the simple mean of the computed shift (geocentric minus local Cartesian coordinates) agrees with the least squares estimates. The Table also shows that the x-component of the shift is the most badly affected estimate when the scale parameters is incorporated in the estimation. This is probably due to the high correlation between x-component of the shift and the scale parameter in the low latitude region. In Table IV, we compare the results obtained when the weight functions are evaluated at the mean and exact positions, respectively. While the rotation parameters remain unchanged, the shift parameters change appreciably.

Table V shows that a significant variation in the variances of latitude and longitude affects only the Z-component of the rotation and the X- and Y-components of the shift. Although it is not obvious why the increase in the variances of latitudes and longitudes causes substantial variation in the Z-component of the rotation and not in the other two, the variations in the X- and Y-components of the shift corresponding to variation in the Z-component of rotation are self-evident. However, the higher variance of the observations (Table II) in the Z--direction may be responsible for the sensitivity of the Z-component of the rotation to variation in the variances of the latutide and longitude of the points. Both the variation in the number of observations and the variation in the configuration of the observation points affect the results of the estimates significantly. It is, however, apparent that the variation in the configurations affects the results of the estimation more than the variation in the number of observation. This again may be due to the general instability associated with the datum

determination problem. Generally, the amount by which the undulation changed is almost the amount by which the X-component of the shift changed. The other components hardly changed. The lack of the information on the undulation values at observation points will in general affect mainly the accuracy of the estimated X-component of the shift. This is again due to the high correlation between the undulation values and the X-component of the shift parameters in the low latitude region.

4. CONCLUSIONS

We have tried to derive a "best" datum for Nigeria, using the available Doppler observations. This we did by investigating the effects of the number of observations, the configuration of the observation points, and the weighting system adopted, on the estimates. We also considered the number and type of parameters that may be most reasonably estimated. The best way to treat the observations to be incorporated in the observation equations in the estimation was considered. We have arrived at the following conclusions based on the analysis of the results in Section 3.2.

a) The inclusion of scale parameter in the datum determination in Nigeria could lead to large distortion of results.

b) The shift parameters, which are not very sensitive to the weighting system and the model of estimation are the best components to be estimated. However, since there is evidence of rotation in the Nigerian geodetic network the estimation of the shift and rotation parameters is desirable.

c) Since the different sets of the estimated parameters (shift and rotation) may be used to achieve fairly the same results, no particular set may be considered the best at the moment.

d) More observations have to be incorporated in the estimation before a unique choice can be made.

REFERENCES

Chen J Y 1982: Geodetic datum and Doppler positioning. Ph.D. Dissertation of the Technical University at Graz

Ezeigbo C U 1984: Bollettino di Geodesia e Scienze Affini, 43, No. 3.

Ezeigbo C U 1986: The estimation of the transformation parameters in a local geodetic datum determination. A paper presented at the 3rd Symposium on Geodesy in Africa, 1986. Yamoussoukro, Cote d'Ivoire

Fajemirokun F A, Orupabo S 1986: Som theoretical considerations in the transformation of geodetic data from one datum to another. A paper presented at the 3rd Symposium on Geodesy in Africa, 1986. Cote d'Ivoire

Field N J 1977: Adjustment and strength analysis of the primary triangulation network of Nigeria. M.Phil. thesis, University of Nottingham

Heiskanen W A, Moritz H 1967: Physical Geodesy. W H Freeman and Co., San Francisco and London

Moritz H 1978: The definition of a geodetic datum. The second international symposium on problems related to the redefinition of the North American Geodetic Networks (NAD 1978)

Mueller I I 1982: African Doppler Survey. Proceedings of the 3rd international symposium on satellite Doppler position. New Mexico State University

Nagy D 1974: The Canadian Surveyor, 28, No. 5.

Nwilo P 1980: Astrogeodetic geoid in Nigeria. B.Sc. Project report, Dept. of Surveying, University of Lagos

Obenson G, Fajemirokun F A 1979: UNIDOP - A program to strengthen and adjust rigorously the Nigerian geodetic control network. Proceedings of 2nd int. symposium on satellite Doppler positioning, Austin, Texas

Omoigui D A 1973: The Nigerian triangulation and the scale check programme. Proceedings of the Int. Seminar on Electronic Distance Measurements, University of Lagos, Lagos, Nigeria

Oyeneye, G A 1985: Satellite Doppler surveying technique: Theory, methodology and some recent advances in Nigeria. Federal Surveys, Lagos

Acta Geod. Geoph. Mont. Hung., Vol. 25 (3-4), pp. 415-442 (1990)

WEIGHT COEFFICIENTS FOR POINT DETERMINATIONS BASED ON A PRIORI MEAN SQUARE ERRORS

V Vincze

H-1027 Budapest, Mártírok útja 56, Hungary

[Manuscript received December 21, 1988]

As it is known, in the geodesy the weight is first of all a term of reliability by definition, however, at present in the computations there have generally been applied weight factors deduced exclusively under geometric consideration for determination of points.

The author sets out from the a priori standard error of the point determination in question, choosing the reciprocal of its square as a weight, which consequently contains already the standard error of the control points used and of the measurements respectively.

The weights of direction are firstly dealt with, separately treating the weight of the orientation directions and the determining ones, as to the latter distinguishing the cases of angular and distance correction.

Keywords: direction measurement; orientation direction; point error, standard error

As it is known the adjustment made by the least squares method aims at the determination of corrections v_i which yield in case of independent measurements with equal weights, the minimum of $[v_i v_i]$, and in case of measurements with different reliability, i.e. of different weights p_i, the minimum of $[p_i v_i v_i]$.

Though the weight is in the present case according to definition a notion of the character of reliability, it is at present usual to adopt weights deduced from purely geometrical considerations.

Thus I considered worth studying the question how weights could be introduced by strictly keeping the corresponding principles so that they be functions not only of the geometry, but also of the reliability of geodetic data and measurements.

For this purpose I shall at first deal with a mixed

horizontal network and deduce weights for directions, then point weights to be used in basic determinations, starting in each case from the a priori mean square error of the used point determination.

1. WEIGHT OF A DIRECTION

If a point is determined in surveying, generally two kinds of directions are distinguished. A part of the directions are used immediately for the determination of the point, an other group of the directions, for the orientation of the directions in the first group. The two groups differ, however, not only in their role, but also in their character-especially concerning the weights.

In case of directions for orientation, both end points are known, and from one end point of the direction, the other end point can be directly pointed by the instrument. In case of determining directions, however, only one end point is known and the direction can be only found by using orientation directions and measurements. (So-called resection directions are not dealt with here.)

In the first case the weight of the direction increases with the length of the direction, in the second case - in addition to geometrical conditions - the weight of the direction depends on the kind of correction which is to be used for the determination of the resulting point coordinates. Namely the weights of directions follow different laws if the adjustment is made on the basis of the minimum of angle corrections and of distance corrections, respectively.

1.1 Weight of the orientation direction

The reliability of a direction used for the determination of a point depends strongly on the reliability of the orientation direction. But it is immediately evident, too, that the weights of these directions depend in addition to the lengths on the location error of the station and of the point being pointed. In case of careful measurements other errors can be

neglected as they are generally much less than the location errors of the end points.

Be the mean square errors of the coordinates of point A μ_{Ay} and μ_{Ax}, and those of point B to be pointed, μ_{By} and μ_{Bx}. In the calculation of the wieights the average coordinate errors of the points can be used which are defined according to Homoródi (1956) as

$$\mu_{AK} = \sqrt{\frac{\mu_{Ay}^2 + \mu_{Ax}^2}{2}} \qquad \text{and} \qquad \mu_{BK} = \sqrt{\frac{\mu_{By}^2 + \mu_{Bx}^2}{2}} .$$

Thus the a priori mean square direction error of an orientation direction is:

$$\mu_{ABi} = \frac{\sqrt{\mu_{AK}^2 + \mu_{BK}^2}}{t_{AB}} \tag{1}$$

and the weight of an orientation direction:

$$p_{ABi} = \frac{1}{\mu_{ABi}^2} = \frac{t_{AB}^2}{\mu_{AK}^2 + \mu_{BK}^2} . \tag{2}$$

The average coordinate errors of the points are naturally in most cases not exactly known. But even if these errors are taken approximatively into account, - e.g. uniformly for different types of the points - the result will be more reliable, than if they would be fully neglected.

In Hungarian conditions, the points can be separated into three main groups from the present point of view:

1. Points of the filling or K-network of the country; a relatively small amount of Ist order points are also included here.
2. Points of the type B within the K-network, and
3. IVth order points and other E-type points of the same order.

The average mean square coordinate error is supposed to be $\pm$ 0.04 m in group K, $\pm$ 0.05 m in group B, $\pm$ 0.10 m in group E.

Thus e.g. if the station is of the type E, and a point of the type B at a distance of 3.0 km is being pointed to, than the weight of the orientation direction is according to Eq. (2):

$$p_{ABi} = \frac{9}{0.04^2 + 0.05^2} = 2195 .$$

For convenience, this value is divided by 100, and the resulting weight is

$$p_{ABi} = 21.95 \approx 22 .$$

Weights for some other cases computed by the same method are found in Table I.

Table I. Weight of an orienting direction

Station	K			B			E		
Pointed station	K	B	E	K	B	E	K	B	E
t=0.5 km	0.78	0.60	0.40	0.6	0.5	0.35	0.4	0.34	0.3
1.0	3.13	2.95	1.5	2.5	2.0	1.40	1.5	1.35	1.0
2.0	12.25	9.8	6.2	12.5	8.0	5.4	6.2	5.4	4.1
3.0	28.2	22.0	13.8	22.0	18.0	12.2	13.8	12.2	9.2
4.0	50.0	39.0	24.6	39.0	32.0				
5.0	78.0	61.5	38.5						
6.0	113.0	88.0	55.5						

It is naturally possible to use an other grouping for the control points or the actual average coordinate errors can also be used for the calculation, but these possibilities do not change the principle.

If from a point A, n known points are pointed for the orientation of the direction to point P to be determined, further the direction angle of the i-th direction is δ_{Ai}, and the corresponding reading on the limb is l_{Ai}, then the angle

of orientation is:

$$z_{Ai} = \delta_{Ai} - l_{Ai} .$$

The mean orientation angle of the direction to be determined one gets by using the weight values from Table I as:

$$z_{Ai} = \frac{[z_{Ai}\ p_{Ai}]}{[p_{Ai}]} . \qquad (3)$$

Finally the mean square error of this direction is if the correction $v_{Ai} = z_{Ai} - \bar{z}$ is known:

$$\mu_z = M_{AP} = \frac{\mu_o}{\sqrt{[p_i]}} \qquad (4)$$

where

$$\mu_o = \sqrt{\frac{[p_i v_i v_i]}{n-1}} . \qquad (5)$$

If the basic points used in the determination are supposed to be of the same reliability, then Eq. (2) gets the form:

$$p_{ABi} = k\ t_{AB}^2$$

where

$$k = \frac{1}{\mu_{AK}^2 + \mu_{BK}^2} = \frac{1}{2\mu_K^2} .$$

Further if the mean square coordinate errors of the fix points are neglected, then

$$p_{AB} = t_{AB}^2$$

and this value differs considerably from that given by Eq. (2), as it is a better approximation.

1.2 Weight of the determining direction

Before considering further details, let us see the problem of the weight of a direction in a more general form.

It is known that the location of a point can be determined by directions using two different kinds of minimum conditions.

If the linear corrections are denoted by e_i, and the angular corrections by v_i, then directions have to fulfil either the minimum condition of $[p_{ei}e_ie_i]$ or the minimum condition of $[p_{vi}v_iv_i]$, each with a given system of weights p_e and p_v. As the two systems of corrections are related as:

$$v_i = \frac{e_i}{t_i} \tag{6}$$

the corresponding weights are related as

$$p_{vi} = \frac{p_{ei}}{t_i^2} \ . \tag{7}$$

This can be given in a general form for the case of Fig. 1 for two determining directions:

$$[p_{ei}e_ie_i] = p_A\, e_A^2 + p_B(s-e_A)^2 \tag{8}$$

and if

$$p_B = cp_A \tag{9}$$

(where c is a positive number), then Eq. (8) can be written as:

$$[p_ie_ie_i] = p_A\, e_A^2 + cp_A(s-e_A)^2 \ . \tag{10}$$

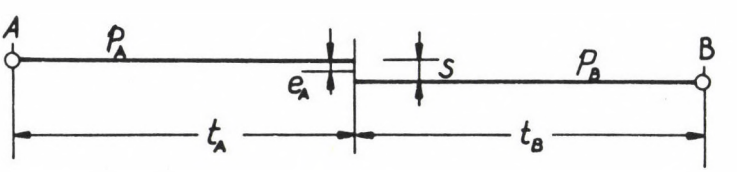

Fig. 1. Role of two directions in the point determination

As the first derivate of Eq. (10) is:

$$e_A - c(s-e_A) = 0$$

the second derivate is a positive number, meaning that Eq. (10) has a minimum at

$$e_A = \frac{c}{c+1} s$$

if Eq. (9) is valid for the weights, i.e. if:

$$\frac{p_B}{p_A} = c \frac{e_A}{s-e_A} .$$

It follows that for any system of corrections a weight system can be naturally found for which Eq. (10) has a minimum.

Let us consider now the sums $[p_i e_i e_i]$ and $[p_i v_i v_i]$ for different weights.

According to Eq. (8):

$$[p_i e_i e_i] = p e_A^2 + p_B (s-e_A)^2 .$$

The sum $[p_i e_i e_i]$ is minimum at

$$e_A = \frac{p_B}{p_A + p_B} . \qquad (11)$$

The sum $[p_i v_i v_i]$ has in case of Fig. 1 the form:

$$[p_i v_i v_i] = p_A \frac{e_A^2}{t_A^2} + p_B \frac{(s-e)^2}{t_B^2} . \qquad (12)$$

This is minimum at

$$e_A = \frac{p'_A}{p'_A + p'_B} s \qquad (13)$$

where p'_A and p'_B are defined by Eq. (7).

1.21 Weight of the determining direction on a geometrical basis

In connection with the purely geometrical weights only a few comments should be made here.

The value of e_A is to be investigated on the basis of Eq. (11) for the length corrections and of Eq. (13) for the angular corrections, if the weights are the lengths of the determining directions, including the case without weights, too. According to Eq. (11).

$$e_A = \frac{p_B}{p_A + p_B} .$$

Let us now consider the following cases:

1. $p_A = \frac{1}{t_A}$ and $p_B = \frac{1}{t_B}$, i.e. $[p_i e_i e_i] = [\frac{1}{t_i} e_i e_i]$.

Thus
$$e_A = \frac{t_A}{t_A + t_B} s . \tag{14}$$

2. $p_A = \frac{1}{t_A^2}$ and $p_B = \frac{1}{t_B^2}$, i.e. $[p_i e_i e_i] = [\frac{1}{t_i^2} e_i e_i] = [v_i v_i]$.

In such a case
$$e_A = \frac{t_A^2}{t_A^2 + t_B^2} s . \tag{15}$$

3. Finally if, $p_A = p_B = 1$, i.e. $[p_i e_i e_i] = [e_i e_i]$

then
$$e_A = \frac{1}{2} s . \tag{16}$$

The following connections are valid among adjustments with length corrections and with angular corrections:

$$[p_i e_i e_i] = [e_i e_i] = [t_i^2 v_i v_i] \tag{17}$$

$$\left[\frac{1}{t_i} e_i e_i\right] = [t_i v_i v_i] \tag{18}$$

$$\left[\frac{1}{t_i^2} e_i e_i\right] = [v_i v_i] . \tag{19}$$

Thus Eq. (17) expresses the case of the length corrections without weights, Eq. (19) the case of angular corrections without weights, and Eq. (18) - as shown by Eq. (14) (Fig. 1) - corresponds to:

$$e_A = \frac{t_A}{t_A + t_B} s$$

that means

$$e_A t_A + e_A t_B = s\ t_A$$

$$t_A\ (s - e_A) = e_A t_B$$

finally

$$\frac{e_A}{t_A} = \frac{s - e_A}{t_B} = \frac{e_i}{t_i} = v \quad \text{(const.)} \tag{20}$$

That means that this adjustment results in a general case in equal angle corrections.

1.22 Direction weight depending on the reliability of the direction

The reliability of a direction used for the determination of a point depends generally on two factors. The first is the error of the coordinates of the station, the second is the angular uncertainty of the direction.

The former is given a priori and it is independent of the observer. The latter contains the uncertainty of the station and of the orientation points - i.e. of the pointed ones - and errors depending on the observer and on external conditions.

The weight of the direction is determined by the common effect of these factors. The cross-error due to the uncertainty of the direction can be computed.

The cross-error is written with the symbols of Fig. 2, as:

$$\Delta_e = \mu^2_{AK} + \mu^2_{Ai}\ t^2_A \tag{21}$$

where

$$\mu_{AK}^2 = \frac{\mu_{Ay}^2 + \mu_{Ax}^2}{2} \tag{22}$$

and μ_{Ai} is the mean square error of the direction AP, discussed in Section 11, and defined by Eqs (4) and (5) respectively.

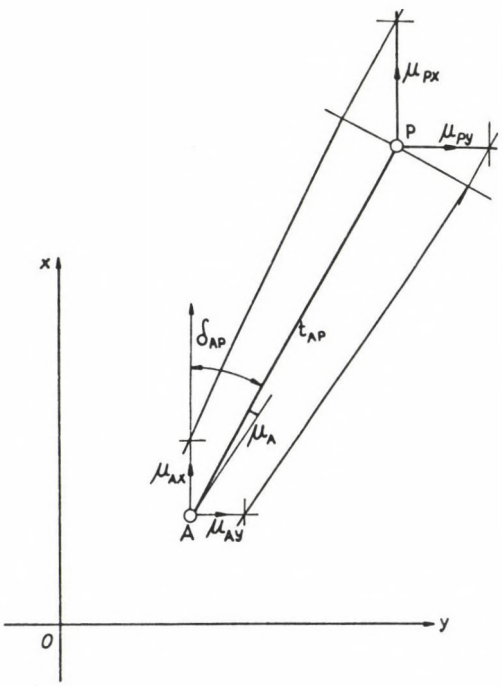

Fig. 2. Coordinate error of a polar point

Using the value of Δ_e, the expected resulting direction error can be computed as:

$$\Delta_v = \frac{\Delta_e}{t_A} . \tag{23}$$

Since the adjusted point location can be obtained by two kinds of corrections, two kinds of weights can be obtained,

too, according to the basis for the computation of the location of the point, i.e. by length corrections or by angular corrections.

The weight of the angular correction v_i is:

$$p_{vi} = \frac{1}{\Delta_v^2} = \frac{t_{AP}^2}{\mu_{AK}^2 + \mu_{Ai}^2 t_{AP}^2} \tag{24}$$

and the weight of the length correction e_i:

$$p_{ei} = \frac{1}{\Delta_e^2} = \frac{1}{\mu_{AK}^2 + \mu_{Ai}^2 t_{AP}^2} . \tag{25}$$

The first case corresponds to the determination of the point location by the minimum of $[p_{vi} v_i v_i]$, the second by the minimum of $[p_{ei} e_i e_i]$.

1.221 Weight of a direction in case of angular corrections

In this case Eq. (24) of the direction weight is in an algebraic system of coordinates:

$$y = \frac{x^2}{ax^2 + b} . \tag{26}$$

This is a second order fracture function which crosses the origin of the coordinate system and has as asymptote a line parallel with the X-axis at a distance of

$$y = \frac{1}{a} = \frac{1}{\mu_{Ai}^2} = p_{max}$$

(Fig. 3).

This curve has an inflexion point at

$$x_o \cong 0.6 \frac{1}{a}$$

and the weight curve has inflexion at

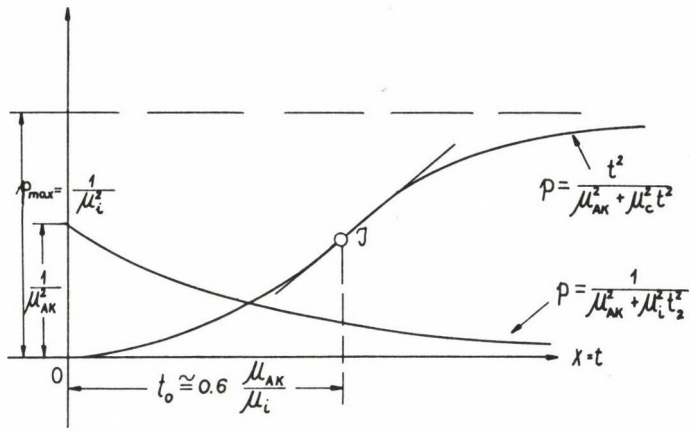

Fig. 3. Weight curves of the determining and orienting directions

$$t_o \cong 0.6\ \frac{1}{\mu_{Ai}^2}\ .$$

At last let us consider the case if the error of the station is neglected, i.e. it is supposed to be errorfree. In this case $\mu_{AK} = 0$, therefore the weight function has the form:

$$p_{AP} = \frac{t_{AP}^2}{\mu_{APi}^2 t_{AP}^2} = \frac{1}{\mu_{APi}^2} = p_{max}\ .$$

The weight of the directions, Eq. (24) can be used in the solution of the normal equations as follows:

$$p_i a_i a_i = 0.1^2\, \varrho''^2\, \frac{\cos^2 \delta_i}{\mu_{Ki}^2 + \mu_i^2 t_i^2} = \frac{0.1^2\, \varrho''^2}{\Delta_i^2} \cos^2 \delta_i$$

$$p_i b_i b_i = 0.1^2\, \varrho''^2\, \frac{\sin^2 \delta_i}{\mu_{Ki}^2 + \mu_i^2 t_i^2} = \frac{0.1^2\, \varrho''^2}{\Delta_i^2} \sin^2 \delta_i$$

$$p_i a_i b_i = -0.1^2 \varrho''^2 \frac{\sin^2 \delta_i \cos^2 \delta_i}{\mu_{Ki}^2 + \mu_i^2 t_i^2} = \frac{-0.1^2 \varrho''^2}{\Delta_i^2} \sin \delta_i \cos \delta_i$$

$$p_i a_i \omega_i = 0.1^2 \varrho''^2 \frac{t_i \cos \delta_i}{\mu_{Ki}^2 + \mu_i^2 t_i^2} \omega_i = \frac{0.1^2 \varrho''^2}{\Delta_i^2} (x_p - x_i) \omega_i$$

$$p_i b_i \omega_i = -0.1^2 \varrho''^2 \frac{t_i \sin \delta_i}{\mu_{Ki}^2 + \mu_i^2 t_i^2} \omega_i = \frac{-0.1^2 \varrho''^2}{\Delta_i^2} (y_p - y_i) \omega_i$$

where δ_i is the preliminary direction angle and

$$\omega_i = \delta_i - l_i \ .$$

The values Δ_i^2 are found in Table II.

Table II. Values Δ_i^2 in the weight formula

t_{km}	K			B			E		
	±2"	±3"	±5"	±3"	±5"	±7"	±5"	±7"	±10"
1	0.17	0.18	0.22	0.27	0.31	0.37	0.55	0.61	0.74
2	0.20	0.25	0.41	0.34	0.50	0.84	0.74	0.98	1.49
3	0.25	0.36	0.72	0.45	0.81	1.35	1.05	1.59	2.74
4	0.32	0.52	1.16	0.61	1.25	2.25	1.49	2.45	4.49
5	0.41	0.72	1.72	0.81	1.81	3.31	2.05	3.55	6.74
6	0.52	0.96	2.41	1.06	2.50	4.66	2.74	4.90	9.49

1.222 Direction weight in case of length corrections

Equation (25) is in an algebraic form:

$$y = \frac{1}{ax^2 + b}$$

and it intersects the Y-axis at

$$Y = \frac{1}{b}$$

that means at

$$p_{ei} = \frac{1}{\mu^2_{AK}}$$

and it approximates asymtotically the X-axis (Fig. 3).

2. WEIGHT OF A POINT

2.1 General aspects

If the semi-major and semi-minor axes of the error ellipse are denoted by a and b, the two conjugated semi-diameters by a_1 and b_1, further the errors of the coordinates of the determined point by μ_{Py} and μ_{Px}, then the following connections are valid for the mean coordinate errors:

$$\mu_{PK} = \frac{\mu^2_{Py} + \mu^2_{Px}}{2} = \frac{a^2 + b^2}{2} \qquad (27)$$

and according to Apollonius:

$$\frac{a^2 + b^2}{2} = \frac{a_1^2 + b_1^2}{2} = \mu^2_{PK} \; . \qquad (28)$$

Thus it is possible to determine the a priori point errors for the determining directions at least with an accuracy which is needed for the weights.

When knowing the expected average mean square errors of the coordinates, the weight of the point is expressed by:

$$p = \frac{1}{\mu^2_K} = \frac{2}{a^2 + b^2} = \frac{2}{a_1^2 + b_1^2} \; . \qquad (29)$$

If the weights are known, weighted algebraic means of the point coordinates computed in different combinations lead to the coordinates of the adjusted location of the point according to Jakobi's principle.

If the coordinates obtained in different combinations are $y_1, y_2, y_3, \ldots y_n$ and $x_1, x_2, x_3, \ldots x_n$, respectively, and the weights of these points are $p_1, p_2, p_3, \ldots p_n$, then the coordinates of the adjusted point can be computed as a weighted average as:

$$y_p = \frac{[py_i]}{[p_i]} \qquad \text{and} \qquad x_p = \frac{[p_i x_i]}{[p_i]} \,. \tag{30}$$

The weights of the points are after Jakobi:

$$p_{12} = \frac{\sin^2 \omega_{12}}{t_1^2 \, t_2^2} \,, \qquad p_{23} = \frac{\sin^2 \omega_{23}}{t_2^2 \, t_3^2} \,, \tag{31}$$

where $t_1, t_2, t_3, \ldots t_n$ are the lengths of the determining directions, and ω_{12}, ω_{23}, ... are the intersection angles of the directions 1-2, 2-3 ....

Jakobi's mean square error, Eq. (31) is, however, in no accordance with the weight of the point deduced from the mean square error of the point as accepted in geodesy. It is known namely that the mean square error of a point determined by two directions is:

$$M = \frac{[aa] + [bb]}{D} \mu_o \tag{32}$$

where μ_o is the mean square error of a measurement result and the other factors are in case of two directions the following:

$$[aa] + [bb] = \frac{1}{t_1^2} + \frac{1}{t_2^2} \tag{33}$$

and

$$D_{12} = \frac{\sin^2 \omega_{12}}{t_1^2 \, t_2^2} \tag{34}$$

respectively. Taking all these formulas into account one obtains:

$$M_{12}^2 = \frac{t_1^2 + t_2^2}{\sin^2 \omega_{12}} \mu_o \tag{35}$$

and from this, the weight of the point coordinates is in contrast to Jakobi's point weight given by Eq. (31), the following:

$$p_{12} = \frac{1}{\mu_{12}^2} = \frac{\sin^2 \omega_{12}}{\mu_o^2 t_1^2 + \mu_o^2 t_2^2} . \tag{36}$$

It should be mentioned here that Hazay's static adjustment (1938) is supported by the fact that the sum $[p \lambda\lambda]$ is fully analogous with the second order intertial moment.

The system of forces p_1, p_2, ... p_n consists of the forces in the plane of Fig. 4 being parallel with each other; the resultant force P is in a distance of l_P from an arbitrary straight line 0 - 0 and the distances of the forces from the same line are l_1, l_2, ... l_n. In case of an equilibrium it is evidently:

$$[l_i P_i] = l_P [P_i]$$

and the location of the resultant is:

$$l_P = \frac{[l_i P]}{[P_i]} . \tag{37}$$

Let us denote the distance of the forces from the resultant by:

$$\lambda_1 = l_P - l_1, \quad \lambda_2 = l_P - l_2, \ \ldots \ \lambda_n = l_P - l_n .$$

Supposing that these distances λ_i are corrections, it can be written formally in accordance with the principle of least squares, as a second order equation of moment:

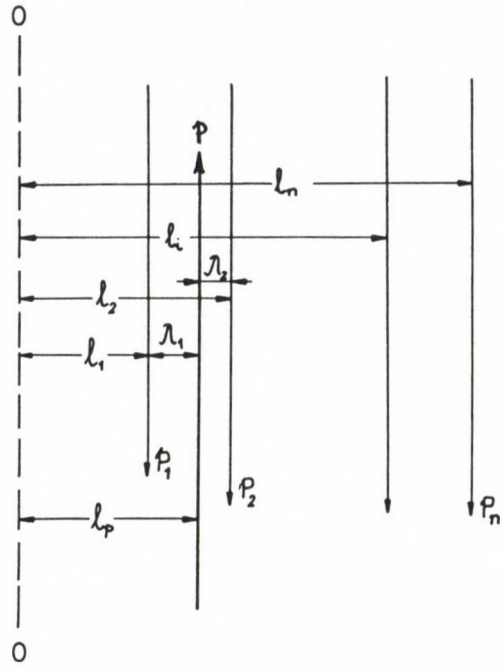

Fig. 4. Weight factors as forces

$$[P\lambda\lambda] = P_1(l_P-l_1)^2 + P_2(l_P-l_2)^2 + \ldots + P_n(l_P-l_n)^2 .$$

After simplification one gets the general form:

$$[P\lambda\lambda] = [P_i l_P^2] - 2[P_i l_i l_P] + [l_i P_i] . \qquad (38)$$

The minimum of Eq. (38) is

$$d[P\lambda\lambda] = 2[P_i]l_P - 2[P_i l_i] = 0$$

and

$$l_P = \frac{[P_i l_i]}{[P_i]}$$

as

$$\frac{d^2[P\lambda\lambda]}{[d^2 l_P]} = 2[P_i] > 0 \ .$$

This formula corresponds to that obtained from the static coordinate adjustment.

2.2 Basic cases of the horizontal point determination

The determination of the coordinates of horizontal control points can be reduced to the following cases:

1. Measurement of direction and length from a single known point
2. Measurement of direction from two known points (intersection by directions)
3. Distance measurement from two known points (intersection by lengths).

In the practice combinations of these methods occur, too, or the same method can also be repeated several times. Thus traverses can be supposed as repeated utilization of the first method, triangulation as that of the second, and trilateration as that of the third, at least from the point of view of the present investigation. All the three methods have, however, in common that they fulfil an elementary condition as follows:

For the determination of an unknown point in an arbitrary system of coordinates at least one control point, the distance of two points and the direction of the line between them are necessary.

This condition is fulfilled in a direct way by the first method. In case of the other ones, two control points are needed, and the distance (in case of intersection by directions) - or the direction (in case of intersection by lengths) is indirectly obtained.

2.21 The weight of the point in case of point determinations by direction and distance measurements

In the present case the coordinates of the station are given and the direction of the line to point P to be determined

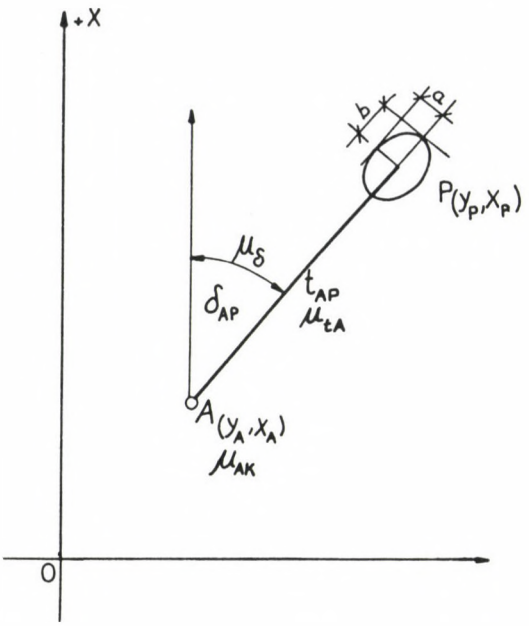

Fig. 5. Error ellipse of a polar point

as well as the distance AP are known (Fig. 5). The coordinates of point P to be determined are then:

$$y_P = y_A + t_{AP} \sin \delta_{AP}$$
$$x_P = x_A + t_{AP} \cos \delta_{AP} \tag{39}$$

and the errors of the coordinates are:

$$\mu_{Py}^2 = \mu_{Ay}^2 + \mu_T^2 \sin^2 \delta_{AP} + \mu_i^2 t_{AP}^2 \cos^2 \delta_{AP}$$
$$\mu_{Px}^2 = \mu_{Ax}^2 + \mu_T^2 \cos^2 \delta_{AP} + \mu_i^2 t_{AP}^2 \sin^2 \delta_{AP} \tag{40}$$

where μ_{Ay} and μ_{Ax} are the coordinate errors of the control point, μ_i is the error of the direction and μ_T the error of the distance t_{AP}.

Thus the mean coordinate error of the point is:

$$\mu^2_{PK} = \frac{\mu^2_{Py} + \mu^2_{Px}}{2} = \frac{\mu^2_{Ay} + \mu^2_{Ax} + \mu^2_T + \mu_i t_{AP}}{2} \qquad (41)$$

Let us introduce the mean coordinate error

$$\mu^2_{AK} = \frac{\mu^2_{Ay} + \mu^2_{Ax}}{2}$$

in case of point A, too, and the error of the distance be deduced from the error of the unit length μ_c, thus if

$$\mu_T = \mu_o t_{AP}$$

then Eq. (41) can be written as:

$$\mu^2_{PK} = \frac{2\mu^2_{AK} + \mu^2_o t^2_{AP} + \mu^2_i t^2_{AP}}{2} . \qquad (42)$$

The nominator of the fracture can be split into two parts in the following form:

$$\mu^2_{PK} = \frac{a^2 + b^2}{2}$$

where

$$a^2 = \mu^2_{AK} + \mu^2_i t^2_{AP} \qquad \text{and} \qquad b^2 = \mu^2_{AK} + \mu^2_o t^2_{AP} . \qquad (43)$$

The values a and b in Eq. (43) are evidently the components of the point error perpendicular to the direction AP and parallel with it, respectively, and these are the semi-major and semi-minor axes of the error ellipse of point P.

The weight of point P is then:

$$p_P = \frac{1}{\mu^2_{PK}} = \frac{2}{2\mu^2_{AK} + \mu^2_i t^2_{AP} + \mu^2_o t^2_{AP}} . \qquad (44)$$

2.22 Weight of a point determined by direction intersection

In the present case the unknown point P is determined by

direction measurements at two known points, A and B as the intersection of two oriented directions (Fig. 6).

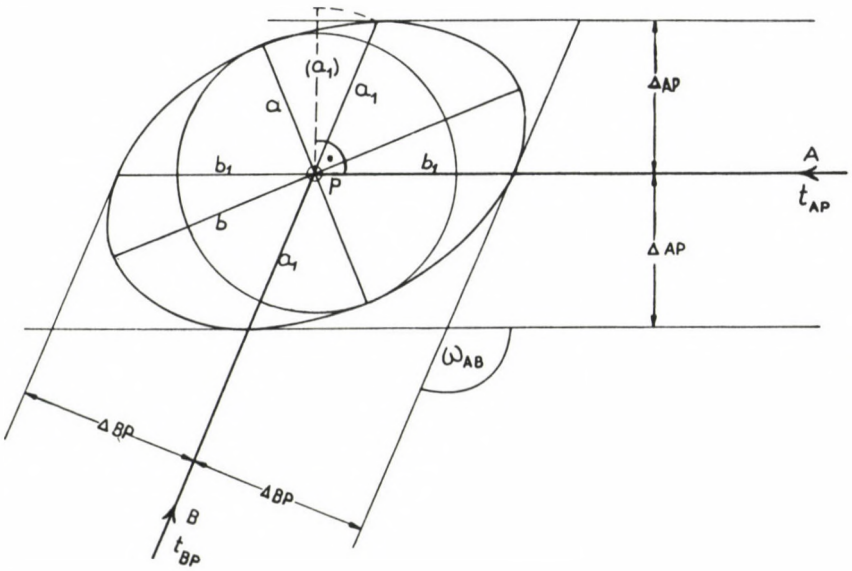

Fig. 6. Error ellipse of a point determined by direction intersection

It is characteristic for this method of the point determination that the angular error of the two directions separately causes a distance error in the other direction and these two distance errors give at the same time a conjugated pair of diameters of the error ellipse in point P.

The cross-error caused by the determining directions is with the symbols of Fig. 6 the following:

$$\mu_{AP} = \sqrt{\mu_{AK}^2 + \mu_{APi}^2 t_{AP}^2}$$
$$\mu_{BP} = \sqrt{\mu_{BK}^2 + \mu_{BPi}^2 t_{BP}^2} \qquad (45)$$

where μ_{AK} and μ_{BK} are the mean coordinate errors of the control points, further μ_{APi} and μ_{BPi} are the angular mean square errors of the determining directions. From the cross-errors in Eq. (1) a conjugated pair of diameters of the error ellipse can be expressed:

$$a_1 = \frac{\mu_{AP}}{\sin\omega_{AB}} \qquad \text{and} \qquad b_1 = \frac{\mu_{BP}}{\sin\omega_{AB}} . \tag{46}$$

According to Eq. (28) in Section 2.1:

$$\frac{a_1^2 + b_1^2}{2} = \frac{a^2 + b^2}{2} = \mu_{PK}^2$$

therefore the weight of the point is:

$$p_P = \frac{1}{\mu_{PK}^2} = \frac{2\sin^2\omega_{AB}}{\mu_{AP}^2 + \mu_{BP}^2} = \frac{2\sin^2\omega_{AB}}{\Delta_A^2 + \Delta_B^2} \tag{47}$$

where

$$\Delta_A^2 = \mu_{AK}^2 + \mu_{APi}^2 t_{AP}^2 \qquad \text{and} \qquad \Delta_B^2 = \mu_{BK}^2 + \mu_{BPi}^2 t_{BP}^2 . \tag{48}$$

The values in Eq. (48) can be taken from Table II.

If the control points are considered as errorfree, then:

$$p_P = \frac{2\sin^2\omega_{AB}}{\mu_{APi}^2 t_{AP}^2 + \mu_{BPi}^2 t_{BP}^2} \tag{49}$$

further if the directions are considered as of the same accuracy i.e. if:

$$\mu_{APi} = \mu_{BPi} = \mu_i$$

then the weight of the point is as follows:

$$p_P = \frac{2 \sin^2 \omega_{AB}}{\mu_i^2 (t_{AP}^2 + t_{BP}^2)} \cdot \qquad (50)$$

2.23 The weight of a point determined by distance intersection

In case of this point determination the unknown point P is obtained by two distance measurements from two control points, essentially as the intersection of two circles (Fig. 7).

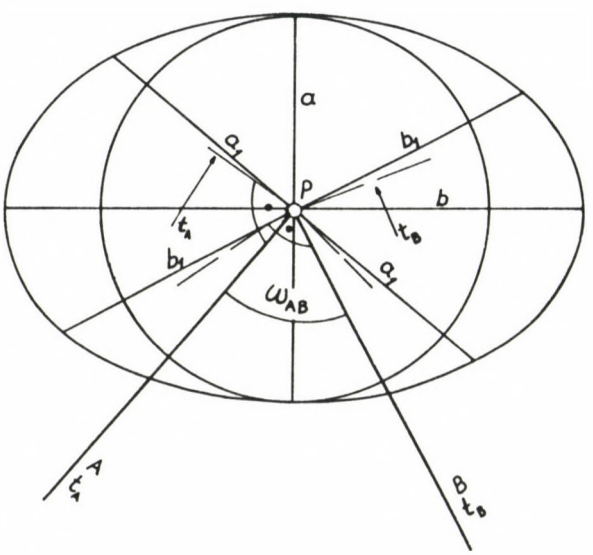

Fig. 7. Error ellipse of a point determined by distance intersection

In this case two conjugated diameters of the error ellipse fit to circular arcs through point P - and due to the big radius and to the small lengths of the arcs - to straight lines being perpendicular to the directions, respectively. In this case a distance error in one of the lengths causes a direction error in the other direction and vice versa.

The full distance error of the leg is then the following:

$$\mu_{AP} = \sqrt{\mu_{AK}^2 + \mu_{HA}^2 t_A^2}$$

and (51)

$$\mu_{BP} = \sqrt{\mu_{BK}^2 + \mu_{HB}^2 t_B^2}.$$

The values μ_{AK} and μ_{BK} below the root are the mean coordinate errors of the control points, μ_{HA} and μ_{HB} are the measurement errors of the distances.

The conjugated semi-diameters are the following:

$$a_1 = \frac{\mu_{AP}}{\sin \omega_{AB}}$$

and (52)

$$b_1 = \frac{\mu_{BP}}{\sin \omega_{AB}}$$

where ω_{AB} is the angle between the two directions.

Thus the mean coordinate error of point P is:

$$PK = \sqrt{\frac{\mu_{AK}^2 + \mu_{HA}^2 t_{AP}^2 + \mu_{BK}^2 + \mu_{HB}^2 t_{BP}^2}{2 \sin^2 \omega_{AB}}}. \quad (53)$$

and the weight of point P:

$$p_P = \frac{1}{\mu_{PK}^2} = \frac{2 \sin^2 \omega_{AB}}{\mu_{AK}^2 + \mu_{hA}^2 t_{AP}^2 + \mu_{BK}^2 + \mu_{hB}^2 t_{BP}^2}. \quad (54)$$

If the control points are considered as errorfree and distance measurements as of equal accuracy, i.e. if

$$\mu_{hA} = \mu_{hB} = \mu_H$$

then the weight of the point is:

$$p_P = \frac{2 \sin^2 \omega_{AB}}{\mu_H^2 (t_{AP}^2 + t_{BP}^2)} \quad (55)$$

3. SUMMARY OF THE RESULTS

The investigations presented in this paper include two parts. The first part deals with direction weights, the second with point weights, in both cases with the new idea that weights are deduced from a priori error estimates. Results obtained so are compared with present methods of weighting.

The results about direction weights can be summarized as follows.

The weight of an orienting direction is:

$$p_{AB} = \frac{t_{AB}^2}{\mu_{AK}^2 + \mu_{BK}^2} . \tag{56}$$

The weight of a determining direction with angular correction:

$$p_{AP} = \frac{t_{AP}^2}{\mu_{AK}^2 + \mu_{Ai}^2 t_{AP}^2} . \tag{57}$$

The weight of a determining direction with distance correction:

$$p_{AP} = \frac{1}{\mu_{AK}^2 + \mu_{Ai}^2 t_{AP}^2} . \tag{58}$$

Figure 8 shows the curves of the direction weights in the two cases supposing that in the one case the mean coordinate error of the station is ± 0.05 cm, in the other case ± 0.15 cm. The error of the direction is in the same cases ± 10 and ± 15 seconds of arc, respectively. The weight curve without taking these errors into account is also shown:

$$p_{AP} = \frac{1}{\mu_{AP}^2} . \tag{59}$$

The figure shows that in the latter case the error is represented by a single line, while in case of the consequent

application of the reliability parameters the weight can be anywhere in an area between the two curves. This weight reflects the reality closer, as it is influenced not only by the geometry, but also by the reliability of the network and of the measurements.

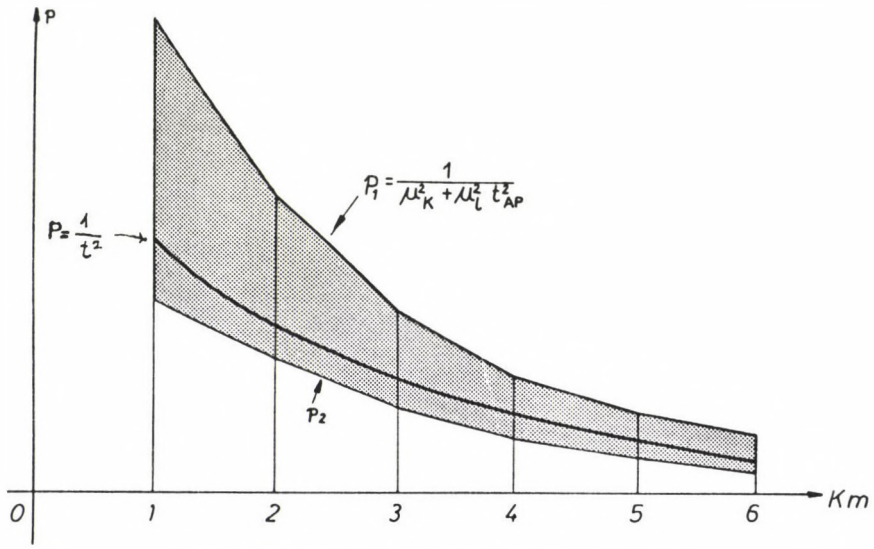

Fig. 8. Curves of the weight factors

The weight of the point is also the reciprocal square of the a priori point mean square error and of the mean coordinate error, respectively - the latter can be advantageously used here. One has then:

Weight of a polar point:

$$p_P = \frac{1}{2\mu_{AK}^2 + \mu_{APi}^2 t_{AP}^2 + \mu_o^2 t_{AP}^2} . \tag{60}$$

Weight of a point from intersection by directions:

$$p_P = \frac{2 \sin^2 \omega_{AB}}{\mu_{AK}^2 + \mu_{APi}^2 t_{AP}^2 + \mu_{BK}^2 + \mu_{BPi}^2 t_{BP}^2} . \tag{61}$$

Weight of a point from intersection by distances:

$$p_P = \frac{2 \sin^2 \omega_{AB}}{\mu_{AK}^2 + \mu_A^2 t_{AP}^2 + \mu_{BK}^2 t_{BP}^2 + \mu_{BK}^2} \quad (62)$$

Hazay (1958) gave the weight of a point, deduced from the mean square error M determined by two directions:

$$p_P = \frac{1}{M^2} = \frac{\sin^2 \omega_{AB}}{\mu_c (t_A^2 + t_B^2)} \quad (63)$$

and Jakobi's point weight:

$$p_P = \frac{\sin^2 \omega_{AB}}{t_A^2 t_B^2} \quad (64)$$

Both formulas have the common disadvantage that - among others - the coordinate errors of the control points do not appear in them.

Finally, it is to be remarked that the formulas for the point weight show clearly the uniformity of these point determinations. This uniformity is proved by the fact that for the determination of a point in each case two basic points and two directions and distances, respectively, are necessary. Even the polar determination of a point is no exception from this rule, as though here one has only one control point, but it appears in two roles, first in the angle measurement, then in the distance measurement (that is why the factor $2\mu_{AK}$ appears in the denominator of the expression).

Further it can be supposed that here one has two directions, too, the second imaginary one intersecting the first one perpendicularly (and the factor $\sin^2 \omega_{AB}$ does not appear in the denominator only as it is equal 1).

The independence of the elements can be supposed in operations connected with the mean square errors, but it was not necessary to investigate them, as the deduced mean square errors are used only for the determination of the weights and it is sufficient to ensure the correct ratio of the weight factors.

That is why the approximation is allowed that the reliability of the different points has been qualified uniformly in point types.

REFERENCES

Hazay I 1938a: Adjustment in the practice of geodesy (in Hungarian). Budapest

Hazay I 1938b: Adjustment of coordinates on a static principle (in Hungarian). Budapest

Hazay I 1959: Mechanic principle of adjustment (in Hungarian). Geod. és Kart., 1, 2.

Homoródi L 1956: Error ellipse and point error (in Hungarian). Geod. és Kart., 1.

Acta Geod. Geoph. Mont. Hung., Vol. 25 (3-4), pp. 443-451 (1990)

ELECTROMAGNETIC STUDIES IN THE TEST-FIELD AT FRUNZE

I. ON THE RELATIONSHIP BETWEEN RESISTIVITY VARIATIONS, DEFORMATION PROCESSES AND EARTHQUAKES

V D Bragin, E P Velikhov, A M Volikhin, V A Zeigarnik, N A Koshkin, Y A Trapeznikov, G G Tchelochkov

Institute of High Temperatures, USSR Academy of Sciences, 127412 Moscow, Izhorskaya 13/19, USSR

[Manuscript received May 16, 1989]

In the paper some results of the electromagnetic studies obtained in a test field near Frunze are presented. Time variations of resistivity records are shown to be related first of all to deformational processes. Active deformations in the uppermost section are not always accompanied by earthquakes. Prior to earthquakes low-frequency resistivity decrease was observed at sites close to the epicentre.

Keywords: earthquake prediction; electromagnetic sounding; MHD-generator; test-field at Frunze

INTRODUCTION

Electromagnetic methods by using artificial current sources have been extensively used for earthquake prediction at a number of test-fields in the Soviet Union (Barsukov 1970, Avagimov et al. 1984, Shanotko et al. 1986, Yakovenko 1958). One such place is the "Frunze" test-field, lying within the Northern Tien Shan seismogenic region at a distance 30 km south of Frunze the capital of Kirghizia. Powerful current sources such as MHD-generator and current impulse generating systems are used there. Besides resistivity measurements the horizontal movements of the upper crust are studied by using laser distance meters; variations of the total geomagnetic vector, the radon concentration in the soil, air and the inclination are also observed. Seismological observations are carried out by the Seismological Institute of the Kirghiz Academy of Sciences. In this area, at the Geophysical Observatory of the Seismological Institute various complex observations, including strain and inclination measurements are carried out. In

addition, several other institutions measure the groundwater level fluctuations in boreholes and the vertical movements of the ground surface. There are several hydrometeorological stations at the investigated area, too.

Owing to wide variety of methods involved it is possible to analyze the complex data set, taking into account possible hydrometeorological and hydrogeological effects.

Electromagnetic studies at the test-field were initiated in 1982. Nowadays a large volume of experimental data is available, which would be the subject of future publications.

Our paper deals with several characteristics of rock resistivity changes, recorded during 1986-1987. They provide evidence of their possible relation to deformation and earthquake generation process.

ELECTROMAGNETIC RESULTS

Among variety of electromagnetic methods involved frequency sounding (FS) is the most significant. Current sources are the MHD-generator "Pamir 2" ("hot shot") and the capacity banks of the MHD primary excitation system ("cold shot"). The duration of the "hot" impulse is 10 sec, the current amplitude is up to 2.6 kA. "Cold" one's duration is 0.4 sec, and the current amplitude reaches 5 kA. The load is an electric dipole having a length of 4.2 km and an electric resistance of 0.4 Ohm. The "hot" operation is made once in a month; the "cold" one several times a day. Besides these two systems, soundings are made also by using an electric impulse generating system, supplied with electric power lines. This third system is able to supply into the current dipole a series of heteropolar impulses of controlled duration, having an amplitude of 800 A.

Resistivity variations are recorded at 5 permanent stations and several other sites, equipped with portable measuring instrumentation. The number of temporary measuring sites and their position depend on the type of survey used. Figure 1 shows the arrangement of the current dipole and the measuring sites during 1986-1987.

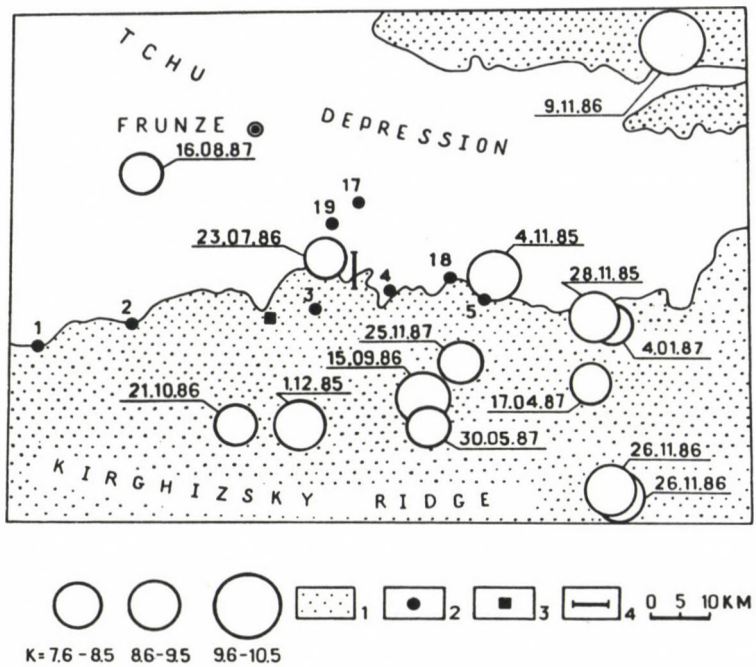

Fig. 1. Electromagnetic network in the Test-Field at Frunze. Earthquake epicentres, indicated by circles, are based on data of the Seismological Institute of the Kirghiz Academy of Sciences (KAS). 1. Premesozoic basement outcrop; 2. observational sites; 3. Geophysical Observatory, Seismological Institute, KAS; 4. current dipole

Electric dipoles oriented meridionally with a length from several hundred meters to one kilometer were used as receivers. The current in the current dipole and the voltage in the receiving dipoles are measured by means of specially-designed digital instruments.

In this paper the variational pattern at site 3, 11 km south-west ward from the current dipole is discussed. Resistivity curves are demonstrated in Fig. 2. The resistivity measurement error can be estimated from Fig. 3, which shows "2σ" changes in percents versus frequency. According to Fig. 3 within the frequency range 1-8 Hz the value 2σ does not exceed 2 p.c. of ϱ_a, and in the range 0.1-1 Hz and 9-10 Hz - 3 p.c. of ϱ_a.

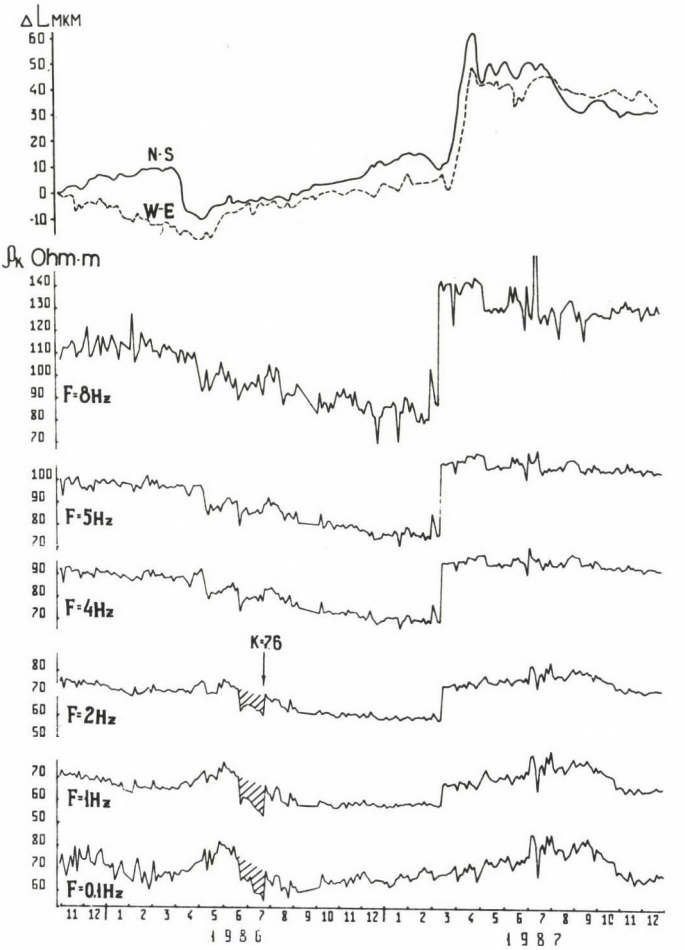

Fig. 2. ΔL deformations recorded at the Observatory [μm] and ρ_a resistivity records observed at several different frequencies at site 3

Resistivity variations at site 3 are characterized by a sudden increase within the frequency range 1-10 Hz, recorded in March, 1987. It was preceeded by a long-term resistivity decrease. The sharpest resistivity increases are observed at high frequencies, and its amplitude decreases with the frequency. It was apparently induced by a certain process in the upper section, propagating downward.

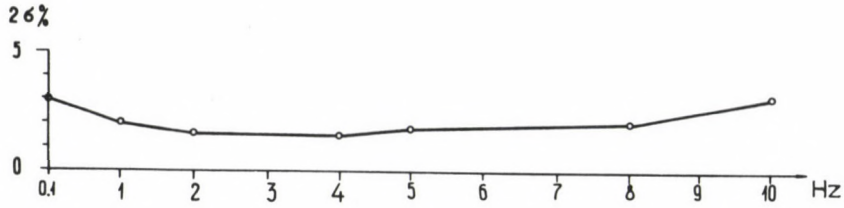

Fig. 3. Resistivity measurement error 2 δ vs. frequency at site 3

At the same time no significant seismic activity was observed. The earthquake intensity in energetic scale ($K = \lg E \cdot J$) was not higher than 9-10. According to Fig. 1 (with exception of an earthquake K = 7.6 July 23, 1986) all other earthquakes were at a considerable distance from site 3. The number of earthquakes increased toward the end of 1985, 1986. The step-like resistivity increase was observed during a seismic gap, and it was not accompanied by hydrometeorological and groundwater anomalies.

The results of deformational and inclination observations in a geophysical observatory 10 km westward from site 3 were published by the Seismological Institute of the Kirghiz Academy of Sciences (Yakovenko 1988). Strain was measured by means of a rod strain meter (RS) having a base of 30 m, placed in an adit. The deformational curves for March and April 1987 shown in Fig. 2 indicate a sharp change in the ground surface deformation which is accompanied by high amplitude inclination changes. These subsurface deformational changes were observed simultaneously with the step-like resistivity increase at site 3. It is assumed that the same deformational changes are responsible for both phenomena. Hence, from curves in Fig. 2 it is evident, that

- as the resistivity variations are caused by deformational changes, resistivity records at various frequencies help to follow the propagation of the deformation with depth;
- deformational changes in the Observatory reflect the deformational processes in the uppermost section;
- extrapolation of deformational changes to greater depths is

impossible without certain additional measurements, in particular without electromagnetic soundings;
- for earthquake predictions it must be taken into account that the very active deformational changes in the uppermost section are not accompanied by earthquakes. Simultaneous anomalies of different geophysical and geodetical parameters, related to local deformations are sometimes erroneously connected with distant earthquakes;
- prognostic abilities of shallow-depth soundings, e.g. vertical electromagnetic soundings are limited.

It is necessary to mention one further characteristic of resistivity records at site 3. In June 1986, at lower frequencies, first of all at 1-2 Hz, the resistivity decreased by 15-30 p.c. (the parameter 2δ was only 2 p.c.), and by the end of July the resistivity returned to its initial level. The ground surface deformation did not have any anomalous behaviour, which refers to the deep origin of the resistivity anomaly. This resistivity anomaly was observed prior the event July 23, 1986 (K = 7.6) between site 3 and the current dipole. The resistivity records were not influenced by earthquakes at greater distances. Figure 4 shows the time evolution of the resistivity variation as a function of frequency. As it can be seen, the resistivity began to decrease in the middle of June at first at frequencies 1-2 Hz and later it extended toward lower frequencies. Above 4 Hz the variations remain isnignificant. By July 20 the resistivity value at 1 Hz decreased from 70 Ohm·m to 50 Ohm·m, i.e. almost by 30 p.c. Immediately after the earthquake a sharp resistivity increase was recorded.

For comparison, in Fig. 5 a time evolution based on diurnal data, recorded at site 3 every hour during the seismic gap is shown.

Similar resistivity variations were observed only at site 19, located to the north-west of the current dipole. In that case, the earthquake epicentre was also between the current and the receiving dipoles. At site 19 only DC resistivity variations were measured by using an electrical impulse generating system as a current source. The resistivity measurement error at this site was about ±1.6 p.c. The resistivity record is

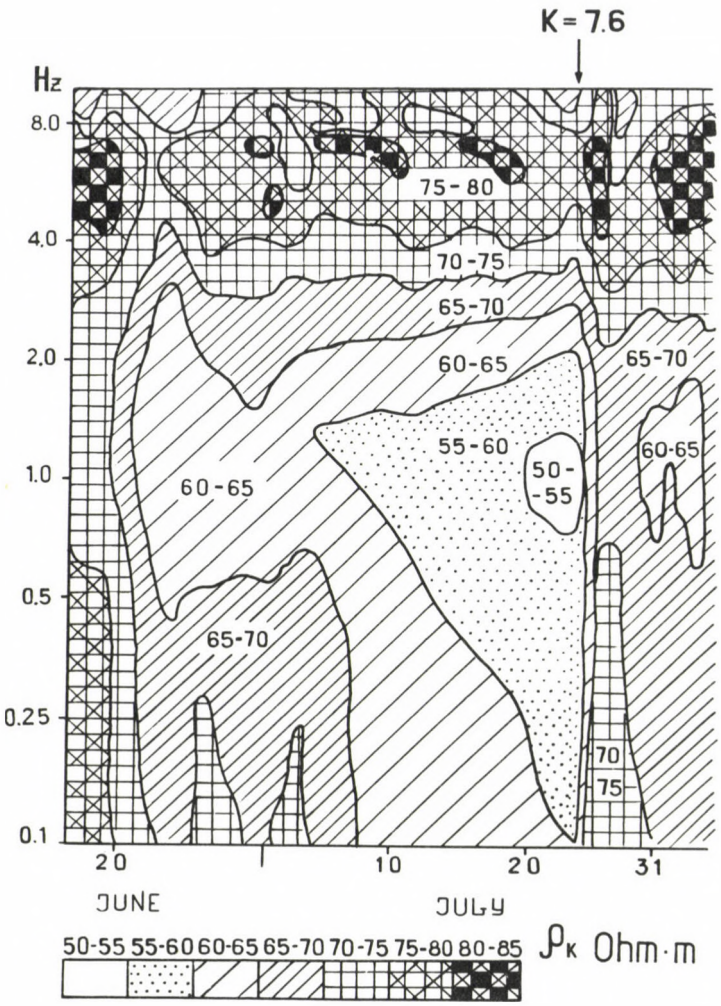

Fig. 4. Time-evolution of resistivity variations at site 3 in June and July 1986, on basis of frequency sounding results. The seismic moment of the event July 23, 1986 is shown by arrow

shown in Fig. 6. Before the earthquake a resistivity increase and then a rapid resistivity decrease was observed. After the seismic event the resistivity values returned to their initial level.

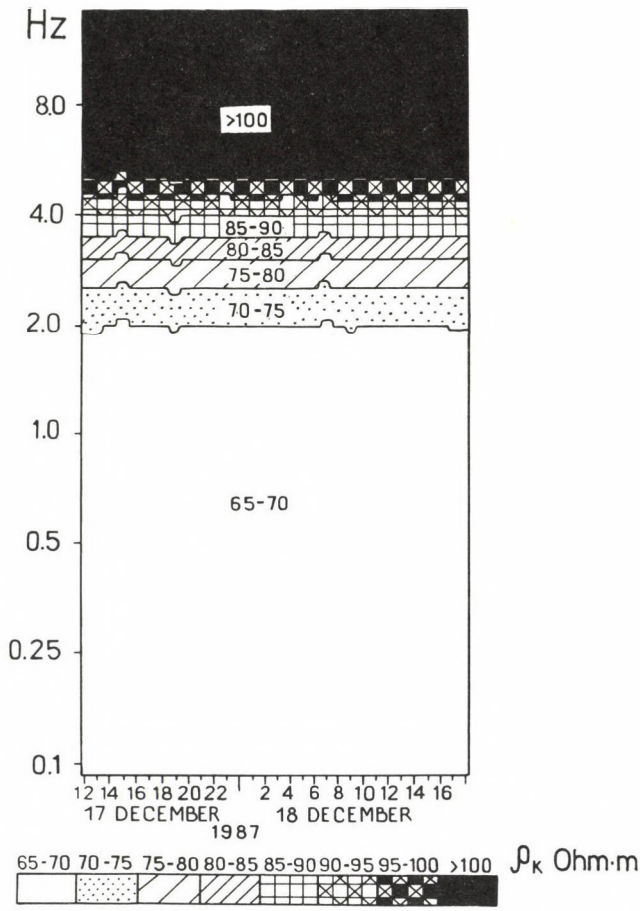

Fig. 5. Resistivity-time-evolution of frequency sounding results on basis of diurnal data at site 3 recorded with a sampling time of one hour during a seismic gap

SUMMARY

Resistivity variations of similar pattern and amplitude were observed only at sites 3 and 19, which are the closest to the epicentre of the event July 23, 1986. It is assumed that they are induced by deformation processes resulting in this earthquake. Their appearance at lower frequencies refers to their deep origin and the fact that they were observed only at

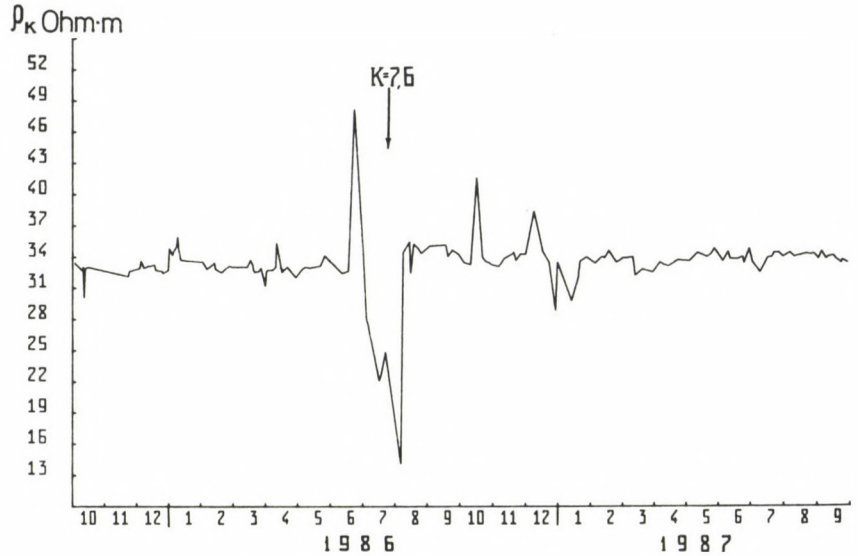

Fig. 6. Resistivity variations based on direct current measurements at site 19. Seismic moments of the event July 23, 1986, K-7,6 are indicated by an arrow

3 and 19 supports their local character. In this case it is assumed that resistivity decrease at sites 3 and 19 was a result of some activity, taking place to the west of current dipole, i.e. close to the epicentre.

REFERENCES

Avagimov A A, Atayev A K, Suhomlin 1984: Izv. of the Tadzhik Acad. of Sci., Series Phys.-Techn., Chem. and Geol. Sci., 4, 64-70.

Barsukov O M 1970: Izv. AN SSSR, Fizika Zemli, I, 84-89.

Sidorin A Y 1986: Dokl. AN SSSR, 290, I. 81-84.

Shamotko V I, Sapuzhak Y S, Markovich B L 1986: In: Recent geodynamic processes and their relation with earthquake-prediction. Kiev, Naukova Dumka, 11-17.

Yakovenko V S 1988: In: Geological structure and seismicity of the test-fields at Toktogul and Frunze. Materials of the International Aero and Cosmic Experiment "Tien-Shan-Intercosmos-88". Frunze, Ilim, 82-85.

Acta Geod. Geoph. Mont. Hung., Vol. 25 (3-4), pp. 453-458 (1990)

ANALYTICAL RELATIVE ORIENTATION WITH ROBUST ESTIMATION

J Kalmár

Geodetic and Geophysical Research Institute of the Hungarian Academy of Sciences, H-9401 Sopron, POB 5, Hungary

[Manuscript received January 13, 1989]

The least squares method yields an unbiased (linear) estimation with minimum scatter if the distribution of the measurement results is normal. This method has gained popularity due to its comfortable use and wide field of application. The weights enable us to introduce a priori information into the processing, thus open new ways for improving the results. Investigations carried out in recent years confirmed a setback of the method, namely that if the distribution of the errors differs slightly from the normal one, the results deviate from the optimum ones, even more if the measurement results contain outliners. For the elimination of these disadvantages several robust estimation methods have been developed.

Keywords: analytical orientation; Hampel's estimation; Huber's estimation; robust estimation

Robust methods include two big groups: the first group uses Lp ($1 \leqslant p \leqslant 2$) norm in the adjustment (the least squares method, as L2-norm, belongs to this group, too). The second group contains estimations of the maximum likelihood type (the least squares method can be included in this group, too, as it yields the maximum likelihood estimation of a random variable with normal distribution). The latter group contains the different weighting algorithms, too, one of them is the Danish method when a weighted least squares adjustment is made in each step and weights are derived from the deviations in the previous iteration step (initial weights have naturally the value 1). The weight function is to be determined separately for each adjustment problem, i.e. no "ideal", always valid weight function exists (Kubik et al. 1987).

The present paper describes a programme for the robust adjustment of analytic relative orientation based on Huber's

(1964) and Hampel's (1973) estimation theories. The estimations are of the maximum likelihood type as the target functions can be essentially considered as the inverse of the logarithm likelihood function of a certain type of random distributions.

The target functions are the following:

Huber's method:

$$\phi(\underline{v}) = \begin{cases} v_i/2 & \text{if } |v_i| < a \\ a\,(|v_i| - a/2) & \text{else.} \end{cases}$$

Hampel's method:

$$\phi(\underline{v}) = \begin{cases} v_i^2/2 & \text{if } |v_i| < a \\ a\,(|v_i| - a/2) & \text{if } a \leqslant |v_i| < b \\ a\,[(c - |v_i|)^2/(b-c) + (b+c-a)]/2 & \text{if } b \leqslant |v_i| < c \\ a\,(b+c-a)/2 & \text{else.} \end{cases}$$

A solution based on the minimum condition $\Sigma\, \phi(v_i)$ is looked for being equivalent to the solution of:

$$\Sigma\, \phi(v_i)/\, \partial t_j = 0, \quad j = 1, \ldots$$ (with $\underline{t}$ as the parameter vector needed).

If the error function $\underline{v}(\underline{t})$ is linear (or it can be made linear) i.e. if $\underline{v} = A\underline{t} - 1$, then condition for zero partial derivates yields a linear system of equations having the form $B\underline{t} = \underline{d}$, where $B = A^T P\, A$ and P is a diagonal weight matrix in which

$$p_{ii} = \begin{cases} 1 & \text{if } |v_i| < a \\ a/(b-c) & \text{if } b \leqslant |v_i| < c \\ 0 & \text{else} \end{cases}$$

and $\underline{d} = A^T P\, \underline{1} - a\, A^T Q\, \text{sign}\, \underline{v}$,
where Q is a further diagonal weight matrix in which

$$q_{ii} = \begin{cases} 1 & \text{if } a \leqslant |v_i| < b \\ c/(c-b) & \text{if } b \leqslant |v_i| < c \\ 0 & \text{else.} \end{cases}$$

The formulas refer to Hampel's estimation, but Huber's method is a special case ($b = c = \infty$) of it. The formulas contain as special case the least squares method, too, as in that case $a = b = c = \infty$, thus $B = A^TA$, $\underline{d} = A^T \underline{l}$. Some further, theoretically interesting cases can be deduced from Hampel's method by selecting appropriate limits of the intervals a, b, c. For example $a = b = c$ gives a robust estimation if "good" measurements are adjusted according to the least squares method, "bad" ones are simply omitted. The cases $a = b$ or $b = c$ correspond to the deletion of the relevant row in the target function. The computation of the robust Hampel estimation is most advantageously started with the parameters $b = 2a$, $c = 2b$, and the value of the parameter a depends on the actual task to be solved (in the relative orientation e.g. a parallax error of $a = 10\ \mu$ has been used).

Due to rapid development of the technical aids (digital data processing, remote sensing, computer technics), analytic photogrammetry gets more and more important in the interpretation of aerial and space images. With the increase of the work and with the spread of automatization, the necessity for filtering gross errors gets imperative. The use of robust estimates in geodesy has been discussed several times (Borre et al. 1983, Carusio 1982, Somogyi and Kalmár 1988), in this paper a robust solution is given for the analytic relative orientation.

The mathematical principles of analytic relative orientation are summarized after Somogyi (1966). Be x, y the coordinates of a point P on the left photo (with the origin in the main principal point of the image) and x', y' are the coordinates of the same point on the right-side photo. If the origins are shifted to the projection centres and the coordinate system of the right-side photo is rotated into parallel position with that of the left-side photo, then the image coordinates are in this system:

$$\begin{matrix} x \\ y \\ z \end{matrix} = \begin{matrix} x \\ y \\ f \end{matrix} \qquad \begin{matrix} x' \\ y' \\ z' \end{matrix} = H \begin{matrix} x' \\ y' \\ f' \end{matrix}$$

where f is the camera constant (focal distance), and H the rotation matrix. If the rotation angles of the axes are ω, φ and $\varkappa$, then (supposing small angles) the rotation matrix has the form:

$$H = \begin{matrix} 1 & -\varkappa & \varphi \\ \varkappa & 1 & -\omega \\ -\varphi & \omega & 1 \end{matrix} .$$

If the coordinates of the projection centre of the right-side image are in a coordinate system coinciding with the projection centre of the right-side photo b_x, b_y, b_z then according to the condition of complanarity:

$$b_x (yz'-y'z) + b_y (x'z-xz') + b_z (xy'-yx') = 0 .$$

Supposing that b_x is known, b_y, b_z and the orientation parameters as approximately known (they are to be corrected), the correction equations are from a linearization of the previous system of equations:

$$\begin{aligned} &[b_x (yy'+zz') + b_y (-xy') + b_z (-xz')] \Delta \omega + \\ &[b_x (-yx') + b_y (xx'+zz') + b_z (-yz')] \Delta \varphi + \\ &[b_x (-zx') + b_y (-zy') + b_z (xx'+yy')] \Delta \varkappa + \\ &(zx'-xz') \Delta b_y + (xy'-yx') \Delta b_z + \\ &b_x (yz'-y'z) + b_y (zx'-xz') + b_z (xy'-x'y) = 0 \end{aligned}$$

where the initial values for b_y, b_z, ω, φ and $\varkappa$ are supposed to be zero.

Using five points for fitting, corrections can be computed from these equations for the orientation parameters, in case of more than five points, an adjustment is to be carried out for the determination of the orientation parameters. A few initial steps are made with the traditional least squares method as

long as approximate orientation parameters reach the necessary accuracy. After that, the robust estimation is used for the elimination of gross errors. The parameter vector

$$t = \langle \Delta\omega, \Delta\varphi, \Delta x, \Delta b_y \Delta b_z \rangle^T$$

is to be substituted into the general formulas of the robust estimation, the row vectors of matrix A contain the coefficients of the correction equations, the column vector $\underline{l}$ contains the free terms of the equations (condition of complanarity).

The efficiency of robust estimations is shown by a numerical example (Table I). The table contains the image coordinates

Table I. A Numerical example

Identifier	Left side photo image		Right side photo image		Parallax		
	x	y	x	y	L2	Hampel	Huber
Image main point	119.534	120.668	120.312	121.817			
9114	23.184	188.647	106.366	192.821	-5	0	1
9113	24.441	97.611	107.472	101.502	1	-4	0
9033	25.236	37.405	107.909	41.024	3	-2	0
9032	79.021	73.574	162.23	77.162	-17	-24	-20
9031	116.425	120.199	200.163	123.863	-2	-9	-4
9030	138.327	169.47	222.285	173.299	4	1	4
9039	64.565	170.136	147.917	174.13	15	15	17
341	107.023	23.741	190.451	26.865	5	-3	1
331	117.225	225.452	201.159	229.566	-5	1	-1

of the points and the parallax errors after adjustments with different methods. The table does not contain the computed model coordinates as in the comparison of the different methods they do not give new information. The data of the example are not simulated ones, the accuracy of the measurements was $\pm$ 2 μ.

Robust estimations enhance the errors in points 9032 and 9039 and the effect of the gross errors is less felt in the stable points. Huber's method is the most stable one, but Hampel's method seems also to be more advantageous than the least squares method. The effectivity of the different methods cannot be judged from a single example, as on the one hand the choice of the limits a, b, c influences significantly the results, on the other correct proof could be obtained from a statistical sample when the measurement errors are produced e.g. by Monte Carlo-simulation. Nevertheless, the advantage of the robust estimation is shown by this example, too.

REFERENCES

Borre K, Jorgensen P C, Kubik K 1983: Scientific Bulletins of the Stanislaw Staszic University of Mining and Metallurgy, Cracow, 57-69.

Carusio A 1982: Vermessung, Photogrammetrie, Kulturtechnik, 6, 196-200.

Hahn M: Comparison of Different Methods and Strategies for Detecting Outliers in Data. Manuscript.

Hampel F R 1973: Robust Estimation. Z. Wahrscheinlichkeitstheorie Verw. Geb., 27, 87-104.

Huber P J 1964: Robust Estimation of a Location Parameter. The Annals of Mathematical Statistics

Kubik K, Merchant D, Schenk T 1987: Photogrammetric Engineering and Remote Sensing, 53, 167-169.

Somogyi J 1966: Theory and practice of analytical aerotriangulation (in Hungarian). Dissertation

Somogyi J, Kalmár J 1988: AVN, No. 4, 141-146.

Werner H 1984: Automatic Gross Error Detection by Robust Estimators, Presented Paper to Comission III. 15th ISPRS Congress, Rio de Janeiro

BOOK REVIEWS

E BAUMANN: Vermessungskunde. Lehr- und Übungsbuch für Ingenieure. Band 1-2. Dümmler-Verlag, Bonn, 1988, 1989. 213 pp. 121 figs, 269 pp, 154 figs

This book is a revised and extended edition of the textbook from 1986 following the up-to-date claims. It gives a basic description of the problems of surveying. Volume 1 contains 12 chapters with the following topics:

Chapter 1 gives a brief view about the surveying.
Chapter 2 summarizes the basis of surveying.
Chapter 3 describes the direct distance measurement.
Chapter 4 deals with the angle measurement.
Chapter 5 treats the setting out problems.
Chapter 6 deals with planimetric survey.
Chapter 7 summarizes the computations connected to the measurements.
Chapter 8 deals with the calculation of areas.
Chapter 9 treats the setting out of circular curves.
Chapter 10 summarizes the problem of error theory.
Chapter 11 describes the levelling methods.
Chapter 12 deals with the ground surveying.

Volume 2 contains 10 chapters with the following topics:

Chapter 13 gives a brief description about linear adjustment.
Chapter 14 treats the angle and direction measurements.
Chapter 15 deals with optical distance measurements.
Chapter 16 gives a review about the tacheometric survey.
Chapter 17 describes the electronic distance measurements.
Chapter 18 deals with indirect measurements.
Chapter 19 treats the traverses.
Chapter 20 summarizes the trigonometric heighting.
Chapter 21 treats the tracing with clothoide.
Chapter 22 summarizes the two dimensional transformation.
Chapter 23 gives a brief view of the point determination by trilateration and triangulation.

The book is clearly written and will help all geodesists both who are young and practitioners.

J Somogyi

T J BLACHUT and R BURKHARD: Historical Development of Photogrammetric Methods and Instruments. American Society for Photogrammetry and Remote Sensing, 1989. 157 pp, 84 figs, 8 tables

This book deals with the history of the development of the photogrammetric discipline. The knowledge of the past is very important for the future. Many of the historical details are contained in old publications of various languages. This book summarizes the history of photogrammetry.

Chapter 1 deals with the early days of photogrammetry, prior to the application of airplanes.

Chapter 2 gives a very comprehensive overview of analogue methods and instruments.

J Somogyi

E GROTEN, R STRAUSS eds: GPS-Techniques Applied to Geodesy and Surveying. Lecture Notes in Earth Sciences 19. Springer-Verlag, Berlin, Heidelberg, 1988. 532 pp, 163 figs, 106 tables

This book contains the proceedings of the International GPS-Workshop Darmstadt, April 10 to 13, 1988. The articles join the following sessions:
1. General Aspects
2. Application of GPS
3. GPS-Campaigns
4. Kinematic Applications
5. Software
6. Geodynamics
7. Special Applications and Orbits

Session 1 contains 4 lectures with the following topics: Geodetic Applications with GPS, GPS Geodesy with Centimeter Accuracy, Relativistic Effects in GPS.

Session 2 collects 5 lectures about the different applications of GPS.

12 lectures deal with the GPS campaigns. The session Kinematic Applications comprises 9 lectures with the following topics: Status of Dual Frequency GPS Development, Kinematic Surveying.

The session Software collects 4 lectures with different program developments.

The session Geodynamics give 5 lectures about the geodynamical applications.

The session Special Applications and Orbits contains 6 lectures with the topics of Determination of Azimuths from GPS. European Tracking Network. World Geodetic System.

At the end of the book one can find a brief summary of the panel discussion and the recommendations.

The book is an up-to-date work and gives a useful help to the readers involved in these subjects.

J Somogyi

S HEITZ: Coordinates in Geodesy. Springer-Verlag, Berlin, Heidelberg, New York, London, Paris, Tokyo, 1988. 255 pp, 20 figs

The points of the earth's surface are represented in earth-fixed three-dimensional coordinate systems, so they play an important role in the geodesy. This kind of coordinate systems are generally related to a reference surface, which roughly represents equipotential surfaces near the earth's surface. The book deals with the geometric principles of the coordinates of this coordinate systems.

Chapter 1 as introduction gives a general view about the regional and global representation of point fields of the earth surface in three dimensional curvilinear coordinates.

Chapter 2 deals with the general fundamentals of surface coordinates. The definition and construction of surface coordinate systems are the fundamental problems in the theory of surfaces therefore it is presented

the bases of this theory.

Chapter 3 deals with the application of power series representing the transformation equations between surface coordinates. It gives a review on constructing surface coordinates, representing power series and transformation between different geodetic coordinates and arbitrary surface coordinates.

Surface coordinates on ellipsoids of revolution are dealt with in Chapter 4. Beside a description of the general principles, nearly all the interesting possibilities for application in practical geodetic surveying are included.

Chapter 5 deals with three-dimensional coordinates in Euclidean spaces, first in general form, then specialized to surface-normal coordinates.

Finally the book ends by references and index.

The book is an English translation of the original German edition Koordinaten auf geodaetischen Bezugsflaechen with certain changes.

The book is an op-to-date, well compiled, clearly written work. It gives useful help to scientists who are interested in this problem.

J Somogyi

H M KARARA ed.-in-Chief: Non-Topographic Photogrammetry. American Society for Photogrammetry and Remote Sensing, second edition 1989. 445 pp, 457 figs, 17 plates, 16 tables

This book is the first in the new "Science and Engineering Series" from the American Society for Photogrammetry and Remote Sensing. As compared to the first edition (1979) the scope is greatly expanded, reflecting many new devices and techniques developed since 1979.

Chapter 1 (author: H M Karara) gives a short introduction to non-topographic photogrammetry.

Chapter 2 (author: E M Mikhail) deals with metrology concepts.

Chapter 3 (author: K B Atkinson) summarizes the instrumentation for non-topographic photogrammetry.

Chapter 4 (author: J C McGlone) includes the analytic data-reduction schemes in non-topographic photogrammetry.

Chapter 5 (author: J G Fryger) is focussed on problems of camera calibration.

Chapter 6 (author: W Faig) deals with non-metric and semi-metric cameras: data reduction.

Chapter 7 (author: K J Torlegard) treats the theory of image coordinate errors.

The topic of Chapter 8 (author: C S Fraser) is the optimalization of networks in non-topographic photogrammetry.

Chapter 9 (author: V Kratky) deals with on-line non-topographic photogrammetry.

Chapter 10 (author: H Ruther) gives an overview of software.

Chapter 11 (author: I Newton) summarizes the problems of underwater photogrammetry.

Chapter 12 (author: S A Veres) treats the X-ray photogrammetry, systems and applications.

Chapter 13 (author: S K Ghosh) gives a detailed description of electron microscopy: systems and applications.

Chapter 14 (author: R J Pryputniewitz) deals with hologrammetry: systems and applications.

Chapter 15 (co-authors: J R Pekelsky, M C Van Wijk) gives a brief account on Moire topography: systems and applications.

Chapter 16 (author: E Hierholzer) treats the raster photogrammetry.

Chapter 17 (co-authors: S F El-Hakim, A Bruner and R R Real) deals with video technology and real-time photogrammetry.

Chapter 18 (author: G R Robertson) collects the problems of ultrasonic technology: systems and applications.

Chapter 19 (author: M Carbonnel) gives a survey of architectural photogrammetry.

Chapter 20 (author: L P Adams) deals with industrial photogrammetry.

Chapter 21 (co-authors: D B Sheffer and R Eitterron) gives a brief view about biostereometrics.

Chapter 22 (author: D C Brown) analyses the emerging trends in non-topographic photogrammetry.

Chapter 23 (author: W Wester-Ehlinghaus) discusses the trends in non-topographic photogrammetrie systems.

Appendix A (co-authors: J Whitnall, F H Moffit) treats the reverse projection technique in forensic photogrammetry.

Appendix B (co-authors: J R Pekelsky, M C Van Wijk) gives a detailed analysis of Moire topography: systems and applications.

The text book is a clearly edited up-to-date work. One can find detailed bibliography and reference at the end of the chapters.

J Somogyi

I I MUELLER, S ZERBINI eds: The Interdisciplinary Role of Space Geodesy. Springer-Verlag, Berlin, Heidelberg, New York, London, Paris, Tokyo, Hongkong, 1988. 300 pp, 51 figs, 27 tables

This book is Vol. 22 of Lecture Notes in Earth Sciences and collects the proceedings of an International Workshop held at International School of Geodesy, Italy, July 23-29, 1988.

The purpose of the workshop was to recommend geodetic and geomagnetic programs and missions, and the development of methods and instrumentation for their implementation. The lectures have been grouped under the next main topics.

Chapter 1 Introduction gives a brief summary of the Earth's rotation and core-mantle interaction, mantle convection, regional tectonics and earthquakes, ocean dynamics and Venus-Earth differences.

Chapter 2 Short-Term Dynamics of the Solid Earth includes the following themes. Precession and nutation, polar motion, axial rate of spin of the earth, earth tides and time variation in the gravity field.

Chapter 3 deals with the Long-Term Dynamics of the Solid Earth involving the following topics. Implication of precise positioning, gravity and geoid, topography and bathymetry.

Chapter 4 Interaction with other disciplines and programs includes geodynamics, earth structure, ocean physics, atmosphere and climate, extension to the planets and fundamental physics.

Chapter 5 summarizes the instrumentation related to the problems. There are discussed the scientific and measurement requirements, laser ranging techniques, microwave techniques, topographic mapping techniques, potential field measurement systems, data management systems, conclusions and recommendations.

Chapter 6 collects the problem of data analysis.

Chapter 7 deals with the Reference Coordinate Systems. One can read

about Conventional Inertial Systems (CIS), Conventional Terrestrial Systems (CTS), Reference Frame Ties, Reference Frame Requirements.

Chapter 8 gives short information about education.

At the end of the book the appendices contain useful information. Among others information about the Earth Observation Activities of the European Space Agency, role of NASA in geodynamics research, the Glonass Satelite Navigation System, space geodesy in France, the Lageos II program and the Wegener programme.

Every chapter ends with references. It is well compiled and gives a useful help to scientists who are interested in the problems of different areas of geosciences.

J Somogyi

Photogrammetry. Volume 1. Baltimore, Maryland, April 2-7, 243 pp, 74 figs, 45 tables

This book is the first volume of the Proceedings of the Technical Sessions of the 1989 Annual Convention of the American Society for Photogrammetry and Remote Sensing and the American Congress on Surveying and Mapping held in Baltimore, Maryland.

The book collects the papers presented on photogrammetry.

There are 8 papers on the topic of photogrammetric systems, among others a PC based version of the planicomp analytical plotter, a modern analytical stereoplotter integrated in a GIS, digital monoplotting.

The second topic was focussed on the problem of photogrammetric control extensions. There are several papers on the problem of robust estimation.

The third topic dealt with close range photogrammetry focussed on engineering problems.

Some papers dealt with general information, data processing and ACID deposition.

The proceedings are well-edited and the papers refer to very actual problems.

J Somogyi

Image Data Processing. Volume 2. Baltimore, Maryland. 171 pp, 76 figs, 14 tables

This book is the second Proceedings of the Technical Sessions of the 1989 Annual Convention of the American Society for Photogrammetry and Remote Sensing and the American Congress on Surveying and Mapping held in Baltimore, Maryland.

The book collects the papers on image data processing with the following topic:

A) Spatial Processing and Applications
B) Image Transforms
C) Data Display
D) Computer Aided Mapping
E) Digital Imaging Systems.

The collected 16 papers deal with the actual problems of image data

processing and could be very useful who are interested on this topic.

J Somogyi

Remote Sensing. Volume 3. Baltimore, Maryland, April 2-7, 437 pp, 129 figs, 59 tables

The book is the third volume of the Proceedings of the Technical Session of the 1989 Annual Convention of the American Society for Photogrammetry and Remote Sensing and the American Congress on Surveying and Mapping held in Baltimore, Maryland.

This volume contains the papers dealing with remote sensing divided into the following topics:

I. Ground Processing with 11 papers
II. Plant Sciences with 7 papers
III. Environmental Management with 3 papers
IV. Thermal Infrared: History and Application with 7 papers
V. Knowledge Based Expert Systems with 4 papers
VI. Coastal Environments with 7 papers
VII. Geology and Engineering with 5 papers.

The Proceedings give a very informative summary about the remote sensing problems in USA.

J Somogyi

GIS/LIS. Volume 4. Baltimore, Maryland, April 2-7. 292 pp, 75 figs, 22 tables

The book is the fourth volume of the Proceedings of the Technical Session of the 1989 Annual Convention of the American Society for Photogrammetry and Remote Sensing and the American Congress on Surveying and Mapping held in Baltimore, Maryland. It collects the papers dealing with Geographic Information Systems and Land Information Systems. The reader gets information about the GIS techniques and applications, GIS/LIS and geodetic control, GIS development designs, data structures and data bases, GIS/LIS in the military, a LIS network joint partnership between local, state, regional and federal governments and the private sector, and about the Land Informations Systems.

The proceedings contain 39 papers from the listed topics.

J Somogyi

Surveying and Cartography. Volume 5. Baltimore, Maryland, April 2-7, 369 pp, 64 figs, 43 tables

The book is the fifth volume of the Proceedings of the Technical Session of the 1989 Annual Convention of the American Society for Photogrammetry and Remote Sensing and the American Congress on Surveying and Mapping held in Baltimore, Maryland. The topics of the papers are the following:

1. Training, Education and Privatization: A Look at the Agenda for the 90's.
2. AM/FM Automated Mapping-Facilities Management

3. Cartography and Artificial Intelligence
4. Multipurpose Cadastral Systems
5. Cartography, Mapping and Graphics in Transition
6. The Proposed Digital Cartographic Data Standard and Results of Testing
7. Engineering, Land Surveys and Adjustments
8. Transportation Surveys
9. Workshop: Understanding Modern Total Station use
10. Recent Results in the Mapping Sciences at the Ohio State University
11. Charting the Coast and Coastal Waters
12. Concerns of the Legal Profession in regard to Surveying Procedures, Practices and Standards.

The proceedings contain 56 papers from the listed topics. The papers deal with very interesting up-to-date geodetic problems.

J Somogyi

Auto-Carto 9, Proceedings, Ninth International Symposium on Computer-Assisted Cartography. Baltimore, Maryland, April 2-7. Sponsored by American Society for Photogrammetry and Remote Sensing, American Congress on Surveying and Mapping. 1989. 879 pp, 280 figs, 44 tables

This book contains papers from the Ninth International Symposium on Computer-Assisted Cartography held in Baltimore, Maryland.

The topic of the papers are the following: Advanced Data Display, Data Bases, GIS Education and Training, Generalization, Data Structures and Parallel Processing, Data Structures and Post-Processing for Digital Terrain, Topics in GIS and Automated Cartography, AGIS Curriculum for Universities, Automated Names Placement, Digital Terrain, GIS Design: Examing the Alternatives, Algorithms, Three Dimensional GIS, Data Capture Techniques, Environmental Applications of GIS, Data Structures and Spatial Query Techniques, Structuring Large Spatial Data Bases, GIS Applications, International Perspectives, Quality Control Issues, Spatial Relations and Data Base Models, Object-Oriented Approaches to GIS, Educational Tools for GIS, Challenges for the Future, Automated Mapping Applications, Standards and Their Use, GIS: Direction for the Future, GIS Performance, System Design, AM/FM and GIS, Displays for Spatial Data.

In the last few years the GIS has played a very important role in geo-sciences. The Proceedings summarize the present day situation and gives a very useful help to people who are working in this field.

J Somogyi

NAVGRAV Navigation and Gravimetric Experiment at the North Sea. Netherlands Geodetic Commission. Publication on Geodesy. New Series, Number 32, 1988. 135 pp, 83 figs, 8 tables

The publication contains five papers which summarize the results of test measurements. The experiment was carried out with the aim of getting accurate gravity information at sea. Gravity measurements at sea are not too easy. It is complicated to separate the disturbing effects from measurements while moving. Modern gravitymeters largely eliminate these disturbances, however, there remains an effect that cannot be eliminated instrumentally, the Eötvös correction. It can only be determined if very

precise navigation is available. With the Global Positioning System (GPS), precise navigation became feasible.

J Somogyi

W H CAMPBELL ed.: Quiet Day Geomagnetic Fields. Reprinted from Pure and Applied Geophysics, Vol. 131, No. 3. Birkhäuser, Basel, 1989, 230 pp, many figs

Birkhäuser has continued with this book a most valuable series of reprints from Pure and Applied Geophysics. These volumes cover some smaller fields of geophysics which can thoroughly discussed in a collection of papers like this. Quiet day geomagnetic field has been a favourite for geomagnetic research in the first half of this century, as many techniques developed for analysis (e.g. spherical harmonics, Fourier transform, special methods for lunar variations etc.) could be very well exercised on this problem. In spite of the very detailed investigations, many questions remained open, not to mention else then the day-to-day variability of the focus position at low-latitudes. Thus it was really time to summarize recent results in this field and as the volume shows it was worth summarizing.

After a historic introduction (W Campbell), the selection criteria of quiet days is discussed by Jocelyn and Hruska & Hruska. These papers show that the selection is far from being unambiguous. Spherical harmonic analysis methods are treated by Kawasaki, Matsushita and Cain.

Polar region Sq problems are the topic of papers by Xu and Kroehl. They summarize current ideas on the different components of Sq in polar regions which have special significance in connection with the interplanetary magnetic field.

Mid-latitude Sq problems start with Richmond's review on modeling the ionosphere with wind dynamo, then Fukushima discusses the effect of the dawn-to-dusk electric field in the magnetosphere through the day/night asymmetry on the Sq-field. Olson presents a paper on the contribution of magnetospheric currents to Sq. Butcher deduces the abnormal Sq from small amplitude substorms appearing at times outside the normal maximum range of Sq. This interpretation may be partly valid, but if one looks at his figure (p. 464) one asks if the decrease of the Sq-amplitude is also caused by this substorm? And if not, what is the cause for the change of the Sq amplitude from one day to the other? Or what is the cause for the change of the focus position? I think that some other influence should be added to the small substorm.

The equatorial electrojet is discussed by Reddy and by Onwumechili & Ozoemena. As last topics, lunar daily variations are treated in three papers by Xu, Tschu and Winch. In the case of the last paper, the very illustrative representation of the lunar variation, more exactly of its effect on the solar Sq and the separation of the 27-day solar rotation from the lunar daily variation are of special interest.

This book gives a complete and uptodate review on problems connected to Sq and thus it deserves attention of all who are interested in geomagnetism and magnetospheric physics.

J Verő

H HÖLDER: Kurze Geschichte der Geologie und Paläontologie. Ein Lesebuch. Springer, Berlin, 244 pp, 39 figs

This is a most interesting book on the history of geology and paleontology, but it is also worth reading for other geoscientists and even for a wider circle of interested people. The author has chosen an ingenuous method to present different chapters from the broad field of geology: he starts from a problem which is crucial for the understanding of the process or situation, then it traces the later history evolving from the given problem. Such central problems are Glossopteri, shark teeth which opened the way for the correct organic interpretation of fossils; the "Greifensteine" in the Saxonian Ore Mts which were supposed witnesses of the deluge, and later initiated detailed investigations on the origin of granite; the basaltic cone of the Scheibenberg which played a central role in the discussions about the origin of basalt; Goethe's ideas on the origin of trapp-basalts; faults near Lake Vierwaldstätter, starting point for the discovery of tectonic events; Escher von der Linth's observation on the Glarn overthrust; Glen Roads, a place where the glaciation in Europe became evident; salt domes in Northern Germany, as example of a non-volcanic intrusion; Wegener's fitting of the shorelines of Africa and America as the starting point of plate tectonics; the Nördlinger Ries, one of the first meteoric craters found on the Earth - to list only a few of the many stories told in the book, in most cases accompanied by original texts, fulfilling what is promised in the title "Lesebuch". Witty and ingenious drawings, mostly from original sources help the understanding of the text, and even add in many cases to the joy of reading.

J Verő

Scattering and Attenuation of Seismic Waves
Part I, KEIITI AKI and RU-SHAN WU eds, Reprint from Pure and Applied Geophysics (PAGEOPH), Vol. 128, No. 1/2, 1988. 447 pp, 168 figs, 16 tables
Part II, RU-SHAN WU and KEIITI AKI eds, Reprint from Pure and Applied Geophysics (PAGEOPH), Vol. 131, No. 4, 1989. 551-739 pp, 53 figs, 6 tables
Part III, RU-SHAN WU and KEIITI AKI eds, Reprint from Pure and Applied Geophysics (PAGEOPH), Vol. 132, No. 1/2, 1990. 437 pp, 170 figs, 26 tables
Birkhäuser Verlag, Basel, Boston, Berlin

The interest of geophysicists in seismic wave scattering and attenuation has grown rapidly. This reflects the broad applications and great potential of this field for many geophysical problems, such as the lithospheric and mantle heterogeneities, identification and monitoring underground nuclear explosions, oil and mineral exploration, earthquake prediction and hazard. The three-volume special issue of PAGEOPH entitled "Scattering and attenuation of seismic waves" contains a total of 18 invited review papers and 28 contributed papers, all the contributed papers in volumes I and III most of the review papers in volume II.

The special issue covers a wide range of the field of seismic scattering and attenuation. They include:

- elastic wave perturbation theory and methods for weak scattering
- time domain and space domain multiple scattering theory
- high frequency asymptotic and approximate theory and methods
- crack and wedge scattering
- coda generation, coda envelope decay and coda Q (including local and regional phases)

- phase and amplitude fluctuations of transmitted waves
- scattering from the core-mantle boundary
- 1-D scattering and the stratigraphic filtering
- array processing and polarization analysis
- numerical simulation of seismic scattering
- laboratory model experiment on seismic scattering
- wave scattering in composite media and the effective parameters
- crack scattering and the effective anisotropy
- scattering and nonlinearity
- scattering attenuation and the separation from intrinsic attenuation
- laboratory Q measurements of rock samples
- anelastic attenuation mechanism
- elastic medium full-wave inversion theory (including attenuation)
- travel time and amplitude inversion.

Gy Szeidovitz

K R KOCH: Parameter Estimation and Hypothesis Testing in Linear Models. Springer Verlag, Berlin, Heidelberg, New York, London, Paris, Tokyo, 1988, 378 pp, 17 figs

This is the English translation of the author's book published in German by Dümmlers Verlag, 1987.

In Chapter 1 (Vector and Matrix Algebra) and Chapter 2 (Probability, Theory) introductory knowledge is discussed rather clearly and at the same time exactly.

In Chapter 3 the parameter estimation in linear models based on the method of least squares and maximum-likelihood is treated. The author gives definition of the Gauss-Markoff model with full rank and presents a numerical computation of the estimates and their covariances. He gives the relationships of the best linear unbiased estimation in a Gauss-Markoff model with constraints.

The establishment of the Gauss-Markoff model not of full rank, just as the completion of this with linear constraints makes complete the treatment of this theme.

Especially, the application of the Gauss-Markoff theory is demonstrated on the example of polynomial interpolation.

If the unknown parameters are considered as random variables in a Gauss-Markoff model then generalized linear models are obtained which go over in special cases into regression models. If the error vector in the Gauss-Markoff model is interpreted by linear combination, then one becomes the mixed model which contains the Gauss-Helmert model, in particular.

In this chapter the fundamental formulas of the estimation of variance and covariance components are given in the case of the best invariant quadratic unbiased estimation and of locally best estimation.

In course of the multivariate parameter estimation it is dealt with the multivariate Gauss-Markoff model. We find the estimation of the vectors of parameters and their covariance matrix.

The title of Chapter 4 is: Hypothesis testing, interval estimation and test for outliers in the Gauss-Markoff model. In connection with this chapter I cannot contest my subjectivity, my interest was totally captivated by it. The observations can be grossly falsified by outliers. Our task is to find and eliminate false observations, in order to estimate the parameters without distortion. I should like to emphasize the statistical test of the author for one outlier and the percentage points of

the outliers.

In Chapter 5 the discriminant analysis is dealt with if the observations belong to different populations. The goal is to classify the observations. The author discusses the Bayes strategy and gives the classifier algorithms based on the normal distribution with known and unknown parameters. The book is closed with rich references and contains an index for the search of the frequently occurring ideas.

Recently more books have been published on the field of the adjustment. However, I recommend this book to a serious researcher or aspirant, I hold it for the best suitable subject-matter to study a powerful topic, further to master deep technics.

Structure, clear style and correct draft of the book make private learning possible. The book surely counts on wide interest among students, engineers, and researchers, too.

J Závoti

S MEIER and W KELLER: Geostatistics. Introduction to the theory of random processes. Akademie Verlag, Berlin, 1990, 206 pp, 34 figs (in German)

There has been available a rather small number of books on random processes that deal with both one-dimensional and multi-dimensional processes accessible for practising geophysicists. The present volume is an introductory work for not only geophysicists and space researchers but readers from other fields. Examples are from at least two geosciences.

To read the book, the usual basic knowledge in analysis, mathematics and mathematical statistics are assumed.

The first chapter outlines the topic of random processes in geosciences as well as a historical reflexion.

The second chapter assembles the necessary matematical tools for the remaining part (distributions, correlations, special functions and transformations etc.). With these means it is possible to describe one--dimensional random processes (Chapter 3) e.g. stationary processes, band filters. More important for use are the processes in the Euclidean space and those on the sphere (Chapter 4).

The discussed special problems concerning Markoff processes and partial differential equations are of special interest e.g. the statistical derivation of the heat convection equation or that of Wiener's equation.

The last chapter is about the statistics of random processes. The concept of ergodicity, signal reconstruction from digital samples and distinguishing signal and noise are useful for all practising specialists.

The main text is completed with an appendix of the discussed models.

The structure of the text is logical, the rather mathematical approach subtracts nothing from its usefulness. The book gives a clear, brief insight into nature and application.

T Steiner

R A PLUMB and R A VINCENT eds: Middle Atmosphere. Birkhäuser, Basel, 1989, 616 pp, SFR 74

This volume contains papers presented at workshops held consecutively at the University of Adelaide in May 1987 and published now as a special issue of PAGEOPH (Pure and Applied Geophysics). The articles deal with the

results of investigations carried out in the framework of the MAP (Middle Atmosphere Program) subprograms GRATMAP (Gravity Waves and Turbulence) and MASH (Middle Atmosphere of the Southern Hemisphere). Thus, the volume can be considered as an up-to-date picture of our knowledge concerning these two important areas of the dynamics of the stratosphere and mesosphere.

The series of papers is introduced by a retrospect by C O Hines in which the history of gravity wave research is outlined. In the paper by H R Phillpot some early radiosonde temperature observations in the Antarctic lower stratosphere are discussed in connection with the springtime warming, which was more regular in 1959 similarly to the years 1985 and 1986. A stratospheric circulation statistics for the Southern Hemisphere including mean fields, transient eddy statistics, Eliassen-Palm flux diagnostics and vorticity fields is presented by D J Karoly. W L Grose and A O'Neill compare data of different satellites and quantities derived from them for the middle atmosphere of the Southern Hemisphere finding substantial quantitative differences in fields of Eliassen-Palm flux divergence and Ertel's potential vorticity. In the paper of D G Andrews the zonal-mean climatological state, stationary and transient waves of different types, stratospheric warmings and polar ozon minima in the Southern and Northern Hemispheres are compared. The seasonal cycle of stratospheric planetary waves is discussed by R A Plumb showing that contrary to the Northern Hemisphere, in the Southern Hemisphere there is a midwinter minimum due to the opacity to stationary wave propagation caused by strong westerlies. The body force circulation problem of Eliassen is generalized to include the effects of mechanical friction and Newtonian cooling in the paper by T J Dunkerton. The ozone differences in the Northern and Southern Hemispheres are analyzed by means of satellite data in the paper by M A Geller, M F Wu and E Nash. They found that the interhemispheric differences in the annual variation of total ozone can well be explained by the interhemispheric differences in stationary planetary waves. T Hirooka and I Hirota present further evidence of normal mode Rossby waves in their paper. Monthly mean winds in the mesosphere measured at 78 S are compared with the results of simultaneous measurements at 44 S by G J Fraser. A Phillips and R A Vincent report on radar observations of prevailing winds and waves in the Southern Hemisphere mesosphere and lower thermosphere and compare them with Northern Hemisphere data and satellite-derived circulation models. Geostrophic and nonlinear balanced winds from LIMS data are compared in the paper by T Miles and W L Grose. Gravity wave saturation processes, their effects (on wave amplitude, momentum and energy fluxes, the diffusion of heat and constituents, the establishment of the vertical wave number spectrum) and variability in the middle atmosphere are discussed by D C Fritts and several saturation mechanisms, as well as their effects (convection, H instability, vortical mode, parametric subharmonic instabilities, mean flow interaction) by T J Dunkerton. A theory of enhanced saturation of the gravity wave spectrum due to increases in atmospheric stability are expounded in the paper by Th E van Zandt and D C Fritts. Effects of horizontal resolution on internal gravity waves simulated by the 40 level GFDL "SKYHI" general circulation model are studied by Y Hayashi, D G Golder, J D Mahlman and S Miyahara. D P Delisi and T J Dunkerton report on laboratory observations of gravity wave critical-layer flows showing in the early evolution turbulent wavebreaking, as well as mean flow modifications and in the late-time critical layer flow internal mixing regions phase locked to the incoming gravity wave. S Fukao, M D Yamanaka, H Matsumoto, T Sato, T Tsuda and S Kato describe wind fluctuations near a cold vortex-tropopause funnel system observed by an MST radar, while wavelike wind variations in the lower stratosphere are analyzed by M D Yamanaka, S Fukao,

H Matsumoto, T Sato, T Tsuda and S Kato assuming monochromatic internal inertio-gravity wave generation. T Tsuda, Y Masuda, H Inuki, K Takahasi, T Takami, T Sato, S Fukao and S Kato report on a high time resolution monitoring of tropospheric temperature with a radio acoustic sounding system. Falling sphere observations of anisotropic gravity wave motions in the upper stratosphere over Australia are analyzed by S D Eckermann and R A Vincent suggesting that the dissipation of gravity waves in a significant source of momentum residuals found in studies of satellite data. A review of important constraints on gravity wave induced diffusion of minor constituents (H_2O, CO), heat and momentum is given in the paper by D F Strobel. C Sidi and F Dalaudier publish results of a study of temperature and heat flux spectra in the buoyancy subrange indicating the need for an anisotropic theory of buoyancy range of turbulence. Interpretation, reliability and accuracies of parameters deduced by the spaced antenna method in the middle atmosphere are discussed by W K Hocking, P May and J Röttger and it is shown that the spaced antenna technique gives reliable estimates of the neutral air motion enabling also the measurement of pattern scale, rate of fading and angle of arrival. Finally, in the paper by M Yamamoto, T Sato, T Tsuda, S Fukao and S Kato a full correlation analysis of turbulent scattering layers in the mesosphere is presented, which has been applied to echo power fluctuations observed by a MST radar.

P Bencze

W SCHRÖDER ed.: Past, present and future trends in geophysical research. Interdivisional commission on history of IAGA, Bremen-Roennebeck, 1988

This book contains 14 papers presented at historical symposia of the Vancouver IUGG General Assembly. A part of the papers deal with purely historical topics, e.g. Börner commemorates Ludwig Biermann, the discoverer of the solar wind; Wiederkehr reports on the activity of Georg Neumayer, a pioneer of geomagnetic observation in Australia. Gadsden presents some remarks on Kepler's atmospheric physics, elucidating the source of some interesting ideas by Kepler.

Brush and Bannerjee give a most comprehensive review on the history of the theories of geomagnetic secular variation. This is an excellent survey till the very first ideas of the phenomenon of the secular variation which was counted for some time as one of the greatest enigmas of modern physics. Heikkila describes the history of magnetic reconnection at the magnetospheric boundary. It is important to read this story from one of the participants in the discussion.

The second half of the book goes over pure history and tries to use historical data for collecting information on processes being active in some field of the Earth's environment.

A group of papers deals with historical auroras, mainly those observed during the Maunder minimum, and other aspects of the recent history of solar activity (Kopecky and Kuklin, Ribes, Ribes and Berthalot, Débarbat, Legrand and Simon). Hersé's paper on bright nights, a nearly forgotten phenomenon concludes this series.

A very active Italian group presented four papers, partly dealing with the methods to interprete historical point-like data, partly they use the methods presented here for several meteorological data sets, e.g. on the floods of the rivers Tevere and Tanaro. Due to the activity of this group, historical sources from Italy get more and more accessible to research, a fact which is welcome in this field where primary data and methods for

their processing are of vital importance.

The editor of the book, W Schröder should be congratulated to this wide-ranging selection of historical papers.

J Verő

Invitation

The Association of Hungarian Geophysicists decided at its annual meeting to establish a "Foundation for Hungarian Geophysicists" and elected a first Advisory Board for 3 years. The foundation could be started with a moderate initial capital of 300 000 HUF, but it is open for everybody.

The aim of the foundation is to help Hungarian geophysicists in the present difficult social and economical situation of the country. There are two main target groups whose application for grants will be accepted with preference: young geophysicists needing assistance (travels, participation at conferences, publications, post-graduate education etc.) at the beginning of their professional life as well as retired and unemployed colleagues whose economical and social position became especially unfavourable.

The nine members of the Advisory Board invite everybody to join this foundation; donations should be communicated with the Board. Organisations and persons donating sums exceeding the initial capital will have the opportunity to delegate representatives into the Board. Detailed information is available at the following address:

Advisory Board of the
"Foundation for Hungarian Geophysicists"
H-1368 Budapest, P.O.B. 240.
Budapest, VI. Anker köz 1.
Telephone 142-9754
Telex 22-5369
Telefax 156-1215

PRINTED IN HUNGARY

Akadémiai Kiadó és Nyomda Vállalat, Budapest

— treble underlining: bold-face italics
— red underlining: Greek letters
— green underlining: script letters.

Rules for mathematical-physical notations:

— trigonometric, logarithmic, analytic symbols, symbols for units and functions are in roman type (not underlined)
— letter symbols in mathematical and physical formulas, scalars, and subscripts of algebraic and physical quantities are in italics (underlined)
— vectors, matrices, operators in probability theory are in bold-face roman type (double underlining)
— tensors, operators and some special functions are in script letters (green underlining). These cannot be bold.
— Greek letters (red underlining) cannot be bold or extra bold type (thus they cannot be used for vectors or tensors)
— void upper lines e.g. for vectors
— avoid possible confusion between o (letter) and 0 (zero), l (letter) and 1 (one), ν (Greek nu) and v, u (letters) etc.
— explain ambiguous or uncommon symbols by making marginal notes in pencil
— be careful about superscripts and subscripts
— formulae must be numbered consecutively with the number in parentheses to the right of the formula. References in text to the equations may then usually be made by the number in parenthesis. When the word equation is used with a number, it is to be abbreviated, Eq. or Eqs in the plural
— the International System of Units (SI) should be used.

Authors are liable for the cost of alteration in the *proofs*. It is, therefore, the responsibility of the author to check the text for errors of facts before submitting the paper for publication.

3. *References* are accepted only in the Harvard system. Citations in the text should be as:

. . . (Bomford 1971) . . . or Bomford (1971)

. . . (Brosche and Sündermann 1976) . . .

. . . (Gibbs et al. 1976b) . . .

The list of references should contain names and initials of all authors (the abbreviation et al. is not accepted here); for *journal articles* year of publication, the title of the paper, title of the journal abbreviated, volume number, first and last page.

For *books* or *chapters in books*, the title is followed by the publisher and place of publication.

All items must appear both in the text and references.

Examples:

Bomford G 1971: Geodesy. Clarendon Press, Oxford

Brosche P, Sündermann J 1976: Effects of oceanic tides on the rotation of the earth. Manuscript. Univ. of Bonn

Buntebarth G 1976: Temperature calculations on the Hungarian seismic profile-section NP-2. In: *Geoelectric and Geothermal Studies (East-Central Europe, Soviet Asia), KAPG Geophysical Monograph.* Akadémiai Kiadó, Budapest, 561–566.

Gibbs N E, Poole W G, Stockmeyer P K 1976a: An algorithm for reducing the bandwidth and profile of a sparse matrix. *SIAM J. Number. Anal.*, 13, 236–250.

Gibbs N E, Poole W G, Stockmeyer P K 1976b: A comparison of several bandwidth and profile reduction algorithms. *ACM Trans. on Math. Software*, 2, 322–330.

Szarka L 1980: Potenciáltérképezés analóg modellezéssel (Analogue modeling of potential mapping). *Magyar Geofizika*, 21, 193–200.

4. *Footnotes* should be typed on separate sheets.

5. *Legends* should be short and clear. The place of the tables and figures should be indicated in the text, on the margin.

6. *Tables* should be numbered serially with Roman numerals. Vertical lines are not used.

All the illustrations should contain the figure number and author's name in pencil on the reverse.

Figures will be redrawn. Therefore the most important point is clearness of the figures, even pencil-drawings are accepted (with a duplicate).

Photographs and *half-tone* illustrations should be sharp and well contrasted.

If a specific reduction or enlargement is required, please indicate this in blue pencil on the figure.

The editors will send information to the first author about the *arrival* and acceptance of the papers. A galley proof is also sent to the first author for *correction*. Hundred *offprints* are supplied free of charge.

Periodicals of the Hungarian Academy of Sciences are obtainable at the following addresses:

AUSTRALIA
C.B.D. LIBRARY AND SUBSCRIPTION SERVICE
Box 4886, G.P.O., *Sydney N.S.W. 2001*
COSMOS BOOKSHOP, 145 Ackland Street
St. Kilda (Melbourne), Victoria 3182

AUSTRIA
GLOBUS, Hochstadtplatz 3, *1206 Wien XX*

BELGIUM
OFFICE INTERNATIONAL DE LIBRAIRIE
30 Avenue Marnix, *1050 Bruxelles*
LIBRAIRIE DU MONDE ENTIER
162 rue du Midi, *1000 Bruxelles*

BULGARIA
HEMUS, Bulvar Ruszki 6, *Sofia*

CANADA
PANNONIA BOOKS, P.O. Box 1017
Postal Station "**B**", *Toronto, Ontario M5T 2T8*

CHINA
CNPICOR, Periodical Department, P.O. Box 50
Peking

CZECHOSLOVAKIA
MAD'ARSKÁ KULTURA, Národní třida 22
115 66 Praha
PNS DOVOZ TISKU, Vinohradská 46, *Praha 2*
PNS DOVOZ TLAČE, *Bratislava 2*

DENMARK
EJNAR MUNKSGAARD, Norregade 6
1165 Copenhagen K

FEDERAL REPUBLIC OF GERMANY
KUNST UND WISSEN ERICH BIEBER
Postfach 46, *7000 Stuttgart 1*

FINLAND
AKATEEMINEN KIRJAKAUPPA, P.O. Box 128 *SF- 00101 Helsinki 10*

FRANCE
DAWSON-FRANCE S. A., B. P. 40, *91121 Palaiseau*
EUROPÉRIODIQUES S. A., 31 Avenue de Versailles, *78170 La Celle St. Cloud*
OFFICE INTERNATIONAL DE DOCUMENTATION ET LIBRAIRIE, 48 rue Gay-Lussac
75240 Paris Cedex 05

GERMAN DEMOCRATIC REPUBLIC
HAUS DER UNGARISCHEN KULTUR
Karl Liebknecht-Straße 9, *DDR-102 Berlin*
DEUTSCHE POST ZEITUNGSVERTRIEBSAMT Straße der Pariser Kommüne 3-4, *DDR-104 Berlin*

GREAT BRITAIN
BLACKWELL'S PERIODICALS DIVISION
Hythe Bridge Street, *Oxford OX1 2ET*
BUMPUS, HALDANE AND MAXWELL LTD.
Cowper Works, *Olney, Bucks MK46 4BN*
COLLET'S HOLDINGS LTD., Denington Estate *Wellingborough, Northants NN8 2QT*
WM. DAWSON AND SONS LTD., Cannon House *Folkstone, Kent CT19 5EE*
H. K. LEWIS AND CO., 136 Gower Street
London WCIE 6BS

GREECE
KOSTARAKIS BROTHERS INTERNATIONAL BOOKSELLERS, 2 Hippokratous Street, *Athens-143*

HOLLAND
MEULENHOFF-BRUNA B. V., Beulingstraat 2,
Amsterdam
MARTINUS NIJHOFF B.V.
Lange Voorhout 9-11, *Den Haag*
SWETS SUBSCRIPTION SERVICE
347b Heereweg, *Lisse*

INDIA
ALLIED PUBLISHING PRIVATE LTD., 13/14
Asaf Ali Road, *New Delhi 110001*
150 B-6 Mount Road, *Madras 600002*
INTERNATIONAL BOOK HOUSE PVT. LTD.
Madame Cama Road, *Bombay 400039*
THE STATE TRADING CORPORATION OF INDIA LTD., Books Import Division, Chandralok 36 Janpath, *New Delhi 110001*

ITALY
INTERSCIENTIA, Via Mazzé 28, *10149 Torino*
LIBRERIA COMMISSIONARIA SANSONI, Via Lamarmora 45, *50121 Firenze*
SANTO VANASIA, Via M. Macchi 58
20124 Milano
D. E. A., Via Lima 28, *00198 Roma*

JAPAN
KINOKUNIYA BOOK-STORE CO. LTD.
17-7 Shinjuku 3 chome, Shinjuku-ku, *Tokyo 160-91*
MARUZEN COMPANY LTD., Book Department, P.O. Box 5050 Tokyo International, *Tokyo 100-31*
NAUKA LTD. IMPORT DEPARTMENT
2-30-19 Minami Ikebukuro, Toshima-ku, *Tokyo 171*

KOREA
CHULPANMUL, *Phenjan*

NORWAY
TANUM-TIDSKRIFT-SENTRALEN A.S., Karl Johansgatan 41-43, *1000 Oslo*

POLAND
WĘGIERSKI INSTYTUT KULTURY, Marszalkowska 80, *00-517 Warszawa*
CKP-I W, ul. Towarowa 28, *00-958 Warszawa*

ROUMANIA
D. E. P., *Bucuresti*
ILEXIM, Calea Grivitei 64-66, *Bucuresti*

SOVIET UNION
SOJUZPECHAT — IMPORT, *Moscow*
and the post offices in each town
MEZHDUNARODNAYA KNIGA, *Moscow G-200*

SPAIN
DIAZ DE SANTOS, Lagasca 95, *Madrid 6*

SWEDEN
GUMPERTS UNIVERSITETSBOKHANDEL AB
Box 346, *401 25 Goteborg 1*

SWITZERLAND
KARGER LIBRI AG, Petersgraben 31, *4011 Basel*

USA
EBSCO SUBSCRIPTION SERVICES
P.O. Box 1943, *Birmingham, Alabama 35201*
F. W. FAXON COMPANY, INC.
15 Southwest Park, *Westwood Mass. 02090*
READ-MORE PUBLICATIONS, INC.
140 Cedar Street, *New York, N. Y. 10006*

YUGOSLAVIA
JUGOSLOVENSKA KNJIGA, Terazije 27, *Beograd*
FORUM, Vojvode Mišića 1, *21000 Novi Sad*

Index: 26.031